Forces Applied and Space Required Relationship for Four Caster Vehicle Manoeuvres

Brian Bernard Abraham

DOCTOR OF PHILOSOPHY

School of Mechanical and Systems Engineering
Newcastle University
May 2012

Abstract

Four-caster manually manoeuvred vehicles are ubiquitous with functions varying from goods movement to transport devices for disabled people. Manual handling related health and safety concerns have been raised but no theoretical study has been published. The few empirical studies which exist have not related dynamics to kinematics and no substantive guidance exists for disability adaptation planning for these vehicles.

A novel graphical method of inspecting the kinematics is developed: the vehicle translational velocity regions in which different combinations of wheel angular velocity directions occur are identified. Theory predicts that these varying combinations of wheel angular velocity directions, along with the caster orientations which arise from them, result in 1) different motion resistance reactions at each of the four caster assembly contacts with the vehicle-frame, 2) a variation in the proportion of the summation of those reactions to the resulting moment acting on the vehicle-frame and 3) substantial variation in the handle-forces required to balance these two motion resistance effects.

An empirical study is devised from the theory. Sixteen subjects made planar manoeuvres from static equilibrium with a maximum comfortable load while attempting to maintain eleven (maximum) different centres of zero velocity which related to the velocity regions. Results showed substantial inter-manoeuvre differences in maximum comfortable load: the loads of the manoeuvres with the two largest maximum comfortable loads are approximately 100% greater than the loads of the two manoeuvres with the smallest maximum comfortable load. The four-caster manually manoeuvred vehicle is mechanically omni-directional but the human operator is effectively constrained. The results confirm the predictions for the first-order effect.

The results are important for adaptation planning: environments can be planned to maximise the operator's load capacity. As the study is based on the relative difference between manoeuvres the results are applicable to various floor coverings and vehicles. The forces-applied and space-required relationship for these vehicles is not intuitive but the results are presented graphically and are therefore accessible to those in adaptation planning services. Further work includes investigation of second-order effects and the effects of wall constraints rather than maintenance of centres of zero velocity. In loose but concise terms this work shows how the architectural spaces which make manoeuvres easy or difficult can be identified.

'All this to bless your fellow man!'

Peter Bull (1998)

IN DEDICATION

Acknowledgements

Thanks be to God, Father, Son and Spirit: the universe to astound us and the discipline of science to humble us. For the many who have played a part in my beginning, persevering and reaching the summit of my small mountain, I give thanks: for Rob's rash, but ultimately justified, spur to begin, for the Dobies' generous encouragement, for the example of fellow travellers (not least Stuart and Andreas), for the prayers of many, for the patience of subjects, for the many 'lifts' from work colleagues (including Julia, and Shan's sympathy over 'hard sums'), for Cynthy's lengthy bearing with me (and without me), for Richard's maths tuition (till I left *him* behind) and proof reading, for Beccy's chilli to sustain me and finally, and far from least, for Garth's confidence in me.

Contents

Nomenclature

Symbols are ordered according to English then Greek alphabet with trailing subscript and then, if required, trailing superscript defining order.

Terms

(a.)	Appended to manoeuvre r, i.e. manoeuvre r (a.) indicating an experimentally attempted manoeuvre r.
ACMV	All caster manual vehicle, vehicle with only passive caster assemblies.
active wheel	Force from ground acting at G_i on wheel is determined by vehicle dynamics.
caster global orientation	Scalar of orientation vector of caster assembly about $\hat{\boldsymbol{S}}$ relative to the ground-plane, denoted θ_{si}.
caster global rotation	Scalar of angular velocity of caster assembly about $\hat{\boldsymbol{S}}$ relative to the ground-plane, denoted $\dot{\theta}_{si}$.
caster orientation	Scalar of orientation vector of caster assembly relative to vehicle-frame about $\hat{\boldsymbol{S}}$ denoted ${}^{B}\theta_{si}$.
caster rotation	Scalar of angular velocity of caster assembly relative to vehicle-frame about $\hat{\boldsymbol{S}}$ denoted ${}^{B}\dot{\theta}_{si}$.
caster steady-state	Idealised condition at which ${}^{B}\dot{\theta}_{si} = 0$, denoted ${}^{B}\theta_{steadi}$
caster near steady-state	Data point for θ_0 at which ${}^{B}\theta_{si}$ data is 90% of average ${}^{B}\theta_{si}$ data at end of manoeuvre r (attempted) , in respect of experimental-FCMV or $0.9{}^{B}\theta_{steadi}$ in respect of Zmodel-FCMV.

COM	Centre of mass
CoZV	Centre(s) of zero velocity
DOF	Degree(s) of freedom.
FCMV	Four caster manual vehicle, vehicle with four passive caster assemblies and two points of force applications at the rear of the vehicle.
Fixed wheel	Where roll heading is constant with respect to the vehicle-frame.
FWV	Manual or non-manual vehicle with caster assemblies and fixed wheels.
handle-forces	With respect to 1) the Dynamics Chapter P_{QLv}, P_{QRv}, P_{QLu} and P_{QRu}, 2) the Methods Chapter P_{Lv}, P_{Rv}, P_{Lu} or P_u, P_v and P_{uCs}, and 3) the Results Chapter P_u, P_v and P_{uCs}.
initial period	Data range for θ_0 from motion start data point to ${}_{ss1}\theta_0^r$ data point.
later period	Data range for θ_0 from data point after ${}_{ss1}\theta_0^r$ to near steady-state data point.
manoeuvre r	A Zmodel-FCMV manoeuvre with fixed CoZV.
manoeuvre r (attempted)	A experimental-FCMV manoeuvre based on manoeuvre r but with an approximate CoZV.
MDF	Medium Density Fibre board as used for the experimental floor-covering.
model-FCMV	FCMV with the assumptions as defined.
motion end	Data point for θ_0 after which all data is disregarded.
motion start	Data point for θ_0 at which all subsequent θ_0 are more negative, defined as $\theta_0 = 0$.
near steady-state	Data point for θ_0 at which all four caster assemblies achieve caster near steady-state.

nonholonomic constraint	Constraint: no $\hat{\boldsymbol{t}}$ direction relative velocity between wheel and ground at G_i.
passive wheel	Horizontal force from ground acting at G_i on wheel is determined by wheel dynamics.
PDF	Supplementary volume on the enclosed computer disc providing additional graphical inspections.
real-FCMV	FCMV without simplifying assumptions.
roll heading	Direction of $\hat{\boldsymbol{n}}_i$.
roll resistance	Motion resistance to wheel roll which arises from wheel and ground deformations or ground conformability which are not perfectly elastic.
rot-roll directions	$[\text{sgn}(\dot{\theta}_{si}), \text{sgn}(\dot{\theta}_{ti})]$
scrub friction	motion resistance effect on caster assembly about $\hat{\boldsymbol{s}}_i$.
start-steady period	Data range for θ_0 from motion start data point to near steady-state data point.
steady-state	When all caster assemblies are in caster steady-state.
steady-state period	Data range for θ_0 from data point after near steady-state data point to motion end data point.
vehicle-frame orientation	Scalar of orientation vector of vehicle-frame about $\hat{\boldsymbol{S}}$ denoted θ_0.
vehicle-frame rotation	Scalar of angular velocity of vehicle-frame about $\hat{\boldsymbol{S}}$ denoted $\dot{\theta}_0$.
walled-manoeuvres	The manoeuvre of real-FCMV in architectural space constrained by walls in contrast to manoeuvres r.
wheel orientation	Scalar of angular displacement vector of caster wheel about $\hat{\boldsymbol{t}}_i$ denoted θ_{ti}.
wheel roll	Scalar of angular velocity of caster wheel about $\hat{\boldsymbol{t}}_i$ denoted $\dot{\theta}_{ti}$.

wheel roll constraint	Constraint: no $\hat{\boldsymbol{n}}$ direction relative velocity between wheel and ground at G.
wheel rotation	The term for the scalar measure of the global angular velocity of a wheel about $\hat{\boldsymbol{S}}$.
Zmodel-FCMV	The equations and assumptions as defined for a model-FCMV with CoZV.

Symbol convention

Over-dotting	Where x is any variable, $\dot{x} = \frac{dx}{dt}$ and $\ddot{x} = \frac{d^2x}{dt^2}$.

Symbols

a_{1i}	Indexed set $\{1, -1, -1, 1\}$.
a_{2i}	Indexed set $\{1, 1, -1, -1\}$.
A_i	y-intercept of linear equation on $\dot{\boldsymbol{x}}_B$ plane derived from $\dot{\theta}_{si} = 0$.
B_i	y-intercept of linear equation on $\dot{\boldsymbol{x}}_B$ plane derived from $\dot{\theta}_{ti} = 0$.
c	Scalar of $\mathbf{c}$.
$\mathbf{c}$	Displacement vector measure from $\mathrm{C_O}$ to $\mathrm{G_O}$.
C_i	Point of geometric centre of caster wheel i.
$\mathrm{C_O}$	Point indicating centre of combined vehicle-frame and load mass.
$\overrightarrow{\mathrm{C_O S}_i}$	Displacement vector from point $\mathrm{C_O}$ to point S_i.
$\overrightarrow{\mathrm{C}_i \mathrm{W}_i}$	Displacement vector from point C_i to point W_i.
$f()$	Function of θ_0 in terms of ${}^B\theta_{si}$.
$f(M_{QPu})$	Function of scalar of moment produced by P_{Qu} when produced by handle-forces P_{QLu} and P_{QRu}.
$f_{Zr}()$	Function providing a handle-force measure for each manoeuvre r when $\lvert\boldsymbol{P}_{Qi}\rvert = 1$.
$f_{Zrmax}()$	Function providing maximum $f_{Zr}()$.
F_{Sni}	Scalar of contact force at point S_i, positive in the $\hat{\boldsymbol{n}}_i$ direction on caster stem and negative in the $\hat{\boldsymbol{n}}_i$ direction on vehicle-frame.

F_{Sti}	Scalar of contact force at point S_i, positive in the $\hat{\boldsymbol{t}}_i$ direction on the caster stem and negative in the $\hat{\boldsymbol{t}}_i$ direction on vehicle-frame.
F_{Gni}	Scalar of contact force at point G_i, negative in the $\hat{\boldsymbol{n}}_i$ direction on the caster wheel.
F_{Gti}	Scalar of contact force at point G_i, negative in the $\hat{\boldsymbol{t}}_i$ direction on the caster wheel.
F_x	Scalar of force measured by sensor, positive in $-\hat{\boldsymbol{u}}$ direction.
F_z	Scalar of force measured by sensor, positive in $\hat{\boldsymbol{v}}$ direction.
$g()$	Function expressing ${}^{B}\theta_{si}$ in terms of θ_0.
G_i	Point of ground-wheel contact line centre.
$\mathrm{G_O}$	Point of vehicle-frame geometric centre.
h_{L}	Positive scalar of $\hat{\boldsymbol{u}}$ component from S_4 to $\mathrm{P_L}$.
h_{R}	Positive scalar of $\hat{\boldsymbol{u}}$ component from S_3 to $\mathrm{P_R}$.
hw	Positive scalar of half-width between $\mathrm{P_L}$ and $\mathrm{P_R}$.
l	Positive scalar of vehicle-frame length
I	Mass moment of inertia of combined vehicle-frame and load mass.
$\Im()$	Imaginary component of the operand.
L_{Mmaxi}	Maximum comfortable load selection (kg) for each subject i for all manoeuvres r (attempted).
L^r_{Mi}	Maximum comfortable load selection (kg) for each subject i for each manoeuvre r (attempted).
L^r_{Mnormi}	Maximum comfortable load selection for each subject i for each manoeuvre r (attempted) as a percentage of L_{Mmaxi}.
L^r_{Mnormm}	The median L^r_{Mnormi} for each manoeuvre r (attempted).
m	Mass of combined vehicle-frame and load.
M_{QC}	Scalar of moment about $\hat{\boldsymbol{S}}$ required to balance motion resistance moment effects.

M_{QPu2}	Scalar of the minimum moment created by $\hat{\boldsymbol{u}}$ components of handle-forces to balance motion resistance moment effects.
M_{uCs}	Scalar of moment about $\hat{\boldsymbol{S}}$ required to balance sensor measures for transformation to handle-forces.
M_y	Scalar of moment measured by sensor about $\hat{\boldsymbol{S}}$ direction.
$\hat{\boldsymbol{n}}_i$	Unit vector of tns_i indicating roll-heading.
O_i	Points in $\dot{\boldsymbol{x}}_B$ plane, fixed by graphic inspection method.
P	Point midway between $\mathrm{P_L}$ and $\mathrm{P_R}$ in $\hat{\boldsymbol{v}}$ direction.
P_a	Scalar of handle-force where a is any of P_{uCs}, P_u or P_v.
${}^{nth}_{ar}P^r_a$	Percentile measure where nth is any percentile, a is any of P_{uCs}, P_u or P_v, r is any manoeuvre r and ar is any θ_0 range of data points.
${}^{mth}_{ar}P^r_{amax}$	Maximum magnitude ${}^{nth}_{ar}P^r_a$ for all subjects, where nth is either or $+90^{th}$ or -90^{th}.
${}^{mth}_{ar}P^r_{amaxi}$	Maximum magnitude ${}^{nth}_{ar}P^r_a$ for each subject, nth as above.
${}^{mth}_{ar}P^r_{amin}$	Minimum magnitude ${}^{nth}_{ar}P^r_a$ for all subjects, nth as above.
${}^{mth}_{ar}P^r_{amini}$	Minimum magnitude ${}^{nth}_{ar}P^r_a$ for each subject, nth as above.
$\mathrm{P_L}$	Point of left handle-force contact.
P_{Lu}	Scalar measure of $\hat{\boldsymbol{u}}$ directed left handle-force
P_{Lv}	Scalar measure of $\hat{\boldsymbol{v}}$ directed left handle-force
$\mathrm{P_R}$	Point of right handle-force contact.
P_{QH}	Positive scalar, summed magnitudes of handle-forces to balance motion resistance effects for quasi-static case.
P_{QHmin}	P_{QH} using a minimisation procedure.
P_{QH1}	P_{QH} for the limited case where $P_{QuCs} = 0$.
$\boldsymbol{P}_{Qi}$	Force required at S_i to balance motion resistance effect at caster assembly i.

P_{QLv}	Scalar of handle-force in $\hat{\boldsymbol{v}}$ direction at $\mathrm{P_L}$ required to balance motion resistance for quasi-static case.
P_{QLu}	Scalar of handle-force in $\hat{\boldsymbol{u}}$ direction at $\mathrm{P_L}$ required to balance motion resistance for quasi-static case.
P_{QRv}	Scalar of handle-force in the $\hat{\boldsymbol{v}}$ direction at $\mathrm{P_R}$ required to balance motion resistance for quasi-static case.
P_{QRu}	Scalar of handle-force in $\hat{\boldsymbol{u}}$ direction at $\mathrm{P_R}$ required to balance motion resistance for quasi-static case.
P_{QuCs}	Positive scalar, summed magnitudes of $\hat{\boldsymbol{u}}$ components of handle-forces producing a force-couple for quasi-static case.
P_{Qv}	Scalar of force at COM in $\hat{\boldsymbol{v}}$ direction for quasi-static case.
P_{Qvi}	Scalar of $\boldsymbol{P}_{Qi}$ in $\hat{\boldsymbol{v}}$ direction for caster assembly i.
P_{Qu}	P_u for quasi-static case.
P_{Qui}	Scalar of $\boldsymbol{P}_{Qi}$ in $\hat{\boldsymbol{u}}$ direction for caster assembly i.
P_u	Scalar of force in $\hat{\boldsymbol{u}}$ direction at either $\mathrm{C_O}$ for the Zmodel-FCMV or at S for experimental-FCMV.
P_{uCs}	Scalar of $\hat{\boldsymbol{u}}$ directed handle-forces which contribute to a couple as defined in Section 5.3.1 (page 116).
P_{Ru}	scalar measure of $\hat{u}$ directed right handle-force
P_{Rv}	scalar measure of $\hat{v}$ directed right handle-force
P_v	Scalar of force in $\hat{\boldsymbol{v}}$ direction at either $\mathrm{C_O}$ for the Zmodel-FCMV or at S for experimental-FCMV.
${}^{large}_{ss1}\mathbf{P}^{\mathrm{r}}_i$	Cuboid boundary enclosing ${}^{mth}_{ar}P^r_{amini}$-${}^{mth}_{ar}P^r_{amaxi}$ range for each subject for each manoeuvre r (attempted).
${}^{large}_{ss1}\mathbf{P}^{\mathrm{r}}$	Cuboid boundary enclosing ${}^{mth}_{ar}P^r_{amin}$-${}^{mth}_{ar}P^r_{amax}$ range for all subjects for each manoeuvre r (attempted).
r	Positive scalar of caster wheel radius.

$\boldsymbol{R}_{Fi}$	Moment of caster assembly motion resistance about $\hat{\boldsymbol{S}}$ termed scrub friction.
R_{Fi}	Scalar of $\boldsymbol{R}_{Fi}$.
$\boldsymbol{R}_{Li}$	Moment of caster wheel motion resistance about $\hat{\boldsymbol{t}}_i$.
R_{Li}	Scalar of $\boldsymbol{R}_{Li}$.
s	Positive scalar dimension between P and S $\hat{\boldsymbol{u}}$ direction.
S	Point of origin of sensor axes.
$\hat{\boldsymbol{S}}$	Unit vector of uvs, perpendicular to the ground plane with positive upwards.
$\hat{\boldsymbol{s}}_i$	Unit vector of tns_i, perpendicular to ground plane with positive upwards.
S_i	Point, idealised, of caster-stem–vehicle-frame contact.
$[\mathrm{sgn}(\dot{\theta}_{si}),$ $\mathrm{sgn}(\dot{\theta}_{ti})]$	rot-roll directions.
t	Positive scalar of caster trail or variable for polynomial fit function.
T	Scalar of torque on vehicle-frame about the $\hat{\boldsymbol{S}}$ direction.
$t_i()$	Time duration function for $\Delta\theta_0$.
$\hat{\boldsymbol{t}}_i$	Unit vector of tns_i, perpendicular to $\hat{\boldsymbol{n}}_i$.
tns_i	Orthonormal triad formed with right hand rule fixed to point S_i.
$\hat{\boldsymbol{u}}$	Unit vector of uvs, forward direction viewed by FCMV operator.
$\hat{\boldsymbol{v}}$	Unit vector of uvs, positive to left as viewed by FCMV operator.
uvs	Orthonormal triad formed with right hand rule fixed to vehicle-frame at $\mathrm{C_O}$.
W_i	Point on caster wheel surface.
w_v	Scalar of vertical displacement of W_i of caster wheel i.
w	Positive scalar of half vehicle-frame width: between S_1 and S_2 or S_3 and S_4.

x	Variable denoting real number.
$\hat{\boldsymbol{X}}$	Unit vector of ground plane co-directional with $\hat{\boldsymbol{u}}$ at $\theta_0 = 0$.
$\dot{\boldsymbol{x}}_B$	Translational velocity of $\mathrm{C_O}$ on vehicle-frame.
$\ddot{\boldsymbol{x}}_B$	Translational acceleration of $\mathrm{C_O}$ on vehicle-frame.
$\dot{x}_{Bu}$	Scalar of $\hat{\boldsymbol{u}}$ component of $\dot{\boldsymbol{x}}_B$.
$\ddot{x}_{Bu}$	Time derivative of $\dot{x}_{Bu}$.
$\dot{x}_{Bv}$	Scalar of $\hat{\boldsymbol{v}}$ component of $\dot{\boldsymbol{x}}_B$.
$\ddot{x}_{Bv}$	Time derivative of $\dot{x}_{Bv}$.
$\dot{\boldsymbol{x}}_{ci}$	Translational velocity of C_i point.
$\dot{x}_{Cni}$	Scalar of $\dot{\boldsymbol{x}}_{ci}$ in $\hat{\boldsymbol{n}}_i$ direction for caster assembly i.
$\dot{x}_{Cti}$	Scalar of $\dot{\boldsymbol{x}}_{ci}$ in $\hat{\boldsymbol{t}}_i$ direction for caster assembly i.
$\dot{x}_G()$	Scalar magnitude of translational velocity of geometric centre of vehicle-frame at θ_0 data point based on $\dot{\theta}_0$.
$\dot{\boldsymbol{x}}_{Si}$	Translational velocity of S_i point.
$\hat{\boldsymbol{Y}}$	Unit vector of ground plane co-directional with $\hat{\boldsymbol{v}}$ at $\theta_0 = 0$
z	Variable denoting complex number.
$\overrightarrow{\mathrm{Z}_r\mathrm{C_O}}$	Displacement vector from point Z_r to point $\mathrm{C_O}$.
$\overrightarrow{\mathrm{Z}_r\mathrm{S}_i}$	Displacement vector from point Z_r to point S_i.
Z_r	Point of CoZV, viewed as either on vehicle-frame or ground-plane.
Z_{ri}	Scalar of $\overrightarrow{\mathrm{Z}_r\mathrm{S}_i}$.
Z_{tri}	$(t^2 - Z_{ri}^2)$.
Δ	Numerical change in a variable.
ρ	1) Test statistic in statistical significance context, 2) as ρ_i in some Figures.
ρ_i	(1) Scalar of orientation vector from $\hat{\boldsymbol{n}}_i$ to direction of combined effects of $\boldsymbol{R}_{Fi}$ and $\boldsymbol{R}_{Li}$ acting on vehicle-frame at S_i. (page 90) (2) When defined as a constant this defines the scrub friction to roll resistance proportion at $\mathrm{sgn}(\dot{\theta}_{si}) = \mathrm{sgn}(\dot{\theta}_{ti}) = 1$ and the numerical value is then redefined for sign changes.

θ_0	Scalar of vehicle-frame orientation vector about $\hat{\boldsymbol{S}}$.
θ_{00}	Lower bound θ_0 for integration.
θ_{01}	Upper bound of θ_0 for integration.
$\dot{\theta}_0$	Time derivative of θ_0
$\ddot{\theta}_0$	Time derivative of $\dot{\theta}_0$.
$\{\theta_{0n}\}$	Set of θ_0 measures comprising of all instances of $\Delta\text{sgn}(\dot{\theta}_{si})$ and $\Delta\text{sgn}(\dot{\theta}_{ti})$ for all manoeuvres r.
θ_{0rti}	θ_0 for $\Delta\text{sgn}(\dot{\theta}_{ti})$ for manoeuvre r and caster assembly i.
θ_{si}	Scalar of orientation vector of caster assembly i about $\hat{\boldsymbol{S}}$ with respect to ground-plane, termed caster global orientation.
$\dot{\theta_{si}}$	Time derivative of θ_{si}, termed caster global rotation.
θ_m	Scalar of orientation vector from $-\hat{\boldsymbol{n}}_i$ axis to W_i.
θ_{ti}	Scalar of orientation vector of caster wheel about $\hat{\boldsymbol{t}}_i$ direction.
θ_{ti0}	Lower bound of θ_{ti} for integration.
θ_{ti1}	Upper bound of θ_{ti} for integration.
$\dot{\theta_{ti}}$	Time derivative of θ_{ti}, termed wheel roll.
${}^B\theta_{si}$	Scalar for orientation vector from $\hat{\boldsymbol{u}}$ direction to $\hat{\boldsymbol{n}}_i$ direction termed caster orientation.
${}^B\theta_{si0}$	Lower bound of ${}^B\theta_{si}$ for integration.
${}^B\theta_{si1}$	Upper bound of ${}^B\theta_{si}$ for integration.
${}^B\theta_{sip}$	${}^B\theta_{si0}$ or ${}^B\theta_{si0}$.
${}^B\dot{\theta}_{si}$	Time derivative of ${}^B\theta_{si}$ termed caster rotation.
${}^B\theta_{steadi}$	${}^B\theta_{si}$ at which caster steady-state occurs for caster assembly i.
${}^B\theta_{zi}$	Scalar of orientation vector from $\hat{\boldsymbol{u}}$ to the direction of $\dot{\boldsymbol{x}}_{Si}$.
${}^B\theta_{zi1}$	Interim value for calculating ${}^B\theta_{zi}$.

Subscripts leading

$ss1$	Data point set for initial period.
$ss1a$	Data point set for initial period disregarding a small $\Delta\theta_0$ from motion start.
ssi	Data point set for start-steady period.

Subscripts trailing

i	Caster assembly or caster wheel index.
n	Index for $\{\theta_{0n}\}$, $[n = 1, \ldots, 44]$.
r	1) Any of [A, ..., M] in respect of the Dynamics Chapter and any of [A, ..., L] in respect of the Results Chapter.

Superscripts leading

B	Measures viewed from uvs frame.

Superscripts trailing

r	Indicating any of [A, ..., L] for manoeuvres r (attempted)
A	Relating to manoeuvre A (attempted).
B	Relating to manoeuvre B (attempted).
C	Relating to manoeuvre C (attempted).
D	Relating to manoeuvre D (attempted).
E	Relating to manoeuvre E (attempted).
F	Relating to manoeuvre F (attempted).
G	Relating to manoeuvre G (attempted).
H	Relating to manoeuvre H (attempted).
J	Relating to manoeuvre J .
K	Relating to manoeuvre K or manoeuvre K (attempted).
L	Relating to manoeuvre L or manoeuvre L (attempted).
M	Relating to manoeuvre M.

Chapter 1–Introduction

1.1. **Foreword**

The impact of disabilities on those with the disability and those who support them is, for good or ill, partly a consequence of technology and the environment. Wheeled vehicles and suitable architectural spaces have made a huge contribution to the wellbeing of people with disabilities and those who support them.

If the streamline vehicle shapes of Olympic wheelchair sprinters are at one end of the occupant wheeled vehicle spectrum then there is at the other end, hidden from public view, a wheeled vehicle of rudimentary technology but of considerable importance: the all-caster manual vehicle serves for showering, over-toilet use and as indoor transport in confined spaces such as between bed and armchair and living room and dining room.

Somewhere in the process of obtaining wheeled vehicles for disability access and determining architectural spaces for their use a decision has to be made regarding vehicle-space compatibility: a commonplace domestic analogy with relatively minor implications on failure is making sure, before purchase, that a settee can be moved from the corridor into its designated room. The author's role as an occupational therapist in a property adaptation service for disabled people means that colleagues and he have to make such vehicle-space compatibility decisions on a daily basis. Experience indicates that space is often confined, occupants may be heavy, operators are often challenged by the forces which have to be applied, collisions have to be avoided and there is often uncertainty as to how to predict whether or not a particular architectural space and vehicle combination would produce an easy or a difficult manoeuvre. Additionally, no methods have been published as to how vehicle-space compatibility uncertainty can be reduced for all-caster manual vehicles.

1.2. Objectives

The primary objective of this investigation is to contribute to the understanding of adaptation planning for all-caster manual vehicles in a way which assists decision-making for vehicle-architectural compatibility, i.e. adaptation planning.

A secondary objective is to ensure that the results can be conveyed graphically and understood intuitively by those, non-engineers, who are responsible for adaptation planning.

1.3. Thesis Structure

A Preliminary Chapter presents some basic mechanical and wheeled vehicle related matters which are considered in the Literature Chapter.

The Literature Chapter outlines the experiential starting point, details reports of all-caster manual vehicle manoeuvring difficulties, describes the background context to disability adaptation planning, reviews the state of the art for adaptation planning and the mechanical literature for the all-caster manual vehicle, concludes that existing literature on vehicle-space compatibility for these vehicles is inadequate, considers current knowledge in terms of motion resistance and makes a necessary methodological conclusion to study the vehicle as a complete system.

The Dynamics Chapter presents a novel graphical method of interpreting all-caster manual vehicle dynamics and this leads to a specific investigative method based on centres of zero velocity. Theoretical analysis taking account of uncertainty regarding empirical measures of motion-resistance is conducted and it is concluded that substantial differences in handle-force measures should be expected for the different manoeuvres.

The Methods Chapter details an investigative method based on the model developed in the Dynamics Chapter. The psychophysical approach is used: this requires motivated subjects to find a maximum comfortable load for eleven different manoeuvring tasks after which the manoeuvres are repeated while force, moment and displacement measurements are made.

The Results Chapter reports the load selections and handle-forces for three manoeuvres in detail: as the results presentation process is largely identical for

each manoeuvre the results for the other eight manoeuvres are given in detail in Appendix D. The result summary for all manoeuvres is presented and this indicates that there are substantial differences in the inter-manoeuvre handle-force measures and these are associated with differences in load selection.

A Discussion Chapter examines and demonstrates the robustness of the results, summarises the findings, demonstrates that the results are important for adaptation planning, illustrates some adaptation planning applications, considers the generalisation of the results, outlines further work with the existing data and and describes future investigations.

A Conclusion Chapter summarises the findings and their importance. This includes a summary of the application of the findings for adaptation planning. Acknowledgement of contributors to the work is included.

Four Appendices are provided: Appendix A provides supplementary mathematical or mechanical information, Appendix B details the structured Literature Review, Appendix C details computerised processes and Appendix D details the data not included in the Results Chapter.

A computer disc is also enclosed. This contains 1) further details relating to the methods, 2) a PDF document which contains the large number of data related graphs and some model related graphs which were inspected and 3) the computer program files and data files which were used.

Chapter 2–Preliminaries

2.1. **Introduction**

This chapter comprises three sections. A brief first section introduces conventions used in the text. The second section introduces the mechanical concepts which are foundational to understanding manual wheeled vehicles. This requires the application of elementary mechanics as provided in basic statics and dynamics literature such as Meriam and Kraige (2003): specifically plane kinematics of particles and rigid bodies, plane kinetics of rigid bodies and work. The only exception to elementary dynamics is the need to consider nonholonomics: this is treated in sufficient depth in Greenwood (1965). Additionally the hysteresis effect and other motion resistance related phenomenon are considered qualitatively. The third section introduces wheeled vehicles: particularly those related to disability access. The existing terminology for these vehicles is considered, found to be inadequate for the investigative purposes, and a mechanical classification is defined. With a small number of mechanical concepts defined and definitions made it is then possible to consider the literature.

2.2. **Conventions**

For the purposes of consistency, conciseness and avoiding ambiguity a number of conventions are used throughout this text as follows. Firstly, all defined terms, and symbols which appear on pages distant to the original definition are included in a single nomenclature. The nomenclature is placed at the end of this chapter and provides a single reference point to support the frequent back-referencing to matters considered in earlier parts of the thesis. Where verbal discussion relating to symbols is envisaged the symbols are given a textual term. As nomenclature descriptions are terse page reference is given to the original definition on some occasions. Secondly,

while the main text is complete in itself, at many points further explanation is given in Appendix A, for example, details of algebraic manipulation or further elaboration: this is indicated by '(page *no.*)' where '*no.*' is a subsequent page. Other conventions are introduced as they arise.

2.3. Vehicle Wheel Mechanisms

The following sections present basic concepts of wheel mechanics as a preliminary to considering the literature for wheeled vehicles relevant to disability uses.

2.3.1. *Coulomb friction*

It is useful to begin by considering friction forces. For body contacts not separated by fluid (dry contacts) this is typically modelled with the Coulomb friction law (Tariku and Rogers, 2001) as follows. Figure 2.1 (page 6) illustrates the free body diagram of body A–represented by a cylinder–which has a line contact contact with body B (not shown). Body B is and remains in static equilibrium. The rigid body assumption is made for both bodies. (Vectors are indicated by bold font in the text but to avoid any ambiguity arising from printing, an over-bar is added in the illustrations: unit vectors are hatted in both text and illustrations.) Body A is defined as: 1) having one degree of freedom (DOF) in the $\hat{\boldsymbol{n}}$ direction with, 2) the velocity relative to body B defined by $\dot{x}\hat{\boldsymbol{n}}$, 3) subject to a force with scalar measure F in direction $\hat{\boldsymbol{n}}$, 4) subject to loading force $\boldsymbol{L}$ which accounts for the body A mass and external forces in direction $-\hat{\boldsymbol{S}}$, 5) subject to the reaction of body B acting on body A, one component of which is indicated by $\boldsymbol{R}$ (Coulomb friction reaction) which acts in the $\hat{\boldsymbol{n}}$ direction and 6) a second component defined by $F_G\hat{\boldsymbol{S}}$ which is the reaction to $\boldsymbol{L}$ and maintains body A in static equilibrium in the $\hat{\boldsymbol{S}}$ direction. As body A is defined as having one DOF, moments need not be considered. For this arrangement using a Coulomb friction model, $\boldsymbol{R}$ is defined as:

$$\boldsymbol{R} = \begin{cases} -F\hat{\boldsymbol{n}} & \dot{x}\hat{\boldsymbol{n}} = 0\text{: } |F\hat{\boldsymbol{n}}| \leq f_1(|\boldsymbol{L}|) \\ -\mathrm{sgn}(\dot{x}\hat{\boldsymbol{n}}) f_2(|\boldsymbol{L}|)\hat{\boldsymbol{n}} & \dot{x}\hat{\boldsymbol{n}} \neq 0. \end{cases} \tag{2.1}$$

For the first condition $\boldsymbol{R}$ may be viewed as balancing $F\hat{\boldsymbol{n}}$ with the restriction that this state can only exist if $F\hat{\boldsymbol{n}}$ does not exceed the 'breakaway force' (as

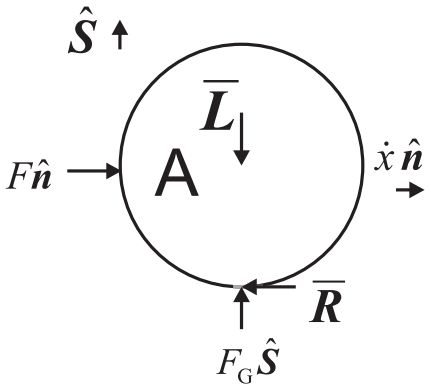

Figure 2.1 – Shows the free-body arrangement for analysis of the Coulomb friction law.

termed by Karnopp (1985)) defined by $f_1(|\boldsymbol{L}|)$ (often shown as μL) which is a function of the loading and the surface properties of the two bodies. In this text the term 'balancing' is used to refer to the actions required to maintain or exceed the breakaway force for the dynamic case. Two functions of $\boldsymbol{L}$ are used in Equation 2.1 as the maximum magnitude of $\boldsymbol{R}$ is typically larger for the first condition than for the second condition (Karnopp). Equation 2.1 indicates that for the dynamic equilibrium case, if $\dot{x}\hat{\boldsymbol{n}}$ is not to tend to zero the magnitude of $F\hat{\boldsymbol{n}}$ must balance (or exceed for the dynamic case) the magnitude of $\boldsymbol{R}$. (Further elaboration, page 231) The wheel may now be considered.

2.3.2. *Wheel roll*

Figure 2.2 (page 7) (left) illustrates a single-wheel vehicle model defined as follows: 1) neither wheel material nor ground (not shown) are subject to deformation (the rigid body assumption), 2) the wheel is an ideal cylinder of homogeneous material with radius r, 3) a line contact exists between wheel and ground, the centre point of which is denoted G_i, 4) the wheel is defined as having one translational DOF as indicated by the axis of $\hat{\boldsymbol{n}}_i$ with scalar measure x_{Cni} and 5) one angular DOF, with scalar measure θ_{ti}, about the axis of $\hat{\boldsymbol{t}}_i$ with, 6) $\hat{\boldsymbol{t}}_i$ perpendicular to the wheel face and positive moving into the page, 7) the geometric centre of the wheel is denoted C_i, 8) loading force $\boldsymbol{L}$ acts acts through point C_i in direction $-\hat{\boldsymbol{S}}$ and 9) static equilibrium in the $\hat{\boldsymbol{S}}$ direction is maintained by the ground reaction $F_{GS}\hat{\boldsymbol{S}}$ which acts along the contact line and balances both the effect of wheel mass and $\boldsymbol{L}$.

For the illustration (left) the wheel is defined as being in dynamic equilibrium with a constant angular velocity denoted $\dot{\theta}_{ti}\hat{\boldsymbol{t}}_{\boldsymbol{i}}$ and with point C_i having a constant translational velocity denoted $\dot{x}_{Cni}\hat{\boldsymbol{n}}_i$. Throughout this text the scalar of $\dot{\theta}_{ti}\hat{\boldsymbol{t}}_{\boldsymbol{i}}$ is termed 'wheel roll' and $\hat{\boldsymbol{n}}_i$ is termed 'roll heading'. If it is also defined that there is no relative velocity between point G_i on the wheel, denoted $\dot{x}_{Gi}\hat{\boldsymbol{n}}_i$, and point G_i on the ground it follows that $\dot{x}_{Gi} = \dot{x}_{Cni} - \dot{\theta}_{ti}r = 0$ and

$$\begin{aligned} \dot{x}_{Cni} &= \dot{\theta}_{ti}r \\ \Rightarrow x_{Cni} &= \theta_{ti}r. \end{aligned} \tag{2.2}$$

Equation 2.2 is termed 'wheel roll constraint' in this text and the implication is made by integration. While the wheel in Figure 2.2 requires two coordinates to define the configuration, x_{Cni} and θ_{ti}, when the wheel is to subject Equation 2.2 only one coordinate is required to define the system configuration so the system now has one DOF.

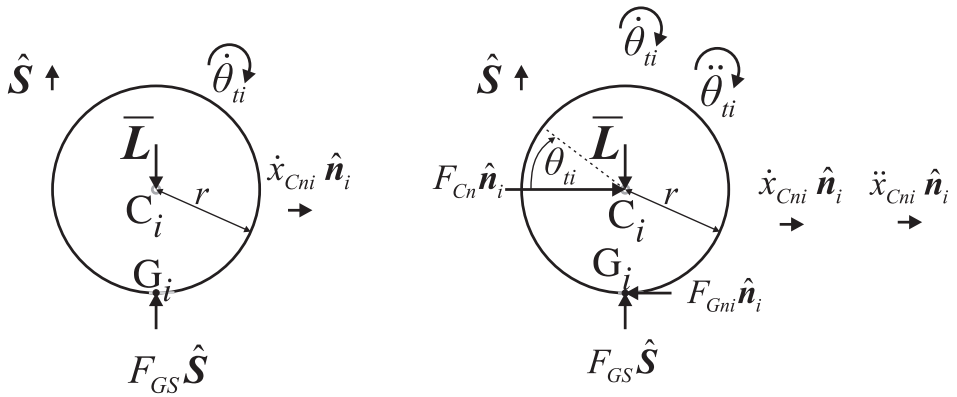

Figure 2.2 – Shows a single-wheel vehicle model: (left) for dynamic equilibrium and (right) for dynamic state.

Figure 2.2 (right) shows the arrangement when a force is applied at point C_i as indicated by $F_{Cn}\hat{\boldsymbol{n}}_i$. Three notable features can be demonstrated for this system. Firstly, it can be shown that the reaction force $F_{Gni}\hat{\boldsymbol{n}}_i$ converts linear work to angular work without energy loss. (page 232) Secondly, $F_{Gni}\hat{\boldsymbol{n}}_i$ is nevertheless a friction force acting in accordance with the first condition of Equation 2.1 since this system is defined with $\dot{x}_{Gi} = 0$. Thirdly, increasing the magnitude of $\boldsymbol{L}$, for example, adding load to the vehicle, increases the maximum magnitude of $F_{Gni}\hat{\boldsymbol{n}}_i$ available to produce angular work but does not increase the magnitude of $F_{Gni}\hat{\boldsymbol{n}}_i$.

A wheel system with these features is termed a 'passive wheel' in this text. The horizontal ground reactions for a passive wheel are therefore related to the dynamics of the wheel and not the loading of the wheel though loading affects the maximum magnitude of this reaction.

An alternative to a passive wheel is termed an 'active wheel' in this text and this occurs if the moment which produces $\ddot{\theta}_{ti}$ is the result of actions occurring within the vehicle; for the passive wheel the action force $F_{Cn}\hat{\boldsymbol{n}}_i$ is external to the vehicle. To represent the active wheel based on Figure 2.2 (right) it would be necessary to remove $F_{Cn}\hat{\boldsymbol{n}}_i$ and set $F_{Gni}\hat{\boldsymbol{n}}_i$ to be directed as $\ddot{x}_{Cni}$; a suitable moment would also need to be added since the moment effect of $F_{Gni}\hat{\boldsymbol{n}}_i$ is now opposed to $\ddot{\theta}_{ti}$. The force component of the equations of motion for this system would then, where m is the vehicle mass, be $F_{Gni}\hat{\boldsymbol{n}}_i = m\ddot{x}_{Cni}\hat{\boldsymbol{n}}_i$ and since the wheel roll constraint can be differentiated this equation of motion is also given by $F_{Gni}\hat{\boldsymbol{n}}_i = mr\ddot{\theta}_{ti}\hat{\boldsymbol{n}}_i$. It then follows that it is possible for $\ddot{\theta}_{ti}$ to have a magnitude such that the $|F_{Gni}|$ required to balance $mr\ddot{\theta}_{ti}\hat{\boldsymbol{n}}_i$ exceeds the maximum magnitude indicated by the first condition of Equation 2.1. The ground reactions for an active wheel are therefore related to the dynamics of the vehicle. The drive wheels of an automobile are active wheels and the operation of the second condition of Equation 2.1 is visible when the automobile vehicle body is in and remains in static equilibrium on an iced road but wheel roll occurs.

Whether or not a wheel is passive or active is not necessarily intrinsic to the mechanical system. Consider the wheeled vehicle illustrated in Figure 2.6(g) (page 17). If an occupant applies a force to the large rear wheels producing a moment about the $\hat{\boldsymbol{t}}_{\boldsymbol{i}}$ direction (as previously defined) then the wheels function as active wheels since the reaction force acting on the wheel at the wheel-ground contact is a function of the vehicle dynamics. However, if forces are applied to the handles of the vehicle by someone assisting the occupant then functionally the rear wheels are passive wheels.

Where $\hat{\boldsymbol{n}}_i$ is constant with respect to the vehicle to which the wheel is attached this is termed a 'fixed wheel' in this text. The rear wheels of Figure 2.5 (page 13) are fixed wheels.

2.3.3. *Nonholonomics*

Examination of the wheel defined for Figure 2.2 (page 7) when subject to general plane motion makes another feature evident and Figure 2.3 (page 9) shows a top view of the idealised wheel with direction $\hat{\boldsymbol{t}}_i$ perpendicular to $\hat{\boldsymbol{n}}_i$ and parallel with the ground-plane. It is evident, since the wheel-ground contact may be viewed as subject to Coulomb friction, that the breakaway force magnitude acting at G_i (not shown but directly beneath C_i as shown in Figure 2.2) that would be required in the axis of $\hat{\boldsymbol{t}}_i$ is a function of $\boldsymbol{L}$, with $\boldsymbol{L}$ as shown in Figure 2.2. Therefore, where $\boldsymbol{L}$ is large compared with the wheel mass, this is typical for most wheeled vehicles, the breakaway force required to create a nonzero $\dot{x}_{Cti}\hat{\boldsymbol{t}}_i$ is relatively large compared with the force magnitude at point C_i which would be required to change the system from static equilibrium to a nonzero wheel roll. In loose language it takes a much larger force to make a wheel move sideways compared to making it roll. An idealisation of this effect defines a second constraint for the wheel

$$\dot{x}_{Cti}\hat{\boldsymbol{t}}_i = 0 : \tag{2.3}$$

this is an example of a constraint class termed nonholonomic and this is termed the 'nonholonomic constraint' in this text. These constraint classifications provide

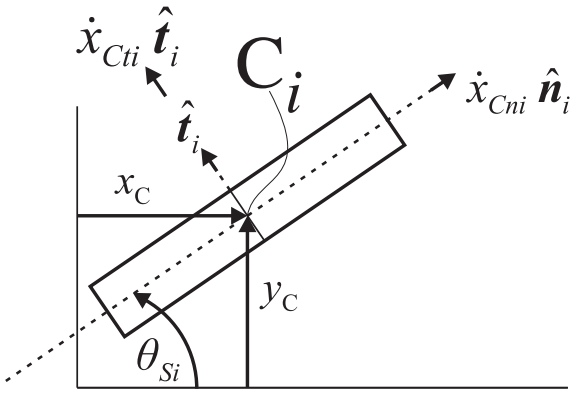

Figure 2.3 – Shows, viewed from the top, the arrangement for a general motion with wheel roll on the plane.

a useful means of distinguishing the behaviour of mechanical systems and this applies to the wheel as follows. Before considering the nonholonomic constraint it is useful to consider a constraint which is not nonholonomic: the system illustrated in Figure 2.2 for the wheel roll constraint. For this system there are two configuration coordinates (θ_{ti} and x_{Cni}), one constraint and a resulting one DOF, i.e. one

constraint removed one DOF. The wheel illustrated in Figure 2.3 (page 9) requires four coordinates to specify the configuration (x_C, y_C, θ_{Si} and θ_{ti}) if not subject to the wheel roll constraint and three configuration coordinates if the system is subject to the wheel roll constraint: $\dot{x}_C$, $\dot{y}_C$ and θ_{Si} can be used to determine $\dot{x}_{Cni}\hat{\boldsymbol{n}}_i$ and consequentially $\dot{\theta}_{ti}$ and so θ_{ti}. Thus, despite there being two *two* DOF (one in the $\hat{\boldsymbol{n}}_i$ direction and one about $\hat{\boldsymbol{S}}$) there are *three* configuration coordinates (x_C, y_C, θ_{Si}): this is a feature of a system with a nonholonomic constraint. The practical implication is that the nonholonomic system is one where the kinematics permit the configuration coordinates to have arbitrary values without violating the constraint: Johnson (2007) has shown this for a sphere but the example may be extended to a wheel system with a line contact. In loose language the wheel which is subject to Equation 2.3 may be displaced to any position on the plane even though it cannot be moved directly to the side. Mathematically the nonholonomic constraint is a function of the form $f(x, \dot{x}, t)$=0, where t is time and where the $\dot{x}$ term cannot be integrated to provide only x Greenwood (1965), i.e. the velocity term is constrained without any mathematical means of expressing this in terms of displacement.

2.3.4. *Caster assembly*

A caster assembly is illustrated in Figure 2.4 (page 12): labelling for the left and middle illustrations follows British Standards Institution (2007b) and the right illustration incorporates the definitions previously used for the wheel as relating to Figures 2.2-2.3. Two axes perpendicular to the ground plane are shown (left). One axis passes through the geometric centre of the caster stem. The second axis, assuming it follows the idealised arrangement shown on the right, passes through the caster wheel geometric centre and COM, indicated by C_i (right sub-Figure) and through the centre of the ground-wheel contact line, previously indicated by G_i but not shown here: the minimum dimension between these two axes is termed the caster trail and denoted by t in this text. With respect to the kinematics it is evident that, for example, point S_i at the geometric centre of the caster stem may have an arbitrary velocity since it is given by $\dot{x}_{Cni}\hat{\boldsymbol{n}}_{\boldsymbol{i}} + \dot{\theta}_{Si}t\hat{\boldsymbol{S}}$, where $\dot{\theta}_{Si}$ is the time derivative of θ_{Si}. Thus while the caster assembly may be defined with a wheel with a nonholonomic constraint, a body attached at point S_i is not subject to a

nonholonomic constraint: the constraint which does exist is that the displacement of S_i in the $\hat{\boldsymbol{t}}_i$ direction and the orientation of the caster assembly (θ_{Si}) cannot be controlled independently. (The kinematics of the caster wheel under various S_i velocities is considered in the Dynamics Chapter.) In this text the caster assembly is fixed to what is termed the 'vehicle-frame'. Thus points on a vehicle-frame to which only caster assemblies are fixed are not subject to a nonholonomic constraint even when the caster wheels are. Such a vehicle may therefore be described as omni-directional.

In this text the scalar of the angular velocity of the caster assembly about the vertical axis through S_i with respect to the ground-plane is termed 'caster global rotation' and the related displacement is termed 'caster global orientation'. The scalar of the angular velocity of the caster assembly about the vertical axis through S_i with respect to the vehicle-frame is termed 'caster rotation' and the related displacement is termed 'caster orientation'. For the fixed wheel, in contrast to caster assemblies, there is only one rotation term, 'wheel rotation' as exampled by $\dot{\theta}_{Si}$ in the consideration of the previous paragraph. It is therefore emphasised that the term caster rotation relates to a relative measure where as the term wheel rotation, in respect of a fixed wheel, relates to a global measure.

The caster wheel axis ($\hat{\boldsymbol{t}}_i$) may not be parallel to the ground plane and perpendicular to the axis of t: British Standards Institution (2008) define caster wheel orientation variations with respect to the ground plane (tilted axle) and with respect to the axis of t (oblique axis). Additionally these standards identify that the wheel centre may be displaced along the wheel axis so that the $\hat{\boldsymbol{n}}_i$ direction if viewed as fixed to the caster wheel at C_i would not pass through the vertical axis through point S_i .

2.3.5. *Vehicle fixing of caster assemblies*

British Standards Institution (2007b) also defines a number of caster assembly related fixing variations for occupied vehicles ('wheelchairs'). Firstly, the vertical axis through point S_i can be out of perpendicular to the ground plane: the front-rear angular displacement of the axis is termed rake and the lateral angular displacement is termed cant.

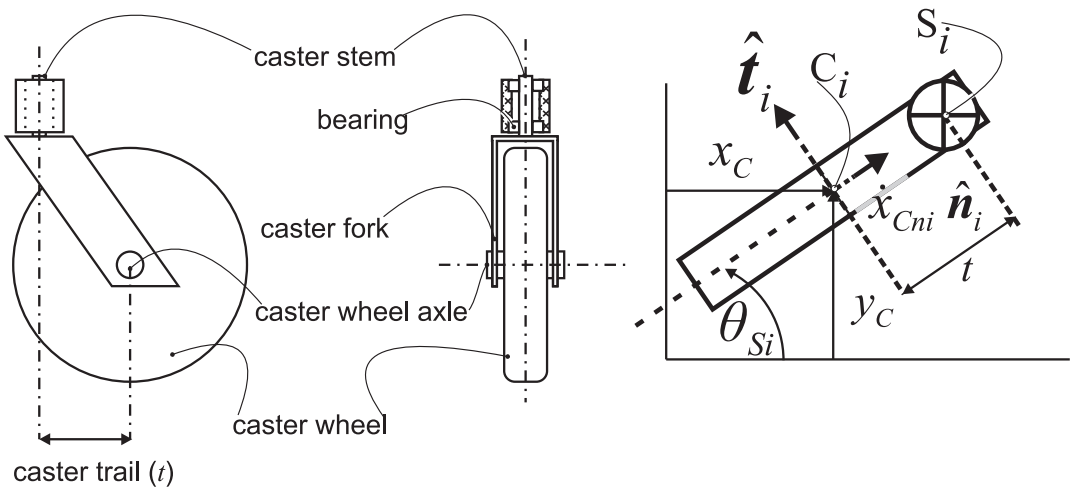

Figure 2.4 – Shows (left) the labelling for the caster assembly and (right) a top view with the kinematics.

The orientation of the caster assembly on the vehicle is defined as follows. Figure 2.5 (page 13) illustrates a wheeled vehicle with occupant. The vehicle comprises of four wheels and a vehicle-frame. Disregarding the asymmetry of the lower limbs and assuming that the occupant was so positioned that left and right sides were symmetrical, the anatomical plane, termed the sagittal plane, would cut through the body producing identical left and right halves. The front and rear of the sagittal plane are then defined by the front and rear of the human body. Assuming that the sagittal plane symmetrically divides the vehicle-frame then the caster assemblies are defined as being in the 'forward trailing position' when the caster wheel $\hat{\boldsymbol{n}}_i$ direction is parallel with the sagittal plane with positive $\hat{\boldsymbol{n}}_i$ towards the front. A vertical axis through the caster stem is then forward of a vertical axis through the caster wheel ground contact as shown. The caster assembly 'rearward trailing position' is then defined as π rad change about the vertical axis from the forward trailing position. For occupant vehicles the front of the vehicle is therefore defined in terms of the occupant's sagittal plane.

2.3.6. *Motion resistance*

The presentation has assumed that wheel and ground do not deform (the rigid body assumption) and that therefore the wheel (as a cylinder) and the ground have a line of contact. In reality this is not the case as some deformity occurs in ground and wheel at wheel-ground contact due to the elasticity of the materials. Additionally, some ground types, for example, sand or a shagpile carpet are

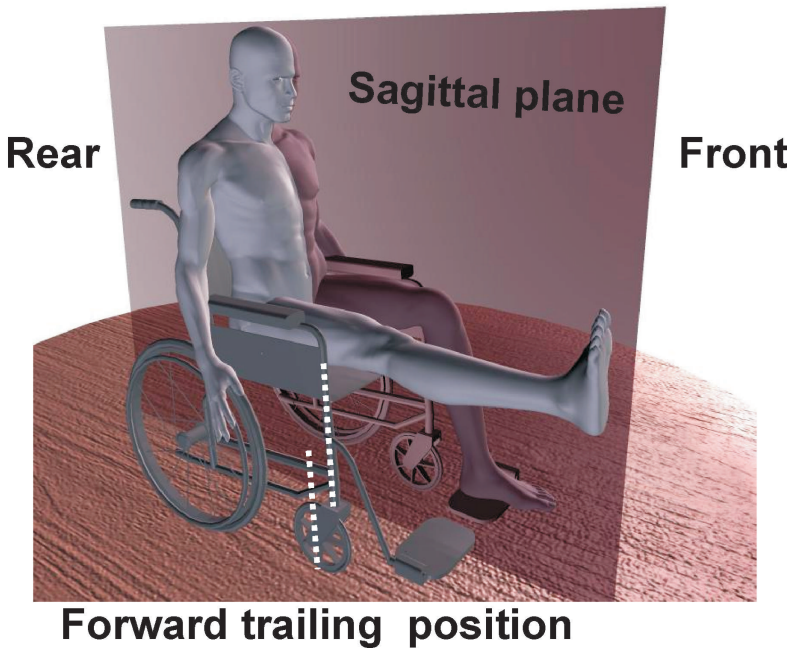

Figure 2.5 – Shows: a) the sagittal plane, b) the rear and front of the vehicle as defined by the occupant, c) the forward trailing position, i.e. a vertical axis through the caster stem is closer to the vehicle front than an axis through the caster wheel ground contact, patch, d) the right leg with knee in extension (the foot-rest replacement to support the leg is not shown) and the left leg with knee in a typical seated position and e) the vulnerability of the left foot to collision trauma.

relatively (compared with, for example, concrete) highly conformable: ground effects will be considered further in the Literature Chapter. Unlike, for example, the wheels of railway vehicles, the manual vehicle of investigative interest have wheels with a distinct outer rim material, a non-pneumatic tyre.

For the passive wheel with a non-pneumatic tyre the primary cause of resistance to wheel roll is hysteresis which arises from elastic effects of the tyre material (Kauzlarich and Thacker, 1985). Elasticity is a phenomenon of solid materials whereby stress or pressure (force over an area) produces strain (a dimensional change directed by the stress or pressure) while applied. When vertical loading is applied, the idealised line contact, described for the wheel in previous sections, deforms into a contact patch. The pressure acting on the wheel in the $\hat{\boldsymbol{S}}$ direction at the wheel-ground contact varies along the $\hat{\boldsymbol{n}}_i$ direction (terms as previously defined for Figure 2.2) as the outer circumference of the wheel, moving from either end towards the centre of the contact patch in the $\hat{\boldsymbol{n}}_i$ axis, is displaced increasingly vertically. Assuming negligible ground deformity then the pressure distribution

acting on a passive wheel will be symmetrical along the $\hat{\boldsymbol{n}}_i$ axis of the contact patch: Pacejka (2000) describes this in terms of the unchanging verticality of the 'tread elements' entering the contact patch during passive wheel roll: the tread elements would not remain vertical with an active wheel as the ground contact end of the wheel material is subject to a ground reaction force with a non negligible magnitude related to the vehicle dynamics.

If strain is viewed in terms of elastic work then on stress removal perfectly elastic materials do work of equal magnitude when returning to the original shape; wheel material is not perfectly elastic. Thus as the wheel rolls and tyre material enters the contact patch more work is done in compressing the tyre than is recovered when the material emerges from the high stress contact areas. So the front contact patch has higher stresses and the centre of pressure of the ground reactions (in the vertical direction) on the wheel is not at the point where a vertical axis passing through the geometric centre of the wheel intersects with the ground-plane: it is on the $+\hat{\boldsymbol{n}}_i$ direction (for $\dot{\theta}_{ti} > 0$: following Figure 2.2) of that point and this produces a moment opposing the wheel roll direction. This is an energy loss effect and the term hysteresis is used to describe this energy loss: the critical effect of hysteresis is that it results in motion resistance to wheel roll. This effect is termed 'roll resistance' in this text.

It is also evident from Figure 2.3 (page 9) that apart from the centre point G_i all the other points on the line contact must have a velocity with respect to the ground as a result of $\dot{\theta}_{Si}$ and that therefore a balancing force related to these frictions must be present. Thus even with a simple model, accounting for $\dot{\theta}_{Si}$ introduces Coulomb friction in the second condition. It is evident given the account of the previous paragraph that as each tread element enters the contact patch under the combined effects of wheel roll and $\dot{\theta}_{Si}$ that the elastic changes in the tyre material is more complex than occurs for wheel roll without $\dot{\theta}_{Si}$. This effect is considered further in the Literature Chapter. The overall motion resistance resulting from the relative velocity of tyre and ground at the wheel ground contact due to a caster global rotation is termed 'scrub friction' in this text.

If a caster assembly with a passive caster wheel is fixed to a vehicle-frame the force to balance scrub friction must be transmitted through the vehicle-frame to

the caster stem and the relevant component would be in the axis of $\hat{\boldsymbol{t}}_i$. If the caster wheel was pneumatic then it would be essential to consider the $\hat{\boldsymbol{S}}$ axis elasticity of the wheel. In the case of the automobile tyre this elasticity is the basis of the cornering force, i.e. under the action of a relatively small force in this axis applied by the steering system an elastic deformation at the tyre-ground contact, in the presence of wheel roll, produces a force large enough to change the direction of the automobile: a measure of this elastic effect is termed the slip angle (Wong, 2008). However, in the case of the non-pneumatic caster wheel, which is the wheel on the vehicles of investigative interest, the slip angle effect is negligible (Karnopp, 2004) and in this work it is disregarded.

The caster assembly also has two bearings which may be a source of motion resistance: the caster bearing and the wheel bearing. It is to be noted that in a simple model the moment contribution, summed about $\hat{\boldsymbol{t}}_i$, to any motion resistance arising from the wheel bearing is a linear function of the bearing radius which is a relatively small measure compared with the radius r. It is also to be noted that the moment contribution, summed about $\hat{\boldsymbol{S}}$, to any motion resistance arising from the caster bearing is a linear function of the bearing radius which is a relatively small measure compared with t. For bearings in good order roll resistance and scrub friction are likely to be responsible for the motion resistance first-order effects.

In conclusion the wheel roll constraint and the nonholonomic constraint are useful kinematics approaches easily explicated by simple models utilising the Coulomb friction model. However, motion resistance requires a more complex model. For general plane motion for the passive wheel as each differential element of the wheel passes through the contact patch it is subject to varying external pressures and internal stresses as a result of the elasticity of the tyre material. Additionally, the ground material will have elastic and possibly relatively large other effects due to conformability and together with the wheel material these combine to produce scrub friction and roll resistance which require an overall balancing action for the dynamic case. This completes the examination of basic mechanical concepts of the wheel.

2.4. **Equipment and Terminology**

The term 'community equipment' is the preferred label for the wide range of low technology (for example, a walking stick) to more complex assistive devices (for example, speech recognition environmental control) used by people with disabilities or health problems who live 'in the community', i.e. outside of residential, nursing and hospital settings (though the equipment is also in use in those settings). Figures 2.6(a)– 2.6(h) (page 17) show a number of manual vehicles which are included under the community equipment umbrella. The vehicles of Figures 2.6(a), 2.6(b), 2.6(e) and 2.6(g) are designated for use in showers. If the toilet pan is suitably arranged the vehicles in Figure 2.6(a) and 2.6(g) may be manoeuvred over the toilet to assist toilet use. Figure 2.6(c) is designated for indoor general mobility. Figure 2.6(f) shows a mobile hoist: guidance indicates that journey lengths should be minimised but some manoeuvring is always required to transfer from one surface to another. The vehicles of Figures 2.6(g) and 2.6(h) have fixed wheels and caster assemblies but all the other vehicles only have caster assemblies. Apart from the vehicle in Figure 2.6(h) all these equipments are designated for indoor use.

A number of classification and or terminology systems exist for community equipment. The Disabled Living Foundation (DLF) on-line data base is *the* structured source of information regarding community equipment in the UK. While it has a thesaurus of terms (Mandelstam (1989b)) it describes itself a record of the 'natural language' of those who are involved with community equipment supply or use. As natural language is used vehicles do not have an exclusive label: in, for example, DLF terms Figure 2.6(c) may be described as a 'caster wheelchair' or a 'glideabout wheelchair'. DLF classifications are not linked in terms of wheel types so Figure 2.6(f) is termed as 'mobile hoist' and Figures 2.6(a) and 2.6(b) are termed as a 'sanitary chair': the common mechanical link of both being vehicles with only caster wheels only vehicles is not noted. The British Standards Institution (2007a) provides a numerical classification system though this is blunter than the DLF system, for example, one class is 'commode chairs (with or without castors wheel assemblies)'. The US DLF equivalent is AbleData (2011) and this uses 'wheelchair' and 'caster' as adjective modifiers for 'chairs' and it is reasonable to assume, though

(a) (b) (c)

(d) (e)

(f) (g) (h)

Figure 2.6 – Various wheeled community equipment: (a) complex needs shower chair with over toilet facility, (b) shower chair with commode facility (c) general access chair (d) bed (e) shower trolley (f) mobile hoist (g) shower chair with over toilet facility (h) wheelchair.

no definition is supplied, that the former comprises of two fixed wheels and two caster wheels assemblies where as the latter comprises of four caster wheel assemblies: there are therefore, for example, '*wheelchair* shower chairs' and '*wheelchair* commodes' and '*caster* shower chairs' and '*caster* commodes' (emphasis added) but like the DLF there is no classification link to Figure 2.6(f) which is termed a 'powered transfer lift'. There is therefore no pre-existing terminology which makes

(a)

(b)

Figure 2.7 – Various wheeled equipment: (a) an ACMV: shopping trolley (with permission M. Wardle©), (b) an ACMV: refuse collector

a consistent classification in terms of the mechanical features of investigative interest: caster assemblies, fixed wheel, passive and active wheel.

In the absence of a serviceable pre-existing terminology the following usage is adopted. Vehicles subject to a nonholonomic constraint are designated as fixed wheel vehicles (FWV). Vehicles which have only passive caster assembles are denoted as all caster manual vehicles (ACMV): it follows that Figures 2.6(a)– 2.6(f) are ACMV. The term 'manual' in the context of ACMV is used in respect of an operator applying forces to the vehicle: all of the chair type vehicles in Figures 2.6 may be propelled by use of the feet (Mandelstam (1989b): cites foot propulsion as a category) and an occupant may apply hand forces to an external object but neither of these actions are considered in this text. As shown in Figures 3.1(a) and 3.1(b) (page 18) ACMV use is much broader than just community equipment use. As the classifications FWV and ACMV are internal to this text it follows that they do not appear in the literature. In referring to the literature it will be useful to interpret the text and use the FWV or ACMV terms as appropriate as this maintains focus on the mechanical interest of this work. However two exceptions are useful. Firstly, in this text the term 'wheelchair' (i.e. wheelchair with quotes surrounding) indicates that the reference uses the term wheelchair without defining the type of vehicle. Secondly, if the term wheelchair appears in this text (i.e. no surrounding quotes) with respect to an empirical study it indicates that a specific FWV was used: one with two front caster assemblies and two fixed rear wheels. Where someone occupies a vehicle this person is termed 'occupant'

and vehicles which are controlled by the occupant are termed 'occupant controlled'. Where the occupant does not control the vehicle or there is no occupant the vehicle is operator controlled: automated control vehicles are not considered.

Chapter 3–Literature

3.1. **Introduction**

Five sections follow: the first section details the originating motivation for the investigation and demonstrates the importance of the ACMV for disabled people. The second section, since the intending desire is to inform architectural planning for adaptations for ACMV use, reviews the state of the art for ACMV adaptation planning: no suitable method exists. The third section details the results of a structured review of the mechanical literature regarding ACMV: there are no theoretically based empirical investigations of the ACMV. The fourth section, presents the details of studies with elements relevant to an ACMV investigation and this is organised in terms of motion resistance effects. Fifthly and finally, given that there are no precursory ACMV studies, consideration is given as to whether a first study should begin by examining a single caster assembly or an ACMV: it is concluded that an ACMV study is more useful.

3.2. **Background**

3.2.1. *Motivation*

The initial motivational seeding for this investigation was experiential. As an occupational therapist the author assesses and recommends provision of indoor disability-access vehicles and adaptations (for example, door widening and wall moving) to accommodate those vehicles. There were occasions when an ACMV was recommended in preference to a wheelchair (see Figure 2.6(g), page 17) because of its omni-directional ability. However, while the ACMV was omni-directional when unoccupied, when occupied – putting this in the terms in which it would have been expressed at the time – it sometimes seemed as if it was stuck; yet it moved relatively easily in some directions though not necessarily in the direction

which one wished. Difficulties manoeuvring the ACMV are not unique to the author. Abel (1983) identifies the manoeuvrability of the ACMV (a hospital porter chair) as desirable but describes control as problematic though the occasions of difficulty are not elaborated. King (1985) found that shopping trolleys which were ACMV were second choice to FWV. Rodgers (1986) recommends that ACMV (for commercial materials transport) should be avoided unless space restrictions make them essential. A survey by Mack et al. (1995) identified difficulties manoeuvring the ACMV compared with other manual vehicle types. Conneeley (1998) comments on ACMV manoeuvring difficulties in respect of mobile patient hoists. Petzäll and Petzäll (2003) reports ACMV (hospital bed) manoeuvring difficulties which prompts a new design. While Ferreira et al. (2004) recommends the use of ACMV (citing Lawson et al. (1993)) in confined spaces, Ferreira et al. also repeatedly comments on the difficulties of manoeuvring vehicles in confined spaces. Finally, Abraham and Johnson (2010) provide a purely theoretical account as to why the handle-forces for some ACMV manoeuvres may vary substantially as a function of displacement direction. Cross-slope – when the ground plane is rotated about a horizontal axis in the sagittal plane–ACMV use has also been explicitly examined and found problematic (for example, Wilkinson (1998)) and it is possible that Abel, Rodgers and Ferreira et al. include cross-slope manoeuvring as part of the ACMV difficulties but the comments also appear to relate to use on level ground. There is something about the dynamics of an ACMV on level ground which is worthy of further examination.

3.2.2. *A brief history of omni-directional vehicles*

A structured study of the history of the development of the ACMV is not necessary but the following provide some historical context:

> This was the appearance and structure of the wheels... As they moved, *they would go in any one of the four directions*... (Ezekiel 1:16-17, New International Version)(emphasis added)

This ancient text describes an omni-directional vehicle (a throne) as part of a claimed revelation of God: assuming that wheeled vehicles, circa 600 BC, were nonholonomic (for example, chariots) it is credible that an omni-directional land vehicle would not be out of place in the literary context. An early example of

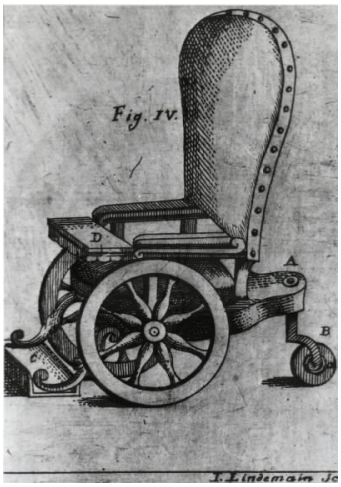

(a)

(b)

Figure 3.1 – Shows: (a) an early disability access vehicle with a caster wheel (image provision by National Library of Medicine acknowledged), (b) Community Equipment (mobile hoist) with two active caster assemblies and two passive caster assemblies

the caster appears to be shown in an illustration by (Soldi and Rondinelli, 1766), (Figure 3.1, page 22); caster assemblies were sufficiently established towards the end of the 19th century for an improvement to a 'furniture caster' to be patented (Fisher, 1876). The ACMV is now ubiquitous as the extensive variety shown in the previous chapter demonstrates. All of the omni-directional vehicles in the DLF index are ACMV, i.e. there are no omni-directional vehicles with all passive wheels which are not caster assemblies, for example, no ball-caster (Townsend, 1964) vehicles. However, a recent commercial development is that an indoor, disability related omni-directional vehicle with two active wheels is now available though prices are manyfold the passive caster wheel equivalent: approximately £12000 compared with £500 for a mobile hoist (see Figure 3.1(b) for an example of the former).

3.2.3. *Numbers of ACMV in use*

Even if an estimation ACMV usage is restricted to community equipment there are substantial numbers in use. There are two sources for ACMV for disability-access in the UK, disregarding a small number of hybrid schemes: firstly private purchase and secondly through a regional NHS Wheelchair Service or through 'community equipment' (a more local arrangement between the local authority and health trusts). Regional NHS Wheelchair Services primarily supply wheelchairs rather than ACMV but estimates of FWV usage provide an indication of

ACMV usage since as noted by Ham et al. (1998) some proportion of FWV users will require an ACMV due to the space constraints on using a FWV indoors. Wheelchair use in the UK was estimated by the Audit Comission (2000) as a maximum of $\frac{3}{4}$ million and by Care Services Improvement Partnership (2006) as 1.2 million. Based on a Netherlands study Van der Woude et al. (2006) extrapolates a European wheelchair using population of 3.3 million from a 2002 study. The Rehabilitation Engineering & Assistive Technology Society of North America (2011) reports an estimated community based wheelchair use of 2.8 million in the US. A guide to the numbers of ACMV in domestic (UK) use is gained by extrapolating from ACMV on loan in Newcastle upon Tyne: this provides a guide number of 320 000 ACMV for UK domestic use (page 234): Figures 2.6(a)–2.6(g) (page 17)). To these ACMV uses may be added users who privately purchased, those in residential care, nursing homes and hospitals and extending use beyond disability-access to include any ACMV there are the numerous material handling vehicles from bins to dining trolleys.

With regards to the commercial implications, with respect to the UK, Consumer Focus (2010) reports that the public spending on community equipment is approximately £318 million annually and that wheelchair services expenditure was £126 million (2006/2007). Even restricting attention to disability-access, the indications are that ACMV usage is an important component of a larger mobility market.

3.2.4. *Health and Safety*

The Health and Safety Executive (UK) reviewed manual vehicle use (Ferreira et al. (2004)) due to accident levels and possible links to musculo-skeletal problems. Subsequently a means of identifying high risk pushing and pulling of manual vehicles was produced (Ferreira and Smith, 2007): one high risk feature was manual vehicle use in confined spaces which is where ACMV are specifically commended (Ferreira et al. (2004)). In the US the NORA Musculoskeletal Disorders Team (2001) reported almost 80,000 injuries related to pushing and pulling tasks. It is not possible to pinpoint if the ACMV is more problematic than other manual vehicles since vehicle types are unspecified but it is possible to say that manual vehicles in general are source of concern in respect of both accidents and

musculo-skeletal injury.

3.2.5. *Exacerbating factors*

There are also a number of factors which may mean that manual vehicle difficulties have a greater impact in the disability-access setting. Cowan et al. (2009) reports that the over-65 age group are the largest manual wheelchair user group in the USA: some proportion of these will be assisted by partners who may also be elderly. Thus older operators with reduced strength and greater propensity to injury are more likely than would occur in industry where the operator will be of sufficient health to gain employment. Where care is provided by employees then the same concerns which exist in industry apply. In industry it may be possible to divide a load but in disability-access the load [1] is a person so this is obviously indivisible. In similar fashion the occupant's shape is largely unalterable: if a knee is in extension (see Figure 2.5 page 13) then this cannot be changed and the opportunities to re-orientate the occupant to suit the space are limited. Furthermore the load may be increasing: the 100kg wheelchair test dummy is no longer considered sufficient. (Cooper et al. (1999)). Hitchcock et al. (2006) in a study of 1356 wheelchair users identified a significant increase (13.85kg) in the 95^{th} percentile of occupant controlled manual wheelchairs and an increase of (9.7kg) in the 95^{th} percentile of operator controlled manual wheelchairs compared with a previous study (1995): both occupant and operator controlled manual wheelchair users may be ACMV users: for example, either group may require a mobile hoist for transfers.

3.2.6. *Community Care*

The National Health Service and Community Care Act 1990 (Great Britain, Parliament, 1990) produced a substantial change in where people with disabilities lived: since that time the primary care location is in the community, i.e. in domestic properties where space is more limited than would occur in a public building. There may be concerns about collisions (for example, with walls) (Northern Ireland Housing Executive, 2006): the ACMV load is a human being

[1] Using 'load' for a disabled person is identified as 'unethical' by Benedict et al. (2006): however, while the use of a depersonalised term is both unnecessary and unjustified in a text dealing solely with persons this text considers vehicles carrying either objects or persons. Additionally, the term 'load' is standard within the mechanical discipline.

who by virtue of needing to use an ACMV may have medical conditions which make the consequences of skin damage much more serious than would occur in the non-wheeled-chair using population: see Figure 2.5 (page 13) for an illustration which conveys the toe collision risks. Also, pain sensitivity may be reduced and limbs may be deformed so as to extend substantially beyond the typical envelope of the ACMV such as occurs when a knee is in fixed extension. Since many of the tasks relate to activities of daily living such as showering and sleeping, the protection offered by for example shoes may not be present. Confidence in workers coming into a domestic home may be undermined if plasterwork is gouged or paint scratched. In domestic properties the devices used to prevent collision damage to the property which are found in industrial or hospital settings are unlikely to be acceptable or practical. Thus the level of manoeuvring precision which is required may be greater than that which occurs in other settings. Additionally, doors may have to be opened and closed and mechanically automated doors are unlikely to be present.

3.2.7. *Daily living impact*

It is also important to note that whatever the difficulties, commercial factors necessitate that loads in industrial settings are moved: this is not a necessity in the disability setting. However high a value is set on maintaining activities the difficulties may be overwhelming. Thus, for example, if vehicle access to the toilet is too difficult the necessary proximity will be lost and incontinence may result (Mandelstam, 1989a) so it follows that the commode may be brought to the person rather than the person to the toilet. In similar fashion there is always the possibility that showering may be replaced by being washed down in bed and living-room access may be replaced by remaining in the bedroom. An understanding of the operation of the ACMV has a wide application but it is has a particular importance in the disability-access setting.

3.2.8. *Conclusion on problem and approach*

ACMV use in the domestic disability-access setting can involve manoeuvring large loads, in confined space where the operator may be an older person and where collisions are unacceptable: this is the ACMV-use of investigative interest. Furthermore there is evidence that despite the apparent omni-directional ability

there is something about manoeuvring ACMV which is judged to be difficult. The problem of interest can therefore be viewed as an interaction of three components:

1. As an issue of dynamics and design: the ACMV is a mechanism with tendencies to resist or maintain motion as the wheels interact with floor covering. (Ground and floor covering effects are considered in a later section.)
2. As a matter of operator biomechanics and motor control: the abilities of the operator to apply the necessary actions to achieve the required motions.
3. As an access planning problem: the physical environment which sets space constraints on the occupied ACMV and operator by virtue of walls and other fixtures.

It follows that while any investigation must take account of all three aspects, with respect to seeking a solution to the manoeuvring problem it is sufficient to frame the investigation in terms of one component. Thus while ACMV design and operator training or selection are both pertinent routes to a solution, access planning is chosen as the solution area of interest and the state of the art for adaptation planning is considered in the next section.

3.3. State of the Art: Adaptations Planning

3.3.1. *Property adaptation*

One means of improving disability-access for ACMV is adaptations to the architecture: for example, moving walls and widening doorways. Adaptations to properties can have a crucial role in supporting people with disabilities in the community (Heywood, 1994) and as a means of avoiding the substantial additional expenditure which other forms of care incur (Heywood and Turner, 2007). It therefore follows that there has to be some means of determining which adaptation to carry out. The state of the art for adaptation planning for disability-access for ACMV manoeuvres is now considered: it will be shown that no satisfactory method exists for determining the spaces required for ACMV manoeuvres.

3.3.2. *Adaptation planning*

Firstly, there is the use of architectural guidelines such as *Design of buildings and their approaches to meet the needs of disabled people-code of practice* (British

Standards Institution, 2010). Architectural guidelines can function in two ways. One function is as a standard, that is, an external requirement: sometimes the requirement is legal (Disability Discrimination Act: Great Britain, Parliament (1995)) and sometimes the requirement has the weight of being good practice without legal enforcement as has been the case of Department of Environment Transport and Regions (1999) in respect of adaptations. The second function is as a source of solutions for disability-access problems. Older UK based guidelines (for example, Department of Environment Transport and Regions (1999)) provide a single guideline for disability-access: for example, it does not contain a list of dimension variables in order for the reader to select in accordance with the type of wheeled vehicle in use. More recent architectural guidelines do provide variable guidance to take account of FWV size, for example, Goldsmith (1997) provides advice for four FWV sizes (the ACMV is not included) and *Design of buildings ...* describes guidelines in term of the percentile of FWV users whose needs will be met; the ACMV is not included.

Three forms of architectural guideline development can be discriminated. Firstly, feedback on the use of previous guidelines can influence the development of new guidelines (Northern Ireland Housing Executive, 2006). Secondly, empirical studies of manoeuvring space have been carried out. This approach has been used with eclectic groups of disability-access vehicle users, this was the case for Feeney (2003) as part of the development of *Design of buildings ...*, or it can target a specific group, for example, spinal injury (Fujiie et al., 1996). These studies use various measurements: for example, Ownsworth (1973) identified collisions and used qualitative measurements of FWV user experience of difficulty as spaces were incrementally reduced: this method is termed a wall-collision study in this text. Wall-collision studies continue to be used, for example, Center for Inclusive Design and Environmental Access (2010). No studies of this type were identified for the ACMV though British Standards Institution does provide some guidance for an ACMV (mobile hoist). As no space studies of the ACMV were identified and there is no intention of developing an architectural guideline using the approach, as exampled by Ownsworth, an examination of the methodology of the space studies is not considered necessary. A third method of guideline development is through the

application of expert clinical experience, for example, Harpin (2000) (specifically for muscular dystrophy). Abraham and Johnson (2006) identify limitations using architectural guidelines to determine adaptations: the limitations relate to the difficulty modifying their use for specific individuals, vehicles and environments.

A second approach is by physical simulation: carrying out the manoeuvre in an equivalent space to the proposed adaptation. This is a wall-collision study with one subject. However, this depends upon the vehicle and operator being available at the time of the planning which may not be the case. Physical simulations may also be costly in terms of time and physically difficult to achieve since space-constraints may need to be constructed.

An alternative to physical simulation is virtual simulation as exampled by Harrison et al. (2010) inter alios: the set-up used by Harrison et al. requires the individual to propel the wheelchair wheels which are subject to the appropriate reactions (force feedback calculated as part of the virtual settings) including those which arise from constraints while the wheelchair seat remains in static equilibrium: large display screens simulate the motion through architectural space. A recent addition to the mechanical theory relating to these set-ups is the incorporation of caster assembly motion resistances (Chénier et al., 2011). However, neither operator controlled FWV users nor ACMV users have been incorporated into this approach for reasons which will be demonstrated in the next section of this chapter.

The third approach described by Abraham and Johnson (2006) is based on the human ability to experientially develop the ability to predict that a particular vehicle manoeuvre is possible. For occupant controlled wheelchairs, though the kinematics are different, there is some overlap with the skills required to park or garage a car when space is limited. For an ACMV the situation has the added complexity that the operator must also have the ability to apply the necessary handle forces. Furthermore, while it is a desirable ability for those in adaptations services to be able to view an architecture or an architectural proposal and conclude, based on experience, that a particular operator, occupant and wheeled vehicle will succeed (however success is defined), there are a number of limitations. Firstly, the ability of itself does not offer any straightforward way of sharing the ability. Secondly, the ability does not of itself allow anyone to participate in the

decision making process. Also, when a new situation is unlike any previous situation, for example, a wider or longer vehicle than previously experienced, there is uncertainty.

A common practice (amongst occupational therapists in adaptations services) is placing scale cut-outs on plans as part of adapations planning (Eriksson and Johansson, 1996). The imposition of circles on a plan indicating manoeuvring spaces is suggested by Goldsmith (1976). It is not clear how the proposals suggested by Goldsmith or Eriksson and Johansson take account of the manoeuvring space. Abraham and Johnson (2006) develop simple rules by which a scale wheelchair cut-out may be moved on the plan in accordance with the wheelchair kinematics and the abilities of the occupant. Tanimoto et al. (2009) has integrated wheelchair kinematics rules into into a computer based visualisation. Pan et al. (2010) has created software which automates the identification of wheelchair access paths by inputting wheelchair kinematics data along with architectural data. Neither Abraham and Johnson, Tanimoto et al. nor Pan et al. include operator controlled FWV users or ACMV users. Eriksson et al. (2000) also developed software which would readily incorporate ACMV. However, as this was purely an illustration tool for adaptations the placement of the ACMV, or any fixture or fitting, is a function of the software interface and is not related to the dynamics of the object placed.

While the ACMV is an essential part of disability-access and while manual handling concerns exist regarding ACMV use, no methods of determining the space requirements and hence the adaptation requirements of specific vehicles with specific occupants have been found in the architectural and adaptations literature. While the manual handling concerns are biomechanical in nature, i.e. it is the operator who is subject to any problematic effects, and social in consequence, i.e. the impact of an access failure falls on the disabled occupant, the phenomenon of ACMV manoeuvring is dynamical. Thus while the various citations of concern regarding the ACMV (Abel (1983), Rodgers (1986), Mack et al. (1995), Conneeley (1998), Petzäll and Petzäll (2003), Ferreira et al. (2004) and Abraham and Johnson (2010)) may be noted by the architectural or adaptations disciplines, the manner in which ACMV use impacts on adaptation planning requires the application of mechanics.

3.4. **Mechanical Review**

A structured search of the engineering literature, details in Appendix B, was followed by ad hoc follow-up of citations and subsequent searches (final search 26.11.11): this demonstrated that only four published works related to the ACMV and of these, only two related directly to ACMV manoeuvres. Firstly, Abel (1983) provides comment in respect of patient transport hospital chairs on the difficulties manoeuvring the ACMV: no observations are reported and neither theory nor measurements are cited. Secondly, Frank and Abel (1989) used an ACMV to make empirical measurements of roll resistance. Thirdly, Inoue et al. (2000) briefly reports (three pages) on an ACMV (mobile hoist) manoeuvre by a skilled and an unskilled domestic hoist user: a *single* trial for each of the two subjects. Inoue et al. reports both vehicle-frame displacement and estimated planar forces and moment about the vertical axis (determined by inverse dynamics using a theoretical model for motion resistance). The information is too slight and difficult to interpret to allow a reconstruction of the displacement. Differences in force, moment and displacement are identified for the two operators: the skilled operator had a peak moment of 42Nm compared with 69Nm for the unskilled operator: load is not reported. Fourthly and lastly, Abraham and Johnson (2010) present a theoretical account of the ACMV at impending motion which assumes that the contribution of inertial forces to handle-forces (as defined) is relatively small compared with the handle-forces required to balance motion resistance. They then argue that acceleration direction differences produce substantial differences in the magnitude of a handle-force measure (as defined). (This theory is restated in terms of vehicle-frame velocity and developed further in the next chapter.)

With only one empirically based and one theoretically based paper concerned with ACMV manoeuvres (the structured literature review Appendix B substantiates this), and only one prior to 2010, it would not be unreasonable or over dramatic to describe the engineering literature as paltry. Why are there so few engineering papers where as, for example, inserting *wheelchair* in the topic field of the Web of Science data base yields over four thousand references? Only speculation is possible: one explanation is that from a theoretical approach, as a mechanism, the ACMV appears too simple and that approached as on object of empirical study

it is too indeterminate. As a mechanism the ACMV has not attracted the interest of dynamicists cf. the spinning top (Kane and Levinson (1978) inter alios). From the empirical view-point the reverse situation exists: Abel and Frank (1991) state that (in contrast to translational displacements for which a small number of studies exist) investigating assisted wheelchair manoeuvres (translation and orientation change) would be difficult: the set of experimental possibilities is so large; the experimental possibilities would only increase for the omni-directional ACMV. Whatever the reasons the resulting effect is that no substantive theoretically based empirical study has been made of ACMV manoeuvres despite the importance of this vehicle.

Given the few texts available it is useful to examine the literature more widely than would be necessary with an established engineering topic. There are therefore two strands to the following examination of the literature. The first strand is an examination of ACMV texts whatever the background discipline and the following rule is applied. Results and comments relating to the ACMV are reported whether or not they are supported by dynamic theory or rigorous empirical study. Even if the reporting relates to material of lesser scientific substance, with respect to the needs of this investigation, it may well meet the needs of the authors, the phenomenon which prompted the reporting has taken place and this is useful given the initial knowledge level regarding the ACMV. The second strand is that, again irrespective of the background discipline, there are non-ACMV studies which contain elements which are pertinent to an ACMV investigation.

3.4.1. *ACMV in the literature*

The previous chapter categorised wheeled vehicles in terms of fixed wheels, caster assembly, passive and active wheels. The literature is imprecise with respect to these categories, this is in addition to terminological differences. While Jansen et al. (2002) provides precise details of three 'carts': one with four caster assemblies, one with four caster assemblies and an option to convert a front caster assembly to a fixed wheel and lastly one with four caster assemblies and a central fixed wheel, such precision is frequently absent. For example, Jäger et al. (2007) and Glitsch et al. (2007) used identical vehicles in an aircraft study but no textual reference was made to the manual vehicle category to which the 'trolley' belonged: a picture

in the former indicates that the vehicles had four caster assemblies. Hoozemans et al. (2004) referred to a 'cart' with the 'casters' at 90° to the motion direction but whether or not this is two or four caster assemblies is not stated or illustrated: nor is this clarified in Van der Beek et al. (2000) to which Hoozemans referred readers for vehicle clarification. Lawson et al. (1993) in a hospital setting (Australia) examined 'trolleys' and 'carts' and considered the typical arrangement to be' two casters and two fixed wheels' but the location, front or rear, is not stated or illustrated; in contrast another hospital based study (UK) of portering 'chairs' (Abel, 1983) noted the presence and discussed the relative advantages of having the caster assemblies at the front or rear of a chair with two caster assemblies and two fixed wheels. The account of ACMV publications which follows may therefore include non-ACMV.

It is also necessary to note that terminological differences: King (1985) (US) described 'supermarket shopping carts' as either having 'two front casters and two rear fixed wheels' or having 'four casters' where as both Barthorpe (1994) and Abel (1983) (both UK) and Wilkinson (1998) (Australia) assumed the shopping trolley to be an ACMV.

Studies reported in 'ergonomics' texts (for example, titles such as Ergonomics or Human Factors) that included an ACMV are concerned with the forces exerted by the operator and the consequential biomechanical effects. For example, in three aircraft studies (Jäger et al. (2007), Glitsch et al. (2007) and Winkel (1983)) the ACMV was displaced along the length of a space which represented the aircraft gangway but no measurement of the vehicle-frame orientation or lateral displacement on the gangway was made nor is there any report of the forces required to maintain the ACMV on a purely translational displacement along gangway length. The vehicle was not a direct object of study: the object of study was the resulting effect on the operator. One exception was identified: the King (1985) study of the effects of shopping trolley type included ACMV and two vehicles with two front caster assemblies and two rear fixed wheel of different sizes. Deviation from a route indicated by a line was measured, there was more deviation with ACMV, and the subjective evaluation of the operators was sought: thirteen of the fifteen participants gave the ACMV the lowest preference rating. No force measurements were made and path deviation reporting does not permit extrapolation to other

ACMV. The King study is further evidence that the ACMV has characteristics which affect path following in a way which does not occur with non-ACMV but how handle forces are related to this phenomenon is not addressed.

Jansen et al. (2002) studied wheeled vehicle handling tasks with translational displacement and with a 90° change of vehicle-frame orientation: handle force measures are classified in terms of tasks with and without vehicle-frame orientation change but handle force measure differences between these two tasks are not discussed. However, the effect of vehicle type on handle force measures for tasks with vehicle-frame orientation change is discussed by Jansen et al.: the results indicated that the ACMV required larger forces than other vehicles. Once again a phenomenon of interest to this investigation is indicated but this was not the direct object of study.

Translational displacement tasks with the caster assemblies initially displaced from forward trailing position also feature in ergonomics studies. This was a common variable for Hoozemans et al. (2004) (90°), Jansen et al. (2002) (180°) and Al-Eisawi et al. (1999) (combinations of: front only, rear only and all at 90°): this was considered to produce a more difficult biomechanical task. The Al-Eisawi et al. findings supported this: 'pull-forces are consistently higher' when all four caster assemblies were initially displaced 90° from the forward trailing position compared with the other initial caster assembly orientations. Al-Eisawi et al. also reports, though no measurements were made, that changes to vehicle-frame orientation were observed (despite the task being designated as translation only) and identifies the cause as caster assemblies not being in the forward trailing position. So the Al-Eisawi et al. study provides observational evidence that vehicle-frame orientation and translational displacements are related to initial caster orientation but the motions are not measured and the implications to handle forces of ensuring no vehicle-frame orientation displacements are not considered.

In a study of cross-slopes Wilkinson (1998) (*33rd Ergonomics Society of Australia Conference*) compared handle forces for three vehicles: ACMV, vehicles with two front caster assemblies and two fixed wheels and a vehicle with a fifth fixed wheel (whether or not the first to fourth wheels were caster assemblies is not stated). The task was to make a translational displacement with the gradient

directed along the vehicle width. The ACMV is reported as having required a substantially greater handle force perpendicular to the direction of motion compared with the other vehicles. No investigation was made of ACMV use on level ground. Petzäll and Petzäll (2003) (*Applied Ergonomics*) made a hospital based study of manoeuvring ACMV beds and non-ACMV beds and observations are presented along with qualitative statistical material. All the material indicates that there are differences manoeuvring ACMV compared with non-ACMV.

In a survey, Mack et al. (1995) (*Applied Ergonomics*) identified difficulties manoeuvring the ACMV compared with other vehicle types. Winkel (1983) also speculates that the difficulties manoeuvring the ACMV in confined spaces is related to the narrow width and long body of the vehicle (a gangway aircraft ACMV). Mobile hoists are also a subject of interest for health-background investigators such as Conneeley (1998) inter alios but again the contribution regarding manoeuvring difficulties is observational.

All of these ergonomics or health based texts contribute evidence towards the view that the ACMV mechanism may produce interesting and important effects at initial motion related to initial caster orientation and during changes of vehicle-frame orientation but no substantive study of the phenomenon was intended.

3.5. **Motion Resistance**

Motion resistance may be viewed as a central phenomenon around which most aspects of manual vehicle motion related to the investigative interest may be deemed to be elements. In this section the literature for any wheeled vehicle is considered since elements of other studies are relevant to an ACMV investigation. The organising frame work is therefore to view these elements as aspects of motion resistance.

For manual vehicle manoeuvres the ideal arrangement for motion resistance has a 'wanting to have it both ways' quality. On the one hand motion resistance is desirable: Ciriello et al. (2001) considers both the problem of insufficient foot-floor contact friction and the usefulness of motion resistance in providing decelerations when required and Wilkinson (1998) overcomes an unwanted cross-slope effect on ACMV by introducing a fifth fixed wheel to benefit from the nonholonomic

constraint. On the other hand motion resistance is often undesirable: many of the difficulties manoeuvring vehicles in confined spaces described by Ferreira et al. (2004) can be viewed as motion prohibitions (the nonholonomic nature of the vehicle) or as difficulties due to the retarding effects of motion resistance.

Throughout this section the literature is examined in terms of the implications for ACMV investigation. This is carried out in the following sections in respect of motion resistance effects: those which can be disregarded, wheels and bearing, floor coverings, architectural constraints, operator skills, mass and mass distribution, start-up effects and handle height and loading.

3.5.1. *Motion resistance effects which may be disregarded*

There are five motion resistance effects which, with respect to the area of investigative interest, may be disregarded: one is air resistance since this is velocity related and velocity magnitudes in the area of investigative interest are assumed to be small. While wind speed is not applicable to an indoor study and it is reasonable to assume that velocities are small with respect to air resistance it is useful to consider relevant studies which take account of velocity since it provides an indication of possible velocities for ACMV use in the area of investigative interest.

At the upper limit Van der Woude et al. (2001) reports wheelchair athletes achieving velocity magnitudes of 4.2m/s (15.1 km/h). In a study of eight able-bodied non-athletes Reid et al. (1990) sets the task to 0.6m/s, Glaser et al. (1981) sets the task to 3km/h (0.83m/s) and in a multi-study of coast down calibration De Groot et al. (2006) records maximum velocity magnitude as 4km/h (1.11m/s). However, these studies were conducted in spaces which were designed to allow motion free from collision concerns: the manoeuvres of interest to this investigation occur when space is confined and collisions are likely. Also while Reid et al. included a manoeuvring element to the study the smallest radius of track was 1.35m radius which is impracticable in a typical domestic property: for an occupant controlled wheelchair user a typical radius may be zero as occurs with a 'turning circle' as defined by Abraham and Johnson (2006). Thus even 0.6m/s may be an over estimation of the vehicle-frame velocity magnitude of the ACMV in the area of investigative interest. While no recording method is reported, Reid

et al. also reports self selected self-propelling velocity magnitudes of severely disabled people in a hospital setting of 0.3-0.4 m/s. As the operators are reported as 'severely disabled' this may suggest that higher velocity magnitudes may be found for ACMV-use where the operators are able bodied. However, it is reasonable to assume that Reid et al. estimated velocity in a hospital corridor or ward from translational vehicle-frame displacements which once again is different from the investigative interest where both translation and orientation change are required. MacPhee et al. (2001) measured mean vehicle-frame rotations of 1.7-2.5 rad/sec for 20 able bodied subjects in wheelchairs. While the task included attempting to remain in a circular area there were no possibilities of collisions and as the task objective was maximal angular velocity these results are only useful as an indication of upper limit for non-athletes. Frank and Abel (1991) estimate that at a 1m/s ('a slow walking pace') an operator controlled wheelchair may experience approximately 0.55 N of air related drag. Velocity magnitudes in the area of investigative interest are therefore expected to be less than 1m/s.

Secondly, the indoor setting also makes some other motion resistance effects of negligible impact. While cross-slopes have a considerable bearing on ACMV (Wilkinson, 1998) as do gradients (Jäger et al. (2007) inter alios) these are a feature of outdoor motion and would not be typical indoors. Some older properties such as hospitals may have floor gradients and domestic level access shower systems will have gradients to allow water drainage but these features can be disregarded by restricting the investigation to level floors.

Thirdly, while no empirical measurements are made Van der Woude et al. (2003) expects the backrest deformation of a folding wheelchair to make a negligible contribution to motion resistance: the investigative chair of interest is non-folding (for example, Figures 2.6(a)– 2.6(c)) so any effects would be even smaller than Van der Woude et al. envisages. As roll resistance is defined as an energy loss effect it is consistent to consider backrest deformation in a motion resistance context.

Fourthly while caster shimmy[2] is relevant to wheelchair use (Kauzlarich et al., 2000) it is not relevant to the area of investigative interest. As considered in respect of air drag the ACMV velocity, in the area of interest, is assumed to be small

[2]A self-excited motion and not a resonance effect Kauzlarich et al. (2000)

compared to other manual vehicle use. An examination of the graphed relationship of vehicle-frame velocity to caster trail length in Kauzlarich et al. indicates that shimmy will not occur. The caster trail of the ACMV of investigative interest is typically 35mm or greater for which the estimated critical velocity for shimmy is estimated at over 1m/s which is much greater than the expected velocity magnitude. However, an additional consideration does exist: the shimmy predictions are based on a constant vehicle-frame translational velocity direction. If the manoeuvre includes a change of vehicle-frame orientation then it is caster stem velocity which is relevant. There is however, no need to consider these complexities since, as will be shown, it is the start-up forces which the literature suggests are of greatest importance and all velocities can be assumed to be small at start-up. Thus the combined effects of both translational and angular vehicle-frame displacement should not produce large caster stem velocities in the area of investigative interest.

Fifth and finally, the caster wheel used for the vehicle of interest, Figures 2.6(a)– 2.6(c)) and 2.6(e), is solid in contrast to a typical FWV for disability access (Figures 2.6(g) and 2.6(h)) so issues relating to tyre pressure (Sawatzky (2005) inter alios) are not relevant.

3.5.2. *Wheels and bearings*

This section considers wheel related motion resistances and initially three simplifying assumptions are applied. Firstly, ideal revolute joints are assumed for wheel roll and caster global rotation. Secondly, it is assumed that wheel roll occurs about an axis parallel to the ground plane and that caster global rotation occurs about an axis normal to the ground plane. Thirdly and finally, it assumed that the motion resistance effects related to wheel roll and caster global rotation, or wheel rotation in respect of fixed wheel, may be considered independently of each other. The contradictory evidence to these assumptions and the greater complexity which exists when these assumptions are removed are considered in a later section.

Genta (1997) defines the motion resistance to wheel roll as the force at the wheel centre which would produce the equivalent combined moment effect of bearing friction, hysteresis and air drag. In this work air effects are disregarded as only small vehicle-frame velocities are of investigative interest but in order to take

account of floor coverings such as carpets, ground firmness effects are included in the roll resistance effects in this work. Additionally in this work, rather than representing the roll resistance as a force, it is represented by a moment acting against the roll direction. Roll resistance is thus defined as a counter moment to wheel roll resulting from bearing friction, hysteresis and ground firmness effects.

For the case where the ground or floor covering is firm (for example concrete rather than a shagpile carpet) and assuming that the wheels are in good repair, the primary causes of motion resistance, for wheel roll, apart from wheel bearing friction is hysteresis (Kauzlarich and Thacker, 1985).

The variability of the hysteresis effect for non-pneumatic caster wheels has been demonstrated by Frank and Abel (1989). The roll resistance of eleven caster wheels (ten had rolling element wheel bearings and one had a plain wheel bearing) using a ramp which permitted travel over various floor coverings (for example, vinyl) and on a treadmill: all measurements were made when the wheels had a non-negligible wheel roll, i.e. the breakaway force was not measured. The wheel bearing resistances for each wheel were determined separately at negligible wheel roll. Frank and Abel report two relevant matters. Firstly, motion resistance force (as defined by Genta (1997)) acting on the wheels for a 200N loading varied considerably on a single ground, for example, (the treadmill) from approximately 2N to 6N not including wheel bearing resistances. Secondly, motion resistance was approximately linear to load. As total motion resistance to wheel roll was measured at non-negligible velocity where as the wheel bearing resistance was measured at negligible velocity this may affect the results. However, the comparative results, that one wheel had three times the roll resistance of another, is not compromised. Large variations in hysteresis losses occur with caster wheels: an ACMV investigation should either avoid or take account of wheel variation.

While Genta (1997), in respect of automobile wheels, describes the contribution of wheel bearing friction to roll resistance as a 'few percent' this is not necessarily the case for manual vehicle wheels. In the 1989 study by Frank and Abel it was found that wheel bearings may account for 50% of the rolling motion resistance effect. Frank and Abel (1991) cites Frank and Abel (1989) as having reported that the use of rolling element wheel bearings may result in a 14 times

reduction in wheel bearing friction compared with plain wheel bearings. However, examination of Frank and Abel (1989) indicates that this is a comparison with the rolling element wheel bearing with the lowest friction result, i.e. some rolling element wheel bearings may produce similar results to the plain wheel bearing. Bearing friction measures are not of direct interest to this investigation. However, as the vehicles of investigative interest may have wheels with plain or rolling element wheel bearings it is important, as with the wheel type, that an ACMV investigation is either consistent in respect of the specific wheel bearing type or takes account of any variation.

The final contribution to roll resistance relates to ground firmness. Wong (2008) introduces a theoretical basis and reports on empirical studies for the passive solid wheel in soft ground. Analysis is considered to be 'complex' by Wong and theory is restricted to wheels greater than 250mm radius (a typical ACMV wheel radius is 50-75mm): additionally, caster assemblies are not considered. Nevertheless, it is relevant to note that two ground conformability effects relating to roll resistance are described. Firstly, there is impaction resistance acting radially to the wheel. Secondly, related to the depth of sinkage a 'bulldozing' effect is described, i.e. there is a resistance ahead of the wheel acting parallel to the horizontal ground plane. Genta (1997) describes the wheel in conformable material in words to the effect of digging a rut which it then tries to climb out of. Stolarski and Tobe (2000) describes a ball rolling on a rubber surface in terms of the hysteresis effects taking place in the rubber surface. The empirical consequences of the theory presented by Stolarski and Tobe is found in Minns and Tracey (2010). Minns and Tracey found that significantly greater motion resistance occurred for an operator controlled wheelchair for forward translation, so motion resistance is primarily a result of wheel roll from front caster assemblies and pneumatic rear fixed wheels, on an energy absorbing material designed to minimise fracture risks during falls. These texts confirm the common experience that greater motion resistance exists moving a wheeled vehicle over a conformable ground or floor covering even if the wheels are hard: a complex process with relatively high motion resistance arises when floor surfaces are highly conformable even if the wheel related hysteresis losses are low. While outdoor grounds such as sand, wood chips, gravel

and soil are outside the area of investigative interest, floor coverings can vary from concrete to cushioned vinyl to shagpile carpets. Furthermore, in domestic settings the carpet may be with or without underlay, stretched tight or so loosely fitting that the carpet ahead of the wheel projects vertically from the floor: the need to avoid loose carpet is detailed in by British Standards Institution (2010) in respect of disability access. It is therefore likely that hysteresis losses in the wheel and bearing friction do not account for all the rolling motion resistance effects for the ACMV. In a first ACMV study it is prudent to circumvent the possible additional complexity of relatively conformable floor coverings as relatively non-conformable floor coverings, for example, wood laminate and thin vinyl are popular in domestic settings.

The final wheel motion resistance considered here relates to wheel rotation, in respect of fixed wheels, or caster global rotation. Frank and Abel (1989) and Kauzlarich et al. (1984) measured this effect for non-rolling non-pneumatic caster wheels (removed from the caster assemblies) by determining the peak force required to initiate motion from static equilibrium for various loads: the load to scrub friction relationship is approximately linear. The results from Frank and Abel (1989) and Kauzlarich et al. (1984) demonstrate that the wheel type also has implications for scrub friction. Neither study considers the caster bearing friction: these are always rolling element for the ACMV of investigative interest. So as with wheel bearing friction and roll resistance also in respect of caster bearing friction and scrub friction, the caster assembly type must be controlled in an ACMV investigation.

Scrub friction and roll resistance have been considered independently in the previous paragraphs. However, when a vehicle with fixed wheels is in general planar motion there will be both wheel rotation and wheel roll. For an ACMV, unless caster assemblies and vehicle-frame motion are configured so that only wheel roll occurs, there will be global caster rotation and wheel roll. So for both fixed wheels and caster assemblies the wheel-ground interaction at the contact patch is a consequence of two angular motions. Related to this, Stout (1979) comments, though no measurements or theory are presented, that scrub friction is highest when there is no wheel roll. Inoue et al. (2000) models scrub friction as a function

of the proportion of global caster rotation to wheel roll though no details are given of the study results on which this approach was based.[3] A possible counter case to the assertion of Stout may exist in Kauzlarich et al. (1984) who reports an experimental manoeuvre: this was made in order to test the motion resistance effects of a new caster assembly design. The study, a *single* test with two different caster assemblies, was with one wheel of a wheelchair constrained to pivot about the contact patch of the rear wheel without wheel roll while a horizontal force was applied to the opposite wheel hub to produce vehicle-frame orientation change: Kauzlarich et al. reports that the maximum force to continue the vehicle-frame rotation does not occur immediately but when the caster orientation on the force applied side was 30° (initial caster orientation appears to have been the forward trailing position). Thus wheel roll was probably not negligible at the point of greatest motion resistance. A further possible counter case is provided by Reid et al. (1990). This study found that significantly increased physiological energy costs occurred for occupant controlled 'wheelchair' users on a track with 1.35m radius curved compared with those with a longer radius for velocity magnitudes above 0.6m/s. In both Kauzlarich et al. and Reid et al. it is possible that other effects were present (gross vehicle dynamics for both and biomechanical and physiological for the latter) and that these effects overwhelmed any motion resistance reduction of scrub friction due to wheel roll.

There are no empirical or theoretical accounts of the contact mechanics of an ACMV caster assembly. However, Johnson (1958) considers the sphere with a constant translational velocity while rotating (termed 'spin') and Pacejka (2000) considers the pneumatic tyre rotating about the vertical axis while rolling and in both cases roll and rotation are considered simultaneously in determining the effects. Taking account of the theory of Johnson and Pacejka and the phenomenon indicated by Stout and Inoue et al. there is sufficient evidence to suggest that an ACMV investigation should permit measurement of the combined effects of roll resistance and scrub friction rather than independent measurement as exampled by Frank and Abel (1989).

The overall motion resistance effect of floor covering on the wheels of manual

[3]The citation relates to a Japanese language publication with no straightforward means of sourcing: given this and the need for translation it was not obtained.

vehicles is considered in a number of studies, for example, for occupant controlled wheelchair users (Cowan et al., 2009) and for 'catering cart' users (Das et al., 2002). Das et al. reports twice the force on carpet over tile to 'push' or 'pull' the cart. Limiting this investigation to relatively non-conformable floor coverings excludes the motion resistances produced by carpet. While increased loading will increase the motion resistance effects of relatively non-conformable floor coverings the extent to which these effects are similar to a smaller load on, for example, carpet is not known: the scrub friction and roll resistance may be in different proportions for conformable and non-conformable floor coverings and that could result in different demands on the operator.

It is useful to note that in all the studies mentioned (Cowan et al, Das et al., Minns et al. and Kauzlarich et al.) the motion resistance effects are viewed as a limiting factor on the task where as in Ciriello et al. (2001) insufficient friction between floor surface and shoe sole is the limiting factor. For the ACMV user both floor-sole friction effects and motion resistance effects have implications. This completes the consideration of motion resistance effects.

3.5.3. *Spatial constraints and manoeuvres*

A number of comments are made in the literature regarding spatial constraints and the relationship with manoeuvring problems: Frank and Abel (1989) identifies the situation where the operator has to stand too close, Lawson et al. (1993) observed the nonholonomic constraint being broken by trolley lifting in order to achieve a manoeuvre, Rodgers (1986) states that space and manoeuvring forces are linked, and Ferreira et al. (2004) (citing Rodgers (1986)) refer to the situation where the vehicle is positioned in such a way that the operator is unable to stand in their preferred position to make the manoeuvre. By way of explanation Rodgers (1986) further comments that operators are unable to bring their body weight into play as a force component. Ferreira et al. (2004) considers it necessary to define a further force in addition to starting and stopping forces: the manoeuvring force.

However, it is not clear what the empirical basis of the above conclusions are. For example, while Rodgers cites Strindberg and Petersson (1972) this is a

study of maximal strength pushing test of 10 healthy subjects and body position was not considered in this study nor was this studied in two of the other three citations provided by Rodgers (Haisman et al. (1972) and Ciriello and Snook (1978) and the third citation (incomplete) could not be obtained: 'Nielsen and Faulkner, Eastman Kodac Company'). That spatial constraints affect operator positioning and produce problematic manoeuvres seems to be a de facto position (Rodgers is cited in Ferreira et al. (2004) which is a Health and Safety Executive publication) in the absence of empirical study. On the other hand, it is not controversial to state that a task where only one operator position may be adopted could produce different results from the same task if the operator is free to choose their position. For example Kumar et al. (1995) in a study of forty healthy subjects where lower limbs were constrained found a statistical difference in the maximum push strength in the sagittal plane compared with force directions at 60° from the sagittal plane.

However, manual vehicle manoeuvring is acknowledged to lack data (Rodgers, 1986), to be without investigation and difficult to investigate (Abel and Frank, 1991) and lacking clarity of understanding (Van der Woude et al., 1995). No relevant studies of manoeuvring subsequent to these publications are identified by Abraham and Johnson (2010). The need for the operator to make a non-sagittal motion, as suggested by a number of commentators (Frank and Abel, Lawson et al. and Ferreira et al. and Rodgers) may account for some difficulties but there is no empirical basis for this conclusion: while it has been demonstrated, for example, Kumar et al. (1995), that strength in a non-sagittal direction is limited compared with a sagittal direction the application to manual manoeuvres has not been established empirically. Thus while ACMV manoeuvring difficulties are reported (Abel (1983) (porter chairs), Rodgers (1986) (carts), Mack et al. (1995), Conneeley (1998) (mobile hoists), Petzäll and Petzäll (2003) (hospital beds)) there is no empirical basis for understanding the difficulties.

All of the references in this section substantiate the relevance of the area of investigative interest, i.e. an ACMV manoeuvre in a confined space. These references also highlight that a constraint may be a constraint on the operator (unable to get into a preferred position) or a constraint on the vehicle or both. For a first ACMV investigation a useful simplification to any experimental design

would be to ensure that all subjects share a common type of constraint. For example taking the illustration by Frank and Abel where an operator is unable to get behind the ACMV due to lack of space: it would multiply the variables if the body shape of some operators permitted getting behind the ACMV where as that of others did not.

3.5.4. *Operator skills*

The study by Inoue et al. (2000) found lower force measures for a skilled operator compared with an unskilled ACMV operator albeit only a single trial took place. Only speculation as to the origin of the difference is possible: lower accelerations, different paths, or a random variation are all possibilities. Kirby et al. (2004) reports improved manoeuvring skills within spatial constraints for wheelchairs operators after training. The skill level of operators may have an impact on any measures made and selection of subjects or provision of training is required in any experimental design.

3.5.5. *Mass and mass distribution*

The vehicle-mass is defined in this text as the combined mass of the vehicle, without a load, and the load mass. The vehicle-mass in combination with any force and or moment effects which alter the vertical ground reaction at the wheel-ground contact, result in what may be termed wheel loading. Up to some maximum after which the mechanism may be damaged an approximately linear relationship between wheel loading and both roll resistance and scrub friction has been found for non-pneumatic caster wheels (Frank and Abel (1989) and Kauzlarich et al. (1984)). It follows that vehicle mass and load mass are important factors in an ACMV investigation. There is no controversy in stating that increasing load mass will increase motion resistance which in turn increases the force and or moment required to balance these motion resistances. (This is not to suggest that situations cannot exist where increased loading reduces motion resistance, a vehicle might clear an over hanging obstacle loaded but not unloaded, but such particulars are not of investigative interest. Nor is it being asserted that all increases in loading necessarily makes a task more difficult for the operator.) So, while determining the extent to which specific components of a manual vehicle mechanism contribute to increased motion resistance requires theory and empirical study, that increasing

mass requires an increased magnitude of force or moment to balance those motion resistances is intuitive and consistent with the considerations of motion resistance which have been made.

Mass distribution is also relevant and both Van der Woude et al. (2006) and Abel and Frank (1991), in respect of the wheelchair, are of the opinion that placing the COM closer to the rear wheels unloads the wheels which have higher roll resistance, the caster assemblies, in favour of the wheels which have lower roll resistance, the larger, fixed, pneumatic rear wheels and thus this reduces the overall motion resistance of the vehicle. While this is not controversial the only quantification of this effect comes from occupant controlled wheelchair studies and not from operator controlled wheelchairs. For example, in a study of occupant controlled wheelchair use with 53 subjects (relative to other wheelchair studies, a high number) Cowan et al. (2009) found that changing the front-rear position of the axle by 80mm produced a significant difference in propulsion forces for a number of floor coverings including carpet: lower measures were found for the forward axle position, i.e. the COM moves backward. However, the effect could also be a biomechanical feature: perhaps operators can apply larger forces when the wheels are closer to the front. Cowan et al. discusses this difficulty, the isolation of mechanism-related axle position effects from the biomechanical one, and argues that seating was tailored to the individual subject so that elbow position was kept within parameters which negated the biomechanical changes of the changed axle position. (It is not directly relevant to this ACMV investigation to come to a decision as to whether or not Cowan et al. has demonstrated mechanism-related effects of COM position: the results are not in the form of wheel loadings versus COM position and it is this which is of direct relevance to this investigation.) For the ACMV case, differences between front and rear wheels types will be negligible; it is the loading differences which are of interest. However, as illustrated by the Cowan et al. study, mass location studies are not in a form which permits extrapolation to the ACMV.

MacPhee et al. (2001) consider mass moment of inertia as part of a study with 20 able-bodied adults investigating the effects of knee extension on wheelchair dynamics. Clinically relevant differences in measures of perceived exertion were found: the task was to make a vehicle-frame orientation change of 900° at maximum

angular velocity with knees fully extended and fully flexed. However, the extent to which this latter result is a consequence of front rear wheel loading or mass moment of inertia effects on the one hand or biomechanical effects which are consequential to differences in posture is not determinable and as with the Cowan et al. study it is not possible to extrapolate to the ACMV.

The extent to which mass distribution affects the ACMV for the area of investigative interest is uncertain so the prudent approach is to assume that it does and to distribute mass consistently in any experimental procedure.

3.5.6. *Start-up*

The ACMV use of investigative interest is one where vehicle-frame displacement precision is imposed by virtue of space constraints. Given this and that doors may need to be managed it is reasonable to assume that a journey may be punctuated by a series of start-ups and stops to an extent which may not occur in some public buildings or in outdoor mobility. Start-up forces therefore have considerable relevance to ACMV-use. Koontz et al. (2005) in a study of eleven disabled but athletic adults measured both the start-up forces and steady-state forces for wheelchair occupant controlled propelling over various grounds and translational displacements (6.1m to 18.3m). Start-up measures were substantially greater than steady state measures: for example, for a concrete ground, mean peak resultant forces on the propelling wheels were 103.2N($\pm$6.7) at the first propulsion stroke compared with an average mean of 63.6N($\pm$2.9) for the last three propulsion strokes. In a study of gender difference involving twelve postal workers Van der Beek et al. (2000) measured forces applied to a 'four wheeled cage': results showed that the mean initial peak force for a group of four women pushing a 130kg load (10 repetitions for each subject) were 167N($\pm$27.9) where as the average force for this group was 52.1N($\pm$2.5). Further citation is not considered necessary as it seems reasonable to assume that for level ground, an absence of obstructions and wheels in good state of repair that start-up force magnitudes would be larger. The relevance of Koontz et al. and Van der Beek et al. is not that they confirm differences at start-up compared with later motion but that they show that these differences may be substantial.

The mechanical origin of the difference between start-up and non-start-up forces is not considered of primary relevance to this investigation since the purpose at hand is to draw on existing literature as a means of shaping an ACMV investigation: the origin of these start-up effects if found in ACMV-use is a secondary matter. Thus for example, even if the start-up effect was partly explained by higher initial accelerations, it presumably is so for wheelchair athlete sprinters as indicated by Tupling et al. (1986), the effect is still present. It is however, relevant to note that for wheel bearings with dry friction, which would be the case for many caster wheels, Sönmez (2003) theorises that the axle is displaced upward on the bearing at start-up: with respect to empirical investigation the wheel bearings types and condition would need to be controlled.

There is however, a feature, peculiar to vehicles with caster assemblies, where the origin of the start-up effect may be visible, i.e. the initial caster orientation and this is now considered, firstly, with respect to translational vehicle-frame displacement and secondly, with respect to vehicle-frame rotation. With respect to translational vehicle-frame displacement Al-Eisawi et al. (1999) found higher forces when all four caster assemblies were initially displaced by 90° from the forward trailing position. Thus, when Hoozemans et al. (2004) reports on the start-up effects in a study of seven healthy adults who made a 4m displacement (probably translational though this is not stated) of three loads (85kg, 135kg and 320kg) with caster orientations initially at 90° (whether two or four and which 90° displacements is not reported) to the forward trailing position, the results are the combined effects of initial caster orientation and other start-up effects: the results reported for two-handed pushing with handles at hip height for the peak exerted force measured for the defined start-up period are modelled as 73N+0.94N/kg compared with 23N+0.23N/kg for the defined sustained phase. However, there is no means of discriminating the caster orientation effect in these measures.

With respect to vehicle-frame rotation, Frank and Abel (1989) state that operator controlled wheelchairs often require a vehicle-frame orientation change at start-up, this is the investigative interest but for ACMV, and that consequentially 'The turning resistance at the beginning of the turn is greatest when the casters are not aligned with the turning circle'; the kinematics elements of this statement

are not defined. The effects of caster orientation at start-up are also considered in Stout (1979): in respect of powered occupant controlled wheelchairs two points are made. Firstly, manoeuvring at '*low* speed, the casters have a significant frictional resistance to turning' (emphasis added). No theoretical explanation to this velocity effect or experimental results accompany the statement and even if this is a useful account of a phenomenon with an electric wheelchair it is not known if it is extant in the ACMV. Stout also defines a method for measuring 'caster turning friction coefficient' for the non-rolling caster wheel: this includes displacing the caster bearing housing of the wheelchair by $\frac{1}{2}$" by a measured force applied at the caster bearing housing. It is to be noted that the front caster wheels are typically without brakes, none are in evidence in the pictures in this article, so it is not clear how wheel roll was prevented or whether negligible wheel roll occurs with this method and that is what is intended by Stout. MacPhee et al. (2001) used a similar approach with an occupant controlled wheelchair, in this case the caster wheel ground contact point is moved by 2.5 cm in a lateral direction, but reports that the test-retest reliability was low. Kauzlarich et al. (1984), cited previously in respect of the relationship between wheel roll and scrub friction, is also relevant to start-up effects since the maximum force to continue the vehicle-frame orientation change does not occur immediately but when the caster orientation, on the force applied side, was 30° (initial orientation appears to have been the forward trailing position): the magnitude of vehicle-frame orientation change when the maximum force to continue occurred is not reported. Whatever the practical value these easily applied measurement methods have they do not assist with a theoretical comprehension of the ACMV. Nevertheless, a start-up caster assembly related phenomenon is in evidence from these publications.

The results from Koontz et al., Van der Beek et al. indicate that an ACMV investigation should consider start-up effects. Additionally, the results from Al-Eisawi et al. and Kauzlarich et al., though caution should be exercised regarding the latter given it is based on a single test, and comments by Frank and Abel (1989) suggest that both initial and subsequent caster orientation may be an important feature of caster assembly effects. More generally the importance of caster orientation on wheelchair dynamics is assumed, most recently, by Chénier et al.

(2011). Furthermore, Kauzlarich et al., Stout and MacPhee et al. all underline the need to consider start-up effects.

3.5.7. *Handle height and loading*

One operator-related and two-mechanism related motion resistance effects linked to handle height are found in the literature. In respect of the operator, in one of the few operator controlled wheelchair studies Van der Woude et al. (1995) examined biomechanical effects of handle height on eight healthy subjects: this study concluded that biomechanical benefits occur with a handle height which is 86.5% of shoulder height. Further citation on the implications of handle height is not necessary since the only investigative requirement is the recognition that handle height may affect the performance of any task which is given to subjects.

The two mechanism-related effects are as follows. Firstly, both Van der Woude et al. (1995) and Abel (1988) report results which indicate that for operator controlled wheelchairs the operators apply vertical forces on the handles when pushing on level ground and that the magnitude of this loading relates to handle height. Secondly, as a matter of theory rather than measurement, Van der Woude et al. (2003) draws attention to the moment effects of handle forces: the planar component of handle forces is vertically displaced from the reactions acting on the vehicle-frame so a couple is formed and the maintenance of equilibrium about axes parallel with the ground plane requires the vertical reactions on the wheel to change.

Two further relevant points may also be added to the above. Firstly, for general planar motion, as opposed to translational motion, the 3D nature of static equilibrium should not be reduced to 2D unless some indication of the resulting error is determined. For the 3D problem with a four wheel device, since there are four wheel reactions and only three equations of static equilibrium, this cannot be determined theoretically without recourse to simplifying assumptions or applying a non-rigid body method: for example, assuming an elastic deformation with a defined stiffness (Genta, 1997) or using loading assumptions (Inoue et al., 2000). However, to ensure a robust empirical investigation it would be necessary to determine first how useful such methods are for the ACMV manoeuvres of in-

vestigative interest: neither Genta nor Inoue et al. consider the extent to which four wheel loading can be usefully estimated by the approaches they use. There is therefore, if a knowledge of individual caster assembly effects is considered necessary to understanding ACMV manoeuvres, a practical consideration as to how the individual loadings on a caster assembly is determined. The second point to note is that the vertical COM height will also affect the outcome of loading since one component would be removed if the planar component of handle forces passes through the vehicle-mass COM. While this is unlikely with a seated occupant, with a mobile hoist occupant, handle heights are higher. The extent to which these mechanism-related handle height effects affect the ACMV is not reported in the literature. Furthermore even a preliminary estimate requires a knowledge of the forces and reactions that occur during the ACMV manoeuvres of investigative interest and this is not available. It is therefore useful in a first investigation to minimise handle height and load mass position variation.

3.6. **Investigative Implications**

Many factors in non-ACMV studies and in ACMV studies outside the area of investigative interest are relevant to an ACMV investigation and the relevances have been noted in each section. However, the literature review has not identified any precursory ACMV studies in the area of investigative interest in the sense that replication or variation can be considered. Given that there are no ACMV studies which combine both theory and empiricism and that motion resistance is considered to be the dominant factor for the area of investigative interest a methodological issue arises: should a first ACMV study which links theory and measurement begin with the caster assembly or the ACMV: these two approaches might be thought of as micro (the former) and macro (the latter) approaches. This final section considers the challenges of both approaches and concludes that a study of the gross dynamics of the ACMV is more useful to the investigative interest.

The motion of the caster wheel of a caster assembly during the general plane motion of the ACMV vehicle-frame to which it is fixed has not been reported. As considered in Section 3.5.2 (page 37) while some caster wheel motion resistance effects have been studied the simplification has been made that roll resistance and

scrub friction are independent; it is imprudent to disregard the interaction between these two effects and a study of the caster assembly is therefore complex. If the micro approach is taken there are three distinct areas of theory and empiricism which are potential sources of prior work on which to build an investigation of caster assembly motion resistance effects: railway vehicle mechanics, automobile dynamics (and related to this bicycles and motorcycles since they have pneumatic tyres) and studies of primitive objects such as the sphere or cylinder. In the first instance, before even a qualitative appreciation of these three theoretical topics is gained, it is useful to consider the location of interest of each of these areas and the relevance to the area of investigative interest. For all three topics the terms of this text, wheel roll and wheel rotation, will be used for the angular velocity motions.

Railway wheel mechanics does account for both wheel roll and wheel rotation but there are four factors which are divergent from the caster assembly. Firstly, the proportions of wheel roll to wheel rotation on a railway vehicle will always be limited by the relatively large radius of track curves. Secondly, the rail track and the wheels of a railway vehicle have a defined geometry which has no counterpart in the ACMV. Thirdly, a flange on the wheel makes rail contact on tight bends. Fourthly, the materials of contact are steel on steel. (See Iwnicki (2006) for all four points.)

The automobile wheel is also subject to wheel roll and wheel rotation. However, the automobile tyre is pneumatic and the relevant caster wheels are not. Disregarding the slip angle effects which arise from the pneumatic tyre, the wheel roll to wheel rotation magnitude differences for parking manoeuvres will not be as large as would occur for a railway wheel. This still contrasts with the ACMV for which it is conceivable that the magnitude of caster global rotation would be greater than that of the magnitude of wheel roll; automobile steering geometry would not permit such proportions. It is relevant to note that Pacejka (2000) specifically disregards motion resistance in the analyses: this indicates the complexity.

The final potential topic source is the study of primitive objects such as spheres and cylinders. For example Johnson (1958) examined the contact mechanics of a sphere with a translational roll (equivalent to wheel roll) and with rotation (so not general plane motion). Before carrying out a structured search for studies

of a primitive mechanisms acting in a manner similar to the caster assembly (for example, a cylinder with wheel roll and wheel rotation) the following is relevant. An ideal geometry has been assumed for the caster assemblies of the ACMV. Certainly, caster rake, a design feature of the wheelchair (Major, 1990), and caster cant are not design features of the ACMV. Also it may be the case that the other deviations noted in British Standards Institution (2008) are all within specification tolerances but the tolerances will allow these effects to some extent: tilted and oblique axle (see Preliminary Chapter). Finally, the ideal revolute joint model is also a simplification: British Standards Institution (2008) identifies caster shift and more generally revolute joints are multi-DOF due to manufacturing tolerances as evidenced by the need for suitable dynamic approaches (Flores et al. (2007) inter alios). In conclusion it would be imprudent to assume that the caster assembly of an ACMV is as determinate as the steel sphere of the rolling element caster bearing which connects the caster assembly to the ACMV frame. It is more prudent to assume that the micro approach would require that a special construction caster assembly closer to the idealised model would be required in order to relate an empirical investigation to a model: a relevant extant model if it exists or one developed if it does not. A first study based on the micro approach could therefore develop an understanding of caster assembly motion resistance but the validity of any extrapolation to ACMV in actual use would be limited by the use of a specially constructed caster assembly. While it would be possible to compare and contrast a specially constructed caster assembly with a proprietary one there is the risk that if results are divergent then extrapolation to the ACMV and the architectural planning issue will not be possible.

Given that the investigative interest is the use of adaptations planning to overcome ACMV manoeuvring difficulties, the most crucial question for a first investigation must be whether or not the manoeuvring difficulties reported are of a type which architectural planning changes could remedy. It is therefore concluded that the macro approach, i.e identifying the gross motion resistance effects are more important than understanding the origin of those effects in detail. If the gross ACMV dynamics are examined and it is found that there is an ACMV behaviour such that architectural planning could influence manoeuvring difficulties,

while the origin of motion resistance would not be fully understood, the findings would be directly valid. Additionally, initial ACMV modelling (developed modelling results are presented in the Dynamics Chapter) indicated the presence of interesting dynamic behaviour. For these reasons it is concluded that the gross motion resistance dynamics should be investigated in a way which takes account of motion resistance uncertainty and the uncertainty regarding individual caster assembly loading.

Given that motion resistance is assumed to be the dominant factor one of way of framing the architectural interest of this investigation is in terms of the relationship between the handle-forces, as will be defined, which must be applied to balance the motion resistances and the space required to carry out the desired manoeuvre: the forces-applied and space-required relationship. A theoretical development of Abraham and Johnson (2010) follows in the next chapter and this leads to a characterisation of the forces-applied and space-required relationship for a model ACMV.

Chapter 4–Dynamics

4.1. **Introduction**

[1] The Literature Chapter has demonstrated that no dynamic account of the ACMV has been published and in particular the relationship between handle-forces and manoeuvring space has not been considered.

Henceforth, the term FCMV (four-caster manual vehicle) will be used. Defining the number of caster assemblies is necessary as the analysis which follows is based on four caster assemblies. Additionally, the term FCMV is used to describe ACMV use, even if it has four caster assemblies, restricted to the case where there are two hand-grasp application areas (handles) at the rear of the vehicle as was typical for many of the disability vehicles considered in the Preliminary Chapter (page 17).

While dynamic models of the FCMV (or ACMV) are not found in the literature it is possible to modify existing published models of non-ACMV: vehicles with caster assemblies and fixed wheels. (Numerous examples exist, for example, Thanjavur and Rajagopalan (1997) who use Kane's formulation.[2]) However, as the FCMV is omni-directional the set of manoeuvres which might be investigated is extremely large for two reasons. Firstly, there are three independent components for general plane motion: as established in the Preliminary Chapter the vehicle-frame is omni-directional on the ground-plane. Secondly, as indicated in the Literature Chapter the four caster orientations seem to have an important effect. Thus while the FCMV has three DOF when subject to the nonholonomic constraints and wheel

[1] A qualitative account of the dynamics is also given for the benefit of the non-technical reader: page 234.

[2] Kane's formulation can assist the formulation of equations of motion for rigid body models with higher levels of detail: the initial ACMV modelling referred to in the Literature Chapter was based on this approach.

roll constraints, the initial caster orientations must also be considered. So the creation of a model does not of itself provide any means of determining whether or not the set of all manoeuvres has any intrinsic subsets and so it does not of itself assist the identification of a finite set of manoeuvres for empirical investigation.

In contrast, the dynamical consideration which is made in this chapter leads to the creation of what is termed the Zmodel-FCMV: this model is selected for two reasons. Firstly, it provides the basis of an empirical investigation of human operation of real-FCMV: to avoid ambiguity, FCMV as an object of empirical study are termed real-FCMV and as an object of modelling are termed model-FCMV. Secondly, it leads to the prediction that the motion resistance effects of some manoeuvres result in substantial differences in a handle-force measure (to be defined) compared with other manoeuvres (on the same floor covering) and these different manoeuvres require different displacement spaces. The term 'substantial' is used to refer to the occurrence of measures where a 100% difference (in handle-force measure) can be demonstrated.

As there are no theoretically-based empirical studies of real-FCMV upon which to make critical developments, it is useful to begin by only considering those effects which are likely to have the greatest impact on results. Thus, while a model without any inhibition on complexity would take account of body deformation and multi-DOF wheel and caster stem joints, only those behaviours which are anticipated as having the most substantive effect are considered. It is the contention of this study that first-order effects are explicable using planar multi-body dynamics and a Coulomb model for motion resistance. Additionally the manoeuvres of interest are those which occur in confined spaces with loads which will be considered heavy by the human operator so accelerations and therefore inertial effects are assumed to be small compared with motion resistance effects: thus accelerations are disregarded and a quasi-static approach is taken.

In order to direct empirical study this chapter therefore develops a model with the following approach. As motion resistance, using a Coulomb model is, in part, a function of velocity direction the three initial sections formulate the model-FCMV kinematics in a way which makes the relevant velocity directions explicit. Firstly, a model-FCMV kinematics system is defined. Secondly, a novel method of graphical

inspection for model-FCMV kinematics is introduced. Thirdly, the kinematics of a model-FCMV subject to a CoZV (centre of zero velocity) are considered: this results in what is termed a 'Zmodel-FCMV'. The subsequent two sections take an inverse dynamics approach, i.e. the kinematics are determined and the dynamics which produce those kinematics are then determined. Firstly, consideration is given to balancing the motion resistance effects by a force at the COM and a torque: the term 'torque' is used in this text in the sense of a force couple, i.e. two forces of equal magnitude and opposite direction applied at different points and not as a synonym for moment: thus in this text a torque, like a force, may be applied to the vehicle-frame. It is demonstrated that for the conditions specified, balancing the motion resistance effects when the model-FCMV is subject to different CoZV requires that varying proportions of torque to force are applied. Secondly, the effect of balancing motion resistance by handle-forces is considered: it is demonstrated that for the conditions specified, with the handle-force measure to be defined, the different CoZV are associated with substantial differences in handle-force measure.

Throughout the chapter while a thorough treatment of the mathematics is made, as the findings will have value to those involved in adaptation planning, visual representation is sought at all times.

The following conventions are used in this chapter. The term 'vehicle-frame' refers to the literal frame of the model-FCMV and not the orthonormal triad attached to the vehicle-frame. Also throughout this chapter measures viewed from the orthonormal triad attached to the vehicle-frame are indicated by a leading 'B' superscript: no leading superscript is used for the global measures. In order to avoid ambiguities which may result from printing reproduction, all vectors are over-barred in Figures even though only bold is used in the text. A nomenclature is found at the end of the Preliminary Chapter. Expressions as well as equalities and inequalities are entitled 'Equation' for the purposes of labelling. No advanced dynamic techniques are used but in addition to those topics indicated in the Preliminary Chapter a number of techniques are applied without explanation of the underlying principles: motion relative to a rotating axis, kinetics of plane motion of rigid bodies, symbolic and numerical integration, complex numbers and a hyperbolic function. The mathematical manipulation not required in the text is made

in Appendix A or, as the case with many of the Figures and for integration, produced within Maple 14.01 (Maplesoft) (computer algebra system) and the folder 'FCMVDynamics' on the accompanying computer disc contains the relevant files.

4.2. **Model-FCMV Kinematics**

The following simplifying kinematics assumptions are used for the model-FCMV:

1. Horizontal ground-plane
2. Rigid bodies
3. Ideal revolute joints
4. Identical caster assemblies
5. Caster orientation is about an axis perpendicular to the ground plane and wheel roll is about an axis parallel to the ground plane
6. Line contact between wheel and ground
7. Point contact between caster-stem and vehicle-frame.

Figure 4.1 (page 58) illustrates: (a) a top view of the vehicle-frame of a model-FCMV, (b) illustrates the caster assembly and (c) tabulates measures for a typical real-FCMV as used for adults with disabilities. The model-FCMV vehicle-frame geometry is defined by positive scalars w, l, hw, h_{L} and h_{R} which are respectively termed: width, length, handle-width, and handle length, left and right respectively. Shown in (a) are the ground plane described by $\hat{\boldsymbol{X}} - \hat{\boldsymbol{Y}}$ with $\hat{\boldsymbol{S}}$ pointing out of the page and the model-FCMV COM at point $\mathrm{C_O}$ located at $[0, 0]$ on the ground plane. The uvs frame (orthonormal triad) with unit vectors $\hat{\boldsymbol{u}}$, $\hat{\boldsymbol{v}}$ and $\hat{\boldsymbol{s}}$ is attached to the vehicle-frame at $\mathrm{C_O}$, with $\hat{\boldsymbol{s}}$ directed as $\hat{\boldsymbol{S}}$, which has a displacement c from the vehicle-frame geometric centre $\mathrm{G_O}$ where $c = \mathbf{c} \cdot \hat{\boldsymbol{u}}$: note, c for the model-FCMV is as defined numerically and not as shown graphically. The COM combines load mass and vehicle-frame mass. The idealised contact between vehicle-frame and caster assembly is at points S_i, $i = [1, ..., 4]$. Handle-force application points are $\mathrm{P_L}$ and $\mathrm{P_R}$, which respectively relate to left and right handles and point is P

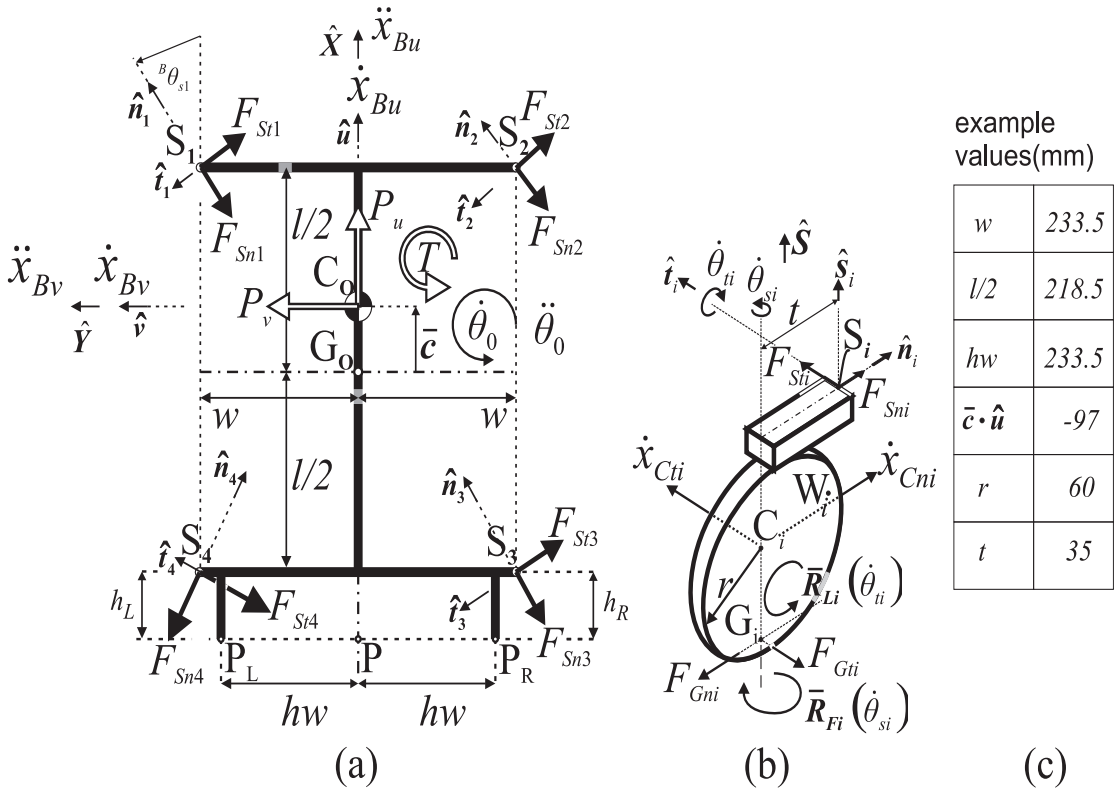

Figure 4.1 – Shows the kinematics and dynamics for the (a) vehicle-frame, (b) caster assembly (c) typical dimensions for a real-FCMV for adult disability use, for example, a shower chair

located midway between points $\mathrm{P_L}$ and $\mathrm{P_R}$. Vehicle-frame motions are therefore described by $\hat{\boldsymbol{u}}$ and $\hat{\boldsymbol{v}}$, forward and left, respectively, with respect to the operator. The angle from $\hat{\boldsymbol{X}}$ to $\hat{\boldsymbol{u}}$ is described by θ_0 (vehicle-frame orientation) and the initial configuration is $\theta_0 = 0$ with positive in the anticlockwise direction. Vehicle-frame angular velocity is $\dot{\theta}_0\hat{\boldsymbol{S}}$ and $\dot{\theta}_0$ is termed vehicle-frame rotation, and translational velocity is $\dot{\boldsymbol{x}}_B$ with components $\dot{x}_{Bu}\hat{\boldsymbol{u}}$ and $\dot{x}_{Bv}\hat{\boldsymbol{v}}$ and with time derivatives of the scalar components given by $\ddot{x}_{Bu}$ and $\ddot{x}_{Bv}$.

Figure 4.1 (b) shows the caster assembly with a tns_i frame with unit vectors $\hat{\boldsymbol{n}}_i$, $\hat{\boldsymbol{t}}_i$, and $\hat{\boldsymbol{s}}_i$ with origin located at S_i on the caster assembly: $\hat{\boldsymbol{s}}_i$ are directed as $\hat{\boldsymbol{S}}$. The caster forks are constrained to the vehicle-frame, with one degree of freedom about an axis normal to the ground plane passing through points S_i. Wheel radius is r, wheel-ground contact points are G_i at the contact line centre, and the geometric wheel centre is C_i. The minimum distance between S_i and the axis through C_i–G_i defines trail length t. The caster assembly $\hat{\boldsymbol{n}}_i$ directions are referred to as roll headings. Caster assembly angular displacements about

the $\hat{\boldsymbol{s}}$ direction as viewed from the vehicle-frame are denoted ${}^{B}\theta_{si}\hat{\boldsymbol{s}}$, measured anti-clockwise from $\hat{\boldsymbol{u}}$ to $\hat{\boldsymbol{n}}_i$ as can be seen in (a) and the time derivative is denoted ${}^{B}\dot{\theta}_{si}\hat{\boldsymbol{s}}$. The term 'caster orientation' refers to ${}^{B}\theta_{si}$ and the term 'caster rotation' refers to ${}^{B}\dot{\theta}_{si}$. The caster assembly angular velocities about $\hat{\boldsymbol{S}}$ as viewed from the ground-plane are denoted $\dot{\theta}_{si}\hat{\boldsymbol{S}}$: this may equally describe the caster wheel angular velocity about $\hat{\boldsymbol{S}}$, the scalar for this vector is termed 'caster global rotation'. Figure 4.1 (b) also shows that the caster wheel directions perpendicular to $\hat{\boldsymbol{n}}_i$ and parallel to the ground-plane are given by $\hat{\boldsymbol{t}}_i$. Caster wheel orientation about $\hat{\boldsymbol{t}}_i$ is denoted θ_{ti}. Caster wheel angular velocities about $\hat{\boldsymbol{t}}_i$ are denoted $\dot{\theta_{ti}}\hat{\boldsymbol{t}}_i$ and $\dot{\theta_{ti}}$ is termed wheel roll. The orientation of $\theta_{ti} = 0$ is indicated by a vector formed from the scalar r directed as -$\hat{\boldsymbol{n}}_i$. The C_i (caster wheel geometric centre) translational velocity is $\dot{\boldsymbol{x}}_{Ci}$ with components $\dot{x}_{Cni}\hat{\boldsymbol{n}}_i$ and $\dot{x}_{Cti}\hat{\boldsymbol{t}}_i$. The velocity of S_i is denoted $\dot{\boldsymbol{x}}_{Si}$ and the scalar is denoted $\dot{x}_{Si}$. (Some terms in Figure 4.1 are considered in later sections.)

The wheel-ground contact G_i has zero velocity with respect to the ground-plane: this is the implication of the nonholonomic constraint and wheel roll constraint as considered in the Preliminary Chapter. Thus, since C_i shares a common planar motion with G_i with respect to $\hat{\boldsymbol{t}}_i$, using the nonholonomic constraint

$$\dot{x}_{Cti}\hat{\boldsymbol{t}}_i = 0 \tag{4.1}$$

and second, the wheel roll constraint

$$\dot{x}_{Cni} = \dot{\theta_{ti}}r. \tag{4.2}$$

The C_i velocity, i.e. $\dot{\boldsymbol{x}}_{Ci}$ may be determined using an absolute motion approach comprising two terms: $\dot{\theta}_{si}\hat{\boldsymbol{S}}$ and the caster stem velocity $\dot{\boldsymbol{x}}_{Si}$. Examination of Figure 4.1 (page 58) shows that the C_i velocity scalar components are then

$$\dot{x}_{Cti} = -\dot{\theta}_{si}t + (-\dot{x}_{Bu} + a_{1i}\dot{\theta}_0 w)\sin({}^{B}\theta_{si}) + \left(\dot{x}_{Bv} + (a_{2i}\frac{l}{2} - c)\,\dot{\theta}_0\right)\cos({}^{B}\theta_{si})$$
$$\begin{cases} a_{11} = a_{14} = a_{21} = a_{22} = 1 \\ a_{12} = a_{13} = a_{23} = a_{24} = -1. \end{cases} \tag{4.3}$$

and

$$\dot{x}_{Cni} = (\dot{x}_{Bu} - a_{1i}\dot{\theta}_0 w)\cos({}^B\theta_{si}) + \left(\dot{x}_{Bv} + \left(a_{2i}\frac{l}{2} - c\right)\dot{\theta}_0\right)\sin({}^B\theta_{si}). \tag{4.4}$$

Substituting Equation 4.1 into Equation 4.3 and Equation 4.2 into Equation 4.4, caster global rotation is

$$\dot{\theta}_{si} = \left\{\left(-\dot{x}_{Bu} + a_{1i}w\dot{\theta}_0\right)\sin\left({}^B\theta_{si}\right) + \left[\dot{x}_{Bv} + \left(a_{2i}\frac{l}{2} - c\right)\dot{\theta}_0\right]\cos\left({}^B\theta_{si}\right)\right\}t^{-1} \tag{4.5}$$

and wheel roll is

$$\dot{\theta}_{ti} = \left\{\left(\dot{x}_{Bu} - a_{1i}w\dot{\theta}_0\right)\cos\left({}^B\theta_{si}\right) + \left[\dot{x}_{Bv} + \left(a_{2i}\frac{l}{2} - c\right)\dot{\theta}_0\right]\sin\left({}^B\theta_{si}\right)\right\}r^{-1}. \tag{4.6}$$

Equations 4.5 and 4.6 indicate that for the model-FCMV, caster global rotation and wheel roll are functions of vehicle-frame velocities and geometry, and caster orientation. This completes the initial consideration of the model-FCMV kinematics system.

4.3. **Graphical Inspection Method**

In this section a novel (Abraham and Johnson, 2010) method of graphical inspection of model-FCMV kinematics is introduced. The value of this method is that it demonstrates that distinct kinematics states exist and it will be shown in later sections that these produce substantially different motion resistance effects. This section demonstrates that caster global rotations and wheel roll directions can be viewed as occurring in vehicle-frame translational velocity regions and a method of inspecting these directions is identified.

The mathematical basis for this is as follows. Equations 4.5 and 4.6, caster global rotation and wheel roll, respectively, may be equated to zero and solving for $\dot{x}_{Bv}$ and $\dot{x}_{Bu}$ respectively, there are points O_i in the $\dot{\boldsymbol{x}}_B$-plane where after cancellation (page 236)

$$\mathrm{O}_i = \left[-\left(a_{2i}\frac{l}{2} - c\right), a_{1i}w\right]\dot{\theta}_0. \tag{4.7}$$

As the ${}^B\theta_{si}$ terms have cancelled out, O_i, illustrated in Figure 4.2 (page 61) for

$\dot{\theta}_0 < 0$, are fixed in the $\dot{\boldsymbol{x}}_B$-plane if $\dot{\theta}_0$ is constant. The other terms are constants.

Setting $\dot{\theta}_{si}$ in Equation 4.5 (page 60) to zero and solving for $\dot{x}_{Bu}$ produces four linear equations in terms of $\dot{x}_{Bv}$.

$$\dot{x}_{Bu} = \text{cotan}\left({}^{B}\theta_{si}\right)\dot{x}_{Bv} + \dot{\theta}_0 A_i \tag{4.8}$$

and setting $\dot{\theta}_{ti}$ in Equation 4.6 (page 60) to zero and solving for $\dot{x}_{Bu}$ produces four more linear equations in terms of $\dot{x}_{Bv}$.

$$\dot{x}_{Bu} = -\tan\left({}^{B}\theta_{si}\right)\dot{x}_{Bv} + \dot{\theta}_0 B_i \tag{4.9}$$

where A_i and B_i comprise of model-FCMV geometry parameter functions and a ${}^{B}\theta_{si}$ term (page 238). It follows that with numerical substitutions made for $\dot{\theta}_0$ and ${}^{B}\theta_{si}$, graphing Equations 4.8 and 4.9 draws the lines at which $\dot{\theta}_{si} = 0$ and $\dot{\theta}_{ti} = 0$ respectively.

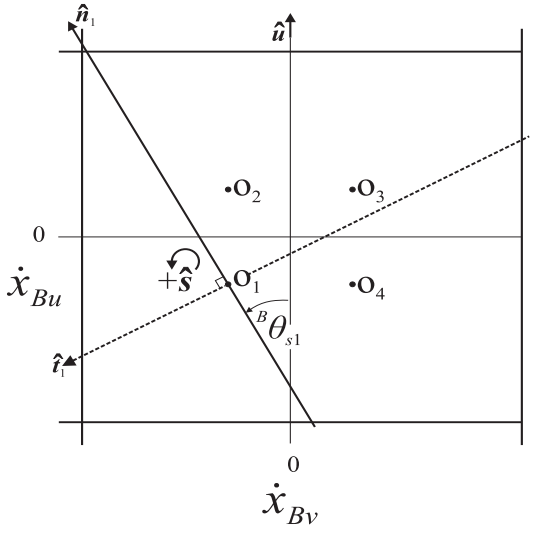

Figure 4.2 – Graphs O_i points and Equations 4.8 and 4.9 with the arbitrary values, ${}^{B}\theta_{s1} = 0.5$ rad and $\dot{\theta}_0$ =-0.4 rad/sec and the parameters of the typical real-FCMV indicated in Figure 4.1 (page 58). The gradient for Equation 4.8, the solid line, is cotan$({}^{B}\theta_{s1})$, so the angle between the equation line and the $\dot{x}_{Bu}$ axis is ${}^{B}\theta_{s1}$. The axis of the roll heading ($\hat{\boldsymbol{n}}_1$) is graphically identical with the gradient of Equation 4.8. The gradient of Equation 4.9 is tan$({}^{B}\theta_{s1})$, which, since it is perpendicular to the gradient of Equation 4.8, describes the $\hat{\boldsymbol{t}}_1$ axis. In loose terms this graph shows for one caster assembly how caster assembly angular velocity directions are determined by vehicle-frame translational velocity.

Using the arbitrary values, ${}^{B}\theta_{s1} = 0.5$ rad and $\dot{\theta}_0$ =-0.4 rad/sec, Equations 4.8 and 4.9 are graphed in Figure 4.2 (page 61). The gradient for Equation 4.8, the solid line, is cotan(${}^{B}\theta_{s1}$) (page 238), so the angle between the equation line and the $\dot{x}_{Bu}$ axis is ${}^{B}\theta_{s1}$. In other words, the axis of roll heading ($\hat{\boldsymbol{n}}_1$) is graphically identical with the gradient of Equation 4.8. The gradient of Equation 4.9 is tan(${}^{B}\theta_{s1}$) (page 239) which, since it is perpendicular to the gradient of Equation 4.8, describes the $\hat{\boldsymbol{t}}_1$ axis. It also follows that the point O_1 is the intersection point of Equations 4.8 and 4.9 for $i = 1$. The same observations may be made of the other axes at the relevant O_i.

Figure 4.2 also shows that Equations 4.8 and 4.9 divide the $\dot{\boldsymbol{x}}_B$-plane into four regions of $[\dot{x}_{Bv}, \dot{x}_{Bu}]$ in each of which there is a unique combination of [sgn($\dot{\theta}_{si}$),sgn($\dot{\theta}_{ti}$)], termed rot-roll directions, as follows. Any $[\dot{x}_{Bv}, \dot{x}_{Bu}]$ can be viewed as a point in the equation lines (Equations 4.8 and 4.9) subject to a variation of either $\dot{x}_{Bu}$ or $\dot{x}_{Bv}$. Thus equating Equation 4.5 (page 60) to zero and varying either $\dot{x}_{Bu}$ or $\dot{x}_{Bv}$, shows that for $0 < {}^{B}\theta_{si} < \pi$, $\dot{\theta}_{si}$ goes positive for coordinates below the line and negative for coordinates above the line; examination of Equation 4.6 (page 60) indicates the reverse for $\dot{\theta_{ti}}$. Hence, Equations 4.8 and 4.9 may be graphed and arrowed in accordance with the tns_i frame with positive $\hat{\boldsymbol{s}}_i$ directed out of the page in accordance with the right-hand rule. Therefore, starting with the quadrant with positive $\hat{\boldsymbol{n}}_i$ and $\hat{\boldsymbol{t}}_i$ and proceeding clockwise for the arrangement shown, [sgn($\dot{\theta}_{si}$),sgn($\dot{\theta}_{ti}$)] are [1, 1], [-1, 1], [-1, -1], and [1, -1]. Thus Figure 4.2 provides a graphical means of determining the initial combination of [sgn($\dot{\theta}_{si}$),sgn($\dot{\theta}_{ti}$)] from the $\dot{\boldsymbol{x}}_B$ components. If for example $\dot{\boldsymbol{x}}_B$ is in the top-left quadrant then there is positive wheel roll ($\dot{\theta}_{t1} > 0$) and a positive caster global rotation ($\dot{\theta}_{s1} > 0$).

Generally $[\dot{x}_{Bv}, \dot{x}_{Bu}]$ cannot be on the equation lines in Figure 4.2 (Equations 4.8 and 4.9) in finite time since this would mean that $\dot{\theta}_{si} = 0$ or $\dot{\theta}_{ti} = 0$ while $\dot{\theta}_0$ is nonzero; $\dot{\boldsymbol{x}}_B$ may pass through $\dot{\theta}_{si} = 0$ or $\dot{\theta}_{ti} = 0$ equation lines as a result of, for example, $\ddot{\boldsymbol{x}}_B$ and thus the time on the line is a differential measure (dt), i.e. tending to zero, but $\dot{\boldsymbol{x}}_B$ cannot be on the line for a finite measure of time. Physically, for example, if $[\dot{x}_{Bv}, \dot{x}_{Bu}]$ is located in the line of Equation 4.9 (apart from at the O_i point), as indicated by the axis of $\hat{\boldsymbol{t}}_1$, in finite time then the caster wheel has a zero wheel roll but a nonzero $\dot{\theta}_{si}$ since it is not located in

the line of Equation 4.8 which, given the nonholonomic constraint and wheel roll constraint, is not possible. However, if $[\dot{x}_{Bv}, \dot{x}_{Bu}]$ is coincident with O_i then $\dot{\theta}_{ti} = 0$ and $\dot{\theta}_{si} = 0$: physically the relevant caster assembly would be in static equilibrium and the vehicle-frame and the other three caster assemblies have nonzero caster global rotation and wheel roll.

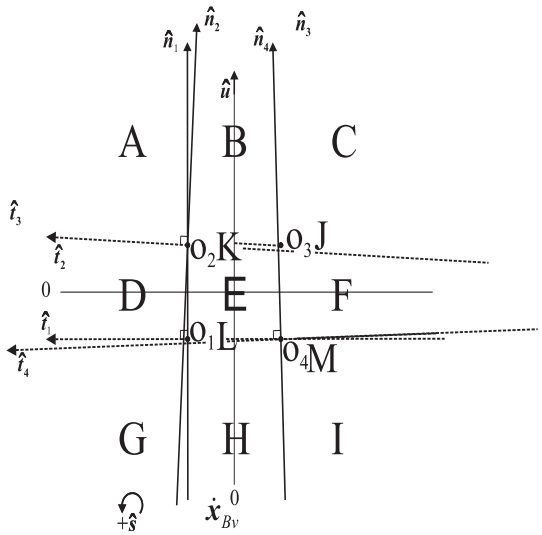

Figure 4.3 – Shows the graphical inspection method for ${}^{B}\theta_{si} \approx 0$, $\dot{\theta}_0 < 0$ and the parameters of a typical real-FCMV indicated in Figure 4.1 (page 58): division of the $\dot{\boldsymbol{x}}_B$-plane into nine regions [A, ...,I] as ${}^{B}\theta_{si}$ approaches zero and four points at O_i, [J, ...,M] are indicated. In loose terms this graph shows how all four caster assembly angular velocity directions are determined by vehicle-frame translational velocity for the case when the caster assemblies are in the forward trail position.

Figure 4.3 (page 63) illustrates the $\dot{\boldsymbol{x}}_B$-plane division for ${}^{B}\theta_{si} \approx 0$ for all four caster assemblies. Although there are 4^4 combinations of [sgn($\dot{\theta}_{si}$),sgn($\dot{\theta}_{ti}$)], the maximum number of regions for L linear equations is defined by Roberts formula (Wetzel, 1978) as R = 1 + L + binomial (L, 2) and so R = 37 for L = 8. Thus, only some [sgn($\dot{\theta}_{si}$),sgn($\dot{\theta}_{ti}$)] combinations are available for specified ${}^{B}\theta_{si}$. Additionally, parallel equation lines and coincident intersection points will reduce R. Figure 4.3 (page 63) illustrates approximately 23 polygon regions: some regions are vanishingly small and difficult to detect by inspection. Irrespective of how many polygon regions exist, for a specified $\dot{\theta}_0$ and ${}^{B}\theta_{si}$ these regions occur in the $\dot{\boldsymbol{x}}_B$-plane and the region in which the choice of $\dot{\boldsymbol{x}}_B$ is located will determine the [sgn($\dot{\theta}_{si}$),sgn($\dot{\theta}_{ti}$)] combination.

It is evident from Figure 4.3 that as ${}^{B}\theta_{si}$ approaches zero the number of

regions in the $\dot{\boldsymbol{x}}_B$-plane with eight components of [sgn($\dot{\theta}_{si}$),sgn($\dot{\theta}_{ti}$)] reduces to nine. These nine regions are labelled [A, B, C, D, E, F, G, H, I] ([A, ..., I]). It follows that as there are nine regions there are nine combinations of [sgn($\dot{\theta}_{si}$),sgn($\dot{\theta}_{ti}$)] arising from them. Additionally, as already demonstrated, $\dot{\boldsymbol{x}}_B$ may be coincidental with the O_i points which are labelled [J, K, L, M] ([J, ...,M]).

With respect to r=[J, ...,M], $\dot{\boldsymbol{x}}_B$ is coincidental with the relevant O_i and the graphic inspection method indicates that $\dot{\theta}_{si} = \dot{\theta}_{ti} = 0$ where i is the i of the O_i at which $\dot{\boldsymbol{x}}_B$ is located so no sign is defined for that caster assembly: the system may then be viewed as a three caster assembly vehicle with a CoZV at the intersection of the ground-plane and a vertical axis through the relevant S_i. While $\dot{\boldsymbol{x}}_B$ is located at a point for r=[J, ...,M] rather than in a region, the point exists within a region and the model-FCMV is subject to the [sgn($\dot{\theta}_{si}$),sgn($\dot{\theta}_{ti}$)] combination for that region. This can be visualised with the assistance of Figure 4.3 by: 1) removing the nts_i frame for the relevant i and 2) with ${}^B\theta_{si} \approx 0$, the initial [sgn($\dot{\theta}_{si}$),sgn($\dot{\theta}_{ti}$)] can then be determined for the remaining nts_i frames. However, with ${}^B\theta_{si} = 0$, a $\hat{\boldsymbol{n}}_i$ axis of one other nts_i frame passes through the O_i point of the chosen caster assembly so the sgn($\dot{\theta}_{si}$) for the caster assembly cannot be determined by the graphic inspection method. An understanding of what is termed caster steady-state in this text is then required to determine sgn($\dot{\theta}_{si}$) and this is considered later.

Thus if ${}^B\theta_{si} = 0$ there are initially thirteen kinematics outcomes with respect to the combinations of [sgn($\dot{\theta}_{si}$),sgn($\dot{\theta}_{ti}$)]: which outcome applies depends on $\dot{\boldsymbol{x}}_B$. Two points should be noted regarding the thirteen initial combinations of [sgn($\dot{\theta}_{si}$),sgn($\dot{\theta}_{ti}$)]. Firstly, these sign combinations may exist even though ${}^B\theta_{si} \neq 0$ in which case other [sgn($\dot{\theta}_{si}$),sgn($\dot{\theta}_{ti}$)] combinations will also exist. Secondly, it can also be seen that as the nts_i frames rotate, the shape of the regions associated with r=[A, ..., M] change and the region will become vanishingly small and cease to exist, i.e. the specific combination of [sgn($\dot{\theta}_{si}$),sgn($\dot{\theta}_{ti}$)] will no longer be a kinematics possibility. The term 'region r' where r =[A, ...,M] denotes those regions present at ${}^B\theta_{si} = 0$ as defined by the combination of [sgn($\dot{\theta}_{si}$),sgn($\dot{\theta}_{ti}$)] for as long as the combination exists in the $\dot{\boldsymbol{x}}_B$-plane irrespective of the change of region shape.

The graphic inspection method indicates that there are three distinct causes of variation to [sgn($\dot{\theta}_{si}$),sgn($\dot{\theta}_{ti}$)] combinations: a fourth possible cause of change

is considered later (Section 4.4.4, page 75). Firstly, the graphic inspection method shows that some $\dot{\boldsymbol{x}}_B$ changes result in a different [sgn($\dot{\theta}_{si}$),sgn($\dot{\theta}_{ti}$)] combination: graphically, for example, with respect to Figure 4.3, if $\dot{\boldsymbol{x}}_B$ is initially located in region A and $\dot{x}_{Bv}$ diminishes it is possible for $\dot{\boldsymbol{x}}_B$ to be in region B. Secondly, if the vehicle-frame rotation ($\dot{\theta}_0$) direction changes, for example, from negative (it is negative in Figure 4.3) to positive then graphically the pattern of O_i points, not the equation lines ($\dot{\theta}_{si} = \dot{\theta}_{ti} = 0$), are rotated by π rad and the graphic inspection method then indicates that $\dot{\boldsymbol{x}}_B$ may then be in a different region and so a different [sgn($\dot{\theta}_{si}$),sgn($\dot{\theta}_{ti}$)] combination exists. Thirdly, the magnitude of $\dot{\theta}_0$ may change; the graphic inspection method indicates that the gradients of the equation lines ($\dot{\theta}_{si} = 0$ and $\dot{\theta}_{ti} = 0$) and the relative positions of the O_i points are unchanged but the scale of the pattern on the $\dot{\boldsymbol{x}}_B$-plane changes: a chosen $\dot{\boldsymbol{x}}_B$ may then be in a different region with a different [sgn($\dot{\theta}_{si}$),sgn($\dot{\theta}_{ti}$)] combination. The second and third points are evident from Equation 4.7 (page 60).

In conclusion where general plane motion occurs from the initial condition ${}^B\theta_{si} \approx 0$, the model-FCMV may be viewed as entering one of thirteen kinematics states depending on vehicle-frame velocities. This has been illustrated for $\dot{\boldsymbol{x}}_B$ but the same case may be made for $\ddot{\boldsymbol{x}}_B$ for impending motion (Abraham and Johnson, 2010). The graphical inspection method therefore provides a means of revealing kinematics characteristics of the model-FCMV namely, caster global rotation directions and wheel roll directions are determined by vehicle-frame translational velocity regions.

4.4. **Centre of Zero Velocity Model**

This section presents a modification to the model-FCMV by the introduction of a CoZV and this is termed Zmodel-FCMV. Introducing a CoZV maintains the [sgn($\dot{\theta}_{si}$),sgn($\dot{\theta}_{ti}$)] combination for $\Delta\theta_0$ irrespective of $\Delta\dot{\theta}_0$ as long as sgn($\dot{\theta}_0$) is constant. The value of such an approach is in the anticipation of empirical investigation since, as will be shown, it provides the opportunity to measure the human operator response to specific kinematics conditions for $\Delta\theta_0$.

It will now be shown that the three changes to the [sgn($\dot{\theta}_{si}$),sgn($\dot{\theta}_{ti}$)] combinations detailed in the previous section are removed when the vehicle-frame or the

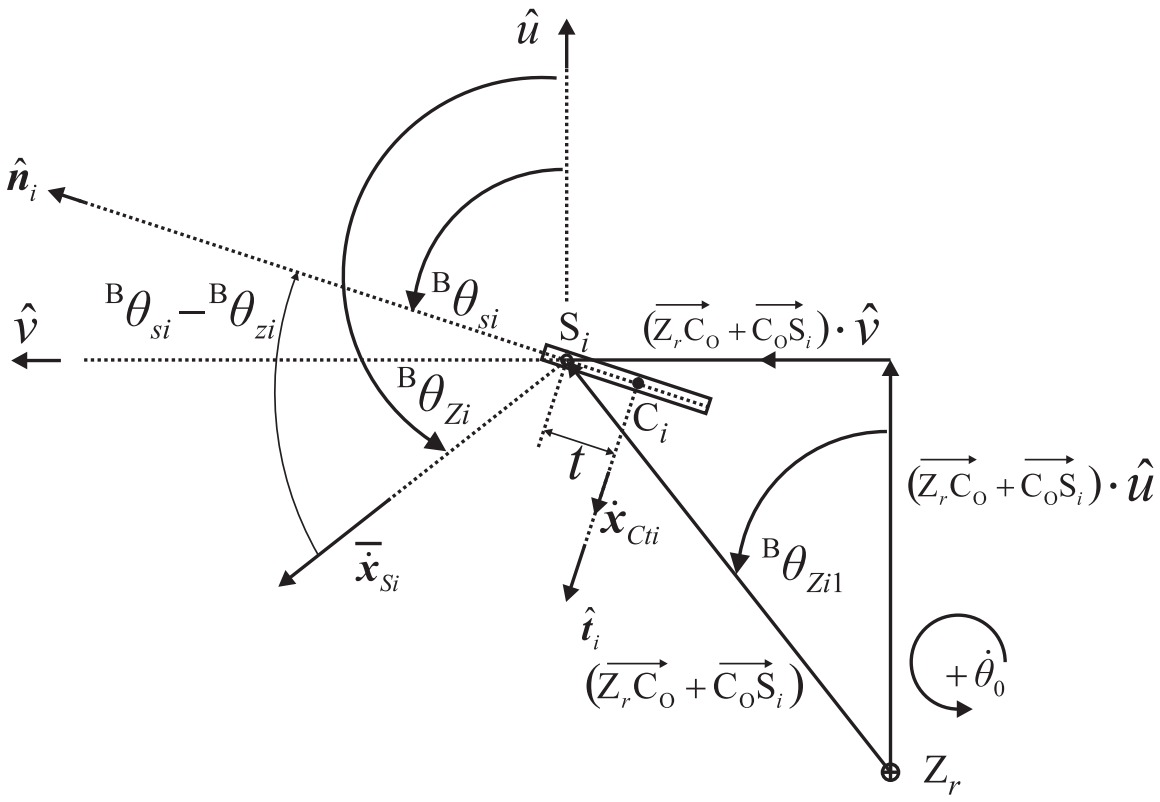

Figure 4.4 – Shows the geometry of caster wheel kinematics for the Zmodel-FCMV, i.e. with a CoZV at Z_r

vehicle-frame extended is subject to a CoZV. The opportunity to introduce this constraint arises, in mathematical terms, because the O_i components both contain a $\dot{\theta}_0$ term (Equation 4.7, page 60) and a magnitude change in $\dot{\theta}_0$ then only changes the scale of the pattern of linear equations and O_i points in the $\dot{\boldsymbol{x}}_B$-plane: the relative positions remain unchanged. It therefore follows that if additionally $\dot{\boldsymbol{x}}_B$ is a linear function of $\dot{\theta}_0$, a magnitude change of $\dot{\theta}_0$ makes no change to the relative positions on the $\dot{\boldsymbol{x}}_B$-plane of: 1) the pattern of linear equations, 2) the O_i point positions or 3) the region r of a chosen $\dot{\boldsymbol{x}}_B$ for a $\Delta\theta_0$ which can be determined. For example, consider the case where the requirement is to maintain $\dot{x}_{Bv}$ at an O_i point: in which case $\dot{x}_{Bv} = -\left(a_{2i}\frac{l}{2} - c\right)\dot{\theta}_0$ and every magnitude change in $\dot{\theta}_0$ adjusts the $\dot{x}_{Bv}$ and O_i point identically. If the CoZV is described by $\overrightarrow{Z_rC_O}$ where $\overrightarrow{Z_rC_O}$ is the vector from any point Z_r on the ground plane to point C_O where C_O is the initial position of the COM projected into the ground plane as defined by Figure 4.1 (page 58) then

$$\dot{\boldsymbol{x}}_B = \dot{\theta}_0 \hat{\boldsymbol{S}} \times \overrightarrow{Z_rC_O} \begin{array}{l} \Rightarrow \dot{x}_{Bu} = \dot{\theta}_0 \overrightarrow{Z_rC_O} \cdot \hat{\boldsymbol{u}} \\ \Rightarrow \dot{x}_{Bv} = \dot{\theta}_0 \overrightarrow{Z_rC_O} \cdot \hat{\boldsymbol{v}} \end{array} \tag{4.10}$$

which confirms that $\dot{\boldsymbol{x}}_B$ becomes a linear function of $\dot{\theta}_0$ with this arrangement: this defines the basis of the Zmodel-FCMV.

The rest of the chapter develops the Zmodel-FCMV, i.e. a model-FCMV with the added constraint that it is subject to a CoZV on the vehicle-frame or vehicle-frame extended. For the Zmodel-FCMV it is useful to disregard the COM position and develop the kinematics system in terms of caster assemblies. With reference to Figure 4.4 (page 66) three points are made. Firstly, $\dot{\boldsymbol{x}}_{si}$ and $\dot{x}_{si}$ are given by

$$\begin{aligned} \dot{\boldsymbol{x}}_{si} &= \dot{\theta}_0 \hat{\boldsymbol{S}} \times \left(\overrightarrow{\mathrm{Z}_r\mathrm{C_O}} + \overrightarrow{\mathrm{C_O S}_i} \right) \\ \Rightarrow \dot{x}_{si} &= \dot{\theta}_0 Z_{ri} \end{aligned} \tag{4.11}$$

where

$$Z_{ri} = \| \overrightarrow{\mathrm{Z}_r\mathrm{C_O}} + \overrightarrow{\mathrm{C_O S}_i} \| \tag{4.12}$$

where $\overrightarrow{\mathrm{C_O S}_i}$ is the vector from point $\mathrm{C_O}$ to point S_i. Secondly, it is evident that the angle from $\hat{\boldsymbol{u}}$ to $\dot{\boldsymbol{x}}_{si}$, denoted ${}^B\theta_{zi}$ is given by

$${}^B\theta_{zi} = \left(\arctan2 \left((\overrightarrow{\mathrm{Z}_r\mathrm{C_O}} + \overrightarrow{\mathrm{C_O S}_i}) \cdot \hat{\boldsymbol{v}}, (\overrightarrow{\mathrm{Z}_r\mathrm{C_O}} + \overrightarrow{\mathrm{C_O S}_i}) \cdot \hat{\boldsymbol{u}} \right) + \mathrm{sgn}(\dot{\theta}_0) \frac{\pi}{2} \right) \tag{4.13}$$

and that the angle from $\dot{\boldsymbol{x}}_{si}$ to $\hat{\boldsymbol{n}}_i$ is therefore ${}^B\theta_{si} - {}^B\theta_{zi}$. Thirdly, $\dot{x}_{Cti}\hat{\boldsymbol{t}}_i$ may be expressed as

$$\begin{aligned} \dot{x}_{Cti}\hat{\boldsymbol{t}}_i &= -\dot{\theta}_0 Z_{ri} \sin\left({}^B\theta_{si} - {}^B\theta_{zi} \right) \hat{\boldsymbol{t}}_i - {}^B\dot{\theta}_{si} \hat{\boldsymbol{s}} \times t\hat{\boldsymbol{n}}_i - \dot{\theta}_0 \hat{\boldsymbol{S}} \times t\hat{\boldsymbol{n}}_i \\ \Rightarrow \dot{x}_{Cti} &= -\dot{\theta}_0 Z_{ri} \sin\left({}^B\theta_{si} - {}^B\theta_{zi} \right) - {}^B\dot{\theta}_{si} t - \dot{\theta}_0 t. \end{aligned} \tag{4.14}$$

Two points are to be made regarding the right hand side of Equation 4.14: 1) the third term takes into account that the second term $({}^B\dot{\theta}_{si}\hat{\boldsymbol{s}} \times t\hat{\boldsymbol{n}}_i)$ is a relative term, i.e. viewed from the vehicle-frame and 2) the sign of $\dot{\theta}_0$ in first term arises because $\left({}^B\theta_{si} - {}^B\theta_{zi} \right)$ in Figure 4.4 is directed clockwise.

The following process is used to determine the Z_r for the CoZV which maintains $\dot{\boldsymbol{x}}_B$ in the chosen region r in the $\dot{\boldsymbol{x}}_B$-plane. There are three steps to this: 1) choose the $\dot{\boldsymbol{x}}_B$ in the region of interest, 2) transform the chosen $\dot{\boldsymbol{x}}_B$ to give Z_r in $\hat{\boldsymbol{X}} - \hat{\boldsymbol{Y}}$ coordinates and 3) transform Z_r from $\hat{\boldsymbol{X}} - \hat{\boldsymbol{Y}}$ coordinates to $\hat{\boldsymbol{v}} - \hat{\boldsymbol{u}}$ coordinates.

A numerical example follows.

Based on the vehicle-frame dimensions as shown in Figure 4.1 (page 58) but with $c = 0$ (C_O at G_O) the locations of the O_i points in the $\dot{\boldsymbol{x}}_B$-plane as per Equation 4.7 (page 60) are in i order: $[0.219, -0.234]\dot{\theta}_0$, $[0.219, 0.234]\dot{\theta}_0$, $[-0.219, 0.234]\dot{\theta}_0$ and $[-0.219, -0.2134]\dot{\theta}_0$. This is illustrated for $\dot{\theta}_0 < 0$ in Figure 4.5 (page 68) which has six other features: 1) the region letters are as indicated for Figure 4.3 (page 63),

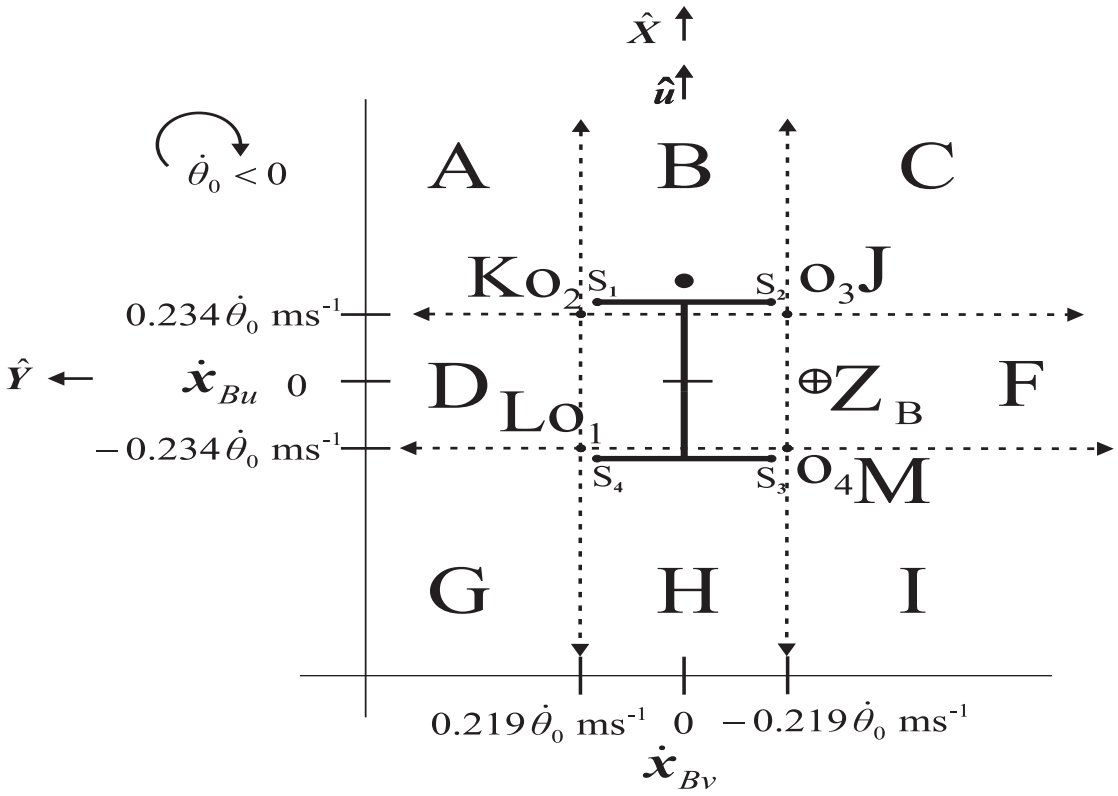

Figure 4.5 – Shows for $\dot{\theta}_0 < 0$: the region and point letters, the ground-plane superimposed on the $\hat{\boldsymbol{v}} - \hat{\boldsymbol{u}}$ plane with coincidental origins and $\hat{\boldsymbol{u}}$ co-directional with $\hat{\boldsymbol{X}}$, the vehicle-frame indicated by black solid lines with the S_i points indicated and G_O located at [0, 0], ${}^B\theta_{si} = 0$ and the CoZV shown by a circled cross marked Z_B. In loose terms this graph relates the graphic inspection method to vehicle position.

2) the $\hat{\boldsymbol{X}} - \hat{\boldsymbol{Y}}$ ground-plane is superimposed on the $\dot{\boldsymbol{x}}_B$-plane which has unit vectors $\hat{\boldsymbol{v}} - \hat{\boldsymbol{u}}$: the two planes have coincidental origins and $\hat{\boldsymbol{u}}$ and $\hat{\boldsymbol{X}}$ are co-directional, 3) the vehicle-frame is indicated by the black solid lines with the S_i points indicated and G_O is located at [0, 0], 4) ${}^B\theta_{si} = 0$, 5) the chosen $\dot{\boldsymbol{x}}_B$ in region B is indicated by a filled black circle and 6) the resulting Z_B, the CoZV, is indicated by a circled cross.

It can be seen that for this arrangement locating Z_B anywhere on

$\left[\overrightarrow{\mathrm{Z}_r\mathrm{C_O}} \cdot \hat{\boldsymbol{Y}} < -0.234, 0\right]$ ensures that $\dot{\boldsymbol{x}}_B$ is in the B region. This is evident since at $\theta_0 = 0$ the displacement in the ground-plane and the translational velocity in the $\dot{\boldsymbol{x}}_B$-plane are linear functions of each other given by

$$\begin{aligned} \dot{\boldsymbol{x}}_B &= \dot{\theta}_0 \hat{\boldsymbol{S}} \times \overrightarrow{\mathrm{Z}_r\mathrm{C_O}} \\ \Rightarrow \begin{bmatrix} \dot{\boldsymbol{x}}_B \cdot \hat{\boldsymbol{v}} \\ \dot{\boldsymbol{x}}_B \cdot \hat{\boldsymbol{u}} \end{bmatrix} &= \dot{\theta}_0 \begin{bmatrix} 0 & \mathrm{sgn}\left(\dot{\theta}_0\right) \\ -\mathrm{sgn}\left(\dot{\theta}_0\right) & 0 \end{bmatrix} \begin{bmatrix} \overrightarrow{\mathrm{Z}_r\mathrm{C_O}} \cdot \hat{\boldsymbol{Y}} \\ \overrightarrow{\mathrm{Z}_r\mathrm{C_O}} \cdot \hat{\boldsymbol{X}} \end{bmatrix} \\ \Rightarrow \dot{\theta}_0 \begin{bmatrix} \overrightarrow{\mathrm{Z}_r\mathrm{C_O}} \cdot \hat{\boldsymbol{Y}} \\ \overrightarrow{\mathrm{Z}_r\mathrm{C_O}} \cdot \hat{\boldsymbol{X}} \end{bmatrix} &= \begin{bmatrix} 0 & -\mathrm{sgn}\left(\dot{\theta}_0\right) \\ \mathrm{sgn}\left(\dot{\theta}_0\right) & 0 \end{bmatrix} \begin{bmatrix} \dot{\boldsymbol{x}}_B \cdot \hat{\boldsymbol{v}} \\ \dot{\boldsymbol{x}}_B \cdot \hat{\boldsymbol{u}} \end{bmatrix}. \end{aligned} \tag{4.15}$$

So the Z_r can be found for any region r by choosing an $\dot{\boldsymbol{x}}_B$ in region r and applying the rotation matrix: graphically this rotates the chosen $\dot{\boldsymbol{x}}_B$ about [0,0] by $\frac{1}{2}\mathrm{sgn}\left(\dot{\theta}_0\right)\pi$ rad. This process is used to calculate the thirteen Z_r scalar components as indicated in Figure 4.6 (page 69). The S_i points provide the four Z_r points located at O_i points, (r=[K,..., M]): rotated about [0, 0] by $\frac{1}{2}\mathrm{sgn}\left(\dot{\theta}_0\right)\pi$ rad.

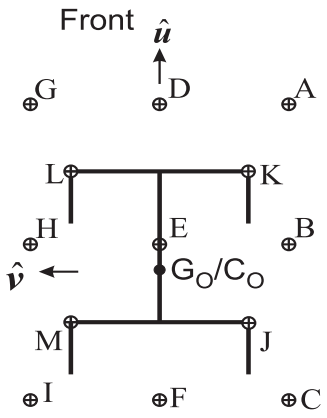

a) Top view of FCMV with centres of zero velocity (manoeuvres)

Z_r	$\hat{\boldsymbol{v}}$	$\hat{\boldsymbol{u}}$
A	340	-408
B	340	-7
C	340	449
D	0	-408
E	0	-7
F	0	449
G	-340	-408
H	-340	-7
I	-340	449
J	233.5	218.5
K	233.5	-218.5
L	-233.5	-218.5
M	-233.5	218.5

b) component measures for Z_r (mm)

Figure 4.6 – Shows a) the location of nine CoZV [A,...,I] which result in nine combinations of [sgn($\dot{\theta}_{si}$),sgn($\dot{\theta}_{ti}$)] which occur for ${}^B\theta_{si} = 0$ and the four CoZV associated with the four points [K, ...,M] which result in a further four combinations of [sgn($\dot{\theta}_{si}$),sgn($\dot{\theta}_{ti}$)] and b) tabulates measures from Z_r to $\mathrm{C_O}$ in the *vus* frame.

For the Zmodel-FCMV the S_i points as illustrated in Figure 4.1 (page 58) are used to form the vector measure $\overrightarrow{\mathrm{C_O S_i}} = a_{1i} w \hat{\boldsymbol{v}} + \left(a_{2i}\frac{l}{2} - c\right)\hat{\boldsymbol{u}}$ and combined with the scalar components given in Figure 4.6 (page 69) the $\overrightarrow{\mathrm{Z}_r\mathrm{S}_i}$ term can be found for the 52 measures of Z_{ri} and ${}^B\theta_{zi}$. This process ensures that the CoZV

which results in the [sgn($\dot{\theta}_{si}$),sgn($\dot{\theta}_{ti}$)] combination selected from those which are extant for the system configuration is maintained for $\Delta\theta_0$.

4.4.1. *Integrating caster rotation*

This subsection determines the function which relates ${}^B\theta_{si}$ (caster orientation) to θ_0 (vehicle-frame orientation). Using the nonholonomic constraint (Equation 4.1) Equation 4.14 may be rewritten as definite integrals

$$\int_{\theta_{00}}^{\theta_{01}} d\theta_0 = -t \int_{{}^B\theta_{si0}}^{{}^B\theta_{si1}} \frac{1}{Z_{ri}\sin\left({}^B\theta_{si} - {}^B\theta_{zi}\right) + t} d{}^B\theta_{si} \tag{4.16}$$

where the lower bounds are defined as (page 240) initial positions given by ${}^B\theta_{si0}$ and θ_{00}. The integral solution thus allows ${}^B\theta_{si1}$ to be defined as a function of θ_{01}.

The integration of the integrals in Equation 4.16 gives

$$\theta_{01} - \theta_{00} \;=\; -2t\left[f\left({}^B\theta_{si1}\right) - f\left({}^B\theta_{si0}\right)\right] Z_{tri}^{-\frac{1}{2}} \tag{4.17}$$

where $f\left({}^B\theta_{sip}\right)$, $p = [0, 1]$, which represents both bounds, is defined as

$$f\left({}^B\theta_{sip}\right) = \arctan\left(\left[\left(Z_{ri}\sin({}^B\theta_{zi}) + t\right)\,\tan\left(0.5{}^B\theta_{sip}\right) + Z_{ri}\cos\left({}^B\theta_{zi}\right)\right] Z_{tri}^{-\frac{1}{2}}\right) \tag{4.18}$$

and $\mathrm{Z}_{tri} = (t^2 - Z_{ri}^2)$. Maple symbolic evaluation was used for the integration of Equation 4.16. While no analytical check is made of the Maple solution the coherence of the numerical results is examined at a later stage as a means of conformation that the symbolic solution is satisfactory: additionally, results based on numerical methods were compared with results based on the symbolic solution.

4.4.2. *Ensuring real solutions*

With respect to Equation 4.17 (page 70) the $\tan\left(0.5{}^B\theta_{si}\right)$ term indicates that the system is not defined at ${}^B\theta_{si} = \pi$. With respect to $\mathrm{Z}_{tri}^{-\frac{1}{2}}$, as t (caster trail), is relatively small compared with Z_{ri} (scalar dimension from the CoZV to the relevant caster stem point S_i) the presence of complex numbers, at least in intermediate calculations, is probable: examination of Equations 4.17–4.18 with regard to non-real solutions is prudent. Assuming that ${}^B\theta_{si} \neq \pi$ and $t^2 > Z_{ri}^2$ then there is a real

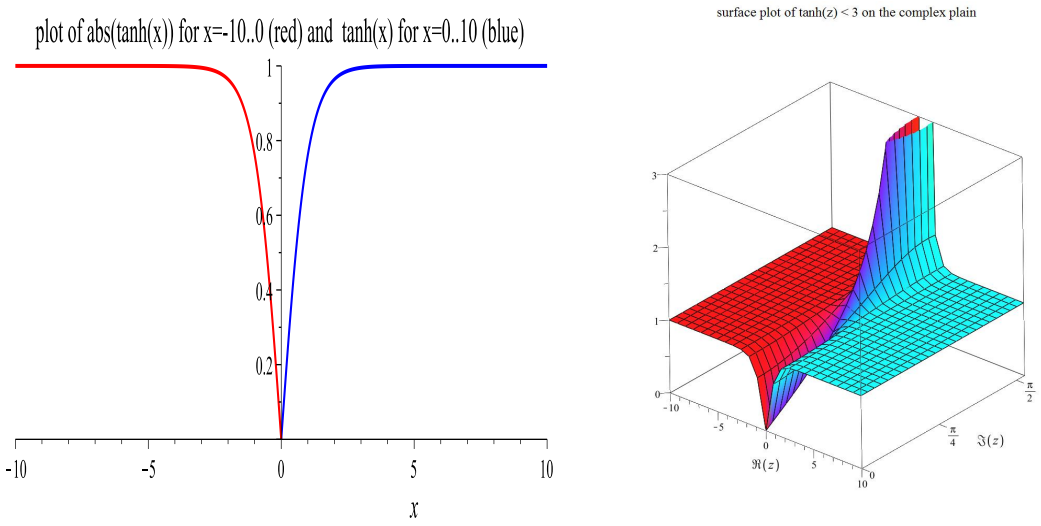

Figure 4.7 – Shows (left) the function tanh(x) and (right) the surface plot of tanh(z)<3 where z is a complex number .

valued solution. Where $t^2 < Z_{ri}^2$, complex solutions may arise so it is necessary to ensure that complex solutions are excluded. Additionally, the examination which is required to achieve this also offers an understanding of what is termed the caster steady-state. To this end, disregarding the coefficient sign each of the two terms of the right hand side of Equation 4.17 are symbolically identical–the numerical values vary since one relates to ${}^B\theta_{si0}$ and one to ${}^B\theta_{si1}$–and may be written as:

$$2tZ_{tri}^{-\frac{1}{2}}\arctan\left(\left[\left(Z_{ri}\sin({}^B\theta_{zi})+t\right)\,\tan\left(0.5{}^B\theta_{sip}\right)+Z_{ri}\cos\left({}^B\theta_{zi}\right)\right]Z_{tri}^{-\frac{1}{2}}\right) \tag{4.19}$$

and where $t^2 < Z_{ri}^2$ and a complex number results the term above may be written as (page 240):

$$-2t|Z_{tri}|^{-\frac{1}{2}}\operatorname{arctanh}\left(\left[\left(Z_{ri}\sin({}^B\theta_{zi})+t\right)\,\tan\left(0.5{}^B\theta_{sip}\right)+Z_{ri}\cos\left({}^B\theta_{zi}\right)\right]|Z_{tri}|^{-\frac{1}{2}}\right) \tag{4.20}$$

One way of considering arctanh() in Equation 4.20 is by first considering the function tanh() for which arctanh() is the inverse function. Firstly, it is known that for tanh(x), x any real number, solutions only exist for $|\tanh(x)| < 1$. This is illustrated in Figure 4.7 (left) (page 71) where $x < 0$ (red) is shown as abs(tanh(x)). So if the surface of tanh(z) is considered, see Figure 4.7 (right), where z is a complex number, it is known that solutions where $\Im\left[\operatorname{arctanh}(\tanh(z))\right] = 0$ occur

at $|\tanh(z)| < 1$. It therefore follows that if the magnitude of the operand of the arctanh() function of Equation 4.20 is ≥ 1 then the solution will be complex but if it is < 1 then a real solution exists. However, as there are two arctanh() terms for Equation 4.20 with opposite sign coefficients, if both operands are >1 then a solution may be found for both terms with identical imaginary parts which then cancel as the sign coefficients are opposite. It follows that real solutions are ensured by choosing ${}^{B}\theta_{si1}$ and ${}^{B}\theta_{si0}$ such that either both or neither angle choice generates a complex value in the operand of arctanh() of Equation 4.20. The boundary values between complex and real solutions for ${}^{B}\theta_{sip}$ are therefore defined by

$$\left| \left[\left(Z_{ri} \sin({}^{B}\theta_{zi}) + t \right) \tan\left(0.5\,{}^{B}\theta_{sip}\right) + Z_{ri} \cos\left({}^{B}\theta_{zi}\right) \right] |Z_{tri}|^{-\frac{1}{2}} \right| = 1. \tag{4.21}$$

In practical terms, if a real solution is sought, which it is, then the numerical values for ${}^{B}\theta_{si1}$ and ${}^{B}\theta_{si0}$ substituted into Equation 4.17 (page 70) must not, in loose terms, straddle these boundary values.

In addition to indicating the transition from real to complex solutions the above boundary values can be shown to be the ${}^{B}\theta_{si}$ values at which ${}^{B}\dot{\theta}_{si} = 0$: this is termed the caster steady-state. An alternative definition is that the caster steady-state occurs when $\dot{\theta}_{si}\hat{\boldsymbol{S}}$ and the vehicle-frame angular velocity equate, i.e. $\dot{\theta}_{si} = \dot{\theta}_0$ and thus ${}^{B}\dot{\theta}_{si} = 0$.

Figure 4.8 (page 73) shows the geometry for the caster steady-state: two caster assembly orientations are shown and it is intuitively evident that for $\dot{\theta}_0 > 0$, as shown, that the orientation shown by the caster assembly in grey is unstable where as the caster assembly in black is not. Physically these two ${}^{B}\theta_{si}$ orientation are given by ${}^{B}\theta_{zi} \pm \arcsin\left(\frac{t}{Z_{ri}}\right)$ but it can be shown (page 241) that where the caster assembly steady-state is denoted ${}^{B}\theta_{steadi}$ it is given by

$${}^{B}\theta_{steadi} = {}^{B}\theta_{zi} - \arcsin\left(\frac{t}{Z_{ri}}\right). \tag{4.22}$$

Using the numerical measures for the typical real-FCMV as displayed in Figure 4.1 (page 58), evaluating Z_{ri} and ${}^{B}\theta_{zi}$ as per Equations 4.12 and 4.13 (page 67) the ${}^{B}\theta_{steadi}$ values are shown in Table 4.1 (page 73). Inputting the numerical values which determined Table 4.1 into Equation 4.21 (page 72) provides identical values

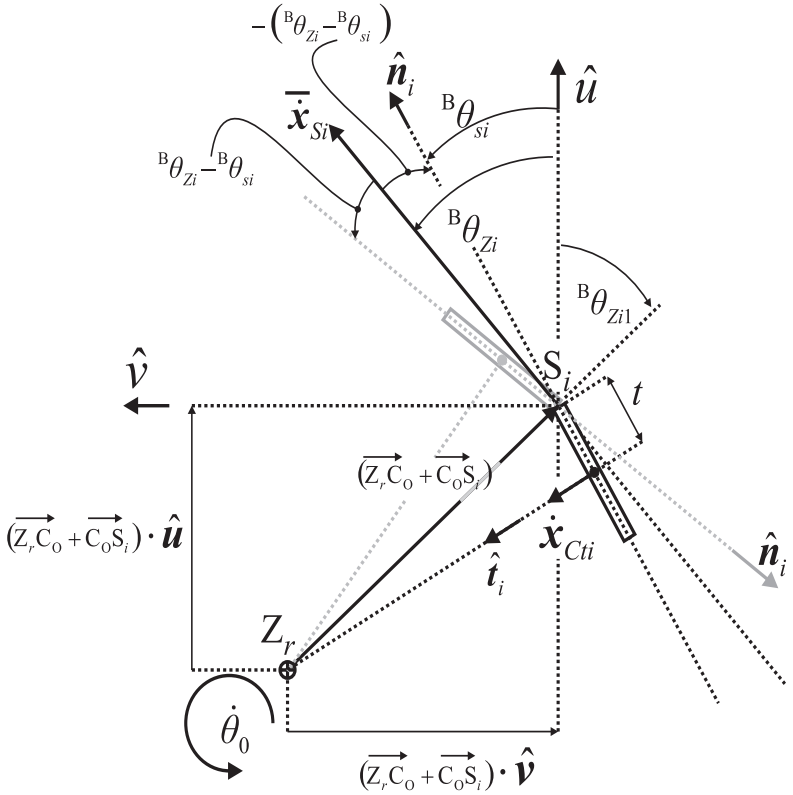

Figure 4.8 – Shows the geometry for Zmodel-FCMV for the kinematics for caster assembly motion with a CoZV at Z_r for the caster steady state ($^{B}\dot{\theta}_{si}=0$) as indicated by the black caster orientation.

r	$^{B}\theta_{stead1}$	$^{B}\theta_{stead2}$	$^{B}\theta_{stead3}$	$^{B}\theta_{stead4}$
A	0.38	1.22	1.46	0.87
B	−0.30	−0.96	1.27	0.43
C	−0.82	−1.36	−1.0	−0.33
D	0.80	2.58	1.98	1.27
E	−0.62	−2.29	2.48	0.88
F	−1.18	−1.86	−2.26	−0.67
G	2.24	2.88	2.35	1.79
H	−1.89	−2.73	2.82	2.15
I	−1.68	−2.24	−2.70	−1.87
J	−0.70	−1.49	0.0	0.08
K	0.08	0.0	1.65	0.81
L	0.0	−3.07	2.44	1.65
M	−1.49	−2.33	−3.07	0.0

Table 4.1 – Shows the caster $^{B}\theta_{steadi}$ measures for all casters and all CoZV for the Zmodel-FCMV.

to Table 4.1 which provides a non-analytical confirmation of the observations which have been made. When all four caster assemblies are in the caster steady-state this

is termed steady-state.

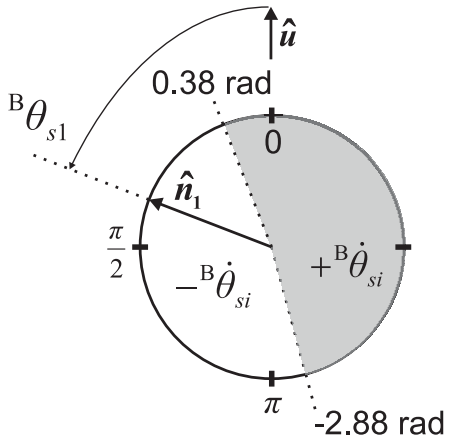

Figure 4.9 – Shows an example of the range division for ${}^{B}\theta_{si}$ created by ${}^{B}\theta_{zi} \pm \arcsin\left(\frac{t}{Z_{ri}}\right)$ which may also be viewed as the complex value boundaries: this is shown for numerical values for $i = 1$ and $\mathrm{Z_A}$.

The relationship between ${}^{B}\theta_{si}$ viewed as boundary values for real solutions and viewed as the caster steady-state is usefully conveyed geometrically. This is illustrated for ${}^{B}\theta_{si}$ in Figure 4.9 (page 74) for $i = 1$ and $\mathrm{Z_A}$: the parameters which provide the numerical values are as explained in the previously explained in this section. The 2π range is divided, as indicated by grey and white shading, by the two dotted lines which may be viewed as the complex value solution boundaries or as the ${}^{B}\theta_{zi} \pm \arcsin\left(\frac{t}{Z_{ri}}\right)$ measures one of which is ${}^{B}\theta_{steadi}$: for this case ${}^{B}\theta_{steadi} = 0.38$ rad. The $\hat{\boldsymbol{n}}_1$ vector which indicates the ${}^{B}\theta_{si1}$ measure (as defined for Equation 4.16, page 70) cannot however be located in the white or grey shaded ranges independently of ${}^{B}\theta_{si0}$ (the initial ${}^{B}\theta_{si}$ position). If ${}^{B}\theta_{si0}$ is in the white shaded range then so is $\hat{\boldsymbol{n}}_1$ since the real system cannot produce complex results.

While it is intuitive that the caster assemblies tend to a steady-state for the Zmodel-FCMV this is yet to be demonstrated: this follows. However, it is also to be noted from Figure 4.9 that since ${}^{B}\theta_{steadi}$ has one solution (0.38 rad for this case) and the complex boundary cannot be traversed for a real system, $\mathrm{sgn}({}^{B}\dot{\theta}_{si})$ is determined by ${}^{B}\theta_{si0}$: as shown $\mathrm{sgn}({}^{B}\dot{\theta}_{si}) = -1$ but if ${}^{B}\theta_{si0}$ is located in the grey shaded range then $\mathrm{sgn}({}^{B}\dot{\theta}_{si}) = 1$.

4.4.3. *Driving the model*

Equation 4.17 (Page 70) may also be manipulated so that ${}^{B}\theta_{si1}$ is expressed in terms of θ_{01} (page 243) and is given by

$$ {}^{B}\theta_{si1} = -2\arctan\left(\frac{\tan\left(\frac{\theta_{01}-\theta_{00}}{2t}Z_{tri}^{\frac{1}{2}} - f\left({}^{B}\theta_{si0}\right)\right)Z_{tri}^{\frac{1}{2}} + Z_{ri}\cos\left({}^{B}\theta_{zi}\right)}{\left(Z_{ri}\sin({}^{B}\theta_{zi}) + t\right)}\right). \quad (4.23) $$

With respect to the description just completed regarding complex solutions resulting from Equation 4.20, if the initial vehicle-frame orientation is defined as $\theta_{00} = 0$ and ${}^{B}\theta_{si0}$ defined as the initial caster orientation then θ_{01}, the vehicle-frame orientation, drives the Zmodel-FCMV and it follows that a solution, where one exists, will always be real and that ${}^{B}\theta_{si1}$ will never cross the boundary values which result in a complex solution.

4.4.4. *Caster global rotation directions*

Using the graphic inspection method it was demonstrated in Section 4.3 (page 60) that three causes of [sgn($\dot{\theta}_{si}$),sgn($\dot{\theta}_{ti}$)] change are evident with the model-FCMV. It has also been demonstrated that these [sgn($\dot{\theta}_{si}$),sgn($\dot{\theta}_{ti}$)] changes do not occur with the Zmodel-FCMV. However, sgn($\dot{\theta}_{si}$) changes do occur with the Zmodel-FCMV and a graphic demonstration for this follows. Figure 4.10 (page 76) reproduces the pertinent parts of Figure 4.5 (page 68) as detailed in Section 4.4 (page 65) including: 1) the relevant $\dot{\boldsymbol{x}}_B$ as indicated by a solid black circle in region A, 2) the CoZV Z_A which produces this $\dot{\boldsymbol{x}}_B$ and 3) the resulting ${}^{B}\theta_{stead1}$ (caster steady-state) for this arrangement as defined by Equation 4.22 (page 72), using the numerical measures for the typical real-FCMV as displayed in Figure 4.1 (page 58).

It can be seen that if the $\dot{\boldsymbol{x}}_B$ choice is as indicated by the solid circle and ${}^{B}\theta_{si0} \approx 0$ then the axis of the $\hat{\boldsymbol{n}}_1$ direction must sweep past the chosen $\dot{\boldsymbol{x}}_B$ point to approach the ${}^{B}\theta_{stead1}$ axis. It follows that since $\dot{\boldsymbol{x}}_B$ becomes located on the other side of the axis described by $\hat{\boldsymbol{n}}_1$ there is a sgn($\dot{\theta}_{s1}$) change. Thus in general the graphic inspection method indicates sgn($\dot{\theta}_{si}$) for the ${}^{B}\theta_{si}$ configuration with which it is graphed and not for the subsequent states which arise from that initial configuration. It also follows that in general sgn(${}^{B}\dot{\theta}_{si}$) $\neq$ sgn($\dot{\theta}_{si}$).

Since at the caster steady-state $\dot{\theta}_{si} = \dot{\theta}_0$ it follows that a change of sgn($\dot{\theta}_{si}$) is related to the region choice as follows. If, using the graphic inspection method

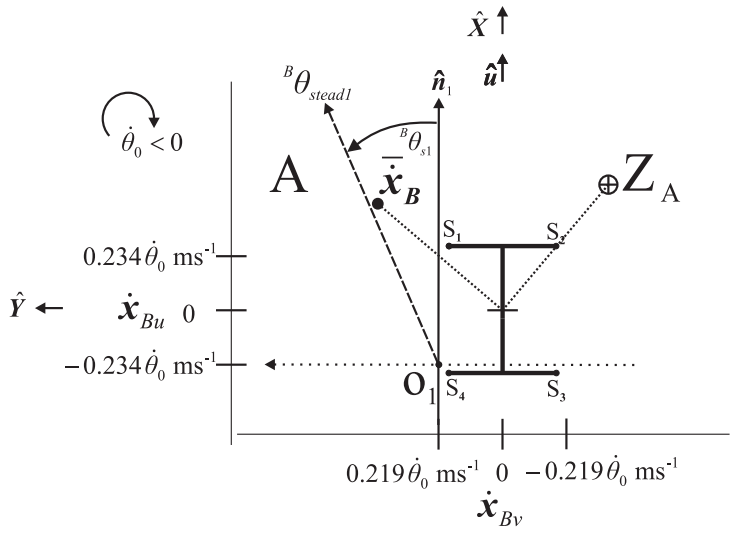

Figure 4.10 – Shows: 1) the relevant $\dot{\boldsymbol{x}}_B$ as indicated by a solid black circle in region A, 2) the CoZV Z_A which produces this $\dot{\boldsymbol{x}}_B$ (circled cross) and 3) the resulting ${}^B\theta_{steadl}$ (caster steady-state) for this arrangement as defined by Equation 4.22 (page 72). In loose terms this graph demonstrates how a change of $\text{sgn}(\dot{\theta}_{si})$ may occur.

for the Zmodel-FCMV, $\dot{\boldsymbol{x}}_B$ is located in a region such that $\text{sgn}(\dot{\theta}_{si}) \neq \text{sgn}(\dot{\theta}_0)$ then $\dot{\theta}_{si}$ must change sign but the sign is constant if initially $\text{sgn}(\dot{\theta}_{si}) = \text{sgn}(\dot{\theta}_0)$.

While in general $\text{sgn}({}^B\dot{\theta}_{si}) \neq \text{sgn}(\dot{\theta}_{si})$; for the limited case where ${}^B\theta_{si} = 0$ it can be shown (page 244) that

$$\Rightarrow {}^B\dot{\theta}_{si} \;=\; \dot{\theta}_{si}\left(1 - \frac{t}{\text{sgn}(\dot{\theta}_0) Z_{ri} \cos({}^B\theta_{zi1})}\right) \quad \{ {}^B\theta_{si} = 0 \qquad (4.24)$$

Since the magnitude of $Z_{ri}\cos\left({}^B\theta_{zi1}\right)$ is large compared to the positive measure t for r =[A,..., I], $\text{sgn}({}^B\dot{\theta}_{si}) = \text{sgn}(\dot{\theta}_{si})$ at ${}^B\theta_{si} = 0$: the large mangitude of $Z_{ri}\cos\left({}^B\theta_{zi1}\right)$ compared with t can be confirmed by examination of the $\hat{\boldsymbol{u}}$ component measures in Figure 4.6 (page 69): in loose terms the CoZV is much further from the caster stems in the $\hat{\boldsymbol{u}}$ direction than the caster trail length.

The situation is more varied for r =[K,..., M] since at $\theta_0 = 0$ and ${}^B\theta_{si} = 0$, as can be seen from Figure 4.6, the denominator is zero for Equation 4.24 (the $\hat{\boldsymbol{u}}$ component difference between Z_r and the relevant S_i position is zero for ${}^B\theta^J_{s4}$, ${}^B\theta^K_{s1}$, ${}^B\theta^L_{s2}$ and ${}^B\theta^M_{s3}$) so the right hand side is mathematically undefined: the trailing superscripts indicate the relevant r for ${}^B\theta_{si}$. For ${}^B\theta^J_{s3}$, ${}^B\theta^K_{s2}$, ${}^B\theta^L_{s1}$ and ${}^B\theta^M_{s4}$ the caster assembly remains in static equilibrium so $\dot{\theta}_{si} = 0$ and $\text{sgn}({}^B\dot{\theta}_{si}) = -\text{sgn}(\dot{\theta}_0)$

since the vehicle-frame is rotating about the relevant caster assembly.

Determining the θ_0 at which $\text{sgn}(\dot{\theta}_{si})$ changes occur proceeds as follows. The θ_0 at which $\dot{\theta}_{si} = 0$ can be determined using the nonholonomic constraint Equation 4.1 (page 59) to set the left hand side of Equation 4.14 (page 67) to zero which may then be written as

$$\dot{\theta}_{si}t = -\dot{\theta}_0 Z_{ri} \sin({}^B\theta_{si} - {}^B\theta_{zi}) \tag{4.25}$$

since $\dot{\theta}_{si} = \dot{\theta}_0 + {}^B\dot{\theta}_{si}$. Thus the solution, for those cases where $\text{sgn}(\dot{\theta}_{si}) \neq \text{sgn}(\dot{\theta}_0)$, after cancellation, is found from

$$0 = \sin({}^B\theta_{si} - {}^B\theta_{zi}). \tag{4.26}$$

Two steps are then required: 1) the numerical values as described in Section 4.4 (page 65) for ${}^B\theta_{zi}$ may be used to determine the ${}^B\theta_{si}$ at which $0 = \sin({}^B\theta_{si} - {}^B\theta_{zi})$ is true and 2), Equation 4.23 (page 75) may be used to determine the θ_0 for that value of ${}^B\theta_{si}$. The resulting measures of θ_0 at which $\dot{\theta}_{si} = 0$ are shown in columns two to five of Table 4.2 (page 78) for those cases where the caster global rotation changes direction. The values (n=43) in Table 4.2 therefore when arranged in order of magnitude therefore represents the discontinuities in any function based on the Zmodel-FCMV: this is so since $\text{sgn}(\dot{\theta}_{si})$ and $\text{sgn}(\dot{\theta}_{ti})$ switch sign at these θ_0 measures.

4.4.5. *Integrating caster rotation: results*

The following process is used to examine a numerical solution to ${}^B\theta_{si1} = f(\theta_{01})$ for $\theta_{01} = 0.. -\frac{\pi}{2}$. Using 1) the numerical measures for the typical real-FCMV as displayed in Figure 4.1 (page 58), 2) evaluating Z_{ri} and ${}^B\theta_{zi}$ as per Equations 4.12 and 4.13 (page 67), 3) evaluating Z_{tri} as indicated in respect of Equation 4.18 (page 70) and 4) driving the model as per Equation 4.23 (page 75) produces caster orientation (${}^B\theta_{si}$) results for r= [A, ...,I] as shown in the multi-Figure 4.11 (page 79) and for r=[J, ...,M] as shown in multi-Figure 4.12 (page 80).

It is useful as a check on the coherence of the analyses to make a cross-check of the ${}^B\theta_{si}$ results (Figure 4.11) against those indicated by the graphical inspection

r	θ_0 at Δ $\text{sgn}(\dot{\theta}_{s1})$	... $\text{sgn}(\dot{\theta}_{s2})$	... $\text{sgn}(\dot{\theta}_{s3})$	... $\text{sgn}(\dot{\theta}_{s4})$	θ_0 at Δ $\text{sgn}(\dot{\theta}_{t1})$	... $\text{sgn}(\dot{\theta}_{t2})$	... $\text{sgn}(\dot{\theta}_{t3})$	... $\text{sgn}(\dot{\theta}_{t4})$
A	-0.11	-0.34	-0.19	-0.13	*NS*	*NS*	*NS*	*NS*
B	*NS*	*NS*	-0.32	-0.12	*NS*	*NS*	*NS*	*NS*
C	*NS*	*NS*	*NS*	*NS*	*NS*	*NS*	*NS*	*NS*
D	-0.23	-0.44	-0.21	-0.17	*NS*	-0.11	-0.02	*NS*
E	*NS*	*NS*	-0.40	-0.23	*NS*	-0.12	-0.09	*NS*
F	*NS*	*NS*	*NS*	*NS*	*NS*	-0.02	-0.11	*NS*
G	-0.48	-0.30	-0.19	-0.21	-0.07	-0.10	-0.03	-0.01
H	*NS*	*NS*	-0.29	-0.43	-0.08	-0.11	-0.09	-0.06
I	*NS*	*NS*	*NS*	*NS*	-0.01	-0.03	-0.10	-0.07
K	*NS*	*NS*	-0.26	-0.15	*NS*	*NS*	*NS*	*NS*
L	*NS*	-0.45	-0.25	-0.26	*NS*	-0.25	-0.05	*NS*
J	*NS*	*NS*	*NS*	*NS*	*NS*	*NS*	*NS*	*NS*
M	*NS*	*NS*	-0.45	*NS*	*NS*	-0.05	-0.25	*NS*

Table 4.2 – Shows the θ_0 (rad) at which $\text{sgn}(\dot{\theta}_{si})$ changes or $\text{sgn}(\dot{\theta}_{ti})$ (wheel roll) direction changes occur for each caster and each r where NS indicates no solution, i.e. there is no change in direction. If these θ_0 measures are ordered from largest to smallest then these are the list of discontinuities which occur in any function based on $\text{sgn}(\dot{\theta}_{si})$ and $\text{sgn}(\dot{\theta}_{ti})$ as θ_0 progresses towards the steady-state: these values are required when the dynamics are considered: there are 43-sub-domains of θ_0.

method (Figure 4.3 page 63) with $\dot{\boldsymbol{x}}_B$ in each of the nine labelled regions [A, ...,I]. Taking account of the relationship between $\text{sgn}({}^B\dot{\theta}_{si})$ and $\text{sgn}(\dot{\theta}_{si})$ indicated in the previous section it can be seen that graphical inspection method correctly describes the ${}^B\theta_{si}$ displacements. Also, even though, ${}^B\theta_{steadi}$ is not displayed in Figure 4.3 and while $\dot{\boldsymbol{x}}_B$ in general may be either side of the axis of ${}^B\theta_{steadi}$, $\dot{\boldsymbol{x}}_B$ does given an indication of the ${}^B\theta_{steadi}$. For example, with respect to Figure 4.3 (page 63), if $\dot{\boldsymbol{x}}_B$ is located at $[0, 0]$ it can seen that caster assemblies one and two rotate clockwise $({}^B\dot{\theta}_{si} < 0\,[i = 1, 2])$, that caster assemblies three and four rotate anti-clockwise $({}^B\dot{\theta}_{si} > 0\,[i = 3, 4])$ and that the magnitudes of the caster steady-state angle for caster assemblies two and three will be approximately double that of caster assemblies one and four: all confirmed by examination of Figure 4.11.

The cross-check can also be make for $\dot{\boldsymbol{x}}_B$ located at the the four O_i points [J, ...,M] and, again taking account of the relationship between $\text{sgn}({}^B\dot{\theta}_{si})$ and $\text{sgn}(\dot{\theta}_{si})$ and the observations about the caster in static equilibrium indicated in the previous

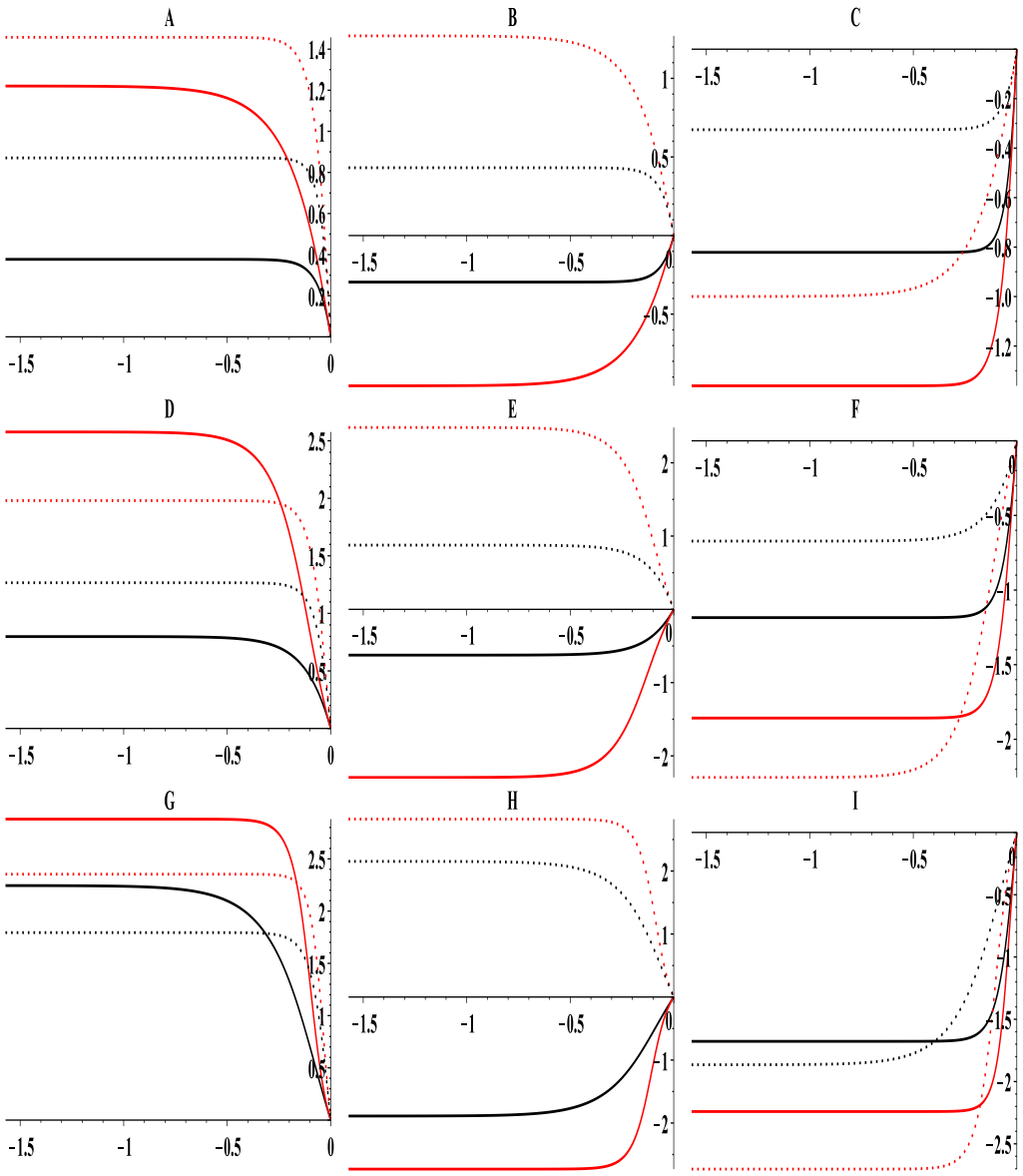

Figure 4.11 – Caster orientation (${}^{B}\theta_{si}$ rad) against vehicle-frame orientation (θ_0 rad) for each caster assembly (1 black solid, 2 red solid, 3 red dotted, 4 black dotted) and for $r = [\mathrm{A},\ldots,\mathrm{I}]$ with ${}^{B}\theta_{si0} = 0$ and $\mathrm{sgn}(\dot{\theta}_0) = -1$

section, it can be seen that graphical inspection method correctly describes the ${}^{B}\theta_{si}$ displacements: the exceptions being ${}^{B}\theta^{J}_{s4}$, ${}^{B}\theta^{K}_{s1}$, ${}^{B}\theta^{L}_{s2}$ and ${}^{B}\theta^{M}_{s3}$ where the absence of mathematical definition at ${}^{B}\theta_{si} = 0$ is also indicated by the visual difficulty of determining ${}^{B}\dot{\theta}_{si}$: no difficulty producing Figure 4.12 exists since the undefined point is ignore. One other feature is that it can be seen from the sub-Figures that for ${}^{B}\theta^{L}_{s2}$ and ${}^{B}\theta^{M}_{s3}$ there is a discontinuity as indicated by the gap (exaggerated for clarity) in the function line: as noted in Section 4.4.2 (page 70) the system is not defined at ${}^{B}\theta_{si} = \pi$. With some limitations the graphical inspection method provides a direct means of indicating caster global rotation and caster rotation.

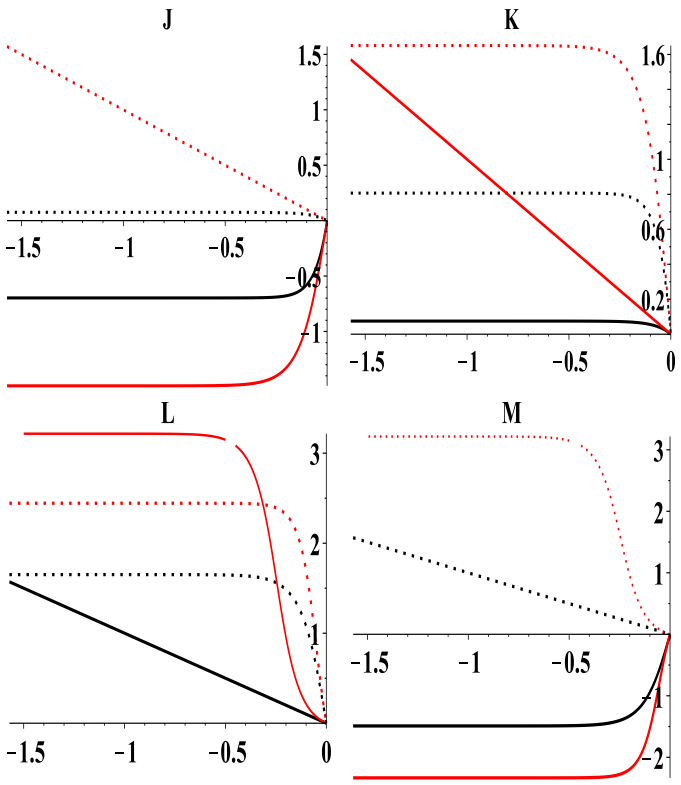

Figure 4.12 – Caster orientation ($^{B}\theta_{si}$ rad) against θ_0 rad for each caster assembly (1 black solid, 2 red solid, 3 red dotted, 4 black dotted) and for $r = [\mathrm{J},\ldots,\mathrm{M}]$ with $^{B}\theta_{si0} = 0$ and $\mathrm{sgn}(\dot{\theta}_0) = -1$.

r	θ_0 at 90% $^{B}\theta_{stead1}$	... $^{B}\theta_{stead2}$	... $^{B}\theta_{stead3}$	... $^{B}\theta_{stead4}$
A	-0.13	-0.38	-0.14	-0.10
B	-0.13	-0.37	-0.33	-0.13
C	-0.09	-0.13	-0.34	-0.13
D	-0.27	-0.35	-0.14	-0.13
E	-0.26	-0.36	-0.31	-0.25
F	-0.12	-0.14	-0.34	-0.25
G	-0.43	-0.21	-0.12	-0.14
H	-0.43	-0.22	-0.20	-0.37
I	-0.14	-0.12	-0.21	-0.40
J	-0.13	-0.21	NS	-0.17
K	-0.17	NS	-0.20	-0.13
L	NS	-0.38	-0.16	-0.20
M	-0.21	-0.17	-0.38	NS

Table 4.3 – Shows θ_0 at the caster near steady-state: θ_0 rad at which 90% of $^{B}\theta_{steadi}$ is achieved for each caster and each r where NS indicates the caster assembly in static equilibrium.

It is also useful to consider the change in θ_0 which occurs before the steady-state exists. It is evident from multi-Figures 4.11–4.12 that, apart from where the caster assembly is in static equilibrium, a substantial proportion of the caster steady-state is reached after a relatively small $\Delta\theta_0$. In order to take this into account the θ_0 at which 90% of ${}^B\theta_{steadi}$ is achieved is determined using Equation 4.17 (page 70) and the results are shown in Table 4.3 (page 80): this is termed caster near steady-state. It can be seen from Table 4.3 that in all cases, 90% of the caster steady-state is achieved by $\theta_0 > -0.43$: the caster assembly in static equilibrium is disregarded.

In general the results from multi-Figures 4.11–4.12 are coherent with both the graphic inspection method and the intuitive expectations for the physical system and it is therefore concluded that the Maple symbolic solution to Equation 4.23 (page 75) is satisfactory.

4.4.6. *Wheel roll*

This section identifies the function which relates θ_{ti} (wheel orientation) to θ_0. With respect to $\dot{x}_{Cni}$ (scalar of roll heading velocity) it is evident from Figure 4.4 (page 66) that:

$$\begin{aligned} \dot{x}_{Cni} &= \dot{\theta}_0 Z_{ri} \cos\left({}^B\theta_{si} - {}^B\theta_{zi}\right) \\ \Rightarrow \dot{\theta}_{ti} r &= \dot{\theta}_0 Z_{ri} \cos\left({}^B\theta_{si} - {}^B\theta_{zi}\right) \end{aligned} \tag{4.27}$$

where the wheel roll constraint (Equation 4.2 page 59) is used for the substitution. After some rearrangement this provides the integral equation:

$$\int_{\theta_{ti1}}^{\theta_{ti0}} d\theta_{ti} = \frac{Z_{ri}}{r} \int_{\theta_{00}}^{\theta_{01}} \cos\left({}^B\theta_{si} - {}^B\theta_{zi}\right) d\theta_0 \tag{4.28}$$

where θ_{ti0} and θ_{ti1} are the initial and final wheel orientations. Utilising the work already done to express ${}^B\theta_{si}$ as a function of θ_0 (Equation 4.23 page 75) and denoting this by $g(\theta_0)$ this provides:

$$\int_{\theta_{ti1}}^{\theta_{ti0}} d\theta_{ti} = \frac{Z_{ri}}{r} \int_{\theta_{00}}^{\theta_{01}} \cos\left(g(\theta_0) - {}^B\theta_{zi}\right) d\theta_0. \tag{4.29}$$

The symbolic solution to Equation 4.29 was determined using Maple. The

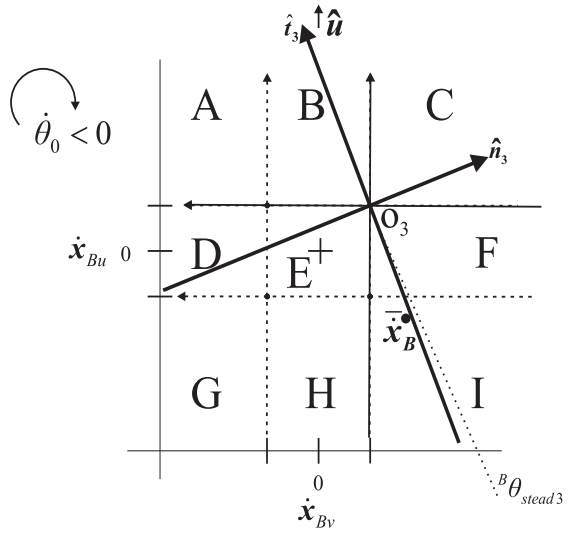

Figure 4.13 – Shows the tns_3 frame, $\dot{\boldsymbol{x}}_B$ as indicated by a solid black circle in region I and the resulting ${}^B\theta_{stead3}$ (caster steady-state) for this arrangement as defined by Equation 4.22 (page 72). This figure illustrates, using the graphic inspection method, how wheel roll can change direction.

solutions were examined to ensure that complex solutions (page 244) did not result.

4.4.7. *Wheel roll directions*

Section 4.4.4 (page 75) indicated the conditions for sgn($\dot{\theta}_{si}$) changes for the Zmodel-FCMV and this section repeats the process for sgn($\dot{\theta}_{ti}$) changes. This is illustrated in Figure 4.13 (page 82) for caster assembly $i = 3$ for a $\dot{\boldsymbol{x}}_B$ in the region I. Figure 4.13 shows the tns_3 frame with ${}^B\theta_{s30} = 0$ indicated by thin lines, $\hat{\boldsymbol{n}}_3$ (${}^B\theta_{s31}$) indicated by thick lines, the ${}^B\theta_{steadi}$ angle indicated by a dotted line and the other tns_i frames indicated by dashed lines: calculated as previously described in respect of Figure 4.3 (page 63). It can be seen that as $\hat{\boldsymbol{n}}_3$ axis sweeps around, in the progression towards the caster steady-state the axis of $\hat{\boldsymbol{t}}_3$ crosses the $\dot{\boldsymbol{x}}_B$ point so sgn($\dot{\theta}_{t3}$) changes.

An examination of Figure 4.3 (page 63) shows that: 1) the page-top regions (r=[A, B, C]) all caster assemblies have a constant sgn($\dot{\theta}_{ti}$), 2) the middle regions (r=[D, E, F]) have a constant sgn($\dot{\theta}_{ti}$) for caster wheels i=[1, 4] (the caster wheels on the operator's left side) and 3) in the page-bottom regions (r=[G, H, I]) no caster wheels have a constant sgn($\dot{\theta}_{ti}$). With respect to the O_i: 1) for the page-bottom O_i points (r=[L, M]), disregarding the caster assemblies in static equilibrium, none of the caster wheels have a constant sgn($\dot{\theta}_{ti}$) and 2) for the page-top O_i points

(r=[K, J]) constant sgn($\dot{\theta}_{ti}$) applies to all caster wheels apart from those in static equilibrium.

The determination of θ_0 at which sgn($\dot{\theta}_{ti}$) change occurs denoted θ_{0rti},where the r subscript indicates the Z_r is obtained from Equation 4.27 (page 81) and setting $\dot{\theta}_{ti} = 0$, which after cancellation and rearrangement (page 245) gives

$$\theta_{0rti} = root\ of\ \left[g\left(\theta_0\right) -^{B} \theta_{zi} - \arccos(0)\right]. \tag{4.30}$$

where the $g\left(\theta_0\right)$ substitution is as defined for Equation 4.29 (page 81) and where $\pi/2$ is chosen for the arccos(0) operand in order to produce a real valued solution if a solution exists.

The resulting measures of θ_0 at which $\dot{\theta}_{ti} = 0$ are shown in columns six to nine of Table 4.2 (page 78) for those cases where wheel roll changes direction: it can be seen that for r=[A,. . . , I] these occur within a relatively small $\Delta\theta_0$.

4.4.8. *Integrating wheel roll: results*

The typical real-FCMV and Z_r related parameters used for obtaining Zmodel-FCMV caster orientation results (Section 4.4.5 page 77) are used to obtain results for the displacement arising from wheel roll ($\dot{\theta}_{ti}$). Additionally the solution to Equation 4.30 (page 83) is used to identify sgn($\dot{\theta}_{ti}$) change where these occur. The results are shown in Figure 4.14 (page 84) for regions r = [A,. . . ,I] and in Figure 4.15 (page 85) for regions r =[J,. . . , M]: where Δsgn($\dot{\theta}_{ti}$) occur they are indicated by vertical dotted lines.

It was noted in Section 4.4.5 (page 77) that while the position of $\dot{\boldsymbol{x}}_B$ in the graphic inspection method does not provide an exact geometric representation of ${}^{B}\theta_{steadi}$ but with ${}^{B}\theta_{si0} = 0$ it does provide an indication of ${}^{B}\theta_{steadi}$ since sgn(${}^{B}\dot{\theta}_{si}$) is indicated. It is therefore possible and useful to crosscheck Figure 4.3 (page 63) with Figures 4.14–4.15: doing so confirms that the graphic inspection method provides a direct means of gaining an indication of wheel roll behaviour. For example, if an $\dot{\boldsymbol{x}}_B = [0, 0]$ is chosen for Figure 4.3 it can be seen that as caster assembly i=[2, 3] rotate clockwise and anticlockwise, respectively, the axes of the $\hat{\boldsymbol{t}}_2$ and $\hat{\boldsymbol{t}}_3$ directions sweep past $\dot{\boldsymbol{x}}_B = [0, 0]$ indicating a sgn($\dot{\theta}_{ti}$) change in wheel roll direction whereas the axes of the $\hat{\boldsymbol{t}}_1$ and $\hat{\boldsymbol{t}}_4$ directions do not cross the $\dot{\boldsymbol{x}}_B = [0, 0]$: examination of

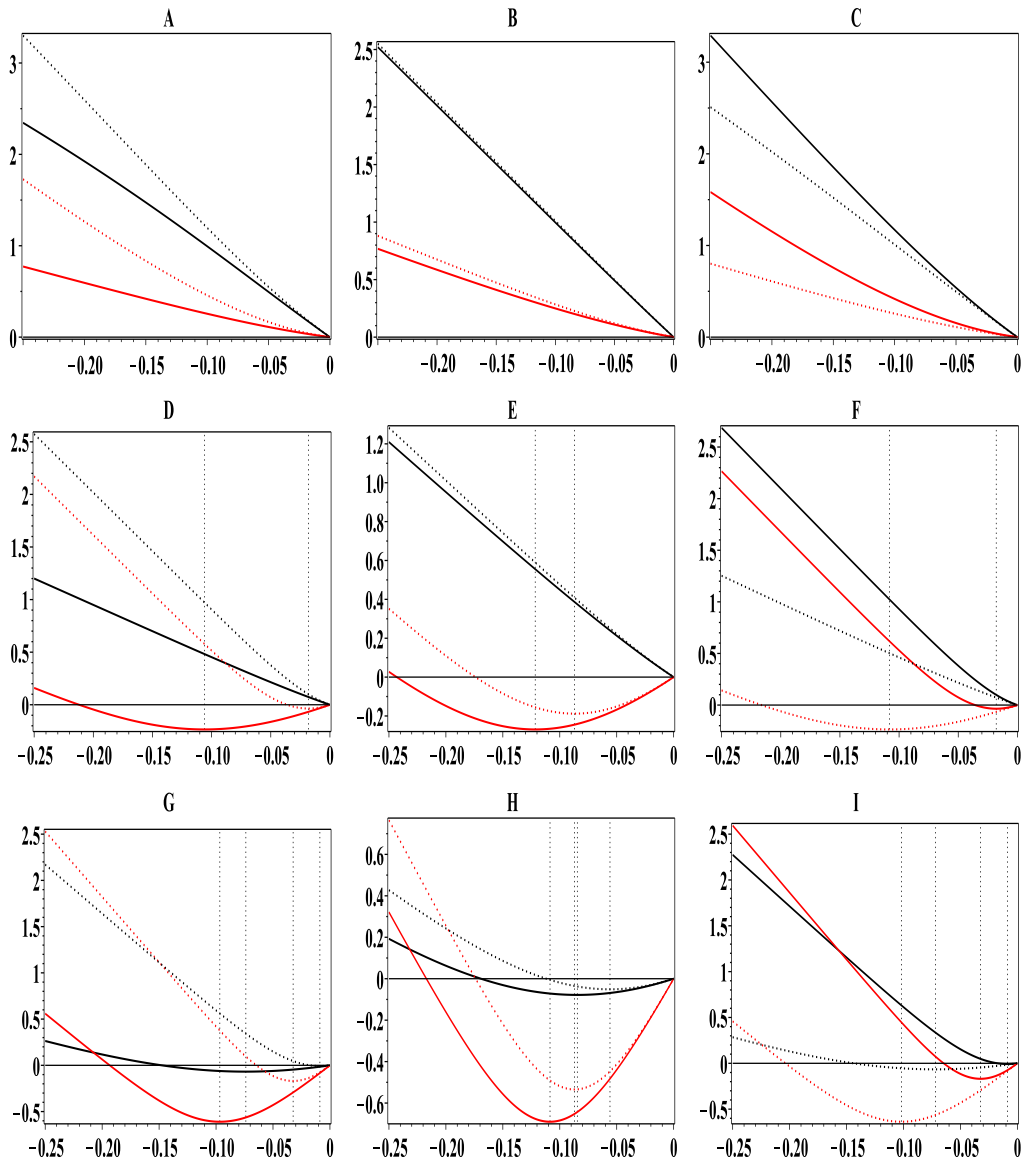

Figure 4.14 – Integration of $\dot{\theta}_{ti}$ (rad) against θ_0 (rad) for each caster assembly (1 black solid, 2 red solid, 3 red dotted, 4 black dotted) for $r =$ [A,. . . ,I] with ${}^{B}\theta_{si0} = 0$ and $\text{sgn}(\dot{\theta}_0) = -1$.

Figure 4.14 for E confirms this is the case. Another approach to describing wheel roll can be gained by determining the vertical displacement of a point W_i on the wheel where $\overrightarrow{\text{C}_i\text{W}_i}$ is the vector from C_i to W_i as indicated in Figure 4.1 (page 58). Thus the scalar measure of vertical displacement of W_i, denoted w_v is given by

$$w_v = \left(\sin\left(\theta_m + \theta_{ti}\right) - \sin\left(\theta_m\right)\right) \left|\overrightarrow{\text{C}_i\text{W}_i}\right| \tag{4.31}$$

where θ_m is the initial angle from $-\hat{\boldsymbol{n}}_i$, i.e. when $\theta_{ti} = 0$, to $\overrightarrow{\text{C}_i\text{W}_i}$. Those manoeuvres which produce no change of $\text{sgn}(\dot{\theta}_{ti})$, i.e. where the wheels roll forwards, oscillate between minimum and then maximum values but the behaviour of the

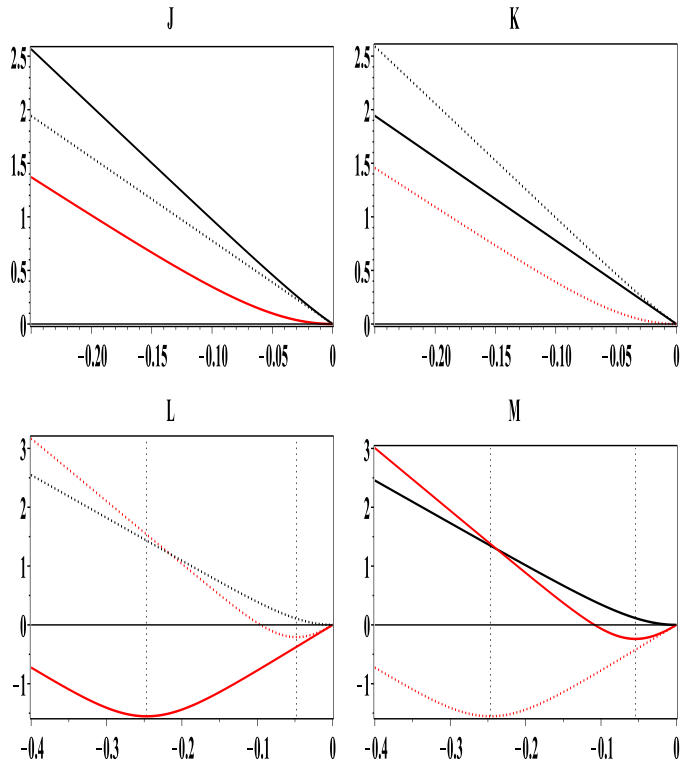

Figure 4.15 – Integration of wheel roll $\dot{\theta}_{ti}$ (rad) against θ_0 (rad) for each caster (1 black solid, 2 red solid, 3 red dotted, 4 black dotted) r = [J,...,M] with ${}^{B}\theta_{si0} = 0$ and $\text{sgn}(\dot{\theta}_0) = -1$.

manoeuvres with change of $\text{sgn}(\dot{\theta}_{ti})$, where the caster wheels initially roll backwards produce an initial positive vertical displacement: this can be deduced from Figure 4.1. Using: 1) the measures as previously described to calculate numerical values for wheel orientation, 2) setting $\theta_m = -\pi$ and 3) setting $\left|\overrightarrow{\text{C}_i\text{W}_i}\right| = 35$ mm, columns six to nine of Table 4.2 (page 78) show the θ_0 values at which $\Delta\text{sgn}(\dot{\theta}_{ti})$ occur. The maximum w_v mm measures for all manoeuvres, where they exist, are shown in Table 4.4 (page 86). A zero indicates no positive vertical movement, i.e. no backward roll. It can be seen from Table 4.4 that some w_v measures are relatively small such as caster $i = [1]$ for Z_I which is 0.27 mm.

4.4.9. *Summarising caster rotation and wheel roll direction changes*

The θ_0 values at which caster wheel angular velocities change direction were presented in Sections 4.4.4 and 4.4.7 (pages 75 and 82). There are 43 unique θ_0 values in Table 4.2 (page 78) associated with these changes. These θ_0 measures may be ordered from largest to smallest value and the resulting set of measures, preceded by $\theta_0 = 0$ and with a final member $\theta_0 < -0.486$, is denoted $\{\theta_{0n}\}$,

	W_1	W_2	W_3	W_4
A	0.0	0.0	0.0	0.0
B	0.0	0.0	0.0	0.0
C	0.0	0.0	0.0	0.0
D	0.0	8.14	1.26	0.0
E	0.0	9.31	6.54	0.0
F	0.0	1.24	8.19	0.0
G	2.39	20.06	5.90	0.28
H	2.73	22.28	17.83	1.79
I	0.27	5.89	20.83	2.31
J	0.0	0.0	0.0	0.0
K	0.0	0.0	0.0	0.0
L	0.0	34.99	7.24	0.0
M	0.0	8.25	34.99	0.0

Table 4.4 – Shows the vertical displacement (mm) of a point W_i on the wheel for each Z_r and i for those cases where an initial upward displacement occurs: 0.0 indicates that the initial displacement is downwards, i.e. positive wheel roll about $\hat{\boldsymbol{t}}_i$ or the caster assembly is in static equilibrium.

n=[2..44]. Thus $\theta_{0n-1}..\theta_{0n}$ provides 43 upper and lower boundaries for piecewise integration of any of the functions of θ_0 which have been developed for the Zmodel-FCMV. Thus each θ_{0n} indicates a change of sgn($\dot{\theta}_{si}$) or sgn($\dot{\theta}_{ti}$). It is therefore to be noted that while the Zmodel-FCMV with ${}^B\theta_{si} = 0$ yields thirteen possible combinations of [sgn($\dot{\theta}_{si}$),sgn($\dot{\theta}_{ti}$)] in general these combinations are not invariant for $\Delta\theta_0$. Nevertheless the labelling of the regions ([A,..., M]) will be used to refer to the manoeuvre which arises from that Z_r even though the initial combination of [sgn($\dot{\theta}_{si}$),sgn($\dot{\theta}_{ti}$)] is not maintained. For example region E refers to a specific combination of [sgn($\dot{\theta}_{si}$),sgn($\dot{\theta}_{ti}$)] but manoeuvre E refers to the resultant kinematics changes to the Zmodel-FCMV including the subsequent changes of [sgn($\dot{\theta}_{si}$),sgn($\dot{\theta}_{ti}$)] when region E vanishes. This completes the kinematics analyses.

4.5. **Dynamics**

4.5.1. *Motion resistance*

As described in the Preliminary Chapter the simplest model of motion resistance is provided by the Coulomb model and for the dynamic case, scrub friction

is denoted $\boldsymbol{R}_{Fi}$ and given by

$$\boldsymbol{R}_{Fi} = -\text{sgn}(\dot{\theta}_{si}) R_{Fi} \hat{\boldsymbol{S}} \tag{4.32}$$

where R_{Fi} is a function of the load with a positive numerical value. Equation 4.32 therefore indicates that the directions of the motion resistance $\boldsymbol{R}_{Fi}$ and the related velocity $\dot{\theta}_{si}\hat{\boldsymbol{S}}$ are coaxial but opposed.

Also as described in the Preliminary chapter the Coulomb model may be used to represent the wheel roll motion resistance, denoted $\boldsymbol{R}_{Li}$ and given by

$$\boldsymbol{R}_{Li} = -\text{sgn}(\dot{\theta}_{ti}) R_{Li} \hat{\boldsymbol{t}}_i. \tag{4.33}$$

4.5.2. *Dynamics of model-FCMV*

With motion resistance terms as defined this section details the model-FCMV as a dynamic system. Using the dynamic method for planar motion as provided by the free body approach the model-FCMV as illustrated in Figure 4.1 (page 58) shows (b) the caster assemblies subject to force components $F_{Gni}\hat{\boldsymbol{n}}_i$, and $F_{Gti}\hat{\boldsymbol{t}}_i$ at G_i and $F_{Sni}\hat{\boldsymbol{n}}_i$, and $F_{Sti}\hat{\boldsymbol{t}}_i$ at S_i and to motion resistance moments $\boldsymbol{R}_{Li}$ and $\boldsymbol{R}_{Fi}$: motion resistance moment directions assume positive $\dot{\theta}_{si}$ and $\dot{\theta}_{ti}$. So setting caster assembly mass to zero, the free body equations for each caster assembly are

$$\left(F_{Sti} - F_{Gti}\right) \hat{\boldsymbol{t}}_i = 0, \tag{4.34}$$

$$\left(F_{Sni} - F_{Gni}\right) \hat{\boldsymbol{n}}_i = 0, \tag{4.35}$$

$$\left(F_{Gni} r - R_{Li}\text{sgn}(\dot{\theta}_{ti})\right) \hat{\boldsymbol{t}}_i = 0 \tag{4.36}$$

and

$$\left(F_{Sti} t - R_{Fi}\text{sgn}(\dot{\theta}_{si})\right) \hat{\boldsymbol{S}} = 0. \tag{4.37}$$

While variation of caster assembly and caster wheel parameters, trail (t) and wheel radius (r) respectively, is not considered in this work it is evident from Equations 4.36 and 4.37 that with the system as defined these parameters make the action force components F_{Sti} and F_{Sni} a linear function of the motion resistance:

trail and wheel radius are recognised design parameters Abel and Frank (1991). As illustrated in Figure 4.1 (page 58) (a) the free body equations for the vehicle-frame are

$$-\sum_{i=1}^{4}\left[F_{Sti}\cos\left({}^{B}\theta_{si}\right)+F_{Sni}\sin\left({}^{B}\theta_{si}\right)\right]\hat{\boldsymbol{v}}+P_{v}\hat{\boldsymbol{v}}=m\left(\ddot{x}_{Bv}+\dot{\theta}_{0}\dot{x}_{Bu}\right)\hat{\boldsymbol{v}}, \tag{4.38}$$

$$\sum_{i=1}^{4}\left[F_{Sti}\sin\left({}^{B}\theta_{si}\right)-F_{Sni}\cos\left({}^{B}\theta_{si}\right)\right]\hat{\boldsymbol{u}}+P_{u}\hat{\boldsymbol{u}} \;=\; m\left(\ddot{x}_{Bu}-\dot{\theta}_{0}\dot{x}_{Bv}\right)\hat{\boldsymbol{u}} \tag{4.39}$$

and for the moment equation

$$-\sum_{i=1}^{4}\left[\begin{array}{c}\left(a_{2i}\frac{l}{2}-c\right)\left[F_{Sti}\cos\left({}^{B}\theta_{si}\right)+F_{Sni}\sin\left({}^{B}\theta_{si}\right)\right]\\ +a_{1i}w\left[F_{Sti}\sin\left({}^{B}\theta_{si}\right)-F_{Sni}\cos\left({}^{B}\theta_{si}\right)\right]\end{array}\right]+T\hat{\boldsymbol{S}}=I\ddot{\theta}_{0}\hat{\boldsymbol{S}} \tag{4.40}$$

where $P_v\hat{\boldsymbol{v}}$ and $P_u\hat{\boldsymbol{u}}$ are the action forces at the COM, $T\hat{\boldsymbol{S}}$ is the action torque, a_{1i} and a_{2i} are as previously defined (page 59), and I is the mass moment of inertia of the combined vehicle-frame and load mass. As there are seven independent Equations (4.34–4.40), four of which have two terms, it is possible and straightforward to solve for the seven components $[F_{Sti}, F_{Sni}, F_{Gti}, F_{Gni}, P_v, P_u, T]$ by substitution. With rearrangement the equations of motion for the vehicle-frame with P_v, P_u and T expressed as functions of velocity and acceleration, and motion resistance, i.e. inverse dynamically, are

$$\begin{aligned}P_{u} &= m\left(\ddot{x}_{Bu}-\dot{\theta}_{0}\dot{x}_{Bv}\right)\\ &\quad+\sum_{i=1}^{4}\left[r^{-1}R_{Li}\mathrm{sgn}(\dot{\theta}_{ti})\cos\left({}^{B}\theta_{si}\right)-t^{-1}R_{Fi}\mathrm{sgn}(\dot{\theta}_{si})\sin\left({}^{B}\theta_{si}\right)\right], \quad (4.41)\\ P_{v} &= m\left(\ddot{x}_{Bv}+\dot{\theta}_{0}\dot{x}_{Bu}\right)\\ &\quad+\sum_{i=1}^{4}\left[r^{-1}R_{Li}\mathrm{sgn}(\dot{\theta}_{ti})\sin\left({}^{B}\theta_{si}\right)+t^{-1}R_{Fi}\mathrm{sgn}(\dot{\theta}_{si})\cos\left({}^{B}\theta_{si}\right)\right] \quad (4.42)\end{aligned}$$

and

$$T=I\ddot{\theta}_{0}+\sum_{i=1}^{4}\left[\begin{array}{c}\left[a_{1i}w\sin\left({}^{B}\theta_{si}\right)+\left(a_{2i}\frac{l}{2}-c\right)\cos\left({}^{B}\theta_{si}\right)\right]t^{-1}R_{Fi}\mathrm{sgn}(\dot{\theta}_{si})\\ +\left[-a_{1i}w\cos\left({}^{B}\theta_{si}\right)+\left(a_{2i}\frac{l}{2}-c\right)\sin\left({}^{B}\theta_{si}\right)\right]r^{-1}R_{Li}\mathrm{sgn}(\dot{\theta}_{ti})\end{array}\right]. \tag{4.43}$$

Equations 4.41–4.43 for P_u, P_v and T may also be written for the quasi-static state, denoted P_{Qu}, P_{Qv} and M_{QC} respectively, and given by

$$P_{Qu} = +\sum_{i=1}^{4}\left[r^{-1}R_{Li}\text{sgn}(\dot{\theta}_{ti})\cos\left({}^{B}\theta_{si}\right) - t^{-1}R_{Fi}\text{sgn}(\dot{\theta}_{si})\sin\left({}^{B}\theta_{si}\right)\right], \quad (4.44)$$

$$P_{Qv} = +\sum_{i=1}^{4}\left[r^{-1}R_{Li}\text{sgn}(\dot{\theta}_{ti})\sin\left({}^{B}\theta_{si}\right) + t^{-1}R_{Fi}\text{sgn}(\dot{\theta}_{si})\cos\left({}^{B}\theta_{si}\right)\right] \quad (4.45)$$

and

$$M_{QC} = \sum_{i=1}^{4}\begin{bmatrix} \left[a_{1i}w\sin\left({}^{B}\theta_{si}\right) + \left(a_{2i}\frac{l}{2} - c\right)\cos\left({}^{B}\theta_{si}\right)\right]t^{-1}R_{Fi}\text{sgn}(\dot{\theta}_{si}) \\ + \left[-a_{1i}w\cos\left({}^{B}\theta_{si}\right) + \left(a_{2i}\frac{l}{2} - c\right)\sin\left({}^{B}\theta_{si}\right)\right]r^{-1}R_{Li}\text{sgn}(\dot{\theta}_{ti}) \end{bmatrix}. \quad (4.46)$$

The change of symbol from T to M_{QC} is useful since while T was defined as the scalar of an action torque the right hand side of Equation 4.46 is viewed as the scalar of the moment which balances the summation of the moment effects about the COM resulting from the motion resistance effects acting on the vehicle-frame at each caster stem.

In order to explicate the characteristic behaviour of the model-FCMV it will prove useful if the equations of quasi-static motion (Equations 4.44–4.46) are also expressed in a way which views motion resistance effects as reactions on the vehicle-frame at the caster stem points S_i. This is achieved as follows: the motion resistance reactions on the vehicle-frame are also described by F_{Sni} and F_{Sti} so a force $\boldsymbol{P}_{Qi}$ can be defined such that

$$\boldsymbol{P}_{Qi} - F_{Sni}\hat{\boldsymbol{n}}_i - F_{Sti}\hat{\boldsymbol{t}}_i = 0. \quad (4.47)$$

It follows, since F_{Sni} and F_{Sti} are the only reaction forces on the vehicle-frame that

$$\sum_{i=1}^{4}\boldsymbol{P}_{Qi}\cdot\hat{\boldsymbol{u}} = P_{Qu}, \quad (4.48)$$

$$\sum_{i=1}^{4}\boldsymbol{P}_{Qi}\cdot\hat{\boldsymbol{v}} = P_{Qv} \quad (4.49)$$

and

$$\sum_{i=1}^{4}\boldsymbol{P}_{Qi}\times\left[-a_{1i}w\hat{\boldsymbol{v}} + \left(a_{2i}\frac{l}{2} - c\right)\hat{\boldsymbol{u}}\right]\cdot\hat{\boldsymbol{S}} = M_{QC}. \quad (4.50)$$

Thus the application of the $\boldsymbol{P}_{Qi}$ at the relevant S_i is dynamically equivalent to the effect of $P_{Qv}\hat{\boldsymbol{v}}$, $P_{Qu}\hat{\boldsymbol{u}}$ and $M_{QC}\hat{\boldsymbol{S}}$. Therefore Equations 4.48 and 4.49 define the forces required to balance the translational effects of motion resistance and Equation 4.50 defines the moment required to balance the moment produced by the translational motion resistance effects.

Using Equations 4.34–4.37 and Equation 4.47 the magnitude of $\boldsymbol{P}_{Qi}$ is

$$|\boldsymbol{P}_{Qi}| = \sqrt{R_{Fi}^2 t^{-2} + R_{Li}^2 r^{-2}} \tag{4.51}$$

at orientation ρ_i measured from $\hat{\boldsymbol{n}}_i$ given by

$$\rho_i = \operatorname{atan2}\left[\operatorname{sgn}(\dot{\theta}_{si}) R_{Fi} t^{-1}, \operatorname{sgn}(\dot{\theta}_{ti}) R_{Li} r^{-1}\right] \{-\pi < \rho_i \leq \pi \tag{4.52}$$

The orientation of $\boldsymbol{P}_{Qi}$ with respect to the vehicle-frame is therefore ${}^{B}\theta_{si} + \rho_i$ and this scalar angular measure therefore describes the direction of $|\boldsymbol{P}_{Qi}|$ with respect to the vehicle-frame.

4.5.3. *Dynamics-kinematics*

The previous section determined the actions ($\boldsymbol{P}_{Qi}$) at the caster stem (S_i) on the vehicle-frame which are required to balance the motion resistance effects. The $\boldsymbol{P}_{Qi}$ have a magnitude $\sqrt{R_{Fi}^2 t^{-2} + R_{Li}^2 r^{-2}}$ and are at an angle ρ_i (Equation 4.52 page 90) from roll heading ($\hat{\boldsymbol{n}}_i$). The characteristics of the motion resistance effects for the model-FCMV are, in part, explicated by introducing $\boldsymbol{P}_{Qi}$ to the graphic inspection method (Section 4.3, page 60) as this section demonstrates.

Figure 4.16 (page 91) (top) reproduces Figure 4.2 (page 61) but with the addition of the $\boldsymbol{P}_{Qi}$ balancing action with $\dot{\boldsymbol{x}}_B$ as indicated by A and $\rho_i = \frac{\pi}{4}$ as indicated by the black heavy arrow: this and all future definitions of ρ_i as a constant define ρ_i for $\operatorname{sgn}(\dot{\theta}_{si}) = \operatorname{sgn}(\dot{\theta}_{ti}) = 1$, i.e. define the scrub friction to roll resistance proportion and the numerical value is then redefined for sign changes in accordance with Equation 4.52. It is to be noted that the quadrant of the $\hat{\boldsymbol{n}}_1 - \hat{\boldsymbol{t}}_1$ plane in which $\boldsymbol{P}_{Qi}$ occurs is determined by the choice of $\dot{\boldsymbol{x}}_B$. The three other possible orientations for $\boldsymbol{P}_{Qi}$ are indicated by the white filled arrows. This is evident from Equation 4.52 since $\operatorname{sgn}(\dot{\theta}_{si})$ and $\operatorname{sgn}(\dot{\theta}_{ti})$ determine the quadrant in which ρ_i occurs and the selection of a specific combination of $\operatorname{sgn}(\dot{\theta}_{si})$ and $\operatorname{sgn}(\dot{\theta}_{ti})$ is a function of

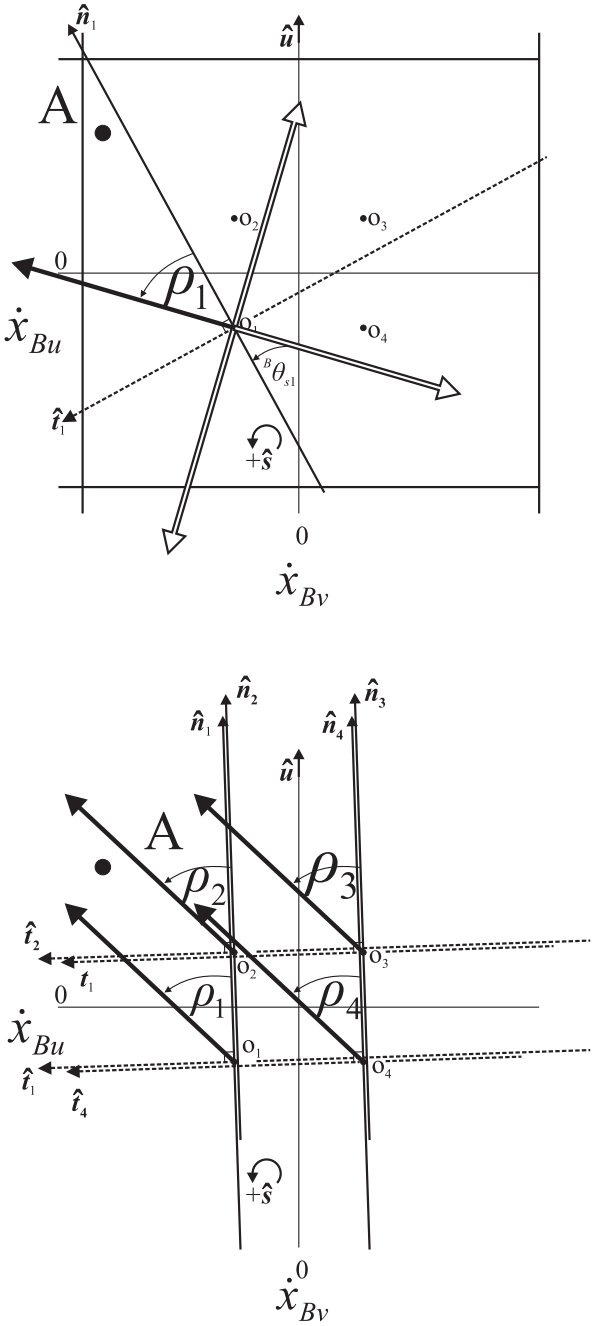

Figure 4.16 – Shows (top) reproduces Figure 4.2 (page 61) with $\dot{\boldsymbol{x}}_B$ as indicated by A and with the addition of the $\boldsymbol{P}_{Qi}$ (balancing action) for $\rho_i = \frac{\pi}{4}$ as indicated by the black heavy arrow: (bottom) illustrates the orientation of the four $\boldsymbol{P}_{Qi}$ with the graphic inspection method with ${}^B\theta_{si} \approx 0$, $\rho_i = \frac{\pi}{4}$ and $\dot{\boldsymbol{x}}_B$ located in region A. This figure incorporates the motion resistance effects into the graphic inspection method and in loose terms shows how the directions of the motion resistance effects can be determined by the graphic inspection method.

the $\hat{\boldsymbol{n}}_1 - \hat{\boldsymbol{t}}_1$ quadrant in which the chosen $\dot{\boldsymbol{x}}_B$ is located, as presented in Section 4.3. Additionally the angular displacement of $\boldsymbol{P}_{Qi}$ within the quadrant is determined by the relative magnitudes of $R_{Fi}t^{-1}$ and $R_{Li}r^{-1}$ and for a real caster assembly neither

component will have a zero magnitude. Thus for the model-FCMV some aspects of the motion resistance effects can be described without specifying numerical values for R_{Li} or R_{Fi}.

Figure 4.16 (bottom) illustrates the orientation of the four $\boldsymbol{P}_{Qi}$ using the graphic inspection method with: 1) ${}^{B}\theta_{si} \approx 0$, 2) $\rho_i = \frac{\pi}{4}$ and 3) $\dot{\boldsymbol{x}}_B$ located in region A.

It is to be noted that as the $\boldsymbol{P}_{Qi}$ are located at O_i and not S_i the graphic illustration Figure 4.16 (top) does not directly convey the moment effects of $\boldsymbol{P}_{Qi}$. To give a direct graphic indication of the moment effects it is necessary to identify the S_i locations on the $\hat{\boldsymbol{v}} - \hat{\boldsymbol{u}}$ plane and reposition the equivalent $\boldsymbol{P}_{Qi}$, as shown at O_i in Figure 4.16 (bottom), at S_i. The S_i locations on the $\hat{\boldsymbol{v}} - \hat{\boldsymbol{u}}$ plane may be directly read from Figure 4.1 (page 58) as these are simply the vehicle dimensions. Alternatively, Equation 4.15 (page 69) may be used to transform the O_i to S_i. This follows since the O_i are the $\dot{\boldsymbol{x}}_B$ at which the $\dot{\theta}_{si} = \dot{\theta}_{ti} = 0$ and Equation 4.15 determines the CoZV on the $\hat{\boldsymbol{X}} - \hat{\boldsymbol{Y}}$ plane for any $\dot{\boldsymbol{x}}_B$.

Figure 4.17 (top) reproduces Figure 4.16 (bottom) but with the equivalent $\boldsymbol{P}_{Qi}$ located at the S_i. This illustration therefore directly indicates the moment effects of the $\boldsymbol{P}_{Qi}$. Figure 4.17 (bottom) repeats the process for $\dot{\boldsymbol{x}}_B$ located in the region E. A comparison of these two illustrations, Figure 4.17 top and bottom, indicates that the proportion of moment to translational motion resistance effects which are balanced vary for the region A and region E location for $\dot{\boldsymbol{x}}_B$. With $\dot{\boldsymbol{x}}_B$ located in region A, relative to the effects when $\dot{\boldsymbol{x}}_B$ is in region E, the moment motion resistance effects which are balanced by the $\boldsymbol{P}_{Qi}$ are of relatively small magnitude and the translational motion resistance effects which are balanced are of relatively large magnitude.

This model-FCMV behaviour, the varying proportions of moment and translational motion resistance effects which have to be balanced for different region r, is the focus of the rest of this chapter and indeed this thesis. It will be demonstrated that the variation in the proportions of motion resistance moment and motion resistance translational effects persists for different ρ_i, different load distributions and as θ_0 is varied. This is demonstrated as follows. Given Equations 4.51-

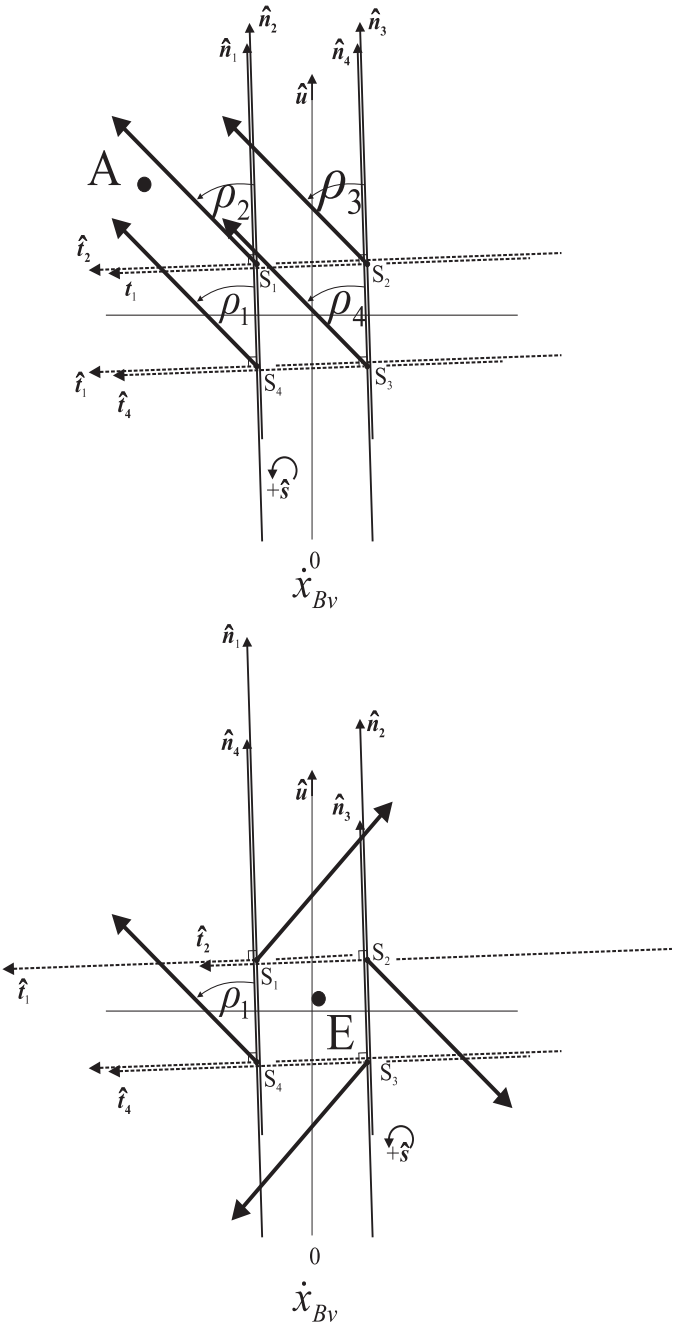

Figure 4.17 – Shows (top) a reproduction of Figure 4.16 (bottom) but with the equivalent $\boldsymbol{P}_{Qi}$ located at the S_i: this directly indicates the moment effects of the $\boldsymbol{P}_{Qi}$. Also shown (bottom) following the same process are the $\boldsymbol{P}_{Qi}$ when $\dot{\boldsymbol{x}}_B$ is located in region E. This figure shows the correct dynamic effect of the motion resistance effects since the motion resistance vectors are located at the S_i and not the O_i.

4.52 (page 90) it follows that the components of motion resistance at each S_i may be expressed as

$$|\boldsymbol{P}_{Qi}|\cos(\rho_i) = R_{Li} r^{-1} \tag{4.53}$$

and

$$|\boldsymbol{P}_{Qi}|\sin(\rho_i) = R_{Fi}t^{-1}, \tag{4.54}$$

and so substituting Equations 4.53 and 4.54 into Equations 4.44–4.46 this gives

$$\frac{P_{Qu}}{|\boldsymbol{P}_{Qi}|} = \sum_{i=1}^{4}\left[\cos(\rho_i)\text{sgn}(\dot{\theta}_{ti})\cos\left({}^{B}\theta_{si}\right) - \sin(\rho_i)\text{sgn}(\dot{\theta}_{si})\sin\left({}^{B}\theta_{si}\right)\right], \tag{4.55}$$

$$\frac{P_{Qv}}{|\boldsymbol{P}_{Qi}|} = \sum_{i=1}^{4}\left[\cos(\rho_i)\text{sgn}(\dot{\theta}_{ti})\sin\left({}^{B}\theta_{si}\right) + \sin(\rho_i)\text{sgn}(\dot{\theta}_{si})\cos\left({}^{B}\theta_{si}\right)\right] \tag{4.56}$$

and

$$\frac{M_{QC}}{|\boldsymbol{P}_{Qi}|} = \sum_{i=1}^{4}\left[\begin{array}{c}\left[a_{1i}w\sin\left({}^{B}\theta_{si}\right) + \left(a_{2i}\frac{l}{2} - c\right)\cos\left({}^{B}\theta_{si}\right)\right]\sin(\rho_i)\text{sgn}(\dot{\theta}_{si}) \\ + \left[-a_{1i}w\cos\left({}^{B}\theta_{si}\right) + \left(a_{2i}\frac{l}{2} - c\right)\sin\left({}^{B}\theta_{si}\right)\right]\cos(\rho_i)\text{sgn}(\dot{\theta}_{ti})\end{array}\right], \tag{4.57}$$

where it is assumed that $|\boldsymbol{P}_{Q1}| = |\boldsymbol{P}_{Q2}| = |\boldsymbol{P}_{Q3}| = |\boldsymbol{P}_{Q4}|$. It then follows that measures of the forces for each manoeuvre r required to balance the translational motion resistance effect is given by $f_{Zr}\left(\sqrt{\left(\frac{P_{Qu}}{|\boldsymbol{P}_{Qi}|}\right)^2 + \left(\frac{P_{Qv}}{|\boldsymbol{P}_{Qi}|}\right)^2}\right)$ and measures of the moments required to balance the motion resistance moment effects is given by $f_{Zr}\left(\left|\frac{M_{QC}}{|\boldsymbol{P}_{Qi}|}\right|\right)$ where the $f_{Zr}()$ function indicates that the operand is to be evaluated for each of the thirteen CoZV. Furthermore, $f_{Zr}()$ for each manoeuvre r may be evaluated under various conditions, for example, varying ρ_i. It then follows that the expression

$$\frac{f_{Zr}\left(\sqrt{\left(\frac{P_{Qu}}{|\boldsymbol{P}_{Qi}|}\right)^2 + \left(\frac{P_{Qv}}{|\boldsymbol{P}_{Qi}|}\right)^2}\right)}{f_{Zrmax}\left(\sqrt{\left(\frac{P_{Qu}}{|\boldsymbol{P}_{Qi}|}\right)^2 + \left(\frac{P_{Qv}}{|\boldsymbol{P}_{Qi}|}\right)^2}\right)} - \frac{f_{Zr}\left(\left|\frac{M_{QC}}{|\boldsymbol{P}_{Qi}|}\right|\right)}{f_{Zrmax}\left(\left|\frac{M_{QC}}{|\boldsymbol{P}_{Qi}|}\right|\right)} \tag{4.58}$$

where $f_{Zrmax}()$ is the measure of the maximum $f_{Zr}()$ measure for the operand for the individual manoeuvre r under whatever varying conditions are set, such as varying ρ_i, allows an inter-manoeuvre r comparison of the proportion of translational motion resistance effects to moment motion resistance effects. In loose terms Equation 4.58 provides a means of comparing the proportions of translational and moment resistance effects which occur for different manoeuvre r under varying conditions. If ${}^{B}\theta_{si}$ in Equations 4.55–4.57 is substituted by a function of ${}^{B}\theta_{si}$ in terms of θ_0, as determined by Equation 4.23 (page 75), then Equation 4.58 may be integrated

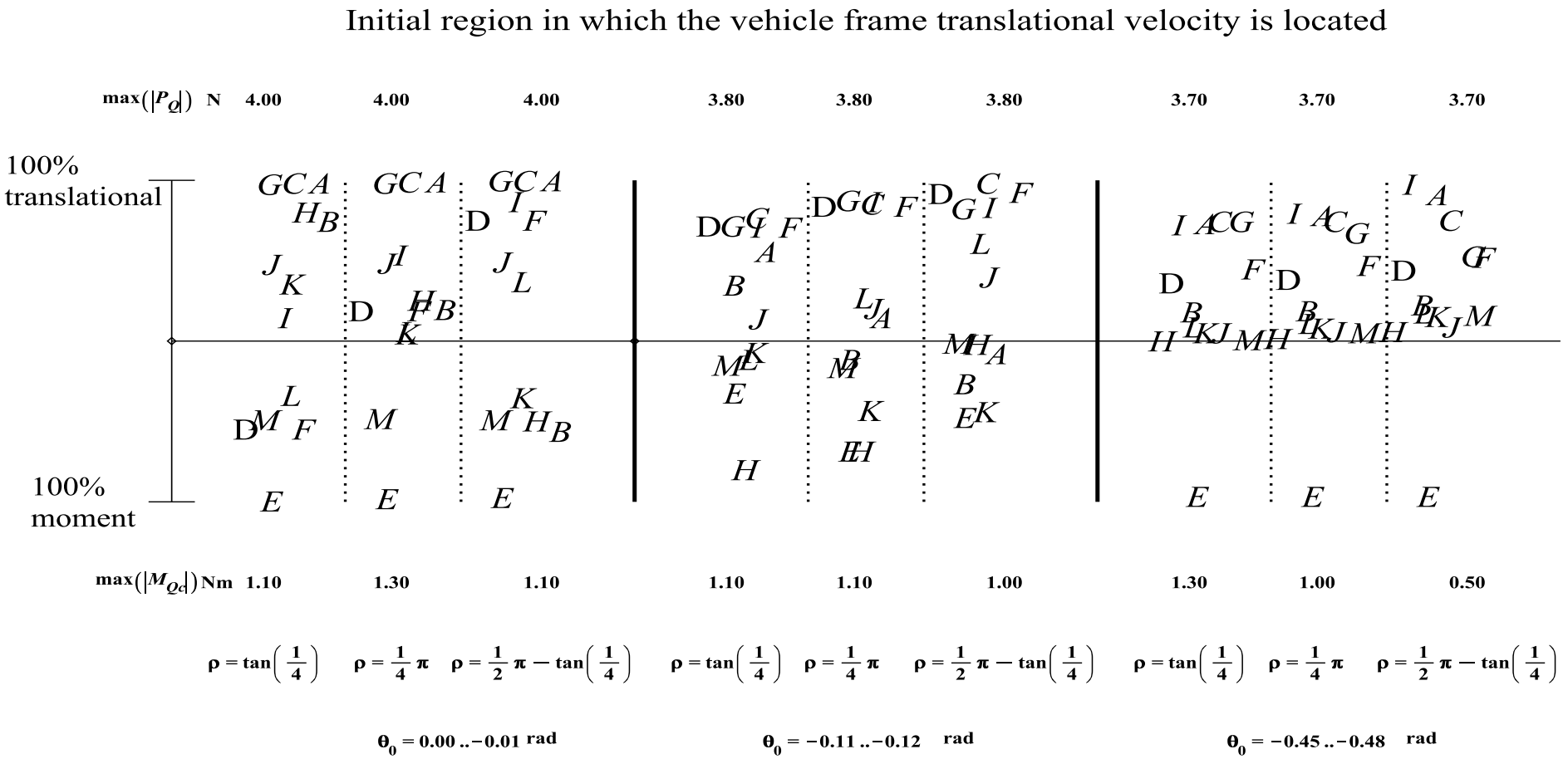

Figure 4.18 – Shows the normalised proportion of translational motion resistance effect to moment motion resistance effect using Equation 4.58 with the results for the 43 sub-domains of θ_0 represented by three subsets of measures, from left to right, for the initial set, the median set and the final set: division between each subset is indicated by a solid vertical line. Each of the three subsets is subdivided into three by vertical dotted lines and these three subdivisions show the results for three ρ_i values as shown ($\rho = \rho_i$). In each of these nine sets of measures the results of Equation 4.58 are shown for the thirteen manoeuvres, r=[A,..., M], and as Equation 4.58 normalises the results the measure can vary from approximately 100% moment motion resistance balance effect to approximately 100% translational motion resistance balance effect. The maximum $|P_Q|$ (top) and maximum $|M_{Qc}|$ (bottom) is also shown. In loose terms this figure demonstrates that for some manoeuvres the motion resistance effects are mostly translational where as for other manoeuvres the effects are mainly a moment effect.

with respect to θ_0. Piecewise integration is then possible using the 43 sub-domains (see Table 4.2 page 78) of θ_0 given by $\{\theta_{0n}\}$ as detailed in Section 4.4.4 (page 75) in respect of $\Delta\text{sgn}(\dot{\theta}_{si})$ and Section 4.4.7 (page 82) in respect of $\Delta\text{sgn}(\dot{\theta}_{ti})$. This was carried out in Maple using: 1) a small offset $(1.000001\theta_{0n0} \ldots 0.999999\theta_{0n1})$ to avoid the discontinuities created by $\text{sgn}(\dot{\theta}_{si})$ and $\text{sgn}(\dot{\theta}_{ti})$, 2) numerical methods as speed of calculation was valuable and the superior accuracy of a symbolic evaluation was not required and 3) $0.999999\theta_{0n1} - 1.000001\theta_{0n0}$ as a divisor to determine an average measure for the sub-domain.

Figure 4.18 (page 95) shows, from left to right, the results for Equation 4.58 for the 1) initial, 2) median and 3) final sub-domain of $\theta_{0n-1}..\theta_{0n}$ where the division between each sub-domain is indicated by a solid vertical line. Each of the three sub-domains is further subdivided into three by vertical dotted lines and these three subdivisions show the results for three ρ_i values as shown. In each of the nine sets of the measures the results of Equation 4.58 are shown for the thirteen manoeuvres r=[A,..., M] and as Equation 4.58 normalises the results the measure can vary from approximately 100% moment motion resistance balance effect, as is frequently the case for manoeuvre E, to approximately 100% translational motion resistance balance effect which is the case, for example, for manoeuvre A in the first subdivision. While the vertical location of the measures for the different CoZV vary it can be seen that the variation persists as θ_0 varies and as ρ_i varies: different maneouvres r produce different proportions of moment and translational motion resistance effects.

In summary it is therefore concluded that the Zmodel-FCMV is a mechanism which is characterised by: 1) having different combinations of [$\text{sgn}(\dot{\theta}_{si}$, $\text{sgn}(\dot{\theta}_{ti}$] in different vehicle-frame translational velocity regions, 2) having motion resistance reactions at S_i vary for the different manoeuvre r, 3) with the resulting moment acting on the vehicle-frame subject to variation, 4) so the proportion of the magnitude of the summation of the reactions at S_i to the moment magnitude varies and 5) requiring different proportions of force and torque to balance these motion resistance effects. The Zmodel-FCMV may be viewed as a mechanism which can transform motion resistance between translational and moment effects. Furthermore this effect perseveres for varying proportions of scrub friction and wheel roll

motion resistance.

4.6. **Handle-forces**

This final section develops the model-FCMV by determining the forces which are required to balance the motion resistance effects of the manoeuvres r when the balancing forces are applied at the handles. It will be shown that the handle-force measure required to balance the motion resistance effects for the varying manoeuvres r can vary substantially.

As in previous sections a geometric approach is taken in order to facilitate a qualitative sense of the transformation. For dynamic equivalence it is necessary, though not necessarily sufficient, that

$$P_{Qv} = P_{QLv} + P_{QRv} \tag{4.59}$$

and

$$P_{Qu} = P_{QLu} + P_{QRu} \tag{4.60}$$

where P_{QLu} and P_{QRu} are the scalars of the $\hat{\boldsymbol{u}}$ components and P_{QLv} and P_{QRv} are the scalars of the $\hat{\boldsymbol{v}}$ components of the handle-forces for the left and right handles respectively, applied at points $\mathrm{P_L}$ and $\mathrm{P_R}$ as shown in Figure 4.1 (page 58).

If $\mathrm{sgn}(P_{QLv})$=$\mathrm{sgn}(P_{QRv})$ where P_{QLv} and P_{QRv} are nonzero and where P_{QRv} or P_{QLv} but not both may be set to zero, then Equation 4.59 may be viewed as the division of P_{Qv} and relocation to one or both handles. The same observation may be extended to P_{Qu} in respect of P_{QLu} and P_{QRu}. If moments are summed at point P then the moment produced by P_{QLv} and P_{QRv} is zero.

The scalar of the moment produced by P_{QLu} and P_{QRu}, denoted $f(M_{QPu})$, is a function of the division of P_{Qu} between $\mathrm{P_L}$ and $\mathrm{P_R}$ and the inequality which bounds the measure is given by

$$-|P_{Qu}|hw \leq f(M_{QPu}) \leq |P_{Qu}|hw. \tag{4.61}$$

In addition to satisfying Equations 4.59 and 4.60 it is necessary that the moment effects of motion resistance are also balanced. No additional handle-forces are

required if there is a solution to

$$M_{QC} + P_{Qv}(0.5l + h + c) = f(M_{QPu}) \tag{4.62}$$

where the second term on the left hand side is required since moments are summed about P and $\mathrm{P}_{Qv}\hat{\boldsymbol{v}}$ was defined as acting at the COM and $(0.5l + h + c)$ is the COM to P dimension. Equation 4.62 will have a solution if $-|P_{Qu}|hw \leq M_{QC} + P_{Qv}(0.5l + h + c) \leq |P_{Qu}|hw$ and if so then a scalar measure of the handle-forces, denoted P_{QH1}, is given by

$$\begin{aligned} P_{QH1} &= |P_{Qu}| + |P_{Qv}| \\ &\quad \{-|P_{Qu}|hw \leq M_{QC} + P_{Qv}(0.5l + h + c) \leq |P_{Qu}|hw \ . \end{aligned} \tag{4.63}$$

P_{QH1} is therefore a measure of handle-forces for the restricted case when the forces required to balance the translational effects of motion resistance by handle-forces may also be used to balance the moment effects of those motion resistances.

In the general case there will be no solution to Equation 4.62 and additional handle-forces are necessary in order to balance the moment effects. For the motion resistance moment effects to be balanced it is necessary that there is a moment with a scalar measure, denoted M_{QPu2}, such that

$$\begin{aligned} M_{QPu2} = \mathrm{sgn}(M_{QC} + P_{Qv}(0.5l + h + c))|M_{QC} + P_{Qv}(0.5l + h + c)| - |P_{Qu}|hw \\ \{|M_{QC} + P_{Qv}(0.5l + h + c)| > |P_{Qu}|hw \end{aligned} \tag{4.64}$$

where M_{QPu2} is minimised, i.e. the largest magnitude moment possible is created from the available $\hat{\boldsymbol{u}}$ directed handle-force components.

The magnitude of one component of the handle-forces producing the moment $M_{QPu2}\hat{\boldsymbol{S}}$ is therefore

$$\frac{|M_{QC} + P_{Qv}(0.5l + h + c)| - |P_{Qu}|hw}{2hw}. \tag{4.65}$$

and it therefore follows that a measure of both components, the summed magnitude

of the two forces producing the force couple, denoted P_{QuCs}, is

$$P_{QuCs} = \frac{|M_{QC} + P_{Qv}(0.5l + h + c)|}{hw} - |P_{Qu}|. \tag{4.66}$$

A measure, denoted P_{QH} of the handle-forces necessary to balance motion resistance effects for the general case is therefore given by

$$P_{QH} = \begin{cases} |P_{Qv}| + |P_{Qu}| & |M_{QC} + P_{Qv}(0.5l + h + c)| \leq |P_{Qu}|hw \\ |P_{Qv}| + |M_{QC} + P_{Qv}(\frac{l}{2} + h + c)|hw^{-1} & |M_{QC} + P_{Qv}(0.5l + h + c)| > |P_{Qu}|hw \end{cases} \tag{4.67}$$

where cancellation removes P_{Qu} from the solution to the second condition.

If Equations 4.49 and 4.50 are substituted into the second term of the second condition of Equation 4.67 then (page 246) this term may be expressed as

$$|w(P_{Qu2} + P_{Qu3} - P_{Qu1} - P_{Qu4}) + (l+h)(P_{Qv1} + P_{Qv2}) + h(P_{Qv3} + P_{Qv4})|hw^{-1} \tag{4.68}$$

where $(\boldsymbol{P}_{Qi} \times \hat{\boldsymbol{u}}) \cdot \hat{\boldsymbol{S}} = a_{2i}P_{Qvi}$ and $(\boldsymbol{P}_{Qi} \times \hat{\boldsymbol{v}}) \cdot \hat{\boldsymbol{S}} = -a_{1i}P_{Qui}$. Equation 4.68 provides a direct appreciation of the motion resistance characteristics of the model-FCMV and the implications of the second condition are now considered. Firstly, with respect to vehicle-frame dimensions, it is to be noted that front caster assemblies, i=[1, 2], have a more substantial effect on the handle-force measure (P_{QH}) since the coefficient of the $\hat{\boldsymbol{v}}$ components in Equation 4.68 is $h+l$ where as the $\hat{\boldsymbol{v}}$ component coefficient for the rear caster assemblies, i=[3, 4], is h: $h = 100$ mm where as $h+l =$ 537 mm for the typical real-FCMV. In looser language, balancing the moment effect of the $\hat{\boldsymbol{v}}$ component of motion resistance of the front caster assemblies requires a larger handle-force measure compared with balancing the same effect from the rear caster assemblies since the former are further away from the operator. Secondly, again with respect to vehicle-frame dimensions, since the second term of the second condition for the handle-force measure (P_{QH}) is divided by the handle-width (hw), mechanically, no assumption is made about the biomechanical implications, larger handle-widths reduce the handle-force measure.

It is to be noted that Equation 4.67 does not produce a physical measure of handle-force, i.e. it is not the force magnitude at each handle which are summed. However, Equation 4.67 is useful since it makes the relationships considered in the

previous paragraph evident: a true handle-force measure is considered in the next section.

With regard to the kinematics, since the signs of the P_{Qui} and P_{Qvi} are related to the directions of the wheel angular velocities there are combinations of rot-roll directions which will tend to increase and combinations of rot-roll directions which tend to decrease the handle-force measure. For example, the P_{Qui} components of the second term of the second condition of Equation 4.67, as expressed in Equation 4.68, are the moment effect of the P_{Qui} components: they will sum when the sign of the left-side $\hat{\boldsymbol{u}}$ components, i= [1, 4] is opposite that of the right-side $\hat{\boldsymbol{u}}$ components, i= [2, 3]. Additionally, the magnitude of the second term of the second condition will be at a maximum magnitude if along with P_{Qui} components being at a maximum, the sign of that maximum magnitude is the same as that of the summation of the P_{Qvi} components.

An indication of the level of variation in the handle-force measure P_{QH} when driving the Zmodel-FCMV with different centres of zero velocities is conveyed by the multi-Figure 4.19 (page 101). There are four steps to the creation of Figure 4.19. Firstly for each of the three proportions of scrub friction to roll resistance (ρ_i) the $\frac{P_{Qu}}{|\boldsymbol{P}_{Qi}|}$, $\frac{P_{Qv}}{|\boldsymbol{P}_{Qi}|}$ and $\frac{M_{QC}}{|\boldsymbol{P}_{Qi}|}$ measures, as described in Equations 4.55–4.57 (page 94), are integrated piecewise with respect to θ_0 in accordance with Section 4.4.9 (page 85). Secondly, the average measure is determined by dividing the result by $\theta_{0n+1} - \theta_{0n}$. Thirdly, the P_{QH} measure is determined in accordance with Equation 4.67 (page 99). Fourthly, the P_{QH} measures for each of the thirteen manoeuvre r are expressed as a percentage of the manoeuvre r with the maximum P_{QH} for each of the $\theta_{0n+1} - \theta_{0n}$ integrations. It is these measure coordinates ($[\theta_0, P_{QH}\%]$) which are connected to provide the thirteen lines in Figure 4.19. It is assumed that $|\boldsymbol{P}_{Q1}| = |\boldsymbol{P}_{Q2}| = |\boldsymbol{P}_{Q3}| = |\boldsymbol{P}_{Q4}|$. In Figure 4.19 the legend (middle figure) is as follows: the nine regions r are indicated by thin lines: with red for the regions on the left (relatively large positive $\dot{x}_{Bv}$ component) of the $\dot{\boldsymbol{x}}_B$-plane, black for the regions in the middle (relatively small $|\dot{x}_{Bv}|$ component) of the $\dot{\boldsymbol{x}}_B$-plane and blue for the regions on the right (relatively large magnitude negative $\dot{x}_{Bv}$ component) of the $\dot{\boldsymbol{x}}_B$-plane. Reading from top to bottom the regions at the top (relatively large positive $\dot{x}_{Bu}$ component) of the $\dot{\boldsymbol{x}}_B$-plane are solid lines, regions

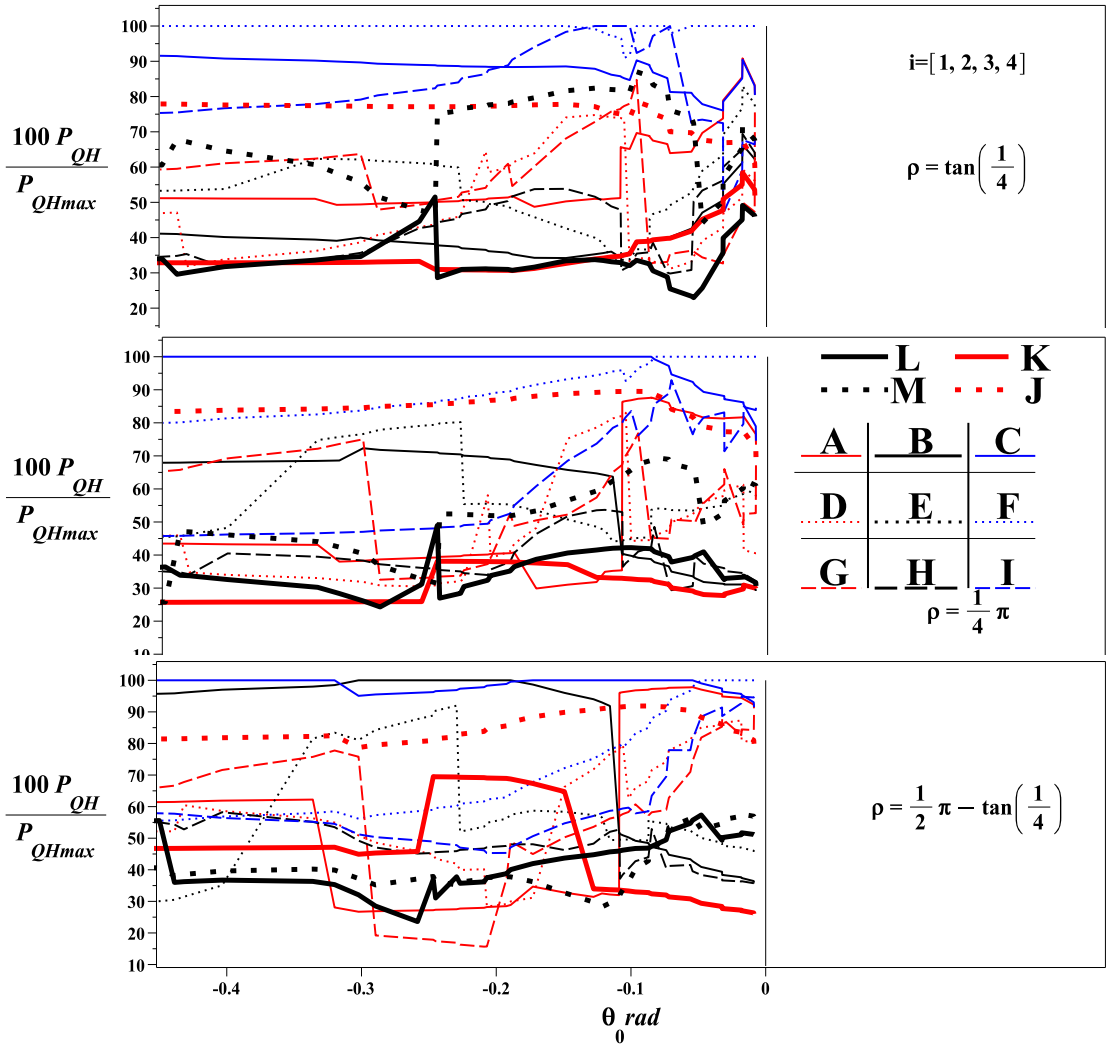

Figure 4.19 – Shows a legend (middle figure) as follows: the nine regions are indicated by thin lines: left-sided regions are red (relatively large $\dot{x}_{Bv}$), middle regions are black (relatively small $|\dot{x}_{Bv}|$) and right-sided regions are blue (relatively large $|\dot{x}_{Bv}|\{\dot{x}_{Bv} < 0)$. Reading from top to bottom, top-ward regions are solid lines (relatively large $\dot{x}_{Bu}$), middle regions are dotted lines (relatively small $|\dot{x}_{Bu}|$) and bottom regions are dashed (relatively large $|\dot{x}_{Bu}|\{\dot{x}_{Bu} < 0)$. The measures for r =[K,...,M] are indicated by thick solid lines for those relating to a front caster assembly in static equilibrium r =[K, L], thick dash lines for those relating to a rear caster assembly in static equilibrium r =[M, J] or alternatively with respect to left and right sides of the vehicle with black for the left side r =[L, M] and red for the right side r =[K, J]. The process is repeated with the three proportions of roll resistance to scrub friction: $\rho_i = [\tan\left(\frac{1}{4}\right)(top), \frac{\pi}{4}(middle), \frac{\pi}{2} - \tan\left(\frac{1}{4}\right)(bottom)]$. The graph lines show P_{QH} measures for each manoeuvre r as a percentage of the manoeuvre with the maximum P_{QH} measure as θ_0 changes for the Zmodel-FCMV. In loose terms this figure shows that the handle-forces vary considerably between manoeuvres irrespective of motion resistance or vehicle-frame orientation.

in the middle (relatively small $|\dot{x}_{Bu}|$ component) of the $\dot{\boldsymbol{x}}_B$-plane are dotted lines and regions in right (relatively large magnitude negative $\dot{x}_{Bv}$ component) of the $\dot{\boldsymbol{x}}_B$-plane. The measures for manoeuvres r= [K,. . . ,M] are indicated by thick solid lines for those with a front caster assembly in static equilibrium (r=[K, L]), thick dash lines for those with a rear caster assembly in static equilibrium (r=[J, M]) or alternatively with respect to left and right sides of the vehicle with black for the left side [L, M] and red for the right side [K, J]. The process is repeated with the three proportions of roll resistance to scrub friction: $\rho_i = [\tan\left(\frac{1}{4}\right), \frac{\pi}{4}, \frac{\pi}{2} - \tan\left(\frac{1}{4}\right)]$.

It is to be noted that value of Figure 4.19 is not that it permits any conclusions about the numerical values of the handle-force measure for different CoZV: the value is that it demonstrates that the Zmodel-FCMV displays substantial differences in handle-force measures which persist for various ρ_i values and θ_0 values. It is not the specific differences which are of interest but that differences exist and that they can be substantial, for example, for $\rho_i = \frac{\pi}{2} - \tan\left(\frac{1}{4}\right)$ (bottom figure) with the $\dot{\boldsymbol{x}}_B$ commencing in region F the measure is 100% at θ_{011} where as for the region K it is approximate 25%.

There are two separate elements which contribute to the variation in handle-force measures which is displayed in Figure 4.19. Firstly, varying proportions of motion resistance moment effects to translational effects occur for varying regions as detailed in respect of Figure 4.18 (page 95). Secondly, as indicated by the consideration of Equation 4.67, balancing the motion resistance effects at the handles also introduces effects which are distinct to the regions r. The graphic inspection method provides a direct visualisation of the way in which handle-force measures vary for varying manoeuvre r. Figure 4.20 (page 103) illustrates the $\boldsymbol{P}_{Qi}$ arrangement for three regions r=[F, D, B] at $\theta_0 = 0$ for $\rho_i = \frac{\pi}{2} - \tan\left(\frac{1}{4}\right)$: $\boldsymbol{P}_{Qi}$ are shown as white filled arrows and the components of $\boldsymbol{P}_{Qi}$ are shown as solid black arrows. While Figure 4.20 illustrates the arrangement for $\theta_0 = 0$ it is to be noted that the measures in Figure 4.19 are all integrations so even within the first stepwise integration the arrangement would be displaced from that shown. Nevertheless the displacements to the ${}^{B}\theta_{si}$ are relatively small and it is useful to treat the initial conditions as if they are continue through the first stepwise integration. It is to be noted that in all three sub-Figures in Figure 4.20 the $\boldsymbol{P}_{Qi}$ are displayed at the S_i

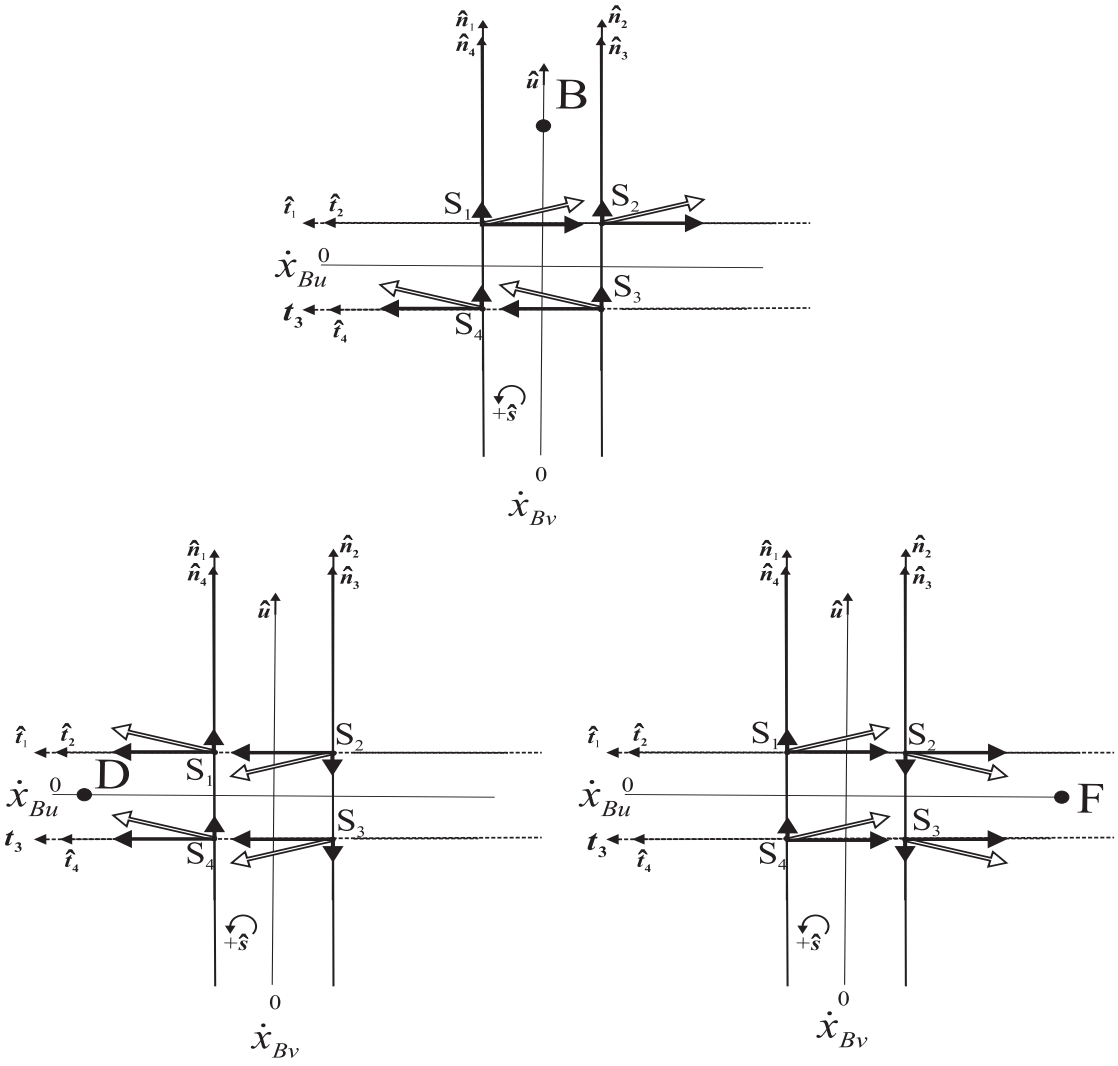

Figure 4.20 – Shows the $\boldsymbol{P}_{Qi}$ arrangement for three regions r=[F, D, B] at $\theta_0 = 0$ for $\rho_i = \frac{\pi}{2} - \tan\left(\frac{1}{4}\right)$: $\boldsymbol{P}_{Qi}$ are shown as white filled arrows and the components are shown as solid black arrows. The $\boldsymbol{P}_{Qi}$ are displayed at the S_i and not the O_i so the correct moment effect of the $\boldsymbol{P}_{Qi}$ can be seen directly. In loose terms this figure shows, using the graphic inspection method, why different manoeuvres have different proportions of translational motion resistance effect to motion resistance moment effect.

and not the O_i so the correct moment effect of the $\boldsymbol{P}_{Qi}$ can be seen.

Considering the manoeuvre B (top sub-Figure) it can be seen that the sum of the $\hat{\boldsymbol{v}}$ components will cancel where as for manoeuvre D (bottom-left sub-Figure) or manoeuvre F (bottom-right sub-Figure) they sum where as the reverse is the case for the $\hat{\boldsymbol{u}}$ components.

With regard to manoeuvre F and manoeuvre D in Figure 4.20 it is useful to consider these together. It can be seen from Figure 4.20 that the P_{Qui} components sum to zero and that the P_{Qvi} sum in both cases to a relatively large magnitude

compared with manoeuvre B. It follows that with a zero P_{Qu} the second condition of Equation 4.67 applies. It is also evident that sgn(P_{Qv})= 1 for manoeuvre D where as sgn(P_{Qv})= -1 for manoeuvre F. It can also be seen that for both manoeuvre F and manoeuvre D the moment effect of the P_{Qui} components is negative (clockwise). Thus the manoeuvre F and manoeuvre D are examples of the two states described in the consideration of Equation 4.68, i.e. the P_{Qui} components and the P_{Qvi} components are so signed in the case of manoeuvre F that the magnitude of the second term is maximised where as cancellation occurs with manoeuvre D. In loose terms handle-forces are maximised if translational displacement is towards $-\hat{\boldsymbol{v}}$ when $\dot{\theta}_0 < 0$ (right and clockwise respectively with respect to Figure 4.20). While this description, in loose form or as the mathematical description which it articulates, is strictly a motion resistance effect there is a straightforward analogy with inertial effects: a lateral force at the handles to the right by the operator tends to produce an anticlockwise moment so if a clockwise moment is required, additional forces must be applied.

It is evident from Figure 4.19 that the magnitude ordering of the handle-forces for the different manoeuvre r vary across ρ_i and θ_0. Nevertheless, disregarding the thick lines which relate to r=[J, K, L, M], certain features can be noted with respect to $\theta_0 > -0.1$ rad. The majority of blue lines, r=[C, F, I], have larger measures in the sub-Figures. The majority of red, r=[A, D, G], and black lines, r=[B, E, H], have either smaller or median measures in the sub-Figures. It is also evident that the black lines, r=[B, E, H], all indicate smaller initial handle-force measures as ρ_i increases, i.e. as scrub friction becomes the more dominant motion resistance effect. With respect to the thick lines it is also noteworthy that initially manoeuvres r=[J, M], related to rear caster assemblies, always incur a higher handle-force measure than those related to front caster assemblies, r=[K, L] and that the latter frequently have small measure and never a large measure. The latter observation is consistent with the note that has already been made regarding the greater effect of the front casters assemblies: with manoeuvres [K, L] one of the front caster assemblies is in static equilibrium.

All of the consideration of handle-force measures has assumed that $|\boldsymbol{P}_{Q1}| = |\boldsymbol{P}_{Q2}| = |\boldsymbol{P}_{Q3}| = |\boldsymbol{P}_{Q4}|$ so it useful to consider if the variation in handle-force

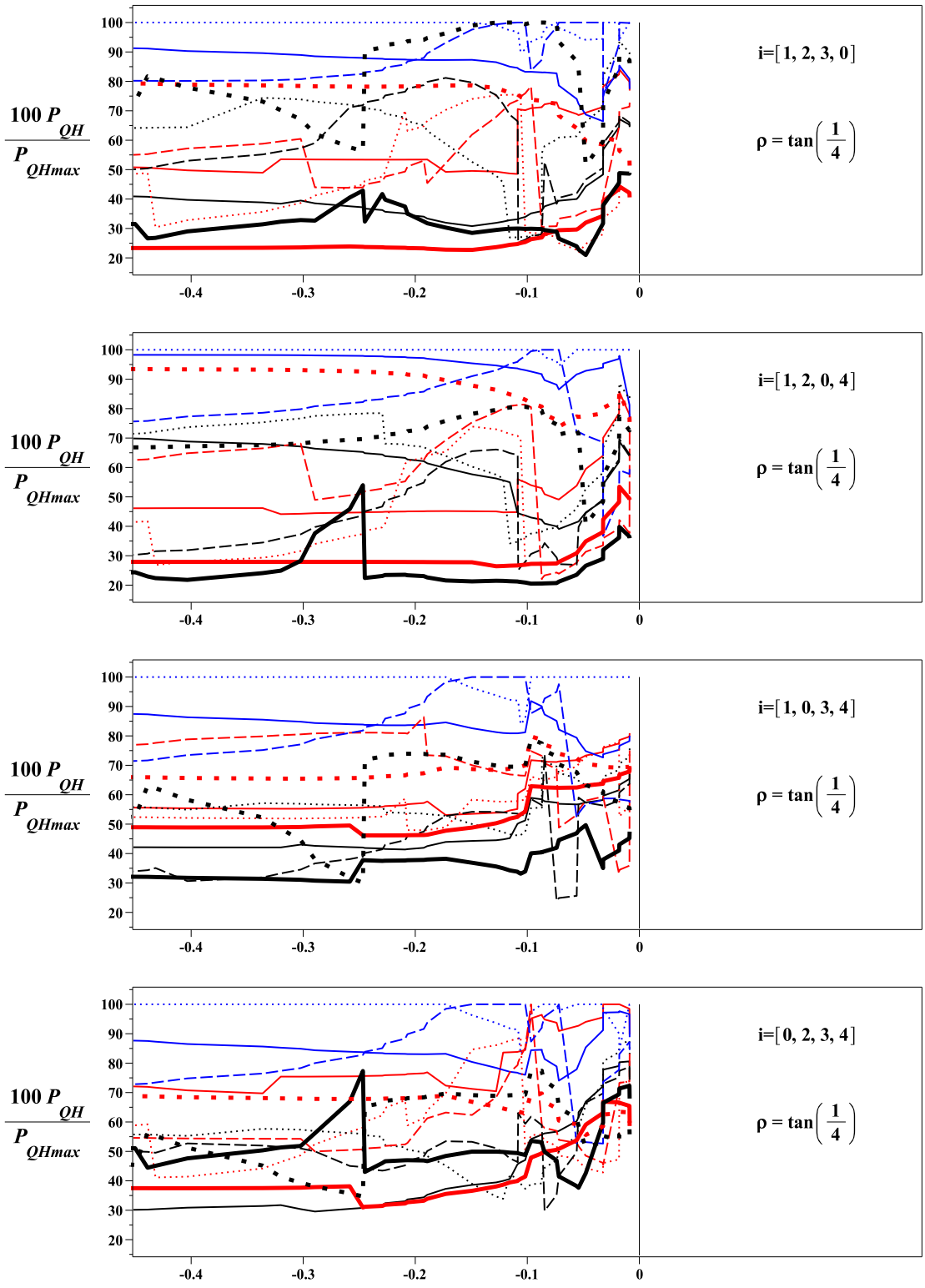

Figure 4.21 – Shows the results for P_{QH} for all manoeuvres r (line legend as per Figure 4.19 page 101) when a single caster assembly is unloaded: the relevant caster assembly is indicated by a zero in the legend and the results are all for $\rho_i = \tan\left(\frac{1}{4}\right)$.

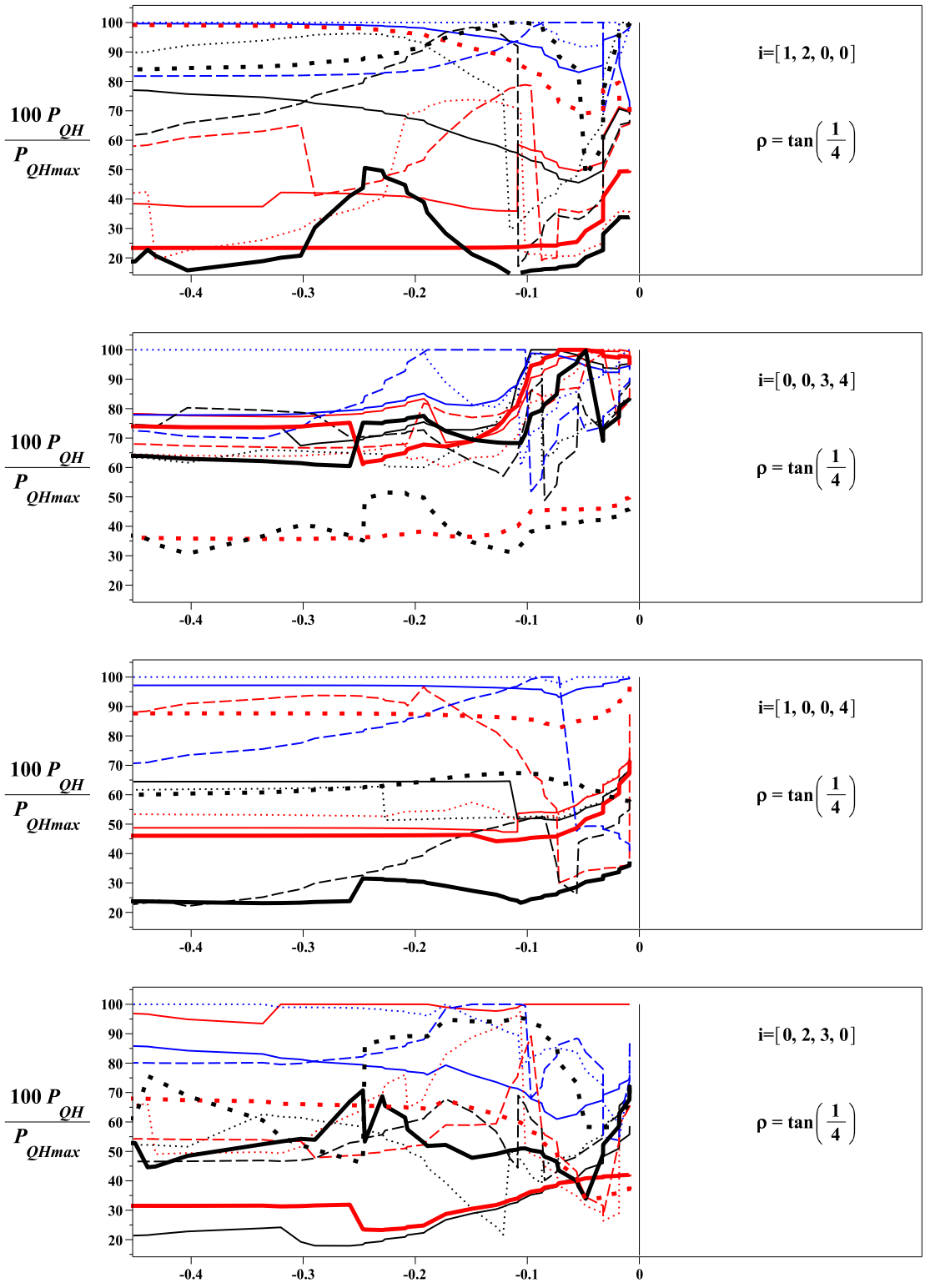

Figure 4.22 – Shows the results for P_{QH} for all manoeuvres r (line legend as per Figure 4.19 page 101) when two caster assemblies are unloaded: the relevant caster assemblies are indicated by a zero in the legend and the results are all for $\rho_i = \tan\left(\frac{1}{4}\right)$.

measure is maintained when this is not the case. Figures 4.21–4.22 (page 105) repeat the process which was used to create Figure 4.19 but in each case different combinations of $\boldsymbol{P}_{Qi}$ are set to zero which would be the case if the individual caster assembly loading was negligible. Figure 4.21 shows the results when a single caster assembly is unloaded: the relevant caster assembly is indicated by a zero in the legend and the results are all for $\rho_i = \tan\left(\frac{1}{4}\right)$. It can be seen that variations in the handle-force measure persist. Figure 4.22 shows the results when one side of the vehicle-frame is unloaded: the relevant caster assemblies are indicated by a zero in the legend and the results are all for $\rho_i = \tan\left(\frac{1}{4}\right)$. It can be seen that handle-force measure variations persist.

4.6.1. *Minimum handle-forces*

A final examination of the persistence of handle-force measure variation for manoeuvre r is to consider the effects when a minimum handle-force measure is calculated. The approach used to determine the handle-force measure P_{QH} has allowed a qualitative appreciation of the relationship between motion resistances and their balancing from the handles: this method does not provide the minimum measure. The following process is used to determine a minimum handle-force measure denoted P_{QHmin} where

$$P_{QHmin} = f_{min}\left(\sqrt{P_{QLu}^2 + P_{QLv}^2} + \sqrt{P_{QRu}^2 + P_{QRv}^2}\right) \tag{4.69}$$

where $f_{min}()$ is a minimisation function. Therefore, P_{QHmin} determines the minimum summation of the magnitudes of the left and right handle force. Equation 4.69 comprises of four unknowns and there are two translational equations of motion (Equations 4.59-4.60 page 97) and T_Q may be related to the handle-forces as

$$T_Q = (P_{QRu} - P_{QLu})\, hw - P_{QLv}\left(\frac{l}{2} + c + h_{\mathrm{L}}\right) - P_{QRv}\left(\frac{l}{2} + c + h_{\mathrm{R}}\right) \tag{4.70}$$

where h_{R} and h_{L} are respectively the h measures for right and left handles as shown in Figure 4.1 (page 58).

The minimisation is achieved as follows: Equations 4.59, 4.60 and 4.70 provide solutions for P_{QRv}, P_{QRu} and P_{QLv} when P_{QLu} is treated as a parameter

and this gives

$$P_{QRv} = \frac{(2P_{QLu} - P_{Qu})hw + T_Q}{h_\mathrm{L} - h_\mathrm{R}} + \frac{(l + 2c + 2h_\mathrm{L})P_{Qv}}{2(h_\mathrm{L} - h_\mathrm{R})} \{h_\mathrm{L} - h_\mathrm{R} \neq 0 \quad (4.71)$$

$$P_{QLv} = \frac{(2P_{QLu} - P_{Qu})hw + T_Q}{h_\mathrm{L} - h_\mathrm{R}} - \frac{(l + 2c + 2h_\mathrm{R})P_{Qv}}{2(h_\mathrm{L} - h_\mathrm{R})} \{h_\mathrm{L} - h_\mathrm{R} \neq 0 \quad (4.72)$$

and

$$P_{QRu} = P_{Qu} - P_{QLu} \quad (4.73)$$

Equations 4.71–4.73 when substituted into the minimisation function Equation 4.69 and differentiated with respect to P_{QLu} and equated to zero, allow solution for P_{QLu}. P_{QLu} may then be substituted into Equations 4.71–4.73 and finally these can be can be substituted into Equation 4.69 to provide a function in terms of T_{Qc}, P_{Qv} and P_{Qu}. The results relating to Figure 4.19 (page 101) (bottom) are then used to provide a $\frac{100P_{QHmin}}{P_{QHminmax}}$ against θ_0 for each region and these are shown for $\rho_i = \frac{\pi}{2} - \tan\left(\frac{1}{4}\right)$ and the resulting graph is shown in Figure 4.23 (page 109). The particular locations of the P_{QHmin} for each manoeuvre r in Figure 4.23 are not of importance; the important feature is that differences between handle-force measures persist when the handle-force measure is minimised.

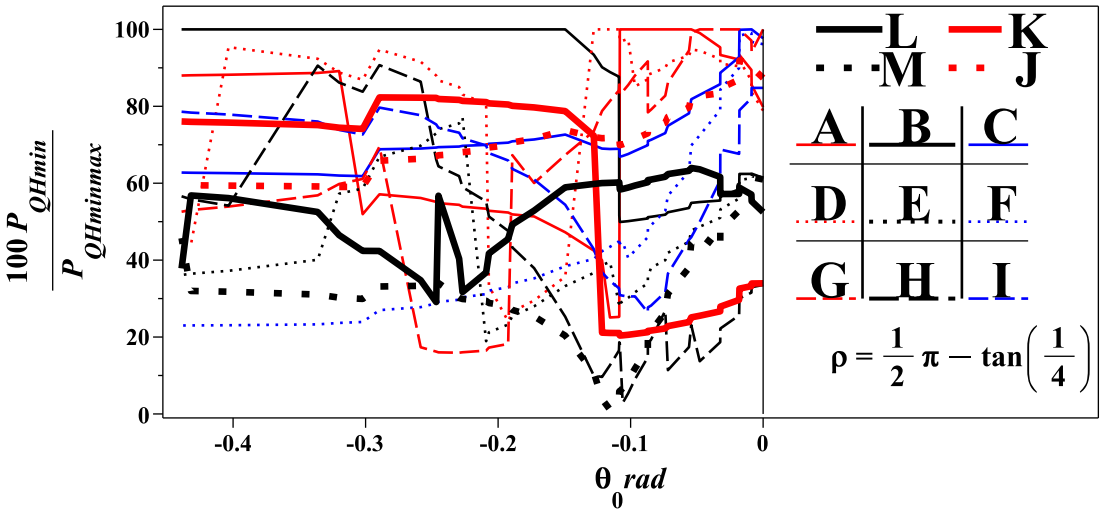

Figure 4.23 – Shows, with legend details as per Figure 4.19 (page 101) and proportion of roll resistance to scrub friction given by $\rho_i = \frac{\pi}{2} - \tan\left(\frac{1}{4}\right)$: the graph lines for P_{QHmin} measures for each manoeuvre r as a percentage of the manoeuvre with the maximum P_{QHmin} measure as θ_0 changes for the Zmodel-FCMV. In loose terms this figure demonstrates that the handle-forces vary between manoeuvres even if the handle-forces are calculated as true measures, i.e. the sum of the two handle force magnitudes.

4.7. **Handle-force Measure Conclusion**

This chapter provides a theoretical account of model-FCMV dynamics which leads to an empirical investigative method: a finite and representative subset of the set of real-FCMV experimental possibilities has been identified for the initial configuration ${}^{B}\theta_{si} \approx 0$, namely those with a CoZV at Z_r, i.e. manoeuvre r. The Zmodel-FCMV demonstrates that the handle-force measure for different manoeuvre r can vary substantially. These substantial differences arise from two distinct processes. Firstly, motion resistance has two effects: 1) the translational motion resistance effect and 2) the moment produced as the motion resistance effect at each caster stem acts on the vehicle frame. Different manoeuvre r require different proportions of torque to force to balance these motion resistance effects. Secondly, producing the equivalent balancing effect by handle-forces can amplify those differences. These differences persist for varying proportions of roll resistance to scrub friction, varying load distributions on the caster assemblies, whether the handle-force measure is minimised or not and as the vehicle-frame orientation changes.

Each manoeuvre r therefore has a space requirement (the displacement space) and an associated handle-force measure. It is a mere tautology to say that different Z_r have different space requirements; however, these different space requirements are associated with substantial handle-force measure variation. This effect on the handle-forces has not been previously noted and at impending motion may be generalised to any initial ${}^{B}\theta_{si}$ (Abraham and Johnson, 2010). In other words, the Zmodel-FCMV displays a forces-applied and space-required relationship which may be important for adaptation planning.

No empirical data has been incorporated into the Zmodel-FCMV: empirical values for the roll resistance to scrub friction proportion are absent and the individual caster assembly loadings which arise from a real-FCMV and the consequential effect on the magnitude of motion resistance acting at individual caster assembly are not incorporated. Therefore, the Zmodel-FCMV does not predict the handle-force measures for different manoeuvre r; the value is that it predicts the occurrence of substantial differences.

As the importance of the start-up period has already been noted in the Literature Chapter, it is noteworthy that Figures 4.19, 4.21 and 4.22 (pages 101, 105 and 106 respectively) indicate that at initial motion, manoeuvres r = [B, E, H, K, L] frequently have a smaller handle-force measure than other manoeuvres and manoeuvres r = [C, F, I, J, M] frequently have a larger handle-force measure than the other manoeuvres. However, these results still do not have a predictive value since *any* empirically based ranking of handle-force measures would conform to the theory if substantial differences are present; the absence of substantial differences would demonstrate that the dynamical effects that have been identified are not of first-order importance.

If the theoretical differences exist empirically then for different manoeuvres r the operator is required to apply different handle-forces. If the operator is required to select a maximum load for each of these manoeuvres then the load selected is the operator load response to the different handle-forces requirements. The definition of 'maximum' would not be important though maintaining the same 'maximum' for all manoeuvres would be.

The findings of this chapter are based on two primary assumptions: 1) no relative velocity occurs between G_i and ground-plane and 2) the first-order effects of motion resistance may be represented by caster orientation, caster global rotation directions and wheel roll directions. The empirical results will demonstrate that these assumptions are justified.

Chapter 5–Methods

5.1. **Introduction**

It is the contention of this thesis that the forces-applied and space-required relationship for real-FCMV is such that it has a substantial impact on adaptation planning. The dynamic analysis predicted substantial variation in the defined handle-force measure for different manoeuvres r. While substantial handle-force variation is predicted it is conceivable that the effect on the human operator is not important: even if statistical differences exist these may not impact on adaptation planning. One approach to investigating the effect on adaptation planning is to make load, the load carried by the real-FCMV, a dependent variable: to allow the operator to select a maximum comfortable load for the manoeuvres r. It follows that if relatively low or relatively high loads are associated with different manoeuvres r and an adaptation plan only permitted manoeuvres associated with, for example, relatively low loads then the different handle-force requirements are important for adaptation planning.

This chapter details the implementation of an experimental method based on the Zmodel-FCMV: handle-forces for different manoeuvres r are measured. This is described in four sections. The first section details the initial considerations: the options and reasons for the choices which were made. The second section gives detailed descriptions of the materials used. The third section describes the data collection process. Finally, the fourth section summarises the post processing which was required to produce a concise and useful account of data collected. Secondary details of materials are included on an accompanying computer disc indicated by '(DISC)'.

5.2. **Experimental Considerations**

5.2.1. *Synopsis of the experiment*

Full details of the experimental method follow but a synopsis and illustration provides useful context before giving more detailed examination. Figure 5.1 shows the experimental set-up.

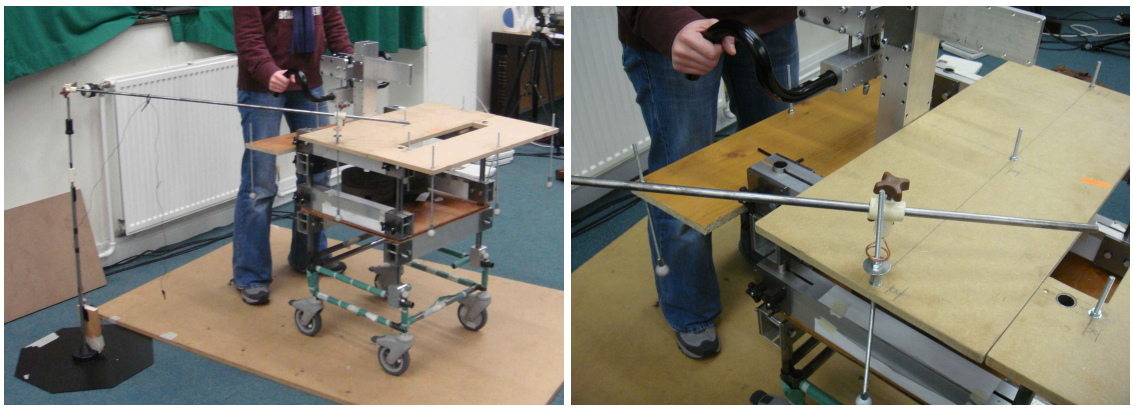

Figure 5.1 – Shows (left) the general arrangement with a modified real-FCMV and a static guide-ring supported by a horizontal and vertical rod terminating in a floor stand (octagonal black base) and (right) a close up showing the experimental-FCMV–fixed rod in the copper guide-ring.

Threaded rods were fixed to the experimental-FCMV at locations corresponding to eleven (explanation to follow) of the thirteen manoeuvre r and a floor stand terminating in a guide-ring was so placed that the experimental-FCMV–fixed rod was in the centre of the guide-ring. The subject changed the vehicle-frame orientation by approximately 0.5π rad while attempting to keep the rod in the guide-ring centre: the experimental-FCMV was loaded with the subject's maximum comfortable load for the manoeuvre r (attempted): the appendage '(attempted)' is necessary since operators were not, unlike the Zmodel-FCMV, subject to a kinematics constraint and thus the CoZV would not necessarily be a fixed point. This was repeated for a maximum of eleven of the thirteen manoeuvres r.

5.2.2. *Psychophysical method, subject selection and participation*

The investigative approach was to make subject load selection the dependant variable of manoeuvres r (attempted). This approach therefore makes use of the psychophysical method. Chaffin et al. (2006) describe the psychophysical method as a "Simulation of a task of interest...[where subjects] adjust the load...until they subjectively believe...[it is the] maximum acceptable" and judge this to be

the most accurate method of strength testing available. Matheson, L. and Mooney, V. Caiozzo, V. and Jarvis, G. Pottinger, J. DeBerry, C. Backlund, K. Klein, K. Antoni, J. (1992) is of the view that the psychophysical method requires "extensive cooperation and motivation" by the subjects. The need for "extensive cooperation" is also heightened by the fact that pilot trials indicated that it would take several hours to carry out measurement of all thirteen manoeuvres r (attempted). It was considered reasonable to assume that the highest motivation would be found in those for whom the findings of the study are directly relevant: those who are connected with adaptation planning, the provision of real-FCMV, or manual handling aspects of real-FCMV. Subjects were therefore recruited from these groups of people. A presentation was made to subjects setting the scene, indicating what the experiment involved and the benefits.

5.2.3. *Ethics*

As only healthy consenting adult subjects would be involved the institutional requirement was (January 2010) that the head of school approved (DISC) the investigation. The choice of subject selection also strengthened the ethical nature of the investigation since the subject selection was of subjects who would minimise personal risks: the subjects were all aware of manual handling risks and received work training or had qualifications which related to assessing manual handling risks. Thus any tendency to select a load which might cause injury would go against manual handling principles with which the subjects would be familiar.

5.2.4. *Sample size*

A pilot study indicated that both handle-forces and load selections varied substantially for some manoeuvres r (attempted) so statistical determination of subject numbers was not considered necessary; subject numbers were determined by a combination of time available to conduct the investigation and the availability of subjects willing to contribute several hours for participation. Nineteen people were identified as potential subjects: these people were in professional contact with the author (occupational therapy context).

5.2.5. *Subject participation and motivation*

As the pilot study indicated that each subject would have to spend approximately four to six hours to complete the data collection it was necessary to consider reducing the participation time in order to minimise the threat to either initial participation or completion. Consideration was therefore given to reducing the number of manoeuvres r (attempted).

Two options existed: either some manoeuvres could have been removed or subjects could have carried out a subset of the thirteen manoeuvres. A practical distinction between the manoeuvres r = [J,...,M] and the other manoeuvres r was relevant. With manoeuvres r = [J,...,M] the maintenance of the relevant CoZV was directly observable: a caster assembly remains in static equilibrium. These four manoeuvres were therefore recognised to have a potential training value. Since the pilot study indicated that manoeuvres r = [K, L] (attempted) were associated with relatively high load selections and trials indicated that manoeuvres r = [J, M] (attempted) were associated with relatively low load selections the latter manoeuvres were considered to be of less interest training-wise: the pilot study indicated that relatively low load selections were represented by a number of the other manoeuvres r (attempted). Manoeuvres r = [J, M] were therefore excluded from the experimentation in order to reduce the time duration of the data capture and henceforth references to manoeuvres r (attempted) is a reference to the eleven manoeuvres r = [A,...,L].

Subjects were assumed to be motivated because the findings were relevant to their work role. Consideration was therefore given to the experimental-FCMV and the extent to which it should be similar to the real-FCMV with which subjects were familiar. It was therefore concluded that however unfamiliar the experimental-FCMV might look, as required by instrumentation, it would be valuable to reinforce motivation by being able to state that the vehicle-frame and caster assemblies were as supplied by a typical shower chair manufacturer. A modification to a standard real-FCMV shower chair base was therefore commissioned: see page 119 for modification details.

The location of the trials was also considered to be pertinent since in addition to the data collection time, travel-time would need to be added. It was therefore

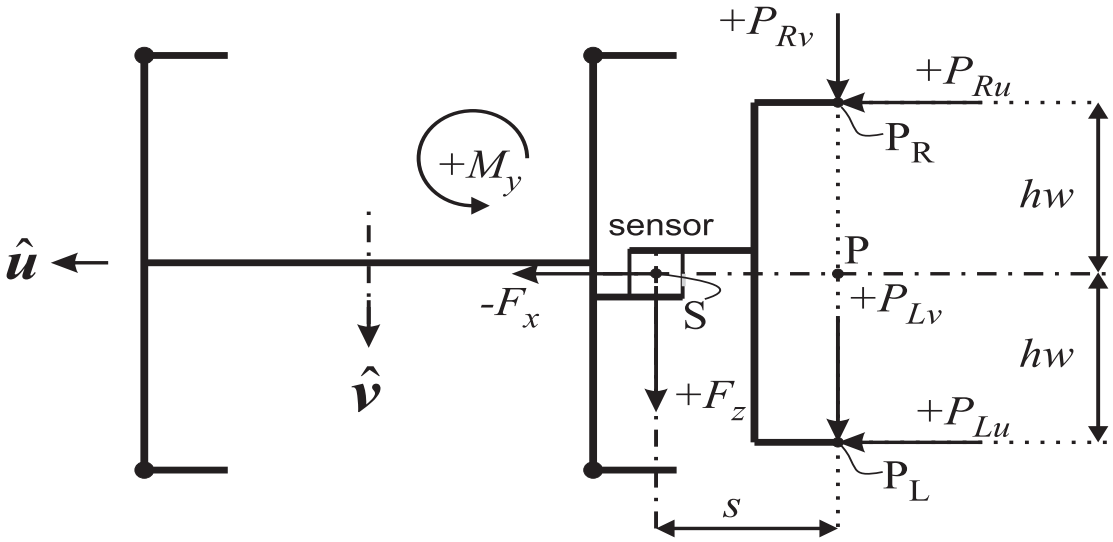

Figure 5.2 – Shows a diagrammatic representation of the experimental-FCMV with sensor and handles, and force and moment measures, and dimension labelling: $\hat{\boldsymbol{S}}$ and $\hat{\boldsymbol{s}}$ comes out of the page.

advantageous to carry out the trials at the place of work of the majority of the subjects and to gain approval for the subjects to participate in work time. The director of Newcastle Adult Services approved (DISC) the use of the Shieldfield Centre (Newcastle upon Tyne) which was a relevant work place site with rooms of suitable size and the relevant manager authorised work time participation for those subjects who did not have the authority to self-authorise this. A practical consequence was that substantial additional time input was required for the experimental set-up at start of day and removal at end of day.

5.3. **Materials**

5.3.1. *Using a single sensor*

This section details the theory underlying the method by which a single sensor was used to determine three components of handle-forces. Assuming that the torques, as defined (page 56), that an operator can apply at a single handle are negligible it follows that any tendency which the vehicle-frame has to rotate about the $\hat{\boldsymbol{S}}$ direction are the result of moment producing handle-forces. While the handle-force at each handle could be sensed individually a useful alternative is possible with a single sensor. The underlying theory for a single sensor alternative follows.

Figure 5.2 provides an illustration of the physical layout indicated by the text following. It is assumed that the sensor can be so fixed to an experimental

vehicle that the three sensor axes are parallel to an orthonormal triad (uvs) with unit vectors $\hat{\boldsymbol{v}}$, $\hat{\boldsymbol{u}}$ and $\hat{\boldsymbol{s}}$ attached to the vehicle-frame so that $\hat{\boldsymbol{u}}$ is in the sagittal plane as previously defined in the Dynamics Chapter. Where $-F_x$ is the scalar measure of the sensor force measure in the $\hat{\boldsymbol{u}}$ direction, F_z is the scalar measure of the sensor force measure in the $\hat{\boldsymbol{v}}$ direction and M_y is the scalar measure of the sensor moment about the $\hat{\boldsymbol{s}}$ direction the following process was used to determine handle-forces in three components. Where P_{Lu} is the scalar measure of the $\hat{\boldsymbol{u}}$ component handle-force on the left handle and where P_{Ru} is the scalar measure of the $\hat{\boldsymbol{u}}$ component handle-force on the right handle then

$$P_{Lu} + P_{Ru} = -F_x. \tag{5.1}$$

Where P_{Lv} is the the scalar measure of the $\hat{\boldsymbol{v}}$ component handle-force on the left handle and where P_{Rv} is the scalar measure of the $\hat{\boldsymbol{v}}$ component handle-force on the right handle then

$$P_{Lv} + P_{Rv} = F_z. \tag{5.2}$$

Where s_L is the dimension magnitude between the application point of P_{Lv} and the sensor and s_R is the dimension magnitude between the application point of P_{Rv} and the sensor, both in the $\hat{\boldsymbol{u}}$ direction axis, and where $s = s_L = s_R$ and where $2hw$ is the dimension magnitude between the application points of P_{Lu} and P_{Ru} in the $\hat{\boldsymbol{v}}$ direction axis then M_y may be expressed in terms of the handle-force components as

$$M_y = -\left(P_{Lv} + P_{Rv}\right) s + \left(P_{Ru} - P_{Lu}\right) hw \tag{5.3}$$

and it follows that from Equation 5.2

$$M_y + F_z s = \left(P_{Ru} - P_{Lu}\right) hw \tag{5.4}$$

It also follows from Equations 5.4 and 5.1 that if

$$|F_x| hw < |M_y + F_z s| \tag{5.5}$$

then even if a force with magnitude $|F_x|$ is applied to whichever handle produces

the necessary moment direction (setting $P_{Lu} = 0$ or $P_{Ru} = 0$) it will be insufficient to balance Equation 5.4. It follows that if Equation 5.5 holds then $\text{sgn}(P_{Lu}) \neq \text{sgn}(P_{Ru})$ in other words the $\hat{\boldsymbol{u}}$ directed handle-force components must, in addition to producing a moment as a consequence of balancing F_x, also produce a couple, denoted M_{uCs}, such that

$$|M_{uCs}| = ||M_y + F_z s| - |F_x| hw| \tag{5.6}$$

on the assumption that $|F_x|$ is assigned to whichever handle minimises $|M_{uCs}|$. In other words it is necessary for $\hat{\boldsymbol{u}}$ directed handle forces to produce a couple with the sign given by

$$\text{sgn}(M_{uCs}) = \text{sgn}\left(M_y + F_z s\right) \tag{5.7}$$

as indicated by Equation 5.4. Given Equation 5.1 and the stipulation that each handle is subject to a single force it follows that

$$\begin{aligned} M_{uCs} &= \left(P_{Lu} - (-F_x)\right) 2hw \ \{ \quad \text{if } \text{sgn}(F_x) = \text{sgn}(M_{uCs}) \\ \Rightarrow P_{Ru} &= -\left(P_{Lu} - (-F_x)\right) \end{aligned} \tag{5.8}$$

or

$$\begin{aligned} M_{uCs} &= \left(P_{Ru} - (-F_x)\right) 2hw \ \{ \quad \text{if } \text{sgn}(F_x) \neq \text{sgn}(M_{uCs}) \\ \Rightarrow P_{Lu} &= -\left(P_{Ru} - (-F_x)\right) \end{aligned} \tag{5.9}$$

where the implications of these two Equations arise since M_{uCs} is a couple and the P_{Lu} or P_{Ru} component with the largest magnitude is already determined. It is then possible to define a force measure of the force components which produce M_{uCs}, denoted P_{uCs}, as follows

$$P_{uCs} = M_{uCs} hw^{-1} \tag{5.10}$$

and the units for P_{uCs} are therefore measures of force and not force distance.

The alternative condition to inequality Equation 5.5 is

$$|F_x| hw \geq |M_y - F_z s| \tag{5.11}$$

and for such a condition $M_{uCs} = P_{uCs} = 0$: physically (F_x) is apportioned to P_{Lu} and P_{Ru} such that Equation 5.4 balances. The transformation of sensor measures in this case produces an integer zero.

(Figure A.5 page 248 for diagrammatic explanation and demonstration of uniqueness of solutions for P_{uCs}).

A limitation of a single sensor is that the decomposition of the F_z measure into $\hat{\boldsymbol{v}}$ handle-force components is not possible since $\text{sgn}(P_{Lv}) = \text{sgn}(P_{Rv})$ is not necessarily true.

5.3.2. *Force and moment measurement*

The AMTI MC3-A-6-500 Force/Torque sensor was chosen to record force data (DISC). The maximum moment range capacity for the three axes was ±56 Nm and the maximum force range capacity for the three axes was ±2200 N. The pilot study confirmed that these capacities were suitable. This sensor is supplied precalibrated. Amplification was provided by the AMTI MSA-6 MiniAmp (DISC). The serial output was utilised and this was inputted into a desktop PC (DISC): thus a real time system was not used and an approximate sampling rate of 50 Hz resulted. A custom LabVIEW application was commissioned (DISC) to manage recording, file saving, provide visual output and to adjust for amplifier gain and excitability settings. An Excel file was written to calculate settings for gain and excitability settings (DISC). This software saved the sensor data as a .dat file comprising of seven data columns: the three handle-force measures (N), the three moment measures (lb inches) and a time stamp provided by the desktop PC operating system. A final feature of this software was the provision of an on-off output signal to the parallel port: this was for the purposes of synchronisation and this is detailed in a later section.

5.3.3. *Experimental vehicle system*

The experimental set-up comprised of six components. The first component is a real-FCMV. This was a special size, lower seat base than standard, and unpainted but otherwise standard shower chair supplied by Westholme Ltd: it consisted of a vehicle-frame made of mild steel tubing (approximately 1" diameter) and four caster assemblies fixed to the vehicle-frame by Allen screws. The instrumented real-

FCMV, the experimental-FCMV, can be seen in Figure 5.3 (page 121): apart from the back rest tubes the real-FCMV parts are those between ground and the second horizontal tubes. The caster assemblies shown in Figure 5.3 were replaced with Steinberg full-lock types with double ball bearing swivel, plain bearing wheel with polypropylene hub, steel bush, 125mm diameter caster wheel, and thermoplastic rubber tyre (DISC): these were typical shower chair caster assemblies at the time of the investigation again supplied by Westholme Ltd. This caster assembly is shown in Figure 5.5 (page 122).

The second component related to the sensor instrumentation and the key elements were, as visible in Figure 5.3, extension tubes clamped to the real-FCMV and stiffened with aluminium box sections, an upright box section to provide optional handle heights, a horizontal mounting plate to provide optional positions from front to back and fixing for a sensor, a sensor to handle assembly and propriety bicycle handles (DISC): this mechanism was commissioned along with fixing to the real-FCMV. The mass of the unloaded experimental-FCMV with instrumentation was approximately 35 kg.

The handle mounting also allowed the opportunity to decouple some handle-force moments by use of a Hooke's joint though this was not used in the investigation: these extra handle DOF were removed by bolts as shown in Figure 5.4 (page 122).

The third component provided a visual means of indicating to an operator that the manoeuvre was a manoeuvre r (attempted). Wooden panels were bolted to the upper box sections at rear, middle and front (DISC). These provided a surface on which to bolt threaded rods (6 mm external diameter) and these were located in accordance with the details shown in Figure 4.6 (page 69). The implementation is shown in Figure 5.1 (page 113). The locations were determined by eye using rulers, set-squares and callipers, so the positions were approximate: r = [C, F, I] to the rear, r = [B, E, H] to the middle section and r = [A, D, G, K, L] to the front. For r=B the threaded rod could be screwed in place by hand as this rod could impede the horizontal arm of the floor stand which is described next. The middle section of the wooden panels was removable in order permit a more convenient access for adding load.

Figure 5.3 – Shows the experimental-FCMV: a modified real-FCMV comprising of a non-standard low-height vehicle-frame and caster assemblies with the addition of height-extension tubing, stiffening boxing, plywood load bearing section, handle-force sensor mounting and sensor.

The fourth component was a floor stand (DISC): it comprised of a base, vertical rod, horizontal rod which was free to rotated about the vertical axis and terminated in an approximately circular winding of copper producing a guide-ring (approximately 20 mm diameter) as can be seen in Figure 5.1 (page 113). The guide-ring could be locked at any position on the horizontal arm and the horizontal arm could be height adjusted: there was no lock to prevent the horizontal arm and guide-ring rotating about the vertical component of the stand. Thus by adjusting the height of the horizontal arm, the guide-ring location on the horizontal arm and the orientation of the arm about the vertical axis, the stand could be placed with the rod in the guide-ring centre without impeding the vehicle-frame when a change

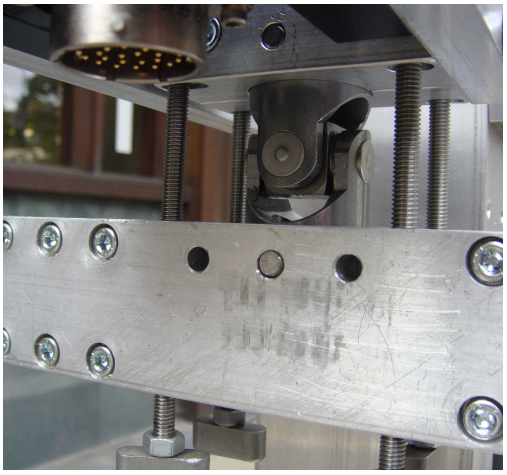

Figure 5.4 – Shows the Hooke's joint option for decoupling two moment effects.

Figure 5.5 – Shows the experimental-FCMV caster assembly

of vehicle-frame orientation occurred. If the operator changed the vehicle-frame orientation while keeping the rod in the guide-ring centre the relevant manoeuvre r (attempted) was achieved.

The fifth component is the floor and this is shown in Figure 5.1 (page 113). A medium density fibre (MDF) board was used as it was readily available, low cost, easily replaced if damaged and enabled pencil marking. It was considered to be reasonable to accept that a $\frac{5}{8}$ inch thickness MDF laid on undamaged, debris free floors of buildings constructed within 60 years would be sufficiently level without the need for measurement. While the experimental-FCMV was manoeuvred on a single MDF board additional boards were available, where required, to allow the subject to step off the manoeuvring board onto a surface of the same height. Also, where the experimental-FCMV might appear as if it could be manoeuvred off the board, additional boards were added to provide assurance to the operator. The manoeuvring board was marked with the approximate starting position which maintained the experimental-FCMV on the board for the manoeuvre r (attempted).

The sixth component were disc-weights which were nominally 4.55kg or 3.22kg. In order to protect the experimental-FCMV from damage the maximum load was set at 170kg. The weights were positioned symmetrically on the plywood at the rearmost vehicle-frame position: when the maximum number of disc-weights

permitted by the middle wood-top section had been reached, they were located on the top of the middle wood-top section directly above the weights below and again symmetrically. The were positioned to produce an approximate load distribution of 60% to the rear and 40% to the front as indicated by a force plate trial (results not presented).

5.3.4. *Determining manoeuvre r success*

Trials indicated a more complex motion resistance effect at the transition from static equilibrium to dynamics than can be represented by the Coulomb based Zmodel-FCMV. Three effects were observable while handle-forces below some maximum were applied. Firstly, relatively large, compared with the other displacements, $\Delta^B\theta_{si}$ occurred. Secondly, relatively small, compared with $\Delta^B\theta_{si}$, $\Delta\theta_{ti}$ and $\Delta\theta_0$ occurred. Thirdly, during these phenomenon the rod could be displaced from the guide-ring centre. On removal of these handle-forces the experimental-FCMV returned towards but did not entirely restore the initial configuration. There was therefore sufficient elasticity in the system for handle-forces which produced negligible permanent $\Delta\theta_0$ to displace the rod while the handle-forces were applied. Thus with for example a 10mm guide-ring diameter it was possible to maintain rod to guide-ring contact as a consequence of system elasticity and the visual feedback which the guide-ring and rod provided was lost. Too large a guide-ring diameter also detracted from the visual feedback as to whether or not the rod was central in the guide-ring. The approximately 20mm guide-ring diameter therefore provided a balance between accommodating elastic effects and maintaining visual feedback.

These elastic effects also meant that there was the possibility that the rod could be displaced from the guide-ring centre and yet the subject would still achieve the required manoeuvre r: a reduction in handle-forces might allow rod displacement and yet not affect [sgn($\dot{\theta}_{si}$), sgn($\dot{\theta}_{ti}$)].

Also, for manoeuvres r (attempted) for r = [A,...,I] while the subject's task was to maintain the rod in the guide-ring centre even if the subject failed to achieve this it was still possible that the [sgn($\dot{\theta}_{si}$), sgn($\dot{\theta}_{ti}$)] combination associated with the relevant manoeuvre r was achieved. This is the case since for regions r = [A,...,I], the required $\dot{\boldsymbol{x}}_B$ is not at a single point in the $\dot{\boldsymbol{x}}_B$-plane but a region

of points. Thus while maintaining the rod in the guide-ring centre is the means of feedback for the subject, it is [sgn($\dot{\theta}_{si}$), sgn($\dot{\theta}_{ti}$)] which is of interest. It was therefore necessary to determine the [sgn($\dot{\theta}_{si}$), sgn($\dot{\theta}_{ti}$)] combination rather than the displacement of the rod. In conclusion the use of rod in guide-ring was a simple visual means of guiding the subject to achieve the intended kinematics task but it was not a sufficient method of determining if the intended kinematics state was achieved. It was necessary to introduce kinematics measurement.

A number of potential measurement methods exist for determining [sgn($\dot{\theta}_{si}$), sgn($\dot{\theta}_{ti}$)]. Instrumenting a real-FCMV for direct measurement of caster global rotation and wheel roll is possible using gyroscopic systems, for example, as provided by Xsens Technologies B.V. However, both the metal vehicle-frame and the proximity of the floor may be problematic (De Vries et al., 2009). Additionally, the caster assemblies are relatively small and subject to $> 360°$ displacement so fixing instruments is not straightforward. Video capture systems exist which do not require markers but while these may be essential where marker attachment is problematic, for example, horses, as there is no great difficulty attaching markers to caster assemblies, marker-based video capture systems are appropriate, for example, Vicon. Video capture marker systems avoid any material change to the caster assembly, do not place any constraint on displacements and are relatively inexpensive if the hardware system is available, which it was. The Vicon Data Station 512 (hardware) and Workstation v4.5 (software) was used with six cameras (50Hz). The camera layout for this system is illustrated in Figure 5.6 (page 125).

5.3.5. *Vicon and displacement data*

The Vicon system depends on 2D sensor (cameras) detection of a spherical marker by a minimum of two cameras: there are also constraints on camera locations since large errors occur if, for example, capture is made with two cameras with only a small angular difference between their field of view. With a suitable calibration, software can then reconstruct the video capture into 3D marker displacements.

Trials indicated two problems using Vicon markers for caster global orientation and wheel orientation measurement. Firstly, unless the caster assembly was

Figure 5.6 – Shows five of the six cameras for the Vicon set-up at the Shieldfield Centre.

modified the wheel orientation detection marker had to be either very small (diameter less than 3mm) to pass between caster fork and caster wheel which then made detection difficult or a larger marker had to be placed within the wheel thickness: the location in the wheel thickness is evident from Figure 5.5 (page 122). The latter option created difficulties for the Vicon system: when caster rotation brought the markers under the vehicle-frame the spherical marker shape was compromised and markers were obscured. Secondly, increasing the number of markers so that some markers were always in view made it difficult to discriminate markers because markers occluded markers. (This investigation contrasts with the typical biomechanical application since multiple markers are potentially passing and remaining under a solid body and remain near the floor at all times.) Trials indicated that these difficulties were minimised if the number of markers was reduced to three per caster assembly and if the inter-marker distance on each caster was not too small: two markers indicated θ_{si} and one marker indicated, indirectly, θ_{ti} as described in the Dynamics Chapter (page 4.4.8).

The two markers (25mm diameter) used to determine θ_{si} were mounted on a balsa wood section using double-sided tape which in turn was screwed to a wood spacer which was attached to the caster assembly by double-sided tape. This is shown in Figure 5.7 (page 126). A single marker (15mm diameter) was used for the indirect determination of θ_{ti}. This single marker was attached using double-sided

tape. The marker was dislodged on contact with the caster fork but the dislodging force was negligible and did not interfere with the manoeuvre. Additionally, this marker was attached by nylon line to the wheel hub centre so when dislodged, it dangled and could not get trapped under the wheel.

Use of single marker for detecting $\Delta\text{sgn}(\dot{\theta}_{ti})$ was possible since, as detailed in Section 4.4.8 (page 83), the change of vertical displacement of a point on the wheel surface would indicate $\text{sgn}(\dot{\theta}_{ti})$ change where it occurred. With suitable selection of the initial position for this marker all $\text{sgn}(\dot{\theta}_{ti})$ changes can be detected before the marker is dislodged by the caster fork. A suitable initial position is shown in Figure 5.7 (page 126) and is indicated by the black, approximately semi-circular, outline. Given that it was the $\Delta\text{sgn}(\dot{\theta}_{ti})$ which was of interest and not $\dot{\theta}_{ti}$ the single marker set-up met the investigative requirements.

As a quasi-static assumption was being made it was necessary to confirm that the vehicle-frame accelerations were negligible. The rods for manoeuvre A and manoeuvre D (front of the vehicle) were extended downwards. Vicon markers (25mm diameter) were screwed into threaded adapters (DISC) which permitted fitting to the rod: these features are shown in Figure 5.1 (page 113). The rods for the other manoeuvres were also extended downwards in order to provide the opportunity to fix a similar marker at the relevant Z_r for each manoeuvre:

Figure 5.7 – Shows the wood spacer glued to the caster fork, the balsa wood section screwed to the wood spacer and the attachment of two 25mm diameter markers by double-sided tape: these are for the detection of caster global orientation. Also shown is a single marker for detection of wheel orientation: the marker initial location, indicated by the black approximately semi-circular outline, occurs when the black spot on the caster wheel is closest to the floor.

5.3.6. *Caster assembly set up*

In order to provide a consistent starting configuration the ${}^{B}\theta_{si} = 0$ position was determined (DISC) and marked on each caster assembly. Indelible pen line-marks were made on the caster-fork and the upper surface of the caster bearing case to indicate ${}^{B}\theta_{si} = 0$. Additionally, the upper surface of the caster bearing case was line-marked as was the vehicle-frame in order to detect any movement between caster assembly and vehicle-frame. This is shown in Figure 5.8 (page 127). In order to ensure a consistent initial θ_{ti} a mark was placed on the caster wheel and the wheel was orientated so that this mark was closest to the floor: this mark can be seen in Figure 5.7 (page 126). To place ${}^{B}\theta_{si}$ and θ_{ti} in the initial position it was necessary to unload the caster assemblies using car-jacks. It was found that raising the rear caster assemblies, adjusting them for initial position, then repeating for the front caster assemblies did not dislodge the rear caster assemblies if done with care: this is also shown in Figure 5.8

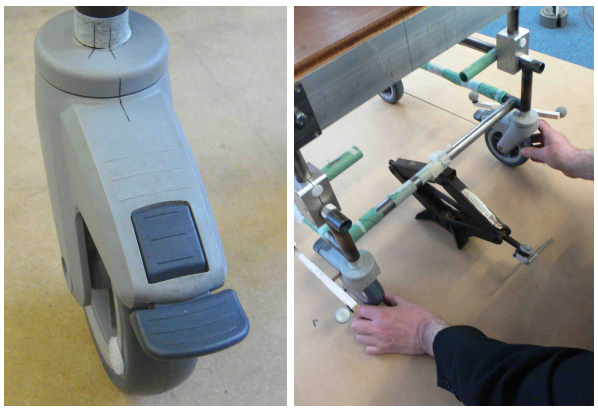

Figure 5.8 – Shows (left) line-marks on the upper surface of the caster bearing case which when aligned with the line-mark of the caster fork indicates ${}^{B}\theta_{si} = 0$. Also shown on the upper surface of the caster bearing case and the caster fork are line-marks which allow detection of movement between caster assembly and vehicle-frame. Shows (right) use of a car-jack to unload the caster assemblies to set the initial position.

5.3.7. *Light interference*

As sunlight could interfere with the marker detection, particularly due to metal reflections, and no provision was available at the Shieldfield Centre temporary blinds were constructed.

5.3.8. *Synchronicity*

In order to synchronise sensor data collection with Vicon data collection the following equipment was used. The software for the sensor data collection produced a voltage output at the parallel port when data was being collected. This signal was used to switch an infra-red LED on and off which was placed in the Vicon cameras field of view (DISC). This appeared as an additional Vicon marker and it was therefore possible to detect when sensor recording began and when it ended.

5.4. **Data Collection**

The data collection was carried out in two distinct stages in order to avoid placing excessive demands on the subjects.

5.4.1. *Load selection*

The first stage of the data collection did not involve any sensor or displacement measurement and the purpose was to determine the subject's maximum comfortable load for each manoeuvre r (attempted). Subjects were instructed as follows:

1. Not to touch the vehicle with any part of their body apart from grasping the handles.
2. To grasp handles in whichever way they found comfortable.
3. To select a maximum comfortable load.
4. To carry out the manoeuvre as slowly as they wished.
5. To abandon the manoeuvre if they felt the initial load could cause self-harm and if so load was removed.
6. To carry out a clock-wise (towards the subject's right side) change of vehicle-frame orientation while maintaining the rod in the guide-ring centre.

The following applied:

1. A load selection sheet (DISC) was completed for each subject detailing the load and the approximate start and stop time for each load selection.

2. The handle, height and front-rear position, was fixed for all subjects in this and subsequent data collections.

3. The vehicle-frame was loaded to bring the total vehicle-frame and load mass to about 40kg.

4. Subjects were not directed to wear any specific footwear.

5. The manoeuvres r (attempted) were carried out in alphabetical order.

6. While subjects were not given any instructions on positioning, apart from the hands-only instruction, where required as part of the learning process subjects were informed of the approximate theoretical directions of forces that produced the relevant manoeuvre r.

7. Subjects were permitted to attempt the manoeuvre r as many times as they wished.

8. The load was initially increased in approximately 18.1kg steps though fine tuning of load selection was done in approximately 9kg steps for loads under 143kg and for above this load fine tuning was done in approximately 6.5kg steps.

9. A pilot study indicated, as was indicated by the start-up effects considered in the Literature Chapter, that the maximum comfortable load was determined by the subject at initial motion: initial motion was deemed to have been completed when the vehicle-frame had reached an approximate steady-state, as judged visually by the experimenter (the author).

10. Once the steady-state was judged to have been achieved strict control was not placed on the amount of vehicle-frame orientation change which was made.

11. The caster assemblies were not unloaded as shown in Figure 5.8 (left) (page 127) on every occasion: this was carried out at the final confirmation of maximum comfortable load or if the subject was uncertain as to which decision to make regarding maximum comfortable load.

12. If the experimenter judged that the rod remained in the guide-ring centre or made only momentary contact with the guide-ring the manoeuvre r (attempted) was deemed a success. If the experimenter judged that the rod made

prolonged contacted with the guide-ring the manoeuvre r (attempted) was deemed a failure. If the subject made prolonged contact with the guide-ring with no additional load and a number of different additional loads without improvement the manoeuvre r was abandoned. If the subject said that a load was the maximum comfortable load and the manoeuvre r (attempted) was deemed a success the load was recorded. Rod guide-ring contact was disregarded after the experimenter judged the steady-state to have been reached.

5.4.2. *Sensor-displacement measurement*

The materials were set-up (DISC) and the following preparatory steps were carried out for each of the manoeuvres r (attempted) which subjects completed at load selection:

1. The subjects carried out a practice trial for the manoeuvre r (attempted).
2. The subjects were free to request that the experimenter add or remove load. The first and second steps were repeated until a maximum comfortable load was selected and the new maximum comfortable load was recorded.
3. The ancillary MDF boards for the subject to step on were arranged to suit the subject.
4. In order to determine the approximate position of the centre of pressure of hand grasp the following was required
   (a) The thumb-finger junction was marked on tape placed on the handles: this became the subject's chosen hand grasp position.
   (b) A fabric measuring tape was used to measure from the handle end (rear), along the top surface of the handle to the thumb-finger junction mark.
   (c) This was repeated for left and right hands for each manoeuvre r (attempted).

The following were carried out for each manoeuvre r (attempted) data collection. These were ordered from smallest load selection to largest load selection: if two selections tied then alphabetical order was followed.

1. The experimental-FCMV was manoeuvred by the experimenter to the required position on the MDF board.
2. The experimenter adjusted the caster assemblies so that ${}^{B}\theta_{si} = 0$ and so that the wheel orientations were in the initial position.
3. Where required the experimenter attached the marker indicating the CoZV.
4. The experimenter attached the θ_{ti} indicating markers and checked that all the caster markers were securely fixed.
5. The experimenter located the stand so that the rod was in the guide-ring centre.
6. The subject stood in position but with hands off the handles.
7. The experimenter set the Vicon system to data collection.
8. The experimenter set the sensor system to data collection and an approximate count of six seconds was made.
9. The subject was instructed to:
   (a) Grasp handles at their chosen position.
   (b) To 'turn to the right' while attempting to keep the rod in the guide-ring centre.
   (c) Do the manoeuvre as slowly as they wished.
   (d) Stop when the experimenter judged that $\Delta\theta_0 \approx 0.5\pi$ rad.
   (e) To remove hands from the handles but otherwise not to move.
10. The experimenter switched off the sensor data collection.
11. The experimenter switched off the Vicon data collection.

These steps were repeated for each of the manoeuvres r (attempted) which was completed. Ad hoc notes were also made by the experimenter. The author was the experimenter.

On completion of all manoeuvres r (attempted) the subject's approximate hand width was determined by the following: while grasping the handle, a measurement was taken from the junction of the base of thumb-forefinger to the maximum width of the hand. This is shown in Figure 5.9 (page 132).

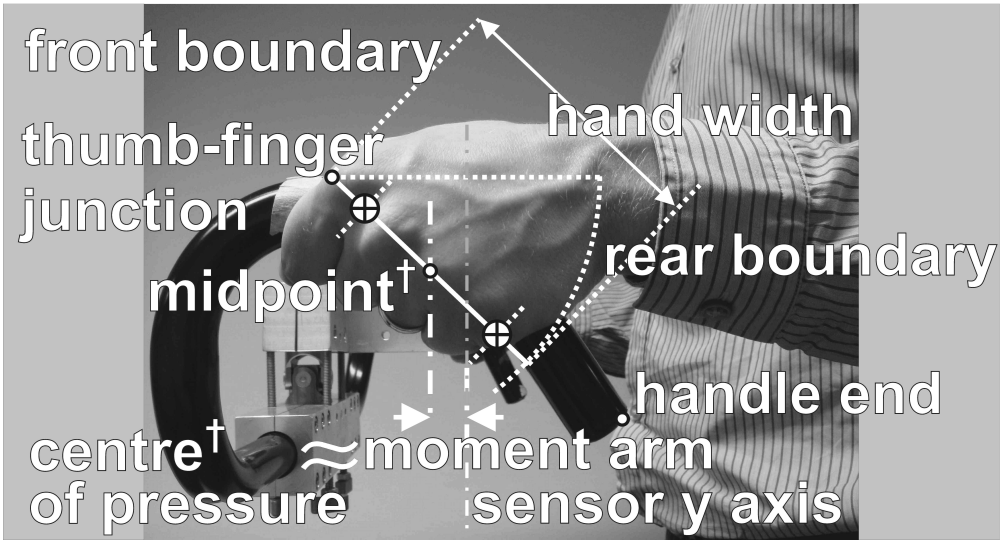

Figure 5.9 – Shows measurement of the hand width and the geometry for estimating the centre of pressure and the resulting moment arm. (Some terms are considered in the Discussion Chapter.)

5.5. Data Processing

A large number of post processing procedures were required and these are summarised here and detailed in Appendix C:

1. Vicon data was trimmed to the sensor on-off signal.
2. The initial vehicle-frame orientation was determined.
3. Gaps were filled in the Vicon data.
4. The motion start of the manoeuvre was defined as the Vicon data point after which all subsequent vehicle-frame orientations were more negative and this was further defined as $\theta_0 = 0$.
5. The vehicle-frame orientation at which 90% of an approximate caster steady-state was achieved for all caster assemblies was determined for each subject and manoeuvre r and this was defined as the near steady-state.

6. The approximate moment arm of the $\hat{\boldsymbol{v}}$ component of handle-forces, with respect to the sensor, was determined.

7. Sensor data was manipulated into a convenient form including normalising against load taking account of the vertical handle-force component. The P_{uCs} measure was determined.

8. The sensor and Vicon data were examined for synchronicity and data lengths were modified to give identical data lengths.

9. Packing all relevant sensor information into a single percentile-related symbol permits conciseness and avoids ambiguity: a percentile measure was created for sensor data as follows.

   (a) Where P is any sensor measure, the percentile measures for a set of P measures for $P > 0$ are denoted ${}^{+nth}P$ where $+nth$ is any percentile integer. For a set of P measures for $P < 0$, the percentile measures determined from $|P|$ are denoted ${}^{-nth}P$ where $-nth$ is any percentile integer: $\text{sgn}({}^{-nth}P)$ is defined as -1.

   (b) The specific sensor measure is indicated by a trailing subscript a where a is any of measures, P_u, P_v or P_{uCs}, respectively $-F_x$, F_Z and as defined (page 118), i.e. ${}^{\pm nth}P_a$ indicates ${}^{\pm nth}P_{Pu}$, ${}^{\pm nth}P_{Pv}$ and ${}^{\pm nth}P_{PuCs}$ respectively where $\pm nth$ indicates $+nth$ or $-nth$.

   (c) Each percentile sensor measure is, by definition, determined from a number of sensor measures and the sensor measures in the Results Chapter are always determined from sensor measures synchronised with $\Delta\theta_0$: the measure-range is indicated by the leading subscript ar, for example, ${}^{+nth}_{ar}P_a$ denotes the measures where $P_a \geq {}^{+nth}P_a$ for sensor measures synchronised with the set of θ_0 data points where ar indicates $\theta_{01} < \theta_0 < \theta_{02}$. Where subjects have a different θ_{02} measure this is indicated by a final i on the leading subscript, i.e. ${}^{+nth}_{ari}P_a$.

   (d) Since percentile measures are determined for each manoeuvre this is indicated by a trailing superscript, for example, ${}^{+nth}_{ari}P^r_a$ where r is any manoeuvre letter [A,..., L].

(e) The trailing subscript appendage 'maxi' is used to denote the intra-subject maximum magnitude and are denoted ${}^{+nth}_{ari}P^{r}_{amaxi}$: the peak measure. Negatively signed actions therefore also have the subscripted appendage 'maxi' where these indicate the maximum negative magnitude, i.e. ${}^{-nth}_{ari}P^{r}_{amaxi}$. The trailing subscript appendage 'max' is used to denote the maximum magnitude inter-subject measure, i.e. the maximum magnitude for all subjects. The trailing subscript appendage 'mini' and 'min' are used in the same way as 'maxi' and 'max' to represent minimum magnitudes for the relevant percentile (page 248).

(f) ${}^{-nth}_{ari}P^{r}_{amini} \geq P_a \geq {}^{-nth}_{ari}P^{r}_{amaxi}$ is therefore a sensor measure range for a specific handle-force measure, vehicle-frame orientation range, which indicates the largest magnitude negative measures for a single subject for a specific manoeuvre r (attempted). Removal of the i trailing subscript therefore provides the same measure for all subjects, i.e. ${}^{-nth}_{ari}P^{r}_{amin} \geq P_a \geq {}^{-nth}_{ari}P^{r}_{amax}$. This may also be used for positive measures, i.e. ${}^{+nth}_{ari}P^{r}_{amini} \leq P_a \leq {}^{+nth}_{ari}P^{r}_{amaxi}$ and ${}^{+nth}_{ari}P^{r}_{amin} \leq P_a \leq {}^{+nth}_{ari}P^{r}_{amax}$ for intra-subject and inter-subject measures respectively.

(g) The P_{uCs} measures can be integer zero (page 118): where this is so these measures are disregarded in the calculation of ${}^{\pm nth}_{ar}P^{r}_{P_{uCs}}$

10. In order to allow for inter-subject comparison of loads for a single manoeuvres r (attempted) the following process was used. The load selection for each subject at sensor measurement is denoted L^{r}_{Mi} (kg) where r is any manoeuvre r (attempted) and i is the subject index. The maximum comfortable load selection for each subject for all manoeuvres is denoted L_{Mmaxi} (kg) where the i is the subject index. The L^{r}_{Mi} for each subject are normalised against that subject's L_{Mmaxi} and these measures are denoted L^{r}_{Mnormi} where the final r is the manoeuvre and are defined as

$$L^{r}_{Mnormi} = 100. \left(\frac{L^{r}_{Mi}}{L_{Mmaxi}} \right) \tag{5.12}$$

The median L^{r}_{Mnormi} for each manoeuvre is denoted L^{r}_{Mnormm}. Details of load selection were output to MiniTab for statistical analyses.

11. Results were output to graphs and tables using Maple.

Chapter 6–Results

6.1. **Introduction**

The data collection included 209 load selection measurement attempts of which 184 were successful manoeuvre r (attempted) and this led to 172 sensor-displacement measurements: measures as described in the Methods Chapter (page 112). In this chapter a representative account of this data is made.

There are four parts to these results: three short and one long. Firstly, the subject participation is reported. Secondly, details of the load selection are given. Thirdly, the kinematics are put in context by indicating the typical vehicle-frame rotation: relative to the velocities noted in the Literature Chapter the manoeuvres are very slow. However, a full kinematics account is delayed until the Discussion Chapter. The reason for doing so is that there is considerable uncertainty regarding the [sgn($\dot{\theta}_{si}$), sgn($\dot{\theta}_{ti}$)] combinations and while this does not undermine the results, as will be demonstrated, a clearer picture of the forces-applied and space-required relationship is achieved by considering forces-applied (handle-forces) in terms of results and kinematics in terms of discussion. Since kinematics conformity to manoeuvres r has not been demonstrated the term '(a.)' indicating 'attempted' is appended to the manoeuvre description, for example, manoeuvre F (a.) is the first manoeuvre considered. Fourthly, the longest part, the handle-force results, preceded by a description of the use of percentiles and the related notation (as described in the Methods Chapter), are presented.

The load selection results show that there is a statistically significant rank ordering for the operator load response (maximum comfortable load) for the eleven manoeuvres.

The handle-force results show that the different manoeuvres have statistic-

ally different handle-force measures and that these handle-force measures have a statistically significant association with load selection, for example, manoeuvres [F, C, I] (a.) are associated with the selection of relatively low loads and manoeuvres [K, L] (a.) are associated with the selection of relatively high loads.

The centres of zero velocity for the eleven manoeuvres are shown in Figure 4.6 (page 69).

6.2. **Subjects and Load**

Nineteen subjects were recruited: fourteen female and five male. Subjects were aged 25–55 (approximately). All subjects were employed with duties relating to FCMV use. Eighteen subjects were employed by a local authority and job titles included: Disability Assessment Officers, Occupational Therapist and Manual Handling Assessors. One subject was employed by the NHS as a Clinical Engineer within a Medical Physics Technical Aids section.

Table 6.1 Page(138) details the participation of the recruited subjects. Sixteen subjects completed the load selection process and the sensor-displacement measurement process which as described in the Methods Chapter were completed on separate occasions: the approximate average time separation between load selection and sensor-displacement measurement was 8 weeks.

Subject[19] was unable to complete load selection process for any of the eleven manoeuvres: approximately 3 to 5 attempts with various loadings for a number of the eleven manoeuvres r were made and on each occasion without improvement no control of the rod in the guide-ring was evident.

Subject[18] completed the load selection process for six manoeuvres (see Table 6.1 (Page 138): the subject stated that she could not determine if the rod was central in the guide-ring for the other five manoeuvres r as she lacked the depth of vision. The manoeuvres for which subject[18] did make load selections took approximately twice as many attempts as other subjects. When subject[18] took part in the sensor-displacement measurement process she was unable to control the rod in the guide-ring without first repeating the load selection process, i.e. she had to begin with no load or a small load and increase load in 14 kg steps, with numerous practice attempts, till she reached her chosen load. The sensor-

subject	initial load selection manoeuvres completed/11	sensor-displacement measurement manoeuvres completed/11
1	11/11	11/11
2	11/11	11/11
3	11/11	11/11
4	11/11	11/11
5	11/11	11/11
6	11/11	11/11
7	10/11 (not F)	10/11 (not F)
8	11/11	11/11
9	11/11	11/11
10	10/11 (not I)	10/11 (not I)
11	11/11	11/11
12	11/11	11/11
13	11/11	11/11
14	10/11 (not B)	10/11 (not B)
15	10/11 (not L)	10/11 (not L)
16	11/11	11/11
17	11/11	none (equipment failure)
18	6/11 (not A, B, C, K, L)	none
19	none	none

Table 6.1 – Shows the participation of each subject at the initial load selection and the later sensor-displacement measurement for each manoeuvre r.

displacement measurement process was abandoned for this subject and the load selections are disregarded in the results.

Subject[17] was the chronologically final subject for the sensor-displacement measurement: the data recording equipment (Vicon) failed and the measurement process was therefore terminated.

Four of the subjects were able to complete load selection for ten of the eleven manoeuvres r (a.) as detailed in Table 6.1 and the remaining twelve subjects completed all eleven load selections. There were therefore 183 load selection results and 172 sensor-displacement measurement results.

Figure 6.1 (Page 139) graphs operator load response at initial load selection (black cross) and at sensor-displacement measurement (red diamond). The intra-subject range magnitudes vary: subject[3] has the longest range and subject[14] has the shortest range. The inter-subject maximum comfortable loads vary: the minimum maximum comfortable load is 107 kg (subject[2]) where as seven subjects[1, 6, 8, 9, 10, 11, 16] reached the maximum comfortable load of 169 kg which was imposed to avoid caster assembly damage. The inter-subject minimums also vary: subject[16] has a minimum of 98 kg where as subject[10] has a minimum of 34 kg.

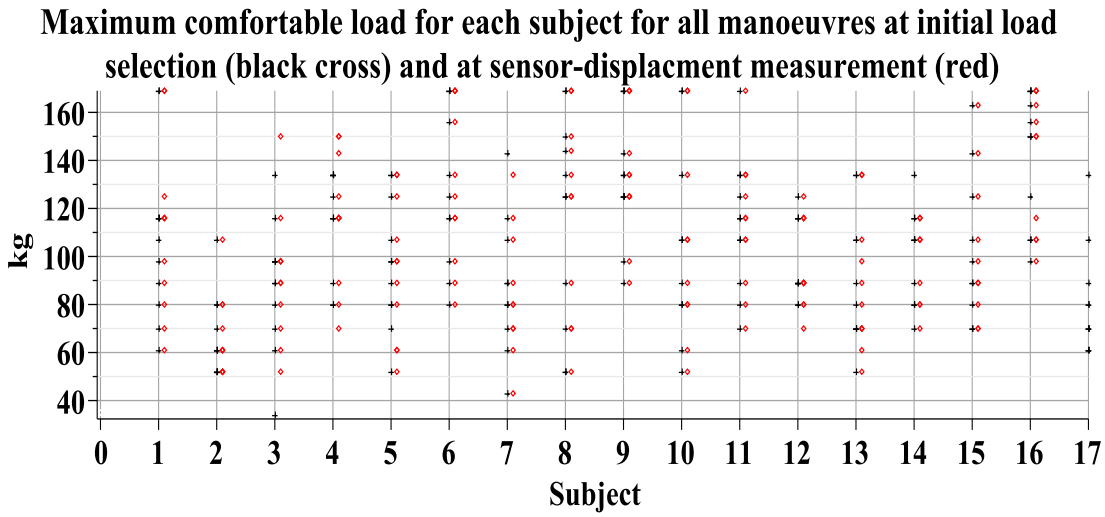

Figure 6.1 – Shows the maximum comfortable load (kg) at initial load selection (black marker) and at sensor-displacement measurement (red marker) for each subject : as subjects could choose identical loads for different manoeuvres the number of markers does not indicate participation.

(For complete load selections details see pages 281–282). As inter-subject strength differences are not being investigated it is more useful to normalise the Figure 6.1 measures against each subject's largest maximum comfortable load (L_{Mmaxi}) (as defined, page 134) and denoted L^r_{Mnormi}. These are shown in Figure 6.2 (page 140).

Figure 6.2 shows the L^r_{Mnormi} with $95^{\%}$ confidence intervals for each manoeuvre for both initial load selection (red thick line) and at the sensor-displacement measurement (blue thin line). Confidence intervals were calculated with the non-parametric one sample Sign Test as examination shows the distributions to be non-normal and variable between manoeuvres. The median (L^r_{Mnormm}) is indicated by a blue or red circle and each load selection is indicated by a black dot: as the selections were for discrete loads some markers are superimposed. The manoeuvres are arranged from left to right with ascending order of lower limit L^r_{Mnormi} for sensor-displacement measurement. In particular the measures for manoeuvre K (a.) are piled up at $100^{\%}$.

The statical analyses is carried out in two stages and given the data distribution characteristics, different non parametric distributions, non parametric tests are used. Firstly, the Skillings-Mack test Skillings (1981), a variant of the Friedman Two-Way Analysis of Variance by Ranks (Daniel, 1990) which allows for the four

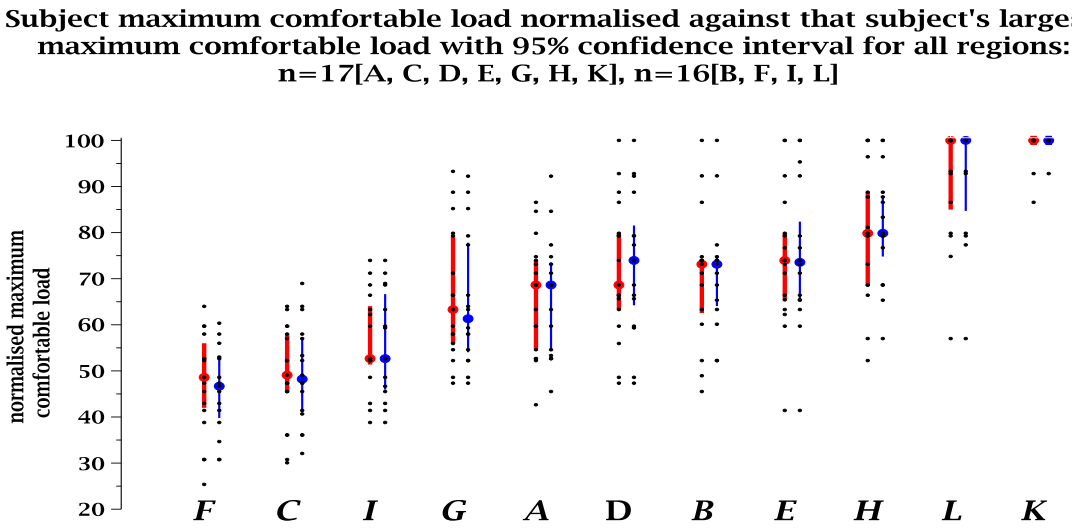

Figure 6.2 – Shows maximum comfortable loads at initial selection (red) and at sensor-displacement measurement (blue) for each manoeuvre r (region) where measures are expressed as a percentage of that subject's largest maximum comfortable load (L^r_{Mnormi}). The median measure (L^r_{Mnormm}) are indicated by a solid circle and the 95% confidence intervals for the median are indicated by lines: as subjects can have identical measures the number of markers does not indicate the participation. The n values are shown for initial caster loading selection. For sensor-displacement measurement $n-1$ applies.

blank entries in the sixteen (subjects) by eleven (manoeuvres) table of results, was used to provide statistical confirmation that the L^r_{Mnormm} are not identical. For the test statistic p, $p < 0.0001$, i.e. there is a negligible possibility that the rank order is a result of chance. This test compares the expected rank positions for all subjects for each manoeuvre with that which would result from chance. Secondly, the visual impression of Figure 6.2 is that the manoeuvres r (a.) are ranked from smallest to largest L^r_{Mnormm} as [F, C, I, G, A, D, B, E, H, L, K]. This was tested (in XLSSTAT) using Page's Test for Ordered Alternatives (Large-Sample Approximation) (Daniel, 1990). The alternative hypothesis is that the rank order is r= [F, C, I, G, A, D, B, E, H, L, K]. For the test statistic p, $p < 0.0001$, i.e. there is a negligible possibility that the rank order is a result of chance.

There is therefore compelling evidence that an association exists between load selection and the manoeuvre r (a.). Furthermore, the clinical implications are substantial: for example, across all subjects the minimum load selection measure for manoeuvre [K] (a.) was $93^{\%}$ where as the maximum selection measure for man-

oeuvre [F] (a.) was 60%. Thus even an extremely and unnecessarily conservative conclusion is that manoeuvre [K] (a.) attracts 50% greater load capacity than manoeuvre [F] (a.).

These results are also potentially conservative since some subjects were willing to to trial loadings greater than the maximum permitted loading (169 kg): manoeuvre B (a.) subject[16], manoeuvre E (a.) subject[6], manoeuvre H (a.) subect[9] and manoeuvres [K, L] (a.) subjects[6, 8, 9, 11, 16].

6.3. **Vehicle-frame Kinematics and Handle-force Measures**

6.3.1. *Vehicle-frame kinematics*

Before presenting handle-force measures, it is useful to set those results in a kinematics context: in loose terms, to indicate the manoeuvring speed. Examination of the handle-force measures will show that there is a dynamic basis for dividing the period from motion start, as defined (page 132), to near steady-state, as defined (page 132), denoted $\theta_{0steadi}$ where i indicates the subject variation at which near steady-state occurs. The period from $\theta_0 = 0$ to $\theta_{0steadi}$ is termed 'start-steady period'. The set of ordered θ_0 measures for the start-steady period is denoted $\{_{ssi}\theta_0^r\}$ where r is any manoeuvre. The $\{_{ssi}\theta_0^r\}$ measures are divided at $\theta_0 = {}_{ss1}\theta_0^r$ and the first part is termed 'initial period' and the second part the 'later period'. The set of θ_0 measures for the initial period is denoted $\{_{ss1}\theta_0^r\}$ and for the later period is denoted $\{_{ss2i}\theta_0^r\}$. The time duration of $\{_{ss1}\theta_0^r\}$ is denoted $t_i(\{_{ss1}\theta_0^r\})$.

For each manoeuvre the subject with the minimum $t_i(\{_{ss1}\theta_0^r\})$ is identified and a representative function for the $\{_{ss1}\theta_0^r\}$ is identified using a third order polynomial in Maple. This is illustrated in Figure 6.3 (Page 142) for manoeuvre C (a.) for subject[15] as this trial had the minimum $t_i(\{_{ss1}\theta_0^r\})$ for all subjects and manoeuvres: loosely, the fastest manoeuvre.

The result, illustrated in Figure 6.3 (page 142) for $\{_{ss15}\theta_0^{\mathrm{C}}\}$, is shown for each of the eleven manoeuvres in Table 6.2 (page 143) which details the results with columns from left to right showing: the manoeuvre label, the subject with the minimum $t_i(\{_{ss1}\theta_0^r\})$ and four measures: 1) $\{_{ss1}\theta_0^r\}$, 2) $\dot{\theta}_0$ at ${}_{ss1}\theta_0^r$ based on the differentiation of the polynomial fit function with respect to t evaluated at ${}_{ss1}\theta_0^r$, 3)

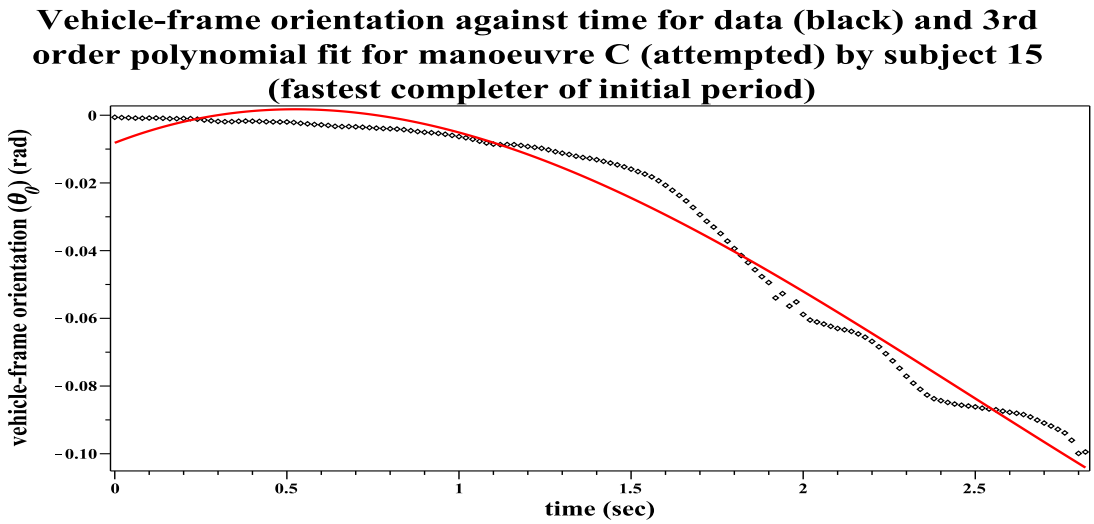

Figure 6.3 – Shows for data subject 15 who completed the initial period $\{{}_{ss1}\theta_0^C\}$ in the minimum$t_i(\{{}_{ss1}\theta_0^r\})$, the $\{{}_{ss1}\theta_0^C\}$ (black) and a third order polynomial fit ($-0.0081+0.0394t-0.0419t^2-0.0056t^3$) (red) against time (sec).

the resulting translational velocity magnitude, denoted $\dot{x}_G({}_{ss1}\theta_0^r)$, of the geometric vehicle-frame centre arising from $\dot{\theta}_0$ evaluated at ${}_{ss1}\theta_0^r$ but disregarding any translational velocities at the nominal centre of zero velocity and 4) $t_i(\{{}_{ss1}\theta_0^r\})$. No particular importance is intended regarding the inter-manoeuvre velocity differences; it is the small magnitudes compared with the translational velocities identified in the Literature Chapter (page 35) which is being noted.

6.3.2. *Presentation of handle-force measures*

The results, presented at the end of this chapter, are an inter-manoeuvre comparison for all subjects for the percentile action measure ${}^{\pm 90th}_{ss1}P_a^r$ (page 133) where a is one of the measures P_u, P_v and P_{uCs}: in loose terms these are the forward handle-force, lateral handle-force and a handle-force measure representing the summed magnitude of the components of the couple (page 118): in non-technical and loose language P_{uCs} is the addition of the push force and pull force which overcomes the motion resistance to the vehicle-frame changing orientation. The ${}^{\pm 90th}_{ss1}P_a^r$ term is simply a percentile measure where the two subscripts and two superscripts keep account of 1) the percentile measure $\pm 90th$, 2) the manoeuvre (r), 3) the action being measured (a) and 4) the range of orientation change of the vehicle-frame ($ss1$ or ssi). In this chapter the term magnitude refers to unsigned scalars.

manoeuvre	*subject*	${}_{ss1}\theta_0^r$ (rad)	$\dot{\theta}_0({}_{ss1}\theta_0^r)$ $(rad\,sec^{-1})$	$\dot{x}_G\,({}_{ss1}\theta_0^r)$ $(m\,sec^{-1})$	$t\,({}_{ss1}\theta_0^r)$ (sec)
A	13	-0.133	-0.0475	0.0252	5.16
B	15	-0.085	-0.0586	0.0199	3.56
C	16	-0.102	-0.0625	0.0352	2.82
D	5	-0.115	-0.0429	0.0175	3.92
E	12	-0.085	-0.0346	0.0002	3.32
F	2	-0.084	-0.0494	0.0222	2.88
G	13	-0.128	-0.0244	0.0129	5.22
H	3	-0.143	-0.0446	0.0152	4.36
I	4	-0.093	-0.0179	0.0101	3.02
K	3	-0.107	-0.1216	0.0389	3.22
L	4	-0.108	-0.1273	0.0407	2.90

Table 6.2 – Shows from left to right: the manoeuvre label, the subject with the minimum $t_i(\{{}_{ss1}\theta_0^r\})$ for the manoeuvre, the period termination angle ${}_{ss1}\theta_0^r$, $\dot{\theta}_0$ at ${}_{ss1}\theta_0^r$ based on the differentiation of the polynomial fit function with respect to t evaluated at ${}_{ss1}\theta_0^r$, the resulting translational velocity magnitude of the vehicle-frame geometric centre arising from $\dot{\theta}_0$, disregarding any translational velocities at the nominal centre of zero velocity at ${}_{ss1}\theta_0^r$, denoted $\dot{x}_G({}_{ss1}\theta_0^r)$ and $t_i(\{{}_{ss1}\theta_0^r\})$

Before presenting the results for the inter-manoeuvre comparison, the results for one manoeuvre are presented in detail in order to demonstrate the basis of the inter-manoeuvre comparison. The results for the ten other manoeuvres can be found in Appendix D.

The detailed results for manoeuvre F (attempted) are presented and these include the following.

1. The three handle-force measures are examined against time and against θ_0: this allows an appreciation of the relatively very slow initial change of vehicle-frame orientation change.

2. A visual inspection is made of the largest magnitudes of handle-force measure (${}^{\pm 90th}_{ssi}P_a^r$ and ${}^{\pm 75th}_{ssi}P_a^r$) against vehicle-frame orientation change from motion start to when all four casters are in the caster near steady-state ($\theta_{0steadi}$), i.e. each caster is at a minimum of 90% of the caster steady-state. The value of this is that it indicates that for at least one of the three handle-force measures a concentration of occurrences of largest magnitudes (${}^{\pm 90th}_{ssi}P_a^r$) exist close to

motion start after which occurrences of these largest magnitudes are then relatively few. For manoeuvre F (attempted) this is most evident for the handle-force measure of the couple (P_{uCs}).

(a) This examination leads to the division of the vehicle-frame orientation change from motion start to near steady state ($\{_{ssi}\theta_0^r\}$) and the identification of vehicle-frame orientation at which this occurs, denoted $_{ss1}\theta_0^r$.

(b) This then allows the relevant percentile measures ($^{\pm 90th}_{ss1}P_a^r$) to be determined: note index change from ssi to $ss1$, i.e. in loose terms it is the $\pm 90th$ percentile measures immediately after motion start which are of interest.

3. While a manoeuvre may be characterised by only magnitudes in one sign subjects sometimes applied small magnitudes of force of the opposite sign when first placing their hands on the handles. In order to avoid the added complication of taking account of these relatively small handle-forces these measures are disregarded. A modified initial period disregarding these measures is defined, for example, manoeuvre F (attempted) begins at -0.01 rad: the new initial period is denoted $\{_{ss1a}\theta_0^r\}$.

6.4. **Manoeuvre F (attempted)**

This subsection presents the results for handle-force measures (P_u, P_v and P_{uCs}) for manoeuvre F (attempted) for the start-steady period. In this subsection 'subjects[F]' or a trailing super or sub script F in a symbol indicates measures from subjects [1,..., 5, 8,..., 16]: subject[7] did not participate and the results for subject[6] were rejected (see PDF page 480).

6.4.1. *Manoeuvre F (attempted) handle-force measures*

It will be shown in the next subsection that examination of the handle-force measures indicates that dividing the data at vehicle-frame orientation $\theta_0 = -0.084$ rad is useful and hence θ_0 measures for manoeuvre F (attempted) are defined for an initial period ($-0.084 < \theta_0 < 0$ rad, denoted $\{_{ss1}\theta_0^{\mathrm{F}}\}$) and for a later period ($\theta_{0steadi} < \theta_0 < -0.084$ rad, denoted $\{_{ss2i}\theta_0^{\mathrm{F}}\}$). There is some variation, related to relatively small handle-force magnitudes, between subjects

immediately after motion start for a small magnitude vehicle-frame orientation (θ_0) displacement: magnitude no greater than 0.01 rad. The range $-0.084 < \theta_0 < -0.01$ rad is denoted $\{_{ss1a}\theta_0^{\mathrm{F}}\}$, i.e. the initial period ($\{_{ss1}\theta_0^{\mathrm{F}}\}$) modified to commence at $\theta_0 = -0.01$ rad rather than motion-start.

Figures 6.4 (page 146) and 6.5 (page 146) illustrates the handle-force measures for one subject[10] against time-steps and θ_0 respectively. For the modified initial period ($\{_{ss1a}\theta_0^{\mathrm{F}}\}$) there are three features of these figures which are common to all subjects[F]. Firstly, in respect of the handle-force measure of the couple, no $P_{uCs} > 0$ occur. Secondly, in respect of the forward force measure, P_u occur in both signs. Thirdly, in respect of the later force measure, positive to the subjects's left, only $P_v < 0$ occur, i.e. directed rightward, The time step figure (top) is read from left to right and the vehicle-frame orientation figure is read from right to left: it can be seen that the initial red bulge (the handle-force measure of the couple:P_{uCs}) in the time step figure is compressed in the vehicle-frame orientation figure but the rest of the graph is less affected: the initial period accounts for a disproportionate amount of time.

6.4.2. *Manoeuvre F (attempted)* P_{uCs}

The presentation begins with P_{uCs} (the summed magnitudes of the $\hat{\boldsymbol{u}}$ directed handle-forces producing a couple). Figure 6.6 (page 147) graphs, against vehicle-frame orientation (θ_0) occurrences of the largest magnitude P_{uCs} ($^{-75th}_{ssi}P^{\mathrm{F}}_{uCs} \geq P_{uCs} > {}^{-90th}_{ssi}P^{\mathrm{F}}_{uCs}$ and of $^{+75th}_{ssi}P^{\mathrm{F}}_{uCs} \leq P_{uCs} < {}^{+90th}_{ssi}P^{\mathrm{F}}_{uCs}$ with black markers and $P_{uCs} \leq {}^{-90th}_{ssi}P^{\mathrm{F}}_{uCs}$ and $P_{uCs} \geq {}^{+90th}_{ssi}P^{\mathrm{F}}_{uCs}$ with red markers) (N/kg) for all subjects[F], where the leading subscript *ssi* indicates the start-steady period for each subject[F]: to assist inspection the measures for each subject are normalised against the subject's P_{uCs} peak magnitude for the start-steady period ($\{_{ssi}\theta_0^{\mathrm{F}}\}$). A dashed vertical line indicates $\theta_0 = -0.084$ rad and this divides $\{_{ssi}\theta_0^{\mathrm{F}}\}$ into the initial period ($\{_{ss1}\theta_0^{\mathrm{F}}\}$) and the later period ($\{_{ss2i}\theta_0^{\mathrm{F}}\}$).

It can be seen from Figure 6.6 that division of the start-steady period ($\{_{ssi}\theta_0^{\mathrm{F}}\}$) locates occurrences of the largest magnitude P_{uCs} ($P_{uCs} \leq {}^{-90th}_{ssi}P^{\mathrm{F}}_{uCs}$ indicated by red markers) in the initial period ($\{_{ss1}\theta_0^{\mathrm{F}}\}$) and thus, despite any variations between subjects, the mechanism is so configured that these measures

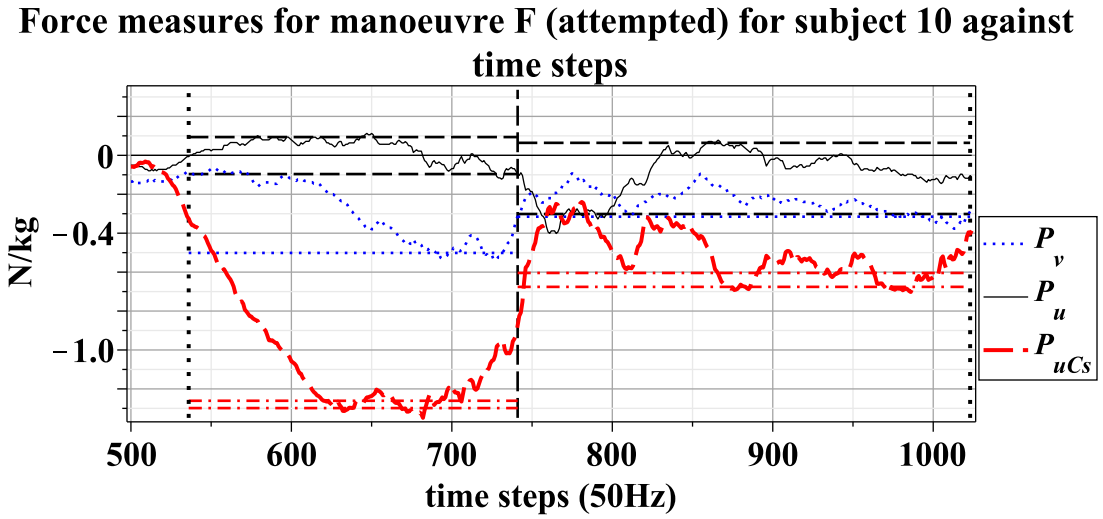

Figure 6.4 – Shows for subject[10] for manoeuvre F (a.), measures: P_v (dotted blue), P_u (thin black) and P_{uCs} (thick red dashed) in N/kg plotted against time-steps (approximately 0.02 seconds) with motion-start line (vertical black dotted: closest to left side), steady-start line (vertical black dotted:closest to right side) and $\theta_0 = -0.084$ rad line (vertical black dashed). The following percentile lines are shown for $\{_{ss1}\theta_0^{\mathrm{F}}\}$: ${}^{-90th}_{ss1}P^{\mathrm{F}}_{uCs}$ and ${}^{-75th}_{ss1}P^{\mathrm{F}}_{uCs}$ (horizontal red dash-dot), ${}^{-90th}_{ss1}P^{\mathrm{F}}_{u}$ and ${}^{+90th}_{ss1}P^{\mathrm{F}}_{u}$ (horizontal black dash) and ${}^{-90th}_{ss1}P^{\mathrm{F}}_{v}$ (horizontal blue dot): these percentile lines are also shown for $\{_{ss2i}\theta_0^{\mathrm{F}}\}$.

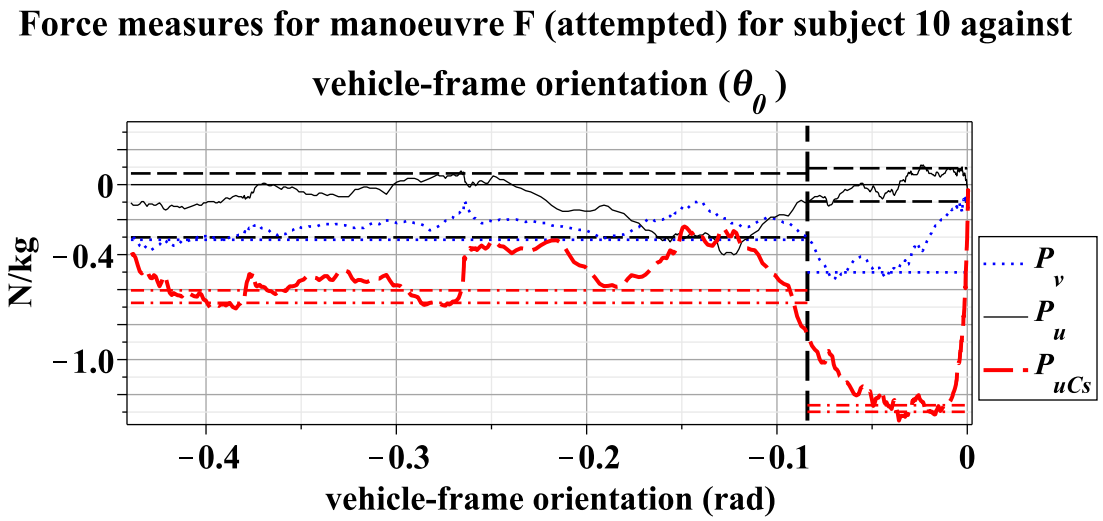

Figure 6.5 – Shows for subject[10] for manoeuvre F (a.), measures plotted against θ_0 with other details as above.

occur by $\theta_0 = -0.084$ rad. Hence division of the start-steady period ($\{_{ssi}\theta_0^{\mathrm{F}}\}$) at this orientation relates to a mechanical property of the system for manoeuvre F (attempted). Additionally, it can be seen that there are no $P_{uCs} > {}^{+75th}_{ssi}P^{\mathrm{F}}_{uCs}$ and hence no $P_{uCs} > 0$ and this confirms the representativeness of Figure 6.5 (page 146) in this respect.

Figure 6.7 (page 147) takes the handle-force measure for the initial period

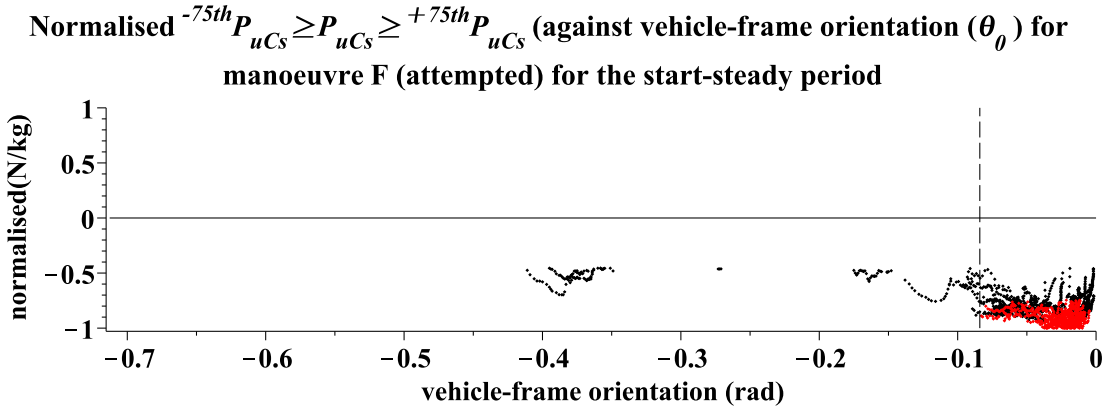

Figure 6.6 – For the manoeuvre F (a.) occurrences of ${}^{-75th}_{ssi}P^{\mathrm{F}}_{uCs} \geq P_{uCs} > {}^{-90th}_{ssi}P^{\mathrm{F}}_{uCs}$ and of ${}^{+75th}_{ssi}P^{\mathrm{F}}_{uCs} \leq P_{uCs} < {}^{+90th}_{ssi}P^{\mathrm{F}}_{uCs}$ (both black markers) and, $P_{uCs} \leq {}^{-90th}_{ssi}P^{\mathrm{F}}_{uCs}$ and $P_{uCs} \geq {}^{+90th}_{ssi}P^{\mathrm{F}}_{uCs}$ (both red markers) in N/kg (normalised against each subject's maximum magnitude P_{uCs} for the start-steady period) against θ_0 for $\{{}_{ssi}\theta^{\mathrm{F}}_0\}$ for each subject: $\theta_0 = -0.084$ line indicated (dashed vertical)

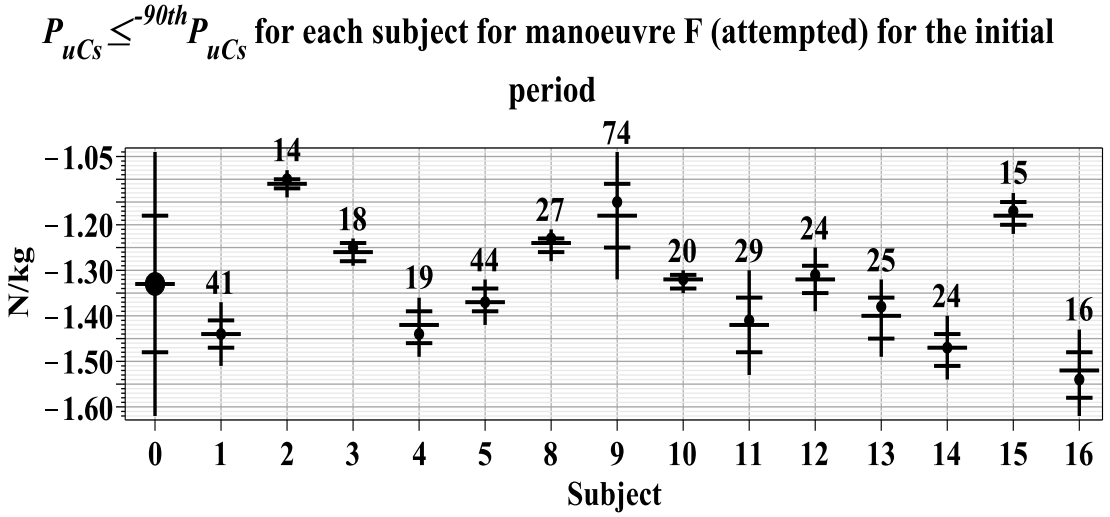

Figure 6.7 – Shows for each subject[F] (i) for $\{{}_{ss1}\theta^{\mathrm{F}}_0\}$ in N/kg: a vertical line indicating the minimum magnitude measure ${}^{-90th}_{ss1}P^{\mathrm{F}}_{uCsmini}$ to the maximum magnitude measure ${}^{-90th}_{ss1}P^{\mathrm{F}}_{uCsmaxi}$, a solid circle indicating the mean ${}^{-90th}_{ss1}P^{\mathrm{F}}_{PuCsmini} \geq P_{uCs} \geq {}^{-90th}_{ss1}P^{\mathrm{F}}_{PuCsmaxi}$, the quarter divisions of the range (horizontal lines), the number of occurrences of $P_{uCs} \leq {}^{-90th}_{ss1}P^{\mathrm{F}}_{uCs}$. Subject[0] shows this data for all subjects[F] with a solid circle indicating the mean of all the mean ${}^{-90th}_{ss1}P^{\mathrm{F}}_{PuCsmini} \geq P_{uCs} \geq {}^{-90th}_{ss1}P^{\mathrm{F}}_{PuCsmaxi}$.

shown in Figure 6.6 and displays it in a different form with two purposes. Firstly, this form is required in order to develop both a symbolic and a numerical account for the inter-manoeuvre comparison which concludes this chapter. Secondly, this form demonstrates inter-subject variation. In Figure 6.7 the measures for the largest magnitude P_{uCs} ($P_{uCs} \leq {}^{-90th}_{ss1}P^{\mathrm{F}}_{uCs}$) are shown for the initial period ($\{{}_{ss1}\theta^{\mathrm{F}}_0\}$) for each and all subjects[F]. (It is to be noted that the percentiles are

based on the initial period: ${}^{-90th}_{ss1}P^{\mathrm{F}}_{uCs}$ not ${}^{-90th}_{ssi}P^{\mathrm{F}}_{uCs}$, i.e. the later period is disregarded since it has already been established that it is the initial period which is of dynamic interest.)

With respect to providing the basis for a symbolic and numerical inter-manoeuvre comparison, Figure 6.7 shows for each subject[F] the measure for the minimum magnitude $P_{uCs} \leq {}^{-90th}_{ss1}P^{\mathrm{F}}_{uCs}$, denoted ${}^{-90th}_{ss1}P^{\mathrm{F}}_{uCsmini}$ may be read and the minimum magnitude ${}^{-90th}_{ss1}P^{\mathrm{F}}_{uCsmini}$ for all subjects[F], denoted ${}^{-90th}_{ss1}P^{\mathrm{F}}_{uCsmin}$, is -1.04 N/kg (subject[9]). The maximum magnitude P_{uCs} for each subject[F], denoted ${}^{-90th}_{ss1}P^{\mathrm{F}}_{uCsmaxi}$ may also be read and the maximum magnitude ${}^{-90th}_{ss1}P^{\mathrm{F}}_{uCsmaxi}$ denoted ${}^{-90th}_{ss1}P^{\mathrm{F}}_{uCsmax}$ is -1.62 N/kg (subject[16]). The mean ${}^{-90th}_{ss1}P^{\mathrm{F}}_{uCsmini} \geq P_{uCs} \geq {}^{-90th}_{ss1}P^{\mathrm{F}}_{uCsmaxi}$ for each subject[F] are indicated by a solid circle and it can be seen that these means are located in the second to third quarters of the intra-subject range. Subject[0], the summary of all subjects, shows the range of ${}^{-90th}_{ss1}P^{\mathrm{F}}_{uCsmin}$ to ${}^{-90th}_{ss1}P^{\mathrm{F}}_{uCsmax}$ and the mean of all the mean ${}^{-90th}_{ss1}P^{\mathrm{F}}_{uCsmini} \geq P_{uCs} \geq {}^{-90th}_{ss1}P^{\mathrm{F}}_{uCsmaxi}$ indicated by a solid circle can be seen to be located centrally in the inter-subject ranges. The inequality ${}^{-90th}_{ss1}P^{\mathrm{F}}_{uCsmini} \geq P_{uCs} \geq {}^{-90th}_{ss1}P^{\mathrm{F}}_{uCsmaxi}$ provides a representative range for each of subjects[F] and the inequality ${}^{-90th}_{ss1}P^{\mathrm{F}}_{uCsmin} \geq P_{uCs} \geq {}^{-90th}_{ss1}P^{\mathrm{F}}_{uCsmax}$ provides a representative range for all subjects[F]. These with the associated numerical values form the basis (for the manoeuvre F (attempted) component) of the inter-manoeuvre comparison at the chapter end.

With respect to variation it can also be seen from Figure 6.7 (page 147) that the range magnitude of 0.58 N/kg i.e. ${}^{-90th}_{ss1}P^{\mathrm{F}}_{uCsmax} - {}^{-90th}_{ss1}P^{\mathrm{F}}_{uCsmin}$ arises from inter-subject variation (subject[9] compared with subject[16]) and is not the result of the ${}^{-90th}_{ss1}P^{\mathrm{F}}_{uCsmaxi} - {}^{-90th}_{ss1}P^{\mathrm{F}}_{uCsmini}$ magnitude of a specific subject. There are therefore substantial differences between subjects for the largest magnitude $P_{uCs} < 0$. The other aspect of variation is variation in the occurrences of largest magnitude P_{uCs} handle-forces. For each subject occurrences of $P_{uCs} \leq {}^{-90th}_{ss1}P^{\mathrm{F}}_{uCs}$ for the initial period are shown above the range line in Figure 6.7. An examination of the data shows (results not presented) that for all subjects[F] for the modified initial period ($\{{}_{ss1a}\theta^{\mathrm{F}}_{0}\}$) there are 23 occurrences of no couple being required ($P_{uCs} = 0$ (integer): see Dynamics Chapter page 97 for the section detailing this effect), 22 of which are produced by subject[4], so the occurrences of largest magnitude P_{uCs} ($P_{uCs} \leq$

${}^{-90th}_{ss1}P^{\mathrm{F}}_{uCs}$) are approximately one tenth of the time duration ($\frac{50}{10} \times t_i(\{_{ss1}\theta^{\mathrm{F}}_0\})$).

6.4.3. *Manoeuvre F (attempted) P_u and P_v*

The same process, without the need to first identify the division of the start-steady period since this has already been achieved for this manoeuvre, is carried for the forward (P_u) and lateral (P_v) handle-force measures using the same division of the start-steady period as was used for the handle-force measure of the couple (P_{uCs}). There are no important further observations of importance to be made in this process, it is simply a repetition of the previous section, and the details are contained in Appendix D; the only difference is that both signs of forward and lateral force need to be accounted for.

6.4.4. *Manoeuvre F (a.) the $P_v - P_{uCs}$ plane*

This final section relating to manoeuvre F (attempted) uses the inequalities, as previously defined, to define a cuboid boundary for the largest magnitude measures for each and all subjects, i.e. this subsection describes the largest handle-force measures occurring during the initial period in terms of a cuboid which encloses the cluster of measures for all subjects and for each subject where the axis of the three dimensions are given by the three handle-force measures.

As some subjects had P_u (see Appendix D) measures in one sign (subjects[2, 12]) and some in two signs this definition requires two sets of three inequalities as follows. For the first set of three inequalities for each of subjects[1,..., 5, 8, 9, 10, 11, 13, 14, 15, 16] the inequalities are:

${}^{-90th}_{ss1}P^{\mathrm{F}}_{uCsmini} \geq P_{uCs} \geq {}^{-90th}_{ss1}P^{\mathrm{F}}_{uCsmaxi}$ (page 145),

${}^{-90th}_{ss1}P^{\mathrm{F}}_{vmini} \geq P_v \geq {}^{-90th}_{ss1}P^{\mathrm{F}}_{vmaxi}$ (page 286) and

${}^{+90th}_{ss1}P^{\mathrm{F}}_{umini} \leq P_u \leq {}^{+90th}_{ss1}P^{\mathrm{F}}_{umaxi}$ (page 283).

For the second set of three inequalities for each of subjects[1, 3, 4, 5, 8,..., 16] the inequalities are as given for P_{uCs} and P_v above and

${}^{-90th}_{ss1}P^{\mathrm{F}}_{umini} \geq P_u \geq {}^{-90th}_{ss1}P^{\mathrm{F}}_{umaxi}$ (page 283).

These two sets of three inequalities define one cuboid boundary for each of subjects[2, 12] and two cuboid boundaries for each of subjects[1, 3, 4, 5, 8, 9, 10, 11, 13, 14, 15, 16]. These two inequality sets provide a representation of

the largest magnitudes of handle-forces for manoeuvre F (a.) for $\{{}_{ss1}\theta_0^{\mathrm{F}}\}$ for each subject. These one set or two sets of three inequalities are denoted ${}^{large}_{ss1}\mathbf{P}_i^{\mathrm{F}}$ where i indicates the subject index. In words ${}^{large}_{ss1}\mathbf{P}_i^{\mathrm{F}}$ indicates the minimum and maximum magnitude values of the largest handle-forces for the initial period for manoeuvre F (attempted) for each subject.

A graphical representation of ${}^{large}_{ss1}\mathbf{P}_i^{\mathrm{F}}$ in the $P_v - P_{uCs}$ plane is shown in Figure 6.8 (page 151): the construction is as follows. For each subject[F] the four vertices of a rectangle are formed with a $[P_v, P_{uCs}]$ coordinate as follows: $[{}^{-90th}_{ss1}P^{\mathrm{F}}_{vmini}, {}^{-90th}_{ss1}P^{\mathrm{F}}_{uCsmini}]$, $[{}^{-90th}_{ss1}P^{\mathrm{F}}_{vmaxi}, {}^{-90th}_{ss1}P^{\mathrm{F}}_{uCsmini}]$, $[{}^{-90th}_{ss1}P^{\mathrm{F}}_{vmaxi}, {}^{-90th}_{ss1}P^{\mathrm{F}}_{uCsmaxi},]$, and $[{}^{-90th}_{ss1}P^{\mathrm{F}}_{vmini}, {}^{-90th}_{ss1}P^{\mathrm{F}}_{uCsmaxi}]$.

Two sets of inequalities define the cuboid boundaries which enclose the measures for all, rather than each of, subjects[F] and this is achieved by removal of the i subscript from the above definitions as follows. For the first set of three inequalities for all of subjects[1,..., 5, 8, 9, 10, 11, 13, 14, 15, 16] the inequalities are:

${}^{-90th}_{ss1}P^{\mathrm{F}}_{uCsmin} \geq P_{uCs} \geq {}^{-90th}_{ss1}P^{\mathrm{F}}_{uCsmax}$ (page 145),

${}^{-90th}_{ss1}P^{\mathrm{F}}_{vmin} \geq P_v \geq {}^{-90th}_{ss1}P^{\mathrm{F}}_{vmax}$ (page 286) and

${}^{+90th}_{ss1}P^{\mathrm{F}}_{umin} \leq P_u \leq {}^{+90th}_{ss1}P^{\mathrm{F}}_{umax}$ (page 283).

For the second set of three inequalities for all of subjects[1, 3, 4, 5, 8,..., 16] the inequalities are as given for P_{uCs} and P_v above and

${}^{-90th}_{ss1}P^{\mathrm{F}}_{umin} \geq P_u \geq {}^{-90th}_{ss1}P^{\mathrm{F}}_{umax}$ (page 283)).

These two sets of three inequalities relating to all subjects[F] are denoted ${}^{large}_{ss1}\mathbf{P}^{\mathrm{F}}$. The numerical values for ${}^{large}_{ss1}\mathbf{P}^{\mathrm{F}}$ are therefore, as detailed in Sections 6.4.2 (Page 145), D.2.2 (Page 286) and D.2.1 (Page 283), respectively:

$-1.04 \geq P_{uCs} \geq -1.62$ (N/kg),

$-0.38 \geq P_v \geq -0.72$ (N/kg),

$0.06 \leq P_u \leq 0.73$ (N/kg) and

$-0.08 \geq P_u \geq -0.33$ (N/kg).

In conclusion ${}^{large}_{ss1}\mathbf{P}^{\mathrm{F}}$ provides a succinct and useful representation of the boundaries of the largest handle-forces for all subjects[F] for manoeuvre F (attempted) which will allow unambiguous symbolic comparison with other manoeuvres.

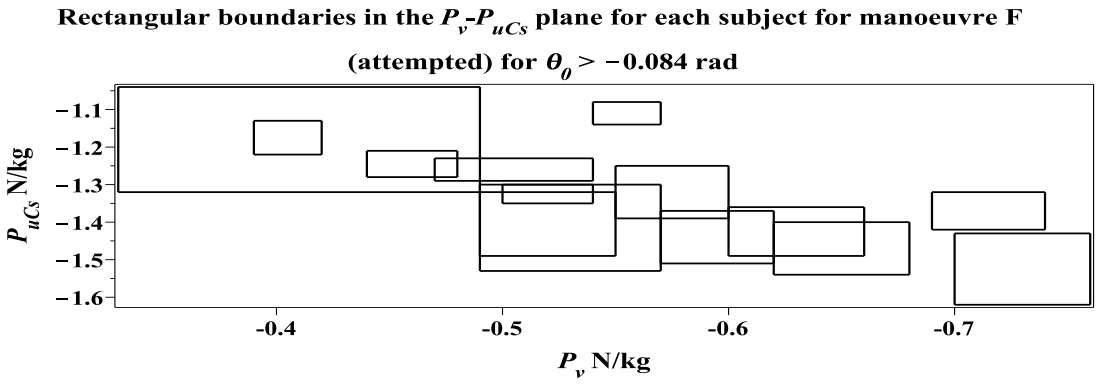

Figure 6.8 – Rectangles formed with vertices of coordinates $[{}^{-90th}_{ss1}P^{\mathrm{F}}_{vmini}, {}^{-90th}_{ss1}P^{\mathrm{F}}_{uCsmini}]$, $[{}^{-90th}_{ss1}P^{\mathrm{F}}_{vmaxi}, {}^{-90th}_{ss1}P^{\mathrm{F}}_{uCsmini}]$, $[{}^{-90th}_{ss1}P^{\mathrm{F}}_{vmaxi}, {}^{-90th}_{ss1}P^{\mathrm{F}}_{uCsmaxi},]$, and $[{}^{-90th}_{ss1}P^{\mathrm{F}}_{vmini}, {}^{-90th}_{ss1}P^{\mathrm{F}}_{uCsmaxi}]$ for all subjects[F]: n=14. In loose terms this figure shows the distribution of the maximum and minimum limits (rectangles) for each subject for this manoeuvre when the largest magnitudes of lateral handle-force (P_v) and handle-force measure of the couple (P_{uCs}) are considered.

In words ${}^{large}_{ss1}\mathbf{P}^{\mathrm{F}}$ indicates the minimum and maximum magnitude values for the largest handle-forces for the initial period for manoeuvre F (attempted) where the maximum and minimum values are for all subjects.

6.5. **Summary of Results**

In this section the results for each manoeuvre are combined in order to show their inter-relationships and relate these inter-relationships to the load measures. In Section 6.4 (page 144) the representation of the largest handle-forces for each subject, denoted ${}^{large}_{ss1}\mathbf{P}^{\mathrm{F}}_{i}$, are graphed in the $P_v - P_{uCs}$ (N/kg) plane for each manoeuvre; in Figure 6.9 (page 158) these eleven results are combined. A number of observations about the inter-relationship of the manoeuvres follow. (The maximum comfortable load measure (L^{r}_{Mnormm}) is shown in the legend rectangles and this will be considered in detail later in this chapter.)

6.5.1. *Qualitative summary of results*

Before proceeding it is useful to provide a qualitative over view of Figure 6.9 which, as it encapsulates all the important results of a complex system, is unavoidably complicated. It should be noted that in this and other related figures in order to maintain the lateral force (P_v) with positive to the left as used in the Dynamics Chapter the horizontal scale goes from right (negative) to left (positive).

As previously described for manoeuvre F (attempted) each rectangle indicates the minimum and maximum magnitude for the largest handle-force measures for the lateral force (P_v) and force measure of the couple (P_{uCs}). It can be seen that in general terms for the different manoeuvres, as indicated by the different colour lines and line type, different line types either cluster together or occupy a similar place on the graph, for example, all the thick lined rectangles (manoeuvres [K, L] (attempted)) are in approximately the same location and additionally both of these manoeuvres attracted the largest maximum comfortable load. In loose terms this figure demonstrates that in order to balance the motion resistance effects, different handle-forces are required and these different handle-forces produce different maximum comfortable load responses. In loose terms manoeuvres [K, L] (thick lines) may be thought of as easy for the subject and manoeuvres [F, C, I] (bottom right corner) may be thought of as difficult, i.e. manoeuvres which require similar handle-force measures are associated with similar levels, hard or easy, of loads. As these manoeuvres have distinct space requirements these findings, as will discussed, are important for adaptation planning. (The non-technical reader may wish to proceed to the Conclusion of Results page 162.)

6.5.2. *Detailed summary of results*

This subsection provides a rigorous account of the results on which the qualitative summary of the previous section is based; it is therefore possible to proceed to the Results Conclusion Section without loss of comprehension of the Discussion Chapter. The legend, top right quadrant, represents the eleven manoeuvres by rectangles with varying colours and line styles. With respect to the P_u component of the ${}^{large}_{ss1}\mathbf{P}^r_i$, the rectangular boundaries are coloured as follows: manoeuvres [A, B, C, K] (a.) which have no inequality for $P_u < 0$ are red, manoeuvres [D, E, F, L] (a.) which have an inequality in both signs for P_u are black and manoeuvres [G, H, I] (a.) which have no inequality for $P_u > 0$ are blue. The legend is arranged so that that manoeuvres [A, B, C, D, E, F, G, H, I] (a.) are positioned in their region position (page 63) and four line types distinguish the ${}^{large}_{ss1}\mathbf{P}^r_i$ with respect to region position or, alternatively, P_v sign component: manoeuvres [A, D, G] (a.) have no $P_v < 0$ are a solid line, manoeuvres [B, E, H] (a.) have P_v components in both signs are dotted lines, manoeuvres [F, C, I] (a.) have no $P_v > 0$ are dashed

lines and finally manoeuvres [K, L] (a.) are thick solid lines.

Firstly, it is evident from Figure 6.9 (page 158) that the ${}^{large}_{ss1}\mathbf{P}^{\mathrm{C}}_i$, ${}^{large}_{ss1}\mathbf{P}^{\mathrm{F}}_i$ and ${}^{large}_{ss1}\mathbf{P}^{\mathrm{I}}_i$ cluster in the same area of the $P_v - P_{uCs}$ plane ($P_{uCs} \leq -0.31$, $P_v \leq -0.33$ N/kg). However, the inequality for the P_u measures for these three representative measures have different combinations of P_u signs as indicated by the colours. This is illustrated in Figure 6.10 (page 159) which shows the ${}^{large}_{ss1}\mathbf{P}^{\mathrm{C}}_i$, ${}^{large}_{ss1}\mathbf{P}^{\mathrm{F}}_i$ and ${}^{large}_{ss1}\mathbf{P}^{\mathrm{I}}_i$ in the $P_{uCs} - P_u$ plane rather than the $P_v - P_{uCs}$ plane. As indicated in the key for Figure 6.10 (right side) the colour and line style representation as used for Figure 6.9 (page 158) is maintained. It is evident that while the ${}^{large}_{ss1}\mathbf{P}^{\mathrm{C}}_i$ and ${}^{large}_{ss1}\mathbf{P}^{\mathrm{I}}_i$ overlap in the $P_v - P_{uCs}$ plane they are separated in the $P_{uCs} - P_u$ plane. Some inter-penetration of ${}^{large}_{ss1}\mathbf{P}^{\mathrm{C}}$ and ${}^{large}_{ss1}\mathbf{P}^{\mathrm{F}}$ is also evident though the central locations appear to be different.

Secondly, it is evident from Figure 6.9 (page 158) that the ${}^{large}_{ss1}\mathbf{P}^{\mathrm{A}}_i$, ${}^{large}_{ss1}\mathbf{P}^{\mathrm{D}}_i$ and ${}^{large}_{ss1}\mathbf{P}^{\mathrm{G}}_i$ cluster in the same area of the $P_v - P_{uCs}$ plane ($P_v \geq 0.28$, $P_{uCs} \geq 0.09$) N/kg. However, the inequality for the P_u measures for these three representative measures have different combinations of P_u signs as indicated by the colours. This is illustrated in Figure 6.11 (page 159) which shows the ${}^{large}_{ss1}\mathbf{P}^{\mathrm{A}}_i$, ${}^{large}_{ss1}\mathbf{P}^{\mathrm{D}}_i$ and ${}^{large}_{ss1}\mathbf{P}^{\mathrm{G}}_i$ in the $P_{uCs} - P_u$ plane. As indicated in the key for Figure 6.11 (right side) the colour and line style representation as used for Figure 6.9 (page 158) is maintained. It is evident from the $P_{uCs} - P_u$ plane view that the ${}^{large}_{ss1}\mathbf{P}^{\mathrm{G}}_i$ do not overlap the ${}^{large}_{ss1}\mathbf{P}^{\mathrm{A}}_i$ or the ${}^{large}_{ss1}\mathbf{P}^{\mathrm{D}}_i$. However, there is an inter-penetration between the ${}^{large}_{ss1}\mathbf{P}^{\mathrm{D}}$ and ${}^{large}_{ss1}\mathbf{P}^{\mathrm{A}}$ though the central location of the latter population appears to have a more positive P_u position.

Thirdly, it is evident from Figure 6.9 (page 158) that the ${}^{large}_{ss1}\mathbf{P}^{\mathrm{E}}$ (black dotted) do not overlap any the other measures in the $P_v - P_{uCs}$ plane. For the purpose of avoiding any ambiguity arising from black and blue colour reproduction it is to be noted that the ${}^{-90th}_{ss1}P^{\mathrm{E}}_{uCsmin}$= -0.95 N/kg where as the ${}^{-90th}_{ss1}P^{\mathrm{H}}_{uCsmax}$= -0.87 N/kg. Also ${}^{large}_{ss1}\mathbf{P}^{\mathrm{E}}$ is clearly separated from ${}^{large}_{ss1}\mathbf{P}^{\mathrm{F}}$ in the $\hat{\boldsymbol{v}}$ direction as the latter has larger magnitude.

Fourthly, it is evident from Figure 6.9 (page 158) that the ${}^{large}_{ss1}\mathbf{P}^{\mathrm{K}}_i$ and ${}^{large}_{ss1}\mathbf{P}^{\mathrm{L}}_i$ are clustered together in the $P_v - P_{uCs}$ plane ($-0.68 \geq P_{uCs} \leq 0$ N/kg and $0.29 \leq$

$P_v \leq 0.54$ N/kg). Some overlap with the ${}^{large}_{ss1}\mathbf{P}^{\mathrm{B}}_i$ and ${}^{large}_{ss1}\mathbf{P}^{\mathrm{H}}_i$ is evident on this plane. Figure 6.12 (page 160) shows the ${}^{large}_{ss1}\mathbf{P}^{\mathrm{K}}_i$, ${}^{large}_{ss1}\mathbf{P}^{\mathrm{L}}_i$, ${}^{large}_{ss1}\mathbf{P}^{\mathrm{H}}_i$ (for $P_v > 0$) and ${}^{large}_{ss1}\mathbf{P}^{\mathrm{B}}_i$ in the $P_v - P_u$ plane. As indicated in the legend for Figure 6.12 (right side) the colour and line style representation as used for Figure 6.9 (page 158) is maintained apart from the thickness of the red rectangle for the ${}^{large}_{ss1}\mathbf{P}^{\mathrm{K}}_i$ which is graphed with a thinner line as this assists discrimination from the ${}^{large}_{ss1}\mathbf{P}^{\mathrm{B}}_i$. It is evident from Figure 6.12 that the ${}^{large}_{ss1}\mathbf{P}^{\mathrm{K}}$ (red solid) are separated from the ${}^{large}_{ss1}\mathbf{P}^{\mathrm{L}}$ (black solid), on the $P_v - P_u$ plane: ${}^{+90th}_{ss1}P^{\mathrm{K}}_{umin}$ is greater than ${}^{+90th}_{ss1}P^{\mathrm{L}}_{umax}$. It is also evident that the ${}^{large}_{ss1}\mathbf{P}^{\mathrm{L}}$ (black solid) are separated from the ${}^{large}_{ss1}\mathbf{P}^{\mathrm{H}}$ (blue dot) on the $P_v - P_u$ plane: the magnitude of ${}^{-90th}_{ss1}P^{\mathrm{L}}_{umax}$ is smaller than the magnitude of ${}^{-90th}_{ss1}P^{\mathrm{H}}_{umin}$. It can also be seen that an overlap occurs between the ${}^{large}_{ss1}\mathbf{P}^{\mathrm{K}}$ (red solid) and the ${}^{large}_{ss1}\mathbf{P}^{\mathrm{B}}$ (red dot). However, only one of the ${}^{large}_{ss1}\mathbf{P}^{\mathrm{B}}_i$, centroid located at $P_v \approx 0.34$ and $P_u \approx 0.39$, is located in the interior of the ${}^{large}_{ss1}\mathbf{P}^{\mathrm{K}}$: the ${}^{large}_{ss1}\mathbf{P}^{\mathrm{K}}_i$ and ${}^{large}_{ss1}\mathbf{P}^{\mathrm{B}}_i$ appear to be distinct populations.

The visual impression of distinct populations of measures for each manoeuvre by can be statistically confirmed as follows. As examination of the ${}^{large}_{ss1}\mathbf{P}^{r}_i$ measures shows varying and non-normal distributions the Sign Test is used to determine $99^{\%}$ confidence intervals for the median location for each handle-force. Where a ${}^{large}_{ss1}\mathbf{P}^{r}_i$ is comprised of a handle-force with inequalities in both signs the confidence interval is established separately for the negative and positive component: when graphed the two components are discriminated by appending a '+' and or '−' to the manoeuvre label. The results are shown for the $P_v - P_{uCs}$ plane in Figure 6.13 (Page 160). It can be seen that only manoeuvres [A, D] (a.) overlap. The process is repeated for $P_{uCs} - P_u$ plane and this is graphed in Figure 6.14 (Page 161) where it can be seen that no overlaps occur. It is therefore concluded for all manoeuvres that, the representative largest measures for the manoeuvres r (a.) (${}^{large}_{ss1}\mathbf{P}^{r}_i$) have at least one of the three handle-force measure components arising from a different population. There are two points to note regarding this result. Firstly, this occurs despite the extensive and substantial inter-subject variations which have been noted. Thus attempting a specific manoeuvre has a more substantial effect on the measures than the inter-subject variation. Secondly, the extent to which the manoeuvre r (a.) achieved the kinematic intention as defined for

manoeuvre r has not been considered in the results. So, even without data indicating the extent to which the kinematics intention was achieved the attempt at manoeuvre r is sufficient to produce distinct populations of measures.

Figure 6.9 (page 158) also shows the median load measure for each manoeuvre L^r_{Mnormm} (as defined, page 134). It has already been established that maximum comfortable load ranking is statistically significant: from small to largest [F ,C , I, G, A, D, B, E, H, L, K] (a.). This ranking will now be related to the handle-force measures.

Firstly, the three smallest L^r_{Mnormm} are manoeuvres [F, C, I] (a.): the range for L^r_{Mnormm} (r =[F, C, I]) range is $47-53\%$. The magnitudes of the ${}^{-90th}_{ss1}P^{\mathrm{C}}_{vmini}$, ${}^{-90th}_{ss1}P^{\mathrm{F}}_{vmini}$ and ${}^{-90th}_{ss1}P^{\mathrm{I}}_{vmini}$ are, with one exception, larger than the ${}^{-90th}_{ss1}P_{vmaxi}$ of the other manoeuvres: the exception is ${}^{-90th}_{ss1}P^{\mathrm{H}}_{vmaxi}$ (subject[11]). Also, the magnitude of the ${}^{-90th}_{ss1}P^{r}_{uCsmin}$ r =[F, C, I] are progressively larger, I then C then F. The ${}^{large}_{ss1}\mathbf{P}^{\mathrm{F}}_{i}$ has the largest magnitude ${}^{-90th}_{ss1}P_{vmin}$ and the largest magnitude ${}^{-90th}_{ss1}P_{uCsmin}$ and it has the smallest L^r_{Mnormm} (47%).

Secondly, as can be seen in Figure 6.9 (page 158), the ${}^{large}_{ss1}\mathbf{P}^{\mathrm{A}}$, ${}^{large}_{ss1}\mathbf{C}^{\mathrm{D}}$ and ${}^{large}_{ss1}\mathbf{P}^{\mathrm{G}}$ have a distinct location in the $P_v - P_{uCs}$ plane since $P_{uCs} > 0$. The associated L^r_{Mnormm} (r =[A D, G]) range is $61-74\%$: these load measures occupy the next three ranks above the load measures for manoeuvres [F, C, I] (a.).

Thirdly, as can be seen from Figure 6.9 (page 158) and Figure 6.12 (page 160), while the ${}^{large}_{ss1}\mathbf{P}^{\mathrm{B}}$ and ${}^{large}_{ss1}\mathbf{P}^{\mathrm{H}}$ do not inter-penetrate, the ${}^{large}_{ss1}\mathbf{P}^{\mathrm{B}}$ and ${}^{large}_{ss1}\mathbf{P}^{\mathrm{H}}$ overlap in the $P_v - P_{uCs}$ plane so it is logical to consider these together. The ${}^{\pm 90th}_{ss1}P^{\mathrm{B}}_{vmax}$ are of smaller magnitude than the other ${}^{\pm 90th}_{ss1}P_{vmax}$. While the magnitudes of ${}^{-90th}_{ss1}P^{\mathrm{H}}_{vmax}$ and ${}^{+90th}_{ss1}P^{\mathrm{H}}_{vmax}$ are not as small as those for manoeuvre B (a.) they are smaller than those of all other manoeuvres apart from manoeuvre E (a.). The associated L^r_{Mnormm} (r =[B, H]) are $73-80\%$ and this overlaps L^{D}_{Mnormm}.

Fourthly, it is evident from Figure 6.9 (page 158) that the measures for manoeuvre E (a.) have a distinct location in the $P_v - P_{uCs}$ plane. Only the magnitude of ${}^{-90th}_{ss1}P^{\mathrm{F}}_{uCsmin}$ is larger than ${}^{-90th}_{ss1}P^{\mathrm{E}}_{uCsmin}$ and the spread in the $\hat{\boldsymbol{v}}$ and the $-\hat{\boldsymbol{v}}$ directions is similar to ${}^{large}_{ss1}\mathbf{P}^{\mathrm{B}}_{i}$. The L^{E}_{Mnormm} is 74% and this load measure is shared by manoeuvre D (a.).

Fifthly and finally, it is evident from Figure 6.9 that manoeuvres [K, L] (a.) occupy the same area on the $P_v - P_{uCs}$ plane. The ${}^{+90th}_{ss1}P^{\mathrm{K}}_{vmin}$ and ${}^{+90th}_{ss1}P^{\mathrm{L}}_{vmin}$ are larger than any other ${}^{+90th}_{ss1}P_{vmin}$ for $P_{uCs} < 0$ apart from one subject for manoeuvre B (a.), centroid located at $[P_v, P_{uCs}] \approx [0.34, -0.29]$. The associated L^r_{Mnormm} (r =[K, L]) measure is 100% for both manoeuvres. It is noteworthy that though the largest L^r_{Mnormm} is associated with manoeuvres [L, K] (a.) an examination of Figure 6.9 (page 158) and Figure 6.12 (page 160) shows that apart from one subject the ${}^{large}_{ss1}\mathbf{P}^{\mathrm{B}}_i$ measures are smaller than the the ${}^{large}_{ss1}\mathbf{P}^{\mathrm{K}}_i$ measures and yet $L^{\mathrm{B}}_{Mnormm} = 73\%$.

There is an apparent association between load measures (L^r_{Mnormm}) and the ${}^{large}_{ss1}\mathbf{P}^r$. As both load and handle-force measures distributions are non-normal and different, a contingency table provides a suitable means of statistical examination as follows. It has been established that the largest rank measure steps occur between manoeuvres [I, G] (a.) and between manoeuvres [H, L] (a.) (page 137). It therefore follows that one approach is to disregard manoeuvres [K, L] (a.), ($L^K_{Mnormm} = L^L_{Mnormm} = 100\%$) as these manoeuvres are associated with the largest load choices, and select a load measure to dichotomise the remaining L^r_{Mnormi}. As it has already been established there is a very low probability that the handle-force measures for each manoeuvre originate from the same populations, the second dichotomy may be viewed in terms of handle-force measures or manoeuvres: the latter approach is more concise since inter-penetrations of ${}^{large}_{ss1}\mathbf{P}^r$ may be disregarded. The contingency table for a dichotomising percentage load measure set to 48.6% is shown in Table 6.3 (page 157). With test statistic p, the resulting $p \approx 0$ of no association confirms the visual impression that the association between manoeuvres [F, C, I] (a.) or viewed in terms of handle-force measures $P_v \leq -0.33$ (N/kg) and low L^r_{Mnormi} is not a random result.

The process is repeated taking account that the rank step for manoeuvres [H, L] (a.) is also relatively large. On this test, manoeuvres [F, C, I] (a.) are disregarded and the dichotomy is between manoeuvres [G, A, D, B, E, H] (a.) and [K , L] (a.). The contingency table for a dichotomising percentage load measure set to 92.2% is shown in Table 6.4 (page157). The resulting $p \approx 0$ of no association confirms the visual impression that the association between manoeuvres [K, L] (a.)

		Manoeuvres	
		r =GADBEH	r =FCI
Load Choice	$L^r_{Mnormi} \leq 48.6\%$	4	22
	$L^r_{Mnormi} > 48.6\%$	89	24

Table 6.3 – Contingency table (excluding manoeuvres [K, L] (a.)) comprising of firstly, rows indicating the frequency of maximum comfortable load for each subject for each manoeuvre as a percentage of the subject's global maximum comfortable load dichotomised about 48.6% into low and not-low measures and secondly columns dichotomised by manoeuvres [F, C, I] and [G, A, D, B, E, H] (a.). $\chi^2 = 38.34$, $p \approx 0$

		Manoeuvres	
		$r = KL$	$r = GADBEH$
Load Choice	$L^r_{Mnormi} \leq 92.2\%$	4	84
	$L^r_{Mnormi} > 92.2\%$	72	11

Table 6.4 – Contingency table (excluding manoeuvres [F, C, I] (a.)) comprising of firstly, rows indicating the frequency of maximum comfortable load for each subject for each manoeuvre as a percentage of the subject's global maximum comfortable load dichotomised about 92.2% into a high and not-high measures and secondly columns dichotomised by manoeuvres [K, L] and [G, A, D, B, E, H] (a.). $\chi^2 = 116.9$, $p \approx 0$

or viewed in terms of handle-force measures $P_v - P_{uCs}$ plane ($-0.68 \leq P_{uCs} \leq 0$ and $0.29 \leq P_v \leq 0.54$) (N/kg) and larger loads is improbably explained by random results.

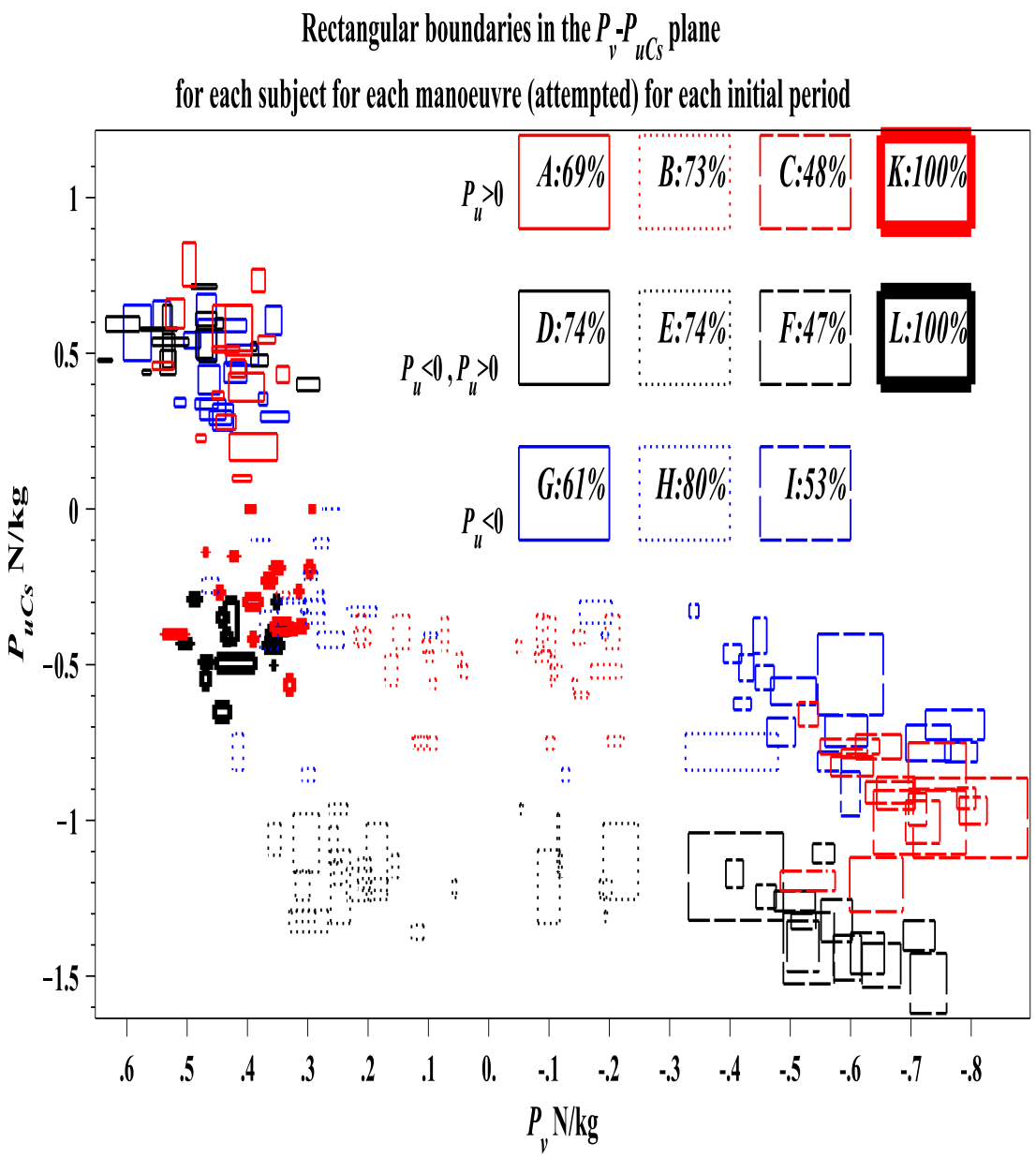

Figure 6.9 – Shows: the eleven ${}^{large}_{ss1}\mathbf{P}^r_i$ results graphed together on the $P_v - P_{uCs}$ plane. The legend indicates by colour manoeuvres [A, B, C, K] (a.) which have no inequality for $P_u < 0$ (red), manoeuvres [D, E, F, L] (a.) which have an inequality in both signs for P_u (black) and manoeuvres [G, H, I] (a.) which have no inequality for $P_u > 0$ (blue) and by line-styles manoeuvres [A, D, G, K, L] (a.) which have no inequality for $P_v < 0$ (solid), manoeuvres [B, E, H] (a.) which have an inequality in both signs for P_v (dotted) and manoeuvres [C, F, I] (a.) which have no inequality for $P_v > 0$ (dashed). The load measures L^r_{Mnormm} are indicated in the legend for each manoeuvre. Each rectangle indicates the minimum and maximum magnitude for the largest handle-force measures for the lateral force (P_v) and force measure of the couple (P_{uCs}). It can be seen that in general terms for the different manoeuvres, as indicated by the different colour lines and line type, different line types either cluster together or occupy a similar place on the graph, for example, all the thick lined rectangles (manoeuvres [K, L] (attempted)) are in approximately the same location and additionally both of these manoeuvres attracted the largest maximum comfortable load. In loose terms this figure demonstrates that in order to balance the motion resistance effects, different handle-forces are required and these different handle-forces produce different maximum comfortable load responses.

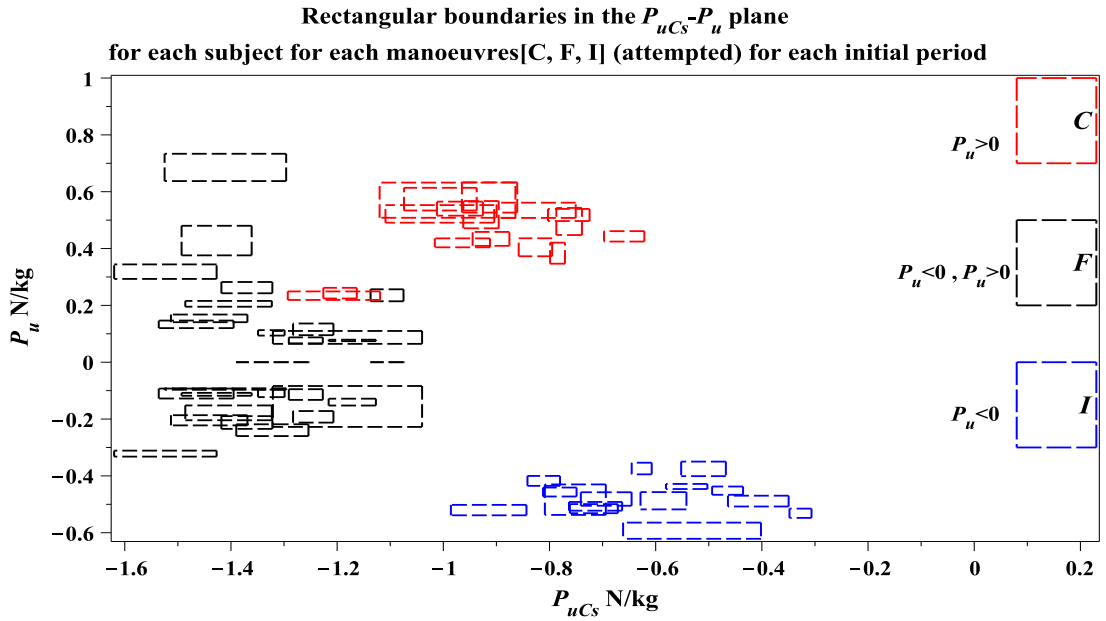

Figure 6.10 – Shows: ${}^{large}_{ss1}\mathbf{P}_i^r$ (r=[F, C ,I] results graphed together on the $P_{uCs} - P_u$ plane with manoeuvre C (a.) (red), manoeuvre F (a.) (black) and manoeuvre I (a.) blue

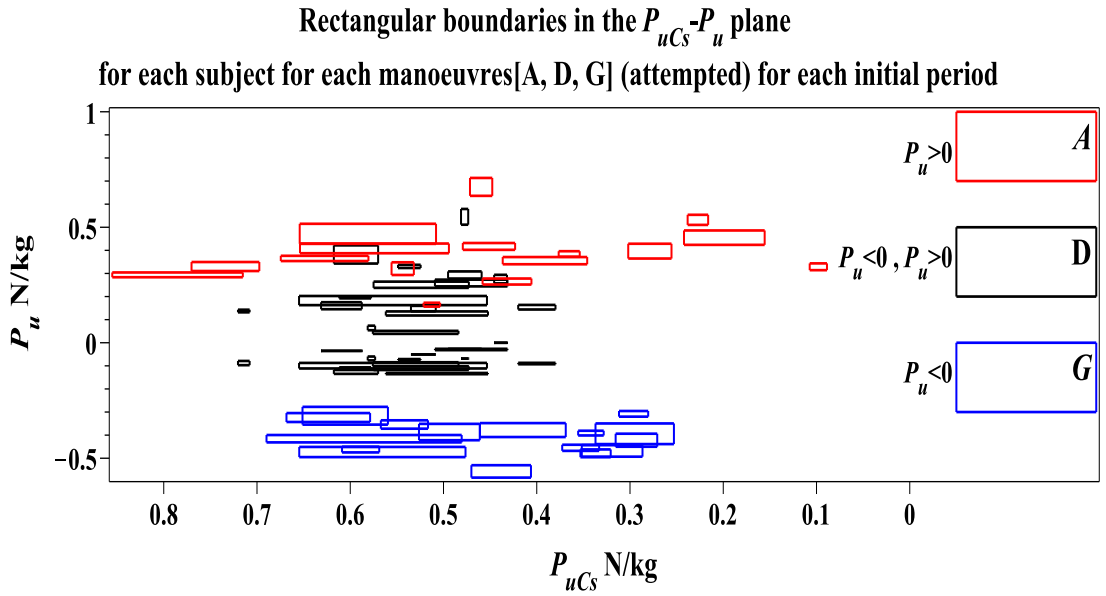

Figure 6.11 – Shows: ${}^{large}_{ss1}\mathbf{P}_i^r$ (r=[A, D ,G] results graphed together on the $P_v - P_u$ plane with manoeuvre A (a.) (red), manoeuvre D (a.) (black) and manoeuvre G (a.) (blue) ($P_v > 0$)

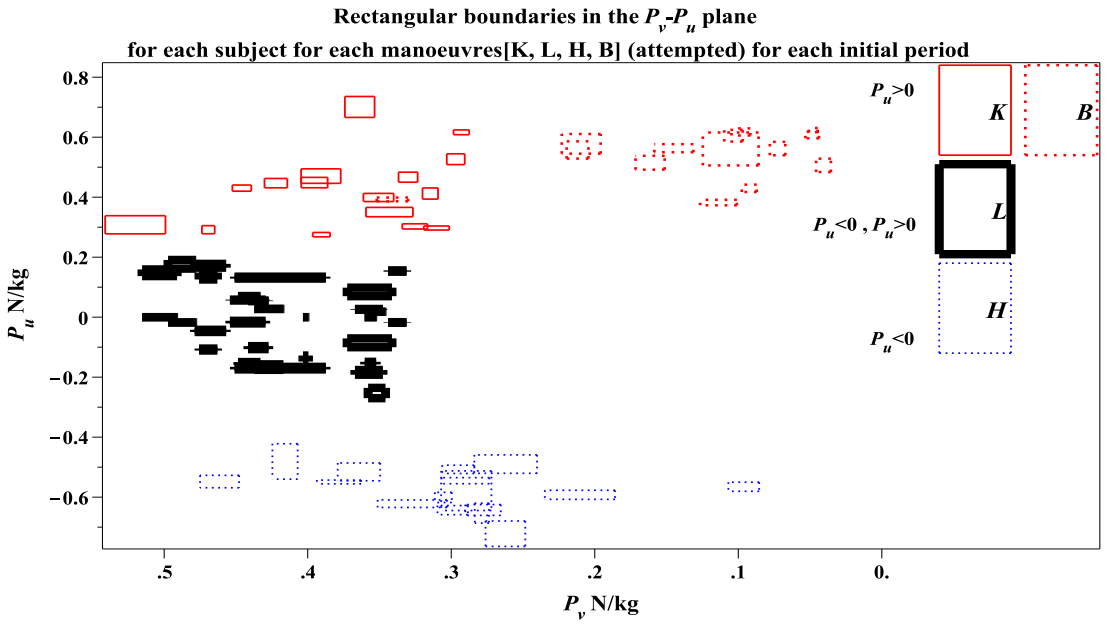

Figure 6.12 – Shows: ${}^{large}_{ss1}\mathbf{P}^r_i$ (r=[K, B, L, H]) results graphed together on the $P_v - P_u$ plane with manoeuvre C (a.) (red), manoeuvre F (a.) (black) and manoeuvre I (a.) blue

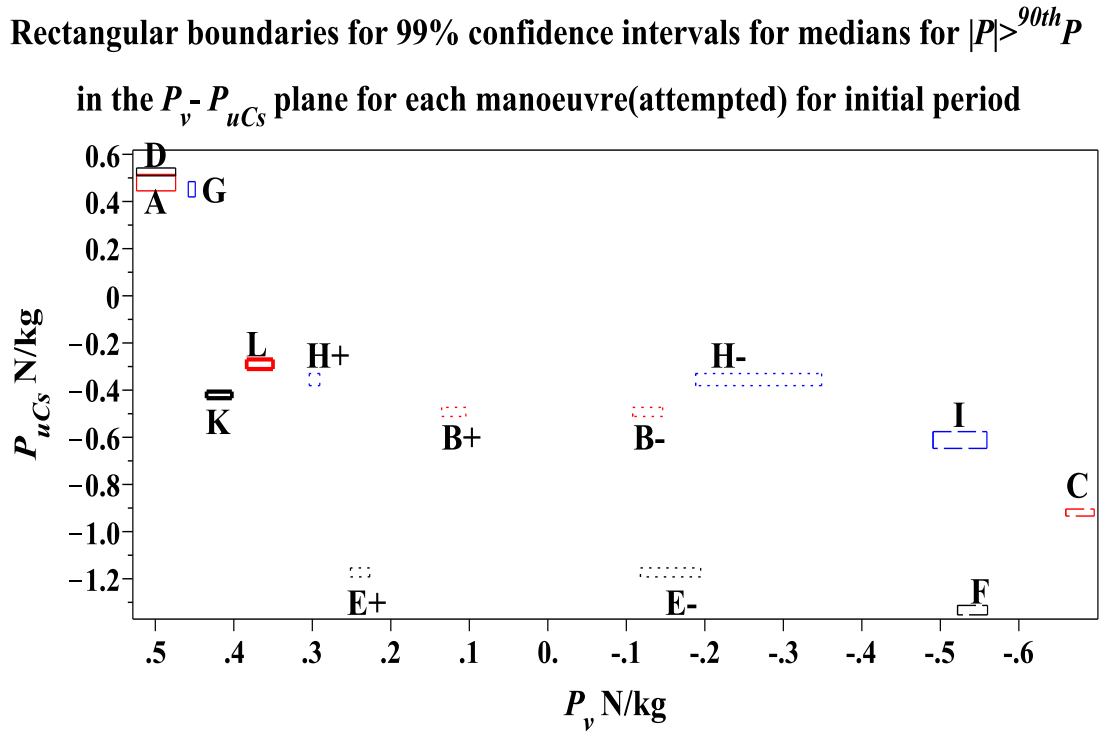

Figure 6.13 – Rectangular boundaries constructed from the upper and lower $99^{\%}$ confidence intervals for medians for each of manoeuvres: for $P_v \geq {}^{+90th}_{ss1}P^r_{vmin}$ for manoeuvres [A, D, B, E, G, H, K, L] (a.), for $P_v \leq {}^{-90th}_{ss1}P^r_{vmin}$ for manoeuvres [B, C, E, H, I, F] (a.), for $P_{uCs} \geq {}^{+90th}_{ss1}P^r_{uCsmin}$ for manoeuvres [A, D, G] (a.) and for $P_{uCs} \leq {}^{-90th}_{ss1}P^r_{uCsmin}$ for manoeuvres [B, C, E, F, G, H, I, K, L] (a.) shown on the $P_v - P_{uCs}$ plane with manoeuvres with measures in both signs of P_v discriminated with a + and −.

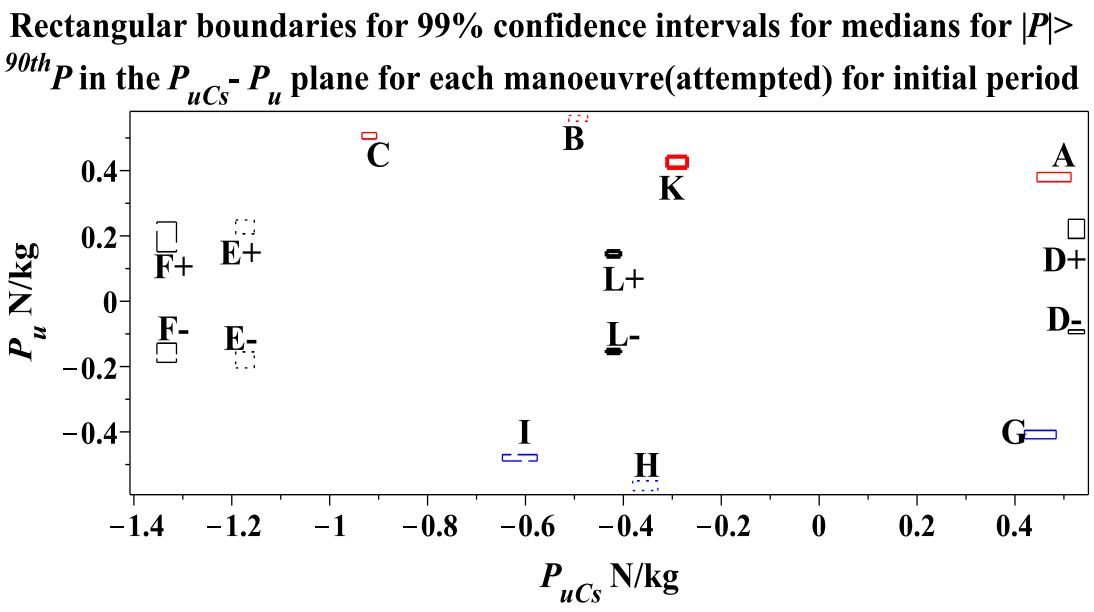

Figure 6.14 – Rectangular boundaries constructed from the upper and lower $99^{\%}$ confidence intervals for medians for each of manoeuvres: for $P_u \geq {}^{+90th}_{ss1}P^r_{umin}$ for manoeuvres [A, B, C, D, E, F, K, L] (a.), for $P_u \leq {}^{-90th}_{ss1}P^r_{umin}$ for manoeuvres [D, E, F, G, H, I, L] (a.), for $P_{uCs} \geq {}^{+90th}_{ss1}P^r_{uCsmin}$ for manoeuvres [A, D, G] (a.) and for $P_{uCs} \leq {}^{-90th}_{ss1}P^r_{uCsmin}$ for manoeuvres [B, C, E, F, G, H, I, K, L] (a.) shown on the $P_{uCs} - P_u$ plane with manoeuvres with measures in both signs of P_u discriminated with a $+$ and $-$.

6.6. **Conclusion of Results**

There are four major results. Firstly, the L^r_{Mnormm} for the manoeuvres (a.) have a rank order from small to large of [F, C, I, G, A, D, B, E, H, K, L]. Secondly, viewed as three sets [F, C, I], [G, A, D, B, E, H] and [K, L] these are associated with small, medium and large loads respectively. Thirdly, these loads are associated with different handle-force measure areas in the $P_v - P_{uCs}$ plane where, in loose terms, relatively large positive P_v combined with relatively small P_{uCs} measures are associated with large loads, relatively large magnitude negative P_v in conjunction with relatively large magnitude negative P_{uCs} are associated with relatively small loads and other combinations are associated with medium loads. Fourthly and finally, these three results occur in the presence of inter-subject variation. In loose terms the key result is that manoeuvres [K, L] were easiest and manoeuvres [F, C, I] were hardest for subjects and hence attracted relatively large and relatively small loads, respectively. Additionally, despite intra-subject differences in handle-force measures the inter-manoeuvre differences are so large that inter-subject differences are of lessor importance compared with inter-manoeuvre differences.

Chapter 7–Discussion

7.1. **Introduction**

This chapter has six components. The first component demonstrates the robustness of a summarising explanation of the results. The second component demonstrates that the results have important adaptation planning implications. The third component presents ergonomic, and health and safety implications. The fourth component considers the generalisation of the results. The fifth component considers further work on the existing data. The sixth and final component sets out some aspects of further work which follow from the results.

7.2. **Summarising Explanation**

The results (Figure 6.9 page 158) indicate substantial differences between some manoeuvres r (attempted): both mechanical and operator load response differences are found. With respect to the mechanical differences, substantially different handle-force measures were found as represented by the handle-force measure ${}^{large}_{ss1}\mathbf{P}^{r}$. With respect to the differences in operator load responses, substantially different load choices were found. On the basis of these findings the following summarising explanation of the forces-applied and space-required relationship for four-caster manual vehicle manoeuvres is made: 1) varying the manoeuvre r (a.) varies the experimental-FCMV motion resistance response which 2) varies the forces required (the handle-forces) which 3) varies the operator load response (the load selections). The primary task is therefore to demonstrate that the evidence for this conclusion is strong and that the counter evidence is weak. There are therefore three parts, the three links in this causal chain, to making this demonstration and these will follow the claimed causal order.

Firstly, related to the manoeuvre r (a.) variation it will be shown that while there is considerable uncertainty as to the extent to which the [sgn($\dot{\theta}_{si}$),sgn($\dot{\theta}_{ti}$)] (rot-roll directions) combinations conform to the Zmodel-FCMV [sgn($\dot{\theta}_{si}$),sgn($\dot{\theta}_{ti}$)] combinations, there is strong evidence that the relationship between the kinematics and motion resistance which is present in the Zmodel-FCMV is present in the results: the inter-manoeuvre handle-force measure differences are related to $\boldsymbol{P}_{Qi}$ orientation differences, i.e. ${}^{B}\theta_{si} + \rho_i$. (This relationship is illustrated for the Zmodel-FCMV for manoeuvres r=[A, E], Figure 4.17, page 93.) Thus, the Zmodel-FCMV and experimental-FCMV results are coherent. This demonstration is unavoidably lengthened, though not undermined, by the need to circumvent uncertainty regarding [sgn($\dot{\theta}_{si}$),sgn($\dot{\theta}_{ti}$)] in the data. As part of this demonstration it is also shown that both the quasi-static assumption and the disregard of caster assembly dynamics is justified.

Secondly, related to the causal link between motion resistance effects and handle-forces, it is demonstrated that the approximation of the handle-force application point is insensitive to error. It is also shown that the ${}^{large}_{ss1}\mathbf{P}^{r}$ are a useful representation.

Thirdly, the load selection process is examined in detail in order to scrutinise any possibility that the operator load response is a result of extraneous causes.

7.2.1. *Model-result coherence: kinematic uncertainty*

The modelling assumes that balancing the reaction of a caster assembly on the vehicle-frame as a result of motion resistance can be represented by $\boldsymbol{P}_{Qi}$ applied at S_i (idealised caster stem vehicle-frame contact point): a force parallel to the ground-plane at an angle ${}^{B}\theta_{si} + \rho_i$ with respect to the vehicle-frame where ${}^{B}\theta_{si}$ is the orientation of the caster assembly with respect to the frame and ρ_i is the angle of $\boldsymbol{P}_{Qi}$ with respect to ${}^{B}\theta_{si}$: ρ_i is determined by the proportions of the scrub friction and roll resistance effects ($\boldsymbol{R}_{Fi}$ and $\boldsymbol{R}_{Li}$) and the wheel angular velocity directions [sgn($\dot{\theta}_{si}$),sgn($\dot{\theta}_{ti}$)] (page 60). On this basis even if $|\boldsymbol{P}_{Qi}|$ is unknown, taking account of ${}^{B}\theta_{si}$, [sgn($\dot{\theta}_{si}$),sgn($\dot{\theta}_{ti}$)] and allowing a range of ρ_i measures, substantial differences in the handle-force magnitudes are demonstrable for different Zmodel-FCMV manoeuvres. The results, the ${}^{large}_{ss1}\mathbf{P}^{r}$, also show substantial vari-

ations in the handle-force measures for the attempted manoeuvres. This section will demonstrate that the ${}^{B}\theta_{si}+\rho_i$ during the occurrences of the largest magnitudes of handle-force (${}^{large}_{ss1}\mathbf{P}^{r}$) also varied between the manoeuvres.

It is to be noted that demonstrating the concurrence of substantial handle-forces differences and substantial ${}^{B}\theta_{si}+\rho_i$ differences for different manoeuvres is not dependent on the extent to which subjects achieved the [sgn($\dot{\theta}_{si}$),sgn($\dot{\theta}_{ti}$)] combinations produced by Zmodel-FCMV manoeuvre. For even if the conformity with Zmodel-FCMV [sgn($\dot{\theta}_{si}$),sgn($\dot{\theta}_{ti}$)] combinations is poor, if there are sufficient inter-manoeuvre variations in ${}^{B}\theta_{si}+\rho_i$, this demonstrates that what was the case for the manoeuvres r is the case for manoeuvres r (attempted). This follows since the general application of the Zmodel-FCMV is that different vehicle-frame velocities require different combinations of $\boldsymbol{P}_{Qi}$ orientations which, for dynamic equivalence to be achieved, result in substantially different handle-forces.

Examples of the roll marker data (black line) along with the model prediction (red line) are shown in Figures 7.1 and 7.2 (page 167) for manoeuvres A and E (a.) respectively, for subjects [1, 16] for all four caster assemblies: this is a single marker where the change of vertical displacement direction indicates sgn($\dot{\theta}_{ti}$) (page 84). Examples of data (black line) for the caster orientation relative to the vehicle-frame (${}^{B}\theta_{si}$) are shown in Figures 7.3 and 7.4 (page 168) along with the model prediction (page 77) (red line) for manoeuvres C and I (a.) respectively, for subjects [6, 12] for all four caster assemblies: while it is the sgn($\dot{\theta}_{si}$) which are of interest – since scrub friction relates to caster global rotation and not caster rotation – it is useful to show the ${}^{B}\theta_{si}$ measures as these indicate the caster steady-state and this provides more straightforward visual identification. (These examples, chosen at random, are representative: see PDF, Vicon-Model Data for other manoeuvres and subjects.) No filtering has been applied to the empirical data. It can be seen that, in a loose sense, the empirical data follows the trend of the model data.

While Figures 7.1–7.4 show that the general data trend conforms to the model data it is not the general trend which is critical but the [sgn($\dot{\theta}_{si}$),sgn($\dot{\theta}_{ti}$)] during the occurrence of ${}^{large}_{ss1}\mathbf{P}^{r}$ since these can make a π difference in ρ_i depending on the sign. Therefore, as is evident from visual inspection, since there are many local variations in displacement directions it follows that alterations to the signal

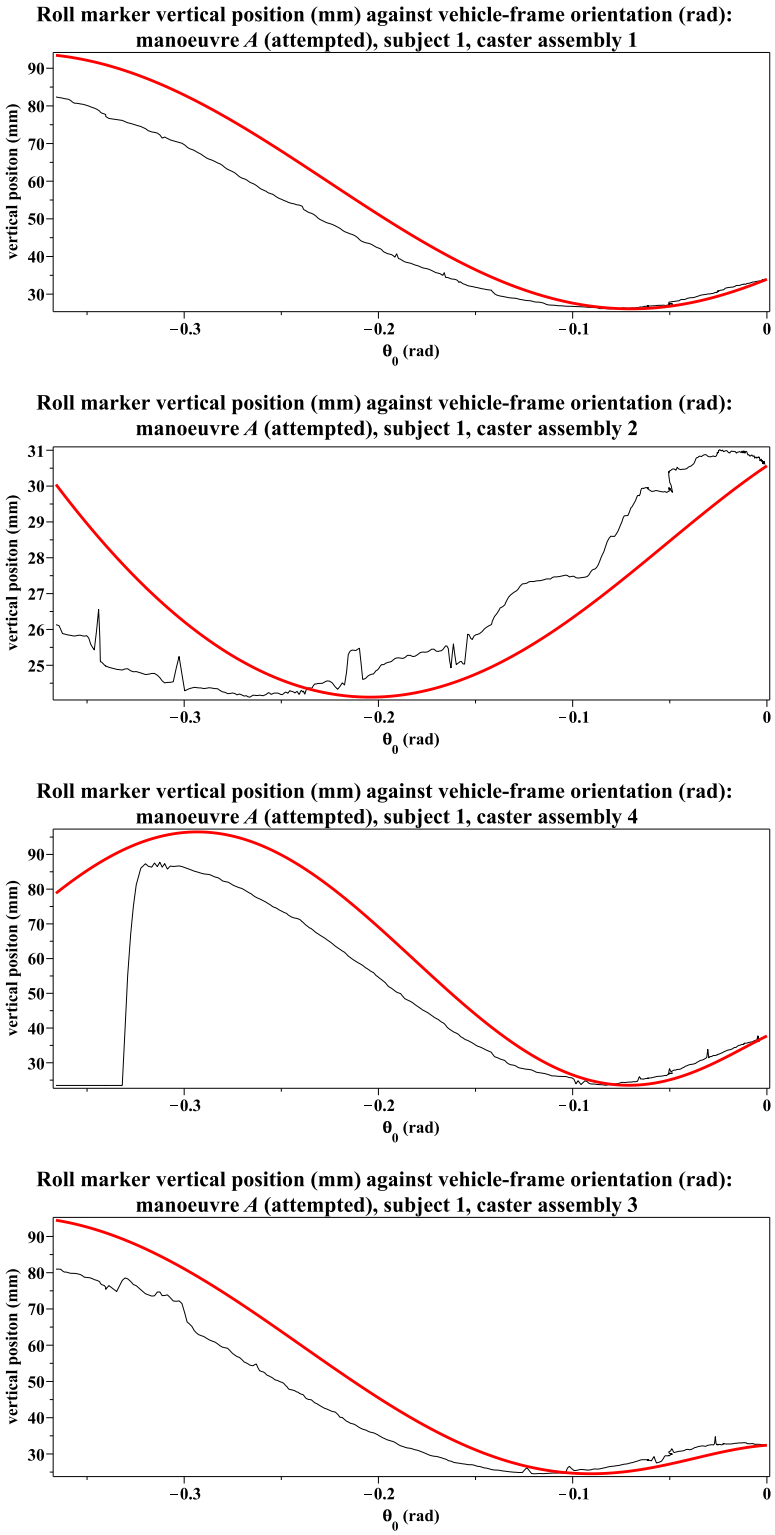

Figure 7.1 – Data (black) and model (red) roll marker vertical position (mm) against vehicle-frame orientation (rads): $\theta_0 = 0$ to right. Marker detachment is evident (second from bottom).

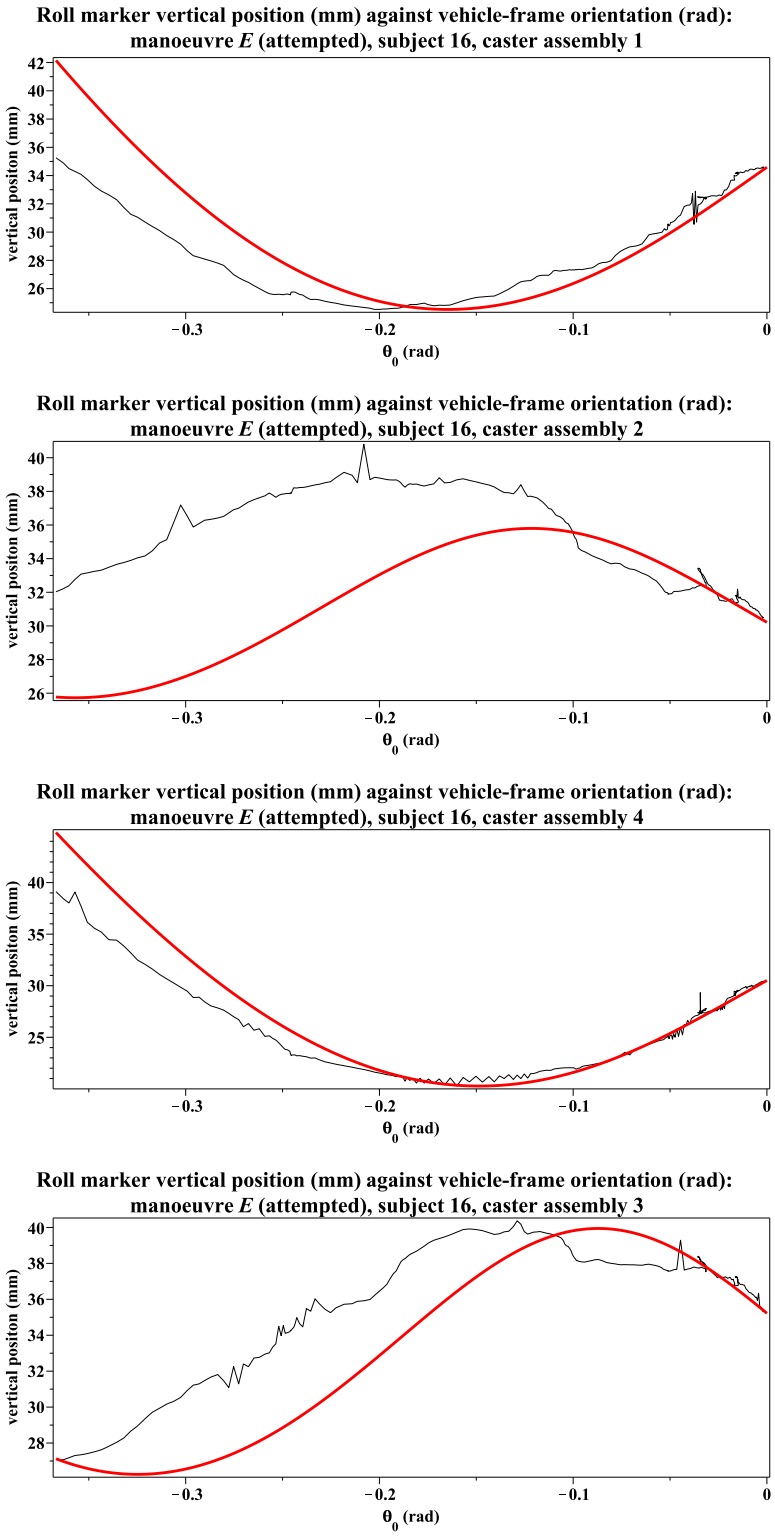

Figure 7.2 – Data (black) and model (red) roll marker vertical position (mm) against vehicle-frame orientation (rads): $\theta_0 = 0$ to right.

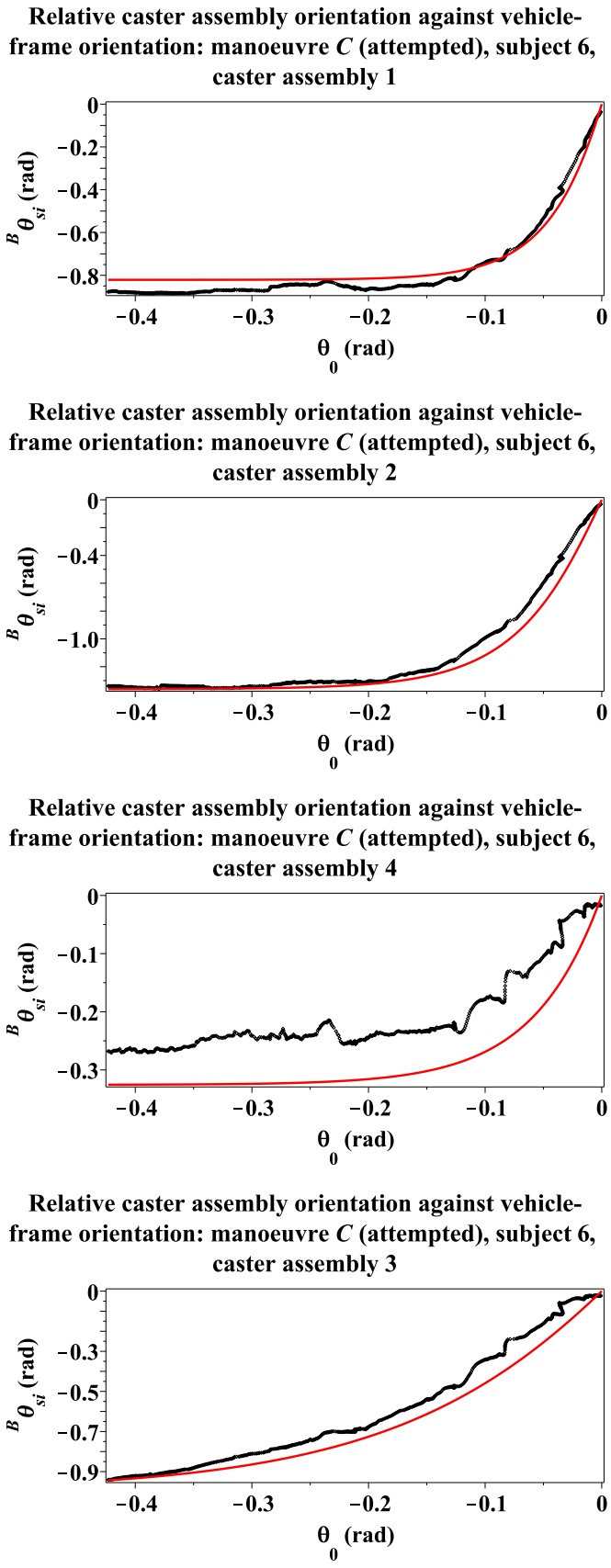

Figure 7.3 – Data (black) and model (red) caster orientation (${}^{B}\theta_{si}$) (rad) against vehicle-frame orientation (rads)

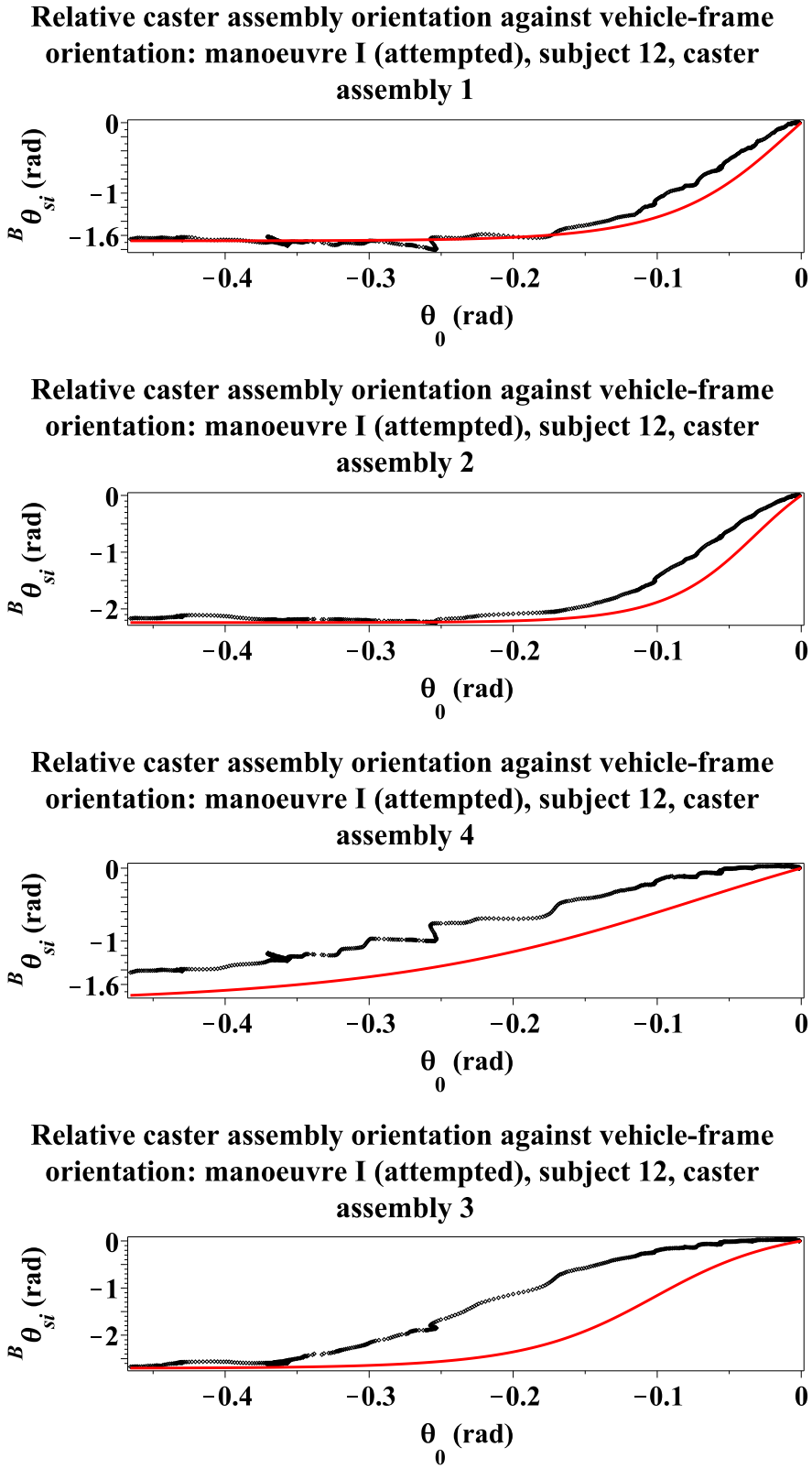

Figure 7.4 – Data (black) and model (red) caster orientation (${}^{B}\theta_{si}$) (rad) against vehicle-frame orientation (rads)

(for example, smoothing) and synchronisation error, since this would shift which kinematic data was relevant, may have a substantial impact on the determination of [sgn($\dot{\theta}_{si}$),sgn($\dot{\theta}_{ti}$)] at the occurrence of the relevant handle-force measures.

A more critical summary appreciation of conformity to the Zmodel-FCMV manoeuvres r is conveyed by Figure 7.5 (page 171) and this has been constructed as follows: in general terms, black lines indicate conformity to the Zmodel-FCMV [sgn($\dot{\theta}_{si}$),sgn($\dot{\theta}_{ti}$)] combinations and the lighter lines do not. The vertical axis indicates the manoeuvre r (a.) and each horizontal line is a subject. The line colour indicates the success of the manoeuvre in terms of conformity with the [sgn($\dot{\theta}_{si}$),sgn($\dot{\theta}_{ti}$)] model output. The line is drawn from left (motion-start) to right (the end of the initial period). Lines are indicative as follows: *thick black* indicates complete conformity (all the [sgn($\dot{\theta}_{si}$),sgn($\dot{\theta}_{ti}$)] match the model), *thin black* indicates conformity with seven angular velocities and one angular velocity was uncertain, *red* indicate nonconformity, *cyan* indicates two or more uncertain angular velocities, *blank* indicates that no conformity was demonstrated with seven angular velocities and that one angular velocity was uncertain. A conservative nonparametric statistical test (Cox and Stuart trend test (Daniel (1990)) with a 20 data point window and a 10 data point step was used to determine [sgn($\dot{\theta}_{si}$),sgn($\dot{\theta}_{ti}$)]. The level $\alpha = 0.05$ was used so any data with a p (the test statistic) result failing to meet α was deemed uncertain.

One relaxation on Zmodel-FCMV expectations is applied: changes in the combination of [sgn($\dot{\theta}_{si}$),sgn($\dot{\theta}_{ti}$)] (page 65) occur in a particular order, apart from manoeuvre C where no changes occur: no check is made on the order of the [sgn($\dot{\theta}_{si}$),sgn($\dot{\theta}_{ti}$)] combinations. If the model indicates that the [sgn($\dot{\theta}_{si}$),sgn($\dot{\theta}_{ti}$)] occurrence occurs within the approximate initial period these were accepted.

In Figure 7.5 the indication of a single uncertainty by a thin black line if all the other [sgn($\dot{\theta}_{si}$),sgn($\dot{\theta}_{ti}$)] conform with the model prediction provides some reduction in the visual impact of the uncertainty. However, even if attention is restricted to the gaps and the red lines, both evidence of nonconformity, it is clear that a substantial proportion of the manoeuvre is accompanied by [sgn($\dot{\theta}_{si}$),sgn($\dot{\theta}_{ti}$)] combinations which do not conform to the Zmodel-FCMV output.

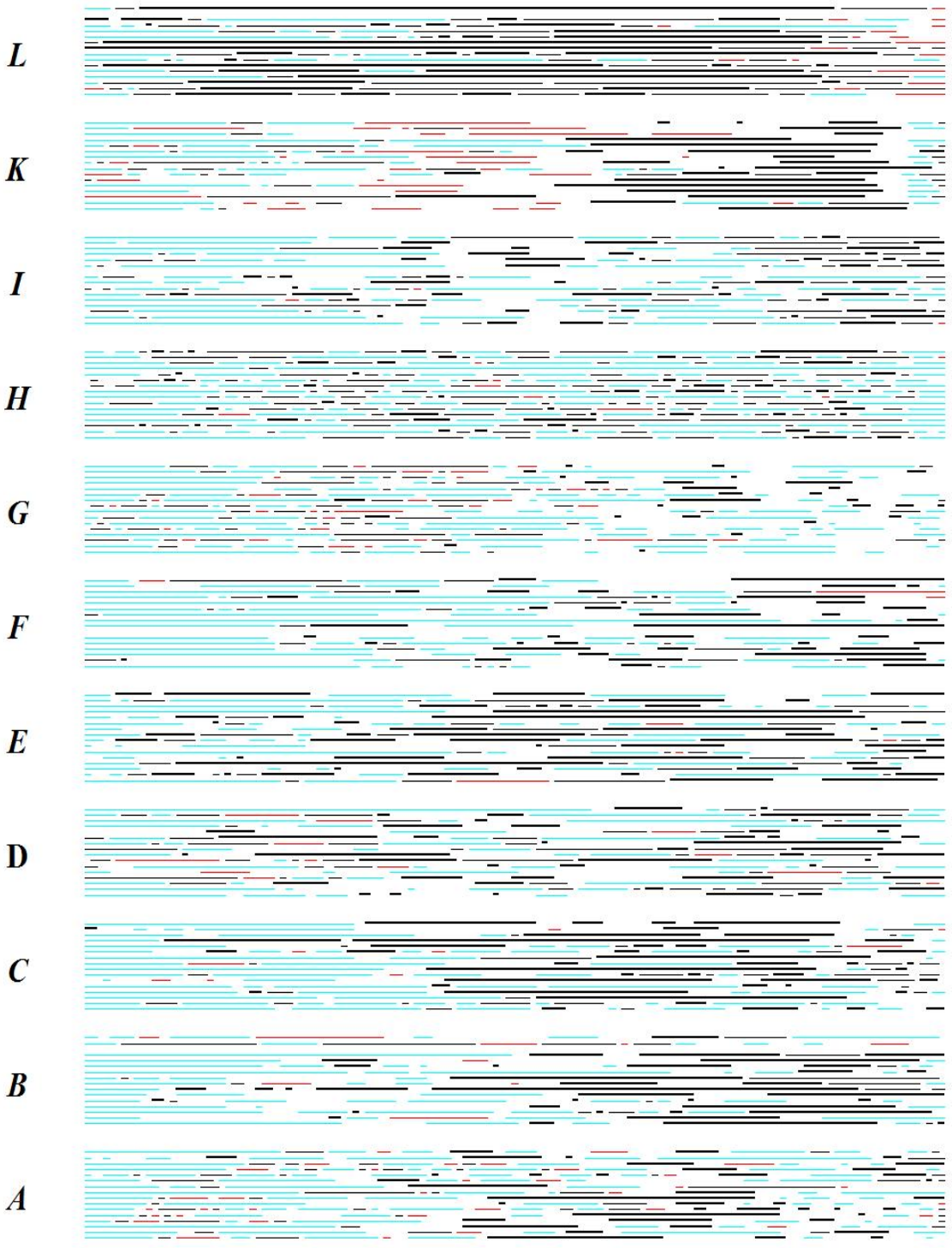

Figure 7.5 – Indicates for initial period (motion start: left) for all subjects and manoeuvres the extent to which manoeuvre r (a.) conformed to the [sgn($\dot{\theta}_{si}$),sgn($\dot{\theta}_{ti}$)] combinations of manoeuvres r. In general black lines indicated conformity but details are as follows: *thick black* indicates complete conformity, *thin black* indicates conformity with seven angular velocities and one angular velocity was uncertain, *red* indicate nonconformity, *cyan* indicates two or more uncertain rot-roll directions, *blank* indicates that no conformity was demonstrated with seven rot-roll directions and that one rot-roll direction was uncertain. This data is based on a 20 data point window, a 10 data point step and $\alpha = 0.05$ with the Cox and Stuart trend test.

The initial high level of nonconformity with model output for manoeuvre K (a.) is noteworthy. An explanation relates to $\dot{\theta}_{s1}$. According to the model this should be a negligible magnitude negative measure during the initial period and examination shows that in practice this value (the red line) is positive. For all the manoeuvres the uncertainty is greatest closer to motion start which may be a result of smaller velocity magnitudes. There is also some variation between manoeuvres: manoeuvres [G, H, I] (a.) show the highest levels of nonconformity with the model output. These three manoeuvres begin with $\text{sign}(\dot{\theta}_{ti}) = -1$ for all four caster wheels so it is possible that this has a bearing on how the manoeuvre is performed: all four $\dot{\theta}_{ti}$ change direction at small θ_0 magnitudes, the largest θ_0 magnitude is 0.11 rad, as shown by Table 4.2 (page 78). While manoeuvre L (a.) has the greatest evidence of conformity to the model manoeuvre and also has three of the four $\text{sign}(\dot{\theta}_{ti}) = -1$ there is other evidence indicating that this manoeuvre is distinctive from [G, H, I]; a possible explanation is considered next.

Figure 7.5 should not be interpreted as indicating that the subject failed to maintain the rod in the 20mm (diameter) guide-ring centre; Table 7.1 (page 173) provides a succinct summary of subject success. The measures in Table 7.1 are the radii (mm) of circle with a centre at the initial position which contains all positions of the CoZV marker during the initial period. In general the displacements from the initial position are relatively small. The displacements for manoeuvres [K, L] (a.) tend to be smaller then the other displacements. While no record was made of subject comments the overall impression gained by the experimenter was that many, if not all subjects, stated that they found it easier to maintain the pin centrally for manoeuvres [K, L] attempted: words to the effect that the pin was self-centring. Statistical analysis of Table 7.1 is not necessary since the only purpose is to convey the general impression that from the subject's perspective, there was considerable success. It is to be noted that the conformity to the Zmodel-FCMV cannot be determined from the CoZV marker for two reasons. Firstly, no examination was made of the relationship between the motion of this marker and $[\text{sgn}(\dot{\theta}_{si}),\text{sgn}(\dot{\theta}_{ti})]$. Secondly, since the $[\text{sgn}(\dot{\theta}_{si}),\text{sgn}(\dot{\theta}_{ti})]$ combinations exist in vehicle-frame translational velocity regions it is possible that the required CoZV is not met but the $[\text{sgn}(\dot{\theta}_{si}),\text{sgn}(\dot{\theta}_{ti})]$ combination is achieved.

	A	*B*	*C*	*D*	*E*	*F*	*G*	*H*	*I*	*K*	*L*	
1	3.5	"*nd*"	4.8	3.2	3.3	5.0	2.5	4.3	3.8	1.3	3.8	3.6
2	3.0	2.7	3.2	3.7	4.6	2.9	3.3	3.0	2.4	1.9	0.9	2.9
3	2.7	0.8	2.7	6.8	3.5	1.5	2.6	3.4	3.4	2.3	1.3	2.8
4	2.6	0.7	3.6	4.4	5.4	2.1	3.3	4.5	3.2	1.8	1.4	3.0
5	4.9	2.7	4.4	4.4	3.0	1.5	3.2	4.5	3.8	0.9	1.8	3.2
6	14.0	2.6	2.8	3.1	3.9	4.2	3.2	1.4	1.8	3.0	2.3	3.8
7	2.7	2.9	3.2	2.9	4.6	"*nt*"	3.6	2.4	4.0	"*nd*"	3.2	3.3
8	2.2	2.0	2.9	3.7	2.8	2.8	3.7	6.4	2.5	1.3	2.4	3.0
9	3.1	7.3	3.6	1.7	"*nd*"	6.3	2.4	3.0	3.1	1.5	1.3	3.3
10	2.4	2.5	2.5	6.7	3.6	4.9	4.6	2.6	"*nt*"	2.2	1.2	3.3
11	4.0	2.3	2.7	2.2	2.7	4.2	5.8	"*nd*"	3.4	1.0	1.8	3.0
12	2.1	3.3	3.0	2.2	4.0	3.1	2.8	2.7	3.9	1.3	2.2	2.8
13	5.0	1.6	4.3	5.9	3.7	2.1	3.9	3.5	3.6	1.6	1.5	3.3
14	3.5	"*nt*"	1.8	3.8	5.2	2.9	2.6	3.7	2.3	"*nd*"	2.1	3.1
15	5.0	13.3	2.7	3.7	3.0	3.2	8.3	"*nd*"	3.1	4.8	"*nt*"	5.2
16	4.3	3.0	2.6	4.7	3.2	3.8	2.1	2.9	3.0	1.1	1.2	2.9
	4.1	3.4	3.2	3.9	3.8	3.4	3.6	3.4	3.2	1.9	1.9	

Table 7.1 – Shows the radius (mm) of the circle containing the CoZV marker position during the initial period for each subject and manoeuvre. The most rightward column shows the mean measure for each subject and the bottom row shows the mean measure for each manoeuvre. The term 'nd' indicates the data was absent and the term 'nt' indicates that the subject did not carry out this manoeuvre

7.2.2. *Theory-result coherence: ρ_i determination*

As with all real data, the measures (for example, Figures 7.1–7.4) comprise of both a true measure and error: in this investigation the most important errors will arise from random effects, limitations on the optical resolution and reconstruction errors arising from marker confusion related to the Vicon system. However, there are also two aspects of the physical system which, in combination, may introduce variations which may be difficult to discriminate, certainly visually, from errors. The first aspect is that the system is controlled by a human being who was free to make discontinuous changes to the handle-forces. The second aspect is that as reported in the Methods Chapter the system has considerable elasticity. Taken together these two aspects make it imprudent to interpret any divergence from smooth curves as error. Unconsidered alteration to the data, by Fourier based

or statistically based smoothing methods, may produce a distorted account of the combinations of [sgn($\dot{\theta}_{si}$),sgn($\dot{\theta}_{ti}$)]. On the one hand removing only higher frequency effects would generally create no change in the direction of the next data point and removing lower frequencies risks obliterating variations which are representative of the physical system. A more cautious approach was therefore implemented as follows.

The bulk of the work arises from the uncertainty of many of the [sgn($\dot{\theta}_{si}$),sgn($\dot{\theta}_{ti}$)] measures: the method of determining uncertainty follows in the next paragraph. However, it is to be noted that the uncertainty conveyed by Figure 7.5 is not an indication of ρ_i uncertainty. In Figure 7.5 a single uncertainty in the eight angular velocity directions creates an uncertainty as to the conformity with the Zmodel-FCMV where as each ρ_i is considered individually: there could be four uncertain angular velocities and two ρ_i could still be certain. With respect to ρ_i the average uncertainty of [sgn($\dot{\theta}_{si}$),sgn($\dot{\theta}_{ti}$)] over all the results was 25%. These were unequally distributed between sgn($\dot{\theta}_{si}$) and sgn($\dot{\theta}_{ti}$) with the former accounting for 25% and the latter 75% of that uncertainty. As will be considered later the Zmodel-FCMV indicates that the $\dot{\theta}_{si}$ are of substantially larger magnitude than the $\dot{\theta}_{ti}$ magnitudes so this difference is explicable. With such a large percentage of uncertainty, particularly for sgn($\dot{\theta}_{ti}$), there is the possibility that whatever conclusions are drawn from the data which are not uncertain, were the uncertain data determined, the conclusions could be overturned. The most robust approach is therefore to assume that the uncertain data always undermines the summarising explanation. Then, if the results still support the summarising explanation there is no dependency on the uncertain data. This approach is implemented as follows: full details of the lengthy process are given in Appendix C.

Firstly, the [sgn($\dot{\theta}_{si}$),sgn($\dot{\theta}_{ti}$)] measures were determined with the nonparametric Cox and Stuart trend test at the level $\alpha \leq 0.05$ (the test is conservative) with two variations in window data size [10, 20] and two variants of step data size [5, 10] resulting in four sets of examination. The procedure utilising the Cox and Stuart test returned a set of eight p values: one for each of the four [sgn($\dot{\theta}_{si}$),sgn($\dot{\theta}_{ti}$)]. If p did not satisfy α the angular velocity direction was deemed uncertain and recorded as a zero but otherwise as 1 or -1 in accordance with the direction. In order to

account for possible synchronisation error (page 250) this was repeated with a data shift of zero and ±25 data points from the indices of the handle force measures which resulted in 12 sets of [sgn($\dot{\theta}_{si}$),sgn($\dot{\theta}_{ti}$)]. This step and all the other steps, which follow, were repeated for each of three handle-force measures: P_u, P_v and P_{uCs} for each trial.

Secondly, for each of the 12 examinations the results for each manoeuvre were combined, i.e. the data for subjects who completed the manoeuvre were combined into a single data set for the manoeuvre. This single set of [sgn($\dot{\theta}_{si}$),sgn($\dot{\theta}_{ti}$)] counts for each manoeuvre was then transformed as follows. The uncertain measures were assigned to the smallest count, for example, if the positive count was 1200 and the negative count was 300 and the count for uncertain data was 300 the final count would be 1200 positive and 600 negative. Thus in the second count the uncertainty was treated as if it was evidence of greater variation in angular velocity direction for the specific sgn($\dot{\theta}_{si}$) or sgn($\dot{\theta}_{ti}$) for that manoeuvre. The positive and negative counts were then converted to percentages. Thus for each manoeuvre a representation of each of the eight angular velocity directions at the handle-force time index was characterised by a percentage of positive and negative directions and this was available in 12 examinations of the kinematics data.

Thirdly, the ${}^{B}\theta_{si}$ values were determined. In order to determine the ρ_i from [sgn($\dot{\theta}_{si}$),sgn($\dot{\theta}_{ti}$)] it is necessary to assume the proportions of the two motion resistance effects ($\boldsymbol{R}_{Fi}$ and $\boldsymbol{R}_{Li}$): the chosen angles were [$\frac{\pi}{8}$, $\frac{\pi}{4}$, $\frac{7\pi}{8}$] so either motion resistance effect could be negligible. This therefore produced 36 examinations of the data. In determining ρ_i if the [sgn($\dot{\theta}_{si}$),sgn($\dot{\theta}_{ti}$)] data was not uncertain this was used but if either component was uncertain then the representative data established by the previous step was used. As this could for certain inter-manoeuvre comparisons result in a larger difference in median ${}^{B}\theta_{si}+\rho_i$ this was repeated using the reverse modification, for example, if the uncertainty was treated as sign($\dot{\theta}_{ti}$) = 1 by the method described in the previous step the opposite sign was used in this step. There were therefore, finally, 72 examinations of the kinematics data for each caster assembly index and at each occurrence of the ${}^{large}_{ss1}\mathbf{P}^{r}$.

Fourthly, the median values of the ${}^{B}\theta_{si}+\rho_i$ for each caster assembly index for each manoeuvre were determined for these 72 examinations: each examination

1.1	–	–	–	–	–	–	–	–	–	B
3.2	2.0	–	–	–	–	–	–	–	–	C
0.1	1.5	3.0	–	–	–	–	–	–	–	D
0.8	0.7	2.2	0.9	–	–	–	–	–	–	E
4.2	2.3	0.6	1.7	1.7	–	–	–	–	–	F
1.3	4.8	6.1	0.9	2.4	2.9	–	–	–	–	G
1.4	2.3	2.6	1.2	1.5	1.1	0.6	–	–	–	H
5.4	4.8	1.8	3.5	4.1	0.3	2.8	1.1	–	–	I
0.8	0.2	1.9	1.6	0.2	1.7	2.2	1.2	3.9	–	K
1.3	0.9	2.2	0.2	0.0	1.4	1.9	1.5	3.8	0.0	L
A	B	C	D	E	F	G	H	I	K	Pu

Table 7.2 – Shows the summed magnitude of the differences of median angle $({}^{B}\theta_{si} + \rho_i)$ (rad) at the occurrence of the P_u component of ${}^{large}_{ss1}\mathbf{P}^r$ for each inter-manoeuvre comparison

0.9	–	–	–	–	–	–	–	–	–	B
3.7	2.6	–	–	–	–	–	–	–	–	C
0.2	1.8	6.3	–	–	–	–	–	–	–	D
0.7	0.0	4.5	1.7	–	–	–	–	–	–	E
2.7	2.3	1.0	3.4	2.2	–	–	–	–	–	F
0.0	1.8	7.6	0.1	1.6	3.4	–	–	–	–	G
0.9	0.0	4.4	1.9	0.1	1.3	1.2	–	–	–	H
2.9	2.8	1.4	3.4	2.5	0.0	2.7	1.6	–	–	I
0.8	0.0	2.8	1.7	0.0	2.3	1.5	0.2	2.6	–	K
1.7	0.3	4.3	1.5	0.2	1.8	1.2	0.2	2.0	0.1	L
A	B	C	D	E	F	G	H	I	K	Pv

Table 7.3 – Shows the summed magnitude of the differences of median angle $({}^{B}\theta_{si} + \rho_i)$ (rad) at the occurrence of the P_v component of ${}^{large}_{ss1}\mathbf{P}^r$ for each inter-manoeuvre comparison

would have as many ${}^{B}\theta_{si} + \rho_i$ as there were data points in the relevant ${}^{large}_{ss1}\mathbf{P}^r$. In each of the 72 examinations the difference magnitude between the median values of the ${}^{B}\theta_{si} + \rho_i$ for each manoeuvre was compared with that of the other manoeuvres and the minimum magnitude of difference was selected: thus the measure which supported the counter-claim was chosen. (PDF, Angular Velocity Direction Data) The magnitude of each ${}^{B}\theta_{si} + \rho_i$ difference for the four caster assembly indices were then summed. The resulting 55 comparisons, each manoeuvre attempted compared with every other manoeuvre, are shown in Tables 7.2–7.4 (page 176) for each of the handle force-measures.

2.4	–	–	–	–	–	–	–	–	–	B
5.2	1.7	–	–	–	–	–	–	–	–	C
0.9	2.6	3.5	–	–	–	–	–	–	–	D
3.9	0.4	1.7	2.2	–	–	–	–	–	–	E
6.0	2.1	0.1	3.3	1.7	–	–	–	–	–	F
2.0	2.6	5.2	0.1	2.4	4.9	–	–	–	–	G
4.1	0.1	1.7	1.9	0.0	1.6	1.3	–	–	–	H
7.5	2.2	0.4	4.3	2.2	0.2	4.1	1.1	–	–	I
2.4	0.0	1.9	2.6	0.4	1.9	2.5	0.2	2.2	–	K
4.0	0.2	1.8	2.2	0.2	2.0	1.8	0.0	1.7	0.2	L
A	B	C	D	E	F	G	H	I	K	$PuCs$

Table 7.4 – Shows the summed magnitude of the differences of median angle $({}^{B}\theta_{si}+\rho_i)$ (rad) at the occurrence of the P_{uCs} component of ${}^{large}_{ss1}\mathbf{P}^{r}$ for each inter-manoeuvre comparison

Tables 7.2 – 7.4 therefore provide a concise representation of the variation in the ${}^{B}\theta_{si} + \rho_i$ between manoeuvres and demonstrate that, despite interpreting the uncertain [sgn($\dot{\theta}_{si}$),sgn($\dot{\theta}_{ti}$)] in a way which minimises variation, the variation is substantial, >1 rad for 40, 37 and 40 of the 55 comparisons for P_u, P_v and P_{uCs} respectively. By way of comparison with the Zmodel-FCMV for ${}^{B}\theta_{si} = 0$ and $\boldsymbol{R}_{Fi} = \boldsymbol{R}_{Li}$ the signs for [sgn($\dot{\theta}_{si}$),sgn($\dot{\theta}_{ti}$)] for manoeuvres A and B are [1, 1, 1, 1, 1, 1, 1, 1] and [1, 1, 1, 1, -1, -1, 1, 1] respectively so the summed difference of ${}^{B}\theta_{si}+\rho_i$ between the manoeuvres is π. An interesting pattern is apparent for the measures<0.6 rad in Tables 7.2–7.4 and this is shown in Table 7.5 (page 178). It can be seen that the distribution of relatively small differences is not random. If the manoeuvre comparisons are viewed in terms of the r location by the graphic inspection method (page 63) it is evident that these low values occur for the comparisons of adjoining regions in the $\hat{\boldsymbol{u}}$ direction. However, this effect is not a feature of the dynamic system but rather a consequence of the method of addressing [sgn($\dot{\theta}_{si}$),sgn($\dot{\theta}_{ti}$)] uncertainty. As 75% of the uncertainty relates to sgn($\dot{\theta}_{ti}$) and 25% to sgn($\dot{\theta}_{si}$) the impact of setting the uncertainty against the claim is greater on those manoeuvres which are distinguished by sgn($\dot{\theta}_{ti}$) than those which are distinguished by sgn($\dot{\theta}_{si}$).

The values in Tables 7.2–7.4 cannot be related to the handle-force measure since these are the difference magnitude and not the $\boldsymbol{P}_{Qi}$ orientations. It would be possible to reconstruct measures of P_u, P_v and T which would arise from these

[]	–	–	–	–	–	–	–	B
[]	[]	–	–	–	–	–	–	C
$[0.1, 0.2]$	[]	[]	–	–	–	–	–	D
[]	$[0.0, 0.4]$	[]	[]	–	–	–	–	E
[]	[]	$[0.1]$	[]	[]	–	–	–	F
$[0.0]$	[]	[]	$[0.1, 0.1]$	[]	[]	–	–	G
[]	$[0.0, 0.1]$	[]	[]	$[0.1, 0.0]$	[]	[]	–	H
[]	[]	$[0.4]$	[]	[]	$[0.3, 0.0, 0.2]$	[]	[]	I
A	B	C	D	E	F	G	H	

Table 7.5 – Shows a summary of results from Tables 7.2 – 7.4 where the result is less than 0.6 rad.

measures but this is unnecessary as the purpose is to evidence that the ${}^{large}_{ss1}\mathbf{P}^{r}$ are accompanied by different $\boldsymbol{P}_{Qi}$ orientations. This examination shows that taking account of synchronisation error, using a counter-claim interpretation of the uncertainty, and four parameter variants of the Cox and Stuart test, ${}^{B}\theta_{si}+\rho_i$ measure differences >1 rad occur with a frequency (Tables 7.2 – 7.4) which is highly improbable in terms of random effects. Additionally, the kinematics data trends follow the model predictions.

While the attempted manoeuvres do produce distinct inter-manoeuvre differences in the $\boldsymbol{P}_{Qi}$ orientations, it is evident from the Figure 7.5 that there is only limited conformity to the model output despite the impression of success indicated by the rod centrality in the guide-ring indicated by Table 7.1. There are a number of factors which may account for this. The Zmodel-FCMV takes no account of system elasticity and a number of kinematics effects are disregarded, for example, caster wheel shift and multiple DOF revolute joints. However, manoeuvres r (a.) has still produced the substantial inter-manoeuvre differences for the same reason as manoeuvres r: the $\boldsymbol{P}_{Qi}$ orientations $({}^{B}\theta_{si} + \rho_i)$ vary.

The following conclusion is made: differences in ${}^{B}\theta_{si} + \rho_i$ (partly resulting from different combinations of [sgn($\dot{\theta}_{si}$),sgn($\dot{\theta}_{ti}$)] and different ${}^{B}\theta_{si}$ both arising from different manoeuvre r (attempted)) between manoeuvres are concurrent with the ${}^{large}_{ss1}\mathbf{P}^{r}$. There is therefore both a theoretical basis and an empirical basis for viewing experimental-FCMV manoeuvring as a system in which vehicle-frame translational velocity has a substantial effect on handle-forces due to the effect on

$\boldsymbol{P}_{Qi}$ orientations.

7.2.3. *Quasi-static assumption*

This section demonstrates the usefulness of the quasi-static assumption. Table 7.6 (page 180) shows a maximum handle-force measure (N/kg) for inertial forces derived by the following process: details, Appendix C. By setting motion resistance effects to zero and $m = 1$, to provide a N/kg measure, the inverse dynamic equations for the model-FCMV (Equations 4.41–4.43, page 88) may be used to produce an inertial measure equivalent of Equation 4.67 (page 99). The three vehicle-frame accelerations are then determined by first establishing a polynomial which fitted the displacement data during the initial period followed by symbolic differentiation. Based on a force platform test (results not reported) the COM position was estimated as $-0.097\hat{\boldsymbol{u}}$ m from the geometric vehicle-frame centre. The mass moment of inertia was estimated as a circular cylindrical shell with a radius of half the vehicle-frame width. The resulting maximum inertial handle-force measure occurring in the initial period are shown in Table 7.6. The largest measure, possibly a statistically extreme measure, is for subject 3 manoeuvre F (attempted), 0.13N/kg. However, using the smallest magnitude result for manoeuvre F (a.) and disregarding the $|P_u|$ component it can be seen from Figure 6.9 (page 158) that $|{}^{-90th}_{ss1}P^{\mathrm{F}}_{uCsmin}| + |{}^{-90th}_{ss1}P^{\mathrm{F}}_{vmin}| > 1.3$ N/kg; so even choosing the extreme value in Table 7.6 and the smallest measure for motion resistance shows an order of magnitude difference between motion resistance and inertial effects.

Neither the COM position nor the mass moment of inertia of the load were measured though the estimate for the latter would tend to overestimate the inertial moment. While these are approximations given that the values indicated by Table 7.6 are so small in comparison to the results, any inaccuracy is irrelevant to the thesis conclusion. Given the order of magnitude difference found using an over estimation of mass moment of inertia and the selection of the maximum inertial effect, it is concluded that the quasi-static assumption is appropriate and usefully concentrates attention on the primary effect: motion resistance.

Caster assembly acceleration magnitudes are not as small as vehicle-frame magnitudes: both the Zmodel-FCMV and the data demonstrate that caster global

0	*A*	*B*	*C*	*D*	*E*	*F*	*G*	*H*	*V*	*K*	*L*
1	0.01	0.01	0.01	0.0	0.0	0.03	0.01	0.02	0.02	0.01	0.03
2	0.01	0.01	0.0	0.01	0.0	0.01	0.02	0.01	0.01	0.03	0.04
3	0.02	0.02	0.06	0.05	0.0	0.13	0.02	0.03	0.02	0.03	0.01
4	0.02	0.04	0.02	0.02	0.03	0.03	0.01	0.03	0.05	0.03	0.12
5	0.01	0.01	0.02	0.02	0.0	0.01	0.01	0.01	0.01	0.03	0.02
6	0.01	0.01	0.01	0.0	0.0	0.0	0.0	0.01	0.01	0.02	0.01
7	0.01	0.02	0.0	0.02	0.01	*nt*	0.03	0.01	0.0	0.02	0.02
8	0.02	0.02	0.03	0.0	0.01	0.01	0.0	0.01	0.0	0.04	0.01
9	0.01	0.01	0.02	0.01	0.01	0.03	0.0	0.0	0.02	0.02	0.01
10	0.01	0.03	0.03	0.01	0.01	0.03	0.03	0.04	*nt*	0.03	0.01
11	0.01	0.01	0.01	0.01	0.0	0.01	0.01	0.0	0.01	0.02	0.02
12	0.01	0.02	0.01	0.01	0.01	0.01	0.01	0.01	0.03	0.02	0.01
13	0.01	0.05	0.04	0.01	0.01	0.04	0.04	0.01	0.04	0.02	0.01
14	0.01	*nt*	0.04	0.0	0.0	0.02	0.02	0.01	0.03	0.02	0.01
15	0.04	0.04	0.03	0.03	0.01	0.06	0.01	0.04	0.03	0.04	*nt*
16	0.01	0.01	0.05	0.01	0.01	0.05	0.01	0.03	0.01	0.02	0.02

Table 7.6 – A maximum handle-force measure (N/kg) for inertial effects during the initial period for each manoeuvre and subject: *nt* indicates no trial.

rotation and wheel roll magnitudes can be relatively large during the initial period compared with vehicle-frame rotation. However, it can be shown (A.6.1) that an overestimate of the component of $\boldsymbol{P}_{Qi}$ which is absent due to neglecting caster dynamics is 0.01N/kg. Compared with motion resistance effects caster assembly dynamic effects are small.

7.2.4. *Handle-forces and hand pressure centre approximation*

The transformation from motion resistance to handle-force measures depends upon three factors: the dynamic formulation of the transformation, the accuracy of the sensor and the approximation of handle-force application areas. These factors are considered in this section.

The dynamic formulation of the transformation is considered elsewhere (page 116) and while this is the application of basic mechanical principles it is important to consider the coherence of the force results. For example, examination of Figure 6.9 (page 158) shows a positive P_{uCs} for manoeuvres [A, D, G] so it is natural to consider how a measure of a positive couple is associated with a negative

vehicle-frame rotation. However, it is the case that the motion resistance effects of the front caster assemblies are not balanced by the rear assemblies for $\hat{\boldsymbol{v}}$ directed actions (page 98) and, as there are relatively large positive P_v actions, the positive P_{uCs} is consistent.

There are three areas of comment to be made in defence of the sensor system. Firstly: 1) the sensor is a high quality pre-calibrated type which is used in similar experimental work, Jansen et al. (2002) is one example, 2) the sensor mounting was designed by a competent person (see Contributors Section), constructed in a dedicated workshop and 3) visual and tactile inspection was maintained throughout the experimental process without any indication of difficulties. Additionally, visual examination of the intra-manoeuvre sensor data (PDF, Sensor Data) is free from gross differences with one exception: subject [8] manoeuvre F (attempted). This data was excluded: the probable cause is a software malfunction.

Secondly, the experimental method is insensitive to a number of errors. Since the key comparison is intra-subject manoeuvre differences, the results of one manoeuvre compared with another for the same subject, inter-subject sensor errors do not effect the results: such errors could be responsible for the variability in Figure 6.9 (page 158) but the variability is not sufficient to overturn the result that the first order effect was due to inter-manoeuvre differences. The variability is considered further under retrospective work.

Thirdly, it is evident from Figure 6.9 that even a highly improbable 10% shift of P_v measures resulting from sensor axes misalignment, due to any elasticity between handles and the rest of the vehicle-frame system would not affect the results. In conclusion given the magnitudes of difference which are relevant to the results further work on these relatively small refinements is not considered necessary.

The determination of P_{uCs}, the $\hat{\boldsymbol{u}}$ directed handle-forces which produce a force couple, relies on an expedient method which only provides an approximation (page 132) of the centre of pressure of the $\hat{\boldsymbol{v}}$ directed handle-forces. Additionally, it may be shown that for the sensor to handle-force transformation (page 116) that non-integer zero P_{uCs} measures can be shown to include the term $P_{Lv}s_L + P_{Rv}s_R$

(page 116) and that therefore the mathematics do permit a substantial variation in P_{uCs} as a consequence of inaccurate s_L or s_R measures. However, it is demonstrable that these methods do not undermined the results as follows.

The hand width measure (Figure 5.9, page 132) range was 0.08–0.096 m: as this measure is at an angle to the ground-plane (see Figure 5.9) the relevant dimension with respect to the $P_{Lv} + P_{Rv}$ moment arm for the hand-grasp position would be smaller than this. An improbable large allowance for error is therefore ±0.03 m, as indicated by the circled cross-hairs in Figure 5.9, since this would mean that the centre of pressure of the hand force was 0.018m (or less given the angle to the ground-plane) from the outer border of the hand. The ${}^{large}_{ss1}\mathbf{P}^r_i$ measures as shown in Figure 6.9 (page158) were recalculated (details: Appendix C) for these modified s_L and s_R values. It can be seen from Figure 7.6 (page 183) that the variation from Figure 6.9 is negligible: no further consideration of the approximate centre of pressure of $P_{Lv} + P_{Rv}$ is required.

Further analysis of the hand-grasp position effect on P_u measures is not considered necessary as the handle width was fixed and any variation in the centre of pressure in the $\hat{\boldsymbol{v}}$ direction must be small compared with the 0.475 m handle width.

7.2.5. *Representativeness of* ${}^{large}_{ss1}\mathbf{P}^r$

The largest magnitude handle-forces are represented by ${}^{large}_{ss1}\mathbf{P}^r$. This measure incorporates three assumptions: firstly, the focus on the initial period, secondly, the use of percentiles and thirdly, that P_u, P_v and P_{uCs} are representative of forces-applied for the experimental-FCMV manoeuvres. The first two assumptions are considered here and the third is considered under future work on existing data. The 'start-up' (with varying or no definition) was identified in the Literature Chapter (page 46) as a period of higher biomechanical demand. These results also assume that the initial period is the most relevant so a justification is necessary: justification exists in terms of work but not impulse as follows.

Page 205 line 3 from bottom, Figure 7.7 (page 207) provides an indication of the comparative size, compared with other periods, of the impulse resulting from the ${}^{large}_{ss1}\mathbf{P}^r$ and it is constructed as follows. Where 1) n_0, n_1, n_2 and n_3 indicate

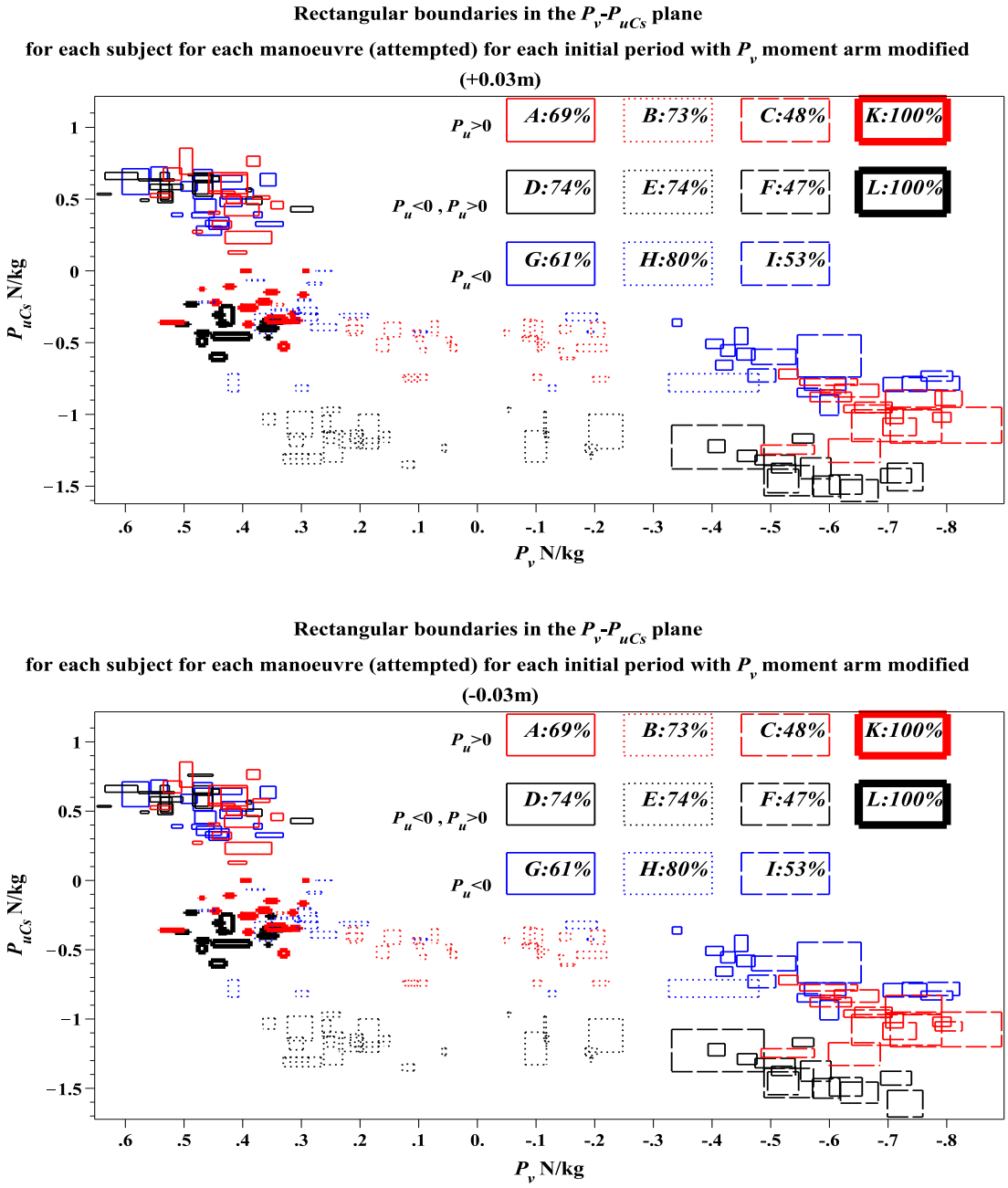

Figure 7.6 – Shows for s_L or s_R values modified by +0.03m (top) and -0.03m (bottom): the eleven ${}^{large}_{ss1}\mathbf{P}^r_i$ results graphed together on the $P_v - P_{uCs}$ plane. The legend indicates by colour manoeuvres[A, B, C, K] (a.) which have no inequality for $P_u < 0$ (red), manoeuvres[D, E, F, L] (a.) which have an inequality in both signs for P_u (black) and maneouvres[G, H, I] (a.) which have no inequality for $P_u > 0$ (blue) and by line-styles manoeuvres[A, D, G, K, L] (a.) which have no inequality for $P_v < 0$ (solid), manoeuvres[B, E, H] (a.) which have an inequality in both signs for P_v (dotted) and maneouvres[C, F, I] (a.) which have no inequality for $P_v > 0$ (dashed). The load measures L^r_{Mnormm} are indicated in the legend for each manoeuvre. The legend is arranged so that that manoeuvres[A, B, C, D, E, F, G, H, I] (a.) are positioned in their region position.

the data points zero, initial period end, later period end and steady-state period end, 2) ${P_{aik}}^r$ is a handle-force measure with action index a, for P_u, P_v, P_{uCs}, subject index i, data point index k and manoeuvre index r, 3) where ${}^{90th}_{n_0..n_3}|{P_{ai}}|^r$ indicates the 90^{th} percentile for handle-force magnitudes from n_0 to n_3 (not a sub-period as previously used) and ${}_jP_{Iai}{}^r$ indicates $\sum_{k=n_{j-1}}^{n_j} \frac{|{P_{aik}}^r| \geq {}^{90th}_{n_0...n_3}|{P_{ai}}^r|}{.02c_j}$ where c_j is the count of $|{P_{aik}}^r| \geq {}^{90th}_{n_0..n_3}|{P_{ai}}^r|$ for $k = n_{j-1} \ldots n_j$ (j=[1, 2, 3]) then the following provides an indication of the impulse difference between a period and the subsequent period: $\sum_{a=1}^{3}(|{}_jP_{Iai}{}^r| - |{}_{j+1}P_{Iai}{}^r|)$ (j=[1, 2]). In words this is a measure for each subject and manoeuvre giving the summation for all actions of the average impulse magnitude difference between a period and the subsequent period for each action for the largest force magnitudes. Red-points indicate the initial–later period comparison and black-points indicate the later–steady-state period comparison with positive measures indicating a decrease and negative measures indicating an increase in the subsequent period measure. If the impulse always reduced as the periods progress then all the results would be positive; there are numerous negative results. If the required handle-forces reduce as the manoeuvre progresses then in general it is not in terms of reducing impulse magnitude.

However, work analysis indicates a consistent change as the manoeuvre progresses through the periods. Figure 7.8 (page 209) provides an indication–no equality is implied since this is the product of angular displacement and force–of the negative angular work done on the vehicle by motion resistance and construction follows a similar process to Figure 7.7. Where $(|\Delta\theta_0|)^{-1}{}_jP^r_{Wai}$ indicates the magnitude of angular work done in the period j, (j=[1, 2, 3]), per rad: using indices as defined for the impulse, where $\Delta\theta_{0j}$ is the angular displacement in period j and ${}_jP^r_{Wai} = (n_j - n_{j-1})^{-1} \sum_{k=n_{j-1}}^{n_j} |{P_{aik}}^r|$, i.e. the average force magnitude in the period, then the following provides an indication of the work difference between a period and the subsequent period: $\sum_{a=1}^{3}((|\Delta\theta_{0j}|)^{-1}\,{}_jP_{Wai}{}^r - (|\Delta\theta_{0(j+1)}|)^{-1}\,{}_{j+1}P_{Wai}{}^r)$, $j = [1, 2]$. Red-points indicate the initial-later period comparison and black-points indicate the later–steady-state period comparison with positive measures indicating a decrease and negative measures indicating an increase in the subsequent period measure. It can be clearly seen, with a small number of exceptions, that

the negative angular work done by motion resistance shows a substantial decrease as the periods progress.

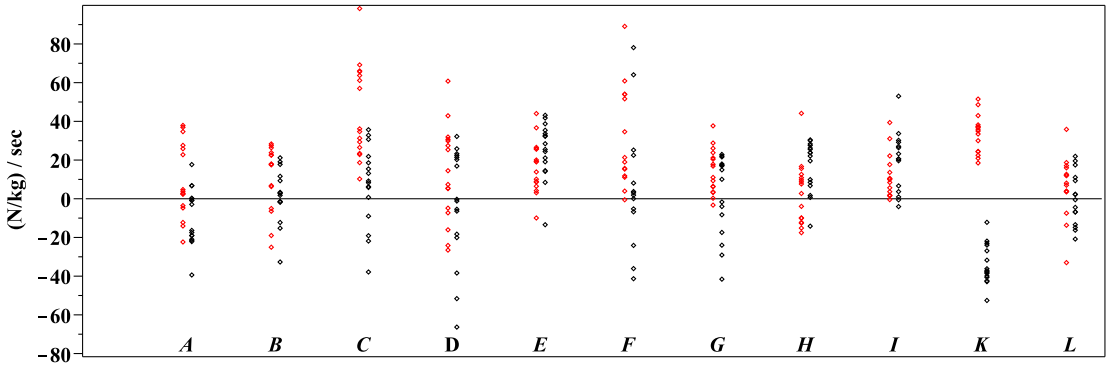

Figure 7.7 – Shows the difference between a representation of the impulse for all subjects for the initial period and later period (red) and the difference between the later period and steady period (black) for each manoeuvre: positive values indicate a decrease in the subsequent period and negative values an increase.

A possible explanation as to why impulse examination does not reveal a reduction as the periods progress is therefore that subjects did not reduce handle-forces as the work done by motion resistance reduced. As this is an intra-manoeuvre comparison an explanation as to why the negative work magnitude by motion resistance decreases as the periods advance is not attempted in terms of $\boldsymbol{P}_{Qi}$ orientation since this was the basis of explaining inter-manoeuvre differences; a possible explanation in terms of elasticity is made in the Prospective Work Section.

These observations do not entirely accord with the start-up considerations in the Literature Chapter (page 46) where experimental results identified higher peak force magnitudes at start-up. However, those results relate to translational displacements rather than real-FCMV manoeuvres. The start-up period, using the Literature Chapter term, is the period of greatest interest with respect to the handle-forces but in these results the distinguishing feature for all manoeuvres is in terms of work.

Figure 7.8 demonstrates progressive decrease in negative work by motion resistance as the periods progress for most subjects, i.e. this is not an inter-manoeuvre examination. It may be possible to demonstrate inter-manoeuvre differences for each subject in terms of work rather than percentiles approach ($^{large}_{ss1}\mathbf{P}^{r}$); this is

not essential. The argument for the use of percentiles is that it demonstrates inter-manoeuvre handle-force differences and provides, by the visual inspection of the previous chapter using ${}^{large}_{ssi}\mathbf{P}^{r}$, the θ_0 measures at which work differences are demonstrable. However, a work approach is considered further in the Retrospective Work Section.

As a single sensor was used and as $|P_{Lv}| + |P_{Rv}| = |P_v|$ may not hold for the general case the representation by P_v does not indicate the occurrence of $P_{Lv} < 0$ and $P_{Rv} > 0$ or $P_{Lv} > 0$ and $P_{Rv} < 0$. However, P_v is a true measure of the dynamic of the experimental-FCMV. It is explanation of load selection variation in terms of operator motor control and biomechanics which is affected but that is not the subject of this thesis.

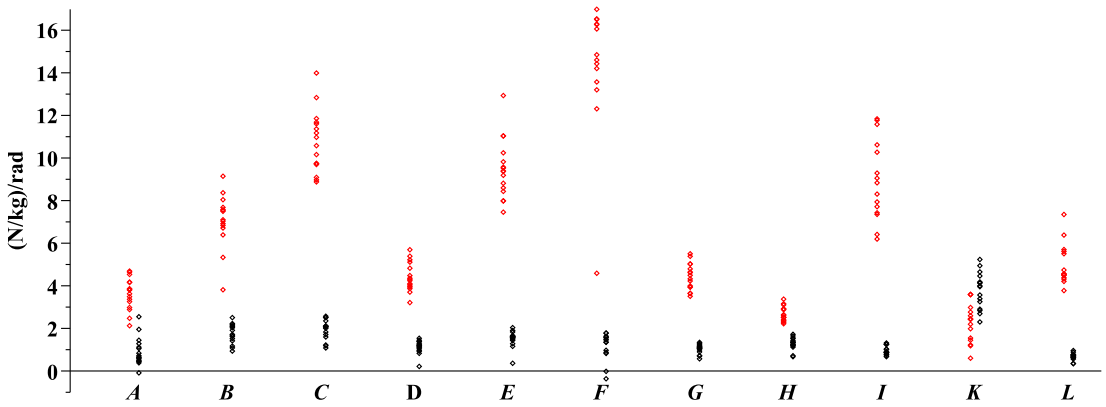

Figure 7.8 – Shows the difference between a representation of the work for all subjects for the initial period and later period (red) and the difference between the later period and steady period (black) for each manoeuvre: positive values indicate a decrease in the subsequent period and negative values an increase.

7.2.6. *Load selection process: motivation*

A key result of this investigation is that variations in the manoeuvre r (a.) are associated with operator load response variations. This section demonstrates that it is improbable that extraneous operator influences, in contrast to changing handle-force requirements produced by the mechanism, would give these results. It follows that the assertion that manoeuvre r (a.) variations cause operator load response variations is strengthened.

One speculation which would undermine the results is that subjects had different levels of motivation for the different manoeuvres: that all subjects were

motivated, for example, to get higher loads for manoeuvre K (a.) compared with manoeuvre F (attempted). But none of the literature, some of which was in non-technical commentary, for example, Abel (1983), and therefore reflects every-day experience, gives any suggestion that the results were anticipated. While the Literature Chapter indicates that difficulties manoeuvring real-FCMV are part of every day experience there is no evidence that there was any prior knowledge of the displacement direction effect reported by Abraham and Johnson (2010) and that publication is neither available to nor intelligible to the non-engineer. As a matter of anecdote, subjects expressed surprise that the manoeuvres with the smaller L^r_{Mnormm} were so difficult. If a motivational bias existed it would seem more likely that subjects would have sought to meet the expectation that the different manoeuvres would have similar load responses.

A motivational bias could also arise if there was an advantage to achieving higher loads with some manoeuvres, for example, if it was a means to increased remuneration (Dempsey, 2004); this is not applicable, there were no such factors.

The only person present who expected that the differing manoeuvres would yield different L^r_{Mnormm} was the experimenter. However, great care was taken to avoid giving clues either verbally, by facial expression or through other reactions. Neither was any feedback given to the subjects until after all subjects had completed the experiments.

The majority of the subjects knew each other. The experimental process included the request not to discuss the load selections. The author's impression was that subjects did not comply and seemed to appear to enjoy comparing which manoeuvres were 'easy' and which were 'difficult'. However, the experimental method was too novel for subjects who had not completed the experiment to appreciate what was being referred to and it is therefore unlikely that anticipation had any effect.

The experimenter's impression was that some subjects were competitive, i.e. they appeared pleased when a relatively large load was selected and appeared disappointed when a relatively small load was selected. However, while there is some variation in the range length for load selection (Figure 6.1, page 139) visual inspec-

tion indicates that even those with a shorter length range still show a substantial variation between minimum and maximum. Furthermore the analysis is insensitive to inter-subject motivation differences since it is N/kg measures which have been used. Given that the subjects not only had manual handling training and were also responsible for minimising the manual handling risks of others it is reasonable to assume that whatever the motivation to achieve higher loads, importance was given to self-care. This was repeatedly stated in the verbal instructions. Related to this while foot-slip and footwear type was not recorded, the experimenter's recollection is that there was no foot-slip despite a wide range of foot wear of various levels of practicality, i.e. the impression was that subjects did not seek to apply such large handle-forces that foot-slip became a problem. However, even if subjects paid insufficient attention to their self-care the results are N/kg measures and there is no intention of determining loading guidelines from this investigation.

In the second session the order of the manoeuvres was from manoeuvre with the smaller load to the manoeuvre with the largest load. Subjects were free to, and some did (Figure 6.1, page 139), alter the load. In the load selection session (the first session) manoeuvres [K, L] came at the end of the session. It would seem more reasonable to expect motivation to reduce at the end of a lengthy trial period (typically two hours) but the largest loads were chosen at the end of the session. Indeed, had the load capacity of the vehicle been greater some subjects would have tried even larger loads (page 141).

Given firstly, the novelty of the results, i.e. the improbability that subjects had an opinion about what they ought to achieve other than having similar loads for all manoeuvres, and secondly, the demonstration of the motivation to maximise the load choice as indicated by the large L^r_{Mnormm}, it is concluded that it is improbable that the load selections are a result of factors other than those related to the changing forces-applied.

7.2.7. *Load selection process: exclusion*

One subject who completed the load selection for manoeuvres [B, E, H, C, F, I] was excluded (page 137): however, the respective L^r_{Mnormi} for this subject were [100, 100, 100, 42, 56, 56]% and as this follows the trend for L^r_{Mnormm}, exclusion

does not compromise the results.

7.2.8. *Reliability*

This section considers how load selection was determined and the limitations to inter-rater reliability. There were two circumstances by which a load trial became the L^r_{Mnormi}. Firstly, subjects maintained the rod in the guide-ring centre, as judged visually by the experimenter, but found it uncomfortable to do so with the selected load and removed some load or decided they were at the limits of comfort and did not want to try a higher load. Secondly, the subject attempted the manoeuvre but the experimenter disqualified the subject from choosing the load as the experimenter judged the deviation of rod from guide-ring centre to be so great that the manoeuvre attempt was counted as a failure. While it would have been valuable to make a kinematic record of this in order to determine the reliability between manoeuvres and between subjects this was not done. The author judged any extension to the time duration of the, typically, two-hour load selection process as creating a potential motivational problem.

There is therefore an uncertainty as to the extent to which the same judgement was applied inter-subject and inter-manoeuvre. It is conceivable that the experimenter applied a stricter control during the small L^r_{Mnormm} and lesser one for the large L^r_{Mnormm}. While this is conceivable, the kinematics results suggest the opposite is the case for manoeuvres r attempted with the largest L^r_{Mnormi}. It can be seen from Table 7.1 (page 173) that Z_r marker displacements were smaller with the largest L^r_{Mnormm} manoeuvres [K, L] and the means are approximately 60% of the radii for the manoeuvres with the smallest L^r_{Mnormm} [F, C, I]. Additionally, the effects of the different manoeuvre r (a.) are not restricted to a change in subject response (load selection) which could be subject to experimenter bias, but are also expressed in terms of the varying handle-force measures which are free from experimenter bias. While it is therefore the case that the experimental method does not provide a robust means of quantifying or ensuring load selection reliability since the experimenter judged success or failure, both the kinematics results and the force measures contradict the view that the results are phenomenon produced by the experimenter. The appropriate conclusion is that further work is required to develop other methods of improving reliability measurement in this experimental

approach.

7.2.9. *Conclusion on summarising explanation*

Given the coherence of theory and results, the value of the quasi-static approach, the robustness of the results to error, the validity of using ${}^{large}_{ss1}\mathbf{P}^r$ as the handle-force representation, and the evidence that the operator load response variation was a consequence of handle-force required variation, it is concluded that the summarising explanation is robust: varying the manoeuvre r (a.) varies the experimental-FCMV motion resistance response which varies the handle-forces required which varies the operator load response.

7.3. **Adaptation Planning**

This section takes the final step in a description of the forces-applied and space-required relationship: it is demonstrated that the results are important to adaptation planning. This requires little work since it has been established that varying manoeuvre r (attempted), i.e. varying Z_r varies the operator load response and by definition varying Z_r varies the manoeuvre space requirements. For $\Delta\theta_0 = -\frac{\pi}{2}$ the resulting variation in space requirements are important given that, for example, a corridor width of 900mm is common in domestic dwellings (Department of Environment Transport and Regions, 1999): Figure 7.10 (page 193) makes this point graphically. This Figure will be introduced and discussed in the next section along with a more detailed account of the forces-applied and space-required relationship.

7.3.1. *Forces-applied and space-required relationship*

The implications of the forces-applied and space-required relationship to adaptation planning is made in three steps. Firstly, as observed in Section 7.2.5 (page 182) all the manoeuvres studied show that when the negative work of motion resistance on the vehicle is examined a substantial magnitude decrease is found as the periods advance. Secondly, handle-forces which result in an approximate manoeuvre r (attempted), as indicated by Table 7.1 (page 173), advance the ${}^{B}\theta_{si}$ towards the steady-state. At the end of the initial period $|\Delta\theta_0|$ is relatively small compared with $|\Delta {}^{B}\theta_{si}|$: this is evident from Figure 7.9 (page 191) which shows the ${}^{B}\theta_{si}$ magnitude measures at the end of the initial period. Since the

maximum $|\Delta\theta_0|$ for the initial period end is 0.133 rad (manoeuvre A (attempted)) the inter-manoeuvre differences in space requirements during this period are not of adaptation planning importance. However, if the specific Z_r *is not* maintained the vehicle is subject to another instance of a larger magnitude of negative work acting on the vehicle by motion resistance. However, thirdly, if Z_r *is* maintained the smaller magnitude of motion resistance work which occurs for the steady-state is incurred. So in summary, in loose terms, the path which is determined in the initial period as a result of maintaining Z_r has to be followed if the reduction in negative work which results from that Z_r is to be incurred. (The existence of paths with superior operator load response is considered in the generality of results section.)

Thus the configuration of ${}^B\theta_{si}$ in the initial period determines the need for substantially different architectural spaces. This observation demonstrates a value of the Zmodel-FCMV as the basis of experimental method compared with the wall-collision approach (page 26); in the latter method distinct kinematics are possible even if very little additional manoeuvring space is available.

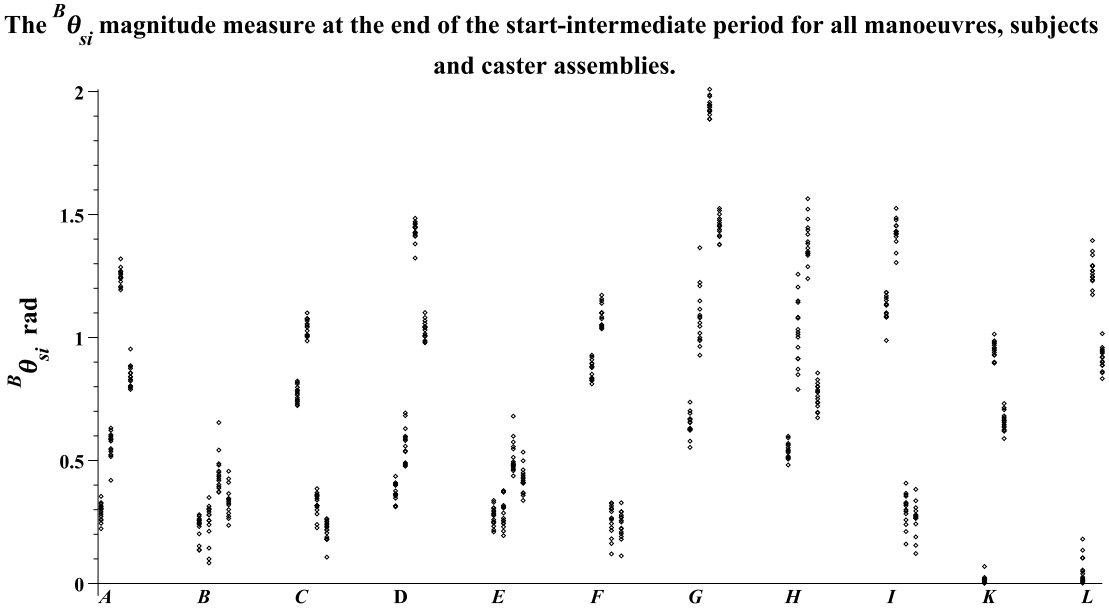

Figure 7.9 – Shows the $|\Delta^B\theta_{si}|$ at the end of the initial period for all subjects and manoeuvres

Figure 7.10 (page 193) illustrates the differing space requirements for two contrasting groups of manoeuvres: those with the two largest [K, L] (blue) and those with the three smallest [F, C, I] (red) L^r_{Mnormm}. The vehicle-frame start

position with vehicle-frame front facing to top of page is shown in black. The vehicle-frame is shown with handles but without caster assemblies. Z_r is indicated by a circled cross and the relevant manoeuvre r letter. The final position of the vehicle-frame front is indicated by an apostrophised manoeuvre r letter. The vehicle-frame point with the greatest displacement is indicated by a dashed line. (This is not intended as an adaptation planning specification since neither operator nor occupant space is accounted for. However, the differing space requirements are evident and important as can be seen from the 900mm measure.) Figure 7.10 also indicates that the forces-applied and space-required relationship is not intuitive; an intuitive access planning relationship would be that larger spaces improve access where as it is evident that the initial location of the vehicle-frame within the space is important: manoeuvre K which had the largest L^r_{Mnormm} is more suited to the 900mm corridor width than manoeuvre F which had the smallest L^r_{Mnormm}.

If the load is a person then the operator must transport the load as a single component so the remaining option, if the operator wishes to apply preferred handle-force magnitudes, is to vary the CoZV. If the architecture is so arranged that the operator can make manoeuvres [K, L] of Figure 7.10 but wishes to make manoeuvres [F, C, I] then it is understandable that the operator perception may be that the real-FCMV is 'stuck' and yet freely moves in unwanted directions; this was the author's originating experience. Operator perception of force application is relevant: results with ten healthy subjects pushing a trolley (Strindberg and Petersson (1972)) showed that the perceived difference between loads considered too large and those which were not, was much higher than the objective difference. Dempsey (2004) describes this phenomenon in terms of the 'psychophysical power law', i.e. the objective difference functions as a power in perceived difference.

A mechanical description of the perception that the real-FCMV can get 'stuck' is therefore that the real-FCMV is (mechanically) omni-directional but that some manoeuvre r (a.) create a dynamic constraint for the operator due to the reduced operator load response to handle-force requirements. This description harmonises with Abel (1983) who identifies real-FCMV manoeuvrability as desirable but control as problematic if the former is interpreted as omni-directional ability and the latter as forces required.

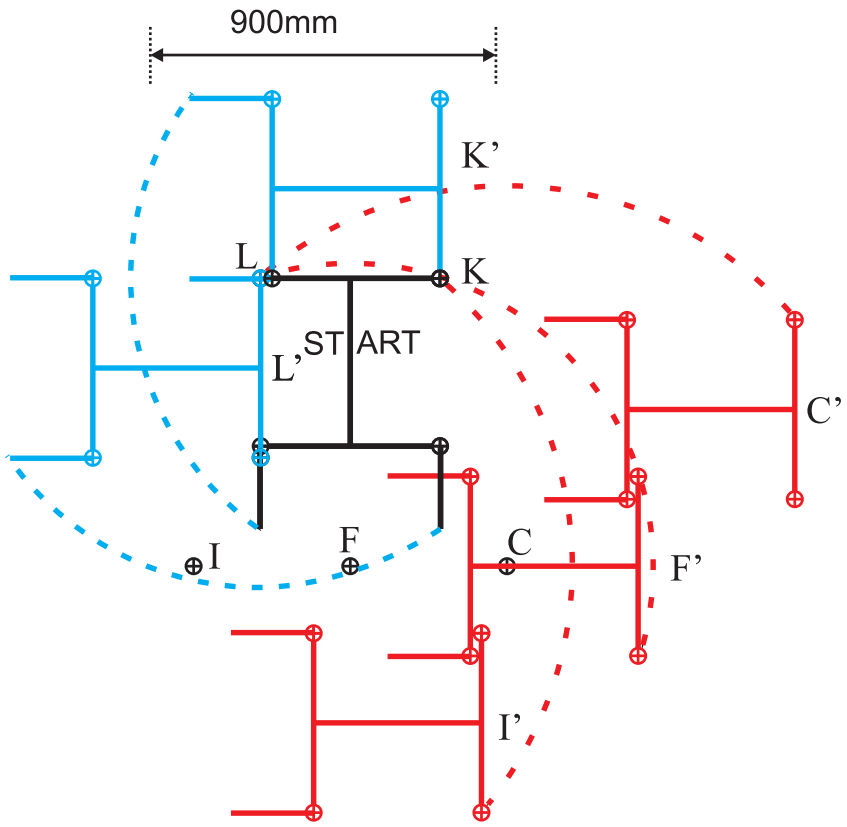

Figure 7.10 – Shows the contrasting adaptation planning spaces for the manoeuvres with the largest [K, L] and the smallest [F, C, I] L^{r}_{Mnormm} as follows: with only vehicle-frame including handles shown but without caster assemblies the original position is shown in black with forward facing top of page, with outer extremity indicated by a dotted line, the Z_r indicated by the manoeuvre letter and circled cross and front facing final position after $\frac{\pi}{2}$ vehicle-frame orientation change indicated by r' where r is the manoeuvre letter, [K, L] are shown by blue lines and [F, C, I] are shown by red lines.

While the mechanics of cross-slope manoeuvres are distinct from level ground manoeuvres r, the change in handle-forces required resulting from a change from non-cross-slope to cross-slope translational displacement are analogous to the changes arising from different manoeuvre r: to balance the gravity effects the operator must introduce relatively large P_v and P_{uCs} components compared to those which occur without a cross-slope and these components will have common signs which is associated with the smallest load capacity in these results.

7.3.2. *Adaptation Planning: applying the results*

Applying the results to specific adaptation planning issues can be achieved with little work and three illustrative case applications are considered here. By the virtue of the investigative approach, the use of manoeuvres r, the illustrations

communicate the adaptation planning objectives without a need to understand the mechanical explanation of the underlying theory and results.

Figure 7.11 (page 195) shows the application of manoeuvre K to create a template to address a hypothetical access requirement. Taking account of the occupant foot length is straightforward and the path of the operator is well-defined, so with the addition of an operator space allowance which could be determined in an ad hoc manner, as part of the assessment, the results provide a powerful solution: powerful in the sense that the results indicate that the L^{r}_{Mnormm} is greatest for this manoeuvre. This does not guarantee the operator can apply the forces required but it does ensure that the allowance for the operator load response has been maximised by the adaptation planning; in contrast the state of the art for adaptations planning has no guidance for real-FCMV which takes account of load. Thus while the ad hoc determination of operator space indicates an area for further work, set against the state of the art for real-FCMV adaptation planning, using manoeuvre K adds substantially to the adaptation planning knowledge since no prior commentary has been made.

This approach extends the 'constrained outlines' approach Abraham and Johnson (2006) which provides a straightforward method of implementation: a scale drawing of the operator and vehicle-frame with occupant is placed on a plan and a pin is located at Z_K so the manoeuvre can be examined with very basic technology.

Figure 7.12 (page 196) combines both a hypothetical manual handling and an adaptation planning issue. The hypothetical situation is that the occupant instructs the operator to manoeuvre the real-FCMV such that he or she is facing the direction of exit as illustrated in Figure 7.12 (top) but the operator says this is too difficult: for this example, the relevant result is $L^{\mathrm{C}}_{Mnormm} = 48\%$. Without understanding why, the operator wishes to use the manoeuvre, for example, shown in Figure 7.12 (middle): for this example the relevant result is $L^{\mathrm{L}}_{Mnormm} = 100\%$. An alternative adaptation planning is shown in Figure 7.12 (bottom) where for this example the relevant result is $L^{\mathrm{H}}_{Mnormm} = 84\%$. For the illustration shown, comparing top and bottom, the results provide an explanation as to why one architectural arrangement might create no operator difficulties where as another

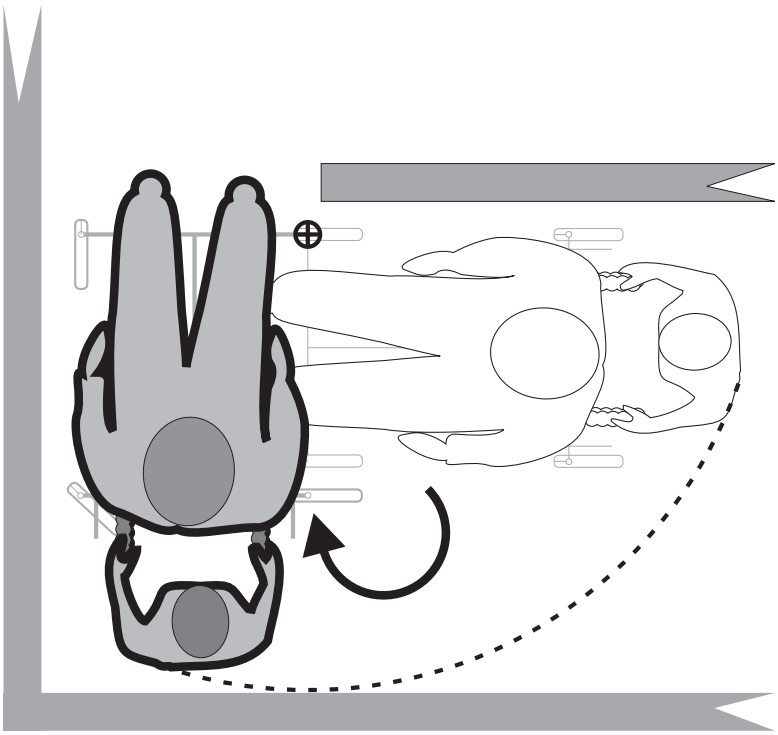

Figure 7.11 – Shows the use of manoeuvre K which had the highest load preference as the basis for creating an adaptation planning template: a constrained outline with the constraint indicated by a circled cross.

architectural arrangement might create considerable difficulties.

The final application relates to the use of a mobile hoist as illustrated in Figure 7.13 (page 196). If the architectural layout or operator routine is such that final position is as indicated Figure 7.13 (left) then in order to orientate the vehicle-frame so that the occupant may be pushed over the armchair it would be necessary to use, for example, manoeuvre F. In contrast if the arrangement is as shown in Figure 7.13 (right) then the same objective is achieved by, for example, manoeuvre D: L^r_{Mnormm} for manoeuvre D was 74% where as the measure for manoeuvre F was 47%. The visual distinction between these two arrangements may be subtle but the results indicate that there are important differences in the handle-forces required. It should also be noted that due to the disproportionate effects of front caster assembly loading (page 98) and the much longer wheel base of the mobile hoist compared with the experimental-FCMV it is reasonable to assume that the inter-manoeuvre differences would be greater for this real-FCMV than indicated by the results.

In each of these three examples it can be seen that the results provide an

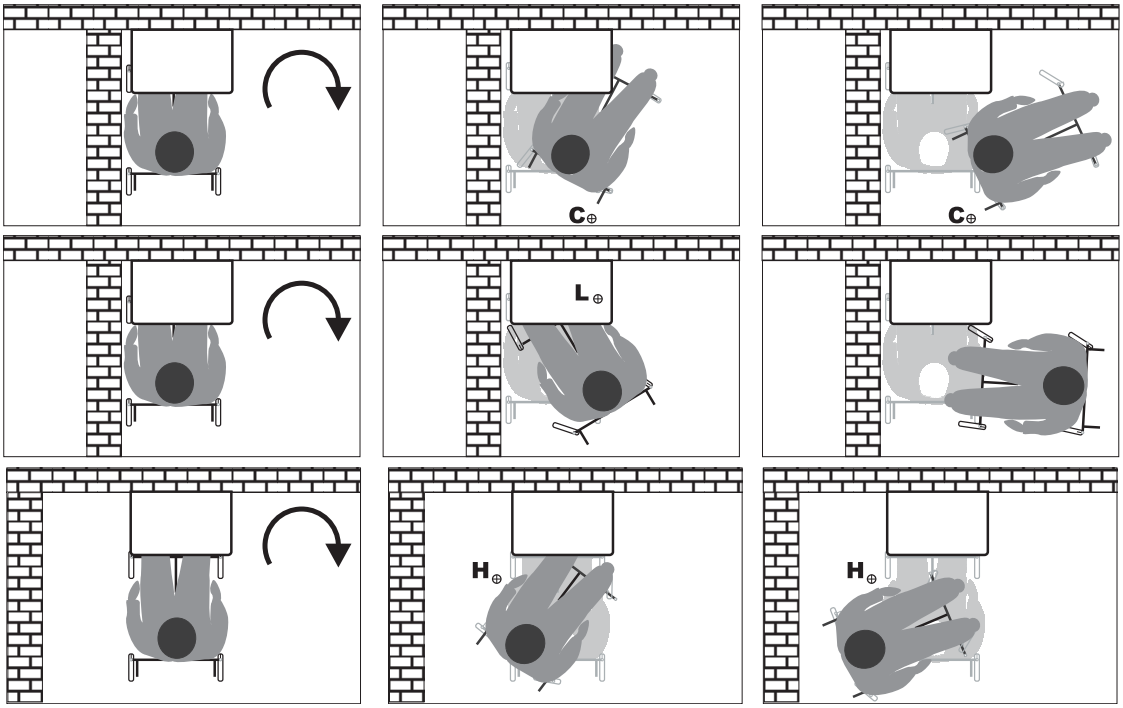

Figure 7.12 – Shows 1) (top) an architectural arrangement whereby to achieve the manoeuvre with the occupant facing the direction of exit, for example, manoeuvre C must be used, 2) (middle) a manoeuvre (r=L) with a possible preferred handle-force measure which may be carried out by the operator contrary to the wishes of the occupant and 3) (bottom) an architectural arrangement whereby to achieve the objective of forward facing, for example, manoeuvre H may be used: manoeuvre C had a L^{r}_{Mnormm} of 48% where as the measure for manoeuvre H was 80% and for L it was 100%.

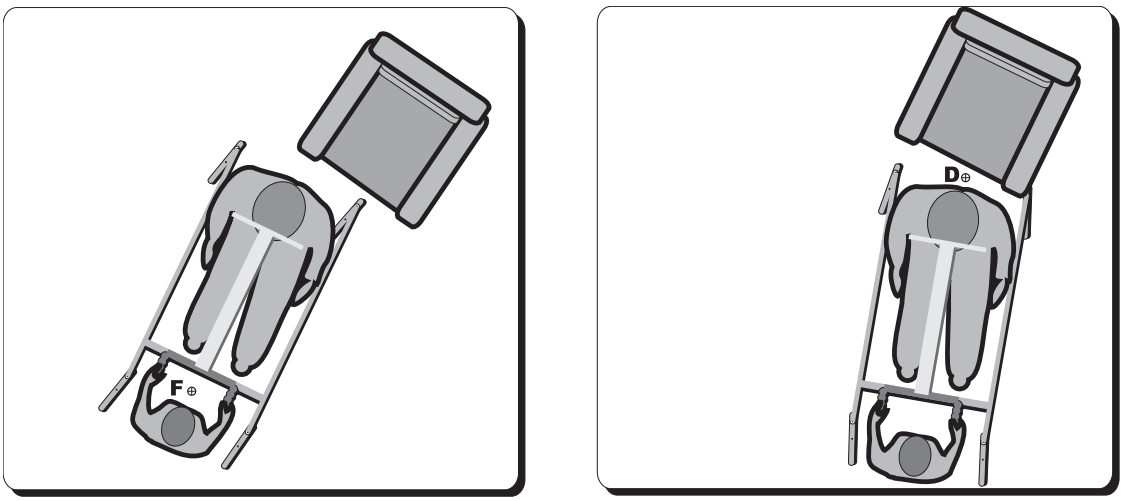

Figure 7.13 – Shows two different mobile hoist positions prior to the final manoeuvring task to bring the occupant over the armchair.

understanding which assists adaptation planning and related manual handling. It can also be seen from these three illustrations that while the underlying theory

and a defence of the results requires a knowledge of dynamics, the applications, if suitably presented and explained, should be able to be intuitively grasped by those who are familiar with these vehicles.

7.4. The Generality of the Results

The results are based on manoeuvre r (a.) in one $\dot{\theta}_0$ direction on MDF flooring with the experimental vehicle and with sixteen subjects after the exclusion of two subjects. Given these factors this section considers the extent to which these results may be applied to the general case. It is concluded that there are good reasons for considering the flooring, vehicle and subjects as generally representative. However, in actual use manoeuvres are constrained by the architectural layout, these are termed walled-manoeuvres, and not necessarily by maintaining a CoZV. It is therefore also concluded that the extent to which and likelihood that the adaptation planning implications arising from the results do not apply to walled-manoeuvres requires further work. Nevertheless the value of the results to adaptation planning is maintained.

7.4.1. *Numbers*

The numbers of subjects (sixteen at sensor-displacement measurement) is typical for this area of investigation. There are two reasons why the generality of the results is not considered to be greatly affected by this number. Firstly, the object of study is a single variable, operator load response to a relatively determined mechanical system given the experimental set-up. Secondly, the focus of interest is the extreme ranks of L^r_{Mnormm} where the differences are extremely large. It is conceivable that there may be individuals for whom manoeuvre F (a.) attracts a 100% larger operator response than manoeuvre K (a.) but there would need to be some features, very specific to the individual, for this to occur.

7.4.2. *Handedness*

All of the manoeuvres were carried out with $\text{sign}(\dot{\theta}_0) = -1$ and it is therefore conceivable that the other direction would have an effect on the results which may be related to differences in hand dominance. However, the task involves the whole body motor system so it is highly improbable that this has an important effect on the results even if there are intra-subject differences for the two directions.

7.4.3. *The ${}^{B}\theta_{si} \approx 0$ and initial static equilibrium assumption*

The manoeuvre r (a.) assume an initial state of ${}^{B}\theta_{si} \approx 0$ and initial static equilibrium. No tracking studies of real-FCMV walled-manoeuvres have been made so only informed speculation is possible. However, the simplifying assumption that ${}^{B}\theta_{si} \approx 0$ seems probable since it can be shown (page 251) that even if ${}^{B}\theta_{si} \approx \pi$ relatively small changes in $\Delta x_{Bu}\hat{\boldsymbol{u}}$ result in ${}^{B}\theta_{si} \approx 0$ if $\dot{x}_{Bv} = 0$ and $\dot{\theta}_0 = 0$: for a caster assembly with 35mm trail, approximately 300 mm of vehicle-frame displacement would achieve this. There are thus good mechanical reasons why many manoeuvres would commence with ${}^{B}\theta_{si} \approx 0$.

As considered in the Literature Chapter (page 25) there are practical reasons, for example, door control and avoidance of collisions which support the assumption that manoeuvre commencement from static equilibrium is representative. Additionally, as it has been demonstrated that the ${}^{large}_{ss1}\mathbf{P}^{r}$ occur after motion start, even if some small positive $\dot{x}\hat{\boldsymbol{u}}$ exists this does not affect the results: this is considered further in the later section on elastic effects. It is therefore concluded that both the ${}^{B}\theta_{si} \approx 0$ and initial static equilibrium assumption do not affect the generality of the results.

7.4.4. *Floor material and vehicle*

While the experimentation occurred on one floor material (MDF) the approach which has been taken is a relative one. The operator load response may be scaled depending on the floor covering but the relative differences will remain: a thick carpet would produce produce a general reduction in operator load response. However, for carpets with a loose fitting it is possible that the motion resistance effects are determined by local variations at each caster assembly so the results may not apply for that situation.

The results do however assume that the caster assemblies are in good repair. Damage to any of the caster assemblies, for example, a seized bearing would produce a different system and the results would not apply.

The results are based on a single vehicle. However, as the results are an inter-manoeuvre comparison which depends on vehicle geometry rather than direct measurement of $\boldsymbol{P}_{Qi}$, the results are applicable to vehicles of similar geometry.

Vehicles with smaller dimensions are unlikely for the adult population but larger dimensions are possible: both mobile hoists and reclining vehicles (see Figure 7.17, page 212) are longer. The results are therefore conservative since these variations will tend to increase the front caster assembly loading (mobile hoists) or the operator distance from the front caster assemblies (mobile hoist and reclined vehicles, the latter is shown in Figure 7.17, page 212 (left)).

Different caster assemblies may have different proportions of scrub friction and roll resistance: as viewed with the simplifying assumption that was applied in the Dynamics Chapter. However, there are three features which suggest that these differences may not be of first-order importance. Firstly, the results indicated that ${}^{B}\theta_{si}$ tend to follow the Zmodel-FCMV so ${}^{B}\theta_{si}$ are independent of motion resistances, as expected. Secondly, it is the rot-roll directions which have the greater effect on ρ_i and not scrub friction to roll resistance proportions since the former vary by π and the latter effect may be as little as $\frac{\pi}{4}$. These features suggest that the impact of the proportion of scrub friction to roll resistance on $\boldsymbol{P}_{Qi}$ orientation $({}^{B}\theta_{si} + \rho_i)$ may not as important as the kinematics. Thirdly, the Zmodel-FCMV identifies the same manoeuvres at the extremities of rank ordering for the handle-force measure P_{QH} (Equation 4.67, page 99) as is found in the results. In the Dynamics Chapter, manoeuvres [K, L, B, H] had a small P_{QH} where as manoeuvres [C, F, I] had a larger P_{QH} and this persisted for various scrub friction to roll resistance proportions during the initial period ($\theta_0 \gtrsim -0.1$ rad), as was subsequently defined with the results: Figure 4.19 (page 101). An estimate of the equivalent measures for the results can be gained by setting $P_{QH} \approx |P_v| + |P_{uCs}| + |P_u|$ (simplifying and modifying Equation 4.67 to accommodate the results) and then using approximations for the medians for P_u, P_v and P_{uCs} (from Figures 6.13-6.14, page 161): for manoeuvre K (a.), $P_{QH} \approx 1.2$: for manoeuvre F (a.), $P_{QH} \approx 1.9$. In conclusion, the Zmodel-FCMV predicts the extremities of the rank ordering for P_{QH} largely independent of scrub friction to roll resistance proportion and the results indicate the same rank ordering at the extremities so it is probable that the scrub friction to roll resistance proportion is not a first-order effect.

7.4.5. *The manoeuvre r (attempted)*

Walled-manoeuvres and manoeuvre r (a.) are different types of constraints: the two subjects who were excluded were physically able to make walled-manoeuvres: they would make walled-manoeuvres in their duties as employees. Their real-FCMV manoeuvring skills may be inferior to the other subjects, particularly if the wall to vehicle-frame dimension is relatively small, but that is not of importance to this consideration; their exclusion demonstrates that an important difference exists between the two constraint types.

For a trial (results not presented) with one of the excluded subjects with substantial free space around the vehicle, a manoeuvre with a [sgn($\dot{\theta}_{si}$),sgn($\dot{\theta}_{ti}$)] combination in accordance with region E was made. Given that this subject did not succeed with the load selection for manoeuvre E (a.) it follows that either some feature of the rod in guide-ring de-skilled her or she could succeed if the guide-ring had a sufficiently large diameter. This explanation may also apply to the four subjects who could not complete one of the manoeuvre r ([B, F, I, L]). There is therefore the possibility that the real-FCMV kinematics during walled-manoeuvres are not distinct from manoeuvre r but that the guide-ring is too demanding a task. It is not known if the subject who made a manoeuvre with a [sgn($\dot{\theta}_{si}$),sgn($\dot{\theta}_{ti}$)] combination in accordance with region E could achieve any other combinations had the shape of the space in which the manoeuvre was carried out changed. It is therefore reasonable to conclude that while the two excluded subjects could not succeed with manoeuvre r this does not indicate that during walled-manoeuvres similarly skilled operators are not subject to the [sgn($\dot{\theta}_{si}$),sgn($\dot{\theta}_{ti}$)] combinations, and hence the dynamics identified in the results, which occur with manoeuvres r.

However, in contrast to the two excluded subjects it should be acknowledged that there may be operators who can produce different results with walled-manoeuvres than occur with manoeuvre r (a.) results. This follows since it is conceivable that an operator could, in an architectural spaces which permitted a manoeuvre r (a.), find a path which did not attempt to maintain a CoZV and produced a superior operator load response. Potential theoretical support to this possibility is found in Abraham and Johnson (2010): in a virtual study of impending motion using estimates for motion resistance it was found that when all the initial config-

urations for ${}^{B}\theta_{si}$ were represented, manoeuvres where $\text{sgn}(P_v) = \text{sgn}(\dot{\theta}_0) = -1$ ([F, C, I] type manoeuvres) could incur small handle-force measures though this was infrequent: frequency in the sense that this effect was present for a small part of the ${}^{B}\theta_{si}$ range. Related to this it is possible that if a larger guide-ring diameter, or no guide-ring, had been used some subjects might have been able to configure the initial ${}^{B}\theta_{si}$ in such a way that superior load capacities were obtained. For these reasons it would be premature to exclude the possibility that some operators can find paths which do not have a fixed CoZV but do use preferred handle-forces. However, either operators generally lack this ability or it is not wholly successful for if it was both a general ability and successful the comments about real-FCMV manoeuvring difficulties would not exist.

While caution should be exercised regarding generalising the results this does not undermine the adaptations planning applications of the earlier section. There may be spaces which provide superior operator load responses than manoeuvre K but if a knowledge of these exists they are unpublished. The state of the art for adaptation planning (page 26) has no research data on real-FCMV manoeuvres so the application of the results in the three illustrations (pages 195-196) constitutes the best research data currently available. The importance of the potential difference between walled-manoeuvres and manoeuvre r is the demonstration that further work is required.

7.5. **Further Work on Existing Data**

There are a number of data observations which have not been analysed as they do not materially affect the results. They are however, interesting and can form the basis of further work. Some preliminary considerations of further work on this data are considered in this section and these include: variability of N/kg measures, alternative action measures and further explanations as to the basis of the inter-manoeuvre operator load response differences. Some of these examinations may guide future work.

7.5.1. *Inter-subject variations*

There is considerable inter-subject action measure variation. For example for manoeuvre B (a.) for subject[9] the $P_{vmini} = 0.33$ N/kg where as for subject[16]

$P_{vmini} = 0.69$ N/kg: an approximately 100% increase. As the results are normalised against the combined effects of load mass, vehicle-frame mass and vertical handle-force loading and the quasi-static approach has been demonstrated to be reasonable, this variation is surprising. A number of potential explanations exist.

Larger loads may produce larger motion resistance effects which would mean that the relative strength differences of subjects was greater than indicated by the results. An examination in terms of kg loads would confirm this.

Apart from incorporating the handle-force vertical loading into the final measure the results disregard the 3D effects so it is possible that a relationship exists between these effects and the variability: one explanation is that some subjects loaded the individual casters in such a way that the forces required were reduced: the incorporation of the Hooke's joint (page 122) into the experimental-FCMV allows for further experimentation.

A physical change in the experimental-FCMV could produce variation, for example, damage to the caster assemblies, would produce inter-subject variation: visual inspection of the experimental-FCMV gives no indication that this is so but further examination of the data is required to see if the variability is chronological. Visual inspection of the floor does not indicate any relevant damage and as the initial position of the caster assemblies on the floor varied, small areas of the flooring were not repeatedly loaded. In a similar way damage to the sensor would produce variation but a visual inspection of the data does not indicate that this is so. A more detailed chronological examination of the data would provide conformation.

Subject freedom as evidenced by different initial ${}^{B}\theta_{si}$ displacements (Figure 7.9, page 191) and the varying kinematics nonconformity (page 171) may be responsible for the measure variations. This is an important result for future work since it has a bearing on the comparison of walled-manoeuvre and manoeuvres r (a.) considered in the previous section, i.e. some subjects may be more skilled than others at reducing the forces required by make changes to the ${}^{B}\theta_{si}$ displacements before ${}^{large}_{ss1}\mathbf{P}^{r}$ occur.

The real system has many more DOF than the Zmodel-FCMV, for example, joints are not ideal revolutes, so one speculation is whether or not the system can

randomly configure in a way that causes motion resistance effects to diminish or increase. The only factor which is excluded is wheel flattening since the wheels were orientated to the same approximate start position for each trial (page 127). No such control existed over initial caster stem axis displacement from the vertical: neither this nor the other DOF not accounted for in the Zmodel-FCMV have been measured and their effect is unknown. While this cannot be investigated directly in the existing data, if all other explanations of variation are excluded then this would indicate that this may be possible cause. This is also considered in the micro approach in the Prospective Work Section.

As none of these potential causes of variation have any material effect on the results, no further consideration is given other than to recognise the importance of this issue for further work: if there are circumstances which reduce the N/kg measures and these can be reproduced this is important as it offers a way of improving the operator load response.

7.5.2. *The inter-manoeuvre load response difference*

Examination of Figure 6.9 (page 158) has some noteworthy features which are worthy of further data examination. Neighbouring ranks of L^r_{Mnormm} share a similar P_v measure or P_{uCs} measure, or both, on the $P_v - P_{uCs}$ plane and some interesting comparisons can be made.

Manoeuvre E (a.) and manoeuvre F (a.) both have relatively large magnitude $-P_{uCs}$ compared with other manoeuvres but the difference in L^r_{Mnormm} between these manoeuvres is large: 74% and 47% respectively. Manoeuvre E (a.) has a relatively small $|P_v|$ with a positive shift for the central measure compared with manoeuvre F (a.) so the difference between these manoeuvres on the $P_v - P_{uCs}$ is the negative P_v magnitude. So large magnitudes of $-P_{uCs}$ are associated with relatively large L^r_{Mnormm} as long as magnitudes of $-P_v$ remain relatively small. A possible implication is that the operator finds some difficulty producing large magnitudes of $-P_{uCs}$ and $-P_v$ in the initial period. It is to be noted that the P_v and P_{uCs} measures are not necessarily concurrent: a check for concurrency (results not presented) indicate that the concurrency was poor.

Another interesting feature of Figure 6.9 is that manoeuvre K (a.) has lar-

ger force measure magnitudes than manoeuvre B (attempted) yet L^{K}_{Mnormm} is the largest measure: Figure 6.12 (page 160) shows that the P_u components are similar. It follows that the distinctive feature of manoeuvre K (a.) is not that the attempted maintenance of one caster assembly in static equilibrium results in lower handle-force measures. It is probable that the maintenance of one caster assembly in static equilibrium requires additional handle-forces. This highlights that increasing operator load response is not a matter of an arbitrary reduction of handle-force magnitudes: it is more accurate to refer to preferred handle-forces. Kumar et al. (1995) found that force applications which are not parallel to the sagittal plane, of the operator and not the occupant as defined in this work, are of smaller magnitude. It is therefore possible that operator orientation with respect to $\hat{\boldsymbol{u}}$ is important. As no measures of operator position were made it is not possible to investigate any relationship between operator sagittal plane and ${}^{large}_{ss1}\mathbf{P}^{\mathrm{K}}$ from existing data so this would need to be a matter for future work.

For manoeuvres [K, L] (a.) the motion resistance effects of the caster assembly in static equilibrium is assisting the maintenance of the CoZV. Comparative examination of the individual subject results for, for example, manoeuvres [F, K] (a.) (pages 146 and 300) indicates that the signal for the latter is smoother than the former and this difference appears to exists for all the manoeuvres [K, L] (a.) compared with the other manoeuvres. It is therefore useful to examine P_{Lu}, P_{Ru} and make some assumption about P_v to provide P_{Lv} and P_{Rv} in order to examine the force at $\mathrm{P_L}$ and at $\mathrm{P_R}$ against time. Such an examination may indicate features of inter-manoeuvre difference which could direct future investigation.

More generally, a further examination of the literature would be valuable in order to develop an understanding of the biomechanical and motor control aspects as to why inter-manoeuvre differences may arise.

7.6. **Ergonomics, and Health and Safety**

In this short section some implications for Ergonomic investigation and Health and Safety are considered.

The Literature Chapter identified ergonomic investigations (page 46) where subjects were tasked with ACMV translational displacement with caster assemblies

initially displaced from the forward trailing position (${}^B\theta_{si} \neq 0$). While manoeuvre r (a.) are different, the theory and results can be applied. If $\dot{\theta}_0 \neq 0$ in the ergonomic studies then the graphic inspection method applies and it follows that the initial displacement of caster assemblies from ${}^B\theta_{si} = 0$ changes the distribution of velocity regions but does not remove them: Figure 4.3 (page 63) may be visualised with ${}^B\theta_{si} = \frac{\pi}{2}$ to convey the effect. Therefore, if experimental methods do not take account of this effect there is the possibility that different tasks with different handle-force requirements are being measured since subjects potentially make manoeuvres with different motion resistance responses. Whether or not this effect is large enough to affect, for example, the Al-Eisawi et al. (1999) results is not known but the possibility exists.

The value of the introduction of a manoeuvring force measure (Ferreira et al. (2004)) for ACMV activity is strongly supported by these results: this work demonstrates that the non-sagittal handle-forces (non-P_u) are critical to understanding ACMV manoeuvres: P_{uCs} should be considered as a non-sagittal measure. However, while recognising a manoeuvring force is an advance on not doing so, it is clear from the results of this investigation that both a couple producing component (P_{uCs}) and a lateral component (P_v) are present so given this, 'manoeuvring force' is a loosely defined term. Related to this Rodgers (1986), Frank and Abel (1989) and Ferreira et al. (2004) provide anecdotal comment on the effects of space constraints on operator position for ACMV use. The distinction between real-FCMV and ACMV, as defined for this work, is relevant to this: the former are assumed to have restricted force applications points, the handles, where as the latter do not, for example, sagittal forces directed away from the operator could be applied anywhere on the refuse collector (page 18). An interpretation of the difficulties created by space constraints on operator position is therefore that in small spaces the operator is prevented from adopting a position in which the forces applied are primarily sagittal. Small spaces may therefore effectively convert an ACMV into a real-FCMV (in terms of fixed force application points, not caster assembly number) with the consequential handle-force requirements as identified in this work. This issue is considered further in the section on design.

7.7. **Prospective Work**

This section considers further areas of investigation which are prompted by this study. These can be divided into three areas: the micro behaviour of the caster assembly, walled-manoeuvres and real-FCMV design.

7.7.1. *Elastic effects*

A hypothesis is made in this section regarding elastic effects which leads to further work. It has been established (page 182) that the distinction between the initial period and later periods can be explained in terms of the negative work by motion resistance: it is of greatest magnitude in the initial period and subsequently diminishes in later periods. An explanation in terms of $\boldsymbol{P}_{Qi}$ orientation is not attempted for while this approach has proved useful in terms of inter-manoeuvre comparison the underlying model for motion resistance is the Coulomb model and it has been demonstrated that this model does not account for the whole phenomenon. Figure 7.14 (page 207) shows the θ_{si} before the occurrences of ${}^{large}_{ss1}\mathbf{P}^r$ for each caster assembly and for each trial grouped horizontally by manoeuvre: a relatively small number of measures greater than 0.15 rad are omitted in order to aid visual inspection. It can be seen that for many trials the caster assemblies have made a non-negligible change in orientation before any ${}^{large}_{ss1}\mathbf{P}^r$ occur and that this is evident for all the manoeuvres: caster assembly [2, 1] are not shown for manoeuvres [K, L] (attempted), respectively. As it has already been established (page 179) that the quasi-static assumption is reasonable the initial occurrence of ${}^{large}_{ss1}\mathbf{P}^r$ after motion start cannot be explained by inertial effects. Thus the ${}^{large}_{ss1}\mathbf{P}^r$ do not occur at impending motion of the caster assemblies as would be the case if the Coulomb model was a complete explanation.

A qualitative explanation to which the data of Figure 7.14 lends support is that the initial θ_{si} displacements are the result of elastic properties but as the displacement progresses the elastic limit is reached and that further θ_{si} displacement produces relative velocity differences between wheel and ground contact points: the actions which produce this displacement are then the ${}^{large}_{ss1}\mathbf{P}^r$. It follows from this that a possible general difference between the motion resistance effects of the initial period and subsequent periods is that the proportions of $\dot{\theta}_{si}$ to $\dot{\theta}_{ti}$ change:

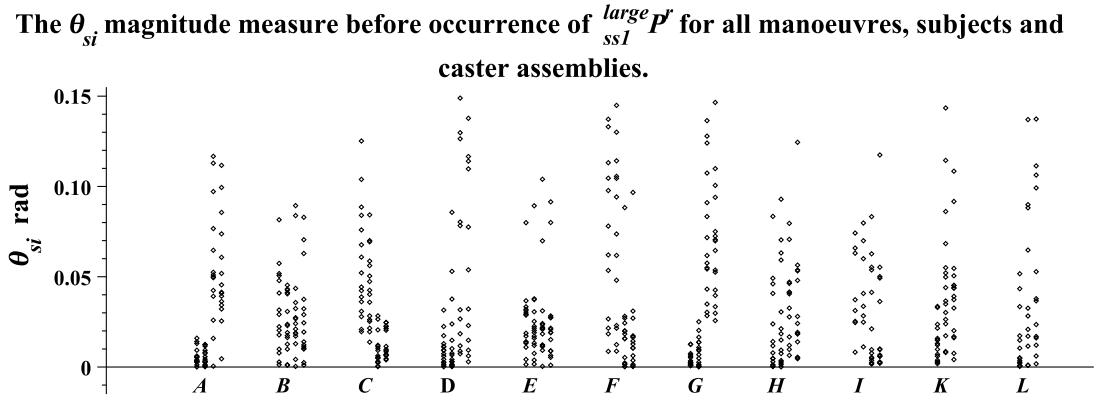

Figure 7.14 – Shows the $|\Delta\theta_{si}|$ before the occurrences of ${}^{large}_{ss1}\mathbf{P}^r$ for each caster assembly and for each trial grouped horizontally by manoeuvre: a relatively small number of measures greater than 0.15 rad are omitted in order to aid visual inspection. Caster assemblies are arranged from left to right and caster assemblies [2, 1] are omitted for manoeuvres [K, L] respectively.

it is a progressively smaller proportion as the CoZV manoeuvre configures the ${}^B\theta_{si}$ towards the steady state. An examination of the data could be made but in order to avoid numerical differentiation, transformation of the single roll marker used to indicate θ_{ti} into angular θ_{ti} data and since the general trend of θ_{si} and θ_{ti} data follows that of the Zmodel-FCMV, the model will be used to examine this relationship.

Based on the Zmodel-FCMV the relationship between caster global rotation and wheel roll is given by $\dot{\theta}_{si} = -\dot{\theta}_{ti}\frac{r}{t}\tan({}^B\theta_{si} - \theta_{zi})$ (page 250). This relationship is graphed in Figure 7.15 (page 208) for manoeuvres [A, E, I] for all four caster assemblies. These are representative of other manoeuvres apart from manoeuvres [K, L] where the i=[1, 2] respectively shows a relatively very small θ_{si} change (PDF, Angular Velocity Proportions). It is evident from Figure 7.15 that as the final ${}^B\theta_{si}$ measure is reached (caster steady state) the magnitude of $\dot{\theta}_{si}$ is a very small proportion of the magnitude of $\dot{\theta}_{ti}$. Given this it is possible that in the steady-state period the elastic limit is never reached since wheel material which is subject to elastic deformation due to $\dot{\theta}_{si}$ (which is of small magnitude) has left the contact zone due to $\dot{\theta}_{ti}$ (which is of large magnitude) before the elastic limit is reached. An examination at ${}^B\theta_{si}$ closer to zero indicates that the magnitude of $\dot{\theta}_{ti}$ is a very small proportion of the magnitude of $\dot{\theta}_{si}$ in which case, in contrast

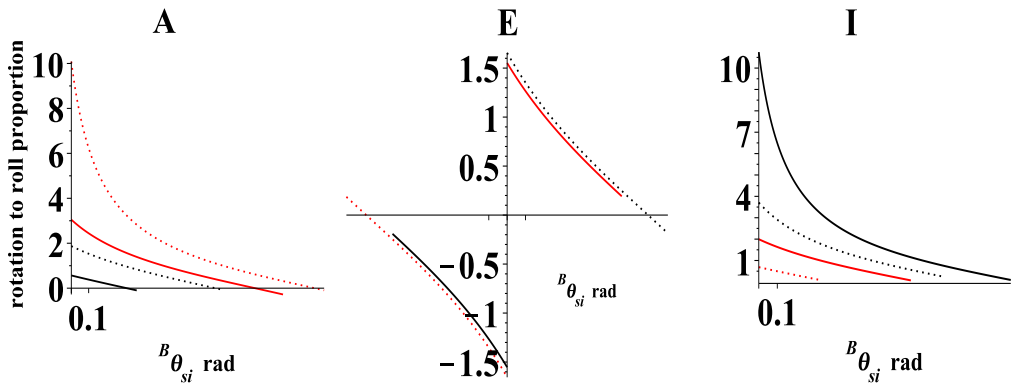

Figure 7.15 – Shows the proportion of $\frac{\dot{\theta}_{si}}{\dot{\theta}_{ti}}$ (caster global rotation to wheel roll) against $^B\theta_{si}$ from $^B\theta_{si} = 0$ to caster steady-state for manoeuvres [A, E, I] for caster assembly i=[1...,4] solid black, solid red, dotted red and dotted black respectively.

to the steady-state period, the replenishment of the wheel material may not occur quickly enough to avoid the elastic limit being reached.

While merely anecdotal one other observation is relevant. One subject, in the load selection, in seeking to change vehicle-frame position appeared to produce oscillatory handle motions along with a relatively (compared with the typical slow rate of change) very slow vehicle-frame rotation. The method was prohibited as the motions would not be acceptable with a human occupant. The subject said it was easier this way. It is possible that this subject was reducing the handle-force magnitudes before any relative velocity occurred between wheel and ground contact points, working up to but not beyond the elastic limit, i.e. before scrub friction occurred, and that the vehicle was therefore very slowly changing orientation as the vehicle did not return to the initial vehicle-frame orientation due to hysteresis. The implications are considered further in the Design Section.

This examination also confirms that shimmy is not a relevant model for the experimental-FCMV during the initial period; wheel roll magnitude is too small.

This above explanation in terms of elastic effects harmonises with the motion resistance calculation method by Inoue et al. (2000) and the comments by Stout (1979) that wheels with negligible wheel roll exhibit greater scrub friction than those with non-negligible wheel roll. The three possible counter examples exist two of which (Kauzlarich et al. (1984) and Reid et al. (1990)) (page 40) should not be given too much weight since their experimental designs are not as focussed on

the phenomenon as Inoue et al., Stout or this work. A third objection may exist in (Karnopp, 2004), since the slip angle was deemed to be negligible. However, while the slip angle of a non-pneumatic wheel may be insufficient to generate a cornering force for an active wheel where wheel roll is non-negligible, it is possible that effects on scrub friction for a passive wheel where wheel roll is negligible is a distinct phenomenon.

As this work has not specifically investigated elastic effects –the methodological decision was taken to use a macro approach (page 50) –this elastic effect may be supported in literature not yet identified. In any case the presence of θ_{si} displacements prior to any ${}^{large}_{ss1}\mathbf{P}^r$ in conjunction with evidence for the appropriateness of the quasi-static approach, the distinctive intra-manoeuvre difference based on motion resistance work, the modelling of the $\dot{\theta}_{ti}$ to $\dot{\theta}_{si}$ proportion and the work cited by Inoue et al. (2000) all lend circumstantial support to the view that elastic effects, in so far as the effects of scrub friction may be reduced, may play an important role in the forces-applied and space-required relationship.

If substantiated this observation has an important limiting effect on the results: the location of the CoZV within the manoeuvre r velocity region is important. Manoeuvres [K, L] are not affected as these are points and manoeuvre E is a bounded region but for manoeuvres [A, B, C, D, F, G, H, I] a CoZV at a relatively large distance from the manoeuvre r (a.) position is possible and this may produce different results. It may, for example, be possible to choose a CoZV for manoeuvre B such that the ${}^{large}_{ss1}\mathbf{P}^r$ are diminished: trials (results not presented) indicate that this may be the case. It is also possible that inter-manoeuvre differences are therefore diminished as the radial arm to the CoZV increases. However, the adaptation planning implications may not be important since the space required for manoeuvres with CoZV at a large displacement from the vehicle-frame, compared with the manoeuvre r, may be too large in respect of domestic dwellings. All these questions suggest important areas for future examination.

A single caster assembly test rig has been both designed and built (Medical Physics Technical Aids Section Newcastle upon Tyne) in order to study these effects: a prototype is shown in Figure 7.16 (page 210). This rig also allows for caster assembly rake (page 11) adjustment.

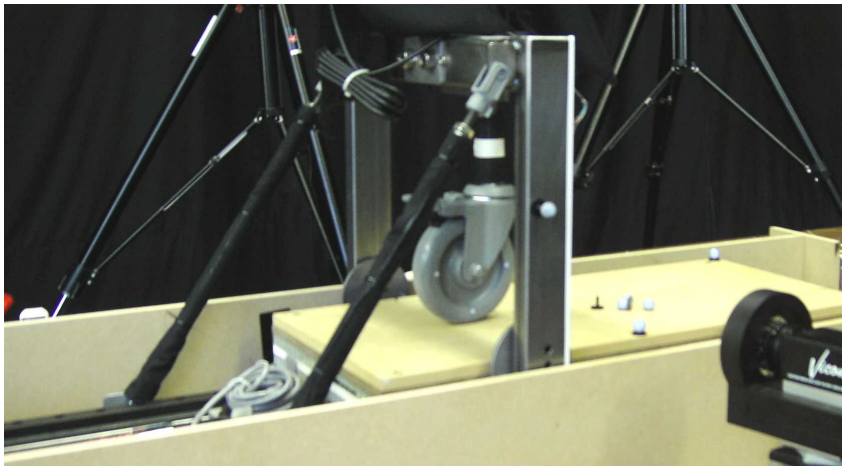

Figure 7.16 – Shows a caster assembly test rig with fixed caster stem and translating floor.

7.7.2. *Walled-manoeuvres*

It was acknowledged in the generality of results section that there may be manoeuvres with superior operator load response than those identified by this work. One potential investigative approach to this would be to provide a space in which, for example, manoeuvre F is possible but not ask the subject to maintain the associated CoZV: load selections for this could then be compared with those for manoeuvre F (attempted). For an initial study only load measures would be required since if no significant difference is found no further work is necessary. If a significant difference is found then a force and kinematics study of these contrasting tasks would be valuable.

Another major element for investigation is the position of the operator and the consequential impact on adaptation planning. As considered in Section 7.6 (page 204) the positions which the the operator can adopt may have an important influence on the load response. A consideration of any walled-manoeuvre investigation is the extent to which the load response is a result of the operator being unable to adopt a preferred position on the one hand and the extent to which it is a result of the handle-force requirements imposed by the motion resistance.

The manoeuvres r approach has considered one manoeuvre type, a vehicle-frame orientation change. There may be other manoeuvre types so further investigation is required to determine the variety of real-FCMV manoeuvres.

7.7.3. *Manoeuvres with only translation*

There are a number of occasions where the primary intention of the operator will be to achieve only translational motions, for example, when pushing a real-FCMV backwards over a toilet, pushing a mobile hoist over a chair or motion along a corridor after making a change in vehicle-frame orientation. Important further work arises from these examples. The first two examples would result in the caster assemblies being set in a reverse trail position when reversing the motion of the vehicle-frame, i.e. coming out. As considered in the Dynamics Chapter this is an unstable position and if space is confined it is possible that, if caster global rotation brings the longer length of the caster assembly outward, there may be a collision with walls or fittings: the real-FCMV may manoeuvre into a narrow passage and there will be no way of manoeuvring out; an understanding and control of the rotation direction would be a valuable area of further study. In the third example the caster assemblies may have various orientations and it would be useful to develop a model which simplifies the understanding of the effects of random initial caster orientation. While the graphical inspection method may be used with varying and different initial orientations, as considered in the Dynamics Chapter the number of regions increases and therefore interpretation is more difficult than occurs when all four caster assemblies begin in the forward trail position.

7.7.4. *Instantaneous centres of zero velocity*

This work has been based on a fixed centre of zero velocity. A more general model would incorporate an instantaneous centre of zero velocity. Both in respect of this issue and examining varied starting caster orientations it may be prudent to develop a more complex motion resistance model since many of the regions may be small and other effects may be more important.

7.7.5. *Design improvements*

This work had no design objectives; however, unexpectedly, a number of potentially important design implications follow from the dynamic examination and arise anecdotally. As no design objectives existed, a structured examination of FCMV design (in respect of design, FCMV are real-FCMV) has not been completed: the knowledge of extant designs in the following consideration is therefore

Figure 7.17 – Shows: (left) a reclining shower chair and (right) the Viking Hoist (Liko) with side arms being used as a walking support but also capable of functioning as a standard mobile hoist. It is to be noted that for the mobile hoist the forward position for the occupant whether supported in a sling or walking, as shown, is reversed, i.e. the occupant faces the operator at transfer on and off seating.

based on and limited to the author's experiences in an adaptation planning service since 1983.

The dynamic analyses (page 98) indicates that the front caster assemblies have a disproportionate effect on handle-forces compared with the rear caster assemblies. There are two potential consequences to this. Firstly, the motion resistance performance of the front caster assemblies is more critical than that of those at the rear. Secondly, it follows that anything which increases the front loading is of importance. This is of particular importance for mobile hoists (page 17). These devices have longer wheel bases than a typical FCMV (as was used for the investigation) and current designs do not appear to be optimised to reduce front caster assembly loading: a design constraint is the need to accommodate the occupant's lower limbs given the presence of what is termed the mast. It follows that occupants of greater size and mass will be further from the mast and therefore create greater front loading. So, unfortunately, mobile hoists for larger masses by having longer wheel bases to accommodate larger people may in part exacerbate the problem which they exist to solve. There is therefore the potential to improve the manoeuvring characteristics by taking account of this effect.

The value of optimising handle-width is also evident from the dynamic analyses since any improvement to the ability to produce a couple is beneficial. Related

to this the experimenter observed the attempted use of the thigh, presumably, to contribute to the couple, though this was prohibited by the experimental method: there is no indication that the potential use of thigh in the initial period has been considered in existing designs.

The dynamic analyses also demonstrated that the inter-manoeuvre difference partly arise because the motion resistance effects are balanced by forces at a distance from the COM, i.e. the location of the force application points is important. The typical FCMV (seat or mobile hoist) has handles at the rear: the application of forces to other parts of the vehicle-frame is possible but there is no evidence to suggest vehicles have been designed to assist this: stability would be an issue. The mobile hoist (page 17) is unusual in that it is available with what are termed side-arms and these are shown in Figure 7.17 (page 212): as shown they are being used for supported walking. Examination of this vehicle by the author indicated, at least for the occupant of the examination, that the side-arm length is insufficient to permit the side-arms to act as an alternative application point for handle-forces: effectively it acts as a half-handle, i.e. one end terminates at a point in line with the vehicle-occupant COM and the other end extends to the mast. More generally, the effective conversion of ACMV to a FCMV due to space constraints also identifies the potential value of designing FCMV such that hand forces can be applied from any side.

It has been identified that the superior operator load response of manoeuvres [K, L] (a.) are not a result of being associated with the smallest handle-forces and that it is possible that additional forces are required to maintain a caster in static equilibrium. This raises the question as to whether or not providing a braking system for the front caster assemblies, the modelling and the results indicate that there is little purpose doing this on the rear caster assemblies, would have a sufficient advantage to justify the cost and maintenance issues. Further work would be required to determine this.

One design approach which is underlined by the results rather than prompted by this work, is the potential value of a FCMV where change of orientation occurs by moving the occupant on the vehicle-frame[1] rather than the vehicle-frame on

[1]Acknowledgement: suggestion by John Snowdon, Adult Services, Newcastle upon Tyne.

the floor. While office-style chairs for assisted occupants do exist the author is not aware of any designs which incorporate over-toilet or shower use.

None of these design observations are straightforward to implement since FCMV design requires a large number of objectives to be optimised. Additionally, since design considerations are unexpected a systematic patent and design investigation has not been made so it is also possible that the above considerations are part of current design knowledge. However, even if no commercial exploitation is possible these design related observation form a criteria for the selection of FCMV, for example, choose as short a mobile hoist wheel base as stability permits.

Finally, a more speculative design issue is whether or not there is any means of developing a drive system taking advantage of what is presumed to be a consequence of the hysteresis effect: it is not known if patents exist for this. This completes both the design considerations and the discussion.

Chapter 8–Conclusion

8.1. **Engineering-based Achievements**

Two major investigative difficulties have been overcome. Firstly, no substantive theoretical or empirical work on this topic existed. Secondly, the set of manoeuvres which can be investigated experimentally is very large. This has been addressed by the development of a novel graphical inspection method: this leads to a finite (thirteen) and representative subset of all the manoeuvres of investigative interest. The members of this manoeuvre subset are distinguished by having the translational velocity of the centre of mass of the combined vehicle and load in different velocity regions.

The dynamic analysis predicts a first order effect for the experimental set-up and this was confirmed empirically. A useful though loose description of the first order effect is that while the four-caster manual vehicle is mechanically omni-directional, there is an effective constraint for the human operator: operators chose substantially smaller maximum comfortable loads for some manoeuvre directions. The maximum comfortable load chosen by the operator can vary by 100% between these different manoeuvres. A more precise summarising explanation of the first order effect is as follows: 1) inertial forces may be disregarded and explanation can be made in terms of motion resistance, 2) motion resistance effects are a result of two effects resulting from the different velocity regions, 3a) the different velocity regions result in varying combinations of the eight (maximum) angular velocity wheel directions which arise from four (maximum) caster assemblies, 3b) the different velocity regions produce varying caster orientations, 4) these motion resistance effects may be viewed as a translational component and the moment component which results from the motion resistance effect of each caster assembly acting on

the vehicle-frame, 5) the proportion of moment to translational effect of motion resistance varies for the different velocity regions, 6) the resulting handle-forces which the operator applies to balance motion resistance can vary substantially for the different velocity regions, and 7) the comparative operator load response varies substantially for some velocity regions.

The forces-applied and space-required relationship identified in this work makes an important and novel contribution to the state of the art for adaptation planning. The different velocity regions have different centres of zero velocity. As vehicle, occupant and operator will typically make a $\frac{\pi}{2}$ rad direction change, there is substantial variation in space requirements for the different manoeuvres. With respect to existing architectural spaces, this understanding of the forces-applied and space-required relationship shows that the space may require the operator to make a manoeuvre for which a relatively large or relatively small comfortable maximum load may be chosen. With respect to disability adaptation planning this understanding identifies spaces which maximise the operator's load capacity.

The visual accounts of the forces-applied and space-required relationship are accessible to the non-engineer, for example, those involved with adaptation planning. The application of forces-applied and space-required relationship to adaptation planning is not intuitive: larger spaces do not necessarily result in improved operator load capacity and small spatial differences can have a substantial load capacity effect. However, the approach taken produces straightforward visual accounts of the forces-applied and space-required relationship.

The results are applicable to a wide range of floor coverings and four-caster manually manoeuvred vehicles. This is achieved by the relative approach which has been taken, an inter-manoeuvre comparison rather than, for example, strength measurement or motion resistance measurement. With respect to varying vehicle types, the results are conservative.

The results are applicable to a wider, non-domestic setting: ergonomists are currently investigating the health and safety of all-caster vehicle manoeuvring. These results provide a fuller account of the importance of the non-sagittal components of force application when caster orientation is not in the forward trailing

position.

This investigation provides the basis for four-caster manual vehicle design development. This is unexpected as this investigation had no design objectives. However, it is implicit in the forces-applied and space-required relationship that certain design features, such as the disproportionate effects of the front caster assemblies, have direct bearing on the design of vehicles which maximises operator load capacity. This could form the basis of commercial exploitation or the development of design criteria for vehicle selection.

8.2. **Adaptation Planning-based Outcomes**

A number of qualitative principles for adaptation planning may be derived from this study which in loose terms are:

The direction of motion, for example, does the FCMV move to the left or to the operator's right, can make the manoeuvre difficult or easy.

Manoeuvres where the operator attempts to keep the front caster assembly from moving will be easiest.

Manoeuvres where the operator attempts to rotate the FCMV around a point at the rear of the vehicle will be the most difficult.

Operators will choose a substantially greater maximum comfortable load with the easier manoeuvres compared with the difficult manoeuvres.

Two important generalities also arise:
The above principles can take account of any vehicle size and operator size or body shape.

The above principles may be applied to any FCMV and floor covering on a level floor.

8.3. **Further Work**

Publications for the adaptation planning, ergonomic and biomechanical communities are in preparation. Investigation of second order effects using a single caster assembly rig is also in preparation. As the results are based on the voluntary maintenance of a centre of zero velocity by the operator and not by wall constraints, further investigation into operator abilities when subject to wall constraints is identified as necessary.

This work also demonstrates a new approach to adaptation planning: the application of engineering methods to low technology access devices. This approach complements a biomechanical based or motor control based approach. In this approach it is not the origins of the operator's abilities which are examined but rather the effects in terms of a load response to the mechanism subject to various space constraints. The longer term intention is to investigate other vehicles such as those with fixed wheels and caster assemblies.

8.4. **Final Statement**

This work achieves a substantial advancement in the understanding of the forces-applied and space-required relationship for four-caster manually manoeuvred vehicles: in loose terms the easiest and most difficult manoeuvres have been identified. This has particular value for adaptation planning for disabled people for whom use of these vehicles has crucial importance in the achievement of and dignity in basic activities of daily living. This work provides an important new approach to adaptation planning.

8.5. **Contributors**

Mr R. I. Davidson, Newcastle University, UK: design of the experimental vehicle.

Dr Z. X. Hu, Newcastle University, UK: software design for sensor interface.

UK Occupational Therapy Research Foundation: funding for sensor.

Bibliography

Abel, E. W., 1983. Survey of attendant propelled mobile chairs used in hospitals. *Health Bulletin (Edinburgh)* 41 (5), 275–277.

Abel, E. W., 1988. *A biomechanical study of the manual pushing of vehicles.* Ph.D. thesis, University of Dundee.

Abel, E. W., Frank, T. G., 1991. The design of attendant propelled wheelchairs. *Prosthetics and Orthotics International* 15 (1), 38–45.

AbleData, 2011. *The guide to AbleData indexing terms.* AbleData Available at: http://www.abledata.com/abledata_docs/2011_AbleData%20_Guide.pdf Accessed on 1 August 2011.

Abraham, B., Johnson, G., 2006. Constrained outlines: a method for creating access guidelines for individual wheelchair users. *British Journal of Occupational Therapy* 69 (8), 379–385.

Abraham, B. B., Johnson, G. R., 2010. A quasi-static state examination of handle forces and translational acceleration at impending planar motion for the four-caster manually manoeuvred vehicle. *Proceedings of the Institution of Mechanical Engineers, Part K: Journal of Multi-body Dynamics* 224 (2), 143–156.

Al-Eisawi, K. W., Kerk, C. J., Congleton, J. J., Amendola, A. A., Jenkins, O. C., Gaines, W., 1999. Factors affecting minimum push and pull forces of manual carts. *Applied Ergonomics* 30, 235–245.

Audit Comission, 2000. *The provision of equipment to older or disabled people by the NHS and social services in England and Wales.* Audit Comission, London.

Barthorpe, F., 1994. Steering shopping down the right track. *Professional Engineering* 7 (16), 2–3.

Benedict, C., Pooley, S., Grisbooke, J., 2006. Ergonomics and housing. *In: Clutton, S., Grisbooke, J., Pengelly, S. (Eds.), Building on firm foundations.* Whurr Publishers Limited, Chichester.

British Standards Institution, 2007a. *Assistive products for persons with disability – classification and terminology.* BSI BS EN ISO 9999:2007, London.

British Standards Institution, 2007b. *Wheelchairs-part 26: vocabulary.* BSI BS ISO 7176-26:2007, London.

British Standards Institution, 2008. *Wheelchairs-part 5: Determination of dimensions, mass and manoeuvring space.* BSI BS ISO 7176-5:2008, London.

British Standards Institution, 2010. *Design of buildings and their approaches to meet the needs of disabled people-code of practice.* BSI BS 8300:2009+A1:2010, London.

Care Services Improvement Partnership, 2006. *Out and about: wheelchairs as part of a whole-systems approach to independence.* Department of Health, London.

Center for Inclusive Design and Environmental Access, 2010. *Anthropometry of wheeled mobility project.* IDeA, New York.

Chaffin, D. B., Andersson, G. B. J., Martin, B. J., 2006. *Occupational biomechanics*, 4th Edition. Wiley-Interscience, New Jersey.

Chénier, F., Bigras, P., Aissaoui, R., 2011. An orientation estimator for the wheelchair's caster wheels. *IEEE Transactions on Control Systems Technology* 19 (6), 1317 –1326.

Ciriello, V. M., Dempsey, P. G., Maikala, R. V., O'Brien, N. V., 2001. Maximum acceptable horizontal and vertical forces of dynamic pushing on high and low coeffient of friction floor. *International Journal of Industrial Ergonomics* 77 (1), 1–8.

Ciriello, V. M., Snook, S. H., 1978. The effects of size, distance, height, and frequency on manual handling performance. *In: Human Factors and Ergonomics*

Society (Ed.), Proceedings of the Human Factors Society-22nd Annual Meeting. Human Factors and Ergonomics Society, Santa Monica, 318–322.

Conneeley, A. L., 1998. The impact of the Manual Handling Operations Regulations 1992 on the use of hoists in the home: the patients perspective. *British Journal of Occupational Therapy* 61 (1), 17–21.

Consumer Focus, 2010. *Equipment for older and disabled people: an analyses of the market.* Consumer Focus, London.

Cooper, R. A., O'Connor, T. J., Gonzalez, J. P., Boninger, M. L., Rentschler, A., 1999. Augmentation of the 100 kg ISO wheelchair test dummy to accommodate higher mass: a technical note. *Journal of Rehabilitation Research and Development* 36 (1), 48–54.

Cowan, R. E., Nash, M. S., Collinger, J. L., Koontz, A. M., Boninger, M. L., 2009. Impact of surface type, wheelchair weight, and axle position on wheelchair propulsion by novice older adults. *Archives of Physical Medicine and Rehabilitation* 90 (7), 1076–1083.

Daniel, W. W., 1990. *Applied nonparametric statistics*, 2nd Edition. The Duxbury Advanced Series in Statistics and Decision Sciences. PWS- KENT Publishing Company, Boston.

Das, B., Wimpee, J., Das, B., 2002. Ergonomics evaluation and redesign of a hospital meal cart. *Applied Ergonomics* 33 (4), 309–318.

De Groot, S., Zuidgeest, M., van der Woude, L. H. V., 2006. Standardization of measuring power output during wheelchair propulsion on a treadmill: pitfalls in a multi-center study. *Medical Engineering & Physics* 28 (6), 604–612.

De Vries, W. H. K., Veeger, H. E. J., Baten, C. T. M., van der Helm, F. C. T., 2009. Magnetic distortion in motion labs, implications for validating inertial magnetic sensors. *Gait & Posture* 29 (4), 535–541.

Dempsey, P. G., 2004. Psychophysical aspects of muscle strength. *In: Kumar, S. (Ed.), Muscle strength.* CRC Press, Boca Raton.

Department of Environment Transport and Regions, 1999. *The Building Regulations 1991 Access and facilities for disable people: approved document M.* HMSO, London.

Eriksson, J., Ek, Å., Johansson, G., 2000. Design and evaluation of a software prototype for participatory planning of environmental adaptations. *IEEE ASSP Magazine Transactions on Rehabilitation Engineering* 8 (1), 94–105.

Eriksson, J., Johansson, G., 1996. Adaptation of workplaces and homes for disabled people using computer-aided design. *International Journal of Industrial Ergonomics* 17 (2), 153–162.

Feeney, R., 2003. BS 8300 - the research behind the Standard. *In: Space requirements for wheeled mobility.* IDeA Center, New York.

Ferreira, J., Smith, M., 2007. *Evaluating the feasibility of developing assessment charts for high risk pushing and pulling operations.* Tech. Rep. RR562, HSE Books, Sudbury.

Ferreira, J. J., Boocock, M. G., Gray, M. I., 2004. *Review of the risks associated with pushing and pulling heavy loads.* Tech. Rep. 228, HSE Books, Sudbury.

Fisher, D. A., 1876. *Improvement in furniture-casters.* US Patent 174,794.

Flores, P., Ambrósio, J., Claro, J. C. P., Lankarani, H. M., 2007. Dynamic behaviour of planar rigid multi-body systems including revolute joints with clearance. *Proceedings of the Institution of Mechanical Engineers, Part K: Journal of Multi-body Dynamics* 221 (2), 161–174.

Frank, T. G., Abel, E. W., 1989. Measurement of the turning, rolling and obstacle resistance of wheelchair castor wheels. *Journal of Biomedical Engineering* 11 (11), 462–466.

Frank, T. G., Abel, E. W., 1991. Drag forces in wheelchairs. *In: van der Woude, L. H., Meijs, P., van der Grinten, B., de Boer, Y. (Eds.), Proceedings of the Workshop Held in Amsterdam October 1991: Ergonomics of Manual Wheelchair Propulsion.* IOS Press, Amsterdam, 255–267.

Fujiie, K., Matico, K., Ide, M., 1996. Doorway designs which allow easy access for people with spinal cord injuries. *Japanese Journal of Ergonomics* 32 (5), 215–222.

Genta, G., 1997. *Motor vehicle dynamics: modelling and simulation.* World Scientific Publishing Co. Pte. Ltd., London.

Glaser, R. M., Sawka, M. N., Wilde, S. W., Woodrow, B. K., Suryaprasad, A. G., 1981. Energy cost and cardiopulmonary responses for wheelchair locomotion and walking on tile and on carpet. *Paraplegia* 19 (4), 220–6.

Glitsch, U., Ottersbacha, H. J., Ellegasta, R., Schaubb, K., Franzc, G., Jäger, M., 2007. Physical workload of flight attendants when pushing and pulling trolleys aboard aircraft. *International Journal of Industrial Ergonomics* 37 (11-12), 845–859.

Goldsmith, S., 1976. *Designing for the disabled*, 3rd Edition. RIBA, London.

Goldsmith, S., 1997. *Designing for the disabled; the new paradigm.* Architectural Press, Oxford.

Great Britain, Parliament, 1990. *National Health Service and Community Care Act 1990.* HMSO, London.

Great Britain, Parliament, 1995. *Disability Discrimination Act 1995.* HMSO, London.

Greenwood, D. T., 1965. *Principles of dynamics.* Prentice-Hall International series in dynamics. Prentice-Hall, New Jersey.

Haisman, M. F., Winsmann, F. R., Goldman, R. F., 1972. Energy cost of pushing loaded handcarts. *Journal of Applied Physiology* 33 (2), 181–183.

Ham, R., Patsy, A., Porter, D., 1998. *Wheelchair users and postural seating.* Churchill Livingstone, London.

Harpin, P., 2000. *Adaptations manual.* Musculor Dystrophy Campaign, London.

Harrison, C. S., Grant, P. M., Conway, B. A., 2010. Enhancement of a virtual reality wheelchair simulator to include qualitative and quantitative performance metrics. *Assistive Technology* 22 (1), 20–31.

Heywood, F., 1994. *Adaptations finding ways to say yes.* SAUS Publications, Bristol.

Heywood, F., Turner, L., 2007. *Better outcomes, lower costs.* Department for Work and Pensions, London.

Hitchcock, D., Hussey, M., Burchill, S., Galley, M., 2006. *A survey of occupied wheelchairs and scooters.* Mobility and Inclusion Unit of the Department for Transport, London.

Hoozemans, M. J. M., Kuijer, P. P. F. M., Kingma, I., van Dieën, J. H., de Vries, W. H. K., van der Woude, L. H. V., Veeger, D. J., van der Beek, A. J., Frings-Dresen, M. H. W., 2004. Mechanical loading of the low back and shoulders during pushing and pulling activities. *Ergonomics* 47 (1), 1–18.

Inoue, T., Fernie, G., Santaguida, P., 2000. Measurement of trajectory and push/pull force for maneuvering a wheeled lifting device. *In: Annual Conference of the Rehabilitation Engineering and Assistive Technology Society of North America (RESNA), Orlando June 2000.* RESNA, Arlington US, 387–389.

Iwnicki, S., 2006. *Handbook of railway vehicle dynamics.* CRC Press.

Jäger, M., Sawatzki, K., Glitsch, U., Ellegast, R., Ottersbach, H. J., Schaub, K., Franz, G., Luttmann, A., 2007. Load on the lumbar spine of flight attendants during pushing and pulling trolleys aboard aircraft. *International Journal of Industrial Ergonomics* 37 (11-12), 863–876.

Jansen, J. P., Hoozemans, M. J., van der Beek, A. J., Frings-Dresen, M. H., 2002. Evaluation of ergonomic adjustments of catering carts to reduce external pushing forces. *Applied Ergonomics* 33 (2), 117–127.

Johnson, B. D., 2007. The nonholonomy of the rolling sphere. *The American Mathematical Monthly* 114 (6), 500–508.

Johnson, K. L., 1958. The effect of spin upon the rolling motion of an elastic sphere on a plane. *Journal of Applied Mechanics* 25, 332–338.

Kane, T. R., Levinson, D. A., 1978. A realistic solution of the symmetric top problem. *Journal of Applied Mechanics* 45, 903–909.

Karnopp, D., 1985. Computer simulation of stick-slip friction in mechanical dynamic systems. *Transactions of the ASME; Journal of Dynamic Systems, Measurement, and Control* 107 (1), 100–103.

Karnopp, D., 2004. *Vehicle stability*. CRC, New York.

Kauzlarich, J. J., Bruning, T., Thacker, J. G., 1984. Wheelchair caster shimmy and turning resistance. *Journal of Rehabilitation Research and Development* 20 (2), 15–29.

Kauzlarich, J. J., Bruning III, T. E., Thacker, J. G., 2000. Wheelchair caster shimmy II: damping. *Journal of Rehabilitation Research and Development* 37 (3), 305–13.

Kauzlarich, J. J., Thacker, J. G., 1985. Wheelchair tire rolling resistance and fatigue. *Journal of Rehabilitation Research and Development* 22 (3), 25–41.

King, L., 1985. A comparative evaluation of three supermarket shopping carts. *In: Brown, I. D., Goldsmith, R., Coombes, K., Sinclair, M. (Eds.), Proceedings of the Ninth Congress of the International Ergonomics Association, Bournmouth September 1985*. Taylor and Francis, London, 625–654.

Kirby, R. L., Mifflen, N. J., Thibault, D. L., Smith, C., Best, K. L., Thompson, K. J., MacLeod, D. A., 2004. The manual wheelchair-handling skills of caregivers and the effect of training. *Archives of Physical Medicine and Rehabilitation* 85 (12), 2011–2019.

Koontz, A. M., Cooper, R. A., Boninger, M. L., Yang, Y., Impink, B. G., van der Woude, L. H. V., 2005. A kinetic analysis of manual wheelchair propulsion during start-up on select indoor and outdoor surfaces. *Journal of Rehabilitation Research and Development* 42 (4), 447–458.

Kumar, S., Narayan, Y., Bacchus, C., 1995. Symmetric and asymmetric two-handed pull-push strength of young adults. *Human Factors* 37 (4), 854–865.

Lawson, J., Potiki, J., Watson, H., 1993. Development of ergonomic guidelines for manually handled trolleys in the health industry. *In: Pollock, C. M., Straker, L. M. (Eds.), Ergonomics in a Changing World Proceedings of the 29th Annual*

Conference of the Ergonomics Society of Australia, December 1993 Perth Australia. Ergonomics Society of Australia, Downer, ACT: Australia, 146–153.

Mack, K., Haslegrave, C. M., Gray, M. I., 1995. Usability of manual handling aids for transporting materials. *Applied Ergonomics* 26 (5), 353–364.

MacPhee, A. H., Kirby, R. L., Bell, A. C., MacLeod, D. A., 2001. The effect of knee-flexion angle on wheelchair turning. *Medical Engineering & Physics* 23 (4), 275–83.

Major, R. E., 1990. Some aspects of wheeled geometry relating to manually propelled wheelchairs. *Physiotherapy* 76 (10), 663–665.

Mandelstam, D., 1989a. *Understanding incontinence*. Chapman and Hall, London.

Mandelstam, M., 1989b. *DLF Thesaurus*. Disabled Living Foundation, London.

Matheson, L. and Mooney, V. Caiozzo, V. and Jarvis, G. Pottinger, J. DeBerry, C. Backlund, K. Klein, K. Antoni, J., 1992. Effect of instructions on isokinetic trunk strength testing variability reliability, absolute value and predictive validity. *Spine* 17 (8), 914–921.

Meriam, J., Kraige, L., 2003. *Engineering mechanics dynamics*, 5th Edition. John Wiley & Sons, Inc., NJ.

Minns, J., Tracey, S., 2010. Wheelchair pushing forces over a vinyl and a new shock -absorbing flooring. *British Journal of Occupational Therapy* 74 (1), 41–43.

NORA Musculoskeletal Disorders Team, 2001. *National occupational research agenda for musculoskeletal disorders: research topics for the next decade*. National Institute for Occupational Safety and Health, Cincinnati.

Northern Ireland Housing Executive, 2006. *Wheelchair user - housing study*. NIHE, Belfast.

Ownsworth, A., 1973. *Housing for the disabled part one: an ergonomic study of the space requirements of wheelchair users for doorways and corridors*. Institute for Consumer Ergonomics Ltd, Loughborough.

Pacejka, H. B., 2000. Modelling of tyre force and moment generation. *In: Jacobson, B., Kalker, J. J. (Eds.), Rolling contact phenomena.* Springer-Verlag Wien, New York.

Pan, X., Han, C. S., Law, K. H., 2010. Using motion planning to determine the existence of an accessible route in a CAD environment. *Assistive Technology* 22 (1), 32–45.

Petzäll, K., Petzäll, J., 2003. Transportation with hospital beds. *Applied Ergonomics* 34 (4), 383–392.

Rehabilitation Engineering & Assistive Technology Society of North America, 2011. *Wheelchair service provision guide.* RESNA, Arlington US.

Reid, M., Lawrie, A. T., Hunter, J., Warren, P. M., 1990. The effect of steering on the physiological energy cost of wheelchair propulsion. *Scandinavian Journal of Rehabilitation Medicine* 22 (3), 139–43.

Rodgers, S. H., 1986. *Ergonomic design for people at work : a source book for human factors practitioners in industry including safety, design and industrial engineers: medical, industrial hygiene, and industrial relations personnel, and management. vol 2, the design of jobs, including work patterns, hours of work, manual materials handling tasks, methods to evaluate job demands, and the physiological basis of work by the Ergonomics Group, Health and Environment Laboratories, Eastman Kodak Company.* Vol. 2. Van Nostrand Reinhold, New York.

Sawatzky, B. J., 2005. Measuring energy expenditure using heart rate to assess the effects of wheelchair tyre pressure. *Clinical Rehabilitation* 19 (2), 182–187.

Skillings, J. H. Mack, G. A., 1981. On the use of a friedman-type statistic in balanced and unbalanced block designs. *Technometrics* 263 (2), 171–177.

Soldi, M., Rondinelli, I., 1766. *Descrizione degl'instrumenti, delle macchine, e delle suppellettili raccolte ad uso chirurgico e medico dal p.don ippolito rondinelli ferrarese.* Faenza.

Sönmez, M., 2003. A study on the combined effect of axle friction and rolling resistance. *International Journal of Mechanical Engineering Education* 31 (2), 101–107.

Stolarski, T. A., Tobe, S., 2000. *Rolling contacts*. Professional Engineering Publishing Limited, Bury St Edmunds.

Stout, G., 1979. Some aspects of high performance indoor/outdoor wheelchairs. *Bulletin of Prosthetics Research* 16 (2), 135–175.

Strindberg, L., Petersson, N., 1972. Measurement of force perception in pushing trolleys. *Ergonomics* 15 (4), 435–438.

Tanimoto, Y., Tokuhiro, A., Yamamoto, H., Nanba, K., Ukida, H., 2009. Measurement of wheelchair turn radius for SCI patient's remodeling house. *In: I2MTC: 2009 IEEE Instrumentation & Measurement Technology Conference, Vols 1-3 Singapore May 2009*. IEEE, New York, 1326–1330.

Tariku, F. A., Rogers, R. J., 2001. Improved dynamic friction models for simulation of one-dimensional and two-dimensional stick-slip motion. *Journal of Tribology* 123 (4), 661–669.

Thanjavur, K., Rajagopalan, R., 1997. Ease of dynamic modelling of wheeled mobile robots (WMRs) using Kane's approach. *In: Proceedings of the 1997 IEEE International Conference on Robotics and Automation, Albuquerque, New Mexico April 1997*. IEEE, New York, 2926–2931.

Townsend, C. M., 1964. *Improvements relating to load bearing balls such as ball-castors*. GB Patent 938675.

Tupling, S. J., Davis, G. M., Pierrynowski, M. R., Shephard, R. J., 1986. Arm strength and impulse generation: initiation of wheelchair movement by the physically disabled. *Ergonomics* 29 (2), 303–311.

Van der Beek, A. J., Kluvers, B. D. R., Frings-Dresen, M. H. W., Hoozemans, M. J. M., 2000. Gender differences in exerted forces and physiological load during pushing and pulling of wheeled cages by postal workers. *Ergonomics* 43 (2), 269–281.

Van der Woude, L. H. V., de Groot, S., Janssen, T. W. J., 2006. Manual wheelchairs: Research and innovation in rehabilitation, sports, daily life and health. *Medical Engineering & Physics* 28 (9), 905–915.

Van der Woude, L. H. V., Geurts, C., Winkelman, H., Veeger, H., 2003. Measurement of wheelchair rolling resistance with a handle bar push technique. *Journal of Medical Engineering & Technology* 27 (6), 249–258.

Van der Woude, L. H. V., van Koningsbruggen, C., Kroes, A., Kingma, I., 1995. Effect of push handle height on net moments and forces on the musculosketal system during standardised wheelchair pushing tasks. *Prosthetics and Orthotics International* 19 (3), 188–201.

Van der Woude, L. H. V., Veeger, H., Dallmeijer, Annet J. Janssen, T. R. L., 2001. Biomechanics and physiology in active manual wheelchair propulsion. *Medical Engineering & Physics* 23 (10), 713–733.

Wetzel, J. E., 1978. On the division of the plane by lines. *The American Mathematical Monthly* 85 (8), 647–656.

Wilkinson, W., 1998. Integrating Human Factors And Engineering Concepts Into Trolley Design. *In: Productivity Ergonomics and Safety - the Total Package. Proceedings of the International Workplace Health and Safety Forum and the 33rd Ergonomics Society of Australia Conference, November 1997, Gold Coast, Australia.* Ergonomics Society of Australia, Downer ACT, Australia.

Winkel, J., 1983. On the manual handling of wide-body carts used by cabin attendants in civil aircraft. *Applied Ergonomics* 14 (3), 162–168.

Wong, J. Y., 2008. *Theory of ground vehicles*, 4th Edition. John Wiley & Sons Inc., New Jersey.

Appendices

Appendix A–Supplementary Details

A.1. **Preliminary**

A.1.1. *Coulomb Friction*

For the arrangement shown in Figure 2.1 (page 6) and defined by Equation 2.1 (page 5) Coulomb friction has two distinct states: applied to the system illustrated one state exists where the relative velocity between the body A and body B is zero and the second state exists where the relative velocity is non-zero. For the case where the relative velocity between body A and body B is zero $\boldsymbol{R}$ displays two features: 1) it acts in the direction opposite to $F\hat{\boldsymbol{n}}$ with a magnitude which equals the magnitude of $F\hat{\boldsymbol{n}}$ but 2) only up to a maximum magnitude which is a function of $\boldsymbol{L}$ and the combined effect of the material properties of body A and body B.

If the magnitude of $F\hat{\boldsymbol{n}}$ increases such that it is greater than the maximum magnitude of $\boldsymbol{R}$ then body A accelerates and develops a relative velocity with respect to body B in which case Coulomb friction operates in the second state: $\boldsymbol{R}$ then acts in a direction opposite to the relative velocity of body A as viewed from body B with a magnitude which is a function of $\boldsymbol{L}$ and the combined effect of the material properties of body A and body B. The maximum magnitude of $\boldsymbol{R}$ may be different in the two states. There is an approximately linear relationship between the maximum magnitude of $\boldsymbol{R}$ and $\boldsymbol{L}$ though it is sufficient for the purposes at hand and more accurate to say that an increase in the latter will produce an increase in the former.

A.1.2. *Wheel*

If it is now assumed that force $F_{Cn}\hat{\boldsymbol{n}}_i$ is applied at point C_i as shown in Figure 2.2 (right), then a change in $\dot{x}_{Cni}$ will occur, i.e. $\ddot{x}_{Cni} \neq 0$. As $\ddot{\theta}_{ti} \neq 0$ and both F_{Cn} and $\boldsymbol{L}$ pass through C_i, the centre of mass, producing no moments, the ground reaction acting at point G_i on the wheel must have a component parallel to the axis of $\hat{\boldsymbol{n}}_i$ to produce this change of angular velocity: this reaction is indicated by F_{Gni} in Figure 2.2 (right): it is assumed that while F_{Gni} acts on a line contact it may be represented as acting through point G_i. As this system is defined as subject to the wheel roll constraint (Equation 2.2, page 7) $F_{Gni}\hat{\boldsymbol{n}}_i$ acts in accordance with the first condition of the Coulomb friction model (Equation 2.1, page 5).

It follows that where Δx_{Cni} is the displacement produced by $\dot{x}_{Cni}$ the negative translational work done by $F_{Gni}\hat{\boldsymbol{n}}_i$ on the wheel is $-F_{Gni}\hat{\boldsymbol{n}}_i \cdot \Delta x_{Cni}\hat{\boldsymbol{n}}_i = -F_{Gni}\Delta x_{Cni}$. The moment about C_i produced by $F_{Gni}\hat{\boldsymbol{n}}_i$ is $rF_{Gni}\hat{\boldsymbol{t}}_i$ which does angular work $rF_{Gni}\hat{\boldsymbol{t}}_i \cdot \Delta\theta_{ti}\hat{\boldsymbol{t}}_i = F_{Gni}r\Delta\theta_{ti}$ on the wheel, where $\Delta\theta_{ti}$ is the angular displacement produced by $\dot{\theta}_{ti}$. By integration, the wheel roll constraint may be expressed in terms of displacements as $\Delta x_{Cni} = r\Delta\theta_{ti}$. Thus the magnitude of negative translational work and positive angular work done by $F_{Gni}\hat{\boldsymbol{n}}_i$ equate and the wheel is shown to be a mechanism which converts linear work to angular work: while friction is an essential part of the system it is not friction in the sense of an energy loss. If the wheel mass is constant and $\boldsymbol{L}$ increases as a result of external forces such as a load added to the vehicle, all other factors unchanged, this increases the maximum magnitude of F_{Gni} before the second condition of Equation 2.1 occurs; it does not increase the magnitude of F_{Gni} since this is not a function of $\boldsymbol{L}$.

A.1.3. *Scalar measures*

In order to avoid all ambiguity the use of the term 'scalar', 'magnitude' and 'vector' and their graphic representation are described. Figure A.1 (page 233) (left) shows two vectors indicating angular measures: $\boldsymbol{\theta}_1$ and $\boldsymbol{\theta}_2$ directed as shown by the arrows with directions $\hat{\boldsymbol{S}}_1$ and $\hat{\boldsymbol{S}}_2$ respectively, where $\hat{\boldsymbol{S}}_2 = -\hat{\boldsymbol{S}}_1$, and with magnitude θ_1 (both vectors). The vectors are over barred and bold in the Figures though not in the text where they are in bold. Figure A.1 illustrates this for angular measures but this is also applied to translational measures. Thus $\boldsymbol{\theta}_1 = \theta_1\hat{\boldsymbol{S}}_1$ and $\boldsymbol{\theta}_2 = \theta_1\hat{\boldsymbol{S}}_2$. In SI units as viewed from $\hat{\boldsymbol{S}}_1$ the scalar measure of $\boldsymbol{\theta}_1$ is therefore

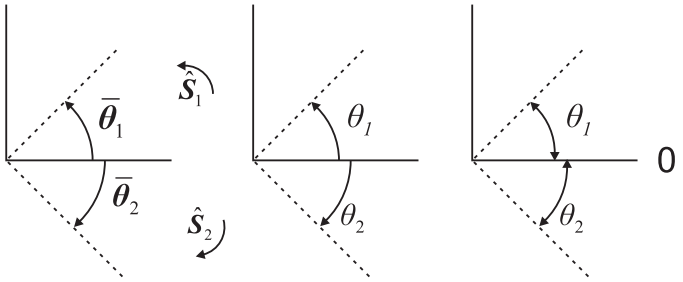

Figure A.1 – Shows the use of vector, scalar and magnitude measures in this text.

θ_1 rad and the the scalar measure of $\boldsymbol{\theta}_2$ is therefore $-\theta_1$ rad. The graphic display of these two *scalar* measures is shown in Figure A.1 (middle): the units are omitted to avoid graphical clutter and an arrow indicates the sign of the scalar measure and the length of the line indicates the magnitude of the scalar. Where a positive scalar measure is indicated then a double headed arrow is used in the illustrations as shown in Figure A.1 (right) and, for example, the wheel radius r is displayed this way with a straight line representing a translational measure. Unless indicated otherwise this convention is followed throughout the text.

A.1.4. *Caster assembly: non-ideal*

Figure A.1.4 illustrates the fixing possibilities of the caster assembly to the vehicle-frame from real-FCMV

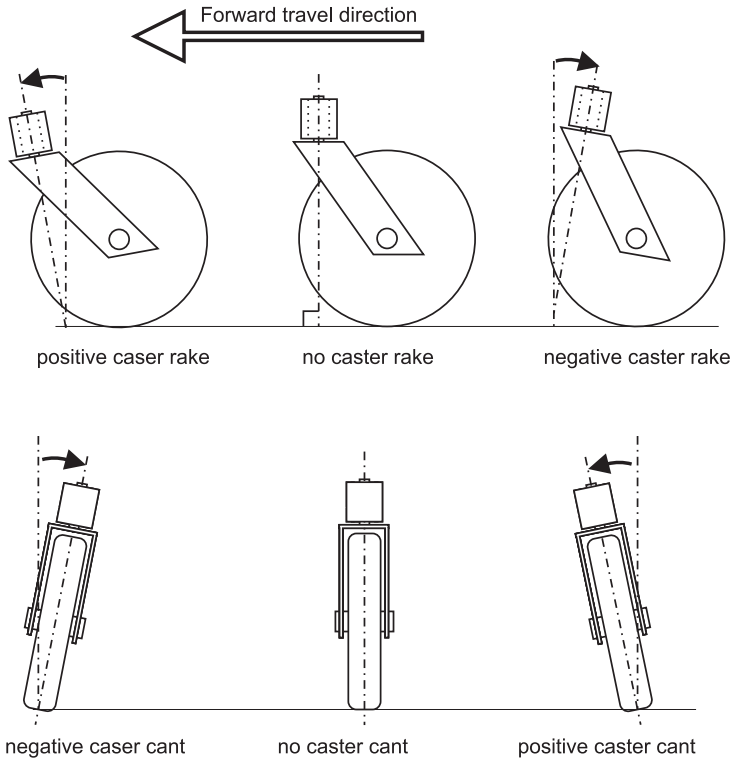

Figure A.2 – Shows the geometry for the fixing for the non-ideal caster assembly: negative cant brings the stem axis through the vehicle-frame

A.2. **Literature: ACMV numbers**

An indication of how much of this wheelchair use is ACMV use in the UK was gained as follows. Newcastle City Loan Equipment Service has on loan [205, 457, 87, 291 589] ACMV: mobile hoists, commodes, standard mobile shower chairs, special order mobile shower chairs, and electric beds, respectively. (Graham A (2011) E-mail communication on 30th November 2011 from Annette Graham, Administration Coordinator, Newcastle City Loan Equipment Service). Special order mobile shower chairs are a combination of FWV and ACMV with an estimated proportion of 40% to 60%, respectively: (Gibson S (2011) E-mail communication on 1st August 2011 from Steve Gibson, Sales Representative, Westholme Ltd.). Newcastle upon Tyne population is approximately 290 000 and the UK population is approximately 62 000 000. A guide to ACMV issue in UK is therefore 320 000.

A.3. **Dynamics**

A.3.1. *Qualitative account*

This section provides an intuitively accessible account of the Dynamics Chapter: there are five steps using intuitively reasonable claims or simple observa-

tions. The first step is the recognition that two distinct conditions could require a operator to apply relatively large forces to the FCMV. One condition exists if, like the wheelchair sprinter, the operator wishes to be as quick as possible: in mechanical terms, if a large acceleration is required. However, as the area of interest is confined spaces where not colliding with walls is essential, the manoeuvres will be slow, i.e. the forces required to produce the necessary accelerations are small compared to the second condition and may be disregarded. The second condition relates to the observation that each caster assembly has two motions with respect to the floor: one motion is that the whole caster assembly changes orientation about a vertical axis as the wheel rubs on the floor and the other motion is that the caster wheel rolls. Some vehicle and occupant weights and floor-covering types may require relatively large handle forces: a very slow manoeuvre with a 150kg (24 stone) occupant on a shag-pile carpet would require relatively large handle forces; a very quick manoeuvre with a 50kg (8stone) occupant on a wood laminate floor would require relatively small forces.

The second step is to recognise that as each caster assembly is connected to the frame of the FCMV a force must be applied by the frame on the caster assembly to overcome the resistance to changes in caster assembly orientation and the resistance to wheel roll. The direction of that force will vary at each caster assembly depending on these resistances and the orientation of the caster assembly with respect to the frame of the FCMV: the distinct feature of caster assemblies compared with self-propelling wheels is that the orientation with respect to the vehicle frame can change. A FCMV manoeuvre may therefore be thought of as the production of the necessary force at each of the four caster assemblies. The operator is not conscious of doing so but from a mechanical view-point that is what occurs.

The third step is the observation that each caster assembly may change orientation in a clockwise or an anti-clockwise direction and that each caster wheel may roll forwards or backwards: there are therefore a finite number of combinations of possible angular motion directions. The importance of this observation is that it can also be shown that the greatest effect on the force at each caster assembly is the combination of angular motion directions. In brief, the direction of these

angular motions has a greater effect on handle forces than anything else.

The fourth step is the observation that the combination of the angular directions (caster assembly orientation direction and wheel roll direction) is dependent on the manoeuvre which the operator makes: for example, if the operator changes the orientation of the frame of the FCMV in the anti-clockwise direction and moves the vehicle frame to the right (manoeuvre F) then one combination of directions will arise but if the vehicle frame is moved in the forward direction (manoeuvre B) another combination of directions will arise. The importance of this observation is the recognition that different forces must therefore exist at each caster assembly connection to the vehicle frame in order to balance the different motion resistance effects and that these forces depend on the manoeuvre. Thus from a specific starting point in a corridor different forces may be required depending on where the door into the desired room is located.

The fifth step is the observation that the operator does not apply the forces directly to the caster assemblies but to the handles so account must be taken of the fact that forces are applied at a distance from the caster assemblies. The implication is intuitively evident when the difference between moving an object using a long stick is compared with moving an object by grasping the object.

With these five observations it is now possible to recognise that forces applied at the handles varies depending on the manoeuvre and that the operator may find that the maximum comfortable weight for different manoeuvres, i.e. different manoeuvres require different combinations of angular motion directions and orientation of caster assembly with respect to the FCMV frame may result, vary.

A.3.2. *O_i points*

The following details the derivation of the O_i points from Equations 4.5 and 4.6 for which Equation 4.7 is the concluding form.

With $\dot{\theta}_{si}$ as given in Equation 4.5

$$\dot{\theta}_{si} = \left\{\left(-\dot{x}_{Bu} + a_{1i}w\dot{\theta}_0\right)\sin\left({}^B\theta_{si}\right) + \left[\dot{x}_{Bv} + \left(a_{2i}\tfrac{l}{2} - c\right)\dot{\theta}_0\right]\cos\left({}^B\theta_{si}\right)\right\}t^{-1} \quad \text{and}$$

setting $\dot{\theta}_{si}$ to zero and expressing in terms of $\dot{x}_{Bu}$ gives

$$\dot{x}_{Bu}\sin\left({}^{B}\theta_{si}\right) = a_{1i}w\dot{\theta}_0, \sin\left({}^{B}\theta_{si}\right) + \dot{x}_{Bv}\cos\left({}^{B}\theta_{si}\right) + \left(a_{2i}\frac{l}{2} - c\right)\dot{\theta}_0\cos\left({}^{B}\theta_{si}\right). \tag{A.1}$$

With $\dot{\theta}_{ti}$ as given in Equation 4.6

$\dot{\theta}_{ti} = \left\{\dot{x}_{Bu} - a_{1i}w\dot{\theta}_0\cos\left({}^{B}\theta_{si}\right) + \left[\dot{x}_{Bv} + \left(a_{2i}\frac{l}{2}c\right)\dot{\theta}_0\right]\sin\left({}^{B}\theta_{si}\right)\right\} r^{-1}$

and setting $\dot{\theta}_{ti}$ to zero and expressing in terms of $\dot{x}_{Bv}$ gives

$$\dot{x}_{Bv} = -\dot{x}_{Bu}\frac{\cos\left({}^{B}\theta_{si}\right)}{\sin\left({}^{B}\theta_{si}\right)} + a_{1i}w\dot{\theta}_0\frac{\cos\left({}^{B}\theta_{si}\right)}{\sin\left({}^{B}\theta_{si}\right)} - \left(a_{2i}\frac{l}{2} - c\right)\dot{\theta}_0. \tag{A.2}$$

Substituting Equation A.2 into Equation A.4 gives

$\dot{x}_{Bu}\sin\left({}^{B}\theta_{si}\right) = a_{1i}w\dot{\theta}_0, \sin\left({}^{B}\theta_{si}\right)$
$+ \left[-\dot{x}_{Bu}\frac{\cos\left({}^{B}\theta_{si}\right)}{\sin\left({}^{B}\theta_{si}\right)} + a_{1i}w\dot{\theta}_0\frac{\cos\left({}^{B}\theta_{si}\right)}{\sin\left({}^{B}\theta_{si}\right)} - \left(a_{2i}\frac{l}{2} - c\right)\dot{\theta}_0\right]\cos\left({}^{B}\theta_{si}\right)$
$+ \left(a_{2i}\frac{l}{2} - c\right)\dot{\theta}_0\cos\left({}^{B}\theta_{si}\right)$
and dividing by $\sin\left({}^{B}\theta_{si}\right)$, cancelling and collecting terms gives
$\dot{x}_{Bu} = a_{1i}w\dot{\theta}_0 - \dot{x}_{Bu}\left(\frac{\cos\left({}^{B}\theta_{si}\right)}{\sin\left({}^{B}\theta_{si}\right)}\right)^2 + a_{1i}w\dot{\theta}_0\left(\frac{\cos\left({}^{B}\theta_{si}\right)}{\sin\left({}^{B}\theta_{si}\right)}\right)^2$
$\Rightarrow \dot{x}_{Bu}\left(1 + \frac{\cos\left({}^{B}\theta_{si}\right)^2}{\sin\left({}^{B}\theta_{si}\right)^2}\right) = a_{1i}w\dot{\theta}_0 + a_{1i}w\dot{\theta}_0\left(\frac{\cos\left({}^{B}\theta_{si}\right)^2}{\sin\left({}^{B}\theta_{si}\right)^2}\right)$
$\Rightarrow \dot{x}_{Bu}\left(1 + \frac{\cos\left({}^{B}\theta_{si}\right)^2}{\sin\left({}^{B}\theta_{si}\right)^2}\right) = a_{1i}w\dot{\theta}_0\left(1 + \frac{\cos\left({}^{B}\theta_{si}\right)^2}{\sin\left({}^{B}\theta_{si}\right)^2}\right)$
so $\dot{x}_{Bu} = a_{1i}w\dot{\theta}_0$

Dividing Equation A.4 by $\sin\left({}^{B}\theta_{si}\right)$ gives

$$\dot{x}_{Bu} = a_{1i}w\dot{\theta}_0 + \dot{x}_{Bv}\frac{\cos\left({}^{B}\theta_{si}\right)}{\sin\left({}^{B}\theta_{si}\right)} + \left(a_{2i}\frac{l}{2} - c\right)\dot{\theta}_0\frac{\cos\left({}^{B}\theta_{si}\right)}{\sin\left({}^{B}\theta_{si}\right)} \tag{A.3}$$

and substituting Equation A.3 into A.2 gives

$\dot{x}_{Bv} = -\left[a_{1i}w\dot{\theta}_0 + \dot{x}_{Bv}\frac{\cos\left({}^{B}\theta_{si}\right)}{\sin\left({}^{B}\theta_{si}\right)} + \left(a_{2i}\frac{l}{2} - c\right)\dot{\theta}_0\frac{\cos\left({}^{B}\theta_{si}\right)}{\sin\left({}^{B}\theta_{si}\right)}\right]\frac{\cos\left({}^{B}\theta_{si}\right)}{\sin\left({}^{B}\theta_{si}\right)}$
$+a_{1i}w\dot{\theta}_0\frac{\cos\left({}^{B}\theta_{si}\right)}{\sin\left({}^{B}\theta_{si}\right)} - \left(a_{2i}\frac{l}{2} - c\right)\dot{\theta}_0$
$\Rightarrow \dot{x}_{Bv} + \dot{x}_{Bv}\left(\frac{\cos\left({}^{B}\theta_{si}\right)}{\sin\left({}^{B}\theta_{si}\right)}\right)^2 = -\left(a_{2i}\frac{l}{2} - c\right)\dot{\theta}_0\left(\frac{\cos\left({}^{B}\theta_{si}\right)}{\sin\left({}^{B}\theta_{si}\right)}\right)^2 - \left(a_{2i}\frac{l}{2} - c\right)\dot{\theta}_0$
$\Rightarrow \dot{x}_{Bv}\left(1 + \left(\frac{\cos\left({}^{B}\theta_{si}\right)}{\sin\left({}^{B}\theta_{si}\right)}\right)^2\right) = -\left(a_{2i}\frac{l}{2} - c\right)\dot{\theta}_0\left(1 + \left(\frac{\cos\left({}^{B}\theta_{si}\right)}{\sin\left({}^{B}\theta_{si}\right)}\right)^2\right)$
so $\dot{x}_{Bv} = \left(a_{2i}\frac{l}{2} - c\right)\dot{\theta}_0$ and $O_i = \left(-\left(a_{2i}\frac{l}{2} - c\right)\dot{\theta}_0, a_{1i}w\,\dot{\theta}_0\right)$ as per equation 4.7.

A.3.3. *Graphic inspection method* ($\hat{\boldsymbol{n}}_i$)

With $\dot{\theta}_{si}$ as given in Equation 4.5

$$\dot{\theta}_{si} = \left\{ \left(-\dot{x}_{Bu} + a_{1i} w \dot{\theta}_0 \right) \sin\left({}^B\theta_{si}\right) + \left[\dot{x}_{Bv} + \left(a_{2i} \tfrac{l}{2} - c \right) \dot{\theta}_0 \right] \cos\left({}^B\theta_{si}\right) \right\} t^{-1}$$

and setting $\dot{\theta}_{si}$ to zero and expressing in terms of $\dot{x}_{Bu}$ gives

$$\begin{aligned}
\dot{x}_{Bu} \sin\left({}^B\theta_{si}\right) &= a_{1i} w \dot{\theta}_0, \sin\left({}^B\theta_{si}\right) + \dot{x}_{Bv} \cos\left({}^B\theta_{si}\right) + \left(a_{2i} \frac{l}{2} - c \right) \dot{\theta}_0 \cos\left({}^B\theta_{si}\right) \\
\Rightarrow \dot{x}_{Bu} &= a_{1i} w \dot{\theta}_0 + \dot{x}_{Bv} \cot\left({}^B\theta_{si}\right) + \left(a_{2i} \frac{l}{2} - c \right) \dot{\theta}_0 \cot\left({}^B\theta_{si}\right) \\
\Rightarrow \dot{x}_{Bu} &= \dot{x}_{Bv} \cot\left({}^B\theta_{si}\right) + \dot{\theta}_0 \left(a_{1i} w + \left(a_{2i} \frac{l}{2} - c \right) \cot\left({}^B\theta_{si}\right) \right) \\
\Rightarrow \dot{x}_{Bu} &= \dot{x}_{Bv} \cot\left({}^B\theta_{si}\right) + \dot{\theta}_0 \mathrm{A}_i \qquad \text{(A.4)}
\end{aligned}$$

where $\mathrm{A}_i = \left(a_{1i} w + \left(a_{2i} \frac{l}{2} - c \right) \cot\left({}^B\theta_{si}\right) \right)$.

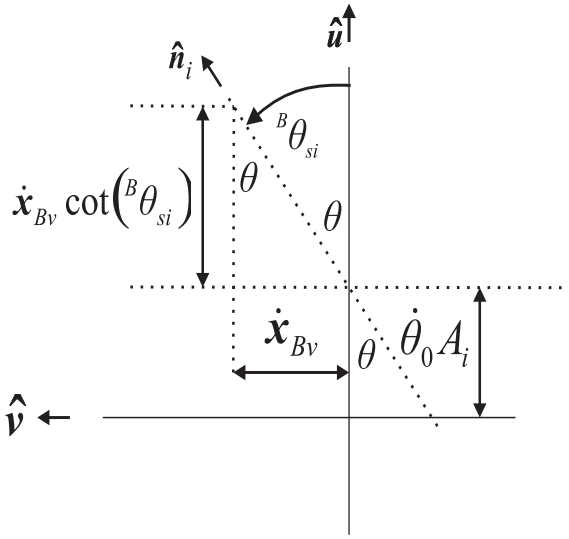

Figure A.3 – Shows the geometric relationship between the gradient of $\theta_{si} = 0$ (dotted diagonal line) and $\hat{\boldsymbol{n}}_i$ on the $\boldsymbol{x}_B$-plane.

It can be seen from Figure A.3 that

$$\begin{aligned}
\tan(\theta) &= \frac{\dot{x}_{Bv}}{\dot{x}_{Bv} \cot\left({}^B\theta_{si}\right)} \\
\Rightarrow \tan(\theta) &= \frac{1}{\cot\left({}^B\theta_{si}\right)} \\
\Rightarrow \tan(\theta) &= \tan({}^B\theta_{si}) \\
\Rightarrow \theta &= {}^B\theta_{si} \qquad \text{(A.5)}
\end{aligned}$$

which confirms the graphic inspection method in respect of $\hat{\boldsymbol{n}}_i$.

A.3.4. *Graphic inspection method* ($\hat{\boldsymbol{t}}_i$)

A similar process is repeated for $\hat{\boldsymbol{t}}_i$ as follows. With $\dot{\theta}_{ti}$ as given in equation 4.6

$$\dot{\theta}_{ti} = \left\{ \left(\dot{x}_{Bu} - a_{1i} w \dot{\theta}_0 \right) \cos\left({}^{B}\theta_{si}\right) + \left[\dot{x}_{Bv} + \left(a_{2i} \tfrac{l}{2} - c \right) \dot{\theta}_0 \right] \sin\left({}^{B}\theta_{si}\right) \right\} r^{-1}$$

and setting $\dot{\theta}_{ti}$ to zero and expressing in terms of $\dot{x}_{Bu}$ gives

$$\begin{aligned} \dot{x}_{Bu}\cos\left({}^{B}\theta_{si}\right) &= a_{1i} w \dot{\theta}_0 \cos\left({}^{B}\theta_{si}\right) - \left(\dot{x}_{Bv} + \left(a_{2i} \frac{l}{2} - c \right) \dot{\theta}_0 \right) \sin\left({}^{B}\theta_{si}\right) \\ \dot{x}_{Bu} &= -\dot{x}_{Bv} \tan\left({}^{B}\theta_{si}\right) + \left(a_{1i} w - \left(a_{2i} \frac{l}{2} - c \right) \tan\left({}^{B}\theta_{si}\right) \right) \dot{\theta}_0 \\ \dot{x}_{Bu} &= -\dot{x}_{Bv} \tan\left({}^{B}\theta_{si}\right) + \dot{\theta}_0 \mathrm{B}_i \end{aligned} \tag{A.6}$$

where $\mathrm{B}_i = \left(a_{1i} w - \left(a_{2i} \frac{l}{2} - c \right) \tan\left({}^{B}\theta_{si}\right) \right)$

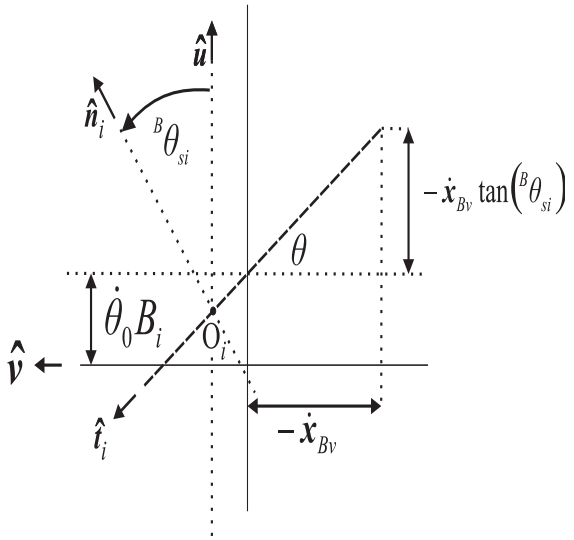

Figure A.4 – Shows the geometric relationship between the gradient of $\theta_{ti} = 0$ (dashed diagonal line) and $\hat{\boldsymbol{t}}_i$ on the $\dot{\boldsymbol{x}}_B$-plane.

It can be seen from Figure A.4 that

$$\begin{aligned} \tan(\theta) &= \frac{-\dot{x}_{Bv}\tan\left({}^{B}\theta_{si}\right)}{-\dot{x}_{Bv}} \\ \Rightarrow \tan(\theta) &= \frac{1}{\cot\left({}^{B}\theta_{si}\right)} \\ \Rightarrow \tan(\theta) &= \tan({}^{B}\theta_{si}) \\ \Rightarrow \theta &= {}^{B}\theta_{si} \end{aligned} \tag{A.7}$$

and by definition $\hat{\boldsymbol{t}}_i$ is directed as ${}^{B}\theta_{si} + \frac{\pi}{2}$ which confirms the graphic inspection method in respect of $\hat{\boldsymbol{t}}_i$.

A.3.5. *Integration bounds*

Equation 4.16 reproduced below

$$\int_{\theta_{00}}^{\theta_{01}} d\theta_0 = -t \int_{^B\theta_{si0}}^{^B\theta_{si1}} \frac{1}{Z_{ri}\sin\left({}^B\theta_{si} - {}^B\theta_{zi}\right) + t} d^B\theta_{si}$$

assumes the manipulation of the bounds on the integral (page 70) for the case where $\dot{\theta}_0 < 0$, $\theta_{00} > \theta_{01}$ so the literal lower bound (i.e. closest to page bottom) has a larger magnitude than the literal upper bound. A check is made here since integration is not made from bounds of smaller to greater magnitude.

For any integral equation of the following form for which an analytical solution exists

$$\begin{aligned} \int_{x1}^{x0} dx &= \int_{y1}^{y0} f(y)dy \\ \Rightarrow g(x0) - g(x1) &= h(y0) - h(y1) \\ \Rightarrow -\left(g(x0) - g(x1)\right) &= -\left(h(y0) - h(y1)\right) \\ \Rightarrow \int_{x0}^{x1} dx &= \int_{y0}^{y1} f(y)dy \end{aligned}$$

and where $x1 < x0$ it can be seen that the equality is maintained if the bound positions on the right hand integral are reversed. Thus where $x1$ is the independent variable, $y1$ is the dependent variable and $x0$ and $y0$ are known initial positions the equality is maintained irrespective of the relative magnitudes of the literal bounds of the left hand integral. Thus the final form maintains the equality irrespective of the relative magnitudes of $x1$ and $x0$.

A.3.6. *Avoiding complex solutions*

The right hand side of Equation 4.17 may be written as:

$$\begin{aligned} &-2tZ_{tri}^{-\frac{1}{2}} f\left({}^B\theta_{si1}\right) + 2tZ_{tri}^{-\frac{1}{2}} f\left({}^B\theta_{si0}\right) \\ =&-2t\left\{\arctan\left(\left[\left(Z_{ri}\sin({}^B\theta_{zi}) + t\right)\tan\left(0.5{}^B\theta_{si1}\right) + Z_{ri}\cos\left({}^B\theta_{zi}\right)\right] Z_{tri}^{-\frac{1}{2}}\right)\right\} Z_{tri}^{-\frac{1}{2}} \\ -[&-2t\left\{\arctan\left(\left[\left(Z_{ri}\sin({}^B\theta_{zi}) + t\right)\tan\left(0.5{}^B\theta_{si0}\right) + Z_{ri}\cos\left({}^B\theta_{zi}\right)\right] Z_{tri}^{-\frac{1}{2}}\right)\right\} Z_{tri}^{-\frac{1}{2}}] \end{aligned}$$

so substituting for $f\left({}^{B}\theta_{si1}\right)$ where ${}^{B}\theta_{sip}$ indicates ${}^{B}\theta_{si0}$ and ${}^{B}\theta_{si1}$ the two terms, disregarding the sign, are given by

$$\begin{aligned}
&2tZ_{tri}^{-\frac{1}{2}}\arctan\left(\left[\left(Z_{ri}\sin({}^{B}\theta_{zi})+t\right)\tan\left(0.5{}^{B}\theta_{sip}\right)+Z_{ri}\cos\left({}^{B}\theta_{zi}\right)\right]Z_{tri}^{-\frac{1}{2}}\right)\\
=&-2t|Z_{tri}|^{-\frac{1}{2}}I\arctan\left(\left[\left(Z_{ri}\sin({}^{B}\theta_{zi})+t\right)\tan\left(0.5{}^{B}\theta_{sip}\right)+Z_{ri}\cos\left({}^{B}\theta_{zi}\right)\right]|Z_{tri}|^{-\frac{1}{2}}(-I)\right)\\
&\left\{t^2<Z_{ri}^2\right.\\
=&-2t|Z_{tri}|^{-\frac{1}{2}}I\arctan\left(I\left[\left(Z_{ri}\sin({}^{B}\theta_{zi})+t\right)\tan\left(0.5{}^{B}\theta_{sip}\right)+Z_{ri}\cos\left({}^{B}\theta_{zi}\right)\right]|Z_{tri}|^{-\frac{1}{2}}\right)\\
=&-2t|Z_{tri}|^{-\frac{1}{2}}\operatorname{arctanh}\left(\left[\left(Z_{ri}\sin({}^{B}\theta_{zi})+t\right)\tan\left(0.5{}^{B}\theta_{sip}\right)+Z_{ri}\cos\left({}^{B}\theta_{zi}\right)\right]|Z_{tri}|^{-\frac{1}{2}}\right)
\end{aligned} \tag{A.8}$$

If $\tanh(x)$ is considered where x is any real number it is known that solutions only exist for $|\tanh(x)|<1$. So if the surface of $\tanh(z)$is considered, where z is a complex number, it is known that solutions where $\Im\left[\operatorname{arctanh}(\tanh(z))\right]=0$ occur at $|\tanh(z)|<1$. It therefore follows that if

$$\left|\left[\left(Z_{ri}\sin({}^{B}\theta_{zi})+t\right)\tan\left(0.5{}^{B}\theta_{sip}\right)+Z_{ri}\cos\left({}^{B}\theta_{zi}\right)\right]|Z_{tri}|^{-\frac{1}{2}}\right|\geq 1$$

then the solution will be complex. If

$$\left|\left[\left(Z_{ri}\sin({}^{B}\theta_{zi})+t\right)\tan\left(0.5{}^{B}\theta_{sip}\right)+Z_{ri}\cos\left({}^{B}\theta_{zi}\right)\right]|Z_{tri}|^{-\frac{1}{2}}\right|<1$$

then a real solution exists. However, as there are two terms of different sign if

$$-\left|\left[\left(Z_{ri}\sin({}^{B}\theta_{zi})+t\right)\tan\left(0.5{}^{B}\theta_{si1}\right)+Z_{ri}\cos\left({}^{B}\theta_{zi}\right)\right]|Z_{tri}|^{-\frac{1}{2}}\right|\geq 1$$

and

$$\left|\left[-\left(Z_{ri}\sin({}^{B}\theta_{zi})+t\right)\tan\left(0.5{}^{B}\theta_{si0}\right)+Z_{ri}\cos\left({}^{B}\theta_{zi}\right)\right]|Z_{tri}|^{-\frac{1}{2}}\right|\geq 1$$

then a solution may be found for both terms with identical imaginary parts which then cancel. It follows that complex solution can be avoided by choosing ${}^{B}\theta_{si1}$ and ${}^{B}\theta_{si0}$ such that either both or neither angle choice generates a complex value.

A.3.7. *Caster steady-state*

This sections details the derivation of the caster steady-state angle for ${}^{B}\theta_{si}$. By inspection of Figure 4.8 (page 73) using the principle of relative motion

$$\begin{aligned}
\dot{\boldsymbol{x}}_{ci} &= \dot{\boldsymbol{x}}_{si}-\dot{\theta}_{si}\hat{\boldsymbol{S}}\times t\hat{\boldsymbol{n}}_i\\
\Rightarrow \dot{\boldsymbol{x}}_{ci} &= \dot{\boldsymbol{x}}_{si}-t\dot{\theta}_{si}\hat{\boldsymbol{t}}_i
\end{aligned} \tag{A.9}$$

and where $\dot{\theta}_{si} = \dot{\theta}_0 +^B \dot{\theta}_{si}$ then $\dot{\theta}_{si} = \dot{\theta}_0 \{^B\dot{\theta}_{si} = 0$ for the caster steady-state definition and thus substituting $\dot{\theta}_{si}$ with $\dot{\theta}_0$ gives

$$\begin{aligned} \dot{\boldsymbol{x}}_{ci} &= -Z_{ri}\dot{\theta}_0 \sin\left({}^B\theta_{zi} -^B \theta_{si}\right) \hat{\boldsymbol{t}}_i - t\dot{\theta}_0 \hat{\boldsymbol{t}}_i + Z_{ri}\dot{\theta}_0 \cos\left({}^B\theta_{zi} -^B \theta_{si}\right) \hat{\boldsymbol{n}}_i \\ \Rightarrow \dot{\boldsymbol{x}}_{ci} \cdot \hat{\boldsymbol{t}}_i &= -Z_{ri}\dot{\theta}_0 \sin\left({}^B\theta_{zi} -^B \theta_{si}\right) - t\dot{\theta}_0 \end{aligned} \tag{A.10}$$

where $\dot{\boldsymbol{x}}_{si}$ substitution is determined by inspection of Figure 4.8 and the final line results since the $\cdot\hat{\boldsymbol{t}}_i$ removes the $\hat{\boldsymbol{n}}_i$ component.

Applying the nonholonomic constraint (Equation 4.1 page 59), Equation A.10 may be written as

$$\begin{aligned} 0 &= Z_{ri} \sin\left({}^B\theta_{zi} -^B \theta_{si}\right) - t \\ \Rightarrow^B \theta_{si} &= {}^B\theta_{zi} - \arcsin\left(\frac{t}{Z_{ri}}\right). \end{aligned} \tag{A.11}$$

By inspection of Figure 4.8 it can be seen that taking account of the caster in the second position (grey) the operand of sin() in the first line is written as $-\left({}^B\theta_{zi} -^B \theta_{si}\right)$ so taking both operands into account then the solutions for ${}^B\theta_{si}$ for Equation A.11 may be written as

$$\left\{{}^B\theta_{si}\right\} =^B \theta_{zi} \pm \arcsin\left(\frac{t}{Z_r}\right). \tag{A.12}$$

However, it can be shown that only one of the two solutions to Equation A.12 is a solution to ${}^B\dot{\theta}_{si} = 0$ as follows. Using Equation 4.14 and applying the nonholonomic constraint to the left hand side

$$\begin{aligned} 0 &= -\dot{\theta}_0 Z_{ri} \sin\left({}^B\theta_{si} -^B \theta_{zi}\right) -^B \dot{\theta}_{si} t - \dot{\theta}_0 t \\ \Rightarrow^B \dot{\theta}_{si} &= -\frac{\dot{\theta}_0}{t}\left[Z_{ri} \sin\left({}^B\theta_{si} -^B \theta_{zi}\right) + t\right] \end{aligned} \tag{A.13}$$

and for the caster steady-state where ${}^B\dot{\theta}_{si} = 0$ it follows that

$$0 = Z_{ri} \sin\left({}^B\theta_{si} -^B \theta_{zi}\right) + t$$

and using ${}^{B}\theta_{si} = {}^{B}\theta_{zi} - \arcsin\left(\frac{t}{Z_r}\right)$ gives

$$\begin{aligned} 0 &= Z_{ri}\sin\left({}^{B}\theta_{zi} - \arcsin\left(\frac{t}{Z_r}\right) - {}^{B}\theta_{zi}\right) + t \\ \Rightarrow 0 &= -\sin\left(\arcsin\left(\frac{t}{Z_r}\right)\right) + \frac{t}{Z_{ri}} \end{aligned} \tag{A.14}$$

which is evidently true where as using ${}^{B}\theta_{si} = {}^{B}\theta_{zi} + \arcsin\left(\frac{t}{Z_r}\right)$ would not provide a zero right hand side. It is therefore concluded that only one solution exists for the caster steady-state which confirms the intuition that the caster orientation indicated by the grey caster is not in caster steady-state.

A.3.8. *Expressing ${}^{B}\theta_{si}$ as a function of θ_0*

The defining equation for expressing θ_{01} as a function of ${}^{B}\theta_{si1}$ is given by equation 4.17 (page 70) which is

$$\theta_{01} - \theta_{00} = -2t\left[f\left({}^{B}\theta_{si1}\right) - f\left({}^{B}\theta_{si0}\right)\right] Z_{tri}^{-\frac{1}{2}}$$

where $f\left({}^{B}\theta_{si}\right)$ is defined as

$$f\left({}^{B}\theta_{si}\right) = \arctan\left(\left[\left(Z_{ri}\sin({}^{B}\theta_{zi}) + t\right)\tan\left(0.5{}^{B}\theta_{si}\right) + Z_{ri}\cos\left({}^{B}\theta_{zi}\right)\right] Z_{tri}^{-\frac{1}{2}}\right)$$

and $Z_{tri} = (t^2 - Z_{ri}^2)$. Equation 4.17 may be expressed in terms of $f\left({}^{B}\theta_{si1}\right)$ thus

$$f\left({}^{B}\theta_{si1}\right) = -\frac{\theta_{01} - \theta_{00}}{2t} Z_{tri}^{\frac{1}{2}} + f\left({}^{B}\theta_{si0}\right)$$

and substituting for $f\left({}^{B}\theta_{si1}\right)$ gives

$$\begin{aligned} &\left[\left(Z_{ri}\sin({}^{B}\theta_{zi}) + t\right)\right. \\ &\quad \cdot\tan\left(0.5{}^{B}\theta_{si}\right) \\ &\quad \left. + Z_{ri}\cos\left({}^{B}\theta_{zi}\right)\right] = -\tan\left(\frac{\theta_{01} - \theta_{00}}{2t} Z_{tri}^{\frac{1}{2}} - f\left({}^{B}\theta_{si0}\right)\right) Z_{tri}^{\frac{1}{2}} \\ &\Rightarrow {}^{B}\theta_{si1} = -2\arctan\left(\frac{\tan\left(\frac{\theta_{01}-\theta_{00}}{2t} Z_{tri}^{\frac{1}{2}} - f\left({}^{B}\theta_{si0}\right)\right) Z_{tri}^{\frac{1}{2}} + Z_{ri}\cos\left({}^{B}\theta_{zi}\right)}{\left(Z_{ri}\sin({}^{B}\theta_{zi}) + t\right)}\right) \end{aligned}$$

as per equation 4.23

A.3.9. *Initial caster rotation direction*

To determine the relationship between $\text{sgn}({}^{B}\dot{\theta}_{si})$ and $\text{sgn}(\dot{\theta}_{si})$ at ${}^{B}\theta_{si} = 0$ the following applies: beginning with Equation A.13 (page 242)

$$0 = -\dot{\theta}_0 Z_{ri} \sin\left({}^{B}\theta_{si} - {}^{B}\theta_{zi}\right) - {}^{B}\dot{\theta}_{si} t - \dot{\theta}_0 t \tag{A.15}$$

and substituting ${}^{B}\theta_{si} = 0$

$$0 = -\dot{\theta}_0 (Z_{ri} \sin\left(0 - {}^{B}\theta_{zi}\right) + t) - {}^{B}\dot{\theta}_{si} t$$

and since $\dot{\theta}_0 = \dot{\theta}_{si} - {}^{B}\dot{\theta}_{si}$

$$\begin{aligned}
0 &= -(\dot{\theta}_{si} - {}^{B}\dot{\theta}_{si})(Z_{ri} \sin\left(0 - {}^{B}\theta_{zi}\right) + t) - {}^{B}\dot{\theta}_{si} t \\
\Rightarrow 0 &= -\dot{\theta}_{si}(Z_{ri} \sin\left(0 - {}^{B}\theta_{zi}\right) + t) + {}^{B}\dot{\theta}_{si}(Z_{ri} \sin\left(0 - {}^{B}\theta_{zi}\right) + t) - {}^{B}\dot{\theta}_{si} t \\
\Rightarrow 0 &= -\dot{\theta}_{si}(Z_{ri} \sin\left(0 - {}^{B}\theta_{zi}\right) + t) + {}^{B}\dot{\theta}_{si} Z_{ri} \sin\left(0 - {}^{B}\theta_{zi}\right) \\
\Rightarrow {}^{B}\dot{\theta}_{si} &= \dot{\theta}_{si} \frac{Z_{ri} \sin\left(0 - {}^{B}\theta_{zi}\right) + t)}{(Z_{ri} \sin\left(0 - {}^{B}\theta_{zi}\right)} \\
\Rightarrow {}^{B}\dot{\theta}_{si} &= \dot{\theta}_{si} \left(1 - \frac{t}{Z_{ri} \sin\left({}^{B}\theta_{zi}\right)}\right)
\end{aligned} \tag{A.16}$$

and as ${}^{B}\theta_{zi} = {}^{B}\theta_{zi1} + \text{sgn}(\dot{\theta}_0)\frac{\pi}{2}$ (Figure 4.4, page 66), $\sin\left({}^{B}\theta_{zi}\right) = \sin\left({}^{B}\theta_{zi1} + \text{sgn}(\dot{\theta}_0)\frac{\pi}{2}\right)$ which after expansion is $\text{sgn}(\dot{\theta}_0)\cos({}^{B}\theta_{zi1})$ which after substitution into Equation A.16 gives

$$\Rightarrow {}^{B}\dot{\theta}_{si} = \dot{\theta}_{si} \left(1 - \frac{t}{\text{sgn}(\dot{\theta}_0) Z_{ri} \cos({}^{B}\theta_{zi1})}\right) \quad \left\{ {}^{B}\theta_{si} = 0 \,.\right.$$

A.3.10. *Real solutions for wheel roll*

As the symbolic solution to the integration of Equation 4.29 is far too voluminous to permit direct inspection of the presence of complex results, necessary given their presence in the orientation equation, examination is carried out after numerical substitution using values for the typical real-FCMV given in Figure Figure 4.1 (page 58) and Z_r related parameters as shown in Figure 4.6 (page 69) and with $\theta_{00} = \theta_{ni0} = 0$. There is no loss to the versatility of the Zmodel-FCMV by setting $\theta_{ni0} = 0$ since any wheel orientation may be deemed to be the zero position without loss. An example result, for caster assembly i=1 and Z_A, with values

shown at one decimal place for conciseness, is:

$$\begin{aligned}\theta_{n1} &= -10.0\,\theta_{01} + 4.3 \\ &\quad +0.6\ln(e^{17.2\theta_{01}-3.7} - 0.0 - 0.1I) \\ &\quad +0.6\ln(e^{17.2\theta_{01}-3.7} - 0.0 + 0.1I) \\ &\quad +(2.7\cdot 10^{-10}I)\,\ln(e^{17.2\theta_{01}-3.7} - 0.0 - 0.1I) \\ &\quad -(2.7\cdot 10^{-10}I)\,\ln(e^{17.2\theta_{01}-3.7} - 0.0 + 0.1I). \end{aligned} \tag{A.17}$$

With respect to complex numbers the first two terms can be disregarded. The third and fourth, and the fifth and sixth terms form pairs where the pairs may be written as

$\ln(re_1 - re_2 I) + \ln(re_1 + re_2 I)$

and

$re_3 I\,(\ln(re_1 - re_2 I) - \ln(re_1 + re_2 I))$

respectively where the re_i represent real numbers. Substitution of $e^{17.2\theta_{01}-3.7} - 0.0$ terms with re_1 is justified since this function of θ_{01} will always evaluate to a real number. Expressing $re_1 - re_2 I$ and $re_1 + re_2 I$ as complex exponentials the laws of complex exponentials indicates that both pairs evaluate to real numbers so there is no boundary analogous to caster orientation change for wheel orientation change. Additionally the $2.7\cdot 10^{-10}I$ term is the result of limited numerical precision, i.e. the exponential integer increases with increasing precision so can be disregarded for that reason but as already indicated these evaluate to negligible real values.

A.3.11. *Wheel roll direction change*

Beginning with Equation 4.27 for $\dot{\theta}_{ti} r = 0$ which defines $\Delta\mathrm{sgn}(\dot{\theta}_{ti})$

$$0 = \dot{\theta}_0 Z_{ri} \cos\left({}^B\theta_{si} - {}^B\theta_{zi}\right) \tag{A.18}$$

$$\Rightarrow 0 = \cos\left({}^B\theta_{si} - {}^B\theta_{zi}\right) \tag{A.19}$$

and expressing ${}^{B}\theta_{si}$ as a function of θ_0 (Equation 4.23 page 75) and denoting this by $g(\theta_0)$ this provides

$$\begin{aligned} 0 &= \cos\left(g(\theta_0) - {}^{B}\theta_{zi}\right) \\ \Rightarrow \arccos(0) &= g(\theta_0) - {}^{B}\theta_{zi} \end{aligned} \tag{A.20}$$

and thus the θ_0 at which $\Delta\text{sgn}(\dot{\theta}_{ti})$ occurs is given by

$$root \quad of \quad \left[g(\theta_0) - {}^{B}\theta_{zi} - \arccos(0)\right]. \tag{A.21}$$

A.3.12. *Expressing* $\mathbf{P}_{Qi}$ *as* P_{Qvi} *and* P_{Qui}

$$\begin{aligned} M_{QC} &= \sum_{i=1}^{4} \boldsymbol{P}_{Qi} \times \left[-a_{1i} w \hat{\boldsymbol{v}} + \left(a_{2i}\frac{l}{2} - c\right)\hat{\boldsymbol{u}}\right] \cdot \hat{\boldsymbol{S}} \\ \Rightarrow M_{QC} &= [\boldsymbol{P}_{Q1} \times -w\hat{\boldsymbol{v}} + \boldsymbol{P}_{Q2} \times w\hat{\boldsymbol{v}} + \boldsymbol{P}_{Q3} \times w\hat{\boldsymbol{v}} + \boldsymbol{P}_{Q4} \times -w\hat{\boldsymbol{v}} \\ &\quad + \boldsymbol{P}_{Q1} \times \left(\frac{l}{2} - c\right)\hat{\boldsymbol{u}} + \boldsymbol{P}_{Q2} \times \left(\frac{l}{2} - c\right)\hat{\boldsymbol{u}} + \boldsymbol{P}_{Q3} \times \left(-\frac{l}{2} - c\right)\hat{\boldsymbol{u}} \\ &\quad + \boldsymbol{P}_{Q4} \times \left(-\frac{l}{2} - c\right)\hat{\boldsymbol{u}}\Big] \cdot \hat{\boldsymbol{S}} \\ \Rightarrow M_{QC} &= -wP_{Qu1} + wP_{Qu2} + wP_{Qu3} - wP_{Qu4} \\ &\quad + P_{Qv1}\left(\frac{l}{2} - c\right) + P_{Qv2}\left(\frac{l}{2} - c\right) + P_{Qv3}\left(-\frac{l}{2} - c\right) \\ &\quad + P_{Qv4}\left(-\frac{l}{2} - c\right) \end{aligned} \tag{A.22}$$

where $(\boldsymbol{P}_{Qi} \times \hat{\boldsymbol{u}}) \cdot \hat{\boldsymbol{S}} = a_{2i} P_{Qvi}$ and $(\boldsymbol{P}_{Qi} \times \hat{\boldsymbol{v}}) \cdot \hat{\boldsymbol{S}} = -a_{1i} P_{Qui}$.

Since $\sum_{i=1}^{4} \boldsymbol{P}_{Qv} \cdot \hat{\boldsymbol{v}} = P_{Qv}$ the P_{Qv} term for the second condition of Equation 4.67 may be written as

$$P_{Qv}(\frac{l}{2} + h + c) = (P_{Qv1} + P_{Qv2} + P_{Qv3} + P_{Qv4})(\frac{l}{2} + h + c) \tag{A.23}$$

So substituting Equations A.23 and A.22 into the second term of the second con-

dition of Equation 4.67 gives, within the magnitude bars, the expression

$$\begin{aligned}
& -wP_{Qu1} + wP_{Qu2} + wP_{Qu3} - wP_{Qu4} \\
& +P_{Qv1}\left(\frac{l}{2} - c\right) + P_{Qv2}\left(\frac{l}{2} - c\right) + P_{Qv3}\left(-\frac{l}{2} - c\right) \\
& +P_{Qv4}\left(-\frac{l}{2} - c\right) + (P_{Qv1} + P_{Qv2} + P_{Qv3} + P_{Qv4})\,(\frac{l}{2} + h + c) \\
= \; & -wP_{Qu1} + wP_{Qu2} + wP_{Qu3} - wP_{Qu4} \\
& +P_{Qv1}(l+h) + P_{Qv2}(l+h) + P_{Qv3}(h) + P_{Qv4}(h) \\
= \; & w(P_{Qu2} + P_{Qu3} - P_{Qu1} - P_{Qu4}) \\
& +(l+h)(P_{Qv1} + P_{Qv2}) + h(P_{Qv3} + P_{Qv4})
\end{aligned} \tag{A.24}$$

A.4. **Methods: Single Sensor Measurement**

It is also evident that with respect to $\hat{\boldsymbol{u}}$ directed handle-forces no other solutions exist for M_{uCs}: this is so since it is not possible to apply $\hat{\boldsymbol{u}}$ directed handle-forces which balance both the force and moment effects if the number of forces applied to each handle is restricted to one. This follows since the whole magnitude of the non-couple component of the $\hat{\boldsymbol{u}}$ directed handle-forces, the handle-force component equivalent to F_x, has to be placed at that handle where it produces a moment in the same direction as the couple component of the $\hat{\boldsymbol{u}}$ directed handle-forces, i.e. this component must minimise the couple component. If this were not so, $\hat{\boldsymbol{u}}$ and $-\hat{\boldsymbol{u}}$ directed force components are applied to one handle which is not possible with the one force per handle condition. It is worth noting that no such condition exists if more than one force is applied to each handle which would be possible if more than one operator produced the actions.

The same argument which has been made in regards of the minimisation of M_{uCs} applies when Equation 5.5 does not hold, that is, no other solution exists since it would be necessary to apply $\hat{\boldsymbol{u}}$ and $-\hat{\boldsymbol{u}}$ directed force components to one handle. It is also noteworthy that when Equation 5.5 does not hold and no couple is required the zero in $M_{uCs} = P_{uCs} = 0$ is integer zero which is distinct from rounding a small sensed measure of M_y to a floating point zero.

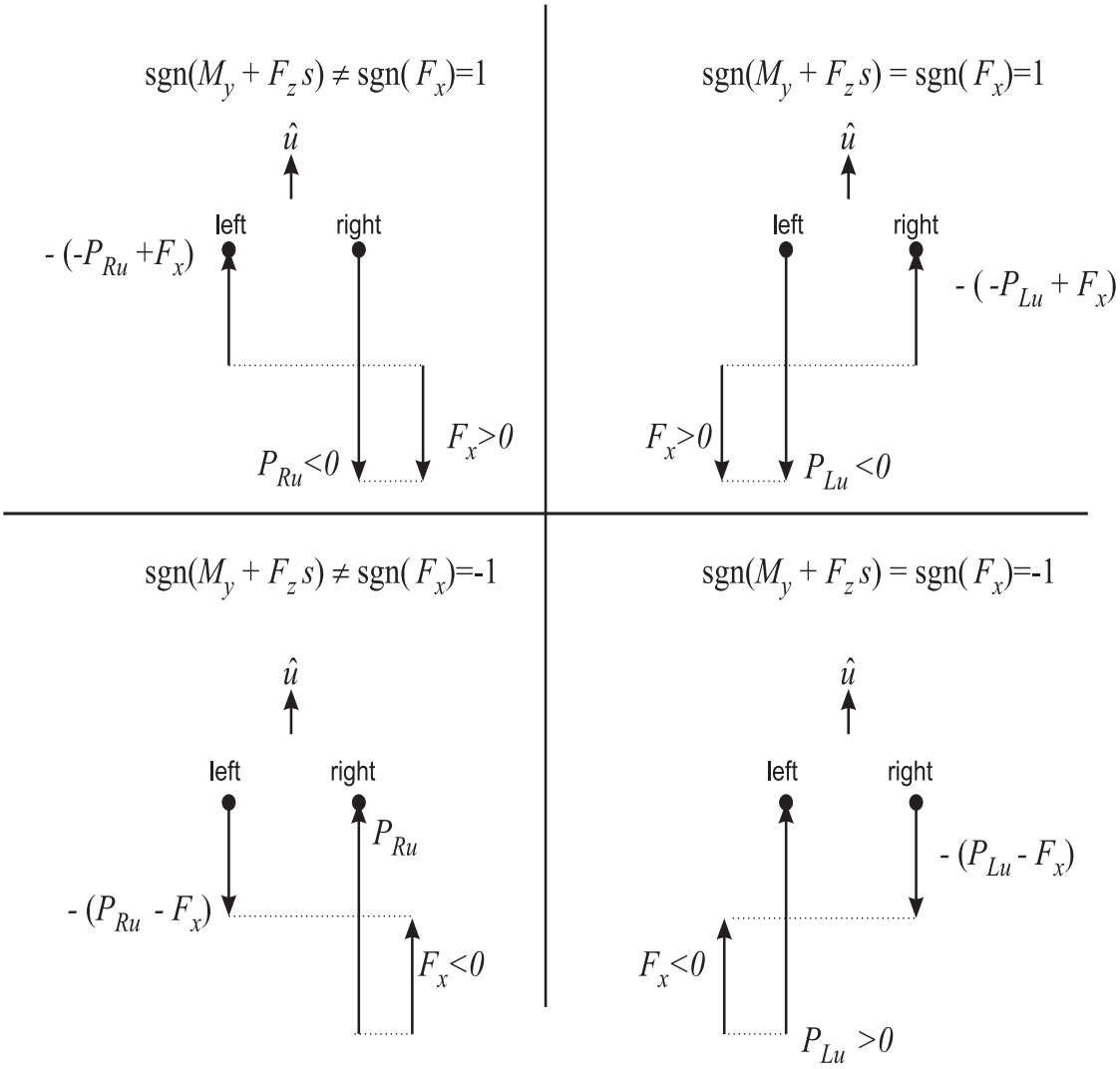

Figure A.5 – Shows that F_x may be viewed as a component of P_{Lu} or P_{Ru} depending on the four conditions resulting from sign$(M_y + F_z s)$ and sgn(F_x).

A.5. **Results**

A.5.1. *Percentiles*

Figure A.6 (page 249) clarifies how ${}^{\pm nth}_{ar}P^{\mathrm{r}}_{a}$ are determined from the data.

A.5.2. *Percentiles interpretation*

For Figure 6.6 (page 147) there are normalised ${}^{-90th}_{ssi}P^{\mathrm{F}}_{uCs} = -1$ (red markers) and no normalised ${}^{+90th}_{ssi}P^{\mathrm{F}}_{uCs}$ occurrences. Assuming that all subjects[F] had P_{uCs} measures, which they did, this arrangement can only occur if all subjects[F] contribute to the red markers for otherwise normalised ${}^{+90th}_{ssi}P^{\mathrm{F}}_{uCs}$ would occur since no matter how small the $P_{uCs} > 0$ measure, it would be the ${}^{+90th}_{ssi}P^{\mathrm{F}}_{uCs}$ measure and would be represented by a red marker.

For Figure D.1 (page 284) red markers occur for both signs of P_u and norm-

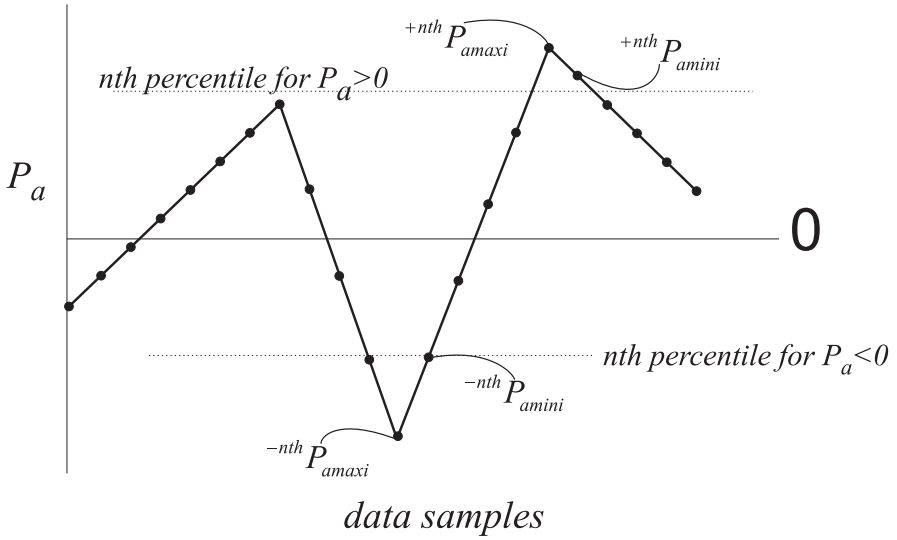

Figure A.6 – Illustrates the definition for ${}^{+nth}P_a$ for $P_a > 0$, ${}^{-nth}P_a$for $P_a < 0$ for the nth percentile.

alised $|{}^{\pm 90th}_{ssi}P^{\mathrm{F}}_{uCs}| \approx 1$ are present in both the initial and later period. Thus, this arrangement could occur because all subjects[F] had ${}^{-90th}_{ssi}P^{\mathrm{F}}_{uCs} \approx -1$ in the initial period and a ${}^{+90th}_{ssi}P^{\mathrm{F}}_{uCs} \approx 1$ in the later period or because some subjects[F] had only ${}^{-90th}_{ssi}P^{\mathrm{F}}_{uCs} \approx -1$ and some subjects had only ${}^{+90th}_{ss1}P^{\mathrm{F}}_{uCs} \approx 1$: this cannot be discriminated in this representation.

A.6. **Discussion**

A.6.1. *Caster dynamics*

Equation 4.25 (page 77) gives

$$\dot{\theta}_{si}t = -\dot{\theta}_0 Z_{ri}\sin({}^{B}\theta_{si} - {}^{B}\,\theta_{zi})$$

and taking the case for an overestimated maximum magnitude $\dot{\theta}_{si}$, Z_{ri} and θ_{zi} are not independent so this maximum cannot occur, this can be simplified to

$$\dot{\theta}_{si} = -\dot{\theta}_0\frac{Z_{ri}}{t} \Rightarrow \ddot{\theta}_{si} = -\ddot{\theta}_0\frac{Z_{ri}}{t}$$

and substituting with the measures for the experimental-FCMV this gives, $\ddot{\theta}_{si} = -25\ddot{\theta}_0$. With regard to Figure 4.1 (page 58)(b) the moment equation for the caster assembly is $F_{Sti} = \ddot{\theta}_{si}\frac{I_C}{t}$ and modelling I_C, the mass moment of inertia of the caster assembly, as a sphere, though as most of the mass would be in the fork this is a further overestimate, then this gives $F_{Sti} = \ddot{\theta}_{si}\frac{2m_C r^2}{5t}$. Substituting,

caster mass $m_C = 1$kg, $\ddot{\theta_{si}} = 25.\ddot{\theta_0}$, $\ddot{\theta_0} = 0.5$ (a gross overestimate since the largest acceleration magnitude based on differentiation of the polynomial fit functions used in respect of Figure 6.3 page 142 is 0.1 rad^{-2}) and with t=0.035m and $r = 0.060$ as for the experimental-FCMV, this evaluates to $F_{Sti} = 0.51$N. The smallest load at sensor-displacement measurement was 43kg so the final result is 0.01N/kg. As $\dot{\theta}_{ti}$ is of small magnitude compared with $\dot{\theta}_{si}$, see next section, it is not considered necessary to examine F_{Sni}, $\dot{\theta}_{si}\hat{\boldsymbol{S}} \times \dot{\theta}_{ti}\hat{\boldsymbol{t}}_{\boldsymbol{i}}$ or $\dot{\theta}_{si}\hat{\boldsymbol{S}} \times \dot{x}_{ci}\hat{\boldsymbol{n}}_{\boldsymbol{i}}$.

A.6.2. *Proportion of caster global rotation to wheel roll*

Equation 4.25 (page 77) gives

$$\dot{\theta}_{si}t = -\dot{\theta}_0 Z_{ri}\sin({}^B\theta_{si} - {}^B\theta_{zi})$$

and using Equation 4.27 (page 81)

$$\begin{aligned} \dot{\theta}_{ti}r &= \dot{\theta}_0 Z_{ri}\cos\left({}^B\theta_{si} - {}^B\theta_{zi}\right) \\ \Rightarrow \dot{\theta}_0 &= \frac{\dot{\theta}_{ti}r}{Z_{ri}\cos\left({}^B\theta_{si} - {}^B\theta_{zi}\right)} \end{aligned}$$

and so substituting back into Equation 4.25 gives

$$\dot{\theta}_{si} = -\dot{\theta}_{ti}\frac{r}{t}\tan({}^B\theta_{si} - {}^B\theta_{zi})$$

A.6.3. *Synchronisation*

The Vicon hardwear time coding system provided a real time calibration against which the sensor timings could be compared. There were two indicators of sensor synchronisation errors. The first and unequivocal indication is the number of data for Vicon (T) and the sensor were sometimes unequal: 48 of the 172 trials had unequal data lengths but of these 45 had 1 frame difference and 1 had 2 frames difference. The final 2 differences were large: 50 and 62 frames extra in the sensor data. The other indication of uncertainty in the sensor timings were the time stamps. Trials indicated that where large frequency variations occurred they occurred at the start of the recording and the following check process was therefore applied. Beginning with the last Vicon (T) and sensor datum the time

stamp change of the latter was compared with the former timings and the index at which the difference between the two timings exceeded 0.01 sec (half the sample frequency) was noted. These timing variations were examined: 31 synchronisation failures occurred but only 9 of these occurred after motion start, i.e. 22 of the failures occurred at a time which is not of interest. Importantly one of the large frame differences (50 frames extra) occurred before motion start. Additionally, 3 of the 9 occurrences of synchronisation failure occurred after motion stop and this included the other large frame difference (62 frames extra). Of the other 6 occurrences of synchronisation failure 3 were a single frame with a time difference $<$0.013sec and 1 was for 2 frames with a time difference $<$0.029sec. The remaining 2 synchronisation failures were for 9 and 10 frames respectively with maximum time differences $<$0.041 sec and $<$0.071 respectively. While there is general uncertainty about the sensor timings the indications are that time differences with the Vicon data were less than 1 frame and where this is not the case the indications are that the most extreme differences are all less than 4 frames for 2 trials during motion. Two points are to be noted before concluding. Firstly, there has been no attempt to balance equations of motion with the experimental data, i.e. no attempt to make use of an exact synchronisation: the kinematics analyses allowed a shift of $\pm$25 frames. Secondly, the motion of interest, the initial period, had a duration of at least 100 frames and often many more frames. It is therefore concluded that the synchronisation was sufficient for the purpose to which it was put.

A.6.4. *The occurrence of* ${}^{B}\theta_{si} \approx 0$

Figure A.7 (page 252) shows a top view of a single caster assembly where S_1 is the caster assembly stem centre with velocity $\dot{\boldsymbol{x}}_{S1}$ where $\dot{\boldsymbol{x}}_{S1} \cdot \hat{\boldsymbol{Y}} = 0$, that is, the caster assembly is constrained to a single non-rotating direction as would occur if the vehicle-frame was constrained to the $\hat{\boldsymbol{u}}$ direction by handle-forces. The geometric centre of the wheel is indicated by C_1 with velocity $\dot{\boldsymbol{x}}_{C1}$. The caster assembly orientation is indicated by θ_1 and caster assembly rotation by $\dot{\theta}_1$ with directions as shown. The trail dimension is indicated by t. For this arrangement as the the nonholonomic constraint applies, the $\hat{\boldsymbol{t}}_1$ component of the C_1 velocity is zero and

$$\dot{\boldsymbol{x}}_{C1} = \dot{x}_{S1x} \cos(\theta_1) \hat{\boldsymbol{n}}_1 \tag{A.25}$$

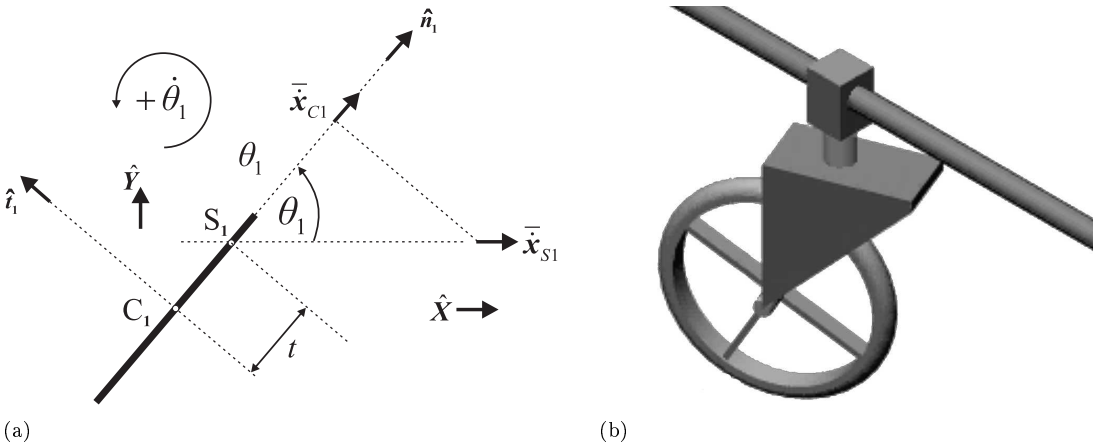

Figure A.7 – Shows: (left) the kinematics for a single caster assembly constrained at the caster stem to a single non-rotating direction (right) an illustration of the physical system

where $\dot{x}_{S1x}$ is the $\hat{\boldsymbol{X}}$ component of $\dot{\boldsymbol{x}}_{S1}$. The relative velocity of the C_1 as viewed from S_1, denoted $\dot{\boldsymbol{x}}_{C1/S1}$, is given by

$$\begin{aligned} \dot{\boldsymbol{x}}_{C1/S1} &= \dot{x}_{S1x}\sin(\theta_1)\hat{\boldsymbol{t}}_1 \\ \Rightarrow -\dot{\theta}_1\, t\hat{\boldsymbol{t}}_1 &= -\dot{x}_{S1x}\sin(\theta_1)\,\hat{\boldsymbol{t}}_1 \\ \Rightarrow \dot{x}_{S1x} &= \frac{\dot{\theta}_1\, t}{\sin(\theta_1)} \end{aligned} \tag{A.26}$$

and so by substitution of Equation A.26 into Equation A.25

$$\begin{aligned} \dot{\boldsymbol{x}}_{C1} = & \quad \frac{\dot{\theta}_1\, t}{\sin(\theta_1)}\cos(\theta_1)\hat{\boldsymbol{n}}_1 \\ \Rightarrow \dot{\boldsymbol{x}}_{C1}\cdot\hat{\boldsymbol{X}} = & \quad \frac{\dot{\theta}_1\, t}{\sin(\theta_1)}\cos(\theta_1)^2 \\ \Rightarrow \int_0^{x_{C1x1}} \mathrm{d}x_{C1x} = & \quad t\int_{\theta_{10}}^{\theta_{11}} \frac{\cos(\theta_1)^2}{\sin(\theta_1)}\mathrm{d}\theta_1 \\ \Rightarrow x_{C1x1} = & \quad -t\ln(\csc(\theta_1)-\cot(\theta_1)) \\ \Rightarrow x_{S1x} = & \quad -t\ln(\csc(\theta_1)-\cot(\theta_1)) + t\cos(\theta_1) \end{aligned} \tag{A.27}$$

where x_{C1x} and x_{S1x} are the scalars of $\hat{\boldsymbol{X}}$ displacement for C_1 and S_1 respectively. Evaluating from $\theta_1 \approx \pi$ to $\theta_1 \approx 0$, Figure A.8 (page 253) shows the resulting displacement graph for the caster stem for both a 35 mm and a 45 mm caster trail.

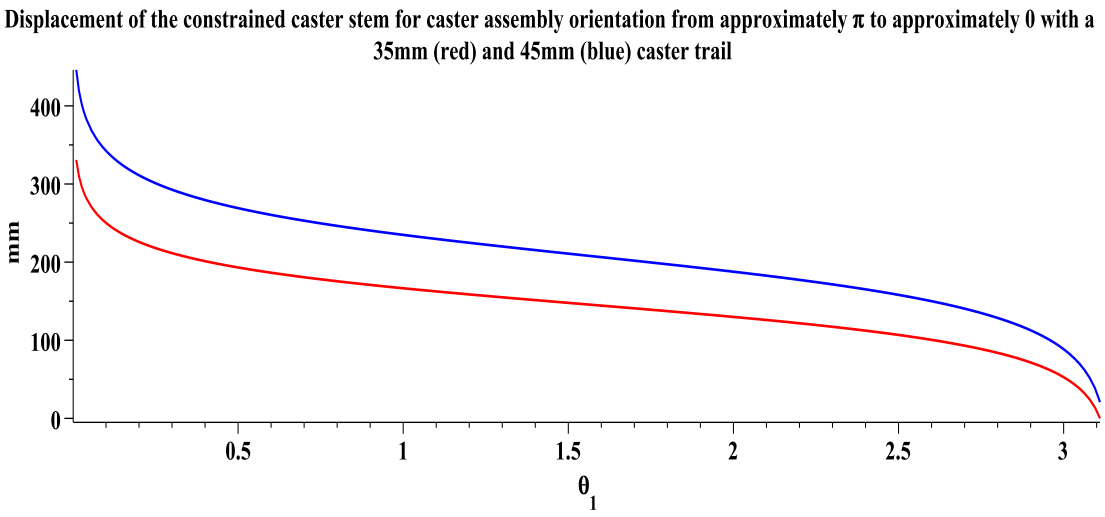

Figure A.8 – Shows the displacement of the caster stem for an approximately π change in θ_1.

Appendix B–Structured Review

As the thesis topic did not appear to have been a subject of study it was prudent to carry out and maintain a structured literature search. The structured review took place as follows. A preliminary combined search of MEDLINE, CINAHL and Inspec was carried out through Ovid. This gave an indication of the size of the literature bank. For all years and for title and abstract two separate searches were made. The first was with

> "(Wheelchair OR (Gurney AND hospital) OR (Cart AND (push or pull)) OR (shopping AND Trolley))"

and 5443 references were returned. The second was with

> "robot$ AND wheel$"

and 3530 references were returned.

In order to reduce references numbers the first search was refined with the following

> "AND (caster OR castor OR tire? OR tyre? OR wheel? OR friction OR resistance OR drag OR aerodynamics OR surfaces OR bearings OR load OR attendant? OR assistant? OR carer? OR manoeuvre$ OR maneuv$ OR turning OR steering OR slope OR push$ OR pull$ OR circular OR driving OR hospital OR shower OR toilet OR treadmill OR coast OR (ramp AND (friction OR resistance OR drag)))"

Further refinement was provided by the exclusion of spurious terms from the title with the addition of

> NOT(vibration? OR blind OR visual? OR impact OR cushion? OR seat$ OR sitting OR tissue? OR joystick? OR stair$ OR vision OR brain OR intelli$ OR neur$ OR cereb$ OR voice? OR thought? OR step? OR lift$ OR balan$ OR crash$ OR finite OR induction OR magnet$ OR muscle$ OR ultra$ OR exercise$ OR pendulum OR virtual OR pain$ or visual$ OR time OR transfer$ OR skin OR autom$ OR rehab$ OR rim path$ or local$ or rim$ OR record$ OR acoust$ OR isch$ OR walk$ OR head$ OR field$ OR filt$ OR fuzzy OR logging).ti.

The final initial structured search was made as

> Years 1865 -2006 (Wheelchair OR (Gurney AND hospital) OR (Cart AND (push or pull)) OR (shopping AND Trolley)) AND (caster OR castor OR tire? OR tyre? OR wheel? OR friction OR resistance OR drag OR aerodynamics OR surfaces OR bearings OR load OR attendant? OR assistant? OR carer? OR manoeuvre$ OR maneuv$ OR turning OR steering OR slope OR push$ OR pull$ OR circular OR driving OR hospital OR shower OR toilet OR treadmill OR coast OR (ramp AND (friction OR resistance OR drag))) NOT(vibration? OR blind OR visual? OR impact OR cushion? OR seat$ OR sitting OR tissue? OR joystick? OR stair$ OR vision OR brain OR intelli$ OR neur$ OR cereb$ OR voice? OR thought? OR step? OR lift$ OR balan$ OR crash$ OR finite OR induction OR magnet$ OR muscle$ OR ultra$ OR exercise$ OR pendulum OR virtual OR pain$ or visual$ OR time OR transfer$ OR skin OR autom$ OR rehab$ OR rim path$ or local$ or rim$ OR record$ OR acoust$ OR isch$ OR walk$ OR head$ OR field$ OR filt$ OR fuzzy OR logging).ti.

which produced 994 references.

This search was repeated, with the necessary alteration of syntax, in Compendex, Scientific Citation Index Expanded and SciVerse Scopus as detailed later. Further refinement within the databases was not carried out. Extending the list of exclusion terms to specifically target spurious references was not generally possible as e.g. Compendex malfunctioned when the number of exclusion terms became too large. Choosing a smaller number of wider terms to establish exclusions was not considered prudent as there was a risk that relevant references would be excluded. The results from all six data bases were exported to a combined Endnote X library where automatic duplication removal was carried out. Titles with explicitly spurious topics were then deleted. Duplicates not detected by automatic duplication detection were also deleted. Abstracts of references with titles which did not explicitly refer to drag, assisted propelling or casters or synonyms were read and irrelevant references were deleted. The guiding decision for inclusion was whether or not the article included some study of the behaviour of the wheelchair as opposed to only a study of the behaviour of the occupant.

For Compendex with Autostemming on the syntax was

> 1884-2006 (Wheelchair OR (Gurney AND hospital) OR (Cart AND (push or pull)) OR (shopping AND Trolley)) AND (cast*r OR t*res OR wheels OR friction OR resistance OR drag OR aerodynamics OR surfaces OR bearings OR load OR attendant OR assistant OR carer OR man*vr* OR turning OR steering OR slope OR pushing OR pulling OR circular OR driving OR hospital OR shower OR toilet OR treadmill OR coast OR (ramp AND (friction OR resistance OR drag)) OR model*) NOT (aircraft OR airfoil OR tree OR wing OR motor-trolley OR cartes OR autonomous OR "robotic wheelchair" OR "wheelchair drive" OR assist) wn KY NOT control wn AB NOT (cushion or seat or sitting or tissue) wn TI

For Scientific Citation Index Expanded the syntax was

> TS = (Wheelchair OR (Gurney AND hospital) OR (Cart AND (push or

pull)) OR (shopping AND Trolley)) AND TS=(caster OR castor OR tire$ OR tyre$ OR wheel$ OR friction OR resistance OR drag OR aerodynamics OR surfaces OR bearings OR load OR attendant$ OR assistant$ OR carer$ OR manoeuvre* OR maneuvr* OR turning OR steering OR slope OR push* OR pull* OR circular OR driving OR hospital OR shower OR toilet OR treadmill OR coast OR (ramp AND (friction OR resistance OR drag))) NOT TI=(stair* OR vision OR brain OR intelli* OR neur* OR cereb* OR voice$ OR thought$ OR step$)

For SciVerse Scopus the syntax was

PUBYEAR BEF 2007 SUBJAREA(mult OR comp OR eart OR ener OR engi OR envi OR mate OR math OR phys) AND TITLE-ABS-KEY ((Wheelchair OR (Gurney AND hospital) OR (Cart AND (push or pull)) OR (shopping AND Trolley)) AND (caster OR castor OR tire? OR tyre? OR wheel? OR friction OR resistance OR drag OR aerodynamics OR surfaces OR bearings OR load OR attendant? OR assistant? OR carer? OR manoeuvre# OR maneuv# OR turning OR steering OR slope OR push# OR pull# OR circular OR driving OR hospital OR shower OR toilet OR treadmill OR coast OR (ramp AND (friction OR resistance OR drag)))) AND NOT TITLE (vibration? OR blind OR visual? OR impact OR cushion? OR seat# OR sitting OR tissue? OR joystick? OR stair# OR vision OR brain OR intelli# OR neur# OR cereb# OR voice? OR thought? OR step? OR lift# OR balan# OR crash# OR finite OR induction OR magnet# OR muscle# OR ultra# OR exercise# OR pendulum OR virtual OR pain# or visual# OR time OR transfer# OR skin OR autom# OR rehab# OR rim path# or local# or rim# OR record# OR acoust# OR isch# OR walk# OR head# OR field# OR filt# OR fuzzy OR logging)

The resulting reference list was compared with references obtained by the ad hoc process. Three drag references were missing from the structured search: one, a

comparison of wheelchair and walking, was excluded by not (walk$), two others were not found by any of the databases.

The process was repeated with Ovid in 2008 with

> Years 2007-May 2008 (Wheelchair OR (Gurney AND hospital) OR (Cart AND (push or pull)) OR (shopping AND Trolley)) AND (caster OR castor OR tire? OR tyre? OR wheel? OR friction OR resistance OR drag OR aerodynamics OR surfaces OR bearings OR load OR attendant? OR assistant? OR carer? OR manoeuvre$ OR maneuv$ OR turning OR steering OR slope OR push$ OR pull$ OR circular OR driving OR hospital OR shower OR toilet OR treadmill OR coast OR (ramp AND (friction OR resistance OR drag))) NOT(vibration? OR blind OR visual? OR impact OR cushion? OR seat$ OR sitting OR tissue? OR joystick? OR stair$ OR vision OR brain OR intelli$ OR neur$ OR cereb$ OR voice? OR thought? OR step? OR lift$ OR balan$ OR crash$ OR finite OR induction OR magnet$ OR muscle$ OR ultra$ OR exercise$ OR pendulum OR virtual OR pain$ or visual$ OR time OR transfer$ OR skin OR autom$ OR rehab$ OR rim path$ or local$ or rim$ OR record$ OR acoust$ OR isch$ OR walk$ OR head$ OR field$ OR filt$ OR fuzzy OR logging).ti.

and on July 30th 2011 with MEDLINE with

> 2007-2011 (Wheelchair OR (Gurney AND hospital) OR (Cart AND (push or pull)) OR (shopping AND Trolley)).m_ttl. AND (caster OR castor OR tire? OR tyre? OR wheel? OR friction OR resistance OR drag OR aerodynamics OR surfaces OR bearings OR load OR attendant? OR assistant? OR carer? OR manoeuvre$ OR maneuv$ OR turning OR steering OR slope OR push$ OR pull$ OR circular OR driving OR hospital OR shower OR toilet OR treadmill OR coast OR (ramp AND (friction OR

resistance OR drag)))m_.titl.

which resulted in 35 references. The titles were read and 5 references were saved for further investigation.

The search with CINAHL was also made (July 30th 2011) with

2007-2011 (Wheelchair OR (Gurney AND hospital) OR (Cart AND (push or pull)) OR (shopping AND Trolley)).m_ttl. AND (caster OR castor OR tire? OR tyre? OR wheel? OR friction OR resistance OR drag OR aerodynamics OR surfaces OR bearings OR load OR attendant? OR assistant? OR carer? OR manoeuvre$ OR maneuv$ OR turning OR steering OR slope OR push$ OR pull$ OR circular OR driving OR hospital OR shower OR toilet OR treadmill OR coast OR (ramp AND (friction OR resistance OR drag)))m_.titl.

which resulted in 24 references. The titles were read and 1 reference was saved for further investigation: 3 others had already been identified in the MEDLINE search.

The search with Scientific Citation Index Expanded was made (July 30th 2011) for

2007-2011 TS = (Wheelchair OR (Gurney AND hospital) OR (Cart AND (push or pull)) OR (shopping AND Trolley)) AND TS=(caster OR castor OR tire$ OR tyre$ OR wheel$ OR friction OR resistance OR drag OR aerodynamics OR surfaces OR bearings OR load OR attendant$ OR assistant$ OR carer$ OR manoeuvre* OR maneuvr* OR turning OR steering OR slope OR push* OR pull* OR circular OR driving OR hospital OR shower OR toilet OR treadmill OR coast OR (ramp AND (friction OR resistance OR drag))) NOT TI=(stair* OR vision OR brain OR intelli* OR neur* OR cereb* OR voice$ OR thought$ OR step$)

which yielded 665 references: titles were read and 21 references were saved. A second search was made (July 30th 2011) with this database with

2007-2011 Caster

which yielded 20 references: none were down loaded as all relevant references were duplicates.

The search with SciVerse Scopus was made (July 30th 2011)

PUBYEAR AFT 2006 SUBJAREA(mult OR comp OR eart OR ener OR engi OR envi OR mate OR math OR phys) AND TITLE-ABS-KEY ((Wheelchair OR (Gurney AND hospital) OR (Cart AND (push or pull)) OR (shopping AND Trolley)) AND (caster OR castor OR tire? OR tyre? OR wheel? OR friction OR resistance OR drag OR aerodynamics OR surfaces OR bearings OR load OR attendant? OR assistant? OR carer? OR manoeuvre# OR maneuv# OR turning OR steering OR slope OR push# OR pull# OR circular OR driving OR hospital OR shower OR toilet OR treadmill OR coast OR (ramp AND (friction OR resistance OR drag)))) AND NOT TITLE (vibration? OR blind OR visual? OR impact OR cushion? OR seat# OR sitting OR tissue? OR joystick? OR stair# OR vision OR brain OR intelli# OR neur# OR cereb# OR voice? OR thought? OR step? OR lift# OR balan# OR crash# OR finite OR induction OR magnet# OR muscle# OR ultra# OR exercise# OR pendulum OR virtual OR pain# or visual# OR time OR transfer# OR skin OR autom# OR rehab# OR rim path# or local# or rim# OR record# OR acoust# OR isch# OR walk# OR head# OR field# OR filt# OR fuzzy OR logging)

and this yielded 380 references: titles were read and 8 references were saved. A second search was made with this data base with

PUBYEAR AFT 2006 (caster)

which yielded 227 references: titles were read and 6 references were saved.

And a search with Compendex was made (July 30th 2011) with

> 2007-2011 (Wheelchair OR (Gurney AND hospital) OR (Cart AND (push or pull)) OR (shopping AND Trolley)) AND (caster OR castor OR tire? OR tyre? OR wheel? OR friction OR resistance OR drag OR aerodynamics OR surfaces OR bearings OR load OR attendant? OR assistant? OR carer? OR manoeuvre$ OR maneuv$ OR turning OR steering OR slope OR push$ OR pull$ OR circular OR driving OR hospital OR shower OR toilet OR treadmill OR coast OR (ramp AND (friction OR resistance OR drag)))

which yielded 349 references: titles were read and 7 references were saved. A second search was made on this data base and date with

> caster wn TI
> yielded 152 references: titles were read and 7 references were saved

After removing duplicates 46 references were examined for the 2007-July 30th 2011 search.

On 26.11.11 the Science Citation Index Expanded was searched with

> TS = (Castor OR Caster OR Wheelchair OR (Gurney AND hospital) OR (Cart AND (push or pull)) OR (shopping AND Trolley)) AND TS=(caster OR castor OR tire$ OR tyre$ OR wheel$ OR friction OR resistance OR drag OR aerodynamics OR surfaces OR bearings OR load OR attendant$ OR assistant$ OR carer$ OR manoeuvre* OR maneuvr* OR turning OR steering OR slope OR push* OR pull* OR circular OR driving OR hospital OR shower OR toilet OR treadmill OR coast OR (ramp AND (friction OR

resistance OR drag))) NOT TI=(stair* OR vision OR brain OR intelli* OR neur* OR cereb* OR voice$ OR thought$ OR step$) Refined by: Subject Areas=(ENGINEERING OR MATERIALS SCIENCE) Timespan=2011. Databases=SCI-EXPANDED, SSCI, A&HCI, CPCI-S. Lemmatization=On

the SciVerse Scopus was searched with

SUBJAREA(mult OR comp OR eart OR ener OR engi OR envi OR mate OR math OR phys) AND TITLE-ABS-KEY((wheelchair OR (gurney AND hospital) OR (cart AND (push OR pull)) OR (shopping AND trolley)) AND (caster OR castor OR tire? OR tyre? OR wheel? OR friction OR resistance OR drag OR aerodynamics OR surfaces OR bearings OR load OR attendant? OR assistant? OR carer? OR manoeuvre# OR maneuv# OR turning OR steering OR slope OR push# OR pull# OR circular OR driving OR hospital OR shower OR toilet OR treadmill OR coast OR (ramp AND (friction OR resistance OR drag)))) AND NOT TITLE(vibration? OR blind OR visual? OR impact OR cushion? OR seat# OR sitting OR tissue? OR joystick? OR stair# OR vision OR brain OR intelli# OR neur# OR cereb# OR voice? OR thought? OR step? OR lift# OR balan# OR crash# OR finite OR induction OR magnet# OR muscle# OR ultra# OR exercise# OR pendulum OR virtual OR pain# OR visual# OR time OR transfer# OR skin OR autom# OR rehab# OR rim path# OR local# OR rim# OR record# OR acoust# OR isch# OR walk# OR head# OR field# OR filt# OR fuzzy OR logging) AND (LIMIT-TO(PUBYEAR, 2012) OR LIMIT-TO(PUBYEAR, 2011))

and Compendex was searched with

(Wheelchair OR (Gurney AND hospital) OR (Cart AND (push or pull)) OR (shopping AND Trolley)) AND (caster OR castor OR tire? OR tyre? OR wheel? OR friction OR resistance OR drag OR aerodynamics OR surfaces OR bearings OR load OR attendant? OR assistant? OR carer? OR manoeuvre$ OR maneuv$ OR turning OR steering OR slope OR push$ OR pull$ OR circular OR driving OR hospital OR shower OR toilet OR treadmill OR coast OR (ramp AND (friction OR resistance OR drag)))

and titles were read resulting in five further articles for examination.

Appendix C–Data Processing

A large number of post processing procedures were required and these are detailed here. The programme files, excluding those related only to graphic outputs or data files, which are identified are all included in the enclosed DISC. In the following the character '␣' is used to represent a space in the file name and `F` is any root directory. The following list is ordered, i.e. each subsequent step may assume the existence of a file output by a previous step. The input files for each step are not listed exhaustively: only those which highlight features of the data processing are included here. The `.mw` extensions indicate files produced with Maple 14.01 and the `.m` extensions are outputs from Maple. Files used in the Dynamics Chapter are also listed here.

1. **Dynamics Chapter:-** The kinematics and dynamics calculations are found in:
   `F:\Shieldfield␣2010\MapleFinal\CheckingCentreofZ05.mw`
   and calculations for the proportions of moment to translational motion resistance effects are found in
   `F:\Shieldfield␣2010\MapleFinal\zModelMomentPorportions0b.mw`
2. **Load recording files:-** Load selection was recorded in two files:
   `F:\Shieldfield␣2010\MapleFinal\Load␣summary.xls`
   `F:\Shieldfield␣2010\MapleFinal\Load␣summary(with␣added␣max).xls`
   The number of disc-weights, large (nominally 4.55kg) or small (nominally, 3.22kg), selected was input and the sheets calculated load (L^r_{Mi}) and a load normalised with the subject's maximum load choice (L_{Mmaxi}), L^r_{Mnormi}. The former file are the loads for load selection and the latter file are the loads for sensor measurement.
3. **Vicon (sensor) data lengths:-**The file
   `F:\Shieldfield␣2010\Patient␣Classification␣1\Vicon␣Force␣start␣end.xls`
   was used to enter the Vicon frames at which the synchronicity LED is identified as on and off. The frames were identified manually from visual examination of the Vicon video signal, i.e. this did not depend on reconstruction. With respect to visual inspection the LED on and off appeared instantaneous.

4. **Vicon file names:-**Data collection files have the following naming conventions: Vicon video files are
   `F:\Shieldfield␣2010\Patient␣Classification␣1\Patient␣s\r\r␣n.tvd`
   and Vicon reconstruction files are
   `F:\Shieldfield␣2010\Patient␣Classification␣1\Patient␣s\r\r␣n.3cd`
   where the `r` of `\r` and the `␣s` are indices for manoeuvres and subjects respectively.

   (a) `␣n`=[1,2,3] indicating which of the data files should be used: occasionally an error was made with the Vicon data collection and a second file was used which incremented the file number, e.g., the Vicon data collection was started and the subject already had put their hands on the handles.

5. **Vicon axes uniformity:-**Uniquely, for subject 17 the data collection took place at the Stephenson building Newcastle University. A different axes configuration was used and the Vicon data was transformed to the axes configuration used at Shieldfield Centre. Maple file
   `F:\Shieldfield␣2010\Maple\ChangeViconAxes01.mw`
   was used and the result was saved back to Vicon parent file with `n`=2.

6. **Vicon reconstruction:-**All Vicon reconstruction data was inspected to determine if data was present. If necessary the reconstruction was repeated with alternative reconstruction parameters until a good balance between minimising missing markers and creating ghost markers was achieved. All ghost markers were deleted leaving 12 caster assembly markers, 2 vehicle-frame markers and 1 CoZV marker except for r= [A, G] where the vehicle-frame marker served as the CoZV marker.

7. **Vicon data trimming:-**Vicon reconstruction files were loaded into Body Builder 3.55-build 136 and were saved with data trimmed to the frames at which the synchronising LED was identified as on and off, in accordance with the `Vicon␣Force␣start␣end.xls` to produce
   `F:\Shieldfield␣2010\Patient␣Classification␣1\Patient␣s\r\r␣n.txt`
   files. No filtering was applied. This data is referred to as Vicon (T) data.

8. A list of trials completed for each subject and each manoeuvre was input into Maple file
   `F:\Shieldfield␣2010\Maple\TrialList\TrialListCreator01.mw`
   with output this in two forms. One is
   `F:\Shieldfield␣2010\Maple\TrialList\TrialList.m`
   and the other is
   `F:\Shieldfield␣2010\Maple\TrialList\TrialListExcl.m`
   The only difference is that the second form sets one completed trial to non completed: the force data for this trial appeared to be subject to a software fault.

9. **Initial vehicle-frame orientation:-**The first 25 frames in the Vicon (T) data were used to determine the initial configuration but in four trials it was not possible to reconstruct the data for these frames without adversely affecting other frames. Alternative frames when the experimental-FCMV was in static equilibrium were identified by visual inspection of the graphed Vicon data. The Vicon (T) data was also inspected to determine when the vehicle returned to static-equilibrium. These frame numbers were input into file

F:\Shieldfield␣2010\Maple\CheckStartEndVehicleRotForData\Check␣for␣data␣01.mw
with output in a required form in respect of motion-start to file
F:\Shieldfield␣2010\Maple\CheckStartEndVehicleRotForData\StartVehRot_LLi.m
and in respect of motion-end to
F:\Shieldfield␣2010\Maple\CheckStartEndVehicleRotForData\GraphIcnspectionMotionStop_LLi.m

10. **Vicon data gaps:-** Inspection of the graphed Vicon (T) data for the vehicle-frame markers showed a small number of gaps in data. These were judged to be unimportant as they did not occur in or close to the initial period but in order to simplify the algorithms for handling the vehicle-frame data these were filled by linear interpolation. Gaps at end or beginning were filled with the nearest extant value. Files
F:\Shieldfield␣2010\Patient␣Classification␣1\Patient␣s\r\r␣n.txt
and
F:\Shieldfield␣2010\Maple\TrialList\TrialList.m
were input into
F:\Shieldfield␣2010\Maple\VehicleRotation\VehicleRotation01.mw
and this provided the output
F:\Shieldfield␣2010\Maple\VehicleRotation\Rr.m
(where the r of \r and the ␣s are indices for manoeuvres and subjects respectively) which provided a list of vehicle-frame orientations without gaps.

11. **Motion-start:-** The manoeuvres r are defined as $\text{sgn}(\dot{\theta}_0) = -1$. However, $\text{sgn}(\dot{\theta}_0) = 1$ are likely at motion-start. In order to provide a consistent selection for vehicle-frame motion-start the following definition was used: motion-start is the Vicon (T) data point after which all subsequent vehicle-frame orientations are more negative. This algorithm was implemented in file
F:\Shieldfield␣2010\Maple\CheckStartEndVehicleRotForData\MotionStart01.mw
which has key inputs
F:\Shieldfield␣2010\Maple\TrialList\TrialList.m
and F:\Shieldfield␣2010\Maple\VehicleRotation\Rr.m
(where the r of Rr is an index for manoeuvres) and outputs to
F:\Shieldfield␣2010\Maple\SynchronicityCheck\VehicleRotationSync\MotionStartSync_LLi.m
which provides a list of the motion-start data points in Vicon (T) data.

12. **Caster steady-state:-**The determination of the vehicle-frame orientation at which 90% of the caster steady-state had been reached was approximated as follows:

    (a) ${}^{B}\theta_{si}$ (caster orientation) was constructed from the Vicon (T) data.

    (b) Visual inspection indicated that the trend of ${}^{B}\theta_{si}$ conformed to the Zmodel-FCMV. Thus after smoothing, directional changes to ${}^{B}\theta_{si}$ contra to the Zmodel-FCMV would only occur at caster steady-state: $|{}^{B}\dot{\theta}_{si}|$ would be sufficiently large prior to that to ensure that noise effects were not dominant. The ${}^{B}\theta_{si}$ data was iteratively smoothed (from greater to lessor) until a direction change of ${}^{B}\theta_{si}$ contra to the Zmodel-FCMV was found.

    (c) The ${}^{B}\theta_{si}$ data from the above data point to motion-end was treated as caster steady-state data and an average was calculated.

    (d) The vehicle-frame orientation at which ${}^{B}\theta_{si}$ was 90% of the above value was determined: this is denoted caster near steady state.

This is implemented in
F:\Shieldfield␣2010\MapleFinal\SteadyStateFind01d.mw
and the key input files were
F:\Shieldfield␣2010\Maple\SynchronicityCheck\VehicleRotationSync\MotionStartSync_LLi.m
and F:\Shieldfield␣2010\Patient␣Classification␣1\Patient␣s\r\r␣n.txt
with an output
F:\Shieldfield␣2010\Maple\CheckStartEndVehicleRotForData.MotionSteadys.m

13. It was found that the output of the above file was not convenient for processing and file
F:\Shieldfield␣2010\Maple\CheckStartEndVehicleRotForData.MotionSteadys.m
was input into
F:\Shieldfield␣2010\Maple\CheckStartEndVehicleRotForData\Convert␣Subject␣to␣Region␣Steady␣␣Lists01
to output file
F:\Shieldfield␣2010\Maple\CheckStartEndVehicleRotForData\SteadyAllRr.m
and this provides a θ_0 data point at which caster near steady-state was reached for each trial collated in terms of manoeuvre r rather than subject. A second output is a list of θ_0 data point at which all four casters were in caster near steady state, denoted near steady-state: this is output to file
F:\Shieldfield␣2010\Maple\CheckStartEndVehicleRotForData\Steady95RrS_LLLif.m
where the r of Rr is an index for manoeuvres.

14. **Centre of pressure:-**The following process was used to estimate the $\hat{\boldsymbol{u}}$ moment arm of the $\hat{\boldsymbol{v}}$ component of the handle-forces. Figure 5.9 (page 132) illustrates this.

    (a) The position of base of thumb-finger junction on the handle top surface was marked at sensor measurement: the measure from this mark along the top surface of the handle to the handle-end was measured with a fabric measuring tape. This was repeated for left and right hands for each manoeuvre r.

    (b) These measures are detailed in file
    F:\Shieldfield␣2010\Patient␣Classification␣s\Patient␣s\Hand␣positions.txt

    (c) The hand-width while grasping the handle was measured, from base of thumb-finger to maximum width, with callipers.

    (d) The handle and sensor were drawn to scale (see DISC) and the location of the sensor y axis (vertical) was determined with respect to handle end.

    (e) The position of thumb-finger junction on the handle top surface was transferred to the drawing.

    (f) The hand width measurement determined a radius.

    (g) The position of thumb-finger junction determined an origin.

    (h) A circle was drawn and the intersection of the circle with the lower handle surface defined the estimated rear hand-handle contact point.

    (i) The mid point between the two marks was determined and this was deemed to be an estimated centre of pressure. A vertical line was drawn through this point.

    (j) The dimension between the vertical line through the estimated centre of pressure and the sensor y axis was measured on the drawing and these measures were input into F:\Shieldfield␣2010\Maple\Handles\HandleData.mw
    and the output of a list of the moment arms in suitable form was made

to file
F:\Shieldfield␣2010\Maple\Handles\HandlePos.m

(k) The process was repeated for subjects with more than one handle grasp position.

(l) Lines in the sagittal plane and perpendicular to the axis through the two marks were deemed to be rear and front lines of handle grasp boundary.

15. **Sensor data storage:-**The sensor data was saved in the form
F:\Shieldfield␣2010\Patient␣Classification␣1\Patient␣s\r\r␣n.dat.
This was loaded into Excel and saved in the form
F:\Shieldfield␣2010\Patient␣Classification␣1\Patient␣s\r\r␣n.csv
where ␣s, \r are indices for manoeuvres and subjects and ␣n are as previously defined.

16. **Sensor data manipulation:-**In order to manipulate the sensor data the file
F:\Shieldfield␣2010\MapleFinal\uvsActionsNNmPerKgFyAdjusted\uvsActionsNNmPerKgFyAdjusted10
input the following files
F:\Shieldfield␣2010\Maple\\Handles\\HandlePos.m,
F:\Shieldfield␣2010\Shieldfield␣2010\Load␣summary(with␣added␣max).xls and
F:\Shieldfield␣2010\Patient␣Classification␣1\Patient␣s\r\r␣n.csv
in order to achieve the following:

(a) Transformation of all data to provide a zero-offset based on the signal before hands-on.

(b) Transformation of sensor measures to the *uvs* frame and sensor moment units (in lb) to SI units (Nm).

(c) Calculation of the force or moment per kg load.

(d) Calculation of the force or moment per kg load with load adjusted for the effects vertical handle-forces.

(e) Calculation of left and right $\hat{\boldsymbol{u}}$ directed handle-force components.

(f) Calculation of $\|P_v\hat{\boldsymbol{v}} + P_u\hat{\boldsymbol{u}}\|$

(g) Determination of indices for $P_{uCs} = 0$.

(h) Calculation of the handle-force measure P_{uCs} when $P_{uCs} \neq 0$.

Results were output as a set of matrices to
F:\Shieldfield␣2010\MapleFinal\ForceMatrices\RrSs.m
where the r and s of RrSs are indices for subjects and manoeuvres and n of n.csv is as previously defined.

17. **Synchronicity:-**The sensor data was collected at approximately 50Hz and the time stamps were an approximate indication of the real time of occurrence. Vicon provides hardware real time control. There was therefore a need to examine the synchronisation of the sensor and Vicon (T) data.

(a) The number of Vicon (T) data frames was checked against the visual inspection record (F:\Shieldfield␣2010\Patient␣Classification␣1\Vicon␣Force␣start␣end.xls) to ensure that no numerical input errors had been made in saving the Vicon data as Vicon (T) data.

(b) The number of Vicon (T) data points was compared with the number of sensor data points.

(c) A synchronisation failure was defined as a time separation of ±0.01sec between the two time signals and as trials indicated that the sensor signal frequency variation seemed to occur at the start of the record the signals were compared from the last datum to the first datum and a list was made of the data indices at which synchronisation failure occurred.

18. The above steps were implemented for each manoeuvre Z_r in file
F:\Shieldfield␣2010\Maple\SynchronicityCheck\SynchronicityCheck01.mw
which provided output file
F:\Shieldfield␣2010\Maple\SynchronicityCheck\Reportr.m
These results for each manoeuvre were examined together in file
F:\Shieldfield␣2010\Maple\SynchronicityCheck\Synchronicity␣summary01.mw
which output details of data manipulations, lengthening and shortening of sensor and Vicon data. If there were no synchronisation failures and Vicon (T) data length varied from sensor data length then the length of the Vicon (T) file was modified at the end by deleting or repeating the final value. If synchronisation failures and data length differences existed the sensor data was deleted at the beginning of the data if the synchronisation failures occurred at the beginning and sensor data was deleted at the end if the synchronisation failures occurred at the end.
F:\Shieldfield␣2010\Maple\SynchronicityCheck\Corrections.m.
These corrections were implemented by
F:\Shieldfield␣2010\MapleFinal\SynchronicityCorrection01.mw
which inputs files:
F:\Shieldfield␣2010\Maple\SynchronicityCheck\Corrections.m,
F:\Shieldfield␣2010\MapleFinal\ForceMatrices\RrSs.m
and F:\Shieldfield␣2010\Maple\VehicleRotation\Rr.m
and outputs these as
F:\Shieldfield␣2010\Maple\SynchronicityCheck\VehicleRotationSync\RrSs.m and
F:\Shieldfield␣2010\MapleFinal\SyncdForceMatrices\RrSs.m
where the r of \Rr.m,Reportr and RrSs and the s of RrSs are indices for subjects and manoeuvres.

19. **Recalculating motion start:-**As the Vicon (T) data lengths had been changed the motion start were recalculated with the modified values. This is carried out in file
F:\Shieldfield␣2010\Maple\MotionStart\MotionStartSync02.mw
which inputs file
F:\Shieldfield␣2010\␣Maple\SynchronicityCheck\VehicleRotationSync\Rr.m
and outputs to file
F:\Shieldfield␣2010\Maple\SynchronicityCheck\VehicleRotationSync\MotionStartSync_LLi.m
where the r of Rr is a manoeuvre index.

20. **Percentiles 1:-**Percentile values for the start-steady period and for the steady-state period were determined from the sensor measures using file
F:\Shieldfield␣2010\MapleFinal\InvestigationNumericalPercentiles03.mw
which input files
F:\Shieldfield2010\MapleFinal\SyncdForceMatrices\RrSs
F:\Shieldfield␣2010\MapleFinal\Kinematics\Steady95RS_LLLif.m
F:\Shieldfield␣2010\Maple\SynchronicityCheck\VehicleRotationSync\MotionStartSync_LLi.m
F:\Shieldfield\2010\Maple\CheckStartEndVehicleRotForData\GraphInspectMotionStop_LLi.
and output files
F:\Shieldfield␣2010\MapleFinal\ForcePercentiles\PreSteadyNRr.m

F:\Shieldfield␣2010\MapleFinal\ForcePercentiles\PreSteadyPRr.m

F:\Shieldfield␣2010\MapleFinal\ForcePercentiles\PostSteadyNRr.m

F:\Shieldfield␣2010\MapleFinal\ForcePercentiles\PostSteadyPRr.m

where the r of Rr is a manoeuvre index and the N and P of NR and PR indicate percentiles for negative and positive measures respectively.

21. **Percentiles 2:-**This second percentile determination followed the previous one but in this case the start-steady period was divided into an initial period and a later period. This was an iterative process based on discriminating different dynamic states. This was carried out in file
F:\Shieldfield␣2010\MapleFinal\InvestigationNumericalPercentilesEL02
which output to files
F:\Shieldfield␣2010\MapleFinal\ForcePercentiles\PreSteadyENRr.m
F:\Shieldfield␣2010\MapleFinal\ForcePercentiles\PreSteadyEPRr.m
F:\Shieldfield␣2010\MapleFinal\ForcePercentiles\PreSteadyLPRr.m
F:\Shieldfield␣2010\MapleFinal\ForcePercentiles\PreSteadyLNRr.m
where the file ending follows the same form as the previous percentiles. The E files provide the values for ${}^{large}_{ss1}\mathbf{P}^{\mathrm{r}}$.
The vehicle-frame orientation at which division of the initial period ends is output to
F:\Shieldfield␣2010\MapleFinal\ForcePercentiles\IntermediateSteady.m

22. **Results outputs:-** A number of files were used to produce graphic outputs for results. These included
    (a) F:\Shieldfield␣2010\MapleFinal\Typeset01.mw which outputted a the file
    F:\Shieldfield␣2010\MapleFinal\typeset01.m
    for display of symbols.
    (b) F:\Shieldfield␣2010\MapleFinal\InvestigationGraphicMotionStartELZ.mw
    where the Z indicates any of the r manoeuvre letters and which graphs sensor data for each subject for each manoeuvre for the start-steady period.
    (c) F:\Shieldfield␣2010\MapleFinal\FinalAnalysesPreSteady␣Z.mw
    which synthesises the results for all subjects, in terms of percentiles for each manoeuvre and graphs and tabulates results (Z indicating as previous).
    (d) F:\Shieldfield␣2010\MapleFinal\FinalAnalysesPreSteady␣ALL0.mw
    which synthesises the results for all subjects and all manoeuvres and graphs and tabulates these results.
    (e) F:\Shieldfield␣2010\MapleFinal\FinalAnalysesKinematicsAll1.mw
    which determines maximum vehicle-frame rotations ($\dot{\theta}_0$) by curve fitting methods and tabulates and graphs results.

23. **Load analyses:-** The file F:\Shieldfield␣2010\MapleFinal\LoadRaw01
analyses the load selections and provides outputs for statistical analyses, tables and graphs.
The inputs are F:\Shieldfield␣2010\MapleFinal\Load␣summary.xls
which is the initial load selection recorded and
F:\Shieldfield␣2010\MapleFinal\Load␣summary(with␣added␣max).xls
which is the load selection recorded at sensor-displacement measurement with outputs

F:\Shieldfield␣2010\MapleFinal\MapleToMiniTab\LoadNorm_M.csv
F:\Shieldfield␣2010\MapleFinal\MapleToMiniTab\LoadMeasureNorm_M.csv
where the first output relates to L^r_{Mnormi} at load selection and the second output repeats this for load selection at sensor-displacement measurement. These were imported into F:\Shieldfield␣2010\MapleFinal\MapleToMiniTab\LoadNormLoadMeasureNorm.xls and the values were pasted into Minitab to determine 95^{th} percentile confidence intervals which were saved as F:\Shieldfield␣2010\MapleFinal\MapleToMiniTab\LoadNorm.MPJ
F:\Shieldfield␣2010\MapleFinal\MapleToMiniTab\LoadMeasureNorm.MPJ
with results pasted to F:\Shieldfield␣2010\MapleFinal\MapleToMiniTab\LoadNormConfidence_M.xls
F:\Shieldfield␣2010\MapleFinal\MapleToMiniTab\LoadMeasureNormConfidence_M.xls
to allow subsequent graphing with these. Final outputs are
F:\Shieldfield␣2010\MapleFinal\MapleToMiniTab\Friedman␣n_M.csv
where the ␣n=[1,2,3] which were required for the Friedman Test in Minitab.

24. **Minitab:-** Was used to carry out the Friedman Test.

25. **Sensor data manipulation with modified handle-force application point:-**This section details the process for determining the insensitivity to errors in determining handle-force application point of P_{Lv} and P_{Rv} by recalculating results with a $\pm$ 0.03 m variation.

    (a) In order to manipulate the sensor data the file
    F:\Shieldfield␣2010\MapleFinal\uvsActionsNNmPerKgFyAdjusted\uvsActionsNNmPerKgFyAdjusted10
    was temporarily modified so that the moment arm was +0.03m or -0.03m and the following files files were input
    F:\Shieldfield␣2010\Maple\\Handles\\HandlePos.m,
    F:\Shieldfield␣2010\Shieldfield␣2010\Load␣summary(with␣added␣max).xls and
    F:\Shieldfield␣2010\Patient␣Classification␣1\Patient␣s\r\r␣n.csv
    in order to achieve the following:

    i. Transformation of all data to provide a zero-offset based on the signal before hands-on.
    ii. Transformation of sensor measures to the *uvs* frame from sensor units to SI units, where required: (in lb) to Nm.
    iii. Calculation of the force or moment per kg load.
    iv. Calculation of the force or moment per kg load with load adjusted for the effects vertical handle-forces.
    v. Calculation of left and right $\hat{\boldsymbol{u}}$ directed handle-force components.
    vi. Calculation of $\|P_v\hat{\boldsymbol{v}} + P_u\hat{\boldsymbol{u}}\|$
    vii. Determination of indices for $P_{uCs} = 0$.
    viii. Calculation of the handle-force measure P_{uCs} when $P_{uCs} \neq 0$.

    (b) Results were outputted as a set of matrices to
    F:\Shieldfield␣2010\MapleFinal\ForceMatrices\PlusRrSs.m
    F:\Shieldfield␣2010\MapleFinal\ForceMatrices\MinusRrSs.m
    where the r and s of RrSs are indices for subjects and manoeuvres and where Plus indicates a +0.03 m modification and Minus indicates a -0.03 m modification.

    (c) In order to duplicate the original process and provide the necessary files synchronisations corrections were made in
    F:\Shieldfield␣2010\MapleFinal\SynchronicityCorrection01Vmoment.mw

with input files:
F:\Shieldfield␣2010\Maple\SynchronicityCheck\Corrections.m,
F:\Shieldfield␣2010\MapleFinal\ForceMatrices\RrSs.m
and output these as
F:\Shieldfield␣2010\MapleFinal\SyncdForceMatrices\PlusRrSs.m and
F:\Shieldfield␣2010\MapleFinal\SyncdForceMatrices\MinusRrSs.m where the r of \Rr.m and RrSs, and the s of RrSs are indices for subjects and manoeuvres.

(d) Percentile measures were determined in
F:\Shieldfield␣2010\MapleFinal\InvestigationNumericalPercentilesEL02vMoment01.mw
with output to files
F:\Shieldfield␣2010\MapleFinal\ForcePercentiles\PreSteadyENPlusRr.m
F:\Shieldfield␣2010\MapleFinal\ForcePercentiles\PreSteadyEPPlusRr.m
F:\Shieldfield␣2010\MapleFinal\ForcePercentiles\PreSteadyENMinusRr.m
F:\Shieldfield␣2010\MapleFinal\ForcePercentiles\PreSteadyEPMinusRr.m

(e) The determination of the ${}^{large}_{ss1}\mathbf{P}^{\mathrm{r}}$ with modified handle-force application point were determined from the above files and these percentile values were input by
F:\Shieldfield␣2010\MapleFinal\FinalAnalysesPreSteady␣ALL0Vmoment.mw
which synthesises the results for all subjects and all manoeuvres and graphs and tabulates these results.

26. **Determination of caster angular velocity directions:-** In the following description of the analyses process, where F is in any root directory the term ROOT1 indicates address
F:\Shieldfield␣2010\MapleFinal\Discussion,
ROOT2 indicates address
F:\Shieldfield␣2010\MapleFinal\ForcePercentiles
and the term ROOT3 indicates
F:\Shieldfield␣2010\Maple\SynchronicityCheck.
Indexed files are indicated by the following addendum to the file names: ␣w␣ (window size), ␣a␣ (action), ␣f␣ (step) ,␣h␣ (α), ␣r␣ (manoeuvres A to L), ␣s␣ (subject) ␣p␣ (percentile window shift).
The angular velocity directions [sgn($\dot{\theta}_{si}$),sgn($\dot{\theta}_{ti}$)] are denoted 'directions' The term 'by trial' indicates that the data for each subject and for each manoeuvre is segregated, i.e. there are 11 by 16 (maximum) data sets. The term 'by manoeuvre' indicates that data for each subject is combined, i.e. there are 11 data sets.

(a) The displacement of the roll marker (as indicated by the vertical displacement of a marker on the wheel face) and global caster orientation were determined in file
ROOT1\KimeaticsData02.mw
with output to files
ROOT1\Roll\R␣r␣S␣s␣.m\\ and ROOT1\GRot\R␣r␣S␣s␣.m
and these are denoted 'roll data' and 'grot data' respectively.

(b) The vehicle-frame orientation is input from ROOT3\VehicleRotationSync\R␣r␣.m and this is denoted 'vehicle-frame orientation data'.

(c) The indices at which the relevant actions (P_v, P_u and P_{uCs}) occurred are input from
ROOT2\PreSteadyENR␣r␣.m
and

ROOT2\PreSteadyEPR␣r␣.m
and these are denoted 'percentile indices'.

(d) As the determination of $\text{sgn}(\dot{\theta}_{ti})$ from the 'roll data' required that the index at which the marker was at the lowest vertical position was known this was determined in file
ROOT1\RollZeroPosition2.mw
and the positions were output to
ROOT1\Roll\RollZero2_LLLi.m
and this is denoted 'roll minimum'. Graphs of these positions were inspected and modification, by use of an exception list, was implemented where the algorithm had failed.

(e) To determine 'directions' the file
ROOT1\DevelopmentKinematics01.mw
functions as follows. The 'roll data', 'grot data', 'roll minimum' and 'percentile indices' were input. For some results positive and negative percentile indices were relevant and a list was written to account for this.

(f) A 'percentile shift' was introduced as follows: the 'directions' were determined from 25 data before the first to 25 data after the last of the 'percentile indices'. The 'directions' were determined from the first to the last data, i.e. a range which contained the 'percentile indices' was used rather than the individual data points of the 'percentile indices' which are not necessarily continuous. The 'directions' were determined using the Cox and Stuart trend test with an $\alpha = 0.05$ level: the 'directions' were indicated by a 1, -1, or 0 depending on whether the Cox and Stuart test determined positive, negative or indeterminate angular velocity, respectively. The Cox and Stuart trend test was constructed with a window size parameter [10, 20] and a step parameter [5, 10]: The output was made to
ROOT1\KinConform2\Act␣a␣Win␣w␣Filt␣f␣Alpha5R␣r␣S␣s␣_M.m

(g) The 'directions' for the 'percentile indices' (the relevant points rather than the whole range) were extracted using file
ROOT1\PercentileRangeToIndexPoints01.mw
using input
ROOT1\KinConform2\Act␣a␣Win␣w␣Filt␣f␣Alpha5R␣r␣S␣s␣_M.m
The 'directions' were determined in three forms: with a ± 25 or zero shift in the index 'by manoeuvre' and output to
ROOT1\PercentileRangeToIndexPoints01\\Act␣a␣Win␣w␣Filt␣f␣Alpha5␣R␣r␣_M.m
and 'by trial' output to
ROOT1\BRotAtPercentilePoints01\\Act␣a␣Win␣w␣Filt␣f␣Alpha5␣R␣r␣S␣s␣_M.m

(h) The most frequent 'directions' in the regions for each caster were determined in file
ROOT1\KinTestPercentilePoints.mw
Inputs were
ROOT1\PercentileRangeToIndexPoints01\Act␣a␣Win␣w␣Filt␣f␣Alpha5R␣r␣_M.m
and the output was a set of two pairs of eleven, two row by eight column matrices. The first of the matrix pair was the count of positive 'directions' for each caster in row one and negative 'directions' in row two. The second of the matrix pair assigned the indeterminate directions to the smaller count of the two directions. This was repeated for the eleven manoeuvres. These counts were in percentage form. The output was to

ROOT1\KinTestPercentilePointsAllr\P␣p␣CountAct␣a␣Win␣w␣Filt␣f␣Alpha5_L.m
each of which contains the data for all manoeuvres based on the different parameters.

(i) Caster orientation, denoted here as 'brot data', at the 'percentile indices' was determined in
ROOT1\BRotAtPercentilePoints01.mw
which took as inputs the 'subject percentile indices', the 'grot data', the 'vehicle-frame orientation data' and output was made to
ROOT1\BRotAtPercentilePoints01\R␣r␣S␣s␣_M.m

i. The orientation of $\boldsymbol{P}_{Qi}$ $(\rho_i +^B \theta_{si})$ are estimated in file
ROOT1\AnalysesByPQiZeroCorrection.mw
which took input
ROOT1\KinTestPercentilePointsAllr\P␣p␣CountAct␣a␣Win␣w␣Filt␣f␣Alpha5_L.m
which was in the form of percentages and produced two new forms of 'directions', denoted 'corrected directions': one where the uncertainty was removed based on reducing the differences and one where the differences between subjects were increased and the output in the form of a list of a combination of eight ± 1 indicating 'directions' was made to
ROOT1\AnalysesByPQiZeroCorrection\Act␣a␣Win␣w␣Filt␣f␣Alpha5.m.

ii. This was read back in and combined with the 'brot data' to determine the $\boldsymbol{P}_{Qi}$ orientation with respect to vehicle-frame for the three ρ_i. There were therefore
$3(\rho_i) \times 2$('corrected directions') $\times$ 2(window) $\times$ 2(steps) $\times$ 3(percentile shift) for each action.

iii. The median $\rho_i +^B \theta_{si}$ measure was determined for each manoeuvre r: the set of measures was for all subjects and each subject would have a number of measures for each action.These were output to file
ROOT1\FinalOut\\a␣Sh␣p␣Win␣w␣Filt␣f␣Ang␣rh␣d.m
where rh is the ρ_i choice and d is the 'corrected directions' choice.

iv. An inter manoeuvre comparison was made of the median $\rho_i +^B \theta_{si}$ and the smallest median magnitude difference was chosen in file
ROOT1\\FinalOut1.mw
which used
ROOT1\\FinalOut\\a␣Sh␣p␣Win␣w␣Filt␣f␣Ang␣rh␣d.m
as input.

27. **Conformity to the Zmodel-FCMV** $[\mathrm{sgn}(\dot{\theta}_{si}),\mathrm{sgn}(\dot{\theta}_{ti})]$ **combinations:-** This was determined in
F:\Shieldfield␣2010\MapleFinal\Discussion\Development\KinSummary0 using the rot-roll directions determined above in **Determination of caster angular velocity directions**

28. **Determination of Zmodel-FCMV roll marker vertical placement based on data initial position:-** As the Vicon markers indicating wheel roll direction were placed by hand neither the initial orientation of θ_{ti} nor the radial distance from caster wheel centre was fixed. In order to determine a Zmodel-FCMV marker displacement curve to compare with the data it was necessary to determined these two values from the data and this was achieved as follows.

(a) The minimum roll marker position was determined in file
`ROOT1\RollZeroPositionForModel01.mw`
which provided output to
`ROOT1\Roll\RollZeroModelR␣r␣_LLi.m`
This provides measures for all marker minimum vertical positions where as the previous measures for the determination of wheel roll direction only made the determination if the largest magnitude percentiles occurred after this position. With minimum roll marker vertical position determined the radial position could be determined since the caster wheel centre on the experimental-FCMV was approximately fixed (disregarding loading effects). With the radial dimension determined it was then possible to determine the initial caster wheel orientation as defined by the roll marker from basic trigonometry.

(b) Data for roll marker and Zmodel-FCMV data could then be plotted using file
`ROOT1\ModelRoll01.mw`
with input from
`ROOT1\Roll\RollZeroModelR␣r␣_LLi.m`

29. **Justifying the quasi-static assumption:-** For the initial period the vehicle-frame accelerations were determined by both numerical and symbolic differentiation in
`ROOT1\ComPrep01.mw`
using vehicle-frame orientation data and inputs taken from
`F:\Shieldfield␣2010\Patient␣Classification␣1\Patient␣s\r\r␣n.txt`,
and
`F:\Shieldfield␣2010\Maple\TrialList\TrialList.m`
using the following process.

(a) For numerical differentiation:

i. The displacement data for the two Vicon markers which determined vehicle-frame orientation (r=[A, G]) were used to determine a virtual point at an equidistant position from these markers (a virtual equivalent to the marker for r=D).

ii. An estimated COM position was then determined in the Vicon frame, denoted XYZ, for the initial period, by 'trial': the estimated COM was located at $-0.505\hat{\boldsymbol{u}}$ m from the virtual D position which is $-0.097\hat{\boldsymbol{u}}$ m from the geometric vehicle-frame centre.

iii. The approximate acceleration of the COM in the initial period was determined in the XYZ frame by 'trial' using the Mean Value Theorem for double numerical differentiation.

iv. The angular acceleration was determined using the same process with θ_0 data.

v. The COM approximate translational acceleration was then transformed to $\hat{\boldsymbol{v}} - \hat{\boldsymbol{u}}$ components.

vi. No smoothing was carried out.

vii. Examination of these accelerations by means of histogram (PDF) by 'trial' indicated that the accelerations had a normal distribution around zero. This was interpreted as an indication that the acceleration magnitudes were small and that noise was being amplified by the numerical differentiation.

(b) Polynomial fitting of the vehicle-frame translational displacements in the XYZ frame and of θ_0 displacement data, each against time, produced small residuals.

(c) Double symbolic differentiation was carried out using the polynomial functions by 'trial' to provide vehicle-frame accelerations in the XYZ frame.

(d) These functions were transformed to $\hat{\boldsymbol{v}} - \hat{\boldsymbol{u}}$ components.

(e) The mass moment of inertia was approximated using circular cylindrical shell mr^2 where $r = \frac{l}{2} = .2185\,m$.

(f) The process which was developed to provide a compact representation of handle-forces, the measure P_{QH} (page 99), was then used to provide a compact measure of the component of handle-forces required for inertial forces. Setting motion resistance effects to zero and $m = 1$, to provide a N/kg measure, the inverse dynamic equations for the model-FCMV (Equations 4.41–4.43, page 88) may be written as

$$P_u = \ddot{\boldsymbol{x}}_B \cdot \hat{\boldsymbol{u}} \tag{C.1}$$

$$P_v = \ddot{\boldsymbol{x}}_B \cdot \hat{\boldsymbol{v}} \tag{C.2}$$

and

$$T = I_m \ddot{\theta}_0 \tag{C.3}$$

where $\ddot{\boldsymbol{x}}_B \cdot \hat{\boldsymbol{u}} = \ddot{x}_{Bu} - \dot{\theta}_0 \dot{x}_{Bv}$, $\ddot{\boldsymbol{x}}_B \cdot \hat{\boldsymbol{v}} = \ddot{x}_{Bv} + \dot{\theta}_0 \dot{x}_{Bu}$ and I_m is I adjusted for $m = 1$: all definitions as given in the Dynamics Chapter. So substituting Equations C.1–C.3 into Equation 4.67 gives an inertial version of P_{QH} for each kg load, denoted as P_{IH}, as

$$P_{IH} = \begin{cases} |\ddot{\boldsymbol{x}}_B \cdot \hat{\boldsymbol{v}}| + |\ddot{\boldsymbol{x}}_B \cdot \hat{\boldsymbol{u}}| & |\ddot{\theta}_0\, I_m + \ddot{\boldsymbol{x}}_B \cdot \hat{\boldsymbol{v}}(0.5l + h + c)| \\ & \leq |\ddot{\boldsymbol{x}}_B \cdot \hat{\boldsymbol{u}}| hw \\ |\ddot{\boldsymbol{x}}_B \cdot \hat{\boldsymbol{v}}| + |\ddot{\theta}_0\, I_m + \ddot{\boldsymbol{x}}_B \cdot \hat{\boldsymbol{v}}(\frac{l}{2} + h + c)| hw^{-1} & |\ddot{\theta}_0\, I_m + \ddot{\boldsymbol{x}}_B \cdot \hat{\boldsymbol{v}}(0.5l + h + c)| \\ & > |\ddot{\boldsymbol{x}}_B \cdot \hat{\boldsymbol{u}}| hw \end{cases} \tag{C.4}$$

(g) The symbolic functions for the accelerations, based on the polynomial fitting, for Equation C.4 were then used to make a numerical evaluation of Equation C.4 at each data point 'by trial'. The largest magnitude occurrence of P_{IH}, with h substituted for subject's estimated centre of pressure of hand contact and c as estimated, for all data points was then selected to represent the subject for the manoeuvre. As this process was automated plots of the XY data, polynomial XY curve, and XY data based on a Zmodel-FCMV were made along with a record of the numerical values of the standard deviations of the polynomial residuals of the XY displacement data fitting (PDF): these were inspected and it was confirmed that the polynomial fits appeared representative.

30. **Determination of the proportion of caster global rotation to wheel roll in the initial period:-** This is calculated in

`F:\Shieldfield␣2010\MapleFinal\Discussion\Development\CheckingCentreofZ05forRot.mw`

C.1. **Processing**

In the following description of the analyses process, where F is in any root directory the term ROOT1 indicates address

F:\Shieldfield␣2010\MapleFinal\Discussion,

ROOT2 indicates address

F:\Shieldfield␣2010\MapleFinal\ForcePercentiles

and the term ROOT3 indicates

F:\Shieldfield␣2010\Maple\SynchronicityCheck.

Indexed files are indicated by the following addendum to the file names: ␣w␣ (window size), ␣a␣ (action), ␣f␣ (step) ,␣h␣ (α), ␣r␣ (manoeuvres A to I), ␣s␣ (subject) ␣p␣ (percentile window shift).

The angular velocity directions [sign($\dot{\theta}_{si}$), sign($\dot{\theta}_{ti}$)] are denoted 'directions' The term 'by trial' indicates that the data for each subject and for each manoeuvre is segregated, i.e. there are 11 by 16(max) data sets. The term by 'manoeuvre' indicates that data for each subject is combined, i.e. there are 11 data sets.

The displacement of the roll marker (as indicated by the vertical displacement of a marker on the wheel face) and global orientation of the caster assembly were determined in file

ROOT1\KimeaticsData02.mw

which outputted to folders

ROOT1\RollR␣r␣S␣s␣.m and ROOT1\GRotR␣r␣S␣s␣.m

and these are denoted 'roll data and' 'grot data' respectively.

The vehicle-frame orientation is input from ROOT3\VehicleRotationSync\R␣r␣.m and this is denoted 'vehicle-frame orientation data'.

The indices at which the relevant actions occurred are input from ROOT2\PreSteadyENR␣r␣.m and ROOT2\PreSteadyEPR␣r␣.m and these are denoted 'percentile indices'.

As the determination of sign($\dot{\theta}_{ti}$) from the 'roll data' required that the index at which the marker was at the lowest vertical position was known this was determined in file

ROOT1\RollZeroPosition2.mw

and the positions were out put to

ROOT1\Roll\RollZero2_LLLi.m

and this is denoted 'roll minimum'. These positions were visually checked and modification by use of an exception list was implemented where the algorithm had failed.

To determine 'directions' the file

ROOT1\DevelopmentKinematics01.mw

functions as follows. The 'roll data', 'grot data', 'roll minimum' and 'percentile indices' were input. For some results positive and negative percentile indices were relevant and a list was written to account for this.

A 'percentile shift' was introduced as follows: the 'directions' were determined from 25 data before the first to 25 data after the last of the 'percentile indices'. The 'directions' were determined from the first to the last data i.e. a range which contained the 'percentile indices' points was used rather than the individual data points of the 'percentile indices' which are not necessarily continuous. The 'directions' were determined using the Cox and Stuart trend test with an $\alpha = 0.05$ level: the 'directions' were indicated by a 1, -1, or 0 depending on whether the Cox and Stuart test determined positive, negative or indeterminate angular velocity. The Cox and Stuart trend test was constructed with a window size parameter [10, 20] and a step parameter [5, 10]: The output was sent to

ROOT1\KinConform2\Act␣a␣Win␣w␣Filt␣f␣Alpha5R␣r␣S␣s␣_M.m

The 'directions' for the 'percentile indices' (the points rather than over the whole range) were extracted using file

ROOT1\PercentileRangeToIndexPoints01.mw

using input

ROOT1\KinConform2\Act␣a␣Win␣w␣Filt␣f␣Alpha5R␣r␣S␣s␣_M.m

The 'directions' were determined in three forms: with a ± 25 or zero shift in the index. The measures for subjects were combined into a single manoeuvre measure to provide these in terms of each manoeuvre i.e. subjects combined output to

ROOT1\PercentileRangeToIndexPoints01\\Act␣a␣Win␣w␣Filt␣f␣Alpha5␣R␣r␣_M.m

and to provide these in terms of each subject for each manoeuvre i.e. subjects not combined combined output to

ROOT1\BRotAtPercentilePoints01\\Act␣a␣Win␣w␣Filt␣f␣Alpha5␣R␣r␣S␣s␣_M.m

The most frequent 'directions' in the regions for each caster were determined in file ROOT1\KinTestPercentilePoints.mw

Inputs were

ROOT1\PercentileRangeToIndexPoints01\Act␣a␣Win␣w␣Filt␣f␣Alpha5R␣r␣_M.m

and the output was a set of two pairs of eleven, two row by eight column matrices. The first of the matrix pair was the count of positive 'directions' for each caster in row one and negative 'directions' in row two. The second of the matrix pair assigned the indeterminate directions to the smaller count of the two directions. This was repeated for the eleven manoeuvres. The output was to

ROOT1\KinTestPercentilePointsAllr\P␣p␣CountAct␣a␣Win␣w␣Filt␣f␣Alpha5_L.m

each of which contains the data for all manoeuvres based on the different parameters.

The relative caster assembly position,denoted 'brot data', at the 'percentile indices' was determined in

ROOT1\BRotAtPercentilePoints01.mw

which took as inputs the 'subject percentile indices', the 'grot data', the 'vehicle-frame orientation data' and output was made to

ROOT1\BRotAtPercentilePoints01\R␣r␣S␣s␣_M.m

A second form of the 'directions', denoted 'corrected directions' was produced. This was based on the counts made in

ROOT1\KinTestPercentilePoints.mw

All indeterminate directions were replaced with a direction which reduced the amount of difference between positive and negative directions. This was carried out for each manoeuvre in file

ROOT1\AnalysesByPQiZeroCorrection.mw

which took as input

`ROOT1\KinTestPercentilePointsAllr\P␣p␣CountAct␣a␣Win␣w␣Filt␣f␣Alpha5_L.m`

and output was made to as lists of signs for each manoeuvre which could replace indeterminate directions

`ROOT1\AnalysesByPQiZeroCorrection\Act␣a␣Win␣w␣Filt␣f␣Alpha5.m`

The orientation of the action of the caster assembly on the vehicle frame relative to the vehicle-frame was estimated as follows in file

`ROOT1\AnalysesByPQiZeroCorrection.mw`

which took inputs ‘brot data’ and ‘corrected directions’

Appendix D–Data

The three tables which follow relate to maximum comfortable load (kg): this is estimated caster loading and therefore includes the vehicle mass.

0	*A*	*B*	*C*	*D*	*E*	*F*	*G*	*H*	*I*	*K*	*L*
1	116	116	61	107	70	80	98	116	89	169	169
2	80	80	61	52	70	52	52	61	52	107	61
3	80	98	61	89	98	34	89	98	70	134	116
4	116	116	80	116	134	80	125	134	89	134	134
5	98	98	70	134	80	80	89	107	52	134	125
6	116	156	80	125	169	89	98	134	116	169	169
7	61	70	43	80	89	*NC*	80	116	89	143	107
8	89	125	52	134	125	52	144	150	70	169	169
9	143	125	98	134	125	89	134	169	125	169	169
10	89	107	61	80	107	52	80	134	*NC*	169	169
11	107	125	80	116	134	70	107	116	89	169	134
12	89	89	80	116	89	80	89	125	89	116	116
13	80	70	70	89	107	52	70	107	70	134	134
14	107	*NC*	80	107	116	70	107	89	80	116	134
15	89	98	80	107	125	70	89	143	70	163	*NC*
16	125	169	107	150	156	98	150	163	107	169	169
17	70	61	61	80	89	61	80	70	70	134	107

Table D.1 – Shows the maximum comfortable load (kg) selected by each subject for each manoeuvre at the initial load selection. *NC* indicates not completed

0	A	B	C	D	E	F	G	H	I	K	L
1	116	116	61	125	70	80	98	116	89	169	169
2	80	80	61	52	70	52	52	61	52	107	61
3	80	98	61	89	98	52	89	98	70	150	116
4	116	116	80	116	143	70	116	125	89	150	150
5	98	98	61	134	80	61	89	107	52	134	125
6	116	156	80	125	169	89	98	134	116	169	169
7	61	70	43	80	89	*NC*	70	116	80	134	107
8	89	125	70	134	125	52	144	150	70	169	169
9	143	125	98	134	125	89	134	169	125	169	169
10	89	107	61	80	107	52	80	134	*NC*	169	169
11	107	125	80	116	134	70	107	116	89	169	134
12	89	89	80	116	89	70	80	125	89	116	116
13	80	70	70	89	98	52	70	107	61	134	134
14	107	*NC*	80	107	116	70	107	89	80	116	116
15	89	98	80	107	125	70	89	143	70	163	*NC*
16	116	169	107	150	156	98	150	163	107	169	169

Table D.2 – Shows the maximum comfortable load (kg) selected by each subject for each manoeuvre at the sensor-displacement measurement. *NC* indicates not completed

0	A	B	C	D	E	F	G	H	I	K	L
1	0	0	0	−18	0	0	0	0	0	0	0
2	0	0	0	0	0	0	0	0	0	0	0
3	0	0	0	0	0	−18	0	0	0	−16	0
4	0	0	0	0	−9	10	9	9	0	−16	−16
5	0	0	9	0	0	19	0	0	0	0	0
6	0	0	0	0	0	0	0	0	0	0	0
7	0	0	0	0	0	*NC*	10	0	9	9	0
8	0	0	−18	0	0	0	0	0	0	0	0
9	0	0	0	0	0	0	0	0	0	0	0
10	0	0	0	0	0	0	0	0	*NC*	0	0
11	0	0	0	0	0	0	0	0	0	0	0
12	0	0	0	0	0	10	9	0	0	0	0
13	0	0	0	0	9	0	0	0	9	0	0
14	0	*NC*	0	0	0	0	0	0	0	0	18
15	0	0	0	0	0	0	0	0	0	0	*NC*
16	9	0	0	0	0	0	0	0	0	0	0

Table D.3 – Shows the difference in maximum comfortable load (kg) selected by each subject for each manoeuvre between load selection and sensor-displacement measurement. *NC* indicates not completed

D.1. **Data**

The results which follow provide, in conjunction with the Results Chapter, a full account of the data for all manoeuvres. Results not included for manoeuvre F (a.) in the Results Chapter are provided here. The results for the first two manoeuvres presented, manoeuvres [B, K] (a.), are given in two sections: first an overview of key points is given and secondly full details of material not covered in the first section are given. The remaining manoeuvres are given in a single section. Most of these results are repetitions but numerous subtleties and exceptions, of no substantial effect but worth noting, exist and these are detailed.

D.2. **Manoeuvre F (a.)**

D.2.1. *Manoeuvre F (a.)* P_u

Figure D.1 (page 284) shows occurrences of ${}^{-75th}_{ssi}P^{\mathrm{F}}_u \geq P_u > {}^{-90th}_{ssi}P^{\mathrm{F}}_u$ and of ${}^{+75th}_{ssi}P^{\mathrm{F}}_u \leq P_u < {}^{+90th}_{ssi}P^{\mathrm{F}}_u$ (both black markers) and, of $P_u \leq {}^{-90th}_{ssi}P^{\mathrm{F}}_u$ and of $P_u \geq {}^{+90th}_{ssi}P^{\mathrm{F}}_u$ (both red markers) (N/kg) against vehicle-frame orientation (θ_0): to aid inspection the measures for each subject are normalised against the subject's P_u peak magnitude for the start-steady period. A dashed vertical line indicates $\theta_0 = -0.084$ rad and this divides $\{{}_{ssi}\theta^{\mathrm{F}}_0\}$ into $\{{}_{ss1}\theta^{\mathrm{F}}_0\}$ and $\{{}_{ss2i}\theta^{\mathrm{F}}_0\}$ as previously defined.

It is evident from Figure D.1 that normalised ${}^{-90th}_{ssi}P^{\mathrm{F}}_u \approx -1$ occur for $\{{}_{ss2i}\theta^{\mathrm{F}}_0\}$ for some subjects[F]. It therefore follows that while Figure D.1 indicates the occurrences of P_u in both signs it is not possible to determine the comparative magnitudes of $P_u \geq {}^{+75th}_{ssi}P^{\mathrm{F}}_u$ and $P_u \leq {}^{-75th}_{ssi}P^{\mathrm{F}}_u$ for the initial period from this Figure (page 248). However, Figure D.2 (page 284) shows measures for ${}^{-90th}_{ss1}P^{\mathrm{F}}_u \geq P_u \geq {}^{+90th}_{ss1}P^{\mathrm{F}}_u$ (N/kg) for all subjects[F] with non-zero occurrences for $\{{}_{ss1}\theta^{\mathrm{F}}_0\}$: no display is shown for subjects with zero occurrences. Representative values for the largest $P_u > 0$ are obtained as follows. For each subject[F] with non-zero occurrences the measure for the minimum ${}^{+90th}_{ss1}P^{\mathrm{F}}_u$, denoted ${}^{+90th}_{ss1}P^{\mathrm{F}}_{umini}$, can be read and the minimum ${}^{+90th}_{ss1}P^{\mathrm{F}}_{umini}$ for all subjects[F], denoted ${}^{+90th}_{ss1}P^{\mathrm{F}}_{umin}$, is 0.06 N/kg (subject[9]). The maximum P_u for each subject[F], denoted ${}^{+90th}_{ss1}P^{\mathrm{F}}_{umaxi}$ can also be read and the maximum ${}^{+90th}_{ss1}P^{\mathrm{F}}_{umaxi}$, denoted ${}^{+90th}_{ss1}P^{\mathrm{F}}_{umax}$, is 0.73 N/kg (subject[11]). The mean ${}^{+90th}_{ss1}P^{\mathrm{F}}_{umaxi} \leq P_u \leq {}^{+90th}_{ss1}P^{\mathrm{F}}_{umaxi}$ for each subject[F] is

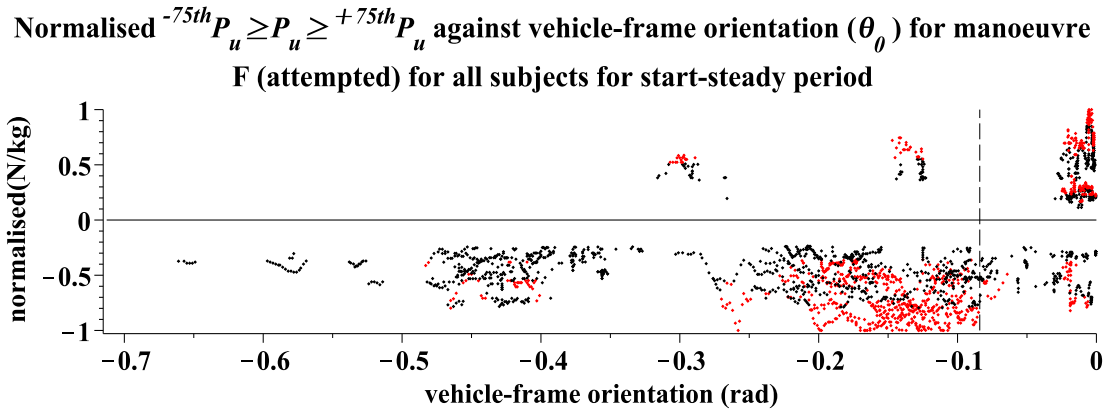

Figure D.1 – For the manoeuvre F (a.) occurrences of ${}^{-75th}_{ssi}P^{\mathrm{F}}_u \geq P_u > {}^{-90th}_{ssi}P^{\mathrm{F}}_u$ and of ${}^{+75th}_{ssi}P^{\mathrm{F}}_u \leq P_u < {}^{+90th}_{ssi}P^{\mathrm{F}}_u$ (both black markers) and, of $P_u \leq {}^{-90th}_{ssi}P^{\mathrm{F}}_u$ and of $P_u \geq {}^{+90th}_{ssi}P^{\mathrm{F}}_u$ (both red markers) in N/kg (normalised against each subject's maximum magnitude P_u for $\{{}_{ssi}\theta^{\mathrm{F}}_0\}$) against θ_0 for $\{{}_{ssi}\theta^{\mathrm{F}}_0\}$ for each subject: $\theta_0 = -0.084$ line indicated (dashed vertical)

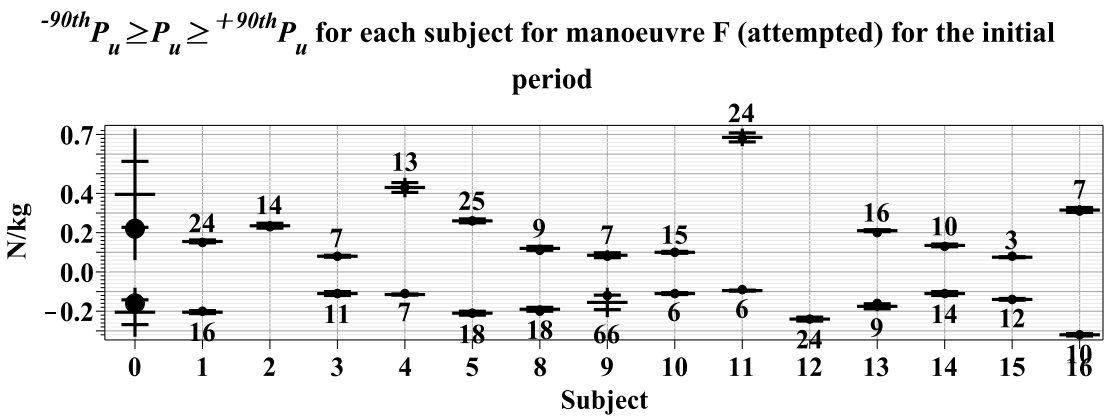

Figure D.2 – Shows for each of subjects[F] (i) for $\{{}_{ss1}\theta^{\mathrm{F}}_0\}$ in N/kg: separately for $P_u > 0$ and $P_u < 0$ for subjects with non-zero occurrences a vertical line indicating the minimum magnitude measure ${}^{\pm 90th}_{ss1}P^{\mathrm{F}}_{umini}$ to the maximum magnitude measure ${}^{\pm 90th}_{ss1}P^{\mathrm{F}}_{umaxi}$, a solid circle indicating the mean ${}^{+90th}_{ss1}P^{\mathrm{F}}_{umini} \leq P_uP \leq {}^{+90th}_{ss1}P^{\mathrm{F}}_{umaxi}$ or ${}^{-90th}_{ss1}P^{\mathrm{F}}_{umini} \geq P_uP \geq {}^{-90th}_{ss1}P^{\mathrm{F}}_{umaxi}$, the quarter divisions of the range (horizontal lines) and the number of occurrences of $P_u \geq {}^{\pm 90th}_{ss1}P^{\mathrm{F}}_u$ shown above the range line for $P_u > 0$ and below for $P_u < 0$. Subject[0] shows this data for all subjects[F] with a solid circle indicating the mean of all the mean ${}^{+90th}_{ss1}P^{\mathrm{F}}_{umini} \leq P_u \leq {}^{+90th}_{ss1}P^{\mathrm{F}}_{umaxi}$ or ${}^{-90th}_{ss1}P^{\mathrm{F}}_{umin} \geq P_uP \geq {}^{-90th}_{ss1}P^{\mathrm{F}}_{umax}$,

indicated by a solid circle but it can be seen that apart from subject[4] the ranges are of such small magnitude that the location of the mean is immaterial. Occurrences of $P_u \geq {}^{+90th}_{ss1}P^{\mathrm{F}}_u$ are shown above the range line for $P_u > 0$ for each subject. Subject[0] shows the range from ${}^{+90th}_{ss1}P^{\mathrm{F}}_{umin}$ to ${}^{+90th}_{ss1}P^{\mathrm{F}}_{umax}$ with the mean for all the mean ${}^{+90th}_{ss1}P^{\mathrm{F}}_{umini} \leq P_u \leq {}^{+90th}_{ss1}P^{\mathrm{F}}_{umaxi}$ located at the boundary of the first

and second quarter as indicated by a solid circle. It can also be seen from Figure D.2 (page 284) that the range magnitude of 0.67 N/kg, ${}^{+90th}_{ss1}P^{\mathrm{F}}_{umax} - {}^{+90th}_{ss1}P^{\mathrm{F}}_{umin}$, arises from inter-subject variation (subject[9] compared with subject[11]) and is not the result of the ${}^{+90th}_{ss1}P^{\mathrm{F}}_{umaxi} - {}^{+90th}_{ss1}P^{\mathrm{F}}_{umini}$ of a specific subject. There are therefore substantial differences between subjects for the largest $P_u > 0$. However, the inequality ${}^{+90th}_{ss1}P^{\mathrm{F}}_{umini} \leq P_u \leq {}^{+90th}_{ss1}P^{\mathrm{F}}_{umaxi}$ provides a representative range for each of subjects[1,..., 5, 8, 9, 10, 11, 13, 14, 15, 16]: subject[12] has no occurrences. Additionally the inequality ${}^{+90th}_{ss1}P^{\mathrm{F}}_{umin} \leq P_u \leq {}^{+90th}_{ss1}P^{\mathrm{F}}_{umax}$ (subject[0]) provides a representative range for all subjects[1,..., 5, 8, 9, 10, 11, 13, 14, 15, 16] for the largest $P_u > 0$ for $\{{}_{ssi}\theta^{\mathrm{F}}_0\}$.

Representative values for the largest magnitude $P_u < 0$ are also read from Figure D.2 (page 284). For each subject[F] with non-zero occurrences the measure for the minimum magnitude ${}^{-90th}_{ss1}P^{\mathrm{F}}_{u}$, denoted ${}^{-90th}_{ss1}P^{\mathrm{F}}_{umini}$ can be read and the minimum ${}^{-90th}_{ss1}P^{\mathrm{F}}_{umini}$ for all subjects[F] with non-zero occurrences, denoted ${}^{-90th}_{ss1}P^{\mathrm{F}}_{umin}$, is -0.08 N/kg (subject[9]). The maximum magnitude $P_u < 0$ for all subjects[F], denoted ${}^{-90th}_{ss1}P^{\mathrm{F}}_{umaxi}$ can also be read and the maximum ${}^{-90th}_{ss1}P^{\mathrm{F}}_{umaxi}$ denoted ${}^{-90th}_{ss1}P^{\mathrm{F}}_{umax}$ is -0.33 N/kg (subject[16]). The occurrences of $P_u \leq {}^{-90th}_{ss1}P^{\mathrm{F}}_{u}$ are shown below the range line. The mean ${}^{-90th}_{ss1}P^{\mathrm{F}}_{umini} \leq P_u \leq {}^{-90th}_{ss1}P^{\mathrm{F}}_{umaxi}$ for each subject[F] is indicated by a solid circle but it can be seen that the ranges (excluding subject[9]) are of such small magnitude that the location is immaterial. Subject[0] shows the range from ${}^{-90th}_{ss1}P^{\mathrm{F}}_{umin}$ to ${}^{-90th}_{ss1}P^{\mathrm{F}}_{umax}$ with the mean of all the mean ${}^{-90th}_{ss1}P^{\mathrm{F}}_{umini} \leq P_u \leq {}^{-90th}_{ss1}P^{\mathrm{F}}_{umaxi}$ indicated by a solid circle located at the first-second quarter boundary.

It can also be seen from Figure D.2 (page 284) that the range magnitude of 0.23 N/kg, ${}^{-90th}_{ss1}P^{\mathrm{F}}_{umax} - {}^{-90th}_{ss1}P^{\mathrm{F}}_{umin}$, arises from inter-subject variation (subject[9] compared with subject[16]) and is not the result of the ${}^{-90th}_{ss1}P^{\mathrm{F}}_{umaxi} - {}^{-90th}_{ss1}P^{\mathrm{F}}_{umini}$ of a specific subject. There are therefore differences between subjects for the largest magnitude $P_u < 0$. However, the inequality ${}^{-90th}_{ss1}P^{\mathrm{F}}_{umini} \geq P_u \geq {}^{-90th}_{ss1}P^{\mathrm{F}}_{umaxi}$ provides a representative range for each of subjects[1, 3, 4, 5, 8,..., 16]. Additionally the inequality ${}^{+90th}_{ss1}P^{\mathrm{F}}_{umin} \leq P_u \leq {}^{+90th}_{ss1}P^{\mathrm{F}}_{umax}$ (subject[0]) provides a representative range for all subjects[F] for the largest $P_u > 0$ for the initial period. Figure D.2 also confirms the representativeness of Figure 6.5 (page 146) for sub-

ject[10] in respect of P_u occurring in both signs for the majority of subjects: not subjects [2, 12].

D.2.2. *Manoeuvre F (a.) P_v*

Figure D.3 (page 287) shows occurrences of ${}^{-75th}_{ssi}P^{\mathrm{F}}_{v} \geq P_v > {}^{-90th}_{ssi}P^{\mathrm{F}}_{v}$ and of ${}^{+75th}_{ssi}P^{\mathrm{F}}_{v} \leq P_v < {}^{+90th}_{ssi}P^{\mathrm{F}}_{v}$ (both black markers) and, of $P_v \leq {}^{-90th}_{ssi}P^{\mathrm{F}}_{v}$ and of $P_v \geq {}^{+90th}_{ssi}P^{\mathrm{F}}_{v}$ (both red markers) against θ_0. To aid inspection the measures (N/kg) for each subject are normalised against the subject's P_v peak magnitude for $\{{}_{ssi}\theta^{\mathrm{F}}_{0}\}$. A dashed vertical line indicates $\theta_0 = -0.084$ rad and this divides the start-steady period into $\{{}_{ss1}\theta^{\mathrm{F}}_{0}\}$ and $\{{}_{ss2i}\theta^{\mathrm{F}}_{0}\}$ as previously defined. It is evident from Figure D.3 that compared with measures for $P_v < 0$, measures for $P_v > 0$ are of small magnitude and few occurrences. An examination of the data shows that for $\{{}_{ss1a}\theta^{\mathrm{F}}_{0}\}$ that there are no $P_v > 0$ and this confirms the representativeness of Figure 6.5 (page 146) for subject[10] in this respect.

Figure D.4 (page 287) shows measures for $P_v \leq {}^{-90th}_{ss1}P^{\mathrm{F}}_{v}$ (N/kg) for each subject [F] and for all subjects[F] (subject[0]). Representative values for the largest magnitude P_v are obtained as follows. For each subject[F] the measure for the minimum magnitude $P_v \leq {}^{-90th}_{ss1}P^{\mathrm{F}}_{v}$, denoted ${}^{-90th}_{ss1}P^{\mathrm{F}}_{vmini}$ may be read and the minimum ${}^{-90th}_{ss1}P^{\mathrm{F}}_{vmini}$ for all subjects[F], denoted ${}^{-90th}_{ss1}P^{\mathrm{F}}_{vmin}$, is -0.33 N/kg (subject[9]). The maximum magnitude P_v for each subject[F], denoted ${}^{-90th}_{ss1}P^{\mathrm{F}}_{vmaxi}$ may also be read and the maximum ${}^{-90th}_{ss1}P^{\mathrm{F}}_{vmaxi}$ denoted ${}^{-90th}_{ss1}P^{\mathrm{F}}_{vmax}$ is -0.76 N/kg (subject[16]). The mean ${}^{-90th}_{ss1}P^{\mathrm{F}}_{vmini} \geq P_v \geq {}^{-90th}_{ss1}P^{\mathrm{F}}_{vmaxi}$ for each subject[F] is indicated by a solid circle: it can be seen that these means are located from the second quarter to the approximate centre of the intra-subject range. Subject[0] shows the range of ${}^{-90th}_{ss1}P^{\mathrm{F}}_{vmin}$ to ${}^{-90th}_{ss1}P^{\mathrm{F}}_{vmax}$ and the mean of all the mean ${}^{-90th}_{ss1}P^{\mathrm{F}}_{vmini} \geq P_v \geq {}^{-90th}_{ss1}P^{\mathrm{F}}_{vmaxi}$ is indicated by a solid circle and this is located approximately centrally in the inter-subject range.

Occurrences of $P_v \leq {}^{-90th}_{ss1}P^{\mathrm{F}}_{v}$ are shown below the line range: these are approximately equal to $\frac{50}{10} \times t_i(\{{}_{ss1}\theta^{\mathrm{F}}_{0}\})$: occurrences are slightly different from Figure 6.7 (page 147) due to the disregard of small magnitude and early occurrences of $P_v \geq {}^{+90th}_{ss1}P^{\mathrm{F}}_{v}$.

It can also be seen from Figure D.4 (page 287) that the range magnitude of

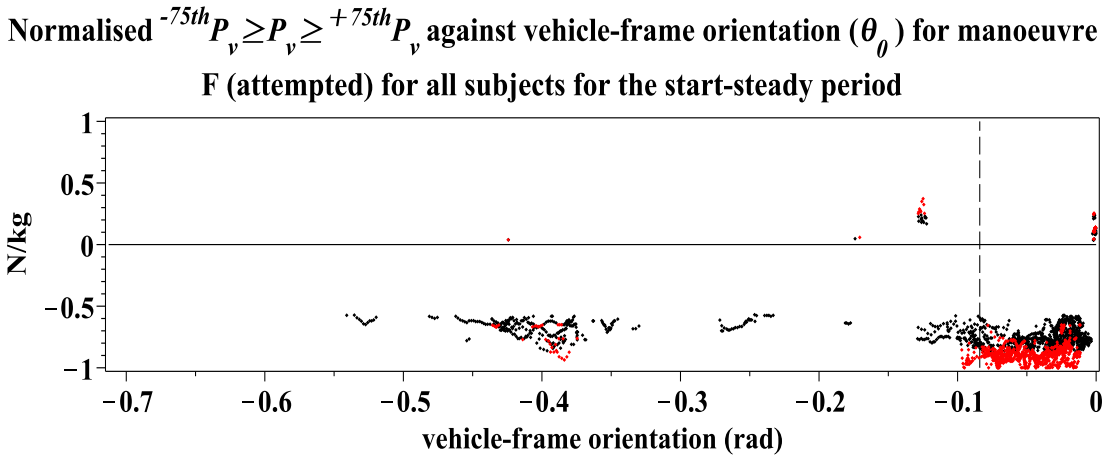

Figure D.3 – For the manoeuvre F (a.) occurrences of ${}^{-75th}_{ssi}P^{\mathrm{F}}_{v} \geq P_v > {}^{-90th}_{ssi}P^{\mathrm{F}}_{v}$ and of ${}^{+75th}_{ssi}P^{\mathrm{F}}_{v} \leq P_v < {}^{+90th}_{ssi}P^{\mathrm{F}}_{v}$ (both black markers) and, of $P_v \leq {}^{-90th}_{ssi}P^{\mathrm{F}}_{v}$ and of $P_v \geq {}^{+90th}_{ssi}P^{\mathrm{F}}_{v}$ (both red markers) in N/kg (normalised against each subject's maximum magnitude P_v for the start-steady period) against θ_0 for $\{{}_{ssi}\theta^{\mathrm{F}}_0\}$ for each subject: $\theta_0 = -0.084$ line indicated (dashed vertical).

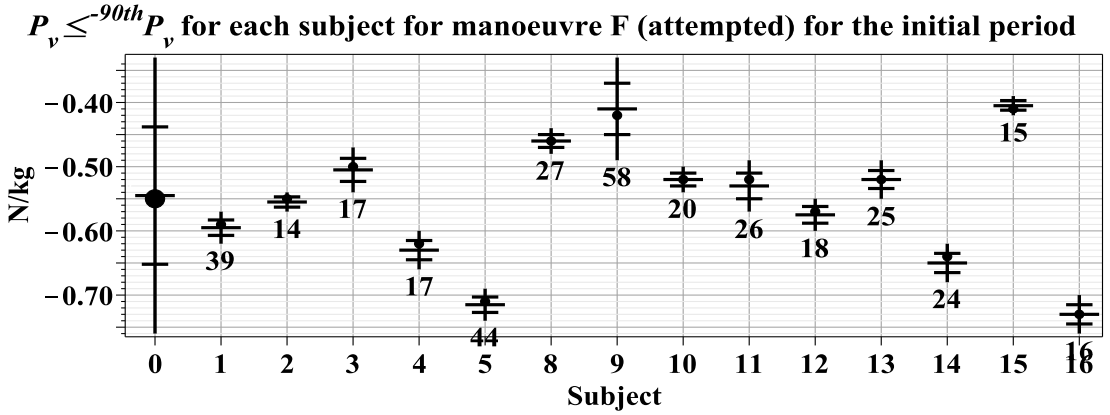

Figure D.4 – Shows for each of subjects[F] (i) for $\{{}_{ss1}\theta^{\mathrm{F}}_0\}$ in N/kg: a vertical line indicating the minimum measure magnitude ${}^{-90th}_{ss1}P^{\mathrm{F}}_{vmini}$ to the maximum measure magnitude ${}^{-90th}_{ss1}P^{\mathrm{F}}_{vmaxi}$, a solid circle indicating the mean ${}^{-90th}_{ss1}P^{\mathrm{F}}_{vmaxi} \geq P_v \geq {}^{-90th}_{ss1}P^{\mathrm{F}}_{vmaxi}$, the quarter divisions of the range (horizontal lines) and the number of occurrences of $P_v \leq {}^{-90th}_{ss1}P^{\mathrm{F}}_{v}$. Subject[0] shows this data for all subjects[F] with a solid circle indicating the mean of all the mean ${}^{-90th}_{ss1}P^{\mathrm{F}}_{vmaxi} \geq P_v \geq {}^{-90th}_{ss1}P^{\mathrm{F}}_{vmaxi}$.

0.43 N/kg, ${}^{-90th}_{ss1}P^{\mathrm{F}}_{vmax} - {}^{-90th}_{ss1}P^{\mathrm{F}}_{vmin}$, arises from inter-subject variation (subject[9] compared with subject[16]) and is not the result of the ${}^{-90th}_{ss1}P^{\mathrm{F}}_{vmaxi} - {}^{-90th}_{ss1}P^{\mathrm{F}}_{vmini}$ magnitude of a specific subject. There are therefore substantial differences between subjects for the largest magnitude $P_v < 0$. However, the inequality ${}^{-90th}_{ss1}P^{\mathrm{F}}_{vmini} \geq P_v \geq {}^{-90th}_{ss1}P^{\mathrm{F}}_{vmaxi}$ provides a representative range for each subject[F]. Additionally the inequality ${}^{-90th}_{ss1}P^{\mathrm{F}}_{vmin} \geq P_v \geq {}^{-90th}_{ss1}P^{\mathrm{F}}_{vmax}$ provides a representative range for all

subjects[F].

D.3. **Manoeuvre B (attempted)**

This section presents the results for handle-force measures (P_u, P_v and P_{uCs}) for manoeuvre B (a.) for the start-steady period. In this subsection 'all subjects[B]' or a trailing super or sub script B in a symbol indicates measures from subjects [1,...,13, 15, 16]: subject[14] did not participate (see Section 6.2).

D.3.1. *Manoeuvre B (a.) handle-force measures*

Examination of the handle-force measures will show that dividing $\{_{ssi}\theta_0^{\mathrm{B}}\}$ at $\theta_0 = -0.085$ rad is useful and hence θ_0 measures for manoeuvre B (a.) are defined for the initial period $-0.085 < \theta_0 < 0$ rad, denoted $\{_{ss1}\theta_0^{\mathrm{B}}\}$ and for the later period $\theta_{0steadi} < \theta_0 < -0.085$ rad, denoted $\{_{ss2i}\theta_0^{\mathrm{B}}\}$. There is some variation between subjects immediately after motion start for a small θ_0 displacement: magnitude no greater than 0.01 rad. The range $-0.085 < \theta_0 < -0.01$ rad is denoted $\{_{ss1a}\theta_0^{\mathrm{B}}\}$ ($\{_{ss1}\theta_0^{\mathrm{B}}\}$ modified to commence at $\theta_0 = -0.01$ rad rather than motion-start). Figure D.6 (page 289) illustrates the handle-force measures for one subject[4] three features of which are common to all subjects[B] for the modified initial period $\{_{ss1a}\theta_0^{\mathrm{B}}\}$. Firstly, the largest magnitudes of P_{uCs} are negatively signed. Secondly, the largest magnitudes of P_u are positively signed. Thirdly, P_v measures are of both signs.

D.3.2. *Manoeuvre B (a.) P_u*

The presentation begins with P_u. Figure D.7 (page 290) shows occurrences of ${}^{-75th}_{ssi}P_u^{\mathrm{B}} \geq P_u > {}^{-90th}_{ssi}P_u^{\mathrm{B}}$ and of ${}^{+75th}_{ssi}P_u^{\mathrm{B}} \leq P_u < {}^{+90th}_{ssi}P_u^{\mathrm{B}}$ (both black markers) and, of $P_u \leq {}^{-90th}_{ssi}P_u^{\mathrm{B}}$ and of $P_u \geq {}^{+90th}_{ssi}P_u^{\mathrm{B}}$ (both red markers): to assist inspection the measures for each subject are normalised against the subject's P_u peak magnitude for $\{_{ssi}\theta_0^{\mathrm{B}}\}$. A dashed vertical line indicates $\theta_0 = -0.085$ rad and this divides $\{_{ssi}\theta_0^{\mathrm{B}}\}$ into $\{_{ss1}\theta_0^{\mathrm{B}}\}$ and $\{_{ss2i}\theta_0^{\mathrm{B}}\}$ as previously defined.

It is evident from Figure D.7 that compared with $P_u > 0$ the magnitudes of $P_u < 0$ are negligible, which confirms the representativeness of Figure D.5 (page 289) in this respect. Two further observations are made. Firstly, it is evident that for the initial period the accumulated occurrences of $P_u \geq {}^{+75th}_{ssi}P_u^{\mathrm{B}}$

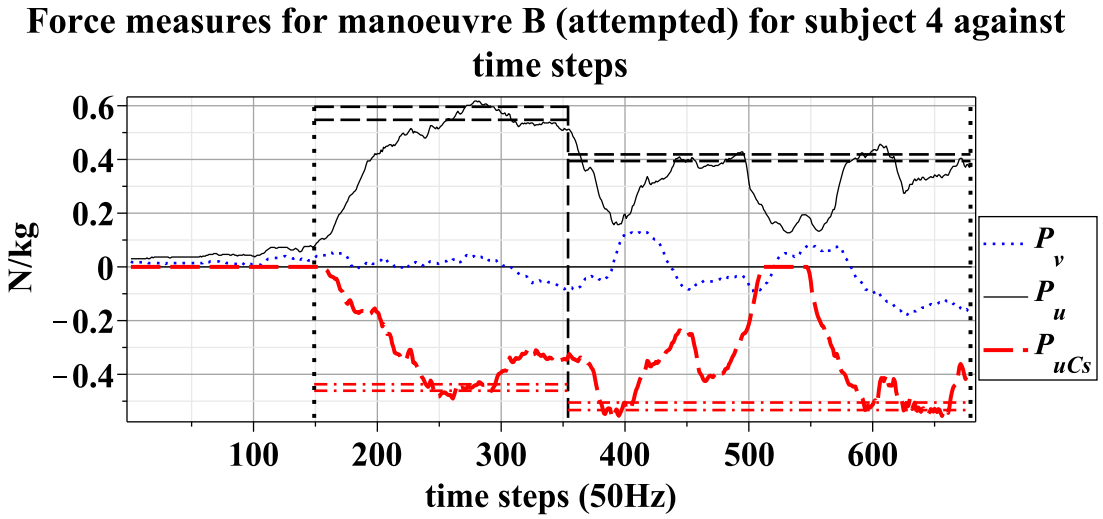

Figure D.5 – For subject[4] for manoeuvre B (a.), measures: P_v (dotted blue), P_u (thin black) and P_{uCs} (thick red dashed) in N/kg plotted against time-steps (approximately 0.02 seconds) with motion-start line (vertical black dotted: closest to left side), steady-start line (vertical black dotted:closest to right side) and $\theta_0 = -0.085$ rad line (vertical black dashed). The following percentile lines are shown for $\{{}_{ss1}\theta_0^{\mathrm{B}}\}$: ${}^{+90th}_{ss1}P_u^{\mathrm{B}}$ and ${}^{+75th}_{ss1}P_u^{\mathrm{B}}$ (horizontal black dash), ${}^{-90th}_{ss1}P_{uCs}^{\mathrm{B}}$ and ${}^{-75th}_{ss1}P_{uCs}^{\mathrm{B}}$ (horizontal red dash-dot): these percentile lines are also shown for $\{{}_{ss2i}\theta_0^{\mathrm{B}}\}$.

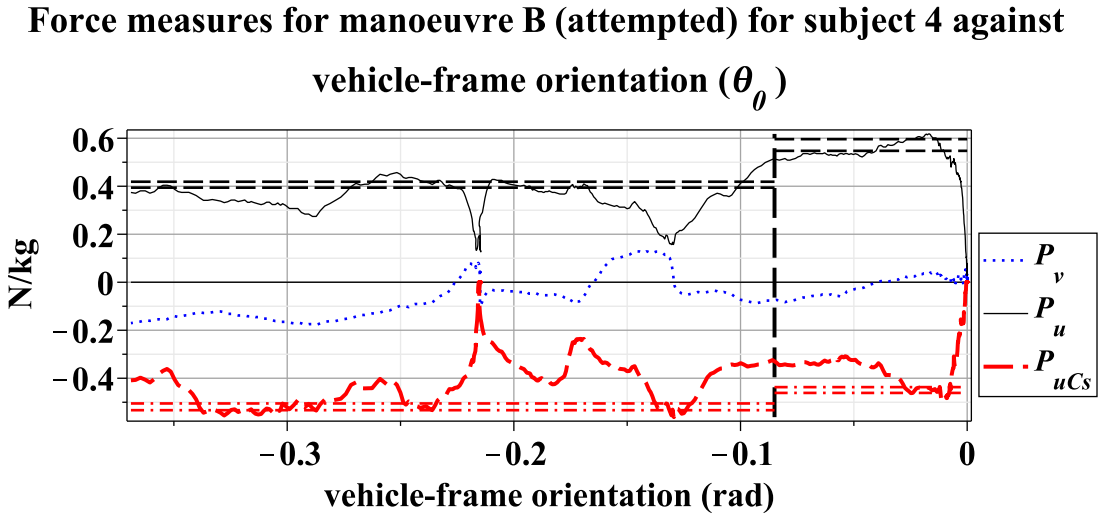

Figure D.6 – Shows for subject[4] for manoeuvre B (a.), measures plotted against θ_0 with other details as above.

from all subjects[B] are contiguous. Secondly, the contiguity of $P_u \geq {}^{+90th}_{ssi}P_u^{\mathrm{B}}$ (red markers are printed on top of black markers) terminates close to $\theta_0 = -0.085$ rad. While it is evident from $\theta_0 < -0.085$ rad that not all peak $P_u > 0$ occur in the initial period examination of the data (results not presented) shows that all subjects[B] contribute to the contiguity. Thus for all subjects[B], despite any variations, the mechanism is so configured that all subjects have occurrences of $P_u \geq {}^{+90th}_{ssi}P_u^{\mathrm{B}}$ by $\theta_0 = -0.085$ rad and subsequent to this, occurrences of $P_u \geq {}^{+75th}_{ssi}P_u^{\mathrm{B}}$ become

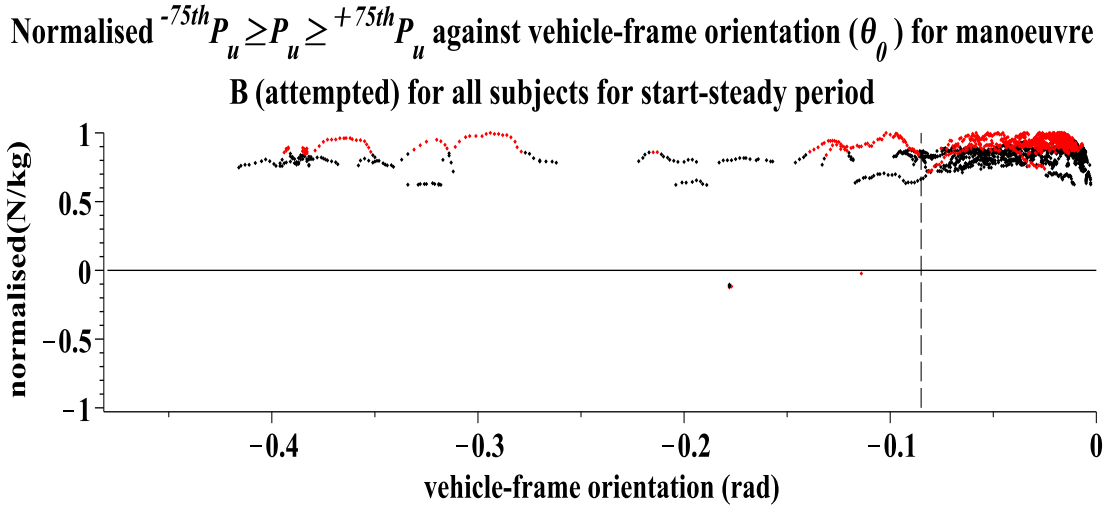

Figure D.7 – Occurrences of ${}^{-75th}_{ssi}P^{\mathrm{B}}_u \geq P_u > {}^{-90th}_{ssi}P^{\mathrm{B}}_u$ and of ${}^{+75th}_{ssi}P^{\mathrm{B}}_u \leq P_u < {}^{+90th}_{ssi}P^{\mathrm{B}}_u$ (both black markers) and, of $P_u < {}^{-90th}_{ssi}P^{\mathrm{B}}_u$ and of $P_u > {}^{+90th}_{ssi}P^{\mathrm{B}}_u$ (both red markers) in N/kg and normalised against each subject's maximum magnitude P_u against vehicle-frame displacement for $\{{}_{ssi}\theta^{\mathrm{B}}_0\}$ for all subjects[B] with $\theta_0 = -0.085$ indicated (dashed vertical) for manoeuvre B (a.)

relatively few compared with the initial period. Thus division of $\{{}_{ssi}\theta^{\mathrm{B}}_0\}$ at this location relates to a mechanical property of the system for manoeuvre B (a.).

D.3.3. *Manoeuvre B (a.) P_{uCs} and P_v*

The process used to produce Figure D.7 (page 290) for P_u is repeated for P_{uCs} and P_v as described for manoeuvre F (a.) in Sections 6.4.2 (page 145) and D.2.2 (page 286) respectively and the resulting graphs are shown in Figures D.8 and D.9 (page 291) respectively. It can be seen from Figure D.8 that $P_{uCs} \leq {}^{-75th}_{ssi}P^{\mathrm{B}}_{uCs}$ continue throughout $\{{}_{ssi}\theta^{\mathrm{B}}_0\}$ though a local trough is apparent at ${}_{ss1}\theta^{\mathrm{B}}_0$. Figure D.9 shows that occurrences of ${}^{-75th}_{ssi}P^{\mathrm{B}}_v \geq P_v > {}^{-90th}_{ssi}P^{\mathrm{B}}_v$ and of ${}^{+75th}_{ssi}P^{\mathrm{B}}_v \leq P_v < {}^{+90th}_{ssi}P^{\mathrm{B}}_v$ occur at many θ_0 during $\{{}_{ssi}\theta^{\mathrm{B}}_0\}$. A detailed account of the measures not considered in detail here follows in the next section.

D.3.4. *Manoeuvre B (a.) the $P_v - P_{uCs}$ plane*

This final section relating to manoeuvre B (a.) uses the inequalities, as previously defined, to define a cuboid boundary for the largest magnitude measures for each and all subjects: this follows the same process as was described for manoeuvre F (a.), though in this case it is P_v and not P_u which occurs in both signs. Taking account of subjects with measures with one sign and two signs of P_v two sets of

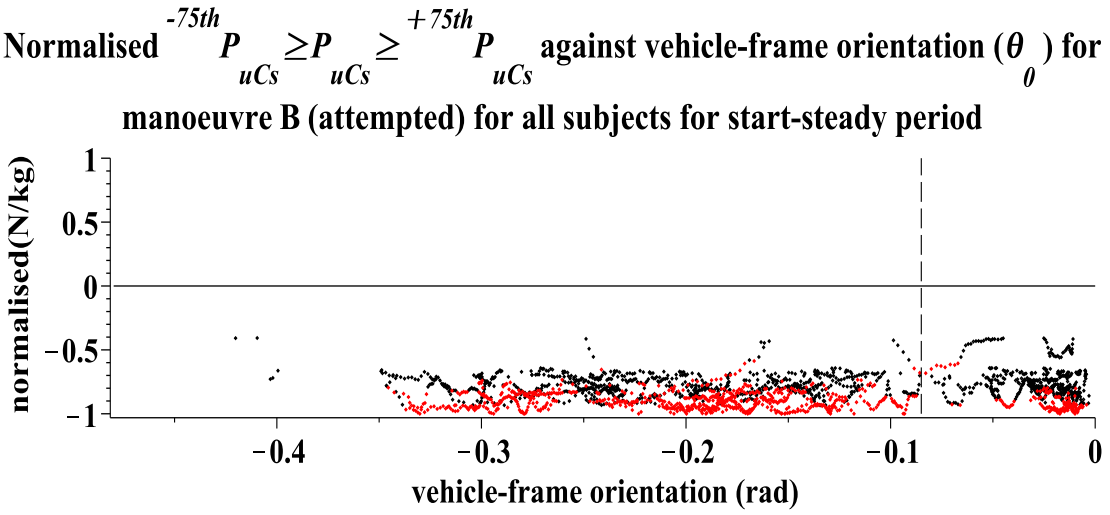

Figure D.8 – Occurrences of ${}^{-75th}_{ssi}P^{\mathrm{B}}_{uCs} \geq P_{uCs} > {}^{-90th}_{ssi}P^{\mathrm{B}}_{uCs}$ and of ${}^{+75th}_{ssi}P^{\mathrm{B}}_{uCs} \geq P_{uCs} \geq {}^{+90th}_{ssi}P^{\mathrm{B}}_{uCs}$ (both black markers) and, $P_{uCs} \leq {}^{-90th}_{ssi}P^{\mathrm{B}}_{uCs}$ and $P_{uCs} > {}^{+90th}_{ssi}P^{\mathrm{B}}_{uCs}$ (red markers) in N/kg and normalised against each subject's maximum magnitude P_{uCs} against θ_0 for $\{{}_{ssi}\theta^{\mathrm{B}}_0\}$ for all subjects[B] with $\theta_0 = -0.085$ indicated (dashed vertical)

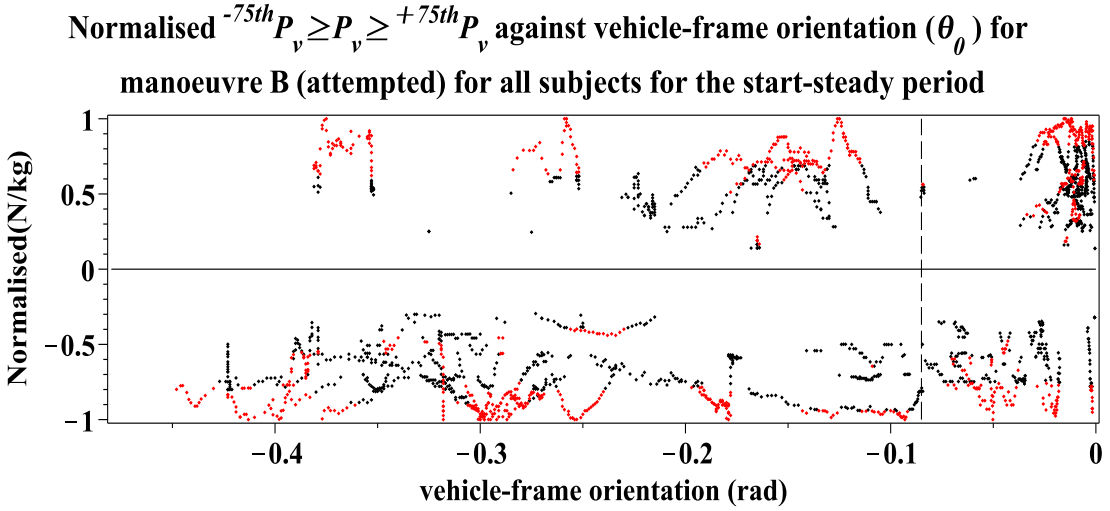

Figure D.9 – Occurrences of ${}^{-75th}_{ssi}P^{\mathrm{B}}_{v} \geq P_{v} > {}^{-90th}_{ssi}P^{\mathrm{B}}_{v}$ and of ${}^{+75th}_{ssi}P^{\mathrm{B}}_{v} \leq P_{v} < {}^{+90th}_{ssi}P^{\mathrm{B}}_{v}$ (both black markers) and, of $P_{v} \leq {}^{-90th}_{ssi}P^{\mathrm{B}}_{v}$ and of $P_{v} \geq {}^{+90th}_{ssi}P^{\mathrm{B}}_{v}$ (both red markers) in N/kg against vehicle-frame displacement for $\{{}_{ssi}\theta^{\mathrm{B}}_0\}$ for all subjects[B]

three inequalities are defined as follows. For the first set of three inequalities for each of subjects[1,..., 5, 7,..., 13, 15, 16] the inequalities are:

${}^{+90th}_{ss1}P^{\mathrm{B}}_{umini} \leq P_u \leq {}^{+90th}_{ss1}P^{\mathrm{B}}_{umaxi}$, (page 293)

${}^{-90th}_{ss1}P^{\mathrm{B}}_{uCsmini} \geq P_{uCs} \geq {}^{-90th}_{ss1}P^{\mathrm{B}}_{uCsmaxi}$ (page 294) and

${}^{+90th}_{ss1}P^{\mathrm{B}}_{vmini} \leq P_v \leq {}^{+90th}_{ss1}P^{\mathrm{B}}_{vmaxi}$ (page 296) .

For the second three inequalities for each of subjects[1,..., 13, 16] the in-

equalities are as given for P_{uCs} and P_u above and

$${}^{-90th}_{ss1}P^{\mathrm{B}}_{vmini} \geq P_v \geq {}^{-90th}_{ss1}P^{\mathrm{B}}_{vmaxi}$$ (page 293).

These two sets of three inequalities define one cuboid boundary for each of subjects[6, 15] and two cuboid boundaries for each of subjects[1,..., 5, 7,..., 13, 16] as the latter have P_v measures in both signs. These one set or two sets of three inequalities are denoted ${}^{large}_{ss1}\mathbf{P}^{\mathrm{B}}_i$ where i indicates the subject index.

A graphical representation of ${}^{large}_{ss1}\mathbf{P}^{\mathrm{B}}_i$ in the $P_v - P_{uCs}$ plane is shown in Figure D.10 (page 293): the construction follows the same process as described in Section 6.4.4 (page 149) for manoeuvre F (a.).

Two sets of inequalities define the cuboid boundaries which enclose the measures for all, rather than each of, subjects[B] and this is achieved by removal of the i subscript from the above definitions as follows. For the first set of three inequalities for all of subjects[1,..., 5, 7,..., 13, 15, 16] the inequalities are:

$${}^{-90th}_{ss1}P^{\mathrm{B}}_{uCsmin} \geq P_{uCs} \geq {}^{-90th}_{ss1}P^{\mathrm{B}}_{uCsmax},$$

$${}^{+90th}_{ss1}P^{\mathrm{B}}_{vmin} \leq P_v \leq {}^{+90th}_{ss1}P^{\mathrm{B}}_{vmax}$$ and

$${}^{+90th}_{ss1}P^{\mathrm{B}}_{umin} \leq P_u \leq {}^{+90th}_{ss1}P^{\mathrm{B}}_{umax}.$$

For the second set of three inequalities for all of subjects[1,..., 13, 16] the inequalities are as given for P_{uCs} and P_u above and

$${}^{-90th}_{ss1}P^{\mathrm{B}}_{vmin} \geq P_v \geq {}^{-90th}_{ss1}P^{\mathrm{B}}_{vmax}.$$

These two sets of three inequalities relating to all subjects[B] are denoted ${}^{large}_{ss1}\mathbf{P}^{\mathrm{B}}$. The numerical values for ${}^{large}_{ss1}\mathbf{P}^{\mathrm{B}}$ are therefore (pages 296, 293, 294 and 293 respectively) are:

$0.04 \leq P_v \leq 0.35$ (N/kg),

$-0.05 \geq P_v \geq -0.22$ (N/kg),

$-0.27 \geq P_{uCs} \geq -0.77$ (N/kg) and

$0.37 \leq P_u \leq 0.63$ (N/kg).

In conclusion ${}^{large}_{ss1}\mathbf{P}^{\mathrm{B}}$ provides a useful representation of the boundaries of the largest handle-forces for all subjects[B] for manoeuvre B (a.).

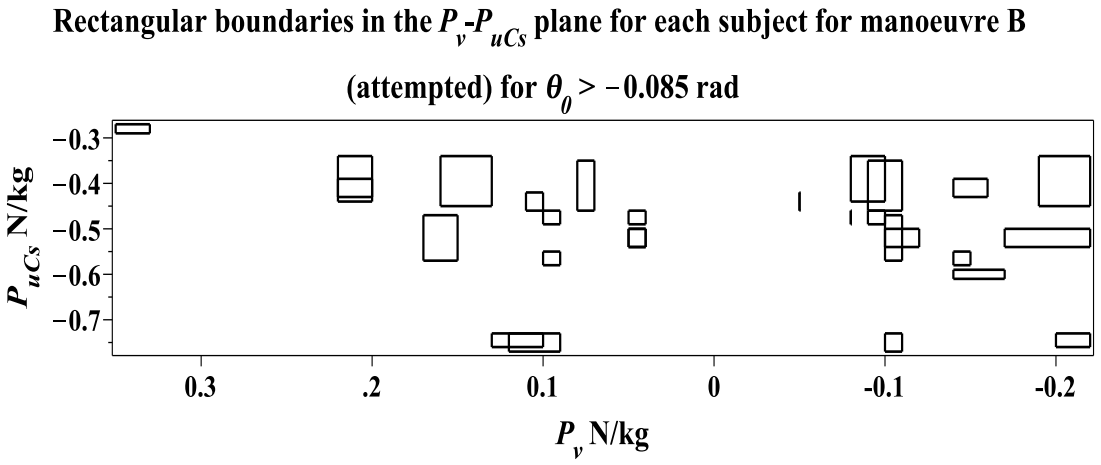

Figure D.10 – Shows relating to $P_v > 0$ for each subject[1,..., 5, 7,..., 13, 15, 16] the four vertices of a rectangle are formed with a $[P_v, P_{uCs}]$ coordinate as follows: $[{}^{+90th}_{ss1}P^{\mathrm{B}}_{vmaxi}, {}^{-90th}_{ss1}P^{\mathrm{B}}_{uCsmini}]$, $[{}^{+90th}_{ss1}P^{\mathrm{B}}_{vmini}, {}^{-90th}_{ss1}P^{\mathrm{B}}_{uCsmini}]$, $[{}^{+90th}_{ss1}P^{\mathrm{B}}_{vmini}, {}^{-90th}_{ss1}P^{\mathrm{B}}_{uCsmaxi},]$, and $[{}^{+90th}_{ss1}P^{\mathrm{B}}_{vmaxi}, {}^{-90th}_{ss1}P^{\mathrm{B}}_{uCsmaxi}]$. It is to be noted that subjects[11,13] occupy the same area on the plane so the graphic display shows 13 and not 14 rectangles: n=14. Relating to $P_v < 0$ for each subject[1,..., 13, 16] the four vertices of a rectangle are formed with a $[P_v, P_{uCs}]$ coordinate as follows: $[{}^{-90th}_{ss1}P^{\mathrm{B}}_{vmini}, {}^{-90th}_{ss1}P^{\mathrm{B}}_{uCsmini}]$, $[{}^{-90th}_{ss1}P^{\mathrm{B}}_{vmaxi}, {}^{-90th}_{ss1}P^{\mathrm{B}}_{uCsmini}]$, $[{}^{-90th}_{ss1}P^{\mathrm{B}}_{vmaxi}, {}^{-90th}_{ss1}P^{\mathrm{B}}_{uCsmaxi},]$, and $[{}^{-90th}_{ss1}P^{\mathrm{B}}_{vmini}, {}^{-90th}_{ss1}P^{\mathrm{B}}_{uCsmaxi}]$: n=14.

D.4. **Manoeuvre B (attempted) Details**

D.4.1. *Manoeuvre B (attempted)* P_u

Figure D.11 (page 294) shows measures for $P_u \geq {}^{+90th}_{ss1}P^{\mathrm{B}}_{u}$ (N/kg) for all subjects[B] for $\{{}_{ss1}\theta^{\mathrm{B}}_0\}$. Representative values for the largest $P_u > 0$ are obtained as follows. For each subject[B] the measure for the minimum ${}^{+90th}_{ss1}P^{\mathrm{B}}_{u}$, denoted ${}^{+90th}_{ss1}P^{\mathrm{B}}_{umini}$ can be read and the minimum ${}^{+90th}_{ss1}P^{\mathrm{B}}_{umini}$ for all subjects[B], denoted ${}^{+90th}_{ss1}P^{\mathrm{B}}_{umin}$, is 0.37 N/kg (subject[16]). The maximum P_u for each subject[B], denoted ${}^{+90th}_{ss1}P^{\mathrm{B}}_{umaxi}$ can also be read and the maximum ${}^{+90th}_{ss1}P^{\mathrm{B}}_{umaxi}$ denoted ${}^{+90th}_{ss1}P^{\mathrm{B}}_{umax}$ is 0.63 N/kg (subjects[1, 11]). The mean ${}^{+90th}_{ss1}P^{\mathrm{B}}_{umini} \leq P_u \leq {}^{+90th}_{ss1}P^{\mathrm{B}}_{umaxi}$ for each subject[B] is indicated by a solid circle and it can be seen , where the range magnitude is not too small, that these are located from first to the third quarter. Subject[0] shows the range from ${}^{+90th}_{ss1}P^{\mathrm{B}}_{umin}$ to ${}^{+90th}_{ss1}P^{\mathrm{B}}_{umax}$ with the mean for all the mean ${}^{+90th}_{ss1}P^{\mathrm{B}}_{umini} \leq P_u \leq {}^{+90th}_{ss1}P^{\mathrm{B}}_{umaxi}$ located in the third quarter as indicated by a solid circle.

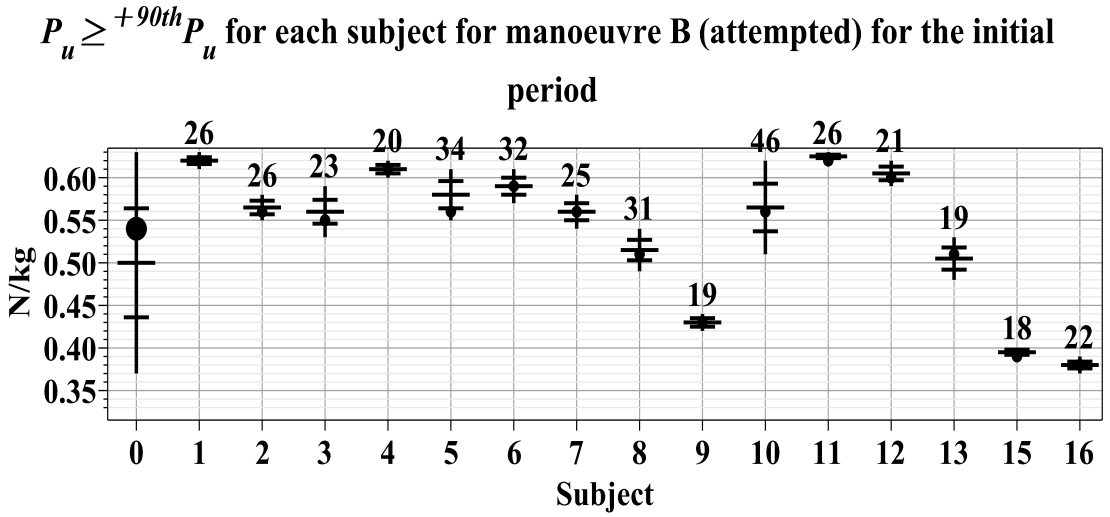

Figure D.11 – Shows for each subject[B] (i) for $\{{}_{ss1}\theta_0^{\mathrm{B}}\}$ in N/kg: a vertical line indicating the minimum magnitude measure ${}^{+90th}_{ss1}P^{\mathrm{B}}_{umini}$ to the maximum magnitude measure ${}^{+90th}_{ss1}P^{\mathrm{B}}_{umaxi}$, a solid circle indicating the mean ${}^{+90th}_{ss1}P^{\mathrm{B}}_{umini} \leq P_u \leq {}^{+90th}_{ss1}P^{\mathrm{B}}_{umaxi}$, the quarter divisions of the range (horizontal lines) and the number of occurrences of $P_u \geq {}^{+90th}_{ss1}P^{\mathrm{B}}_{u}$ shown above the range line. Subject[0] shows these measures with a solid circle indicating the mean of all the mean ${}^{+90th}_{ss1}P^{\mathrm{B}}_{umini} \leq P_u \leq {}^{+90th}_{ss1}P^{\mathrm{B}}_{umaxi}$.

For each subject occurrences of $P_u \geq {}^{+90th}_{ss1}P^{\mathrm{B}}_{u}$ are shown above the range line in Figure D.11: these are approximately equal to $\frac{50}{10} \times t_i(\{{}_{ss1}\theta_0^{\mathrm{B}}\})$. This supports the claim made in respect of Figure D.7 (page 290) that all subjects[B] contribute to the contiguous cluster of $P_u \geq {}^{+90th}_{ssi}P^{\mathrm{B}}_{u}$ in $\{{}_{ss1}\theta_0^{\mathrm{B}}\}$: since ${}^{+90th}_{ss1}P^{\mathrm{B}}_{u}$, as used for Figure D.11, will have a larger value than ${}^{+90th}_{ssi}P^{\mathrm{B}}_{u}$, as used in Figure D.7.

It can also be seen from Figure D.11 (page 294) that the range magnitude of 0.26 N/kg i.e. ${}^{+90th}_{ss1}P^{\mathrm{B}}_{umax} - {}^{+90th}_{ss1}P^{\mathrm{B}}_{umin}$ arises from inter-subject variation (subjects[16] compared with subjects[1, 11]) and is not the result of the ${}^{+90th}_{ss1}P^{\mathrm{B}}_{umaxi} - {}^{+90th}_{ss1}P^{\mathrm{B}}_{umini}$ of a specific subject. While there are differences between subjects for the largest $P_u > {}^{+90th}_{ss1}P^{\mathrm{B}}_{u}$ the intra-subject range magnitude is relatively small. The inequality ${}^{+90th}_{ss1}P^{\mathrm{B}}_{umini} \leq P_u \leq {}^{+90th}_{ss1}P^{\mathrm{B}}_{umaxi}$ provides a representative range for each subject[B]. Additionally the inequality ${}^{+90th}_{ss1}P^{\mathrm{B}}_{umin} \leq P_u \leq {}^{+90th}_{ss1}P^{\mathrm{B}}_{umax}$ (subject[0]) provides a representative range for all subjects[B] for the largest $P_u > 0$ for $\{{}_{ss1}\theta_0^{\mathrm{B}}\}$.

D.4.2. *Manoeuvre B (attempted) P_{uCs}*

Figure D.8 (page 291) shows occurrences for ${}^{-75th}_{ssi}P^{\mathrm{B}}_{uCs} \geq P_{uCs} > {}^{-90th}_{ssi}P^{\mathrm{B}}_{uCs}$ and for ${}^{+75th}_{ssi}P^{\mathrm{B}}_{uCs} \leq P_{uCs} < {}^{+90th}_{ssi}P^{\mathrm{B}}_{uCs}$ (both black markers), and for $P_{uCs} \leq$

${}^{-90th}_{ssi}P^{\mathrm{B}}_{uCs}$ and for $P_{uCs} \geq {}^{+90th}_{ssi}P^{\mathrm{B}}_{uCs}$ (both red markers) (N/kg) against θ_0 for all subjects[B]: to assist inspection the measures for each subject are normalised against the subject's P_{uCs} peak magnitude for $\{{}_{ssi}\theta^{\mathrm{B}}_0\}$. A dashed vertical line indicates $\theta_0 = -0.085$ rad and this divides $\{{}_{ssi}\theta^{\mathrm{B}}_0\}$ into $\{{}_{ss}\theta^{\mathrm{B}}_0\}$ and $\{{}_{ss2i}\theta^{\mathrm{B}}_0\}$ as previously defined.

There are no occurrences of $P_{uCs} \geq {}^{+75th}_{ssi}P^{\mathrm{B}}_{uCs}$ and therefore no occurrences of $P_{uCs} > 0$ and this confirms the representativeness of Figure D.6 (page 289) in this respect. It also evident that there are few $P_{uCs} < {}^{-75th}_{ssi}P^{\mathrm{B}}_{uCs}$ occurring close to $\theta_0 = -0.085$ rad compared with other orientations so this orientation is one at which there is the greatest coincidence of P_{uCs} not reaching ${}^{-75th}_{ssi}P^{\mathrm{B}}_{uCs}$ magnitude for all subjects[B], there is a local trough, and this lends support to the choice of this location to divide $\{{}_{ssi}\theta^{\mathrm{B}}_0\}$ as presented in Sections D.3.3 (Page 290). It is also to be noted that peak magnitudes of P_{uCs} continue in the later period.

Figure D.12 (page 296) shows measures for $P_{uCs} \leq {}^{-90th}_{ss1}P^{\mathrm{B}}_{uCs}$ (N/kg) for all subjects[B] for $\{{}_{ss1}\theta^{\mathrm{B}}_0\}$. Representative values for the largest magnitude P_{uCs} are obtained as follows. For each subject[B] the measure for the minimum magnitude $P_{uCs} \leq {}^{-90th}_{ss1}P^{\mathrm{B}}_{uCs}$, denoted ${}^{-90th}_{ss1}P^{\mathrm{B}}_{uCsmini}$ may be read and the minimum magnitude ${}^{-90th}_{ss1}P^{\mathrm{B}}_{uCsmini}$ for all subjects[B], denoted ${}^{-90th}_{ss1}P^{\mathrm{B}}_{uCsmin}$, is -0.27 N/kg (subject[15]). The maximum magnitude P_{uCs} for each subject[B], denoted ${}^{-90th}_{ss1}P^{\mathrm{B}}_{uCsmaxi}$ may also be read and the maximum magnitude ${}^{-90th}_{ss1}P^{\mathrm{B}}_{uCsmaxi}$ denoted ${}^{-90th}_{ss1}P^{\mathrm{B}}_{uCsmax}$ is -0.77 N/kg (subject[10]). The mean ${}^{-90th}_{ss1}P^{\mathrm{B}}_{uCsmini} \geq P_{uCs} \geq {}^{-90th}_{ss1}P^{\mathrm{B}}_{uCsmaxi}$ for each subject[B] are indicated by a solid circle and it can be seen that these means, ignoring subjects where the range magnitude is relatively small, are located in the second to third quarters of the intra-subject range. Subject[0] shows the range of ${}^{-90th}_{ss1}P^{\mathrm{B}}_{uCsmin}$ to ${}^{-90th}_{ss1}P^{\mathrm{B}}_{uCsmax}$ and the mean of all the mean ${}^{-90th}_{ss1}P^{\mathrm{B}}_{uCsmini} \geq P_{uCs} \geq {}^{-90th}_{ss1}P^{\mathrm{B}}_{uCsmaxi}$ indicated by a solid circle can be seen to be located approximately centrally in the inter-subject ranges.

For each subject occurrences of $P_{uCs} \leq {}^{-90th}_{ss1}P^{\mathrm{B}}_{uCs}$ are shown in Figure D.12. It has already been established that there are no $P_{uCs} > 0$ and an examination of the data shows that all occurrence of $P_{uCs} = 0$ (integer) are confined to $\theta_0 > -0.01$ rad and these are relatively few ([0, 0, 42, 8, 43, 2, 0, 0, 0, 56, 0, 16, 0, 0, 0] for subjects[1, ..., 16] respectively) so the occurrences of $P_{uCs} \leq {}^{-90th}_{ss1}P^{\mathrm{B}}_{v}$ are

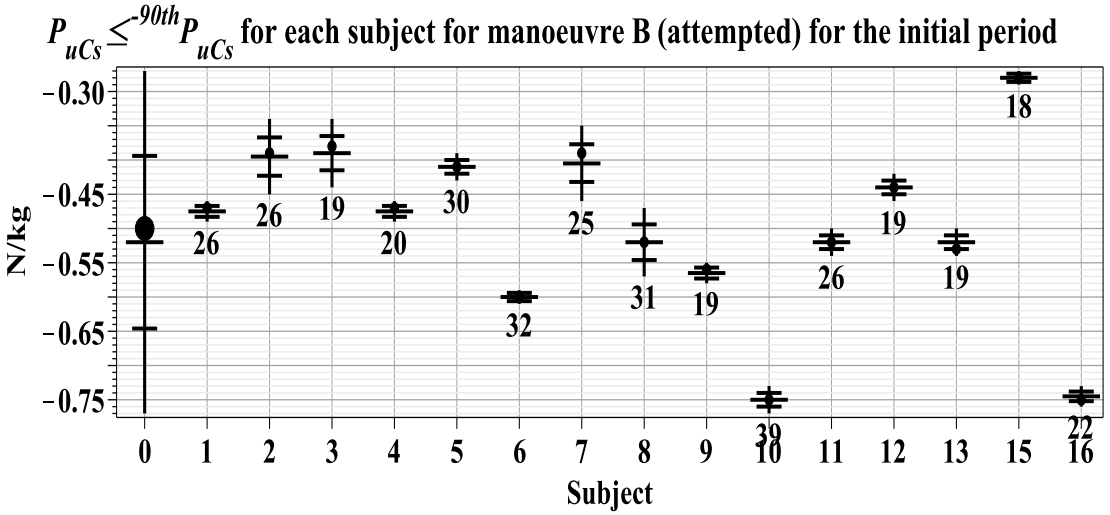

Figure D.12 – Shows for each subject[B] (i) for $\{{}_{ss1}\theta_0^{\mathrm{B}}\}$ in N/kg: a vertical line indicating the minimum magnitude measure ${}^{-90th}_{ss1}P^{\mathrm{B}}_{uCsmini}$ to the maximum magnitude measure ${}^{-90th}_{ss1}P^{\mathrm{B}}_{uCsmaxi}$, a solid circle indicating the mean ${}^{-90th}_{ss1}P^{\mathrm{B}}_{PuCsmini} \geq P_{uCs} \geq {}^{-90th}_{ss1}P^{\mathrm{B}}_{PuCsmaxi}$, the quarter divisions of the range (horizontal lines), the number of occurrences of $P_{uCs} \leq {}^{-90th}_{ss1}P^{\mathrm{B}}_{uCs}$ shown below the range line. Subject[0] shows this data for all subjects[B] with a solid circle indicating the mean of all the mean ${}^{-90th}_{ss1}P^{\mathrm{B}}_{PuCsmini} \geq P_{uCs} \geq {}^{-90th}_{ss1}P^{\mathrm{B}}_{PuCsmaxi}$.

approximately equal to 10% of $50 \times t_i(\{{}_{ss1}\theta_0^{\mathrm{B}}\})$.

It can also be seen from Figure D.12 (page 296) that the range magnitude of 0.50 N/kg, i.e. ${}^{-90th}_{ss1}P^{\mathrm{B}}_{uCsmax} - {}^{-90th}_{ss1}P^{\mathrm{B}}_{uCsmin}$ arises from inter-subject variation (subject[15] compared with subject[10]) and is not the result of the ${}^{-90th}_{ss1}P^{\mathrm{B}}_{uCsmaxi} - {}^{-90th}_{ss1}P^{\mathrm{B}}_{uCsmini}$ magnitude of a specific subject. There are therefore substantial differences between subjects for the largest magnitude P_{uCs}. However, the inequality ${}^{-90th}_{ss1}P^{\mathrm{B}}_{uCsmini} \geq P_{uCs} \geq {}^{-90th}_{ss1}P^{\mathrm{B}}_{uCsmaxi}$ provides a representative range for each subject. In addition the inequality ${}^{-90th}_{ss1}P^{\mathrm{B}}_{uCsmin} \geq P_{uCs} \geq {}^{-90th}_{ss1}P^{\mathrm{B}}_{uCsmax}$ provides a representative range for all subjects[B].

D.4.3. *Manoeuvre B (attempted)* P_v

Figure D.9 (page 291) shows occurrences for ${}^{-75th}_{ssi}P^{\mathrm{B}}_{v} \geq P_v > {}^{-90th}_{ssi}P^{\mathrm{B}}_{v}$ and ${}^{+75th}_{ssi}P^{\mathrm{B}}_{v} \leq P_v < {}^{+90th}_{ssi}P^{\mathrm{B}}_{v}$ (both black markers) and for $P_v \leq {}^{-90th}_{ssi}P^{\mathrm{B}}_{v}$ and $P_v \geq {}^{+90th}_{ssi}P^{\mathrm{B}}_{v}$ (both red markers) (N/kg) against θ_0 for all subjects[B]: to assist inspection the measures for each subject are normalised against the subject's P_v peak magnitude for $\{{}_{ssi}\theta_0^{\mathrm{B}}\}$. A dashed vertical line indicates $\theta_0 = -0.085$ rad and this divides $\{{}_{ssi}\theta_0^{\mathrm{B}}\}$ into $\{{}_{ss1}\theta_0^{\mathrm{B}}\}$ and $\{{}_{ss2i}\theta_0^{\mathrm{B}}\}$ as previously defined.

It is evident that P_v magnitudes and occurrences are non negligible in both signs so it follows that the representation of the largest magnitude P_v must consider both signs: this confirms the representativeness of Figure D.6 (page 289) in this respect.

Figure D.13 (page 298) shows measures for ${}^{-90th}_{ss1}P^{\mathrm{B}}_{v} \geq P_v \geq {}^{+90th}_{ss1}P^{\mathrm{B}}_{v}$ (N/kg) for all subjects[B] with non zero occurrences for $\{{}_{ss1}\theta^{\mathrm{B}}_{0}\}$: no display is shown for subjects with zero occurrences. Representative values for the largest $P_v > 0$ are obtained as follows. For each subject[B] with non zero occurrences the measure for the minimum ${}^{+90th}_{ss1}P^{\mathrm{B}}_{v}$, denoted ${}^{+90th}_{ss1}P^{\mathrm{B}}_{vmini}$ can be read and the minimum ${}^{+90th}_{ss1}P^{\mathrm{B}}_{vmini}$ for all subjects[B], denoted ${}^{+90th}_{ss1}P^{\mathrm{B}}_{vmin}$, is 0.04 N/kg (subjects[4, 11, 13]). The maximum P_v for each subject[B], denoted ${}^{+90th}_{ss1}P^{\mathrm{B}}_{vmaxi}$ can also be read and the maximum ${}^{+90th}_{ss1}P^{\mathrm{B}}_{vmaxi}$ denoted ${}^{+90th}_{ss1}P^{\mathrm{B}}_{vmax}$ is 0.35 N/kg (subject[15]). The mean ${}^{+90th}_{ss1}P^{\mathrm{B}}_{vmaxi} \leq P_v \leq {}^{+90th}_{ss1}P^{\mathrm{B}}_{vmaxi}$ for each subject[B] is indicated by a solid circle though the ranges are of such small magnitude that the location of the mean is immaterial. Occurrences of $P_v \geq {}^{+90th}_{ss1}P^{\mathrm{B}}_{v}$ are shown above the range line for $P_v > 0$ for each subject. Subject[0] shows the range from ${}^{+90th}_{ss1}P^{\mathrm{B}}_{vmin}$ to ${}^{+90th}_{ss1}P^{\mathrm{B}}_{vmax}$ with the mean for all the mean ${}^{+90th}_{ss1}P^{\mathrm{B}}_{vmini} \leq P_v \leq {}^{+90th}_{ss1}P^{\mathrm{B}}_{vmaxi}$ located at the boundary of the first and second quarter as indicated by a solid circle.

It can also be seen from Figure D.13 (page 298) that the range magnitude of 0.31 N/kg i.e. ${}^{+90th}_{ss1}P^{\mathrm{B}}_{vmax} - {}^{+90th}_{ss1}P^{\mathrm{B}}_{vmin}$ arises from inter-subject variation (subjects[4, 11, 13] compared with subject[15]) and is not the result of the ${}^{+90th}_{ss1}P^{\mathrm{B}}_{vmaxi} - {}^{+90th}_{ss1}P^{\mathrm{B}}_{vmini}$ of a specific subject. There are therefore substantial differences between subjects for the largest $P_v > 0$. However, the inequality ${}^{+90th}_{ss1}P^{\mathrm{B}}_{vmini} \leq P_v \leq {}^{+90th}_{ss1}P^{\mathrm{B}}_{vmaxi}$ provides a representative range for each of subjects[1,..., 5, 7,..., 13, 15, 16]. Additionally the inequality ${}^{+90th}_{ss1}P^{\mathrm{B}}_{vmin} \leq P_v \leq {}^{+90th}_{ss1}P^{\mathrm{B}}_{vmax}$ (subject[0]) provides a representative range for subjects[1,..., 5, 7,..., 13, 15, 16] for the largest $P_v > 0$ for $\{{}_{ss1}\theta^{\mathrm{B}}_{0}\}$.

Representative values for the largest magnitude $P_v < 0$ are also read from Figure D.13 (page 298). For each subject[B] with non zero occurrences the measure for the minimum magnitude ${}^{-90th}_{ss1}P^{\mathrm{B}}_{v}$, denoted ${}^{-90th}_{ss1}P^{\mathrm{B}}_{vmini}$, can be read and the minimum magnitude ${}^{-90th}_{ss1}P^{\mathrm{B}}_{vmini}$ for all subjects[B] with non zero occurrences, denoted ${}^{-90th}_{ss1}P^{\mathrm{B}}_{vmin}$, is -0.05 N/kg (subject[12]). The maximum magnitude $P_v < 0$

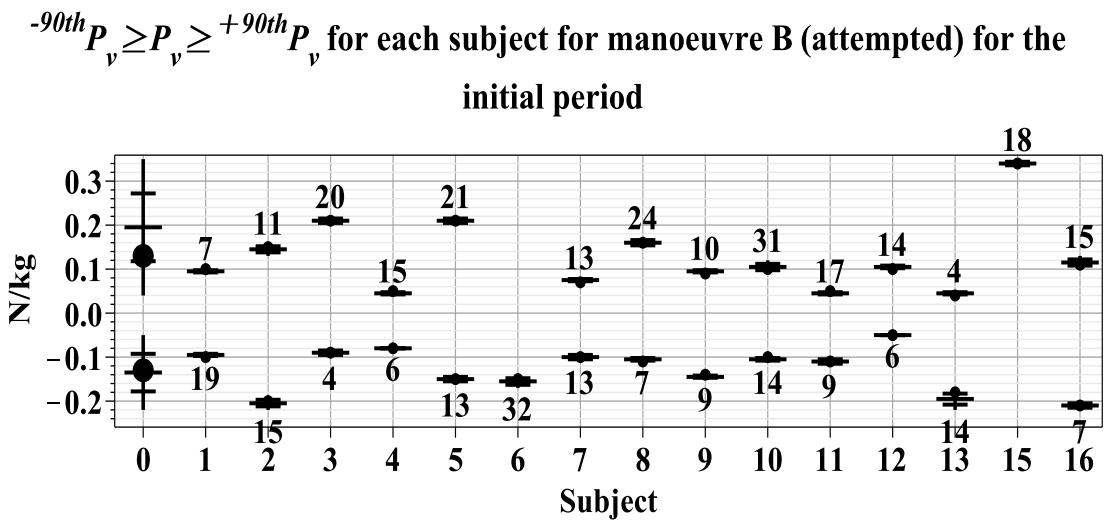

Figure D.13 – Shows for each subject[B] (i) for $\{{}_{ss1}\theta_0^{\mathrm{B}}\}$ in N/kg: for $P_v > 0$ a vertical line indicating the minimum magnitude measure ${}^{+90th}_{ss1}P^{\mathrm{B}}_{vmini}$ to the maximum magnitude measure ${}^{+90th}_{ss1}P^{\mathrm{B}}_{vmaxi}$, a solid circle indicating the mean ${}^{+90th}_{ss1}P^{\mathrm{B}}_{vmini} \leq P_v \leq {}^{+90th}_{ss1}P^{\mathrm{B}}_{vmaxi}$, the quarter divisions of the range (horizontal lines) and the number of occurrences of $P_v \geq {}^{+90th}_{ss1}P^{\mathrm{B}}_{v}$ shown above the range line: for $P_v < 0$ where there are non zero occurrences, a vertical line indicating the minimum magnitude measure ${}^{-90th}_{ss1}P^{\mathrm{B}}_{vmini}$ to the maximum magnitude measure ${}^{-90th}_{ss1}P^{\mathrm{B}}_{vmaxi}$, a solid circle indicating the mean ${}^{-90th}_{ss1}P^{\mathrm{B}}_{vmaxi} \geq P_v \geq {}^{-90th}_{ss1}P^{\mathrm{B}}_{vmaxi}$, the quarter divisions of the range (horizontal lines) and the number of occurrences of $P_v \leq {}^{+90th}_{ss1}P^{\mathrm{B}}_{v}$ shown below the range line. Subject[0] shows these measures for all subjects[B] with a solid circle indicating the mean of all the mean ${}^{+90th}_{ss1}P^{\mathrm{B}}_{vmini} \leq P_v \leq {}^{+90th}_{ss1}P^{\mathrm{B}}_{vmaxi}$ for $P_v > 0$ and the mean of all the mean ${}^{-90th}_{ss1}P^{\mathrm{B}}_{vmini} \geq P_v \geq {}^{-90th}_{ss1}P^{\mathrm{B}}_{vmaxi}$ for $P_v < 0$.

for all subjects[B], denoted ${}^{-90th}_{ss1}P^{\mathrm{B}}_{vmaxi}$ can also be read and the maximum magnitude ${}^{-90th}_{ss1}P^{\mathrm{B}}_{vmaxi}$ denoted ${}^{-90th}_{ss1}P^{\mathrm{B}}_{vmax}$ is -0.22 N/kg (subjects[2, 13, 16]). The occurrences of $P_v \leq {}^{-90th}_{ss1}P^{\mathrm{B}}_{v}$ are shown below the range line. The mean ${}^{-90th}_{ss1}P^{\mathrm{B}}_{vmini} \leq P_v \leq {}^{-90th}_{ss1}P^{\mathrm{B}}_{vmaxi}$ for each subject[B] is indicated by a solid circle but it can be seen that the ranges (excluding subject[13] are of such small magnitude that the location is immaterial. Subject[0] shows the range from ${}^{-90th}_{ss1}P^{\mathrm{B}}_{vmin}$ to ${}^{-90th}_{ss1}P^{\mathrm{B}}_{vmax}$ with the mean of all the mean ${}^{-90th}_{ss1}P^{\mathrm{B}}_{vmini} \leq P_v \leq {}^{-90th}_{ss1}P^{\mathrm{B}}_{vmaxi}$ indicated by a solid circle which is centrally located.

It can also be seen from Figure D.13 (page 298) that the range magnitude of 0.17 N/kg, i.e. ${}^{-90th}_{ss1}P^{\mathrm{B}}_{vmax} - {}^{-90th}_{ss1}P^{\mathrm{B}}_{vmin}$ arises from inter-subject variation (subject[12] compared with subjects[2, 13, 16]) and is not the result of

the ${}^{-90th}_{ss1}P^{\mathrm{B}}_{vmaxi} - {}^{-90th}_{ss1}P^{\mathrm{B}}_{vmini}$ of a specific subject. There are therefore differences between subjects for the largest magnitude $P_v < 0$. However, the inequality ${}^{-90th}_{ss1}P^{\mathrm{B}}_{vmini} \geq P_v \geq {}^{-90th}_{ss1}P^{\mathrm{B}}_{vmaxi}$ provides a representative range for each of subjects[1,..., 13, 16]. Additionally the inequality ${}^{+90th}_{ss1}P^{\mathrm{B}}_{vmin} \leq P_v \leq {}^{+90th}_{ss1}P^{\mathrm{B}}_{vmax}$ (subject[0]) provides a representative range for subjects[1,..., 13, 16] for the largest magnitude $P_v < 0$ for $\{{}_{ss1}\theta^{\mathrm{B}}_0\}$.

D.5. **Manoeuvre K (attempted)**

In this subsection 'all subjects[K]' or a trailing super or sub script K in a symbol indicates measures from subjects [1,..., 16].

D.5.1. *Manoeuvre K (a.) handle-force measures*

Examination of the handle-force measures will show that dividing the start-steady period at $\theta_0 = -0.107$ rad is useful and hence vehicle-frame orientation measures for manoeuvre[K] (a.) are defined for an initial period $-0.107 < \theta_0 < 0$ rad, denoted $\{{}_{ss1}\theta^{\mathrm{K}}_0\}$, and for the later period $\theta_{0steadi} < \theta_0 < -0.107$ rad, denoted $\{{}_{ss2i}\theta^{\mathrm{K}}_0\}$. There is some variation between subjects immediately after motion start for some small θ_0 displacement: magnitude no greater than 0.01 rad. The range $-0.107 < \theta_0 < -0.01$ rad is denoted $\{{}_{ss1a}\theta^{\mathrm{K}}_0\}$ ($\{{}_{ss1}\theta^{\mathrm{K}}_0\}$ modified to commence at $\theta_0 = -0.01$ rad rather than motion-start). Figures D.15 and D.14 (pages 300 and 300) illustrates the handle-force measures for one subject[10]. For the modified initial period $\{{}_{ss1a}\theta^{\mathrm{K}}_0\}$ there are three features of which are common to all subjects[K]. Firstly, there are no occurrences of $P_{uCs} > 0$. Secondly, there are no occurrences of $P_u < 0$ for $\{{}_{ss1a}\theta^{\mathrm{K}}_0\}$. Thirdly, there are no occurrences of $P_v < 0$.

D.5.2. *Manoeuvre K (a.) P_v*

The presentation begins with P_v: the lateral force. Figure D.16 (page 301) shows occurrences of ${}^{-75th}_{ssi}P^{\mathrm{K}}_v \geq P_v > {}^{-90th}_{ssi}P^{\mathrm{K}}_v$ and of ${}^{+75th}_{ssi}P^{\mathrm{K}}_v \leq P_v < {}^{+90th}_{ssi}P^{\mathrm{K}}_v$ (both black markers) and, of $P_v \leq {}^{-90th}_{ssi}P^{\mathrm{K}}_v$ and of $P_v \geq {}^{+90th}_{ssi}P^{\mathrm{K}}_v$ (both red markers). To aid inspection the measures (N/kg) for each subject are normalised against the subject's peak magnitude P_v for $\{{}_{ss1}\theta^{\mathrm{K}}_0\}$: these are the occurrences for all subjects[K]: a dashed line indicates $\theta_0 = -0.107$ rad. It is evident from Figure D.16 that all P_v are $P_v > 0$ and this confirms the representativeness of subject[10] in this respect as shown in Figure D.15 (page 300). While Figure D.16 does not

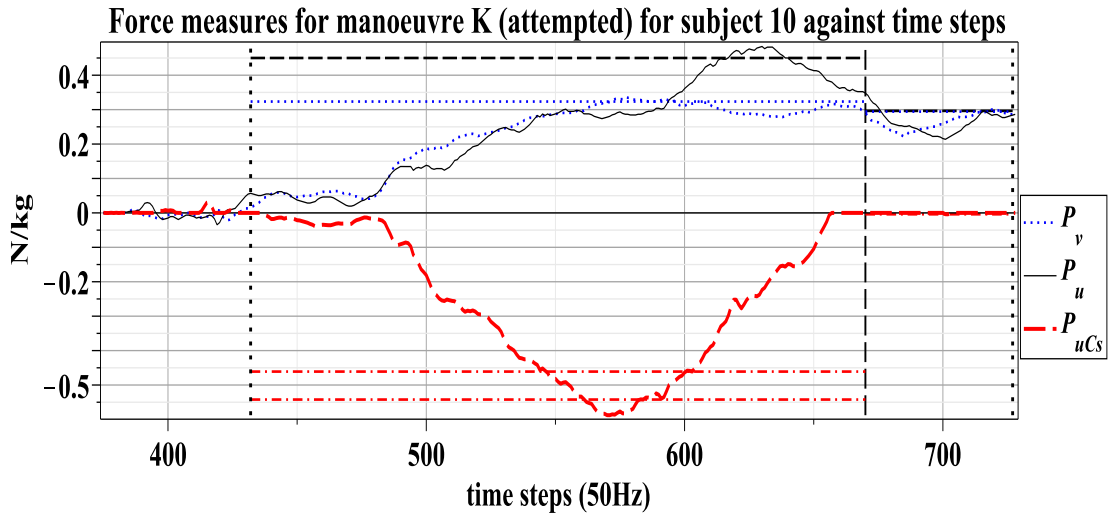

Figure D.14 – For subject[10] for manoeuvre K (a.), measures: P_v (dotted blue), P_u (thin black) and P_{uCs} (thick red dashed) in N/kg plotted against time-steps (approximately 0.02 seconds) with motion-start line (vertical black dotted: closest to left side), steady-start line (vertical black dotted:closest to right side) and $\theta_0 = -0.031$ rad line (vertical black dashed). The following percentile lines are shown for $\{{}_{ss1}\theta_0^{\mathrm{K}}\}$: ${}^{-90th}_{ss1}P^{\mathrm{K}}_{uCs}$ and ${}^{-75th}_{ss1}P^{\mathrm{K}}_{uCs}$ (horizontal red dash-dot), ${}^{+90th}_{ss1}P^{\mathrm{K}}_{u}$ (horizontal black dash) and ${}^{+90th}_{ss1}P^{\mathrm{K}}_{v}$ (horizontal blue dot)

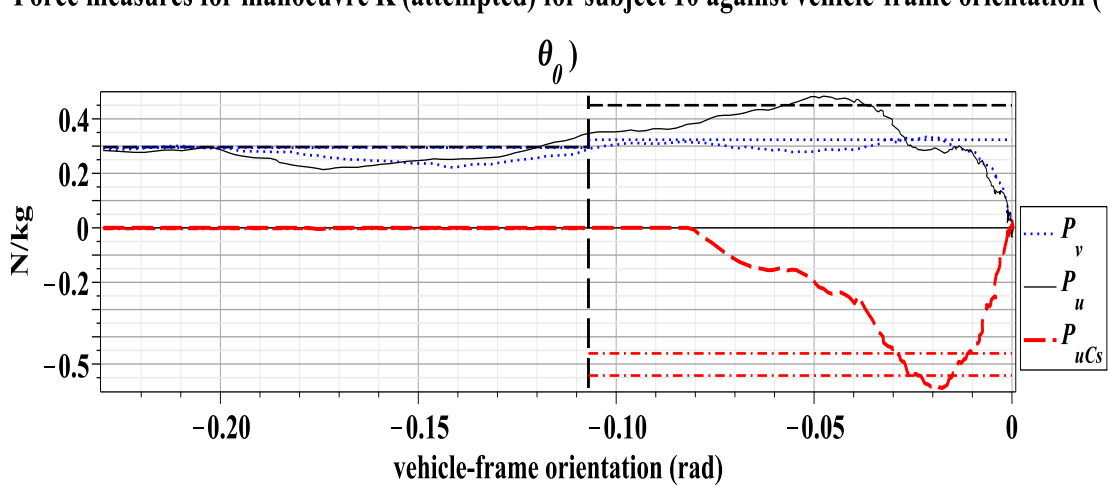

Figure D.15 – For subject[10] for manoeuvre K (a.), measures plotted against θ_0 with other details as above.

demonstrate that all subjects[K] have a peak P_v for $\{{}_{ss1}\theta_0^{\mathrm{K}}\}$ it is evident that $P_v \geq {}^{+90th}_{ssi}P^{\mathrm{K}}_{v}$ do not occur for approximately 0.05 rad after the initial-later period boundary is reached. Thus apart from the minority of occurrences of $P_v \geq {}^{+75th}_{ssi}P^{\mathrm{K}}_{v}$ for $\theta_0 < -0.15$ rad., despite any variations, the mechanism is so configured that the majority of the largest P_v actions occur by $\theta_0 = -0.107$ rad and hence division of the start-steady period at this location relates to a mechanical property of the

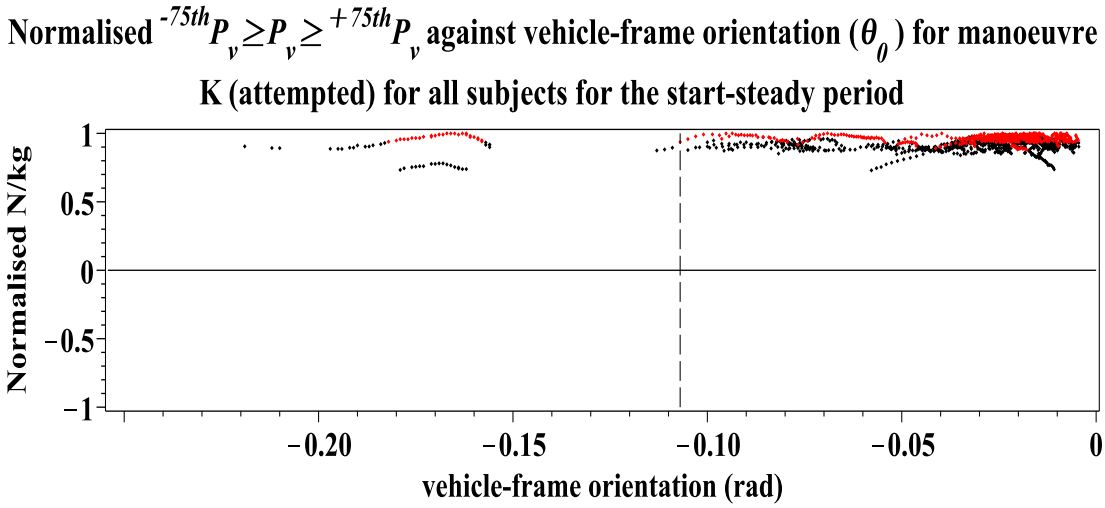

Figure D.16 – For manoeuvre K (a.) occurrences of ${}^{-75th}_{ssi}P^{\mathrm{K}}_v \geq P_v > {}^{-90th}_{ssi}P^{\mathrm{K}}_v$ and of ${}^{+75th}_{ssi}P^{\mathrm{K}}_v \leq P_v < {}^{+90th}_{ssi}P^{\mathrm{K}}_v$ (both black markers) and, of $P_v \leq {}^{-90th}_{ssi}P^{\mathrm{K}}_v$ and of $P_v \geq {}^{+90th}_{ssi}P^{\mathrm{K}}_v$ (both red markers) in N/kg (normalised against each subject's maximum magnitude P_v for the start-steady period) against θ_0 for $\{{}_{ssi}\theta^{\mathrm{K}}_0\}$ for each subject: $\theta_0 = -0.107$ line indicated (dashed vertical).

system for manoeuvre K (a.).

The equivalent process, as was used to graph Figure D.16 (page 301) for P_v is repeated for P_{uCs} and P_u, as described for manoeuvre F (a.) in Sections 6.4.2 (page 145) and D.2.1 (page 283) respectively, and the resulting graphs are shown in Figures D.17 (page 302) and D.18 (page 302) respectively. A detailed account of the measures is included in Appendix B. Figure D.19 (page 303) shows measures for $P_v \geq {}^{+90th}_{ss1}P^{\mathrm{K}}_v$ (N/kg) for each of all subjects[K] and for all subjects[K], denoted subject[0], for $\{{}_{ss1}\theta^{\mathrm{K}}_0\}$. Representative values for the largest P_v are obtained as follows. For each subject[K] the measure for the minimum ${}^{+90th}_{ss1}P^{\mathrm{K}}_v$, denoted ${}^{+90th}_{ss1}P^{\mathrm{K}}_{vmini}$ may be read and the minimum ${}^{+90th}_{ss1}P^{\mathrm{K}}_{vmini}$ for all subjects[K], denoted ${}^{+90th}_{ss1}P^{\mathrm{K}}_{vmin}$, is 0.28 N/kg (subject[6]). The maximum P_v for each subject[K], denoted ${}^{+90th}_{ss1}P^{\mathrm{K}}_{vmaxi}$ may also be read and the maximum ${}^{+90th}_{ss1}P^{\mathrm{K}}_{vmaxi}$ denoted ${}^{+90th}_{ss1}P^{\mathrm{K}}_{vmax}$ is 0.54 N/kg (subject[15]). The mean ${}^{+90th}_{ss1}P^{\mathrm{K}}_{vmaxi} \leq P_v \leq {}^{+90th}_{ss1}P^{\mathrm{K}}_{vmaxi}$ for each subject[K] is is indicated by a solid circle: it can be seen that where the range magnitude is not too small these means are located from the second to the third quarter of the intra-subject range. Subject[0] shows the range of the minimum ${}^{+90th}_{ss1}P^{\mathrm{K}}_{vmini}$ to the maximum ${}^{+90th}_{ss1}P^{\mathrm{K}}_{vmaxi}$ and the mean of all the mean ${}^{+90th}_{ss1}P^{\mathrm{K}}_{vmaxi} \leq P_v \leq {}^{+90th}_{ss1}P^{\mathrm{K}}_{vmaxi}$ is indicated by a solid circle and this is loc-

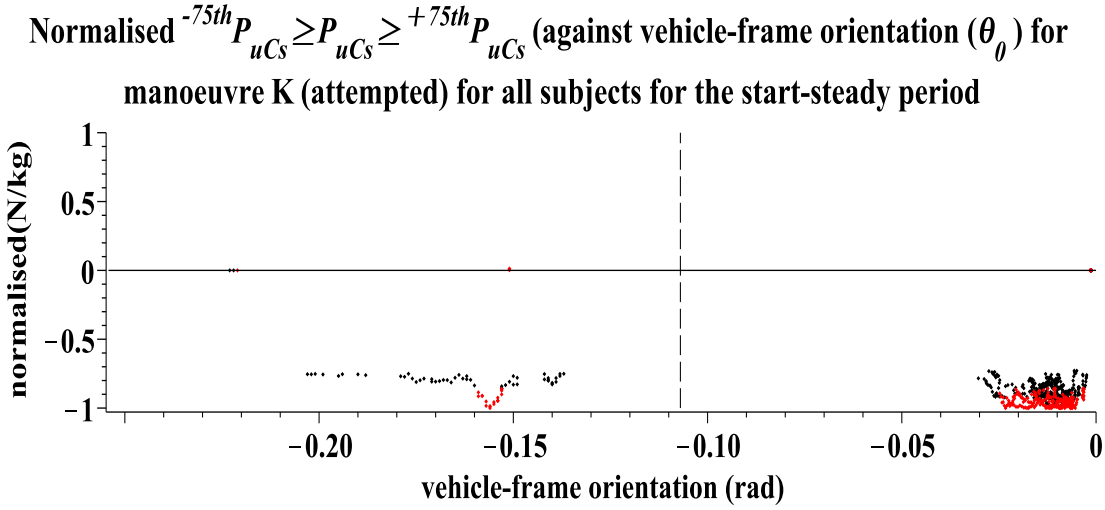

Figure D.17 – For manoeuvre K (a.) occurrences of ${}^{-75th}_{ssi}P^{\mathrm{K}}_{uCs} \geq P_{uCs} > {}^{-90th}_{ssi}P^{\mathrm{K}}_{uCs}$ and of ${}^{+75th}_{ssi}P^{\mathrm{K}}_{uCs} \leq P_{uCs} < {}^{+90th}_{ssi}P^{\mathrm{K}}_{uCs}$ (both black markers) and, $P_{uCs} \leq {}^{-90th}_{ssi}P^{\mathrm{K}}_{uCs}$ and $P_{uCs} \geq {}^{+90th}_{ssi}P^{\mathrm{K}}_{uCs}$ (both red markers) in N/kg (normalised against each subject's maximum magnitude P_{uCs} for $\{{}_{ssi}\theta^{\mathrm{K}}_0\}$, against θ_0 for the start-steady period for each subject: $\theta_0 = -0.107$ line indicated (dashed vertical)

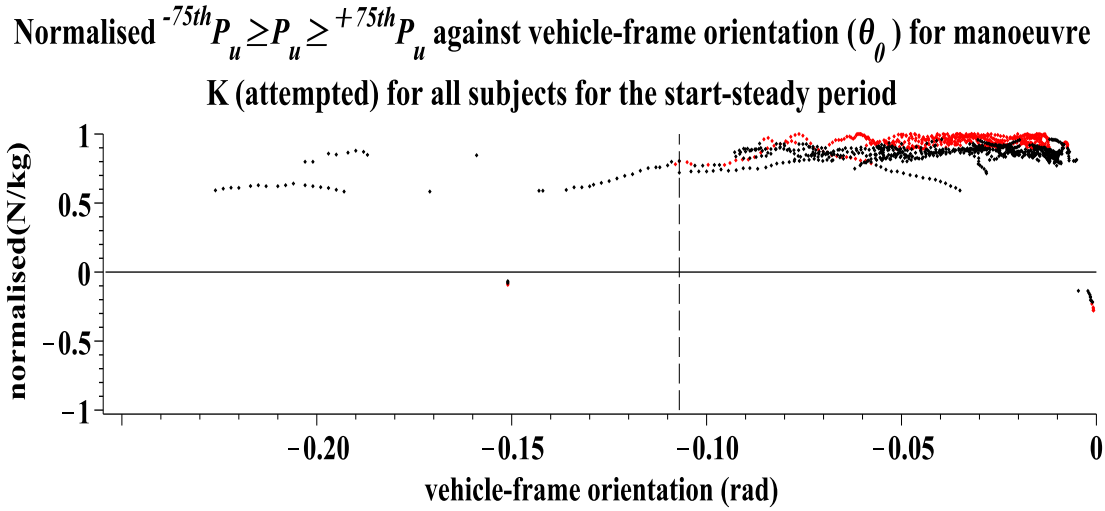

Figure D.18 – For manoeuvre K (a.) occurrences of ${}^{-75th}_{ssi}P^{\mathrm{K}}_{u} \geq P_u > {}^{-90th}_{ssi}P^{\mathrm{K}}_{u}$ and of ${}^{+75th}_{ssi}P^{\mathrm{K}}_{u} \leq P_u < {}^{+90th}_{ssi}P^{\mathrm{K}}_{u}$ (both black markers) and, of $P_u \leq {}^{-90th}_{ssi}P^{\mathrm{K}}_{u}$ and of $P_u \geq {}^{+90th}_{ssi}P^{\mathrm{K}}_{u}$ (both red markers) in N/kg (normalised against each subject's maximum magnitude P_{uCs} for $\{{}_{ssi}\theta^{\mathrm{K}}_0\}$, against θ_0 for the start-steady period for each subject: $\theta_0 = -0.107$ line indicated (dashed vertical)

ated in the second quarter of the inter-subject range. Occurrences of $P_v \geq {}^{+90th}_{ss1}P^{\mathrm{K}}_{v}$ are shown. As there are no $P_v < 0$ for the initial period the occurrences of $P_v \geq {}^{+90th}_{ss1}P^{\mathrm{K}}_{v}$ are approximately equal to $\frac{50}{10} \times t_i(\{{}_{ss1}\theta^{\mathrm{K}}_0\})$. A detailed account of the measures not considered in detail here follows in the next section.

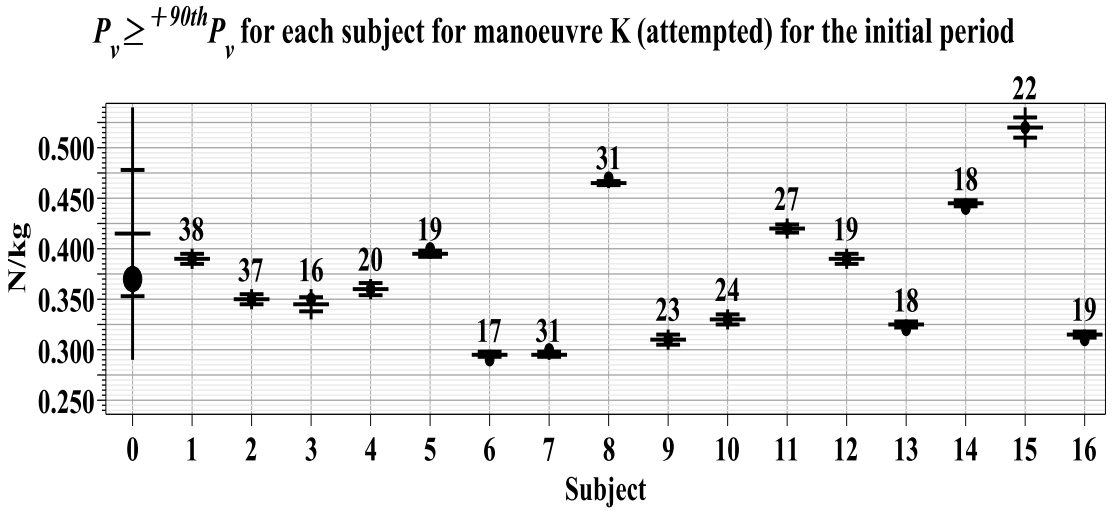

Figure D.19 – Shows for each subject[K] (i) for $\{{}_{ss1}\theta_0^{\mathrm{K}}\}$ in N/kg: a vertical line indicating the minimum measure ${}^{+90th}_{ss1}P^{\mathrm{K}}_{vmini}$ to the maximum measure ${}^{+90th}_{ss1}P^{\mathrm{K}}_{vmaxi}$, a solid circle indicating the mean ${}^{+90th}_{ss1}P^{\mathrm{K}}_{vmaxi} \leq P_v \leq {}^{+90th}_{ss1}P^{\mathrm{K}}_{vmaxi}$, the quarter divisions of the range (horizontal lines) and the number of occurrences of $P_v \geq {}^{+90th}_{ss1}P^{\mathrm{K}}_{v}$. Subject[0] shows these results for all subjects[K] with a solid circle indicating the mean of all the mean ${}^{+90th}_{ss1}P^{\mathrm{K}}_{vmaxi} \leq P_v \leq {}^{+90th}_{ss1}P^{\mathrm{K}}_{vmaxi}$.

D.5.3. *Manoeuvre K (a.) the $P_v - P_{uCs}$ plane*

This final section relating to manoeuvre K (a.) uses the inequalities, as previously defined, to define a cuboid boundary for the largest magnitude measures for each and all subjects. As all measures are in one sign one set of three inequalities is required. For each of subjects[1,..., 16] the following inequalities define the cuboid boundaries:

$${}^{-90th}_{ss1}P^{\mathrm{K}}_{uCsmini} \geq P_{uCs} \geq {}^{-90th}_{ss1}P^{\mathrm{K}}_{uCsmaxi} \text{ (page 304)},$$

$${}^{+90th}_{ss1}P^{\mathrm{K}}_{vmini} \leq P_v \leq {}^{+90th}_{ss1}P^{\mathrm{K}}_{vmaxi} \text{ (page 299) and}$$

$${}^{+90th}_{ss1}P^{\mathrm{K}}_{umini} \leq P_u \leq {}^{+90th}_{ss1}P^{\mathrm{K}}_{umaxi} \text{ (page 306)}.$$

and these three inequalities are denoted ${}^{large}_{ss1}\mathbf{P}^{\mathrm{K}}_i$. A graphical representation of ${}^{large}_{ss1}\mathbf{P}^{\mathrm{K}}_i$ in the $P_v - P_{uCs}$ plane is shown in Figure D.20 (page 304): the construction follows the same process as described in Section 6.4.4 (page 149) for manoeuvre F (a.).

The cuboid boundary for all subjects[K] as opposed to each subject is given by:

$${}^{-90th}_{ss1}P^{\mathrm{K}}_{uCsmin} \geq P_{uCs} \geq {}^{-90th}_{ss1}P^{\mathrm{K}}_{uCsmax},$$

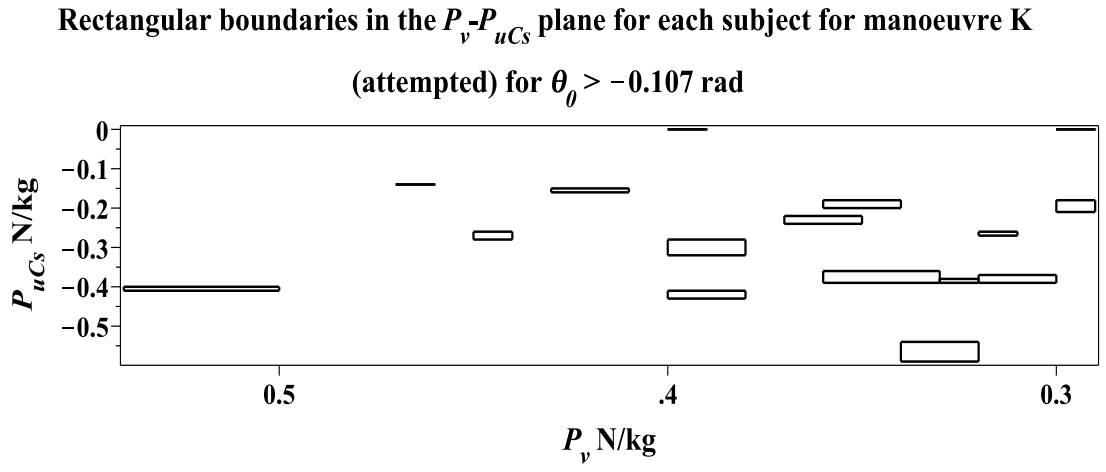

Figure D.20 – Rectangles formed with vertices of coordinates $[{}^{+90th}_{ss1}P^{\mathrm{K}}_{vmini}, {}^{-90th}_{ss1}P^{\mathrm{K}}_{uCsmini}]$, $[{}^{+90th}_{ss1}P^{\mathrm{K}}_{vmaxi}, {}^{-90th}_{ss1}P^{\mathrm{K}}_{uCsmini}]$, $[{}^{+90th}_{ss1}P^{\mathrm{K}}_{vmaxi}, {}^{-90th}_{ss1}P^{\mathrm{K}}_{uCsmaxi},]$, and $[{}^{+90th}_{ss1}P^{\mathrm{K}}_{vmini}, {}^{-90th}_{ss1}P^{\mathrm{K}}_{uCsmaxi}]$ for all subjects[K] i.e. n=16.

$${}^{+90th}_{ss1}P^{\mathrm{K}}_{vmin} \leq P_v \leq {}^{+90th}_{ss1}P^{\mathrm{K}}_{vmax} \text{ and}$$

$${}^{+90th}_{ss1}P^{\mathrm{K}}_{umin} \leq P_u \leq {}^{+90th}_{ss1}P^{\mathrm{K}}_{umax}$$

and this is denoted ${}^{large}_{ss1}\mathbf{P}^{\mathrm{K}}$. In conclusion ${}^{large}_{ss1}\mathbf{P}^{\mathrm{K}}$ provides a useful representation of the boundaries of the largest handle-forces for all subjects[K] for manoeuvre K (a.): the numerical values are:

$0.28 \leq P_v \leq 0.54$ (N/kg),

$-0.14 \geq P_{uCs} \geq -0.59$ (N/kg) and

$0.27 \leq P_u \leq 0.74$ (N/kg).

In conclusion ${}^{large}_{ss1}\mathbf{P}^{\mathrm{K}}$ provides a useful representation of the boundaries of the largest handle-forces for all subjects[K] for manoeuvre K (a.).

D.6. Manoeuvre K (attempted) Details

D.6.1. *Manoeuvre K (attempted)* P_{uCs}

Figure D.17 (page 302) shows occurrences of ${}^{-75th}_{ssi}P^{\mathrm{K}}_{uCs} \geq P_{uCs} > {}^{-90th}_{ssi}P^{\mathrm{K}}_{uCs}$ and of ${}^{+75th}_{ssi}P^{\mathrm{K}}_{uCs} \leq P_{uCs} < {}^{+90th}_{ssi}P^{\mathrm{K}}_{uCs}$ (both black markers), and $P_{uCs} \leq {}^{-90th}_{ssi}P^{\mathrm{K}}_{uCs}$ and $P_{uCs} \geq {}^{+90th}_{ssi}P^{\mathrm{K}}_{uCs}$ (both red markers) in N/kg for all subjects: to assist inspection the measures for each subject are normalised against the subject's P_{uCs} peak magnitude for $\{{}_{ssi}\theta^{\mathrm{K}}_0\}$. A dashed vertical line indicates $\theta_0 = -0.107$ rad and this divides $\{{}_{ssi}\theta^{\mathrm{K}}_0\}$ into $\{{}_{ss1}\theta^{\mathrm{K}}_0\}$ and $\{{}_{ss2i}\theta^{\mathrm{K}}_0\}$ as previously defined. Additionally, an

evaluation of the data (results not presented) shows that for all subjects[K] that there are no $P_{uCs} > 0$ for $\{{}_{ss1a}\theta_0^{\mathrm{K}}\}$ (as previously defined) and this confirms the representativeness of Figure D.15 (page 300) in this respect.

Figure D.21 (page 306) shows measures for $P_{uCs} \geq {}^{-90th}_{ss1}P^{\mathrm{K}}_{uCs}$ (N/kg) for all subjects[K] for $\{{}_{ss1}\theta_0^{\mathrm{K}}\}$. Representative values for the largest P_{uCs} are obtained as follows. For each subject[K] the measure for the minimum ${}^{-90th}_{ss1}P^{\mathrm{K}}_{uCs}$, denoted ${}^{-90th}_{ss1}P^{\mathrm{K}}_{uCsmini}$ may be read and the minimum ${}^{-90th}_{ss1}P^{\mathrm{K}}_{uCsmini}$ for all subjects[K], denoted ${}^{-90th}_{ss1}P^{\mathrm{K}}_{uCsmin}$, is -0.14 N/kg (subject[8]). The maximum P_{uCs} for each subject[K], denoted ${}^{-90th}_{ss1}P^{\mathrm{K}}_{uCsmaxi}$ may also be read and the maximum ${}^{-90th}_{ss1}P^{\mathrm{K}}_{uCsmaxi}$, denoted ${}^{-90th}_{ss1}P^{\mathrm{K}}_{uCsmax}$, is -0.59 N/kg (subject[10]). The mean ${}^{-90th}_{ss1}\geq^{\mathrm{K}}_{uCsmini} P_{uCs} \geq {}^{-90th}_{ss1}P^{\mathrm{K}}_{uCsmaxi}$ for each subject[K] are indicated by a solid circle and it can be seen that these means, ignoring subjects where the range magnitude is relatively small, are located in the first to third quarters of the intra-subject range. Subject[0] shows the range of ${}^{-90th}_{ss1}P^{\mathrm{K}}_{uCsmin}$ to ${}^{-90th}_{ss1}P^{\mathrm{K}}_{uCsmax}$ and the mean of all the mean ${}^{-90th}_{ss1}\geq^{\mathrm{K}}_{uCsmini} P_{uCs} \geq {}^{-90th}_{ss1}P^{\mathrm{K}}_{uCsmaxi}$ indicated by a solid circle can be seen to be located in the second quarter of the inter-subject range.

For each subject occurrences of $P_{uCs} \leq {}^{-90th}_{ss1}P^{\mathrm{K}}_{uCs}$ are shown in Figure D.21 and the percentage of occurrences of $P_{uCs} = 0$ (integer) are shown below the range line. Substantial variation is evident: subjects[5, 6] have 100% occurrences of $P_{uCs} = 0$ (integer), so no occurrences of $P_{uCs} \geq {}^{-90th}_{ss1}P^{\mathrm{K}}_{uCs}$ and subject[7] has 2% occurrences of $P_{uCs} = 0$ (integer). In other words the attempt at manoeuvre[K] by some subjects, to some extent, reduces the occurrences of the couple action.

It can also be seen from Figure D.21 (page 306) that the range magnitude of 0.45 N/kg, ${}^{-90th}_{ss1}P^{\mathrm{K}}_{uCsmax} - {}^{-90th}_{ss1}P^{\mathrm{K}}_{uCsmin}$, arises from inter-subject variation (subject[8] compared with subject[10]) and is not the result of the ${}^{-90th}_{ss1}P^{\mathrm{K}}_{uCsmaxi} - {}^{-90th}_{ss1}P^{\mathrm{K}}_{uCsmini}$ magnitude of a specific subject. There are therefore substantial differences between subjects for the largest magnitude $P_{uCs} < 0$. However, the inequality ${}^{-90th}_{ss1}P^{\mathrm{K}}_{uCsmini} \geq P_{uCs} \geq {}^{-90th}_{ss1}P^{\mathrm{K}}_{uCsmaxi}$ provides a representative range for each subject. In addition the inequality ${}^{-90th}_{ss1}P^{\mathrm{K}}_{uCsmin} \geq P_{uCs} \geq {}^{-90th}_{ss1}P^{\mathrm{K}}_{uCsmax}$ provides a representative range for all subjects[K].

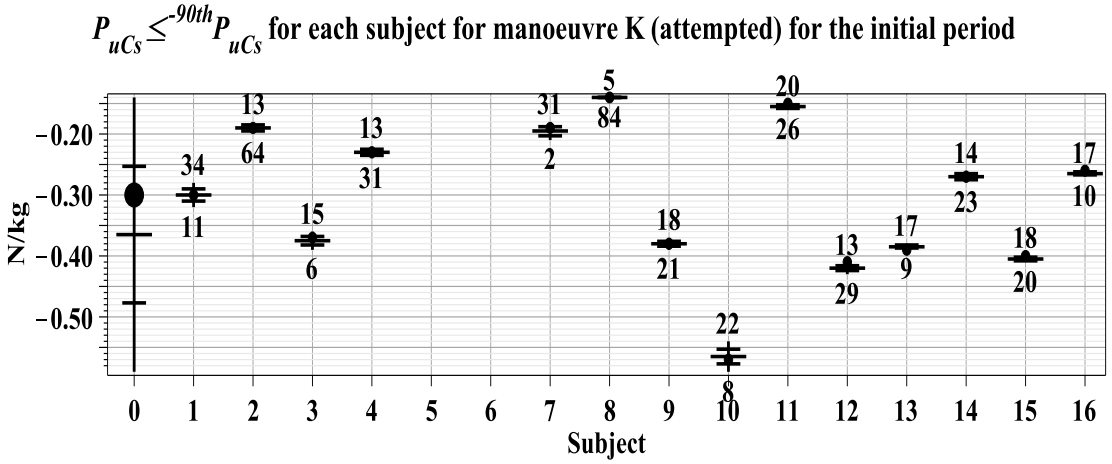

Figure D.21 – Shows for each subject[K] (i), excluding subjects[5, 6] who have no occurrences, for $\{{}_{ss1}\theta_0^{\mathrm{K}}\}$ in N/kg: a vertical line indicating the minimum magnitude measure ${}^{-90th}_{ss1}P^{\mathrm{K}}_{uCsmini}$ to the maximum magnitude measure ${}^{-90th}_{ss1}P^{\mathrm{K}}_{uCsmaxi}$, a solid circle indicating the mean ${}^{-90th}_{ss1}P^{\mathrm{K}}_{PuCsmini} \geq P_{uCs} \geq {}^{-90th}_{ss1}P^{\mathrm{K}}_{PuCsmaxi}$, the quarter divisions of the range (horizontal lines), the number of occurrences of $P_{uCs} \leq {}^{-90th}_{ss1}P^{\mathrm{K}}_{uCs}$ shown above the range line and the percentage of occurrences of $P_{uCs} = 0$ (integer) for the initial period shown below the range line. Subject[0] shows these measures for all subjects[K] with a solid circle indicating the mean of all the mean ${}^{-90th}_{ss1}P^{\mathrm{K}}_{PuCsmini} \geq P_{uCs} \geq {}_{ss1}P^{\mathrm{K}}_{PuCsmaxi}$.

D.6.2. *The K manoeuvre (attempted) P_u*

Figure D.18 (page 302) shows occurrences of ${}^{-75th}_{ssi}P^{\mathrm{K}}_{u} \geq P_u > {}^{-90th}_{ssi}P^{\mathrm{K}}_{u}$ and of ${}^{+75th}_{ssi}P^{\mathrm{K}}_{u} \leq P_u < {}^{+90th}_{ssi}P^{\mathrm{K}}_{u}$ (both black markers) and, of $P_u \leq {}^{-90th}_{ssi}P^{\mathrm{K}}_{u}$ and of $P_u \geq {}^{+90th}_{ssi}P^{\mathrm{K}}_{u}$ (both red markers): to aid inspection the measures for each subject are normalised against the subject's P_u peak magnitude for $\{{}_{ssi}\theta_0^{\mathrm{K}}\}$: these are the occurrences for all subjects[K]. All peak P_u occur in the initial period and are for $P_u > 0$. Additionally, an evaluation of the data (results not reported) shows that for all subjects[K] that there are no $P_u < 0$ for $\{{}_{ss1a}\theta_0^{\mathrm{K}}\}$ and this confirms the representativeness of Figure D.15 (page 300) in this respect.

Figure D.22 (page 307) shows measures for $P_u \geq {}^{+90th}_{ss1}P^{\mathrm{K}}_{u}$ (N/kg) for all subjects[K] for $\{{}_{ss1}\theta_0^{\mathrm{K}}\}$. Representative values for the largest $P_u > 0$ are obtained as follows. For each subject[K] the measure for the minimum ${}^{+90th}_{ss1}P^{\mathrm{K}}_{u}$, denoted ${}^{+90th}_{ss1}P^{\mathrm{K}}_{umini}$, can be read and the minimum ${}^{+90th}_{ss1}P^{\mathrm{K}}_{umini}$ for all subjects[K], denoted ${}^{+90th}_{ss1}P^{\mathrm{K}}_{umin}$, is 0.27 N/kg (subject[12]). The maximum P_u for each subject[K], denoted ${}^{+90th}_{ss1}P^{\mathrm{K}}_{umaxi}$, can also be read and the maximum ${}^{+90th}_{ss1}P^{\mathrm{K}}_{umaxi}$,

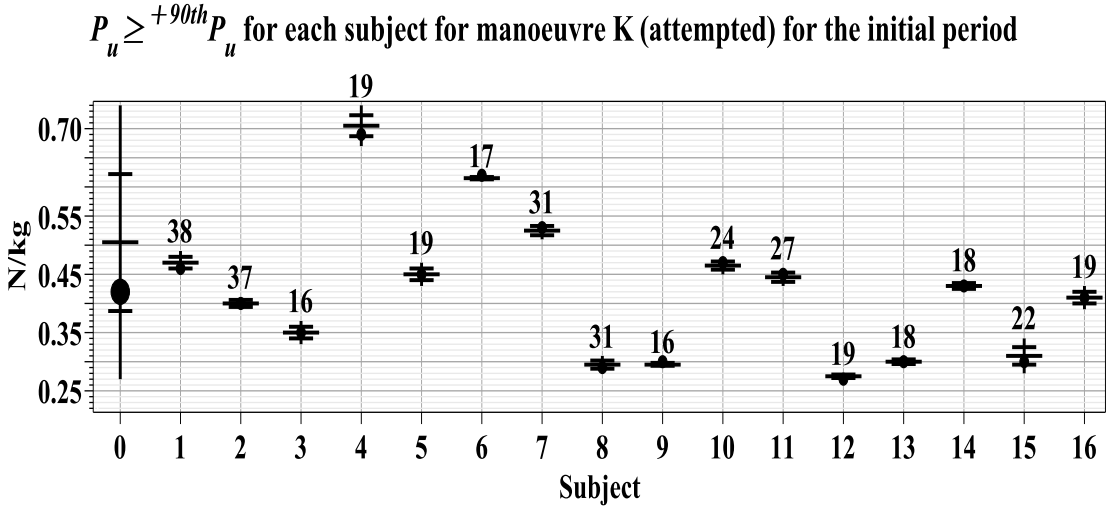

Figure D.22 – Shows for each subject[K] (i) for $\{{}_{ss1}\theta_0^{\mathrm{K}}\}$ in N/kg: a vertical line indicating the minimum magnitude measure ${}^{+90th}_{ss1}P^{\mathrm{K}}_{umini}$ to the maximum magnitude measure ${}^{+90th}_{ss1}P^{\mathrm{K}}_{umaxi}$, a solid circle indicating the mean ${}^{+90th}_{ss1}\leq^{\mathrm{K}}_{umini} P_u \leq {}^{+90th}_{ss1}P^{\mathrm{K}}_{umaxi}$, the quarter divisions of the range (horizontal lines) and the number of occurrences of $P_u \geq {}^{+90th}_{ss1}P^{\mathrm{K}}_{u}$ shown above the range line. Subject[0] shows these measures for all subjects[K] with a solid circle indicating the mean of all the mean ${}^{+90th}_{ss1}\leq^{\mathrm{K}}_{umini} P_u \leq {}^{+90th}_{ss1}P^{\mathrm{K}}_{umaxi}$.

denoted ${}^{+90th}_{ss1}P^{\mathrm{K}}_{umax}$, is 0.74 N/kg (subject[4]). The mean ${}^{+90th}_{ss1}P^{\mathrm{K}}_{umaxi} \leq P_u \leq {}^{+90th}_{ss1}P^{\mathrm{K}}_{umaxi}$ for each subject[K] is indicated by a solid circle but it can be seen that these are located in the first to second quarter apart from where the ranges are of such small magnitude that the location of the mean is immaterial. Subject[0] shows the range from ${}^{+90th}_{ss1}P^{\mathrm{K}}_{umin}$ to ${}^{+90th}_{ss1}P^{\mathrm{K}}_{umax}$ with the mean for all the mean ${}^{+90th}_{ss1}\leq^{\mathrm{K}}_{umaxi} P_u \leq {}^{+90th}_{ss1}P^{\mathrm{K}}_{umaxi}$ located in the second quarter as indicated by a solid circle.

For each subject occurrences of $P_u \geq {}^{+90th}_{ss1}P^{\mathrm{K}}_{uCs}$ are shown above the range line in Figure D.22. As there are no $P_u < 0$ for $\{{}_{ss1a}\theta_0^{\mathrm{K}}\}$ the occurrences of $P_u \geq {}^{+90th}_{ss1}P^{\mathrm{K}}_{u}$ are approximately (since this is based on $\{{}_{ss1a}\theta_0^{\mathrm{K}}\}$) equal to $\frac{50}{10} \times t_i(\{{}_{ss1}\theta_0^{\mathrm{K}}\})$.

D.7. **Manoeuvre C (attempted)**

In this subsection a trailing super or sub script C in a symbol or 'all subjects[C]' indicates measures from subjects [1,. . . , 16].

D.7.1. *Manoeuvre C (a.) handle-force measures*

Examination of the handle-force measures will show that dividing the start-steady period denoted $\{{}_{ssi}\theta_0^{\mathrm{C}}\}$, at $\theta_0 = -0.102$ rad is useful and hence θ_0 measures

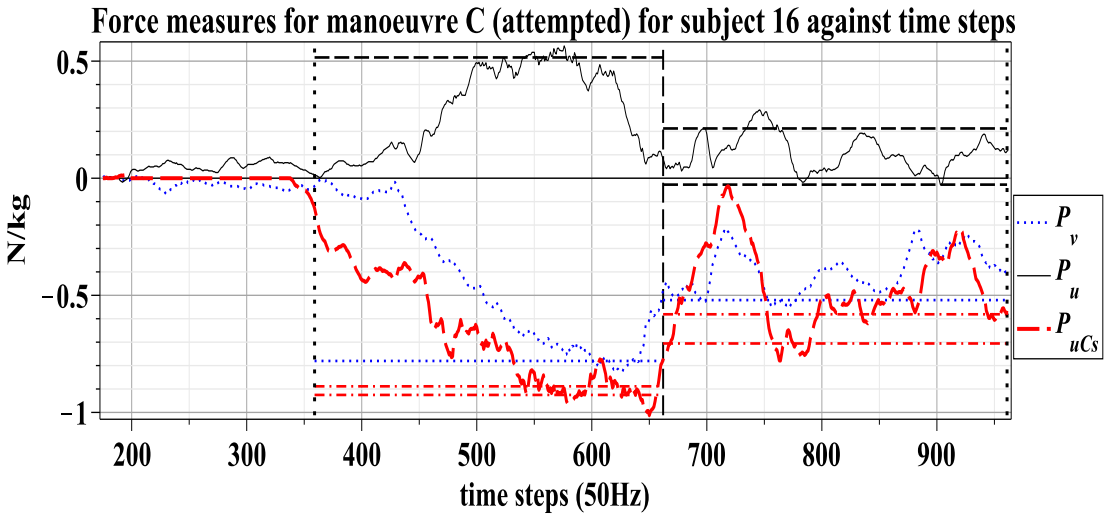

Figure D.23 – For subject[16] for manoeuvre C (a.), measures: P_v (dotted blue), P_u (thin black) and P_{uCs} (thick red dashed) in N/kg plotted against time-steps (approximately 0.02 seconds) with motion-start line (vertical black dotted: closest to left side), steady-start line (vertical black dotted: closest to right side) and $\theta_0 = -0.102$ rad line (vertical black dashed). The following percentile lines are shown for $\{{}_{ss1}\theta_0^{\mathrm{C}}\}$: ${}^{-90th}_{ss1}P^{\mathrm{C}}_{uCs}$ and ${}^{-75th}_{ss1}P^{\mathrm{C}}_{uCs}$ (horizontal red dash-dot), ${}^{+90th}_{ss1}P^{\mathrm{C}}_{u}$ (horizontal black dash) and ${}^{-90th}_{ss1}P^{\mathrm{C}}_{v}$ (horizontal blue dot): these percentile lines are also shown for $\{{}_{ss2i}\theta_0^{\mathrm{C}}\}$.

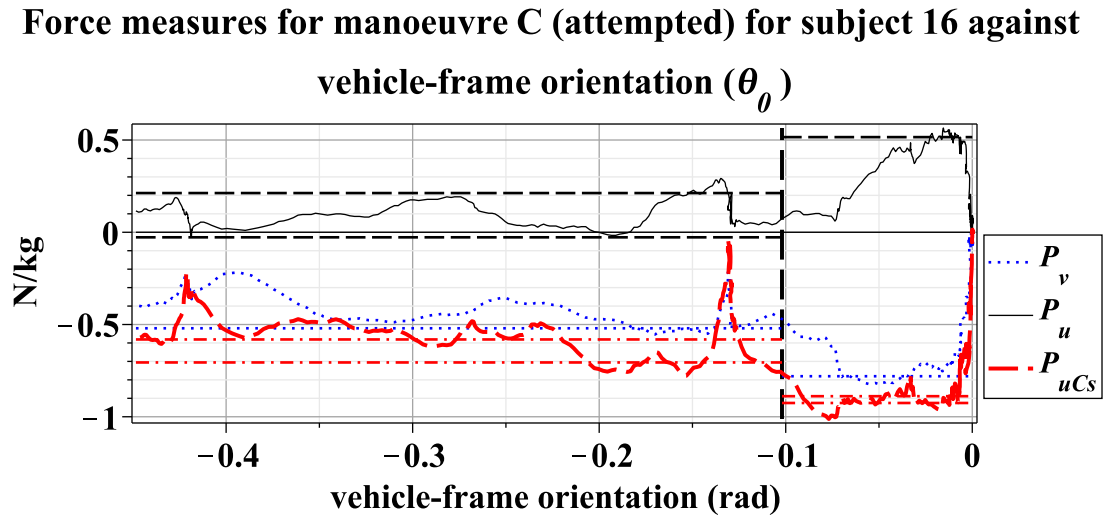

Figure D.24 – For subject[16] for manoeuvre C (a.), measures plotted against θ_0 with other details as above.

for manoeuvre C (a.) are defined for an initial period $-0.102 < \theta_0 < 0$ rad, denoted $\{{}_{ss1}\theta_0^{\mathrm{C}}\}$, and a later period $\theta_{0steadi} < \theta_0 < -0.102$ rad, denoted $\{{}_{ss2i}\theta_0^{\mathrm{C}}\}$. There is some variation between subjects immediately after motion start for a small θ_0 displacement: magnitude no greater than 0.01 rad. The range $-0.102 < \theta_0 < -0.01$ rad is denoted $\{{}_{ss1a}\theta_0^{\mathrm{C}}\}$ ($\{{}_{ss1}\theta_0^{\mathrm{C}}\}$ modified to commence at $\theta_0 = -0.01$ rad

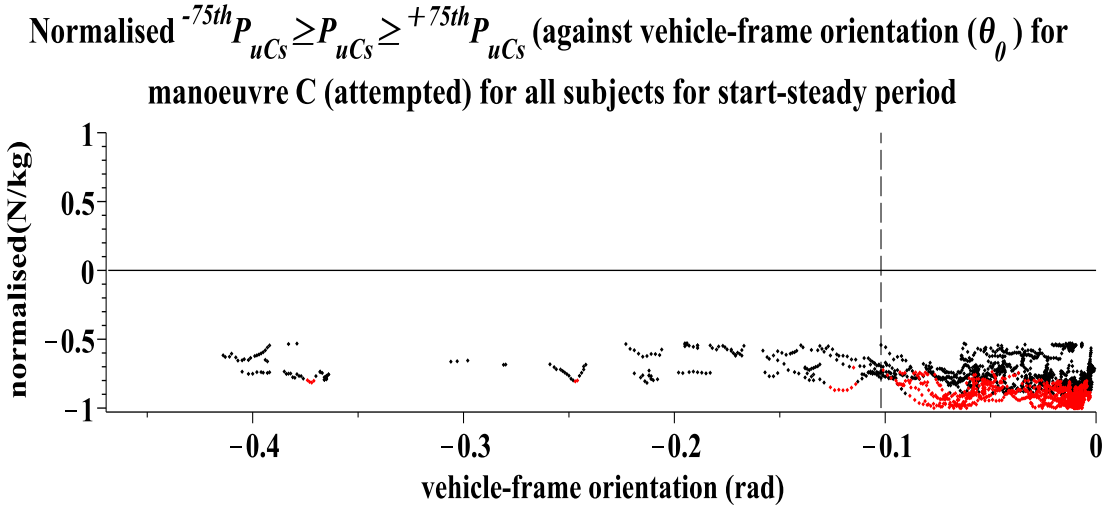

Figure D.25 – For the manoeuvre C (a.) occurrences of ${}^{-75th}_{ssi}P^{\mathrm{C}}_{uCs} \geq P_{uCs} > {}^{-90th}_{ssi}P^{\mathrm{C}}_{uCs}$ and of ${}^{+75th}_{ssi}P^{\mathrm{C}}_{uCs} \leq P_{uCs} < {}^{+90th}_{ssi}P^{\mathrm{C}}_{uCs}$ (both black markers) and, $P_{uCs} \leq {}^{-90th}_{ssi}P^{\mathrm{C}}_{uCs}$ and $P_{uCs} \geq {}^{+90th}_{ssi}P^{\mathrm{C}}_{uCs}$ (both red markers) in N/kg (normalised against each subject's maximum magnitude P_{uCs} for $\{{}_{ssi}\theta^{\mathrm{C}}_0\}$) against θ_0 for $\{{}_{ssi}\theta^{\mathrm{C}}_0\}$ for each subject: $\theta_0 = -0.102$ line indicated (dashed vertical)

rather than motion-start). Figures D.24 (page 308) and D.23 (page 308) illustrate the force measures for one subject[16] against θ_0 and time-steps respectively three features of which are common to all subjects[C] for $\{{}_{ss1a}\theta^{\mathrm{C}}_0\}$. Firstly, there are no occurrences of $P_{uCs} > 0$ for $\{{}_{ss1a}\theta^{\mathrm{C}}_0\}$. Secondly, $P_u < 0$ are negligible for $\{{}_{ss1}\theta^{\mathrm{C}}_0\}$. Thirdly, occurrences of $P_v > 0$ are negligible for $\{{}_{ss1}\theta^{\mathrm{C}}_0\}$.

D.7.2. *Manoeuvre C (a.)* P_{uCs}

The presentation begins with P_{uCs}. Figure D.25 (page 309) graphs occurrences of ${}^{-75th}_{ssi}P^{\mathrm{C}}_{uCs} \geq P_{uCs} > {}^{-90th}_{ssi}P^{\mathrm{C}}_{uCs}$ and of ${}^{+75th}_{ssi}P^{\mathrm{C}}_{uCs} \leq P_{uCs} < {}^{+90th}_{ssi}P^{\mathrm{C}}_{uCs}$ (both black markers), and $P_{uCs} \leq {}^{-90th}_{ssi}P^{\mathrm{C}}_{uCs}$ and $P_{uCs} \geq {}^{+90th}_{ssi}P^{\mathrm{C}}_{uCs}$ (both red markers) in N/kg for all subjects[C]: to assist inspection the measures for each subject are normalised against the subject's P_{uCs} peak magnitude for $\{{}_{ssi}\theta^{\mathrm{C}}_0\}$. A dashed vertical line indicates $\theta_0 = -0.102$ rad and this divides $\{{}_{ssi}\theta^{\mathrm{C}}_0\}$ into $\{{}_{ss1}\theta^{\mathrm{C}}_0\}$ and $\{{}_{ss2i}\theta^{\mathrm{C}}_0\}$ as previously defined: this line is included in the equivalent Figures which follow for P_v and P_u.

It can be seen that this division $\{{}_{ssi}\theta^{\mathrm{C}}_0\}$ places the majority of occurrences of $P_{uCs} \leq {}^{-90th}_{ssi}P^{\mathrm{C}}_{uCs}$ (red markers) in $\{{}_{ss1}\theta^{\mathrm{C}}_0\}$ and that the remaining red markers are not at peak magnitude: the subjects who produced the actions indicated by the red markers in $\{{}_{ss2i}\theta^{\mathrm{C}}_0\}$ have a peak handle-force magnitude before

$\theta_0 = -0.102$ rad. It is also evident that $\theta_0 = -0.102$ rad is located at a local trough. Thus for all subjects[C], despite any variations between subjects, the mechanism is so configured that all subjects[C] have their peak magnitude occurrences of $P_{uCs} \leq {}^{-90th}_{ssi}P^{\mathrm{C}}_{uCs}$ by $\theta_0 = -0.102$ rad. Hence division of $\{{}_{ssi}\theta^{\mathrm{C}}_0\}$ at this location relates to a mechanical property of the system for manoeuvre C (a.). It is also evident that there are no $P_{uCs} > 0$ for $\{{}_{ssi}\theta^{\mathrm{C}}_0\}$ which confirms the representativeness of Figure D.24 (page 308) in this respect.

Figure D.26 (page 311) shows measures for $P_{uCs} \leq {}^{-90th}_{ss1}P^{\mathrm{C}}_{uCs}$ (N/kg) for all subjects[C] for $\{{}_{ss1}\theta^{\mathrm{C}}_0\}$. Representative values for the largest magnitude P_{uCs} are obtained as follows. For each subject[C] the measure for the minimum magnitude $P_{uCs} \leq {}^{-90th}_{ss1}P^{\mathrm{C}}_{uCs}$, denoted ${}^{-90th}_{ss1}P^{\mathrm{C}}_{uCsmini}$, may be read and the minimum magnitude ${}^{-90th}_{ss1}P^{\mathrm{C}}_{uCsmini}$ for all subjects[C], denoted ${}^{-90th}_{ss1}P^{\mathrm{C}}_{uCsmin}$, is -0.62 N/kg (subject[15]). The maximum magnitude P_{uCs} for each subject[C], denoted ${}^{-90th}_{ss1}P^{\mathrm{C}}_{uCsmaxi}$ may also be read and the maximum magnitude ${}^{-90th}_{ss1}P^{\mathrm{C}}_{uCsmaxi}$, denoted ${}^{-90th}_{ss1}P^{\mathrm{C}}_{uCsmax}$, is -1.29 N/kg (subject[7]). The mean ${}^{-90th}_{ss1}P^{\mathrm{C}}_{uCsmini} \geq P_{uCs} \geq {}^{-90th}_{ss1}P^{\mathrm{C}}_{uCsmaxi}$ for each subject[C] are indicated by a solid circle and it can be seen that these means, ignoring subjects where the range magnitude is relatively small, are located in the second to third quarters of the intra-subject range. Subject[0] shows the range of ${}^{-90th}_{ss1}P^{\mathrm{C}}_{uCsmin}$ to ${}^{-90th}_{ss1}P^{\mathrm{C}}_{uCsmax}$ and the mean of all the mean ${}^{-90th}_{ss1}P^{\mathrm{C}}_{uCsmini} \geq P_{uCs} \geq {}^{-90th}_{ss1}P^{\mathrm{C}}_{uCsmaxi}$ indicated by a solid circle can be seen to be located approximately centrally in the inter-subject ranges.

For each subject occurrences of $P_{uCs} \leq {}^{-90th}_{ss1}P^{\mathrm{C}}_{uCs}$ are shown above the range line in Figure D.26. An examination of the data (results not presented) shows that for all subjects[C] there are only four occurrences of $P_{uCs} = 0$ (integer) so the occurrences of $P_{uCs} \leq {}^{-90th}_{ss1}P^{\mathrm{C}}_{uCs}$ are almost exactly equal to $\frac{50}{10} \times t_i(\{{}_{ss1a}\theta^{\mathrm{C}}_0\})$.

It can also be seen from Figure D.26 (page 311) that the range magnitude of 0.67 N/kg, ${}^{-90th}_{ss1}P^{\mathrm{C}}_{uCsmax} - {}^{-90th}_{ss1}P^{\mathrm{C}}_{uCsmin}$, arises from inter-subject variation (subject[15] compared with subject[7]) and is not the result of the ${}^{-90th}_{ss1}P^{\mathrm{C}}_{uCsmaxi} - {}^{-90th}_{ss1}P^{\mathrm{C}}_{uCsmini}$ magnitude of a specific subject. There are therefore substantial differences between subjects for the largest magnitude P_{uCs}. However, the inequality ${}^{-90th}_{ss1}P^{\mathrm{C}}_{uCsmini} \geq P_{uCs} \geq {}^{-90th}_{ss1}P^{\mathrm{C}}_{uCsmaxi}$ provides a representative range for each subject. In addition the inequality ${}^{-90th}_{ss1}P^{\mathrm{C}}_{uCsmin} \geq P_{uCs} \geq {}^{-90th}_{ss1}P^{\mathrm{C}}_{uCsmax}$ provides a

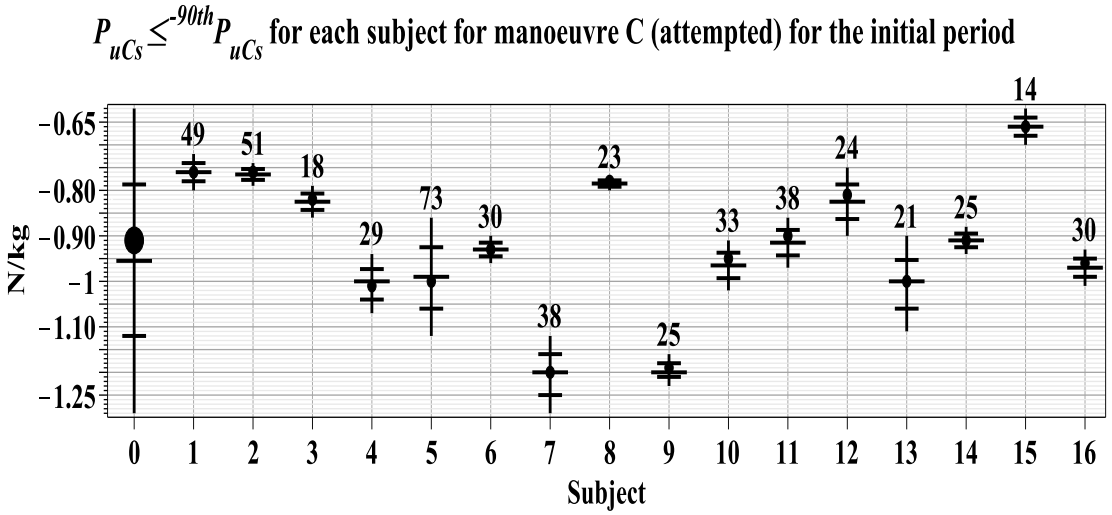

Figure D.26 – Shows for each subject[C] (i) for $\{{}_{ss1}\theta_0^{\mathrm{C}}\}$ in N/kg: a vertical line indicating the minimum magnitude ${}^{-90th}_{ss1}P^{\mathrm{C}}_{uCsmini}$ to the maximum magnitude ${}^{-90th}_{ss1}P^{\mathrm{C}}_{uCsmaxi}$, a solid circle indicating the mean ${}^{-90th}_{ss1}P^{\mathrm{C}}_{PuCsmini} \geq P_{uCs} \geq {}^{-90th}_{ss1}P^{\mathrm{C}}_{PuCsmaxi}$, the quarter divisions of the range (horizontal lines), the number of occurrences of $P_{uCs} \leq {}^{-90th}_{ss1}P^{\mathrm{C}}_{uCs}$. Subject[0] shows these measures for all subjects[C] with a solid circle indicating the mean of all the mean ${}^{-90th}_{ss1}P^{\mathrm{C}}_{PuCsmini} \geq P_{uCs} \geq {}^{-90th}_{ss1}P^{\mathrm{C}}_{PuCsmaxi}$.

representative range for all subjects[C].

D.7.3. *Manoeuvre C (a.) P_u*

Figure D.27 (page 312) shows occurrences of ${}^{-75th}_{ssi}P^{\mathrm{C}}_{u} \geq P_u > {}^{-90th}_{ssi}P^{\mathrm{C}}_{u}$ and of ${}^{+75th}_{ssi}P^{\mathrm{C}}_{u} \leq P_u < {}^{+90th}_{ssi}P^{\mathrm{C}}_{u}$ (both black markers) and, of $P_u \leq {}^{-90th}_{ssi}P^{\mathrm{C}}_{u}$ and of $P_u \geq {}^{+90th}_{ssi}P^{\mathrm{C}}_{u}$ (both red markers): to aid inspection the measures for each subject are normalised against the subject's P_u peak magnitude for $\{{}_{ss1a}\theta_0^{\mathrm{C}}\}$: these are the occurrences for all subjects[C]. As Figure D.27 shows normalised P_u it is evident that the magnitudes of P_u<0 are relatively small and occurrences relatively few compared with $P_u > 0$. Figure D.27 also shows that $\{{}_{ss1}\theta_0^{\mathrm{C}}\}$ includes the majority of $P_u \geq {}^{+75th}_{ssi}P^{\mathrm{C}}_{u}$. An examination of the data (results not reported) indicates that there are negligible occurrences of $P_u < 0$ for $\{{}_{ss1a}\theta_0^{\mathrm{C}}\}$ and this confirms the representativeness of Figure D.24 (page 308) in this respect.

Figure D.28 (page 313) shows measures for $P_u \geq {}^{+90th}_{ss1}P^{\mathrm{C}}_{u}$ (N/kg) for all subjects[C] for $\{{}_{ss1}\theta_0^{\mathrm{C}}\}$. Representative values for the largest $P_u > 0$ are obtained as follows. For each subject[C] the measure for the minimum ${}^{+90th}_{ss1}P^{\mathrm{C}}_{u}$, denoted ${}^{+90th}_{ss1}P^{\mathrm{C}}_{umini}$, can be read and the minimum ${}^{+90th}_{ss1}P^{\mathrm{C}}_{umini}$ for all subjects[C],

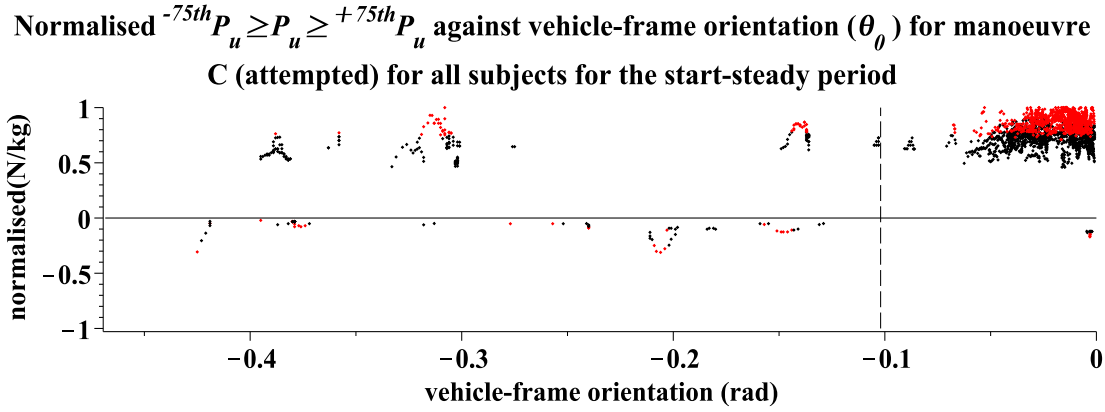

Figure D.27 – For the manoeuvre C (a.) occurrences of ${}^{-75th}_{ssi}P^{\mathrm{C}}_{u} \geq P_u > {}^{-90th}_{ssi}P^{\mathrm{C}}_{u}$ and of ${}^{+75th}_{ssi}P^{\mathrm{C}}_{u} \leq P_u < {}^{+90th}_{ssi}P^{\mathrm{C}}_{u}$ (both black markers) and, of $P_u \leq {}^{-90th}_{ssi}P^{\mathrm{C}}_{u}$ and of $P_u \geq {}^{+90th}_{ssi}P^{\mathrm{C}}_{u}$ (both red markers) in N/kg (normalised against each subject's maximum magnitude P_u for $\{{}_{ss1}\theta^{\mathrm{C}}_0\}$) against θ_0 for $\{{}_{ssi}\theta^{\mathrm{C}}_0\}$ for each subject: $\theta_0 = -0.102$ line indicated (dashed vertical)

denoted ${}^{+90th}_{ss1}P^{\mathrm{C}}_{umin}$, is 0.22 N/kg (subjects[9]). The maximum P_u for each subject[C], denoted ${}^{+90th}_{ss1}P^{\mathrm{C}}_{umaxi}$ can also be read and the maximum ${}^{+90th}_{ss1}P^{\mathrm{C}}_{umaxi}$ denoted ${}^{+90th}_{ss1}P^{\mathrm{C}}_{umax}$ is 0.63 N/kg (subject[5]). The mean ${}^{+90th}_{ss1}P^{\mathrm{C}}_{umini} \leq P_u \leq {}^{+90th}_{ss1}P^{\mathrm{C}}_{umaxi}$ for each subject[C] is indicated by a solid circle and it can be seen that theses are located from the range minimum to the central location. Subject[0] shows the range from ${}^{+90th}_{ss1}P^{\mathrm{C}}_{umin}$ to ${}^{+90th}_{ss1}P^{\mathrm{C}}_{umax}$ with the mean for all the mean ${}^{+90th}_{ss1}P^{\mathrm{C}}_{umini} \leq P_u \leq {}^{+90th}_{ss1}P^{\mathrm{C}}_{umaxi}$ located approximately centrally as indicated by a solid circle.

For each subject occurrences of $P_u \geq {}^{+90th}_{ss1}P^{\mathrm{C}}_{u}$ are shown above the range line in Figure D.28: these are approximately equal to $\frac{50}{10} \times t_i\{{}_{ss1}\theta^{\mathrm{C}}_0\}$).

It can also be seen from Figure D.28 (page 313) that the range magnitude of 0.41 N/kg, i.e. ${}^{+90th}_{ss1}P^{\mathrm{C}}_{umax} - {}^{+90th}_{ss1}P^{\mathrm{C}}_{umin}$ arises from inter-subject variation (subjects[9] compared with subject[5]) and is not the result of the ${}^{+90th}_{ss1}P^{\mathrm{C}}_{umaxi} - {}^{+90th}_{ss1}P^{\mathrm{C}}_{umini}$ of a specific subject. While there are differences between subjects for the largest $P_u > {}^{+90th}_{ss1}P^{\mathrm{C}}_{u}$ the intra-subject range magnitude is relatively small. The inequality ${}^{+90th}_{ss1}P^{\mathrm{C}}_{umini} \leq P_u \leq {}^{+90th}_{ss1}P^{\mathrm{C}}_{umaxi}$ provides a representative range for each subject[C]. Additionally the inequality ${}^{+90th}_{ss1}P^{\mathrm{C}}_{umin} \leq P_u \leq {}^{+90th}_{ss1}P^{\mathrm{C}}_{umax}$ (subject[0]) provides a representative range for all subjects[C] for the largest $P_u > 0$ for $\{{}_{ss1}\theta^{\mathrm{C}}_0\}$.

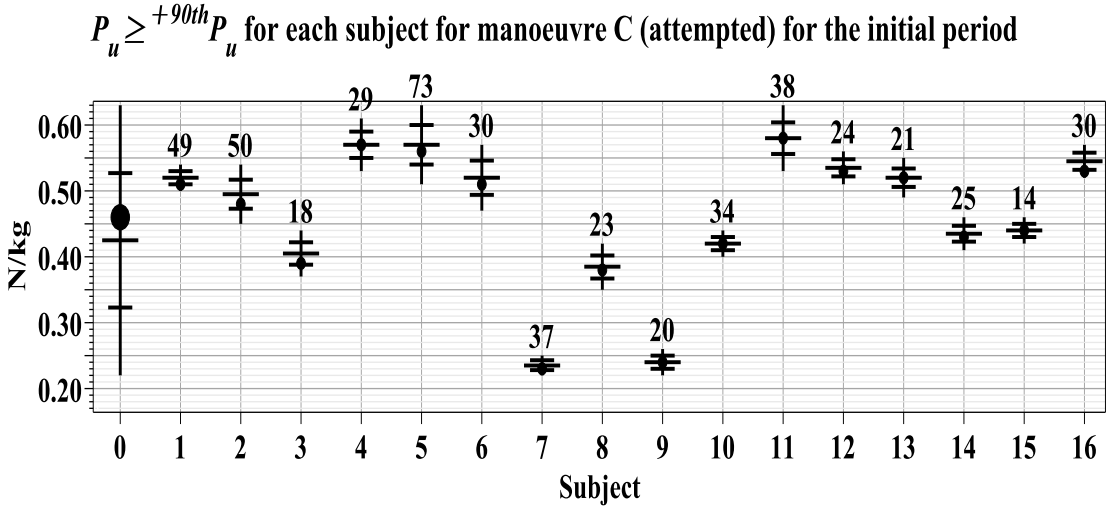

Figure D.28 – Shows for each subject[C] (i) for $\{{}_{ss1}\theta_0^{\mathrm{C}}\}$ in N/kg: a vertical line indicating the minimum magnitude measure ${}^{+90th}_{ss1}P^{\mathrm{C}}_{umini}$ to the maximum magnitude measure ${}^{+90th}_{ss1}P^{\mathrm{C}}_{umaxi}$, a solid circle indicating the mean ${}^{+90th}_{ss1}P^{\mathrm{C}}_{umini} \leq P_u \leq {}^{+90th}_{ss1}P^{\mathrm{C}}_{umaxi}$, the quarter divisions of the range (horizontal lines) and the number of occurrences of $P_u \geq {}^{+90th}_{ss1}P^{\mathrm{C}}_{u}$ shown above the range line. Subject[0] shows this data for all subjects[C] with a solid circle indicating the mean of all the mean ${}^{+90th}_{ss1}P^{\mathrm{C}}_{umini} \leq P_u \leq {}^{+90th}_{ss1}P^{\mathrm{C}}_{umaxi}$.

D.7.4. *Manoeuvre C (a.) P_v*

Figure D.29 (page 314) shows occurrences of ${}^{-75th}_{ssi}P^{\mathrm{C}}_{v} \geq P_v > {}^{-90th}_{ssi}P^{\mathrm{C}}_{v}$ and of ${}^{+75th}_{ssi}P^{\mathrm{C}}_{v} \leq P_v < {}^{+90th}_{ssi}P^{\mathrm{C}}_{v}$ (both black markers) and, of $P_v \leq {}^{-90th}_{ssi}P^{\mathrm{C}}_{v}$ and of $P_v \geq {}^{+90th}_{ssi}P^{\mathrm{C}}_{v}$ (both red markers): to aid inspection the measures for each subject are normalised against the subject's P_v peak magnitude for $\{{}_{ssi}\theta_0^{\mathrm{C}}\}$: these are the occurrences for all subjects[C].

The peak magnitudes for $P_v < 0$ occur in $\{{}_{ss1}\theta_0^{\mathrm{C}}\}$ for all subjects[C]. As P_v is normalised in Figure D.29 it is evident that the occurrences of $P_v > 0$ are few and the peak magnitudes of $P_v > 0$ are small in comparison with those for $P_v < 0$. An examination of the data (results not reported) indicates that there are no occurrences of $P_v > 0$ for $\{{}_{ss1a}\theta_0^{\mathrm{C}}\}$ and this confirms the representativeness of Figure D.24 (page 308) in this respect.

Figure D.30 (page 315) shows measures for $P_v \leq {}^{-90th}_{ss1}P^{\mathrm{C}}_{v}$ (N/kg) for each subject [C] and for all subjects[C] for $\{{}_{ss1}\theta_0^{\mathrm{C}}\}$. Representative values for the largest magnitude P_v are obtained as follows. For each subject[C] the measure for the minimum magnitude $P_v \leq {}^{-90th}_{ss1}P^{\mathrm{C}}_{v}$, denoted ${}^{-90th}_{ss1}P^{\mathrm{C}}_{vmini}$ may be read and the minimum ${}^{-90th}_{ss1}P^{\mathrm{C}}_{vmini}$ for all subjects[C], denoted ${}^{-90th}_{ss1}P^{\mathrm{C}}_{vmin}$, is -0.48 N/kg (sub-

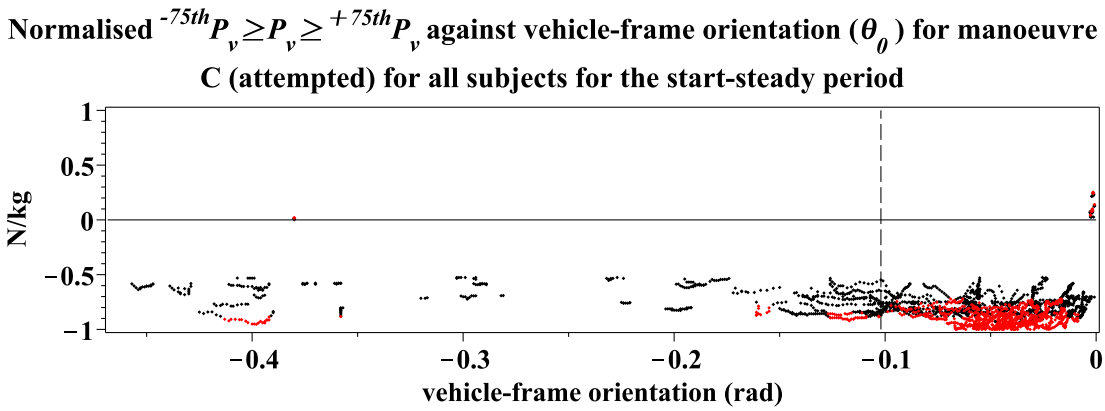

Figure D.29 – For the manoeuvre C (a.) occurrences of ${}^{-75th}_{ssi}P^{\mathrm{C}}_{v} \geq P_v > {}^{-90th}_{ssi}P^{\mathrm{C}}_{v}$ and of ${}^{+75th}_{ssi}P^{\mathrm{C}}_{v} \leq P_v < {}^{+90th}_{ssi}P^{\mathrm{C}}_{v}$ (both black markers) and, of $P_v \leq {}^{-90th}_{ssi}P^{\mathrm{C}}_{v}$ and of $P_v \geq {}^{+90th}_{ssi}P^{\mathrm{C}}_{v}$ (both red markers) in N/kg (normalised against each subject's maximum magnitude P_v for $\{{}_{ssi}\theta^{\mathrm{C}}_0\}$) against θ_0 for $\{{}_{ssi}\theta^{\mathrm{C}}_0\}$ for each subject: $\theta_0 = -0.102$ line indicated (dashed vertical).

ject[9]). The maximum magnitude P_v for each subject[C], denoted ${}^{-90th}_{ss1}P^{\mathrm{C}}_{vmaxi}$, may also be read and the maximum ${}^{-90th}_{ss1}P^{\mathrm{C}}_{vmaxi}$ denoted ${}^{-90th}_{ss1}P^{\mathrm{C}}_{vmax}$, is −0.89 N/kg (subject[5]). The mean ${}^{-90th}_{ss1}P^{\mathrm{C}}_{vmaxi} \geq P_v \geq {}^{-90th}_{ss1}P^{\mathrm{C}}_{vmaxi}$ for each subject[C] is indicated by a solid circle: it can be seen that these means are located from the second quarter to the centre of the intra-subject range. Subject[0] shows the range from ${}^{-90th}_{ss1}P^{\mathrm{C}}_{vmin}$ to ${}^{-90th}_{ss1}P^{\mathrm{C}}_{vmax}$ and the mean of all the mean ${}^{-90th}_{ss1}P^{\mathrm{C}}_{vmaxi} \geq P_v \geq {}^{-90th}_{ss1}P^{\mathrm{C}}_{vmaxi}$ is indicated by a solid circle and this is located approximately centrally in the inter-subject range.

Occurrences of $P_v \leq {}^{-90th}_{ss1}P^{\mathrm{C}}_{v}$ are approximately equal to $\frac{50}{10} \times t_i$ ($\{{}_{ss1}\theta^{\mathrm{C}}_0\}$).

D.7.5. *Manoeuvre C (a.) the $P_v - P_{uCs}$ plane*

This final section relating to manoeuvre C (a.) uses the inequalities, as previously defined, to define a cuboid boundary for the largest magnitude measures for each and all subjects. For each of subjects[1,..., 16] the following inequalities define the cuboid boundaries:

${}^{-90th}_{ss1}P^{\mathrm{C}}_{uCsmini} \geq P_{uCs} \geq {}^{-90th}_{ss1}P^{\mathrm{C}}_{uCsmaxi}$ (page 309),

${}^{-90th}_{ss1}P^{\mathrm{C}}_{vmini} \geq P_v \geq {}^{-90th}_{ss1}P^{\mathrm{C}}_{vmaxi}$ (page 313) and

${}^{+90th}_{ss1}P^{\mathrm{C}}_{umini} \leq P_u \leq {}^{+90th}_{ss1}P^{\mathrm{C}}_{umaxi}$ (page 311)

and these three inequalities are denoted ${}^{large}_{ss1}\mathbf{P}^{\mathrm{C}}_{i}$.

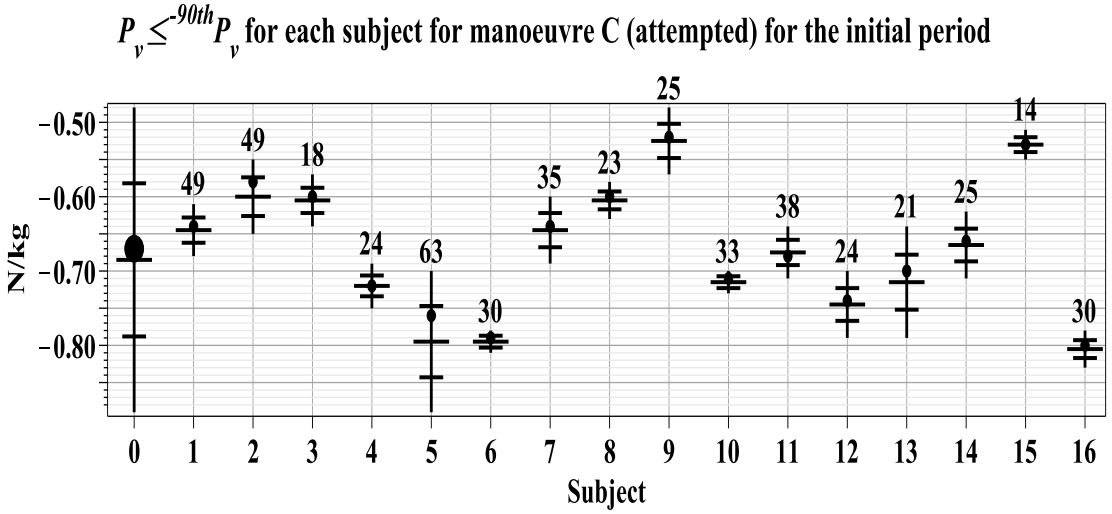

Figure D.30 – Shows for each subject[C] (i) for $\{{}_{ss1}\theta_0^{\mathrm{C}}\}$ in N/kg: a vertical line indicating the minimum magnitude ${}^{-90th}_{ss1}P^{\mathrm{C}}_{vmini}$ to the maximum magnitude ${}^{-90th}_{ss1}P^{\mathrm{C}}_{vmaxi}$, a solid circle indicating the mean ${}^{-90th}_{ss1}P^{\mathrm{C}}_{vmaxi} \geq P_v \geq {}^{-90th}_{ss1}P^{\mathrm{C}}_{vmaxi}$, the quarter divisions of the range (horizontal lines) and the number of occurrences of $P_v \leq {}^{-90th}_{ss1}P^{\mathrm{C}}_{v}$. Subject[0] shows these measures for all subjects[C] with a solid circle indicating the mean of all the mean ${}^{-90th}_{ss1}P^{\mathrm{C}}_{vmaxi} \geq P_v \geq {}^{-90th}_{ss1}P^{\mathrm{C}}_{vmaxi}$.

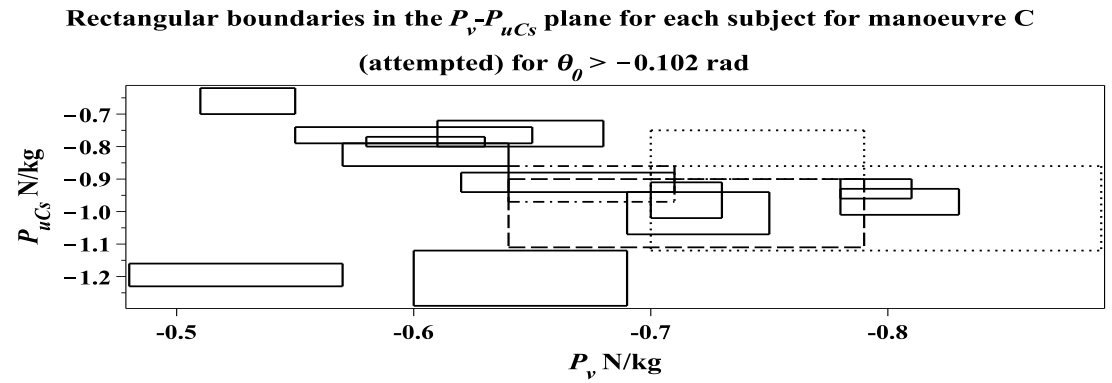

Figure D.31 – Rectangles formed with vertices of coordinates $[{}^{-90th}_{ss1}P^{\mathrm{C}}_{vmini}, {}^{-90th}_{ss1}P^{\mathrm{C}}_{uCsmini}]$, $[{}^{-90th}_{ss1}P^{\mathrm{C}}_{vmaxi}, {}^{-90th}_{ss1}P^{\mathrm{C}}_{uCsmini}]$, $[{}^{-90th}_{ss1}P^{\mathrm{C}}_{vmaxi}, {}^{-90th}_{ss1}P^{\mathrm{C}}_{uCsmaxi},]$, and $[{}^{-90th}_{ss1}P^{\mathrm{C}}_{vmini}, {}^{-90th}_{ss1}P^{\mathrm{C}}_{uCsmaxi}]$ for all subjects[C], i.e. n=16. To assist inspection some enclosures are non solid lines.

A graphical representation of ${}^{large}_{ss1}\mathbf{P}^{\mathrm{C}}_i$ in the $P_v - P_{uCs}$ plane is shown in Figure D.31 (page 315): the construction is as described in Section 6.4.4 (page 149) for manoeuvre F (a.) and where required dotted lines are used to assist inspection.

Three inequalities define the cuboid boundaries which enclose the measures for all, rather than each of, subjects[C] and removal of the i subscript from the

above definitions provides this. and these there inequalities are denoted ${}^{large}_{ss1}\mathbf{P}^{\mathrm{C}}$. In conclusion ${}^{large}_{ss1}\mathbf{P}^{\mathrm{C}}$ provides a useful representation of the boundaries of the largest handle-forces for all subjects[C] for manoeuvre C (a.): the numerical values are:

$-0.48 \geq P_v \geq -0.89$ (N/kg),

$-0.62 \geq P_{uCs} \geq -1.29$ (N/kg) and

$0.22 \leq P_u \leq 0.63$ (N/kg).

D.8. **Manoeuvre I (attempted)**

In this section a trailing super or sub script I in a symbol or 'all subjects[I]' indicates measures from subjects [1,..., 9, 11,..., 16]: subject[10] did not participate (see Section 6.2).

D.8.1. *Manoeuvre I (a.) handle-force measures*

Examination of the handle-force measures will show that dividing the start-steady period, denoted $\{{}_{ssi}\theta_0^{\mathrm{I}}\}$, at $\theta_0 = -0.093$ rad is useful and hence θ_0 measures for manoeuvre I (a.) are defined for an initial period $-0.093 < \theta_0 < 0$ rad, denoted $\{{}_{ss1}\theta_0^{\mathrm{I}}\}$, and a later period $\theta_{0steadi} < \theta_0 < -0.093$ rad, denoted $\{{}_{ss2i}\theta_0^{\mathrm{I}}\}$. There is some variation between subjects immediately after motion start for a small θ_0 displacement: magnitude no greater than 0.01 rad. The range $-0.084 < \theta_0 < -0.01$ rad is denoted $\{{}_{ss1a}\theta_0^{\mathrm{I}}\}$ ($\{{}_{ss1}\theta_0^{\mathrm{I}}\}$ modified to commence at $\theta_0 = -0.01$ rad rather than motion-start). For the modified initial period $\{{}_{ss1a}\theta_0^{\mathrm{I}}\}$ Figure D.33 (page 317) for subject[9] illustrates three features which are common to all subjects[I]. Firstly, occurrences and magnitudes of $P_{uCs} > 0$ are negligible. Secondly, $P_u > 0$ are negligible. Thirdly, occurrences of $P_v > 0$ are negligible.

D.8.2. *Manoeuvre I (a.) P_{uCs}*

The presentation begins with P_{uCs}. Figure D.34 (page 318) shows occurrences of ${}^{-75th}_{ssi}P^{\mathrm{I}}_{uCs} \geq P_{uCs} > {}^{-90th}_{ssi}P^{\mathrm{I}}_{uCs}$ and of ${}^{+75th}_{ssi}P^{\mathrm{I}}_{uCs} \leq P_{uCs} < {}^{+90th}_{ssi}P^{\mathrm{I}}_{uCs}$ (both black markers), and $P_{uCs} \leq {}^{-90th}_{ssi}P^{\mathrm{I}}_{uCs}$ and $P_{uCs} \geq {}^{+90th}_{ssi}P^{\mathrm{I}}_{uCs}$ (both red markers) (N/kg) for all subjects[I] against θ_0: to assist inspection the measures for each subject are normalised against the subject's P_{uCs} peak magnitude for $\{{}_{ssi}\theta_0^{\mathrm{I}}\}$. A dashed vertical line indicates $\theta_0 = -0.093$ rad and this divides the start-steady period into $\{{}_{ss1}\theta_0^{\mathrm{I}}\}$

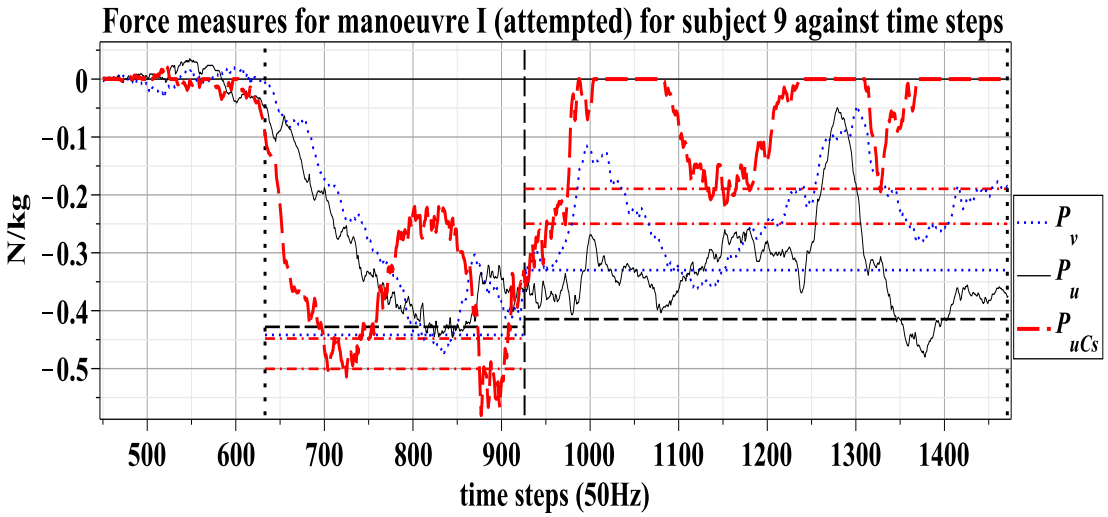

Figure D.32 – For subject[9] for manoeuvre I (a.), measures: P_v (dotted blue), P_u (thin black) and P_{uCs} (thick red dashed) in N/kg plotted against time-steps (approximately 0.02 seconds) with motion-start line (vertical black dotted: closest to left side), steady-start line (vertical black dotted: Closest to right side) and $\theta_0 = -0.093$ rad line (vertical black dashed). The following percentile lines are shown for $\{_{ss1}\theta_0^{\mathrm{I}}\}$: ${}^{-90th}_{ss1}P^{\mathrm{I}}_{uCs}$ and ${}^{-75th}_{ss1}P^{\mathrm{I}}_{uCs}$ (horizontal red dash-dot), ${}^{-90th}_{ss1}P^{\mathrm{I}}_{u}$ (horizontal black dash) and ${}^{-90th}_{ss1}P^{\mathrm{I}}_{v}$ (horizontal blue dot): these percentile lines are also shown for $\{_{ss2i}\theta_0^{\mathrm{I}}\}$.

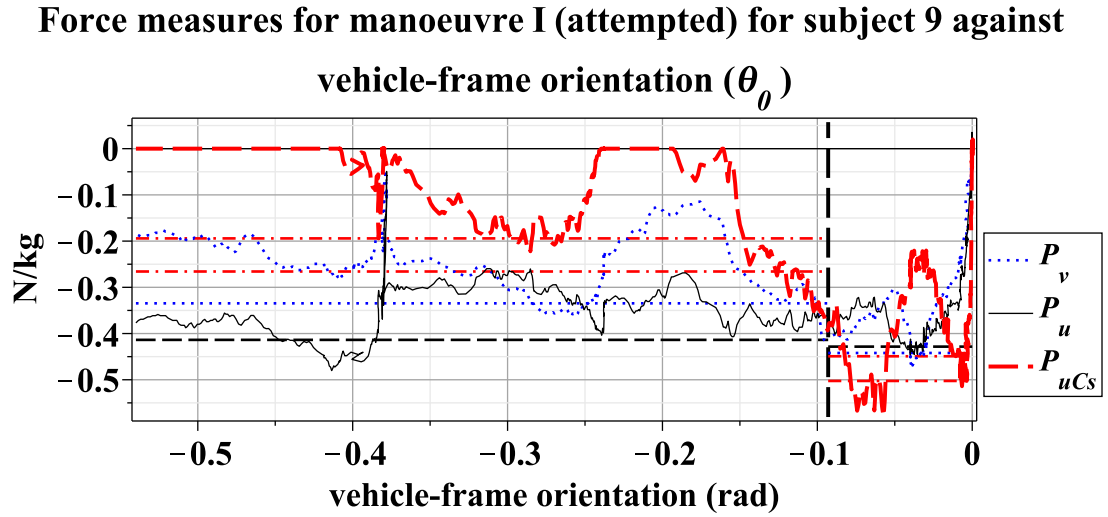

Figure D.33 – For subject[9] for manoeuvre I (a.), measures plotted against θ_0 with other details as above.

and $\{_{ss2i}\theta_0^{\mathrm{I}}\}$ as previously defined: this line is included in the equivalent graphs which follow for P_v and P_u.

This division of $\{_{ssi}\theta_0^{\mathrm{I}}\}$ places the majority of the occurrences of $P_{uCs} \leq {}^{-90th}_{ssi}P^{\mathrm{I}}_{uCs}$ (red markers) in $\{_{ss1}\theta_0^{\mathrm{I}}\}$ without further occurrences for 0.15 rad. Exam-

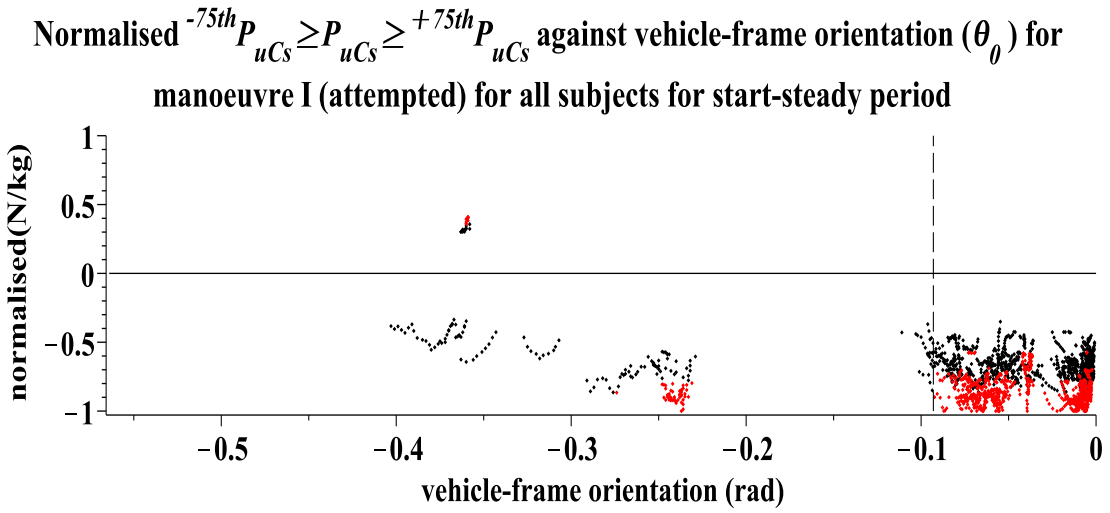

Figure D.34 – For the manoeuvre I (a.) occurrences of ${}^{-75th}_{ssi}P^{\mathrm{I}}_{uCs} \geq P_{uCs} > {}^{-90th}_{ssi}P^{\mathrm{I}}_{uCs}$ and of ${}^{+75th}_{ssi}P^{\mathrm{I}}_{uCs} \leq P_{uCs} < {}^{+90th}_{ssi}P^{\mathrm{I}}_{uCs}$ (both black markers) and, $P_{uCs} \leq {}^{-90th}_{ssi}P^{\mathrm{I}}_{uCs}$ and $P_{uCs} \geq {}^{+90th}_{ssi}P^{\mathrm{I}}_{uCs}$ (both red markers) in N/kg (normalised against each subject's maximum magnitude P_{uCs} for the start-steady period) against θ_0 for $\{{}_{ssi}\theta^{\mathrm{I}}_0\}$ each subject: $\theta_0 = -0.093$ line indicated (dashed vertical)

ination of the data (results not reported) also shows that all subjects contribute to the $\{{}_{ss1}\theta^{\mathrm{I}}_0\}$ occurrences. Thus for all subjects[I], despite any variations, the mechanism is so configured that all subjects[I] have their first occurrences of $P_{uCs} \leq {}^{-90th}_{ssi}P^{C}_{uCs}$ by $\theta_0 = -0.093$ rad. Hence division of $\{{}_{ssi}\theta^{\mathrm{I}}_0\}$ at this location relates to a mechanical property of the system for manoeuvre I (a.). An examination of the data (results not presented) indicates that there are no $P_{uCs} > 0$ for $\{{}_{ss1}\theta^{\mathrm{I}}_0\}$ and this confirms the representativeness of Figure D.33 (page 317) in this respect.

Figure D.35 (page 319) shows measures for $P_{uCs} \leq {}^{-90th}_{ss1}P^{\mathrm{I}}_{uCs}$ (N/kg) for all subjects[I] for $\{{}_{ss1}\theta^{\mathrm{I}}_0\}$. Representative values for the largest magnitude P_{uCs} are obtained as follows. For each subject[I] the measure for the minimum magnitude $P_{uCs} \leq {}^{-90th}_{ss1}P^{\mathrm{I}}_{uCs}$, denoted ${}^{-90th}_{ss1}P^{\mathrm{I}}_{uCsmini}$ may be read and the minimum magnitude ${}^{-90th}_{ss1}P^{\mathrm{I}}_{uCsmini}$ for all subjects[I], denoted ${}^{-90th}_{ss1}P^{\mathrm{I}}_{uCsmin}$, is -0.31 N/kg (subject[15]). The maximum magnitude P_{uCs} for each subject[I], denoted ${}^{-90th}_{ss1}P^{\mathrm{I}}_{uCsmaxi}$, may also be read and the maximum magnitude ${}^{-90th}_{ss1}P^{\mathrm{I}}_{uCsmaxi}$, denoted ${}^{-90th}_{ss1}P^{\mathrm{I}}_{uCsmax}$, is -0.99 N/kg (subject[14]). The mean ${}^{-90th}_{ss1}P^{\mathrm{I}}_{uCsmini} \geq P_{uCs} \geq {}^{-90th}_{ss1}P^{\mathrm{I}}_{uCsmaxi}$ for each subject[I] are indicated by a solid circle and it can

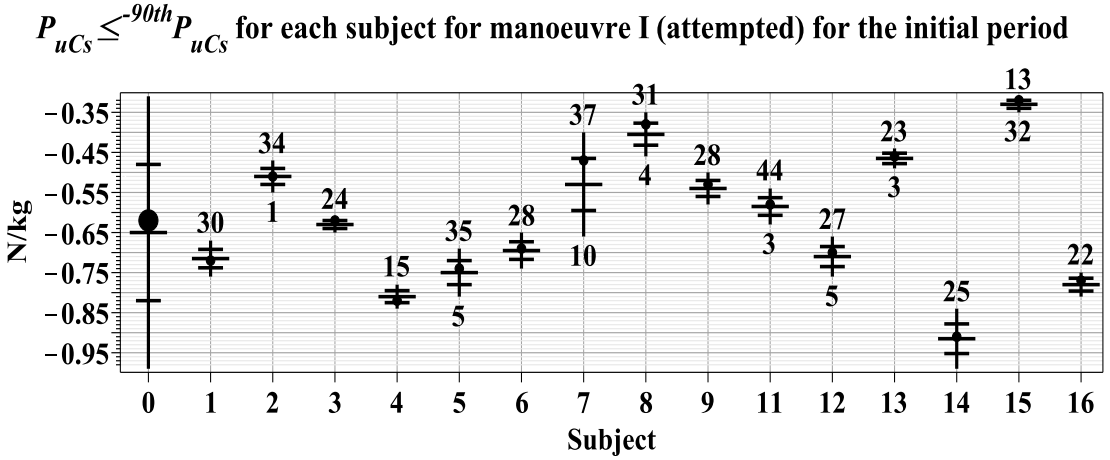

Figure D.35 – Shows for each subject[I] (i) for $\{{}_{ss1}\theta^{\mathrm{I}}_0\}$ in N/kg: a vertical line indicating the minimum magnitude measure ${}^{-90th}_{ss1}P^{\mathrm{I}}_{uCsmini}$ to the maximum magnitude measure ${}^{-90th}_{ss1}P^{\mathrm{I}}_{uCsmaxi}$, a solid circle indicating the mean ${}^{-90th}_{ss1}P^{\mathrm{I}}_{PuCsmini} \geq P_{uCs} \geq {}^{-90th}_{ss1}P^{\mathrm{I}}_{PuCsmaxi}$, the quarter divisions of the range (horizontal lines), the number of occurrences of $P_{uCs} \leq {}^{-90th}_{ss1}P^{\mathrm{I}}_{uCs}$ shown above the range line and the percentage of occurrences of $P_{uCs} = 0$ (integer) for $\{{}_{ss1}\theta^{\mathrm{I}}_0\}$ shown below the range line. Subject[0] shows this data for all subjects[I] with a solid circle indicating the mean of all the mean ${}^{-90th}_{ss1}P^{\mathrm{I}}_{PuCsmini} \geq P_{uCs} \geq {}^{-90th}_{ss1}P^{\mathrm{I}}_{PuCsmaxi}$.

be seen that these means, ignoring subjects where the range magnitude is relatively small, are located in the first to third quarters of the intra-subject range. Subject[0] shows the range of ${}^{-90th}_{ss1}P^{\mathrm{I}}_{uCsmin}$ to ${}^{-90th}_{ss1}P^{\mathrm{I}}_{uCsmax}$ and the mean of all the mean ${}^{-90th}_{ss1}P^{\mathrm{I}}_{uCsmini} \geq P_{uCs} \geq {}^{-90th}_{ss1}P^{\mathrm{I}}_{uCsmaxi}$ indicated by a solid circle can be seen to be located approximately centrally in the inter-subject ranges.

For each subject occurrences of $P_{uCs} \leq {}^{-90th}_{ss1}P^{\mathrm{I}}_{uCs}$ are shown above the range line in Figure D.35 and for those subjects with occurrences of $P_{uCs} = 0$ (integer) the percentage of occurrences for $\{{}_{ssi}\theta^{\mathrm{I}}_0\}$ is shown below the range line. Substantial variation is evident: subjects[1, 3, 4, 6, 7, 14, 16] have no occurrences of $P_{uCs} = 0$ (integer) where as subject[15] has 32% $P_{uCs} = 0$ (integer) occurrences. In other words the attempt at manoeuvre[I] by some subjects, to some extent, reduces the occurrences of the couple action. The occurrences of $P_{uCs} \leq {}^{-90th}_{ss1}P^{\mathrm{I}}_{uCs}$ are therefore not a linear function of $t_i(\{{}_{ssi}\theta^{\mathrm{I}}_0\})$ for subjects[2, 5, 9, 8, 11, 12, 13, 15].

D.8.3. *Manoeuvre I (a.)* P_u

Figure D.36 (page 320) shows occurrences of ${}^{-75th}_{ssi}P^{\mathrm{I}}_u \geq P_u > {}^{-90th}_{ssi}P^{\mathrm{I}}_u$ and of ${}^{+75th}_{ssi}P^{\mathrm{I}}_u \leq P_u < {}^{+90th}_{ssi}P^{\mathrm{I}}_u$ (both black markers) and, of $P_u \leq {}^{-90th}_{ssi}P^{\mathrm{I}}_u$ and of $P_u \geq$

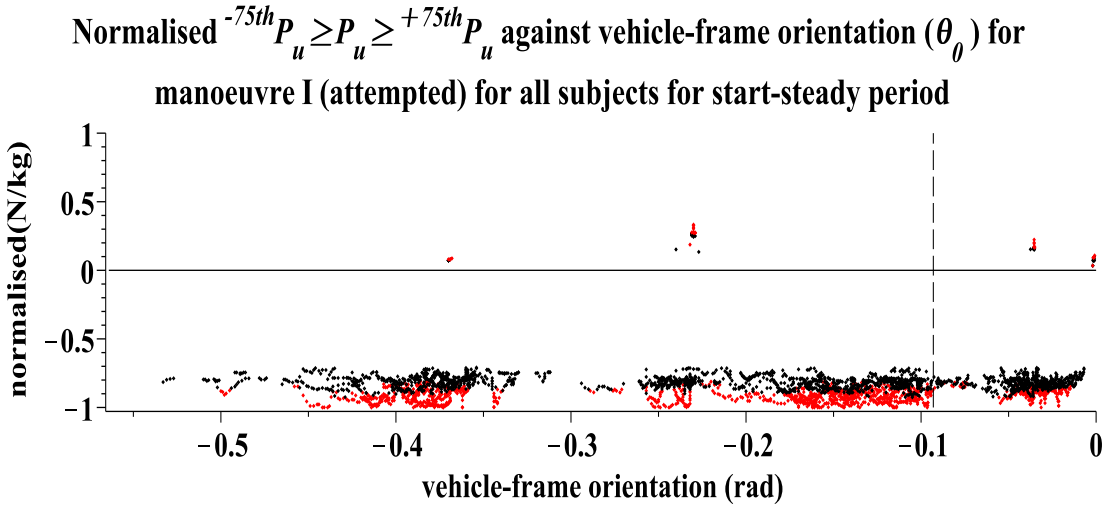

Figure D.36 – For the manoeuvre I (a.) occurrences of ${}^{-75th}_{ssi}P^{\mathrm{I}}_u \geq P_u > {}^{-90th}_{ssi}P^{\mathrm{I}}_u$ and of ${}^{+75th}_{ssi}P^{\mathrm{I}}_u \leq P_u < {}^{+90th}_{ssi}P^{\mathrm{I}}_u$ (both black markers) and, of $P_u \leq {}^{-90th}_{ssi}P^{\mathrm{I}}_u$ and of $P_u \geq {}^{+90th}_{ssi}P^{\mathrm{I}}_u$ (both red markers) in N/kg (normalised against each subject's maximum magnitude P_u for $\{{}_{ssi}\theta^{\mathrm{I}}_0\}$) against θ_0 for $\{{}_{ssi}\theta^{\mathrm{I}}_0\}$ for each subject: $\theta_0 = -0.093$ line indicated (dashed vertical)

${}^{+90th}_{ssi}P^{\mathrm{I}}_u$ (both red markers) (N/kg) for all subjects[I] for $\{{}_{ssi}\theta^{\mathrm{I}}_0\}$ for each subject[I] against θ_0: to assist inspection the measures for each subject are normalised against the subject's P_u peak magnitude for $\{{}_{ssi}\theta^{\mathrm{I}}_0\}$. As Figure D.36 shows normalised P_u it is evident that relative to $P_u < 0$ the $P_u > 0$ magnitudes are relatively small and occurrences are relatively few and this confirms the representativeness of Figure D.33 (page 317) in this respect: $P_u > 0$ are not considered further in the results.

Figure D.37 (page 321) shows measures for $P_u \leq {}^{-90th}_{ss1}P^{\mathrm{I}}_u$ (N/kg) for all subjects[I] for $\{{}_{ss1}\theta^{\mathrm{I}}_0\}$. Representative values for the largest magnitude $P_u < 0$ are obtained as follows. For each subject[I] the measure for the minimum magnitude ${}^{-90th}_{ss1}P^{\mathrm{I}}_u$, denoted ${}^{-90th}_{ss1}P^{\mathrm{I}}_{umini}$, can be read and the minimum magnitude ${}^{-90th}_{ss1}P^{\mathrm{I}}_{umini}$ for all subjects[I], denoted ${}^{+90th}_{ss1}P^{\mathrm{I}}_{umin}$, is −0.35 N/kg (subjects[2, 3]). The maximum magnitude P_u for each subject[I], denoted ${}^{-90th}_{ss1}P^{\mathrm{I}}_{umaxi}$ can also be read and the maximum magnitude ${}^{-90th}_{ss1}P^{\mathrm{I}}_{umaxi}$ denoted ${}^{-90th}_{ss1}P^{\mathrm{I}}_{umax}$ is−0.62 N/kg (subject[7]). The mean ${}^{-90th}_{ss1}P^{\mathrm{I}}_{umini} \geq P_u \geq {}^{-90th}_{ss1}P^{\mathrm{I}}_{umaxi}$ for each subject[I] is indicated by a solid circle and it can be seen that the mean is located in the second to third quarter. Occurrences of $P_u \leq {}^{-90th}_{ss1}P^{\mathrm{I}}_u$ are shown above the range line for each subject. Subject[0] shows the range from ${}^{-90th}_{ss1}P^{\mathrm{I}}_{umin}$ to ${}^{-90th}_{ss1}P^{\mathrm{I}}_{umax}$ with

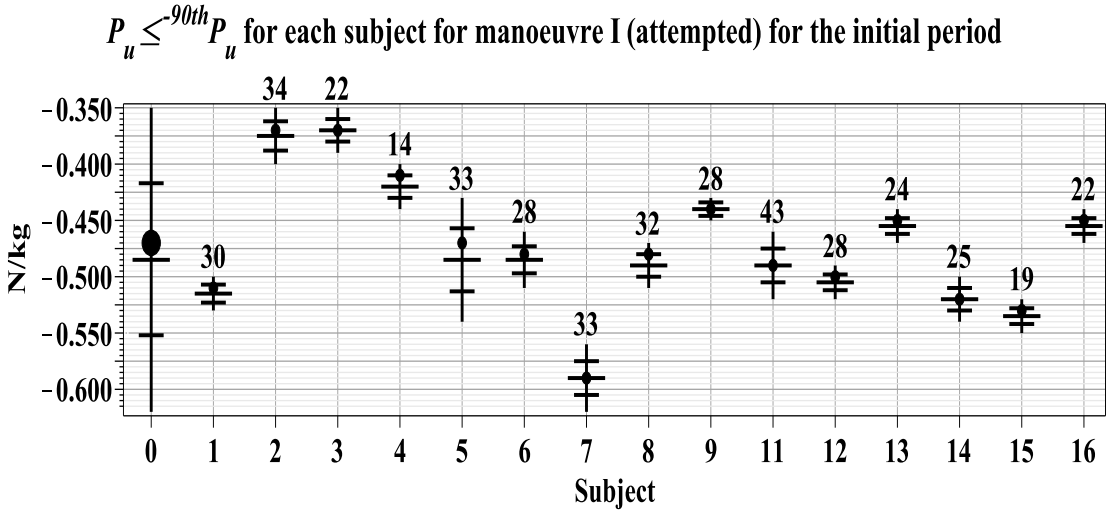

Figure D.37 – Shows for each subject[I] (i) for the initial period $\{{}_{ss1}\theta_0^{\mathrm{I}}\}$ in N/kg: a vertical line indicating the minimum magnitude ${}^{-90th}_{ss1}P^{\mathrm{I}}_{umini}$ to the maximum magnitude ${}^{-90th}_{ss1}P^{\mathrm{I}}_{umaxi}$, a solid circle indicating the mean ${}^{-90th}_{ss1}P^{\mathrm{I}}_{umaxi} \geq P_u \geq {}^{-90th}_{ss1}P^{\mathrm{I}}_{umaxi}$, the quarter divisions of the range (horizontal lines) and the number of occurrences of $P_u \leq {}^{+90th}_{ss1}P^{\mathrm{I}}_{u}$ shown below the range line. Subject[0] shows these measures for all subjects[I] with a solid circle indicating the mean of all the mean ${}^{-90th}_{ss1}P^{\mathrm{I}}_{umini} \geq P_u \geq {}^{-90th}_{ss1}P^{\mathrm{I}}_{umaxi}$.

the mean for all the mean ${}^{-90th}_{ss1}P^{\mathrm{I}}_{umini} \geq P_u \geq {}^{-90th}_{ss1}P^{\mathrm{I}}_{umaxi}$ located approximately centrally as indicated by a solid circle.

Occurrences of $P_u \leq {}^{-90th}_{ss1}P^{\mathrm{I}}_{u}$ are also shown above the range line and examination of the data (results not presented) shows that these are equal to $\frac{50}{10} \times t_i(\{{}_{ss1}\theta_0^{\mathrm{I}}\})$ for subjects[1, 2, 6, 8, 9, 12, 13, 14, 15, 16] and approximately equal for subjects[3, 4, 5, 7, 11] who have some $P_u > 0$.

D.8.4. *Manoeuvre I (a.)* P_v

Figure D.38 (page 322) shows occurrences of ${}^{-75th}_{ssi}P^{\mathrm{I}}_{v} \geq P_v > {}^{-90th}_{ssi}P^{\mathrm{I}}_{v}$ and of ${}^{+75th}_{ssi}P^{\mathrm{I}}_{v} \leq P_v < {}^{+90th}_{ssi}P^{\mathrm{I}}_{v}$ (both black markers) and, of $P_v \leq {}^{-90th}_{ssi}P^{\mathrm{I}}_{v}$ and of $P_v \geq {}^{+90th}_{ssi}P^{\mathrm{I}}_{v}$ (both red markers) (N/kg) for all subjects[I] for $\{{}_{ssi}\theta_0^{\mathrm{I}}\}$ for each subject[I] against θ_0: to assist inspection the measures for each subject are normalised against the subject's P_v peak magnitude for $\{{}_{ssi}\theta_0^{\mathrm{I}}\}$. The peak magnitudes for $P_v < 0$ occur in $\{{}_{ss1}\theta_0^{\mathrm{I}}\}$ for all subjects[I]. As P_v is normalised in Figure D.38 it is evident that the occurrences of $P_v > 0$ are few and the peak magnitudes of $P_v > 0$ are at half-magnitude in comparison with those for $P_v < 0$. This confirms the representativeness of Figure D.33 (page 317) in this respect. Additionally an

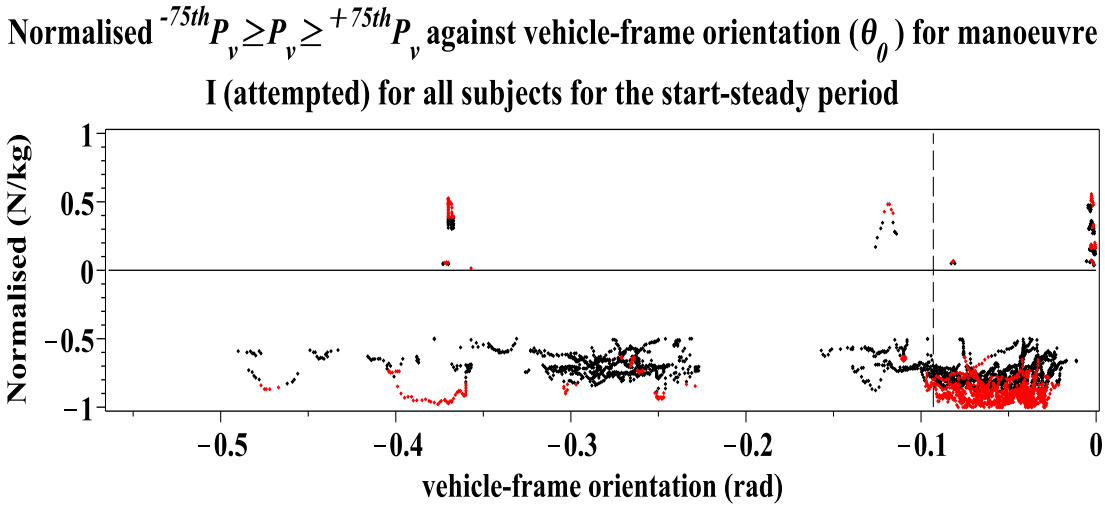

Figure D.38 – For the manoeuvre I (a.) occurrences of ${}^{-75th}_{ssi}P^{\mathrm{I}}_v \geq P_v > {}^{-90th}_{ssi}P^{\mathrm{I}}_v$ and of ${}^{+75th}_{ssi}P^{\mathrm{I}}_v \leq P_v < {}^{+90th}_{ssi}P^{\mathrm{I}}_v$ (both black markers) and, of $P_v \leq {}^{-90th}_{ssi}P^{\mathrm{I}}_v$ and of $P_v \geq {}^{+90th}_{ssi}P^{\mathrm{I}}_v$ (both red markers) in N/kg (normalised against each subject's maximum magnitude P_v for $\{{}_{ssi}\theta^{\mathrm{I}}_0\}$) against θ_0 for $\{{}_{ssi}\theta^{\mathrm{I}}_0\}$ for each subject: $\theta_0 = -0.093$ line indicated (dashed vertical).

examination of the data (results not presented) indicates that there are negligible occurrences of $P_v > 0$ for $\{{}_{ss1a}\theta^{\mathrm{I}}_0\}$ and measures of $P_v > 0$ are not considered further in the results.

Figure D.39 (page 323) shows measures for $P_v \leq {}^{-90th}_{ss1}P^{\mathrm{I}}_v$ (N/kg) for each subject [I] and for all subjects[I], denoted subject[0], for $\{{}_{ss1}\theta^{\mathrm{I}}_0\}$. Representative values for the largest magnitude P_v are obtained as follows. For each subject[I] the measure for the minimum magnitude $P_v \leq {}^{-90th}_{ss1}P^{\mathrm{I}}_v$, denoted ${}^{-90th}_{ss1}P^{\mathrm{I}}_{vmini}$, may be read and the minimum ${}^{-90th}_{ss1}P^{\mathrm{I}}_{vmini}$ for all subjects[I], denoted ${}^{-90th}_{ss1}P^{\mathrm{I}}_{vmin}$, is -0.33 N/kg (subject[15]). The maximum magnitude P_v for each subject[I], denoted ${}^{-90th}_{ss1}P^{\mathrm{I}}_{vmaxi}$, may also be read and the maximum ${}^{-90th}_{ss1}P^{\mathrm{I}}_{vmaxi}$, denoted ${}^{-90th}_{ss1}P^{\mathrm{I}}_{vmax}$, is -0.82 N/kg (subject[6]). The mean ${}^{-90th}_{ss1}P^{\mathrm{I}}_{vmini} \geq P_v \geq {}^{-90th}_{ss1}P^{\mathrm{I}}_{vmaxi}$ for each subject[I] is is indicated by a solid circle: it can be seen that, where the range magnitude is not too small, that these means are located from the second to the third quarter of the intra-subject range. Subject[0] shows the range of ${}^{-90th}_{ss1}P^{\mathrm{I}}_{vmin}$ to ${}^{-90th}_{ss1}P^{\mathrm{I}}_{vmax}$ and the mean of all the mean ${}^{-90th}_{ss1}P^{\mathrm{I}}_{vmini} \geq P_v \geq {}^{-90th}_{ss1}P^{\mathrm{I}}_{vmaxi}$ is indicated by a solid circle and this is located approximately centrally in the inter-subject range. Occurrences of $P_v \leq {}^{-90th}_{ss1}P^{\mathrm{I}}_v$ are shown above the line range: an examination of the the data (results not reported) shows that these are equal to $\frac{50}{10} \times t_i(\{{}_{ss1}\theta^{\mathrm{I}}_0\})$ for subjects [1,

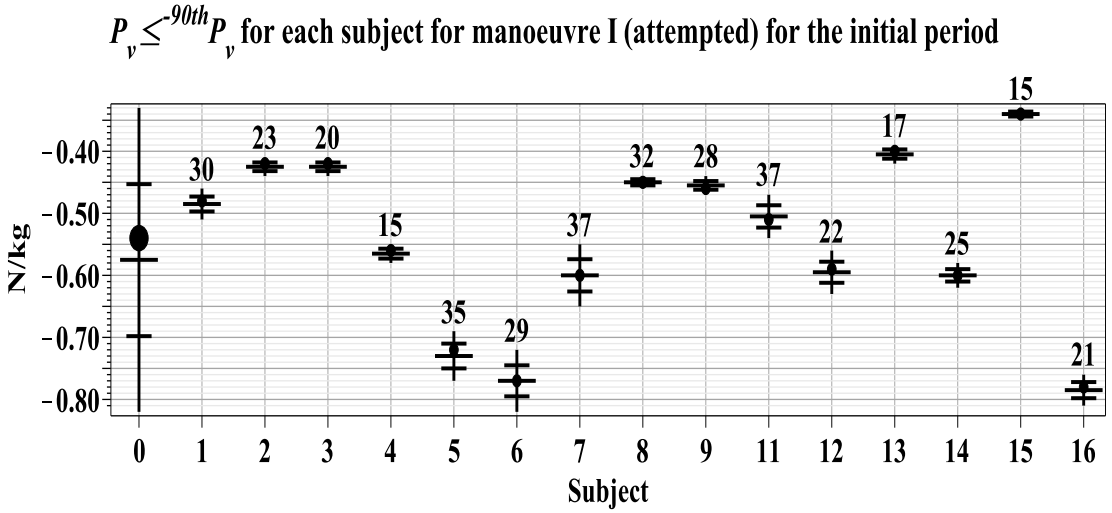

Figure D.39 – Shows for each subject[I] (i) for the initial period $\{{}_{ss1}\theta_0^{\mathrm{I}}\}$ in N/kg: a vertical line indicating the minimum measure magnitude ${}^{-90th}_{ss1}P^{\mathrm{I}}_{vmini}$ to the maximum measure magnitude ${}^{-90th}_{ss1}P^{\mathrm{I}}_{vmaxi}$, a solid circle indicating the mean ${}^{-90th}_{ss1}P^{\mathrm{I}}_{vmaxi} \geq P_v \geq {}^{-90th}_{ss1}P^{\mathrm{I}}_{vmaxi}$, the quarter divisions of the range (horizontal lines) and the number of occurrences of $P_v \leq {}^{-90th}_{ss1}P^{\mathrm{I}}_{v}$ shown above the range line. Subject[0] shows this data for all subjects[I] with a solid circle indicating the mean of all the mean ${}^{-90th}_{ss1}P^{\mathrm{I}}_{vmaxi} \geq P_v \geq {}^{-90th}_{ss1}P^{\mathrm{I}}_{vmaxi}$.

4, 6, 8, 9, 14] and approximately so for subjects [2, 3, 5, 7, 11, 12, 13, 15, 16] who have $P_v > 0$ measures.

It can also be seen from Figure D.39 (page 323) that the range magnitude of 0.49 N/kg, ${}^{-90th}_{ss1}P^{\mathrm{I}}_{vmax} - {}^{-90th}_{ss1}P^{\mathrm{I}}_{vmin}$, arises from inter-subject variation (subject[15] compared with subject[6]) and is not the result of the ${}^{+90th}_{ss1}P^{\mathrm{I}}_{vmaxi} - {}^{-90th}_{ss1}P^{\mathrm{I}}_{vmini}$ magnitude of a specific subject. There are therefore substantial differences between subjects for the largest magnitudes of P_v. However, the inequality ${}^{-90th}_{ss1}P^{\mathrm{I}}_{vmini} \leq P_v \leq {}^{-90th}_{ss1}P^{\mathrm{I}}_{vmaxi}$ provides a representative range for each subject[I]. Additionally the inequality ${}^{-90th}_{ss1}P^{\mathrm{I}}_{vmin} \leq P_v \leq {}^{-90th}_{ss1}P^{\mathrm{I}}_{vmax}$ provides a representative range for all subjects[I].

D.8.5. *Manoeuvre I (a.) the $P_v - P_{uCs}$ plane*

This final section relating to manoeuvre I (a.) uses the inequalities, as previously defined, to define a cuboid boundary for the largest magnitude measures for each and all subjects. For each of subjects[1,..., 9, 11,..., 16] the following inequalities define the cuboid boundaries:

${}^{-90th}_{ss1}P^{\mathrm{I}}_{uCsmini} \geq P_{uCs} \geq {}^{-90th}_{ss1}P^{\mathrm{I}}_{uCsmaxi}$ (page 316),

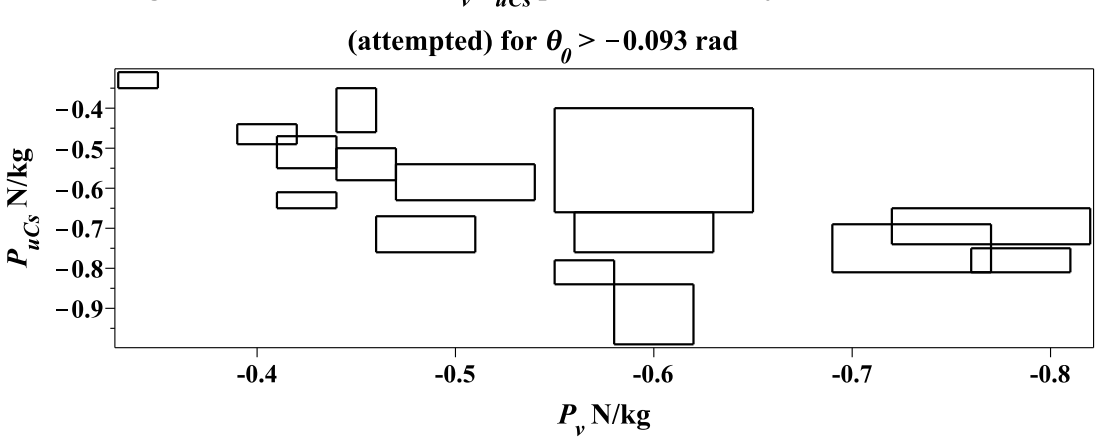

Figure D.40 – Rectangles formed with vertices of coordinates $[{}^{-90th}_{ss1}P^{\mathrm{I}}_{vmini}, {}^{-90th}_{ss1}P^{\mathrm{I}}_{uCsmini}]$, $[{}^{-90th}_{ss1}P^{\mathrm{I}}_{vmaxi}, {}^{-90th}_{ss1}P^{\mathrm{I}}_{uCsmini}]$, $[{}^{-90th}_{ss1}P^{\mathrm{I}}_{vmaxi}, {}^{-90th}_{ss1}P^{\mathrm{I}}_{uCsmaxi},]$, and $[{}^{-90th}_{ss1}P^{\mathrm{I}}_{vmini}, {}^{-90th}_{ss1}P^{\mathrm{I}}_{uCsmaxi}]$ for all subjects[I], i.e. n=15.

${}^{-90th}_{ss1}P^{\mathrm{I}}_{vmini} \geq P_v \geq {}^{-90th}_{ss1}P^{\mathrm{I}}_{vmaxi}$ (page 321) and

${}^{-90th}_{ss1}P^{\mathrm{I}}_{umini} \geq P_u \geq {}^{-90th}_{ss1}P^{\mathrm{I}}_{umaxi}$ (page 319)

and these three inequalities are denoted ${}^{large}_{ss1}\mathbf{P}^{\mathrm{I}}_{i}$.

A graphical representation of ${}^{large}_{ss1}\mathbf{P}^{\mathrm{I}}_{i}$ in the $P_v - P_{uCs}$ plane is shown in Figure D.40 (page 324): the construction follows the same process as described in Section 6.4.4 (page 149) for manoeuvre F (a.).

Three inequalities define the cuboid boundaries which enclose the measures for all, rather than each of, subjects[I] and removal of the i subscript from the above definitions provides this and these three inequalities are denoted ${}^{large}_{ss1}\mathbf{P}^{\mathrm{I}}$. In conclusion ${}^{large}_{ss1}\mathbf{P}^{\mathrm{I}}$ provides a useful representation of the boundaries of the largest handle-forces for all subjects[I] for manoeuvre I (a.): the numerical values are:

$-0.48 \geq P_v \geq -0.89$ (N/kg),

$-0.31 \geq P_{uCs} \geq -0.99$ (N/kg) and

$-0.35 \geq P_u \geq -0.62$ (N/kg).

D.9. Manoeuvre A (attempted)

In this section a trailing super or sub script A in a symbol or'all subjects[A]' indicates measures from subjects [1,..., 16].

D.9.1. *Manoeuvre A (a.) handle-force measures*

Examination of the handle-force measures will show that dividing the start-steady period $\{_{ssi}\theta_0^{\mathrm{A}}\}$ at $\theta_0 = -0.133$ rad is useful and thus two periods are defined: an initial period $-0.133 < \theta_0 < 0$ rad, denoted $\{_{ss1}\theta_0^{\mathrm{A}}\}$, and a later period $\theta_{0steadi} < \theta_0 < -0.133$ rad, denoted $\{_{ss2i}\theta_0^{\mathrm{A}}\}$. There is some variation between subjects immediately after motion start for a small θ_0 displacement: magnitude no greater than 0.013 rad. The range $-0.133 < \theta_0 < -0.013$ rad is denoted $\{_{ss1a}\theta_0^{\mathrm{A}}\}$ ($\{_{ss1}\theta_0^{\mathrm{A}}\}$ modified to commence at $\theta_0 = -0.013$ rad rather than motion-start). For the modified initial period $\{_{ss1a}\theta_0^{\mathrm{A}}\}$ Figure D.41 (page 326) for subject[14] illustrates four features which are common to all subjects[A]. Firstly, occurrences and magnitudes of $P_{uCs} < 0$ are negligible. Secondly, some occurrences of P_{uCs} are integer zero measures. Thirdly, occurrences and magnitudes of $P_u < 0$ are negligible. Fourthly, occurrences and magnitudes of $P_v < 0$ are negligible.

D.9.2. *Manoeuvre A (a.) P_{uCs}*

The presentation begins with P_{uCs}. Figure D.43 (page 327) shows occurrences of ${}^{-75th}_{ssi}P^{\mathrm{A}}_{uCs} \geq P_{uCs} > {}^{-90th}_{ssi}P^{\mathrm{A}}_{uCs}$ and of ${}^{+75th}_{ssi}P^{\mathrm{A}}_{uCs} \leq P_{uCs} < {}^{+90th}_{ssi}P^{\mathrm{A}}_{uCs}$ (both black markers), and $P_{uCs} \leq {}^{-90th}_{ssi}P^{\mathrm{A}}_{uCs}$ and $P_{uCs} \geq {}^{+90th}_{ssi}P^{\mathrm{A}}_{uCs}$ (both red markers) for all subjects[A]: to assist inspection the N/kg measures for each subject are normalised against the subject's P_{uCs} peak magnitude for $\{_{ssi}\theta_0^{\mathrm{A}}\}$. A dashed vertical line indicates $\theta_0 = -0.133$ rad and this divides $\{_{ssi}\theta_0^{\mathrm{A}}\}$ into $\{_{ss1}\theta_0^{\mathrm{A}}\}$ and $\{_{ss2i}\theta_0^{\mathrm{A}}\}$ as previously defined. It can be seen that there are two features resulting from the division of $\{_{ssi}\theta_0^{\mathrm{A}}\}$ at this location. Firstly, all $P_{uCs} \geq {}^{+90th}_{ssi}P^{\mathrm{A}}_{uCs}$ and the majority of $P_{uCs} \geq {}^{+75th}_{ssi}P^{\mathrm{A}}_{uCs}$ occur in $\{_{ss1}\theta_0^{\mathrm{A}}\}$. Secondly, the proximity of occurrences of $P_{uCs} \geq {}^{+75th}_{ssi}P^{\mathrm{A}}_{uCs}$ changes after $\{_{ss1}\theta_0^{\mathrm{A}}\}$ since a $\Delta|\theta_0| \approx 0.09$ rad takes place before further occurrences. Thus for all subjects[A], despite any variations, the mechanism is so configured that all subjects have an occurrence of their peak handle-force magnitude by $\theta_0 = -0.133$ rad and hence division of $\{_{ssi}\theta_0^{\mathrm{A}}\}$ at this location relates to a mechanical property of the system for manoeuvre A (a.). It is also evident that for $\{_{ss1a}\theta_0^{\mathrm{A}}\}$, compared with $P_{uCs} > 0$, measures for $P_{uCs} < 0$ are of very small magnitude and few occurrences.

For each subject occurrences of $P_{uCs} \geq {}^{+90th}_{ss1}P^{\mathrm{A}}_{uCs}$ are shown above the range line in Figure D.44 and the percentage of occurrences of $P_{uCs} = 0$ (integer) are

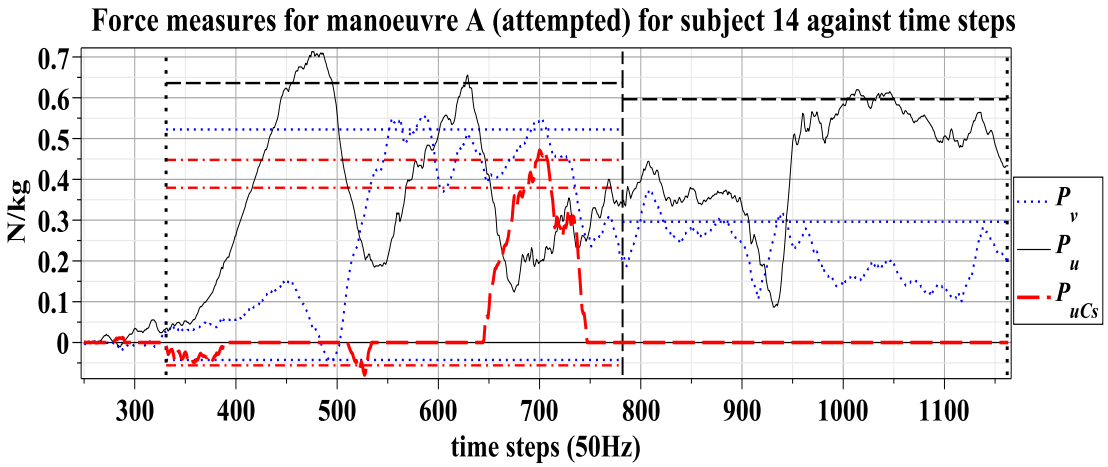

Figure D.41 – For subject[14] for manoeuvre A (a.), measures: P_v (dotted blue), P_u (thin black) and P_{uCs} (thick red dashed) in N/kg plotted against time steps (approximately 0.02 seconds) with $\theta_0 = -0.133$ rad line (vertical black dashed). The following percentile lines are shown for the initial period $\{{}_{ss1}\theta_0^{\mathrm{A}}\}$: ${}^{-90th}_{ss1}P^{\mathrm{A}}_{uCs}$, ${}^{+90th}_{ss1}P^{\mathrm{A}}_{uCs}$ and ${}^{+75th}_{ss1}P^{\mathrm{A}}_{uCs}$ (horizontal red dash-dot), ${}^{+90th}_{ss1}P^{\mathrm{A}}_{u}$ (horizontal black dash) and ${}^{+90th}_{ss1}P^{\mathrm{A}}_{v}$ (horizontal blue dot): these percentile lines are also shown for the later period $\{{}_{ss2i}\theta_0^{\mathrm{A}}\}$

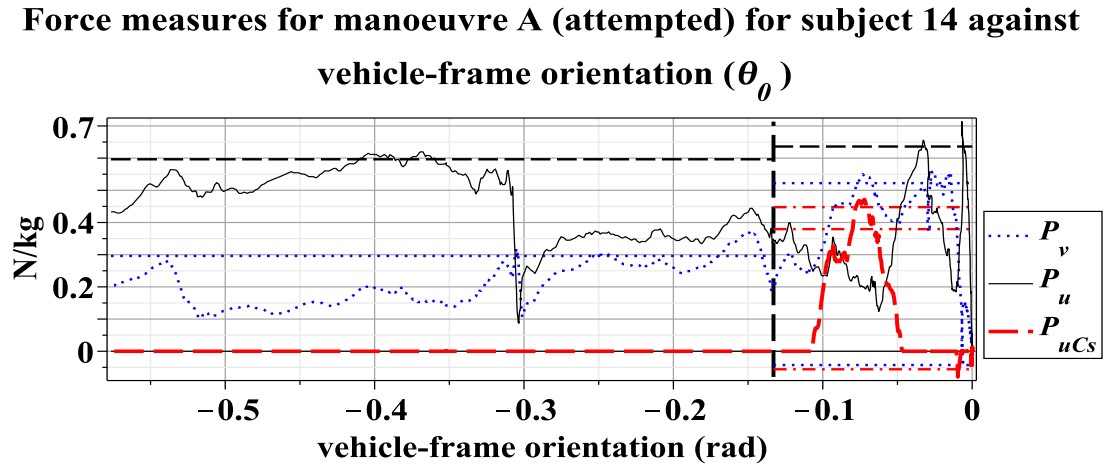

Figure D.42 – For subject[14] for manoeuvre A (a.), measures plotted against θ_0 with other details as above.

shown below the range line. Substantial variation is evident: subject[13] has 10% $P_{uCs} = 0$ occurrences where as subject[2] has 85% $P_{uCs} = 0$ occurrences. In other words the attempt at manoeuvre[A] by some subjects, to some extent, reduces the occurrences of the couple action.

Figure D.44 (page 328) shows measures for $P_{uCs} \geq {}^{+90th}_{ss1}P^{\mathrm{A}}_{uCs}$ (N/kg) for all subjects[A] for $\{{}_{ss1}\theta_0^{\mathrm{A}}\}$. Representative values for the largest P_{uCs} are obtained as follows. For each subject[A] the measure for the minimum ${}^{+90th}_{ss1}P^{\mathrm{A}}_{uCs}$,

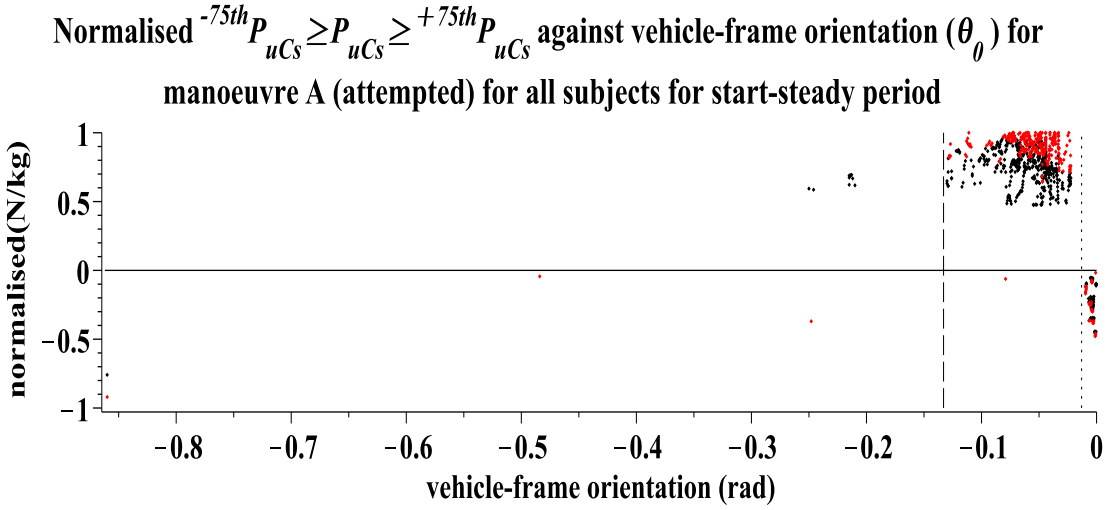

Figure D.43 – For the manoeuvre A (a.) occurrences of ${}^{-75th}_{ssi}P^{\mathrm{A}}_{uCs} \geq P_{uCs} > {}^{-90th}_{ssi}P^{\mathrm{A}}_{uCs}$ and of ${}^{+75th}_{ssi}P^{\mathrm{A}}_{uCs} \leq P_{uCs} < {}^{+90th}_{ssi}P^{\mathrm{A}}_{uCs}$ (both black markers) and, $P_{uCs} \leq {}^{-90th}_{ssi}P^{\mathrm{A}}_{uCs}$ and $P_{uCs} \geq {}^{+90th}_{ssi}P^{\mathrm{A}}_{uCs}$ (both red markers) in N/kg (normalised against each subject's maximum magnitude P_{uCs} for $\{{}_{ssi}\theta^{\mathrm{A}}_0\}$) against θ_0 for $\{{}_{ssi}\theta^{\mathrm{A}}_0\}$ for each subject: $\theta_0 = -0.133$ line (dashed) and $\theta_0 = -0.013$ rad line (dotted) indicated.

denoted ${}^{+90th}_{ss1}P^{\mathrm{A}}_{uCsmini}$, may be read and the minimum ${}^{+90th}_{ss1}P^{\mathrm{A}}_{uCsmini}$ for all subjects[A], denoted ${}^{+90th}_{ss1}P^{\mathrm{A}}_{uCsmin}$, is 0.09 N/kg (subject[6]). The maximum P_{uCs} for each subject[A], denoted ${}^{+90th}_{ss1}P^{\mathrm{A}}_{uCsmaxi}$ may also be read and the maximum ${}^{+90th}_{ss1}P^{\mathrm{A}}_{uCsmaxi}$, denoted ${}^{+90th}_{ss1}P^{\mathrm{A}}_{uCsmax}$, is 0.86 N/kg (subject[11]). The mean ${}^{+90th}_{ss1}P^{\mathrm{A}}_{uCsmaxi} \leq P_{uCs} \leq {}^{+90th}_{ss1}P^{\mathrm{A}}_{uCsmaxi}$ for each subject[A] are indicated by a solid circle and it can be seen that these means, ignoring subjects where the range magnitude is relatively small, are located in the first to third quarter of the intra-subject range. Subject[0] shows the range of ${}^{+90th}_{ss1}P^{\mathrm{A}}_{uCsmin}$ to ${}^{+90th}_{ss1}P^{\mathrm{A}}_{uCsmax}$ and the mean of all the mean ${}^{+90th}_{ss1}P^{\mathrm{A}}_{uCsmini} \leq P_{uCs} \leq {}^{+90th}_{ss1}P^{\mathrm{A}}_{uCsmaxi}$ indicated by a solid circle can be seen to be located approximately at the centre of the inter-subject ranges.

It can also be seen from Figure D.44 (page 328) that the range magnitude of 0.68 N/kg, ${}^{+90th}_{ss1}P^{\mathrm{A}}_{uCsmax} - {}^{+90th}_{ss1}P^{\mathrm{A}}_{uCsmin}$, arises from inter-subject variation (subject[6] compared with subject[11]) and is not the result of the ${}^{+90th}_{ss1}P^{\mathrm{A}}_{uCsmaxi} - {}^{+90th}_{ss1}P^{\mathrm{A}}_{uCsmini}$ magnitude of a specific subject. There are therefore substantial differences between subjects for the largest $P_{uCs} > 0$. However, the inequality ${}^{+90th}_{ss1}P^{\mathrm{A}}_{uCsmini} \leq P_{uCs} \leq {}^{+90th}_{ss1}P^{\mathrm{A}}_{uCsmaxi}$ provides a representative range for each

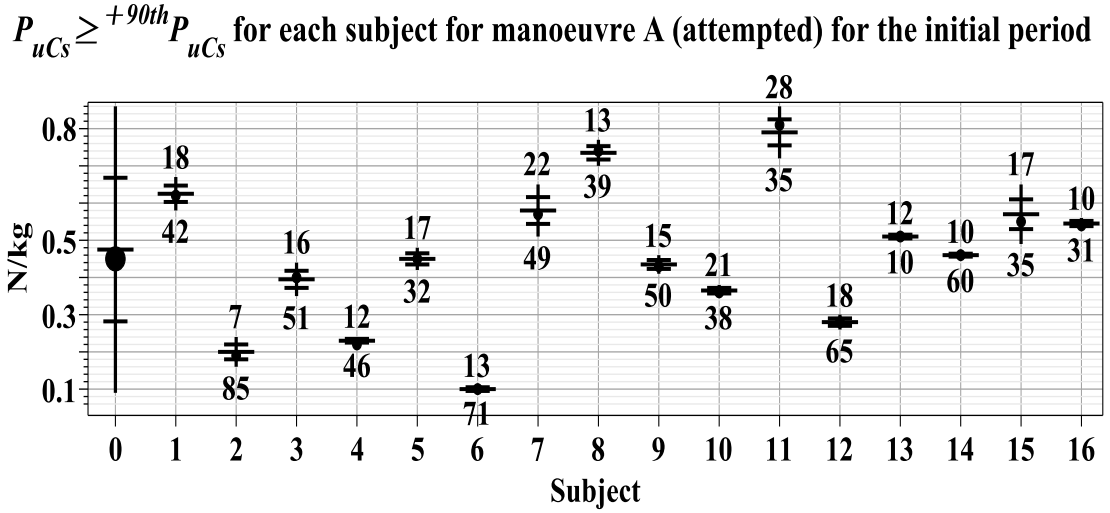

Figure D.44 – Shows for each subject[A] (i) for $\{{}_{ss1}\theta_0^{\mathrm{A}}\}$ in N/kg: a vertical line indicating the minimum ${}^{+90th}_{ss1}P^{\mathrm{A}}_{uCsmini}$ to the maximum ${}^{+90th}_{ss1}P^{\mathrm{A}}_{uCsmaxi}$, a solid circle indicating the mean ${}^{+90th}_{ss1}P^{\mathrm{A}}_{uCsmini} \leq P_{uCs} \leq {}^{+90th}_{ss1}P^{\mathrm{A}}_{uCsmaxi}$, the quarter divisions of the range (horizontal lines), the number of occurrences of $P_{uCs} \geq {}^{+90th}_{ss1}P^{\mathrm{A}}_{uCs}$ shown above the range line and the percentage of occurrences for $P_{uCs} = 0$ (integer) shown below the range line. Subject[0] shows these measures for all subjects[A] with a solid circle indicating the mean of all the mean ${}^{+90th}_{ss1}P^{\mathrm{A}}_{uCsmini} \leq P_{uCs} \leq {}^{+90th}_{ss1}P^{\mathrm{A}}_{uCsmaxi}$.

subject. In addition the inequality ${}^{+90th}_{ss1}P^{\mathrm{A}}_{uCsmin} \leq P_{uCs} \leq {}^{+90th}_{ss1}P^{\mathrm{A}}_{uCsmax}$ provides a representative range for all subjects[A]. As the $P_{uCs} \leq {}^{-90th}_{ss1}P^{\mathrm{A}}_{uCs}$ are disregarded, most $P_{uCs} < 0$ occur before $\theta_0 > -0.013$, this inequality provides a representative range for the largest magnitude P_{uCs}.

D.9.3. *Manoeuvre A (a.) P_u*

Figure D.45 (page 329) shows occurrences of ${}^{-75th}_{ssi}P^{\mathrm{A}}_{u} \geq P_u > {}^{-90th}_{ssi}P^{\mathrm{A}}_{u}$ and of ${}^{+75th}_{ssi}P^{\mathrm{A}}_{u} \leq P_u < {}^{+90th}_{ssi}P^{\mathrm{A}}_{u}$ (both black markers) and, of $P_u \leq {}^{-90th}_{ssi}P^{\mathrm{A}}_{u}$ and of $P_u \geq {}^{+90th}_{ssi}P^{\mathrm{A}}_{u}$ (both red markers): these are the occurrences for all subjects[A]. It is evident from Figure D.45 that for $\{{}_{ss1a}\theta_0^{\mathrm{A}}\}$ that compared with $P_u > 0$ occurrences of $P_u < 0$ are few and magnitudes are small. $P_u < 0$ are disregarded in the results.

It is evident from Figure D.45 that a peak measure occurs in $\{{}_{ss2i}\theta_0^{\mathrm{A}}\}$ for some subjects[A] and that therefore Figure D.45 does not demonstrate that all subject[A] contribute to the peak P_u for $\{{}_{ss1}\theta_0^{\mathrm{A}}\}$. It therefore follows that while Figure D.45 indicates the occurrences of P_u in both signs it is not possible to determine the comparative magnitudes of $P_u \geq {}^{+75th}_{ssi}P^{\mathrm{A}}_{u}$ and $P_u \leq {}^{-75th}_{ssi}P^{\mathrm{A}}_{u}$ for $\{{}_{ss1}\theta_0^{\mathrm{A}}\}$ from this

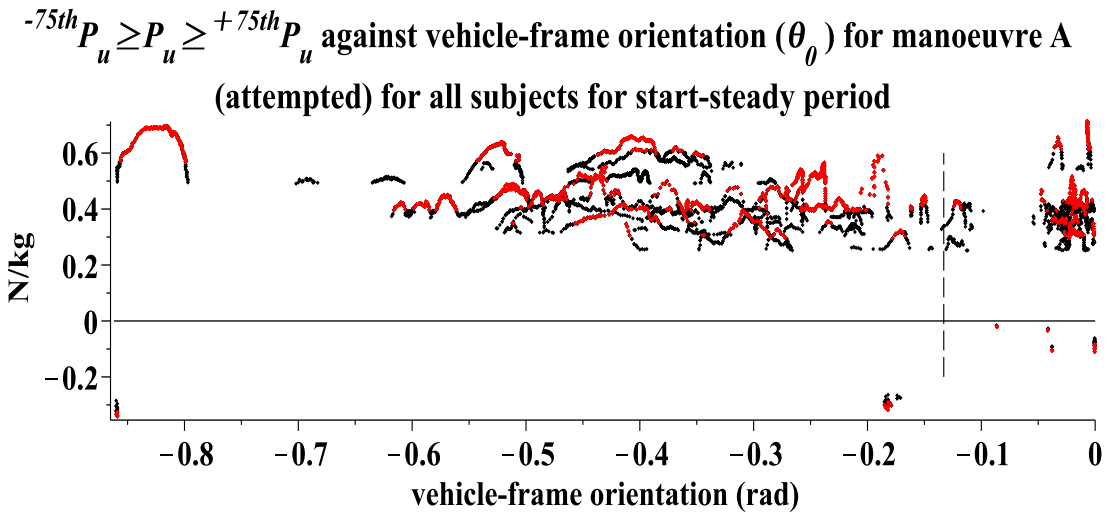

Figure D.45 – Shows for manoeuvre A (a.) occurrences of ${}^{-75th}_{ssi}P^{\mathrm{A}}_{u} \geq P_u > {}^{-90th}_{ssi}P^{\mathrm{A}}_{u}$ and of ${}^{+75th}_{ssi}P^{\mathrm{A}}_{u} \leq P_u < {}^{+90th}_{ssi}P^{\mathrm{A}}_{u}$ (both black markers) and, of $P_u \leq {}^{-90th}_{ssi}P^{\mathrm{A}}_{u}$ and of $P_u \geq {}^{+90th}_{ssi}P^{\mathrm{A}}_{u}$ (both red markers) in N/kg against θ_0 for $\{{}_{ssi}\theta^{\mathrm{A}}_{0}\}$ for each subject: $\theta_0 = -0.133$ line indicated (dashed vertical)

Figure.

However, Figure D.46 (page 330) shows measures for $P_u \geq {}^{+90th}_{ss1}P^{\mathrm{A}}_{u}$ (N/kg) for all subjects[A] for $\{{}_{ss1}\theta^{\mathrm{A}}_{0}\}$. Representative values for the largest $P_u > 0$ are obtained as follows. For each subject[A] the measure for the minimum ${}^{+90th}_{ss1}P^{\mathrm{A}}_{u}$, denoted ${}^{+90th}_{ss1}P^{\mathrm{A}}_{umini}$, can be read and the minimum ${}^{+90th}_{ss1}P^{\mathrm{A}}_{umini}$ for all subjects[A], denoted ${}^{+90th}_{ss1}P^{\mathrm{A}}_{umin}$, is 0.16 N/kg (subject[13]). The maximum P_u for each subject[A], denoted ${}^{+90th}_{ss1}P^{\mathrm{A}}_{umaxi}$, can also be read and the maximum ${}^{+90th}_{ss1}P^{\mathrm{A}}_{umaxi}$, denoted ${}^{+90th}_{ss1}P^{\mathrm{A}}_{umax}$, is 0.71 N/kg (subject[14]). The mean ${}^{+90th}_{ss1}P^{\mathrm{A}}_{umini} \leq P_u \leq {}^{+90th}_{ss1}P^{\mathrm{A}}_{umaxi}$ for each subject[A] is indicated by a solid circle but it can be seen that apart from subjects[2, 7, 12, 14, 16], where it is located approximately centrally, the ranges are of such small magnitude that the location of the mean is immaterial. Occurrences of $P_u \geq {}^{+90th}_{ss1}P^{\mathrm{A}}_{u}$ are shown for each subject. Subject[0] shows the range from ${}^{+90th}_{ss1}P^{\mathrm{A}}_{umin}$ to ${}^{+90th}_{ss1}P^{\mathrm{A}}_{umax}$ with the mean for all the mean ${}^{+90th}_{ss1}P^{\mathrm{A}}_{umaxi} \leq P_u \leq {}^{+90th}_{ss1}P^{\mathrm{A}}_{umaxi}$ located in the second quarter as indicated by a solid circle.

D.9.4. *Manoeuvre A (a.)* P_v

Figure D.47 (page 331) shows occurrences of ${}^{-75th}_{ssi}P^{\mathrm{A}}_{v} \geq P_v > {}^{-90th}_{ssi}P^{\mathrm{A}}_{v}$ and of ${}^{+75th}_{ssi}P^{\mathrm{A}}_{v} \leq P_v < {}^{+90th}_{ssi}P^{\mathrm{A}}_{v}$ (both black markers) and, of $P_v \leq {}^{-90th}_{ssi}P^{\mathrm{A}}_{v}$ and

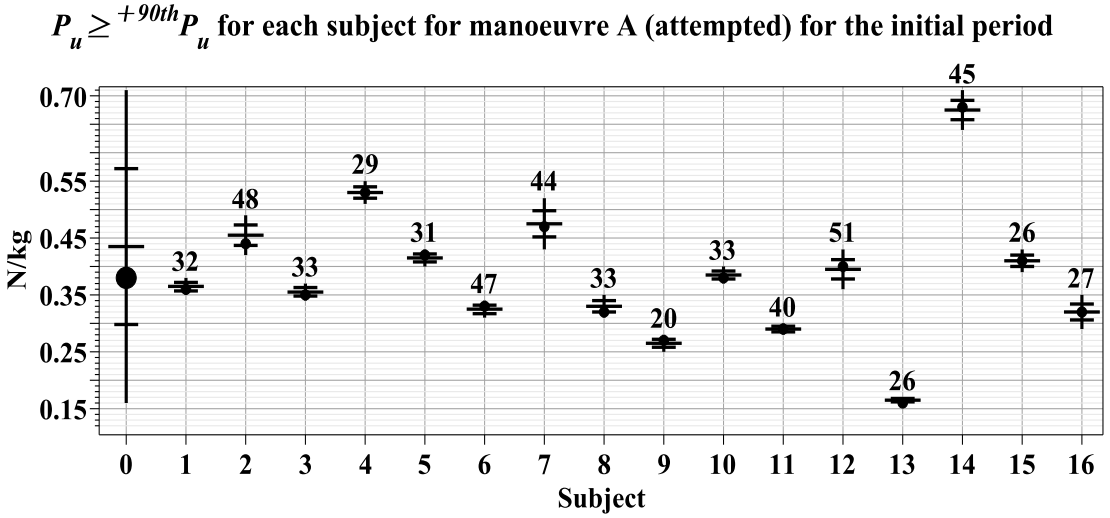

Figure D.46 – Shows for each subject[A] (i) for $\{{}_{ss1}\theta_0^{\mathrm{A}}\}$ in N/kg: for $P_u > 0$ a vertical line indicating the minimum magnitude measure ${}^{+90th}_{ss1}P^{\mathrm{A}}_{umini}$ to the maximum magnitude measure ${}^{+90th}_{ss1}P^{\mathrm{A}}_{umaxi}$, a solid circle indicating the mean ${}^{+90th}_{ss1}P^{\mathrm{A}}_{umini} \leq P_u \leq {}^{+90th}_{ss1}P^{\mathrm{A}}_{umaxi}$, the quarter divisions of the range (horizontal lines) and the number of occurrences of $P_u \geq {}^{+90th}_{ss1}P^{\mathrm{A}}_{u}$: Subject[0] shows these measure with a solid circle indicating the mean of all the mean ${}^{+90th}_{ss1}P^{\mathrm{A}}_{umini} \leq P_u \leq {}^{+90th}_{ss1}P^{\mathrm{A}}_{umaxi}$.

of $P_v \geq {}^{+90th}_{ssi}P^{\mathrm{A}}_{v}$ (both red markers): to aid inspection the measures (N/kg) for each subject are normalised against the subject's P_v peak magnitude for $\{{}_{ssi}\theta_0^{\mathrm{A}}\}$: these are the occurrences for all subjects[A]. It is evident from Figure D.47 that for $\{{}_{ss1}\theta_0^{\mathrm{A}}\}$ compared with $P_v > 0$, the occurrences of $P_v < 0$ are few and the magnitudes are small: as all subjects[A] have a peak P_v in $\{{}_{ss1}\theta_0^{\mathrm{A}}\}$, the $P_v < 0$ are, at maximum, less than a quarter the magnitude of $P_v \geq {}^{+90th}_{ssi}P^{\mathrm{A}}_{v}$. This confirms the representativeness of Figure D.41 (page 326) in this respect.

Figure D.48 (page 331) shows measures for $P_v \geq {}^{+90th}_{ss1}P^{\mathrm{A}}_{v}$ (N/kg) for each subject [A] and for all subjects[A] for $\{{}_{ss1}\theta_0^{\mathrm{A}}\}$. Representative values for the largest P_v are obtained as follows. For each subject[A] the measure for the minimum ${}^{+90th}_{ss1}P^{\mathrm{A}}_{v}$, denoted ${}^{+90th}_{ss1}P^{\mathrm{A}}_{vmini}$, may be read and the minimum ${}^{+90th}_{ss1}P^{\mathrm{A}}_{vmini}$ for all subjects[A], denoted ${}^{+90th}_{ss1}P^{\mathrm{A}}_{vmin}$, is 0.30 N/kg (subject[9]). The maximum P_v for each subject[A], denoted ${}^{+90th}_{ss1}P^{\mathrm{A}}_{vmaxi}$ may also be read and the maximum ${}^{+90th}_{ss1}P^{\mathrm{A}}_{vmaxi}$, denoted ${}^{+90th}_{ss1}P^{\mathrm{A}}_{vmax}$, is 0.56 N/kg (subject[14]). The mean ${}^{+90th}_{ss1}P^{\mathrm{A}}_{vmini} \leq P_v \leq {}^{+90th}_{ss1}P^{\mathrm{A}}_{vmaxi}$ for each subject[A] is indicated by a solid circle: it can be seen that these means are located from the second to the third quarter of the intra-subject range.

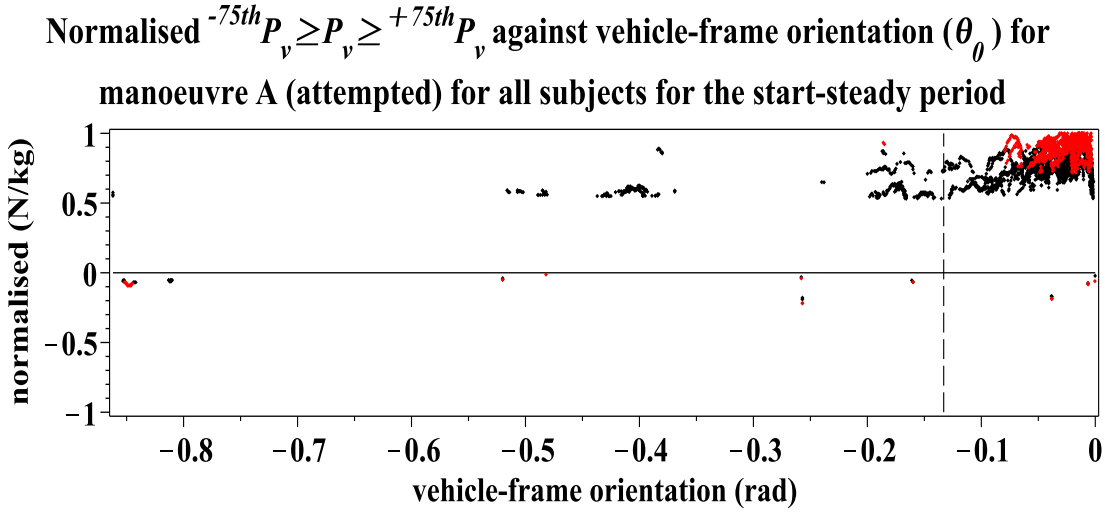

Figure D.47 – For manoeuvre A (a.) occurrences of ${}^{-75th}_{ssi}P^{\mathrm{A}}_{v} \geq P_v > {}^{-90th}_{ssi}P^{\mathrm{A}}_{v}$ and of ${}^{+75th}_{ssi}P^{\mathrm{A}}_{v} \leq P_v < {}^{+90th}_{ssi}P^{\mathrm{A}}_{v}$ (both black markers) and, of $P_v \leq {}^{-90th}_{ssi}P^{\mathrm{A}}_{v}$ and of $P_v \geq {}^{+90th}_{ssi}P^{\mathrm{A}}_{v}$ (both red markers) in N/kg against θ_0 for $\{{}_{ssi}\theta^{\mathrm{A}}_0\}$ for each subject: $\theta_0 = -0.133$ line indicated (dashed vertical)

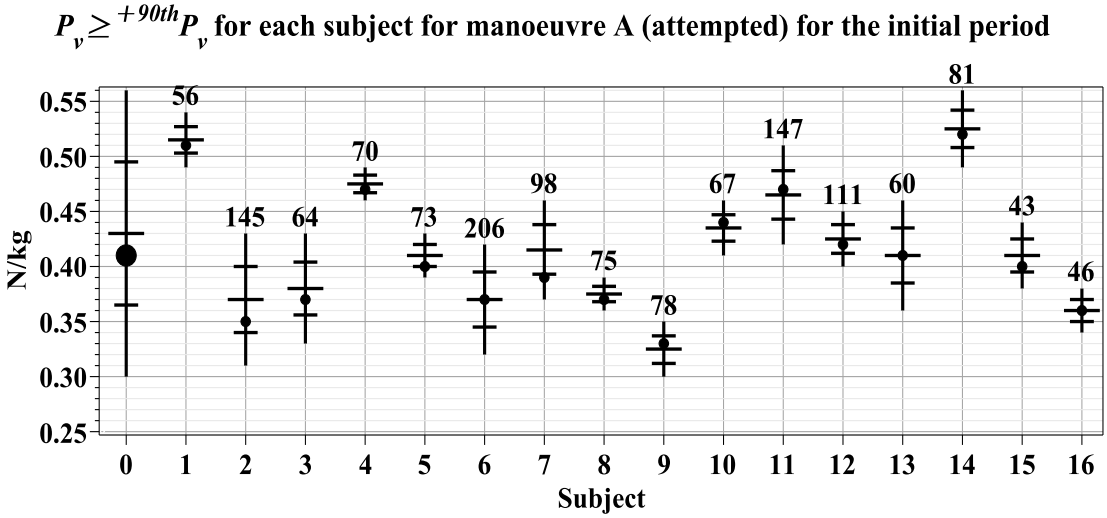

Figure D.48 – Shows for each subject[A] (i) for the initial period $\{{}_{ss1}\theta^{\mathrm{A}}_0\}$ in N/kg: a vertical line indicating the minimum measure ${}^{+90th}_{ss1}P^{\mathrm{A}}_{vmini}$ to the maximum measure ${}^{+90th}_{ss1}P^{\mathrm{A}}_{vmaxi}$, a solid circle indicating the mean ${}^{+90th}_{ss1}P^{\mathrm{A}}_{vmini} \leq P_v \leq {}^{+90th}_{ss1}P^{\mathrm{A}}_{vmaxi}$, the quarter divisions of the range (horizontal lines) and the number of occurrences of $P_v \geq {}^{+90th}_{ss1}P^{\mathrm{A}}_{v}$ shown above the range line. Subject[0] shows this data with a solid circle indicating the mean of all the mean ${}^{+90th}_{ss1}P^{\mathrm{A}}_{vmaxi} \leq P_v \leq {}^{+90th}_{ss1}P^{\mathrm{A}}_{vmaxi}$.

Subject[0] shows the range of the minimum ${}^{+90th}_{ss1}P^{\mathrm{A}}_{vmini}$ to the maximum ${}^{+90th}_{ss1}P^{\mathrm{A}}_{vmaxi}$ and the mean of all the mean ${}^{+90th}_{ss1}P^{\mathrm{A}}_{vmaxi} \leq P_v \leq {}^{+90th}_{ss1}P^{\mathrm{A}}_{vmaxi}$ is indicated by a solid circle and this is located approximately centrally in the inter-subject range. Occurrences of $P_v \geq {}^{+90th}_{ss1}P^{\mathrm{A}}_{v}$ are shown above the line range. As there are few

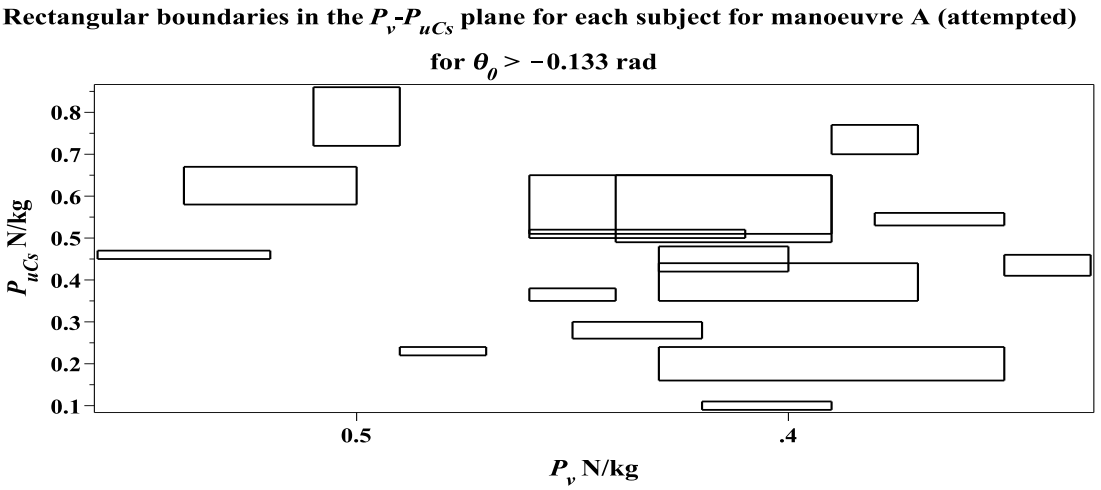

Figure D.49 – Rectangles formed with vertices of coordinates $[{}^{+90th}_{ss1}P^{\mathrm{A}}_{vmini}, {}^{+90th}_{ss1}P^{\mathrm{A}}_{uCsmini}]$, $[{}^{+90th}_{ss1}P^{\mathrm{A}}_{vmaxi}, {}^{+90th}_{ss1}P^{\mathrm{A}}_{uCsmini}]$, $[{}^{+90th}_{ss1}P^{\mathrm{A}}_{vmaxi}, {}^{+90th}_{ss1}P^{\mathrm{A}}_{uCsmaxi},]$, and $[{}^{+90th}_{ss1}P^{\mathrm{A}}_{vmini}, {}^{+90th}_{ss1}P^{\mathrm{A}}_{uCsmaxi}]$ for all subjects[A], i.e. n=16.

$P_v < 0$ for $\{{}_{ss1}\theta^{\mathrm{A}}_0\}$ the occurrences of $P_v \geq {}^{+90th}_{ss1}P^{\mathrm{A}}_v$ are approximately equal to $\frac{50}{10} \times t_i(\{{}_{ss1}\theta^{\mathrm{A}}_0\})$.

It can also be seen from Figure D.48 (page 331) that the range magnitude of 0.26 N/kg, ${}^{+90th}_{ss1}P^{\mathrm{A}}_{vmax} - {}^{+90th}_{ss1}P^{\mathrm{A}}_{vmin}$, arises from inter-subject variation (subject[2] compared with subject[14]) and is not the result of the ${}^{+90th}_{ss1}P^{\mathrm{A}}_{vmaxi} - {}^{+90th}_{ss1}P^{\mathrm{A}}_{vmini}$ of a specific subject. There are therefore substantial differences between subjects for the magnitudes of the largest P_v. However, the inequality ${}^{+90th}_{ss1}P^{\mathrm{A}}_{vmini} \leq P_v \leq {}^{+90th}_{ss1}P^{\mathrm{A}}_{vmaxi}$ provides a representative range for each subject[A]. Additionally the inequality ${}^{+90th}_{ss1}P^{\mathrm{A}}_{vmin} \leq P_v \leq {}^{+90th}_{ss1}P^{\mathrm{A}}_{vmax}$ provides a representative range for all subjects[A].

D.9.5. *Manoeuvre A (a.) the $P_v - P_{uCs}$ plane*

This final section relating to manoeuvre A (a.) uses the inequalities, as previously defined, to define a cuboid boundary for the largest magnitude measures for each and all subjects. For each of subjects[1,..., 16] the following inequalities define the cuboid boundaries:

${}^{+90th}_{ss1}P^{\mathrm{A}}_{uCsmini} \leq P_{uCs} \leq {}^{+90th}_{ss1}P^{\mathrm{A}}_{uCsmaxi}$ (page 325),

${}^{+90th}_{ss1}P^{\mathrm{A}}_{vmini} \leq P_v \leq {}^{+90th}_{ss1}P^{\mathrm{A}}_{vmaxi}$ (page 329) and

${}^{+90th}_{ss1}P^{\mathrm{A}}_{umini} \leq P_u \leq {}^{+90th}_{ss1}P^{\mathrm{A}}_{umaxi}$ (page 328).

and these three inequalities are denoted ${}^{large}_{ss1}\mathbf{P}^{\mathrm{A}}_{i}$.

A graphical representation of ${}^{large}_{ss1}\mathbf{P}^{\mathrm{A}}_{i}$ in the $P_v - P_{uCs}$ plane is shown in Figure D.49 (page 332): the construction follows the same process as described in Section 6.4.4 (page 149) for manoeuvre F (a.).

Three inequalities define the cuboid boundaries which enclose the measures for all, rather than each of, subjects[A] and removal of the i subscript from the above definitions provides this. These three inequalities are denoted ${}^{large}_{ss1}\mathbf{P}^{\mathrm{A}}$. In conclusion ${}^{large}_{ss1}\mathbf{P}^{\mathrm{A}}$ provides a useful representation of the largest handle-forces for all subjects[A] for manoeuvre A attempted: the numerical values are:

$0.30 \leq P_v \leq 0.56$ (N/kg),

$0.09 \leq P_{uCs} \leq 0.86$ (N/kg) and

$0.16 \leq P_u \leq 0.71$ (N/kg).

D.10. **Manoeuvre G (attempted)**

In this section a trailing super or sub script G in a symbol or 'all subjects[G]' indicates measures from subjects [1,..., 16].

D.10.1. *Manoeuvre G (a.) handle-force measures*

Examination of the handle-force measures will show that dividing $\{{}_{ssi}\theta^{\mathrm{G}}_0\}$ at $\theta_0 = -0.128$ rad is useful and hence two periods are defined: $-0.128 < \theta_0 < 0$ rad, denoted $\{{}_{ss1}\theta^{\mathrm{G}}_0\}$, and a later period $\theta_{0steadi} < \theta_0 < -0.128$ rad, denoted $\{{}_{ss2i}\theta^{\mathrm{G}}_0\}$. There is some variation between subjects immediately after motion start for a small θ_0 displacement: magnitude no greater than 0.017 rad. The range $-0.128 < \theta_0 < -0.017$ rad is denoted $\{{}_{ss1a}\theta^{\mathrm{G}}_0\}$ ($\{{}_{ss1}\theta^{\mathrm{G}}_0\}$ modified to commence at $\theta_0 = -0.017$ rad rather than motion-start). For $\{{}_{ss1a}\theta^{\mathrm{G}}_0\}$ the force measures for subject[2], illustrated in Figure D.51 (page 334), are representative of all subjects[G] in three respects. Firstly, occurrences and magnitudes of $P_v < 0$ are negligible. Secondly, compared with $P_{uCs} > 0$, magnitudes of $P_{uCs} < 0$ are small and occurrences are few. Thirdly, occurrences and magnitudes of $P_u > 0$ are negligible.

D.10.2. *Manoeuvre G (a.) P_v*

The presentation begins with P_v. Figure D.52 (page 335) shows, against θ_0, occurrences of ${}^{-75th}_{ssi}P^{\mathrm{G}}_v \geq P_v > {}^{-90th}_{ssi}P^{\mathrm{G}}_v$ and of ${}^{+75th}_{ssi}P^{\mathrm{G}}_v \leq P_v < {}^{+90th}_{ssi}P^{\mathrm{G}}_v$ (both black

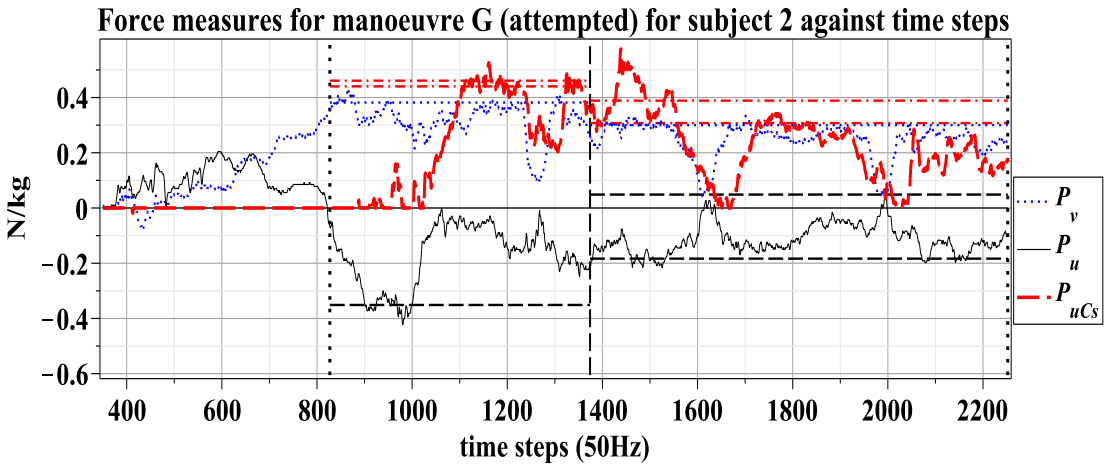

Figure D.50 – For subject[2] for manoeuvre G (a.), measures: P_v (dotted blue), P_u (thin black) and P_{uCs} (thick red dashed) in N/kg plotted against time-steps (approximately 0.02 seconds) with motion-start line (vertical black dotted: closest to left side), steady-start line (vertical black dotted: closest to right side) and $\theta_0 = -0.128$ rad line (vertical black dashed). The following percentile lines are shown for the initial period $\{{}_{ss1}\theta_0^{\mathrm{G}}\}$: ${}^{+90th}_{ss1}P^{\mathrm{G}}_{uCs}$ and ${}^{+75th}_{ss1}P^{\mathrm{G}}_{uCs}$ (horizontal red dash-dot), ${}^{-90th}_{ss1}P^{\mathrm{G}}_{u}$ (horizontal black dash) and ${}^{+90th}_{ss1}P^{\mathrm{G}}_{v}$ (horizontal blue dot): these percentiles are calculated and shown for the later period $\{{}_{ss2i}\theta_0^{\mathrm{G}}\}$ with the addition of ${}^{+90th}_{ss2i}P^{\mathrm{G}}_{u}$ (horizontal black dash).

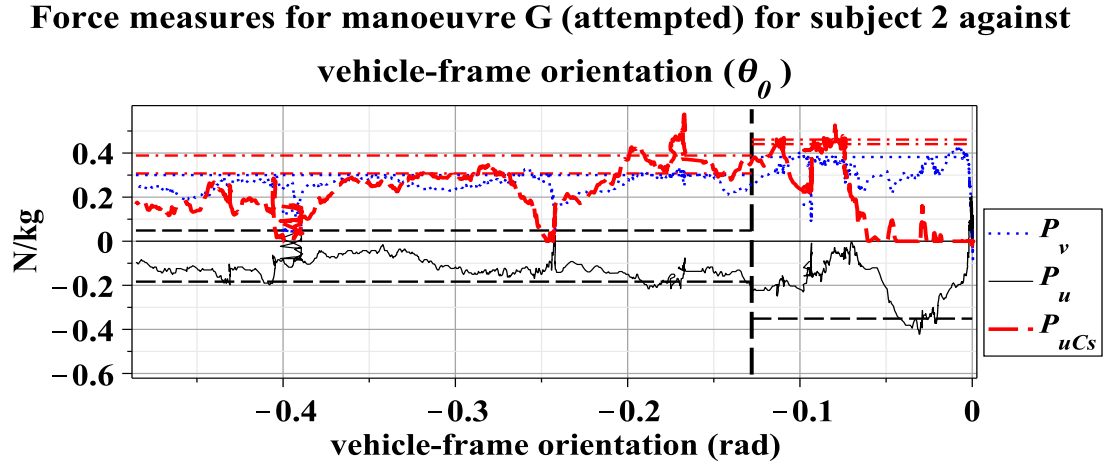

Figure D.51 – For subject[2] for manoeuvre G (a.), measures plotted against θ_0 with other details as above.

markers) and, of $P_v \leq {}^{-90th}_{ssi}P^{\mathrm{G}}_{v}$ and of $P_v \geq {}^{+90th}_{ssi}P^{\mathrm{G}}_{v}$ (both red markers): to aid inspection the measures (N/kg) for each subject are normalised against the subject's P_v peak magnitude for $\{{}_{ssi}\theta_0^{\mathrm{G}}\}$: these are the occurrences for all subjects[G]. A dashed line indicates $\theta_0 = -0.128$ rad. It is evident from Figure D.52 that compared with $P_v > 0$, magnitudes of $P_v < 0$ are small and the occurrences are few and this confirms the representativeness of Figure D.51 (page 334) in this respect. Two

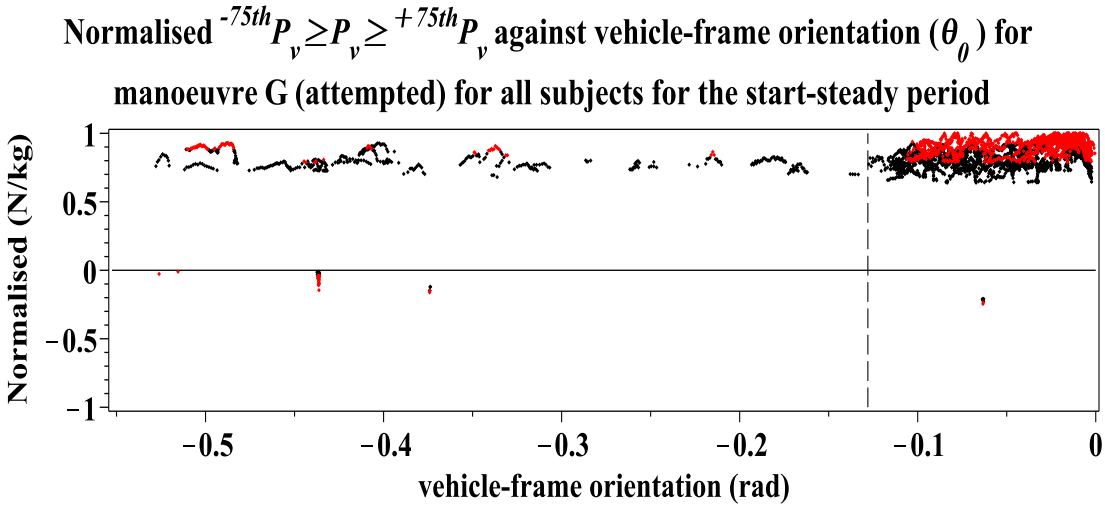

Figure D.52 – For the manoeuvre G (a.) for all subjects [G] occurrences of ${}^{-75th}_{ssi}P^{\mathrm{G}}_{v} \geq P_v > {}^{-90th}_{ssi}P^{\mathrm{G}}_{v}$ and of ${}^{+75th}_{ssi}P^{\mathrm{G}}_{v} \leq P_v < {}^{+90th}_{ssi}P^{\mathrm{G}}_{v}$ (both black markers) and, $P_v \leq {}^{-90th}_{ssi}P^{\mathrm{G}}_{v}$ and $P_v \geq {}^{+90th}_{ssi}P^{\mathrm{G}}_{v}$ (both red markers) in N/kg (normalised against each subject's maximum magnitude P_v for the $\{{}_{ssi}\theta^{\mathrm{G}}_0\}$) against θ_0 displacement for the $\{{}_{ssi}\theta^{\mathrm{G}}_0\}$ for each subject: $\theta_0 = -0.128$ line indicated (dashed vertical)

further observations are made. Firstly, it is evident that for $\{{}_{ss1}\theta^{\mathrm{G}}_0\}$ the accumulated occurrences of $P_v \geq {}^{+75th}_{ssi}P^{\mathrm{G}}_{v}$ from all subjects[G] are contiguous. Secondly, the contiguity includes all the peak P_v for all subjects[G]. These two observations indicate that taking account of all subjects[G], despite any variations between subjects, the mechanism is so configured that the occurrences of the largest $P_v > 0$ is maintained until $\theta_0 = -0.128$ rad and that all the peak $P_v > 0$ have occurred by then and hence division of $\{{}_{ssi}\theta^{\mathrm{G}}_0\}$ at this location relates to a mechanical property of the system for manoeuvre G (a.).

Figure D.53 (page 336) shows measures for $P_v \geq {}^{+90th}_{ss1}P^{\mathrm{G}}_{v}$ (N/kg) for all subjects[G] for the $\{{}_{ss1}\theta^{\mathrm{G}}_0\}$. Representative values for the largest P_v are obtained as follows. For each subject[G] the measure for the minimum ${}^{+90th}_{ss1}P^{\mathrm{G}}_{v}$, denoted ${}^{+90th}_{ss1}P^{\mathrm{G}}_{vmini}$, can be read and the minimum ${}^{+90th}_{ss1}P^{\mathrm{G}}_{vmini}$ for all subjects[G], denoted ${}^{+90th}_{ss1}P^{\mathrm{G}}_{vmin}$, is 0.30 N/kg (subject[13]). The maximum P_v for each subject[G], denoted ${}^{+90th}_{ss1}P^{\mathrm{G}}_{vmaxi}$, can also be read and the maximum ${}^{+90th}_{ss1}P^{\mathrm{G}}_{vmaxi}$ denoted ${}^{+90th}_{ss1}P^{\mathrm{G}}_{vmax}$ is 0.61 N/kg (subject[14]). The mean ${}^{+90th}_{ss1}P^{\mathrm{G}}_{vmini} \leq P_v \leq {}^{+90th}_{ss1}P^{\mathrm{G}}_{vmaxi}$ for each subject[G] are indicated by a solid circle located in the second to third quarter of the intra-subject range. Subject[0] shows the range of

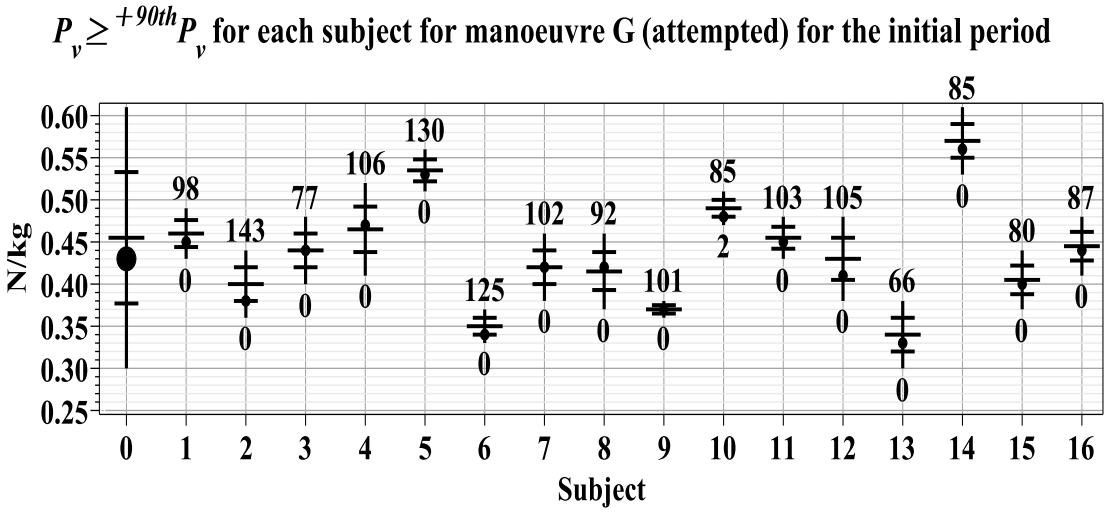

Figure D.53 – Shows for each subject[G] (i) for $\{{}_{ss1}\theta_0^{\mathrm{G}}\}$ in N/kg: a vertical line indicating the minimum measure ${}^{+90th}_{ss1}P^{\mathrm{G}}_{vmini}$ to the maximum measure ${}^{+90th}_{ss1}P^{\mathrm{G}}_{vmaxi}$, a solid circle indicating the mean measure ${}^{+90th}_{ss1}P^{\mathrm{G}}_{vmeani}$, the quarter divisions of the range (horizontal lines), the number of occurrences of $P_v \geq {}^{+90th}_{ss1}P^{\mathrm{G}}_{v}$ shown above the range line and the number of occurrences of $P_v \leq {}^{-90th}_{ss1}P^{\mathrm{G}}_{v}$ shown below the range line. Subject[0] shows these results for all subjects[G] with a solid circle indicating the mean of the mean ${}^{+90th}_{ss1}P^{\mathrm{G}}_{vmini} \leq P_v \leq {}^{+90th}_{ss1}P^{\mathrm{G}}_{vmaxi}$.

the minimum ${}^{+90th}_{ss1}P^{\mathrm{G}}_{vmini}$ to the maximum ${}^{+90th}_{ss1}P^{\mathrm{G}}_{vmaxi}$ and the mean of the mean ${}^{+90th}_{ss1}P^{\mathrm{G}}_{vmini} \leq P_v \leq {}^{+90th}_{ss1}P^{\mathrm{G}}_{vmaxi}$ is indicated by a solid circle and this is located approximately centrally in the inter-subject range.

It can also be seen from Figure D.53 (page 336) that the range magnitude of 0.31 N/kg, ${}^{+90th}_{ss1}P^{\mathrm{G}}_{vmax} - {}^{+90th}_{ss1}P^{\mathrm{G}}_{vmin}$, arises from inter-subject variation and is not the result of the ${}^{+90th}_{ss1}P^{\mathrm{G}}_{vmaxi} - {}^{+90th}_{ss1}P^{\mathrm{G}}_{vmini}$ magnitude of a specific subject. There are therefore substantial differences between subjects for the magnitudes of the largest $P_v > 0$. However, the inequality ${}^{+90th}_{ss1}P^{\mathrm{G}}_{vmini} \leq P_v \leq {}^{+90th}_{ss1}P^{\mathrm{G}}_{vmaxi}$ provides a representative range for each subject[G]. Additionally the inequality ${}^{+90th}_{ss1}P^{\mathrm{G}}_{vmin} \leq P_v \leq {}^{+90th}_{ss1}P^{\mathrm{G}}_{vmax}$ provides a representative range for all subjects[G].

D.10.3. *Manoeuvre G (a.)* P_{uCs}

Figure D.54 (page 337) shows, against θ_0, occurrences of ${}^{-75th}_{ssi}P^{\mathrm{G}}_{uCs} \geq P_{uCs} > {}^{-90th}_{ssi}P^{\mathrm{G}}_{uCs}$ and of ${}^{+75th}_{ssi}P^{\mathrm{G}}_{uCs} \leq P_{uCs} < {}^{+90th}_{ssi}P^{\mathrm{G}}_{uCs}$ (both black markers) and, of $P_{uCs} \leq {}^{-90th}_{ssi}P^{\mathrm{G}}_{uCs}$ and of $P_{uCs} \geq {}^{+90th}_{ssi}P^{\mathrm{G}}_{uCs}$ (both red markers): to aid inspection the measures (N/kg) for each subject are normalised against the subject's P_{uCs} peak magnitude for $\{{}_{ssi}\theta_0^{\mathrm{G}}\}$: these are the occurrences for all subjects[G]. It is evident that peak

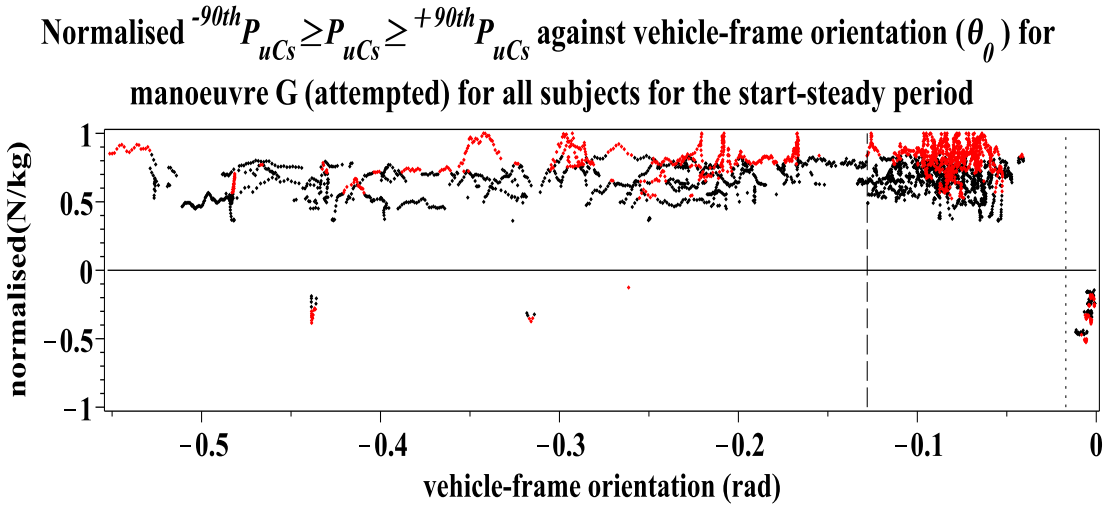

Figure D.54 – For the manoeuvre G (a.) for all subjects[G] occurrences of ${}^{-75th}_{ssi}P^{\mathrm{G}}_{uCs} \geq P_{uCs} > {}^{-90th}_{ssi}P^{\mathrm{G}}_{uCs}$ and of ${}^{+75th}_{ssi}P^{\mathrm{G}}_{uCs} \leq P_{uCs} < {}^{+90th}_{ssi}P^{\mathrm{G}}_{uCs}$ (both black markers) and, $P_{uCs} \leq {}^{-90th}_{ssi}P^{\mathrm{G}}_{uCs}$ and $P_{uCs} \geq {}^{+90th}_{ssi}P^{\mathrm{G}}_{uCs}$ (both red markers) in N/kg (normalised against each subject's maximum magnitude P_{uCs} for the $\{{}_{ssi}\theta^{\mathrm{G}}_0\}$) against θ_0 displacement for the $\{{}_{ssi}\theta^{\mathrm{G}}_0\}$ for each subject: $\theta_0 = -0.128$ line indicated (dashed vertical) and $\theta_0 = -0.017$ line indicated (dotted vertical)

measures occur in $\{{}_{ss2i}\theta^{\mathrm{G}}_0\}$ and that therefore Figure D.54 does not demonstrate that all subject[G] contribute to the $P_{uCs} \geq {}^{+90th}_{ssi}P^{\mathrm{G}}_{uCs}$ for $\{{}_{ss1}\theta^{\mathrm{G}}_0\}$. Relatedly, examination of the data (results not presented) indicates that there are no $P_{uCs} < 0$ for $\{{}_{ss1a}\theta^{\mathrm{G}}_0\}$.

Figure D.55 (page 338) shows measures for $P_{uCs} \geq {}^{+90th}_{ss1}P^{\mathrm{G}}_{uCs}$ (N/kg) for all subjects[G] for $\{{}_{ss1}\theta^{\mathrm{G}}_0\}$. For each subject occurrences of $P_{uCs} \geq {}^{+90th}_{ss1}P^{\mathrm{G}}_{uCs}$ are shown above the range line in Figure D.53 and the percentage of occurrences of $P_{uCs} = 0$ (integer) are shown below the range line. Substantial variation is evident: subject[3] has no occurrences of $P_{uCs} = 0$ where as subject[15] has 76% $P_{uCs} = 0$ occurrences In other words the attempt at manoeuvre[G] by some subjects, to some extent, reduces the occurrences of the couple action.

Representative values for the largest P_{uCs} are obtained as follows. For each subject[G] the measure for the minimum ${}^{+90th}_{ss1}P^{\mathrm{G}}_{uCs}$, denoted ${}^{+90th}_{ss1}P^{\mathrm{G}}_{uCsmini}$, may be read and the minimum ${}^{+90th}_{ss1}P^{\mathrm{G}}_{uCsmini}$ for all subjects[G], denoted ${}^{+90th}_{ss1}P^{\mathrm{G}}_{uCsmin}$, is 0.25 N/kg (subject[8]). The maximum P_{uCs} for each subject[G], denoted ${}^{+90th}_{ss1}P^{\mathrm{G}}_{uCsmaxi}$, may be read and the maximum ${}^{+90th}_{ss1}P^{\mathrm{G}}_{uCsmaxi}$, denoted ${}^{+90th}_{ss1}P^{\mathrm{G}}_{uCsmax}$, is 0.69 N/kg (subject[11]). The mean ${}^{+90th}_{ss1}P^{\mathrm{G}}_{uCsmini} \leq P_{uCs} \leq$

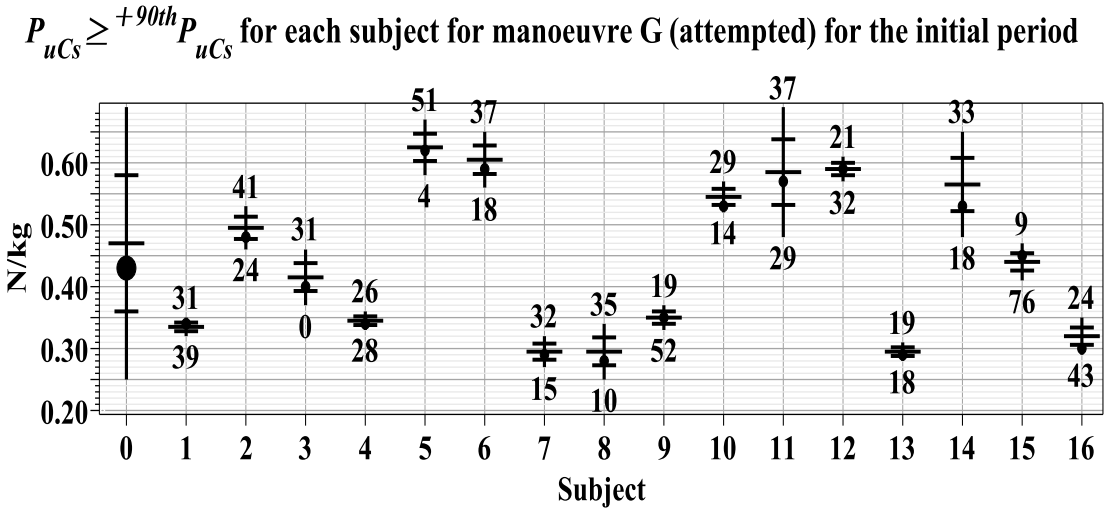

Figure D.55 – Shows for each subject[G] (i) for $\{{}_{ss1}\theta_0^{\mathrm{G}}\}$ in N/kg: a vertical line indicating the minimum measure ${}^{+90th}_{ss1}P^{\mathrm{G}}_{uCsmini}$ to the maximum measure ${}^{+90th}_{ss1}P^{\mathrm{G}}_{uCsmaxi}$, a solid circle indicating the mean measure mean of all the mean ${}^{+90th}_{ss1}P^{\mathrm{G}}_{uCsmini} \leq P_{uCs} \leq {}^{+90th}_{ss1}P^{\mathrm{G}}_{uCsmaxi}$, the quarter divisions of the range (horizontal lines), the number of occurrences of $P_{uCs} \geq {}^{+90th}_{ss1}P^{\mathrm{G}}_{uCs}$ shown above the range line and the number of percentage of occurrences for $P_{uCs} = 0$ (integer) shown below the range line. Subject[0] shows these results for all subjects[G]with a solid circle indicating the mean of all the mean ${}^{+90th}_{ss1}P^{\mathrm{G}}_{uCsmini} \leq P_{uCs} \leq {}^{+90th}_{ss1}P^{\mathrm{G}}_{uCsmaxi}$.

${}^{+90th}_{ss1}P^{\mathrm{G}}_{uCsmaxi}$ for each subject[G] are indicated by a solid circle and it can be seen that these are located in the first to third quarter of the intra-subject range except where the range is of short magnitude. Subject[0] shows the range of the minimum ${}^{+90th}_{ss1}P^{\mathrm{G}}_{uCsmini}$ to the maximum ${}^{+90th}_{ss1}P^{\mathrm{G}}_{uCsmaxi}$ and the mean of all the mean ${}^{+90th}_{ss1}P^{\mathrm{G}}_{uCsmini} \leq P_{uCs} \leq {}^{+90th}_{ss1}P^{\mathrm{G}}_{uCsmaxi}$ is indicated by a solid circle and this is located approximately centrally in the inter-subject range.

D.10.4. *Manoeuvre G (a.) P_u*

Figure D.56 (page 339) shows, against θ_0, occurrences of ${}^{-75th}_{ssi}P^{\mathrm{G}}_{u} \geq P_u > {}^{-90th}_{ssi}P^{\mathrm{G}}_{u}$ and of ${}^{+75th}_{ssi}P^{\mathrm{G}}_{u} \leq P_u < {}^{+90th}_{ssi}P^{\mathrm{G}}_{u}$ (both black markers) and, of $P_u \leq {}^{-90th}_{ssi}P^{\mathrm{G}}_{u}$ and of $P_u \geq {}^{+90th}_{ssi}P^{\mathrm{G}}_{u}$ (both red markers): to aid inspection the measures (N/kg) for each subject are normalised against the subject's P_u peak magnitude for $\{{}_{ssi}\theta_0^{\mathrm{G}}\}$: these are the occurrences for all subjects[G]. It is evident that a peak measure occurs in $\{{}_{ss2i}\theta_0^{\mathrm{G}}\}$ for some subjects[G] and that therefore Figure D.54 does not demonstrate that all subject[G] contribute to the peak P_u for $\{{}_{ss1}\theta_0^{\mathrm{G}}\}$. It is also evident that for $\{{}_{ss1a}\theta_0^{\mathrm{G}}\}$ that magnitudes of $P_u > 0$ are relatively small compared

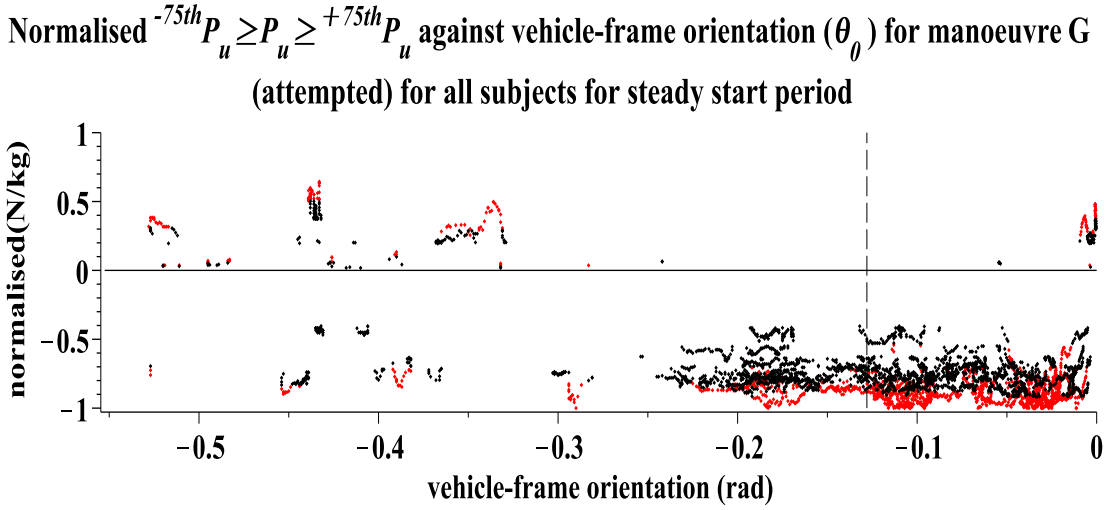

Figure D.56 – Shows for the manoeuvre G (a.) against θ_0 for all subjects[G]: for $\{{}_{ssi}\theta_0^{\mathrm{G}}\}$ occurrences of ${}^{-75th}_{ssi}P_u^{\mathrm{G}} \geq P_u > {}^{-90th}_{ssi}P_u^{\mathrm{G}}$ and of ${}^{+75th}_{ssi}P_u^{\mathrm{G}} \leq P_u < {}^{+90th}_{ssi}P_u^{\mathrm{G}}$ (both black markers), and of $P_u \leq {}^{-90th}_{ssi}P_u^{\mathrm{G}}$ and of $P_u \geq {}^{+90th}_{ssi}P_u^{\mathrm{G}}$ (both red markers) in N/kg (normalised against each subject's maximum magnitude P_{uCs} for $\{{}_{ssi}\theta_0^{\mathrm{G}}\}$): $\theta_0 = -0.128$ line indicated (dashed vertical).

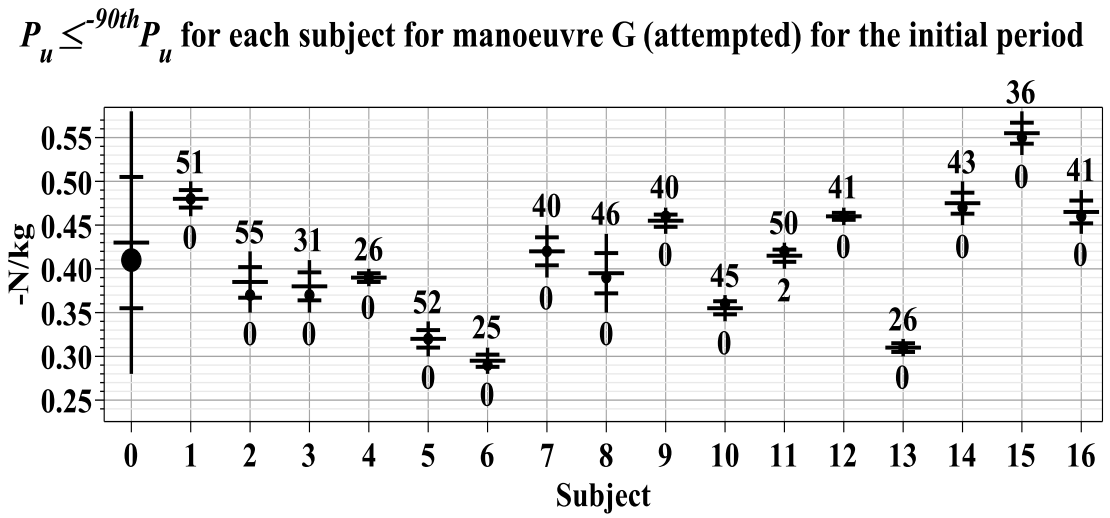

Figure D.57 – Shows for each subject[G] (i) for the $\{{}_{ss1}\theta_0^{\mathrm{G}}\}$ in -N/kg: a vertical line indicating the minimum magnitude measure ${}^{-90th}_{ss1}P^{\mathrm{G}}_{umini}$ to the maximum magnitude measure ${}^{-90th}_{ss1}P^{\mathrm{G}}_{umaxi}$, a solid circle indicating the mean measure, the quarter divisions of the range (horizontal lines), the number of occurrences of $P_{uCs} \leq {}^{-90th}_{ss1}P_u^{\mathrm{G}}$ shown above the range line and the number of occurrences of $P_u \geq {}^{+90th}_{ss1}P_u^{\mathrm{G}}$ for $\{{}_{ss1a}\theta_0^{\mathrm{G}}\}$ (i.e. commencing at $\theta_0 = -0.017$ rad rather than motion-start) shown below the range line. Subject[0] shows these results for all subjects[G] with a solid circle indicating the mean for all the mean ${}^{-90th}_{ss1}P^{\mathrm{G}}_{umini} \leq P_u \leq {}^{-90th}_{ss1}P^{\mathrm{G}}_{umaxi}$.

with magnitudes of $P_u < 0$.

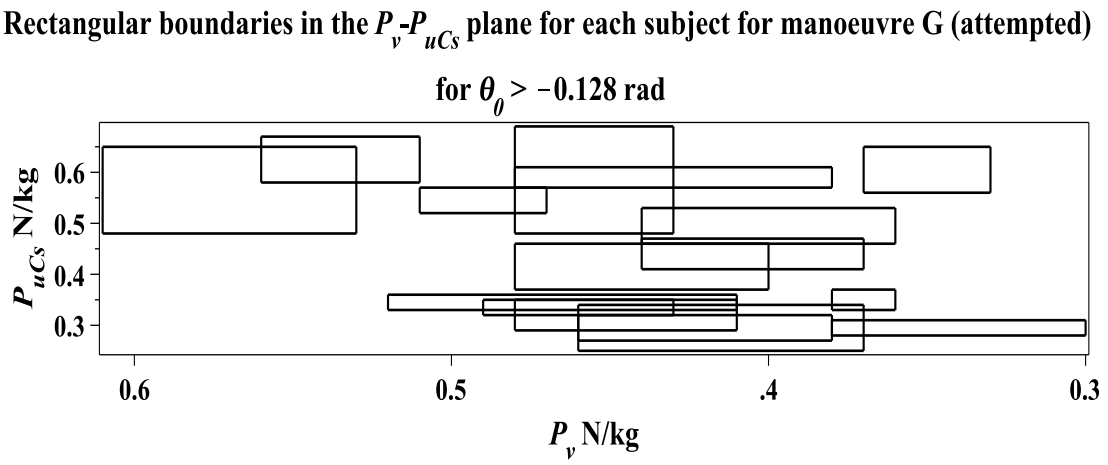

Figure D.58 – Rectangles formed with vertices of coordinates $[{}^{-90th}_{ss1}P^{\mathrm{G}}_{vmini}, {}^{+90th}_{ss1}P^{\mathrm{G}}_{uCsmini}]$, $[{}^{-90th}_{ss1}P^{\mathrm{G}}_{vmaxi}, {}^{+90th}_{ss1}P^{\mathrm{G}}_{uCsmini}]$, $[{}^{-90th}_{ss1}P^{\mathrm{G}}_{vmaxi}, {}^{+90th}_{ss1}P^{\mathrm{G}}_{uCsmaxi},]$, and $[{}^{-90th}_{ss1}P^{\mathrm{G}}_{vmini}, {}^{+90th}_{ss1}P^{\mathrm{G}}_{uCsmaxi}]$ for all subjects[G] i.e. n=16.

Figure D.57 (page 339) shows $P_u \geq {}^{-90th}_{ss1}P^{\mathrm{G}}_{u}$ in (-N/kg) for all subjects[G] for $\{{}_{ss1}\theta^{\mathrm{G}}_0\}$. Representative values for the largest magnitude P_u are obtained as follows. For each subject[G] the measure for the minimum magnitude ${}^{-90th}_{ss1}P^{\mathrm{G}}_{u}$, denoted ${}^{-90th}_{ss1}P^{\mathrm{G}}_{umini}$, can be read and the minimum magnitude ${}^{-90th}_{ss1}P^{\mathrm{G}}_{umini}$ for all subjects[G], denoted ${}^{-90th}_{ss1}P^{\mathrm{G}}_{umin}$, is −0.28 N/kg (subject[6]). The maximum magnitude P_u for each subject[G], denoted ${}^{-90th}_{ss1}P^{\mathrm{G}}_{umaxi}$ can also be read and the maximum magnitude ${}^{-90th}_{ss1}P^{\mathrm{G}}_{umaxi}$, denoted ${}^{-90th}_{ss1}P^{\mathrm{G}}_{umax}$, is −0.58 N/kg (subject[15]). The mean ${}^{-90th}_{ss1}P^{\mathrm{G}}_{umaxi} \leq P_u \leq {}^{-90th}_{ss1}P^{\mathrm{G}}_{umini}$ for each subject[G] are also shown and it can be seen that these are located in the second to third quarter of the intra-subject range. Subject[0] shows the range from ${}^{-90th}_{ss1}P^{\mathrm{G}}_{umin}$ to ${}^{-90th}_{ss1}P^{\mathrm{G}}_{umax}$ with the mean for all the mean ${}^{-90th}_{ss1}P^{\mathrm{G}}_{umini} \leq P_u \leq {}^{-90th}_{ss1}P^{\mathrm{G}}_{umaxi}$ located approximately centrally as indicated by a solid circle.

D.10.5. *Manoeuvre G (a.) the $P_v - P_{uCs}$ plane*

This final section relating to manoeuvre G (a.) uses the inequalities, as previously defined, to define a cuboid boundary for the largest magnitude measures for each and all subjects. For each of subjects[1,..., 16] the following inequalities define the cuboid boundaries:

${}^{+90th}_{ss1}P^{\mathrm{G}}_{uCsmini} \leq P_{uCs} \leq {}^{+90th}_{ss1}P^{\mathrm{G}}_{uCsmaxi}$ (page 336),

${}^{+90th}_{ss1}P^{\mathrm{G}}_{vmini} \leq P_v \leq {}^{+90th}_{ss1}P^{\mathrm{G}}_{vmaxi}$ (page 333) and

$^{-90th}_{ss1}P^{\mathrm{G}}_{umini} \geq P_u \geq {}^{-90th}_{ss1}P^{\mathrm{G}}_{umaxi}$ (page 338)

and these three inequalities are denoted $^{large}_{ss1}\mathbf{P}^{\mathrm{G}}_{i}$.

A graphical representation of $^{large}_{ss1}\mathbf{P}^{\mathrm{G}}_{i}$ in the $P_v - P_{uCs}$ plane is shown in Figure D.58 (page 340): the construction follows the same process as described in Section 6.4.4 (page 149) for manoeuvre F (a.).

Three inequalities define the cuboid boundaries which enclose the measures for all, rather than each of, subjects[G] and removal of the i subscript from the above definitions provides this. These three inequalities are denoted $^{large}_{ss1}\mathbf{P}^{\mathrm{G}}$. In conclusion $^{large}_{ss1}\mathbf{P}^{\mathrm{G}}$ provides a useful representation the largest handle-forces for all subjects[G] for manoeuvre G (a.): the numerical values are:

$0.30 \leq P_v \leq 0.61$ (N/kg),

$0.25 \leq P_{uCs} \leq 0.69$ (N/kg) and

$-0.28 \geq P_u \geq -0.58$ (N/kg).

D.11. **Manoeuvre D (attempted)**

In this section a trailing super or sub script D in a symbol or 'all subjects[D]' indicates measures from subjects [1,. . . , 16].

D.11.1. *Manoeuvre D (a.) force measures*

Examination of the force measures will show that dividing the start-steady period, denoted $\{_{ssi}\theta^{\mathrm{D}}_0\}$, at $\theta_0 = -0.115$ rad is useful and hence θ_0 measures for the manoeuvre D (a.) are defined for an initial period $-0.115 < \theta_0 < 0$ rad, denoted $\{_{ss1}\theta^{\mathrm{D}}_0\}$, and for a later period $\theta_{0steadi} < \theta_0 < -0.115$ rad, denoted $\{_{ss2i}\theta^{\mathrm{D}}_0\}$. There is some variation between subjects immediately after motion start for a small θ_0 displacement: magnitude no greater than 0.028 rad. The range $-0.115 < \theta_0 < -0.028$ rad is denoted $\{_{ss1a}\theta^{\mathrm{D}}_0\}$ ($\{_{ss1}\theta^{\mathrm{D}}_0\}$ modified to commence at $\theta_0 = -0.028$ rad rather than motion-start).

For the modified initial period $\{_{ss1a}\theta^{\mathrm{D}}_0\}$ the force measures for subject[1], illustrated in Figure D.60 (page 342), are representative of all subjects[D] in two respects. Firstly, compared with $P_{uCs} > 0$, magnitudes and occurrences of $P_{uCs} < 0$ are negligible. Secondly, occurrences and magnitudes of $P_v < 0$ are negligible.

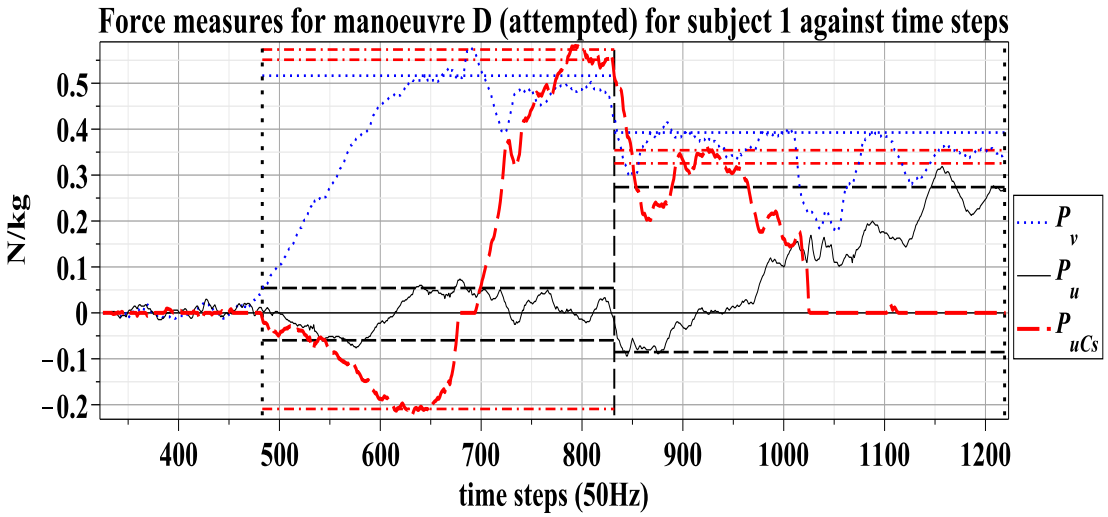

Figure D.59 – For subject[1] for manoeuvre D (a.), measures: P_v (dotted blue), P_u (thin black) and P_{uCs} (thick red dashed) in N/kg plotted against time-steps (approximately 0.02 seconds) with motion-start line (vertical black dotted: closest to left side), steady-start line (vertical black dotted: closest to right side) and $\theta_0 = -0.115$ rad line (vertical black dashed). The following percentile lines are shown for $\{{}_{ss1}\theta_0^{\mathrm{D}}\}$: ${}^{-90th}_{ss1}P^{\mathrm{D}}_{uCs}$, ${}^{+90th}_{ss1}P^{\mathrm{D}}_{uCs}$ and ${}^{+75th}_{ss1}P^{\mathrm{D}}_{uCs}$ (horizontal red dash-dot), ${}^{+90th}_{ss1}P^{\mathrm{D}}_{u}$ and ${}^{-90th}_{ss1}P^{\mathrm{D}}_{u}$ (horizontal black dash) and ${}^{+90th}_{ss1}P^{\mathrm{D}}_{v}$ (horizontal blue dot): these percentile lines are also shown for $\{{}_{ss2i}\theta_0^{\mathrm{D}}\}$.

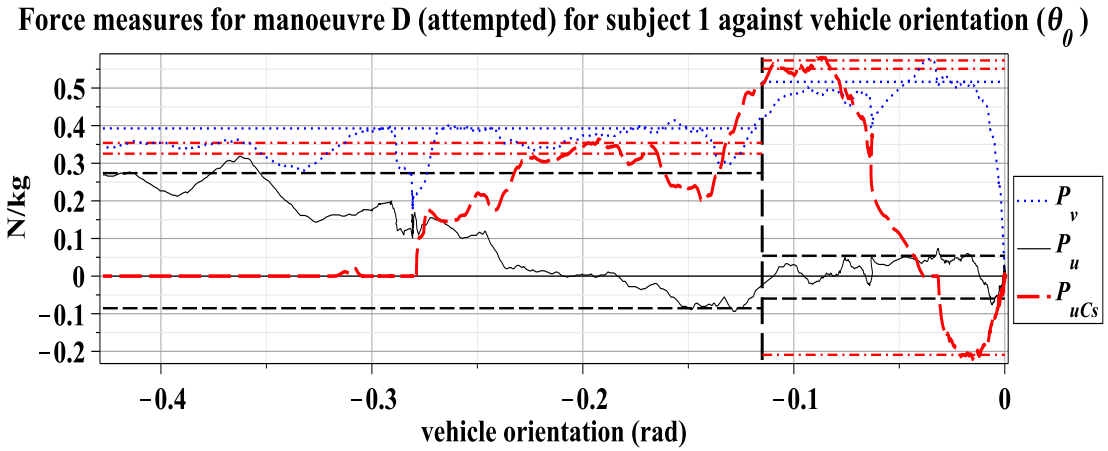

Figure D.60 – Shows for subject[1] for manoeuvre D (a.), measures plotted against vehicle-frame orientation (θ_0) with other details as above.

D.11.2. *Manoeuvre D (a.) P_v*

The presentation begins with P_v. Figure D.61 (page 343) graphs, against vehicle-frame orientation, occurrences of ${}^{-75th}_{ssi}P^{\mathrm{D}}_{v} \geq P_v > {}^{-90th}_{ssi}P^{\mathrm{D}}_{v}$ and of ${}^{+75th}_{ssi}P^{\mathrm{D}}_{v} \leq P_v < {}^{+90th}_{ssi}P^{\mathrm{D}}_{v}$ (both black markers) and, of $P_v \leq {}^{-90th}_{ssi}P^{\mathrm{D}}_{v}$ and of $P_v \geq {}^{+90th}_{ssi}P^{\mathrm{D}}_{v}$ (both red markers): to aid inspection the measures (N/kg) for each subject are normalised

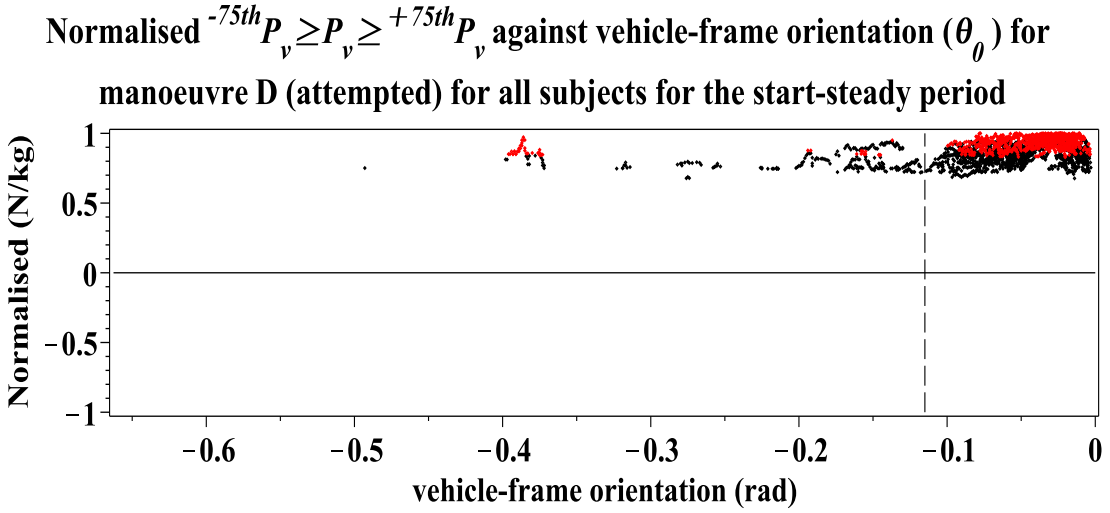

Figure D.61 – For the manoeuvre D (a.) occurrences of ${}^{-75th}_{ssi}P^{\mathrm{D}}_v \geq P_v > {}^{-90th}_{ssi}P^{\mathrm{D}}_v$ and of ${}^{+75th}_{ssi}P^{\mathrm{D}}_v \leq P_v < {}^{+90th}_{ssi}P^{\mathrm{D}}_v$ (both black markers) and, of $P_v \leq {}^{-90th}_{ssi}P^{\mathrm{D}}_v$ and of $P_v \geq {}^{+90th}_{ssi}P^{\mathrm{D}}_v$ (both red markers) in N/kg against θ_0 for $\{{}_{ssi}\theta^{\mathrm{D}}_0\}$ for each subject: $\theta_0 = -0.115$ line indicated (dashed vertical)

against the subject's P_v peak magnitude for $\{{}_{ssi}\theta^{\mathrm{D}}_0\}$: these are the occurrences for all subjects[D]: a dashed line indicates $\theta_0 = -0.115$ rad. It is evident from Figure D.61 that all P_v are $P_v > 0$ and this confirms the representativeness of Figure D.60 (page 342) in this respect. Two further observations are made. Firstly, it is evident that for $\{{}_{ss1}\theta^{\mathrm{D}}_0\}$ the accumulated occurrences from all subjects[D] of $P_v \geq {}^{+75th}_{ssi}P^{\mathrm{D}}_v$ are contiguous. Secondly, the contiguity includes all the peak $P_v > 0$ for all subjects[D]. Thus for all subjects[D], despite any subject variations, the mechanism is so configured that all subjects have an occurrence of their peak handle-force magnitude by $\theta_0 = -0.115$ rad and hence division of the start-steady period at this location relates to a mechanical property of the system for manoeuvre D (a.).

Figure D.62 (page 344) shows measures for $P_v \geq {}^{+90th}_{ss1}P^{\mathrm{D}}_v$ (N/kg) for each of subjects[D] and for all subjects[D], denoted subject[0], for $\{{}_{ss1}\theta^{\mathrm{D}}_0\}$. Representative values for the largest P_v are obtained as follows. For each subject[D] the measure for the minimum ${}^{+90th}_{ss1}P^{\mathrm{D}}_v$, denoted ${}^{+90th}_{ss1}P^{\mathrm{D}}_{vmini}$, may be read and the minimum ${}^{+90th}_{ss1}P^{\mathrm{D}}_{vmini}$ for all subjects[D], denoted ${}^{+90th}_{ss1}P^{\mathrm{D}}_{vmin}$, is 0.28 N/kg (subject[2]). The maximum P_v for each subject[D], denoted ${}^{+90th}_{ss1}P^{\mathrm{D}}_{vmaxi}$, may also be read and the maximum ${}^{+90th}_{ss1}P^{\mathrm{D}}_{vmaxi}$ denoted ${}^{+90th}_{ss1}P^{\mathrm{D}}_{vmax}$ is 0.65 N/kg (subject[4]). The mean ${}^{+90th}_{ss1}P^{\mathrm{D}}_{vmini} \leq P_v \leq {}^{+90th}_{ss1}P^{\mathrm{D}}_{vmaxi}$ for each subject[D] is is indicated by a

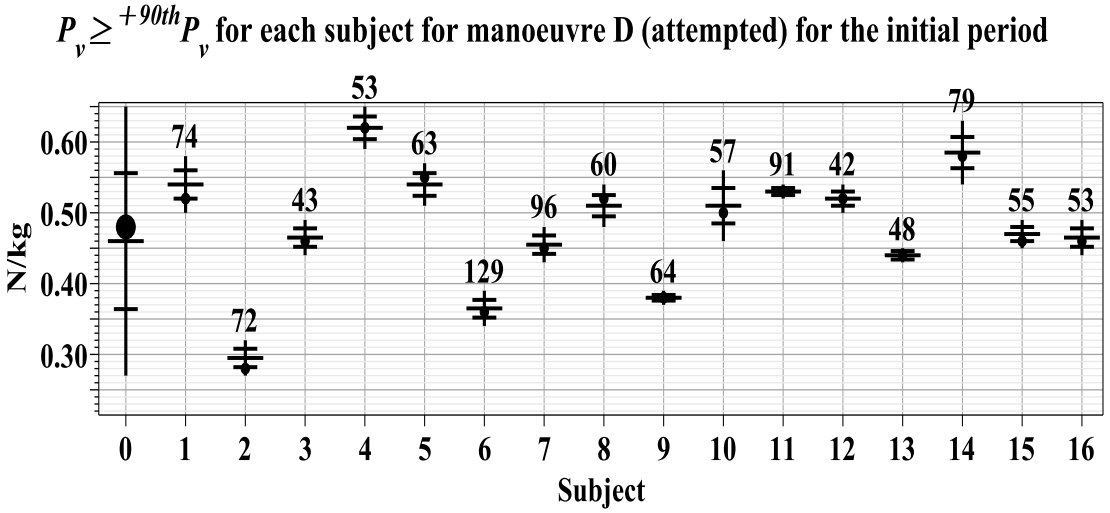

Figure D.62 – Shows for each subject[D] (i) for $\{{}_{ss1}\theta_0^{\mathrm{D}}\}$ in N/kg: a vertical line indicating the minimum ${}^{+90th}_{ss1}P^{\mathrm{D}}_{vmini}$ to the maximum ${}^{+90th}_{ss1}P^{\mathrm{D}}_{vmaxi}$, a solid circle indicating the mean ${}^{+90th}_{ss1}P^{\mathrm{D}}_{vmini} \leq P_v \leq {}^{+90th}_{ss1}P^{\mathrm{D}}_{vmaxi}$, the quarter divisions of the range (horizontal lines) and the number of occurrences of $P_v \geq {}^{+90th}_{ss1}P^{\mathrm{D}}_{v}$. Subject[0] shows these results for all subjects[D] with a solid circle indicating the mean of all the mean ${}^{+90th}_{ss1}P^{\mathrm{D}}_{vmini} \leq P_v \leq {}^{+90th}_{ss1}P^{\mathrm{D}}_{vmaxi}$.

solid circle: it can be seen that these means are located from near the minimum range position to the third quarter of the intra-subject range. Subject[0] shows the range of the minimum ${}^{+90th}_{ss1}P^{\mathrm{D}}_{vmini}$ to the maximum ${}^{+90th}_{ss1}P^{\mathrm{D}}_{vmaxi}$ and the mean of all the mean ${}^{+90th}_{ss1}P^{\mathrm{D}}_{vmini} \leq P_v \leq {}^{+90th}_{ss1}P^{\mathrm{D}}_{vmaxi}$ is indicated by a solid circle and this is located approximately centrally in the inter-subject range. Occurrences are shown above the line range. As there are no $P_v < 0$ for the initial period the occurrences of $P_v \geq {}^{+90th}_{ss1}P^{\mathrm{D}}_{v}$ are equal to $\frac{50}{10} \times t_i(\{{}_{ss1}\theta_0^{\mathrm{D}}\})$

D.11.3. *Manoeuvre D (a.)* P_{uCs}

Figure D.63 (page 345) shows occurrences of ${}^{-75th}_{ssi}P^{\mathrm{D}}_{uCs} \geq P_{uCs} > {}^{-90th}_{ssi}P^{\mathrm{D}}_{uCs}$ and of ${}^{+75th}_{ssi}P^{\mathrm{D}}_{uCs} \leq P_{uCs} < {}^{+90th}_{ssi}P^{\mathrm{D}}_{uCs}$ (both black markers), and $P_{uCs} \leq {}^{-90th}_{ssi}P^{\mathrm{D}}_{uCs}$ and $P_{uCs} \geq {}^{+90th}_{ssi}P^{\mathrm{D}}_{uCs}$ (both red markers) for all subjects[D] : to assist inspection the N/kg measures for each subject are normalised against the subject's P_{uCs} peak magnitude for $\{{}_{ssi}\theta_0^{\mathrm{D}}\}$. A dashed vertical line indicates $\theta_0 = -0.115$ rad and this divides $\{{}_{ssi}\theta_0^{\mathrm{D}}\}$ into $\{{}_{ss1}\theta_0^{\mathrm{D}}\}$ and $\{{}_{ss2i}\theta_0^{\mathrm{D}}\}$ as previously defined. A dotted vertical line indicates $\theta_0 = -0.028$ rad

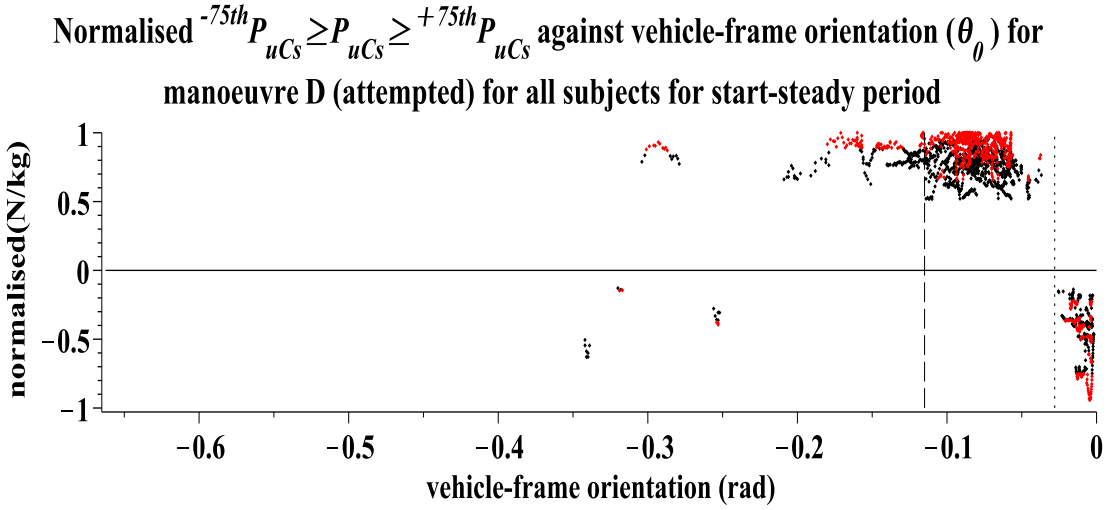

Figure D.63 – For the manoeuvre D (a.) occurrences of $^{-75th}_{ssi}P^{\mathrm{D}}_{uCs} \geq P_{uCs} > {}^{-90th}_{ssi}P^{\mathrm{D}}_{uCs}$ and of $^{+75th}_{ssi}P^{\mathrm{D}}_{uCs} \leq P_{uCs} < {}^{+90th}_{ssi}P^{\mathrm{D}}_{uCs}$ (both black markers) and, of $P_{uCs} \leq {}^{-90th}_{ssi}P^{\mathrm{D}}_{uCs}$ and of $P_{uCs} \geq {}^{+90th}_{ssi}P^{\mathrm{D}}_{uCs}$ (both red markers) in N/kg against vehicle-frame orientation for the start-steady period for each subject: $\theta_0 = -0.115$ line indicated (dashed vertical)

It is evident that peak measures occur in the later period$\{{}_{ss2i}\theta^{\mathrm{D}}_0\}$ and that therefore Figure D.63 does not demonstrate that all subject[D] contribute to the $P_{uCs} \geq {}^{+90th}_{ssi}P^{\mathrm{D}}_{uCs}$ for the initial period $\{{}_{ss1}\theta^{\mathrm{D}}_0\}$. It is also evident that there are no $P_{uCs} \leq {}^{-75th}_{ssi}P^{\mathrm{D}}_{uCs}$ for $\{{}_{ss1a}\theta^{\mathrm{D}}_0\}$ (i.e. commencing at $\theta_0 = -0.028$ rad rather than motion-start): an examination of the data (results not presented) shows that for all subjects[D] that there are no $P_{uCs} < 0$ for $\{{}_{ss1a}\theta^{\mathrm{D}}_0\}$ and this confirms the representativeness of Figure D.60 (page 342) in this respect.

Figure D.64 (page 346) shows measures for $P_{uCs} \geq {}^{+90th}_{ss1}P^{\mathrm{D}}_{uCs}$ (N/kg) for all subjects[D] for $\{{}_{ss1}\theta^{\mathrm{D}}_0\}$. Representative values for the largest P_{uCs} are obtained as follows. For each subject[D] the measure for the minimum ${}^{+90th}_{ss1}P^{\mathrm{D}}_{uCs}$, denoted ${}^{+90th}_{ss1}P^{\mathrm{D}}_{uCsmini}$, may be read and the minimum ${}^{+90th}_{ss1}P^{\mathrm{D}}_{uCsmini}$ for all subjects[D], denoted ${}^{+90th}_{ss1}P^{\mathrm{D}}_{uCsmin}$, is 0.38 N/kg (subject[2]). The maximum P_{uCs} for each subject[D], denoted ${}^{+90th}_{ss1}P^{\mathrm{D}}_{uCsmaxi}$, may also be read and the maximum ${}^{+90th}_{ss1}P^{\mathrm{D}}_{uCsmaxi}$, denoted ${}^{+90th}_{ss1}P^{\mathrm{D}}_{uCsmax}$, is 0.72 N/kg (subject[16]). The mean ${}^{+90th}_{ss1}P^{\mathrm{D}}_{uCsmINi} \leq P_{uCs} \leq {}^{+90th}_{ss1}P^{\mathrm{D}}_{uCsmaxi}$ for each subject[D] are indicated by a solid circle and it can be seen that these means, ignoring subjects where the range magnitude is relatively small, are located in the first quarter to central location of the intra-subject range. Subject[0] shows the range of ${}^{+90th}_{ss1}P^{\mathrm{D}}_{uCsmin}$ to

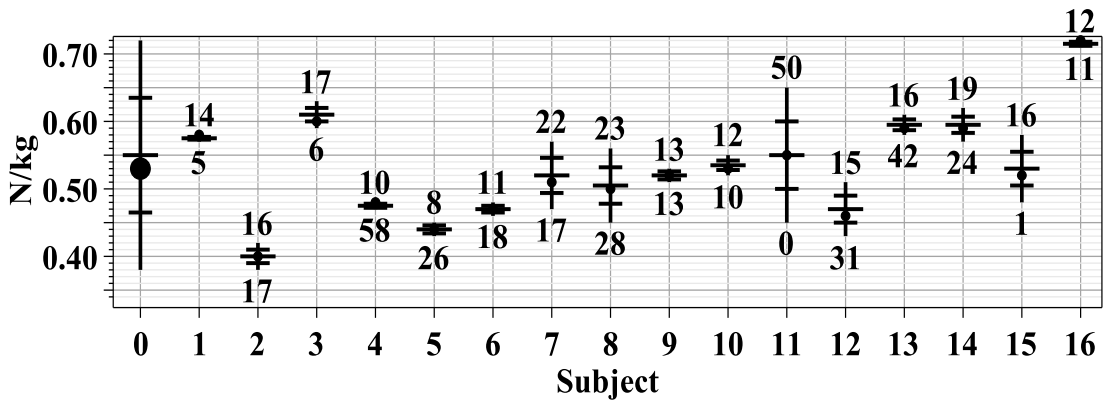

Figure D.64 – Shows for each subject[D] (i) for $\{{}_{ss1}\theta_0^{\mathrm{D}}\}$ in N/kg: a vertical line indicating the minimum ${}^{+90th}_{ss1}P^{\mathrm{D}}_{uCsmini}$ to the maximum ${}^{+90th}_{ss1}P^{\mathrm{D}}_{uCsmaxi}$, a solid circle indicating the mean ${}^{+90th}_{ss1}p^{\mathrm{D}}_{uCsmini} \leq P_{uCs} \leq {}^{+90th}_{ss1}P^{\mathrm{D}}_{uCsmaxi}$, the quarter divisions of the range (horizontal lines), the number of occurrences of $P_{uCs} \geq {}^{+90th}_{ss1}P^{\mathrm{D}}_{uCs}$ shown above the range line and the number of percentage of occurrences for $P_{uCs} = 0$ (integer) shown below the range line. Subject[0] shows these measures for all subjects[D] with a solid circle indicating the mean of all the mean ${}^{+90th}_{ss1}P^{\mathrm{D}}_{uCsmini} \leq P_{uCs} \leq {}^{+90th}_{ss1}P^{\mathrm{D}}_{uCsmaxi}$.

${}^{+90th}_{ss1}P^{\mathrm{D}}_{uCsmax}$ and the mean of all the mean ${}^{+90th}_{ss1}P^{\mathrm{D}}_{uCsmINi} \leq P_{uCs} \leq {}^{+90th}_{ss1}P^{\mathrm{D}}_{uCsmaxi}$ indicated by a solid circle can be seen to be located approximately at the centre of the inter-subject ranges. For each subject occurrences of $P_{uCs} \geq {}^{+90th}_{ss1}P^{G}_{uCs}$ are shown above the range line and the percentage of occurrences of $P_{uCs} = 0$ (integer) are shown below the range line. Substantial variation is evident: subject[11] has no occurrences of $P_{uCs} = 0$ where as subject[4] has 58% $P_{uCs} = 0$ occurrences In other words the attempt at manoeuvre[D] by some subjects, to some extent, reduces the occurrences of the couple action.

It can also be seen from Figure D.64 (page 346) that the range magnitude of 0.34 N/kg, ${}^{+90th}_{ss1}P^{\mathrm{D}}_{uCsmax} - {}^{+90th}_{ss1}P^{\mathrm{D}}_{uCsmin}$, arises from inter-subject variation (subject[2] and subject[16]) and is not the result of the ${}^{+90th}_{ss1}P^{\mathrm{D}}_{uCsmaxi} - {}^{+90th}_{ss1}P^{\mathrm{D}}_{uCsmini}$ of a specific subject. There are therefore substantial differences between subjects for the largest $P_{uCs} > 0$. However, the inequality ${}^{+90th}_{ss1}P^{\mathrm{D}}_{uCsmini} \leq P_{uCs} \leq {}^{+90th}_{ss1}P^{\mathrm{D}}_{uCsmaxi}$ provides a representative range for each subject. In addition the inequality ${}^{+90th}_{ss1}P^{\mathrm{D}}_{uCsmin} \leq P_{uCs} \leq {}^{+90th}_{ss1}P^{\mathrm{D}}_{uCsmax}$ provides a representative range for all

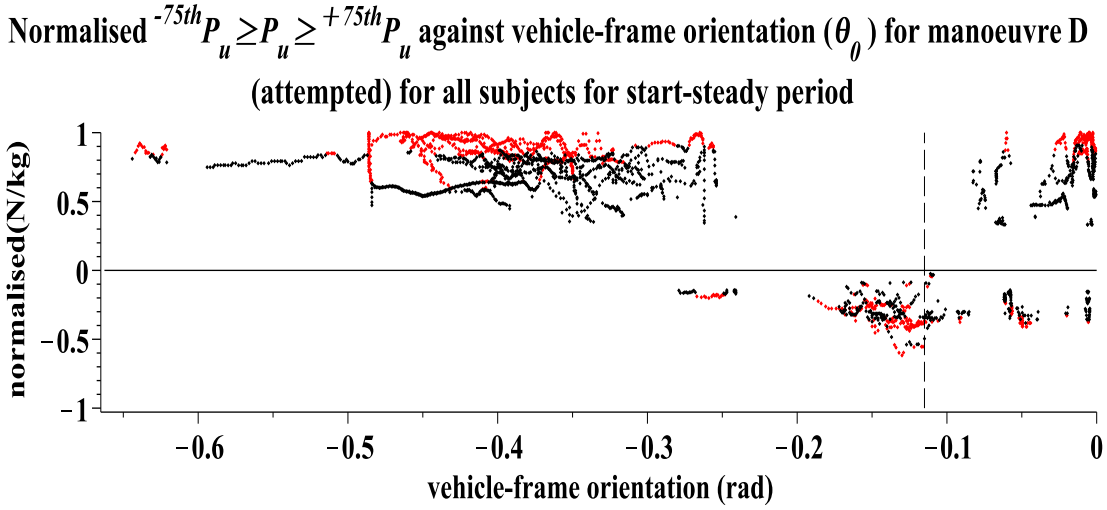

Figure D.65 – Shows for the manoeuvre D (a.) against θ_0 for all subjects[D]: for $\{{}_{ssi}\theta_0^{\mathrm{D}}\}$ occurrences of ${}^{-75th}_{ssi}P_u^{\mathrm{D}} \geq P_u > {}^{-90th}_{ssi}P_u^{\mathrm{D}}$ and of ${}^{+75th}_{ssi}P_u^{\mathrm{D}} \leq P_u < {}^{+90th}_{ssi}P_u^{\mathrm{D}}$ (both black markers), and of $P_u \leq {}^{-90th}_{ssi}P_u^{\mathrm{D}}$ and of $P_u \geq {}^{+90th}_{ssi}P_u^{\mathrm{D}}$ (both red markers) in N/kg (normalised against each subject's maximum magnitude P_u for $\{{}_{ssi}\theta_0^{\mathrm{D}}\}$). $\theta_0 = -0.115$ is indicated (dashed vertical).

subjects[D].

D.11.4. *Manoeuvre D (a.) P_u*

Figure D.65 (page 347) shows, against θ_0, occurrences of ${}^{-75th}_{ssi}P_u^{\mathrm{D}} \geq P_u > {}^{-90th}_{ssi}P_u^{\mathrm{D}}$ and of ${}^{+75th}_{ssi}P_u^{\mathrm{D}} \leq P_u < {}^{+90th}_{ssi}P_u^{\mathrm{D}}$ (both black markers) and, of $P_u \leq {}^{-90th}_{ssi}P_u^{\mathrm{D}}$ and of $P_u \geq {}^{+90th}_{ssi}P_u^{\mathrm{D}}$ (both red markers): to aid inspection the measures (N/kg) for each subject are normalised against the subject's P_u peak magnitude for $\{{}_{ssi}\theta_0^{\mathrm{D}}\}$: these are the occurrences for all subjects[D] and a dashed line indicates $\theta_0 = -0.115$ rad. It is evident that a peak measure occurs for $\{{}_{ss2i}\theta_0^{\mathrm{D}}\}$ for some subjects[D] and that therefore Figure D.65 does not demonstrate that all subject[D] contribute to the peak P_u for $\{{}_{ss1}\theta_0^{\mathrm{D}}\}$. It therefore follows that while Figure D.65 indicates the occurrences of P_u in both signs it is not possible to determine the comparative magnitudes of $P_u \geq {}^{+75th}_{ssi}P_u^{\mathrm{D}}$ and $P_u \leq {}^{-75th}_{ssi}P_u^{\mathrm{D}}$ for $\{{}_{ss1}\theta_0^{\mathrm{D}}\}$.

However, Figure D.66 (page 349) shows measures for ${}^{-90th}_{ss1}P_u^{\mathrm{D}} \geq P_u \geq {}^{+90th}_{ss1}P_u^{\mathrm{D}}$ (N/kg) for all subjects[D] for $\{{}_{ss1}\theta_0^{\mathrm{D}}\}$. Representative values for the largest $P_u > 0$ are obtained as follows. For each subject[D] the measure for the minimum ${}^{+90th}_{ss1}P_u^{\mathrm{D}}$, denoted ${}^{+90th}_{ss1}P^{\mathrm{D}}_{umini}$, can be read and the minimum ${}^{+90th}_{ss1}P^{\mathrm{D}}_{umini}$ for all subjects[D], denoted ${}^{+90th}_{ss1}P^{\mathrm{D}}_{umin}$, is 0.04 N/kg (subject[15]). The maximum P_u for each subject[D], denoted ${}^{+90th}_{ss1}P^{\mathrm{D}}_{umaxi}$, can also be read and the maximum ${}^{+90th}_{ss1}P^{\mathrm{D}}_{umaxi}$,

denoted ${}^{+90th}_{ss1}P^{\mathrm{D}}_{umax}$, is 0.58 N/kg (subject[4]). The mean ${}^{+90th}_{ss1}P^{\mathrm{D}}_{umini} \leq P_u \leq {}^{+90th}_{ss1}P^{\mathrm{D}}_{umaxi}$ for each subject[D] is indicated by a solid circle but it can be seen that with only two exceptions (subjects[4, 13]) the ranges are of such small magnitude that the location of the mean is immaterial. Occurrences of $P_u \geq {}^{+90th}_{ss1}P^{\mathrm{D}}_{u}$ are shown above the range line for $P_u > 0$ for each subject. Subject[0] shows the range from ${}^{+90th}_{ss1}P^{\mathrm{D}}_{umin}$ to ${}^{+90th}_{ss1}P^{\mathrm{D}}_{umax}$ with the mean for all the mean ${}^{+90th}_{ss1}P^{\mathrm{D}}_{umini} \leq P_u \leq {}^{+90th}_{ss1}P^{\mathrm{D}}_{umaxi}$ located in the second quarter as indicated by a solid circle.

It can also be seen from Figure D.66 (page 349) that the range magnitude of 0.54 N/kg, ${}^{+90th}_{ss1}P^{\mathrm{D}}_{umax} - {}^{+90th}_{ss1}P^{\mathrm{D}}_{umin}$, arises from inter-subject variation (subject[15] compared with subject[4]) and is not the result of the ${}^{+90th}_{ss1}P^{\mathrm{D}}_{umaxi} - {}^{+90th}_{ss1}P^{\mathrm{D}}_{umini}$ of a specific subject. There are therefore substantial differences between subjects for the largest $P_u > 0$. However, the inequality ${}^{+90th}_{ss1}P^{\mathrm{D}}_{umini} \leq P_u \leq {}^{+90th}_{ss1}P^{\mathrm{D}}_{umaxi}$ provides a representative range for each subject[D]. Additionally the inequality ${}^{+90th}_{ss1}P^{\mathrm{D}}_{umin} \leq P_u \leq {}^{+90th}_{ss1}P^{\mathrm{D}}_{umax}$ provides a representative range for all subjects[D] for the largest $P_u > 0$ for $\{{}_{ss1}\theta^{\mathrm{D}}_0\}$.

Representative values for the largest magnitude $P_u < 0$ are also read from Figure D.66. For each subject[D] the measure for the minimum magnitude ${}^{-90th}_{ss1}P^{\mathrm{D}}_{u}$, denoted ${}^{-90th}_{ss1}P^{\mathrm{D}}_{umini}$, can be read and the minimum ${}^{-90th}_{ss1}P^{\mathrm{D}}_{umini}$ for all subjects[D] with non-zero occurrences, denoted ${}^{-90th}_{ss1}P^{\mathrm{D}}_{umin}$, is -0.03 N/kg (subject[12]). The maximum magnitude $P_u < 0$ for each subjects[D], denoted ${}^{-90th}_{ss1}P^{\mathrm{D}}_{umaxi}$, can also be read and the maximum ${}^{-90th}_{ss1}P^{\mathrm{D}}_{umaxi}$, denoted ${}^{-90th}_{ss1}P^{\mathrm{D}}_{umax}$, is -0.14 N/kg (subjects[8, 14]). The occurrences of $P_u \leq {}^{-90th}_{ss1}P^{\mathrm{D}}_{u}$ are shown below the range line. The mean ${}^{-90th}_{ss1}P^{\mathrm{D}}_{umaxi} \leq P_u \leq {}^{-90th}_{ss1}P^{\mathrm{D}}_{umini}$ for each subject[D] is indicated by a solid circle but it can be seen that the ranges (excluding subjects[3, 4, 10] who have a single occurrence) are of such small magnitude that the location is immaterial. Subject[0] shows ${}^{-90th}_{ss1}P^{\mathrm{D}}_{umin}$ and ${}^{-90th}_{ss1}P^{\mathrm{D}}_{umax}$ with the mean of all the mean ${}^{-90th}_{ss1}\leq^{\mathrm{D}}_{umaxi} P_u \leq {}^{-90th}_{ss1}P^{\mathrm{D}}_{umini}$ approximately centrally located as indicated by a solid circle.

It can also be seen from Figure D.66 (page 349) that the range magnitude of 0.11 N/kg, ${}^{-90th}_{ss1}P^{\mathrm{D}}_{umax} - {}^{-90th}_{ss1}P^{\mathrm{D}}_{umin}$, arises from inter-subject variation (subject[12] compared with subjects[8, 14]) and is not the result of the ${}^{-90th}_{ss1}P^{\mathrm{D}}_{umaxi} - {}^{-90th}_{ss1}P^{\mathrm{D}}_{umini}$ of a specific subject. There are therefore differences between subjects for the largest

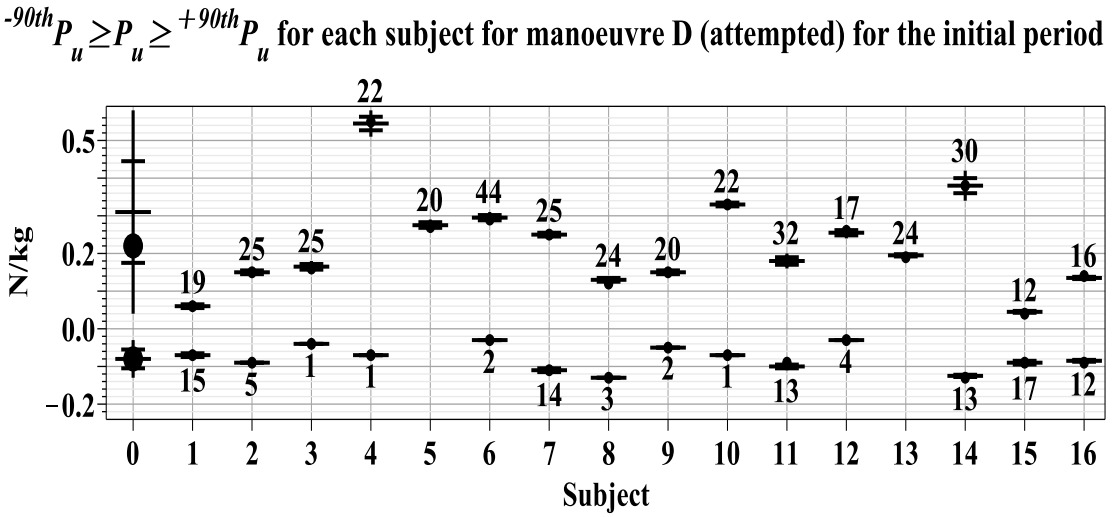

Figure D.66 – Shows for each subject[D] (i) for $\{{}_{ss1}\theta_0^{\mathrm{D}}\}$ in N/kg: for $P_u > 0$ a vertical line indicating the minimum magnitude measure ${}^{+90th}_{ss1}P^{\mathrm{D}}_{umini}$ to the maximum magnitude measure ${}^{+90th}_{ss1}P^{\mathrm{D}}_{umaxi}$, a solid circle indicating the mean ${}^{+90th}_{ss1}P^{\mathrm{D}}_{umini} \leq P_u \leq {}^{+90th}_{ss1}P^{\mathrm{D}}_{umaxi}$, the quarter divisions of the range (horizontal lines) and the number of occurrences of $P_u \geq {}^{+90th}_{ss1}P^{\mathrm{D}}_{u}$ shown above the range line: for $P_u < 0$ where there are non-zero occurrences, a vertical line indicating the minimum magnitude measure ${}^{-90th}_{ss1}P^{\mathrm{D}}_{umini}$ to the maximum magnitude measure ${}^{-90th}_{ss1}P^{\mathrm{D}}_{umaxi}$, a solid circle indicating the mean ${}^{-90th}_{ss1}P^{\mathrm{D}}_{umini} \geq P_u \geq {}^{-90th}_{ss1}P^{\mathrm{D}}_{umaxi}$, the quarter divisions of the range (horizontal lines) and the number of occurrences of $P_u \leq {}^{+90th}_{ss1}P^{\mathrm{D}}_{u}$ shown below the range line. Subject[0] shows these measures for all subjects[D]: for $P_u > 0$ with a solid circle indicating the mean of all the mean ${}^{+90th}_{ss1}P^{\mathrm{D}}_{umini} \leq P_u \leq {}^{+90th}_{ss1}P^{\mathrm{D}}_{umaxi}$: for $P_u < 0$ for subjects with non-zero occurrences a solid circle indicating the mean of all the mean ${}^{-90th}_{ss1}P^{\mathrm{D}}_{umini} \geq P_u \geq {}^{-90th}_{ss1}P^{\mathrm{D}}_{umaxi}$.

magnitude $P_u < 0$. There are also differences of occurrences: subject[15] has 17 occurrences where as subjects[3, 4, 5, 10, 13] have one or zero. The inequality ${}^{-90th}_{ss1}P^{\mathrm{D}}_{umaxi} \leq P_u \leq {}^{-90th}_{ss1}P^{\mathrm{D}}_{umini}$ provides a representative range for each subject[D] with more than one occurrence: one occurrence does not constitute a range. Additionally the inequality ${}^{-90th}_{ss1}P^{\mathrm{D}}_{umax} \leq P_u \leq {}^{-90th}_{ss1}P^{\mathrm{D}}_{umin}$ provides a representative range for all of subjects[1, 2, 6, 7, 8, 9, 11, 12, 14, 15, 16] who have more than one occurrence.

D.11.5. *Manoeuvre D (a.) the $P_v - P_{uCs}$ plane*

This final section uses the inequalities, as previously defined, to define a cuboid boundary for the largest magnitude measures for each and all subjects.

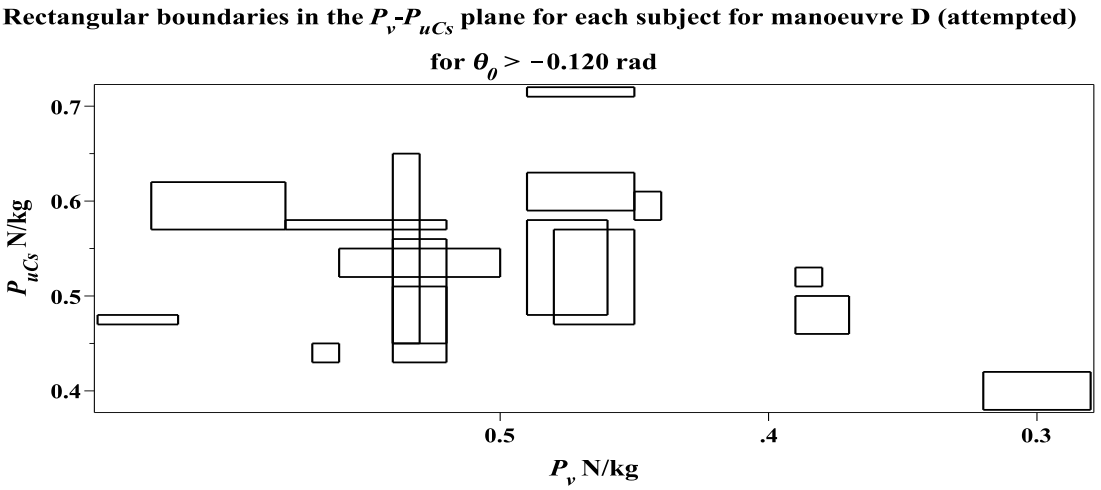

Figure D.67 – Rectangles formed with vertices of coordinates $[{}^{+90th}_{ss1}P^{\mathrm{D}}_{vmini}, {}^{+90th}_{ss1}P^{\mathrm{D}}_{uCsmini}]$, $[{}^{+90th}_{ss1}P^{\mathrm{D}}_{vmaxi}, {}^{+90th}_{ss1}P^{\mathrm{D}}_{uCsmini}]$, $[{}^{+90th}_{ss1}P^{\mathrm{D}}_{vmaxi}, {}^{+90th}_{ss1}P^{\mathrm{D}}_{uCsmaxi},]$, and $[{}^{+90th}_{ss1}P^{\mathrm{D}}_{vmini}, {}^{+90th}_{ss1}P^{\mathrm{D}}_{uCsmaxi}]$ for all subjects[D], i.e. n=16.

As some subjects had P_u measures in two signs ([1, 2, 6, 7, 8, 9, 11, 12, 14, 15, 16]) and some in one sign subjects[3, 4, 5, 10, 13] this definition requires two sets of three inequalities as follows. For the first set of three inequalities for each of subjects[1,..., 16] the inequalities are:

$${}^{+90th}_{ss1}P^{\mathrm{D}}_{uCsmini} \leq P_{uCs} \leq {}^{+90th}_{ss1}P^{\mathrm{D}}_{uCsmaxi} \text{ (page 344)},$$

$${}^{+90th}_{ss1}P^{\mathrm{D}}_{vmini} \leq P_v \leq {}^{+90th}_{ss1}P^{\mathrm{D}}_{vmaxi} \text{ (page 342) and}$$

$${}^{+90th}_{ss1}P^{\mathrm{D}}_{umini} \leq P_u \leq {}^{+90th}_{ss1}P^{\mathrm{D}}_{umaxi} \text{ (page 347)}.$$

For the second set of three inequalities for each of subjects[1, 2, 6, 7, 8, 9, 11, 12, 14, 15, 16] the inequalities are as given for P_{uCs} and P_v above and

$${}^{-90th}_{ss1}P^{\mathrm{D}}_{umini} \geq P_u \geq {}^{-90th}_{ss1}P^{\mathrm{D}}_{umaxi} \text{ (page 347)}.$$

A graphical representation of ${}^{large}_{ss1}\mathbf{P}^{\mathrm{D}}_i$ in the $P_v - P_{uCs}$ plane is shown in Figure D.67 (page 350): the construction follows the same process as described in Section 6.4.4 (page 149) for manoeuvre F (a.). These two sets of three inequalities define one cuboid boundary for each of subjects[1,..., 16] and two cuboid boundaries for each of subjects[1, 2, 6, 7, 8, 9, 11, 12, 14, 15, 16] as they have P_u measures in both signs. These two inequality sets provide a representation of the largest magnitudes of handle-forces for manoeuvre D (a.) for $\{{}_{ss1}\theta^{\mathrm{D}}_0\}$ for each subject. These one set or two sets of three inequalities are denoted ${}^{large}_{ss1}\mathbf{P}^{\mathrm{D}}_i$ where

i indicates the subject index.

Two sets of three inequalities define the cuboid boundaries which enclose the measures for all, rather than each of, subjects[D] and removal of the i subscript from the above definitions provides this. These two sets of three inequalities are denoted ${}^{large}_{ss1}\mathbf{P}^{\mathrm{D}}$. In conclusion ${}^{large}_{ss1}\mathbf{P}^{\mathrm{D}}$ provides a useful representation of the boundaries of the largest handle-forces for all subjects[D] for manoeuvre D (a.): the numerical values are:

$0.28 \leq P_v \leq 0.65$ (N/kg),

$0.38 \leq P_{uCs} \leq 0.72$ (N/kg) and

$0.04 \leq P_u \leq 0.58$ (N/kg).

$-0.03 \geq P_u \geq -0.14$ (N/kg).

D.12. **Manouevre H (attempted)**

A trailing super or sub script H in a symbol or 'all subjects[H]' indicates measures from subjects [1,. . . , 16].

D.12.1. *Manouevre H (a.) handle-force measures*

Examination of the handle-force measures will show that dividing the start-steady period, denoted $\{{}_{ssi}\theta_0^{\mathrm{H}}\}$, at $\theta_0 = -0.143$ rad is useful and hence vehicle-frame orientation (θ_0) measures for manoeuvre H (a.) are defined for $-0.143 < \theta_0 < 0$ rad and denoted $\{{}_{ss1}\theta_0^{\mathrm{H}}\}$ and for $\theta_{0steadi} < \theta_0 < -0.143$ rad and denoted $\{{}_{ss2i}\theta_0^{\mathrm{H}}\}$.

The handle-force measures for subject[5] for manoeuvre H (a.) are shown against time-steps in Figure D.68 (page 352) and against θ_0 in Figure D.69 (page 352). Figure D.69 illustrates four features of which are common to all subjects. Firstly, $P_{uCs} > 0$ are of relatively small magnitude compared with $P_{uCs} < 0$. Secondly, the majority of occurrences of P_{uCs} are of negligible or zero magnitude. Thirdly, the majority of P_u are negative. Fourthly, the majority of P_v are positive.

D.12.2. *Manouevre H (a.) P_u*

The presentation begins with P_u. Figure D.70 (page 353) shows occurrences of ${}^{-75th}_{ssi}P_u^{\mathrm{H}} \geq P_u > {}^{-90th}_{ssi}P_u^{\mathrm{H}}$ and of ${}^{+75th}_{ssi}P_u^{\mathrm{H}} \leq P_u < {}^{+90th}_{ssi}P_u^{\mathrm{H}}$ (both black markers) and, of $P_u < {}^{-90th}_{ssi}P_u^{\mathrm{H}}$ and of $P_u > {}^{+90th}_{ssi}P_u^{\mathrm{H}}$ (both red markers): to assist

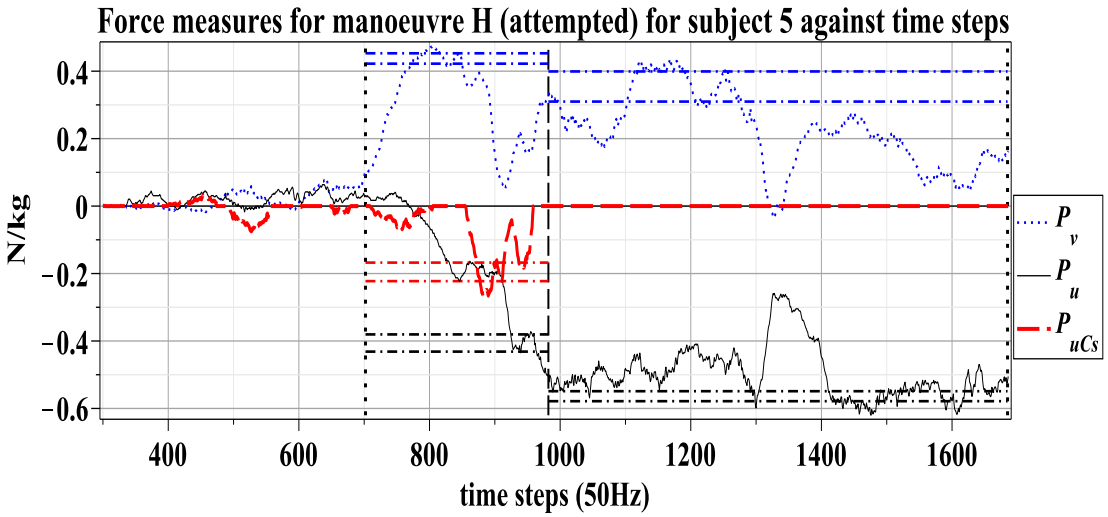

Figure D.68 – Measures P_v (dotted blue), P_u (thin black) and P_{uCs} (thick red dashed) in N/kg plotted against time-steps (approximately 0.02 seconds) with motion-start line (vertical black dotted: closest to zero), steady-start line (vertical black dotted:closest to end), $\theta_0 = -0.143$ rad line (vertical black dashed), percentile lines for ${}^{-75th}P_{uCs}$ and ${}^{-90th}P_{uCs}$ (horizontal red dash-dot), ${}^{-75th}P_u$ and ${}^{-90th}P_u$ (horizontal black dash) and ${}^{+75th}P_v$ and ${}^{+90th}P_v$ (horizontal blue dot) for $(\{{}_{ss1}\theta_0^{\mathrm{H}}\})$ and $(\{{}_{ss2i}\theta_0^{\mathrm{H}}\})$for subject[5] for manoeuvre[H] (a.)

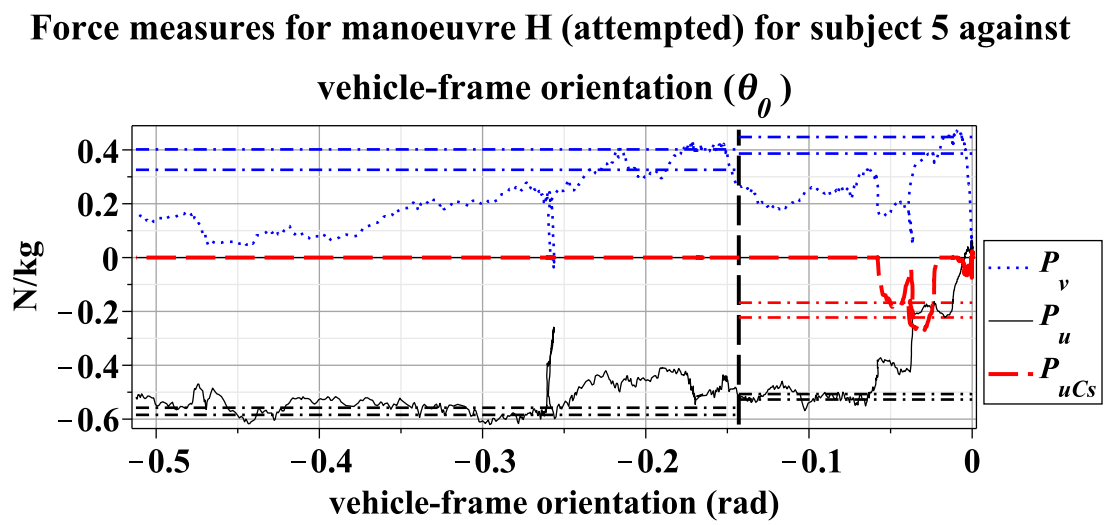

Figure D.69 – Shows for subject[5] for manoeuvre H (a.), measures plotted against θ_0 with other details as above.

inspection the measures for each subject are normalised against the subject's P_u peak magnitude for $\{{}_{ssi}\theta_0^{\mathrm{H}}\}$. A dashed vertical line indicates $\theta_0 = -0.143$ rad and this divides $\{{}_{ssi}\theta_0^{\mathrm{H}}\}$ into $\{{}_{ss1}\theta_0^{\mathrm{H}}\}$ and $\{{}_{ss2i}\theta_0^{\mathrm{H}}\}$ as previously defined. The measures for ${}^{-75th}_{ssi}P_u^{\mathrm{H}} \geq P_u > {}^{-90th}_{ssi}P_u^{\mathrm{H}}$ occurrences (black markers) are printed on top of $P_u < {}^{-90th}_{ssi}P_u^{\mathrm{H}}$ occurrences (red markers). It is evident that compared with $P_u < 0$ the magnitudes and occurrences of measures of $P_u > 0$ are negligible,

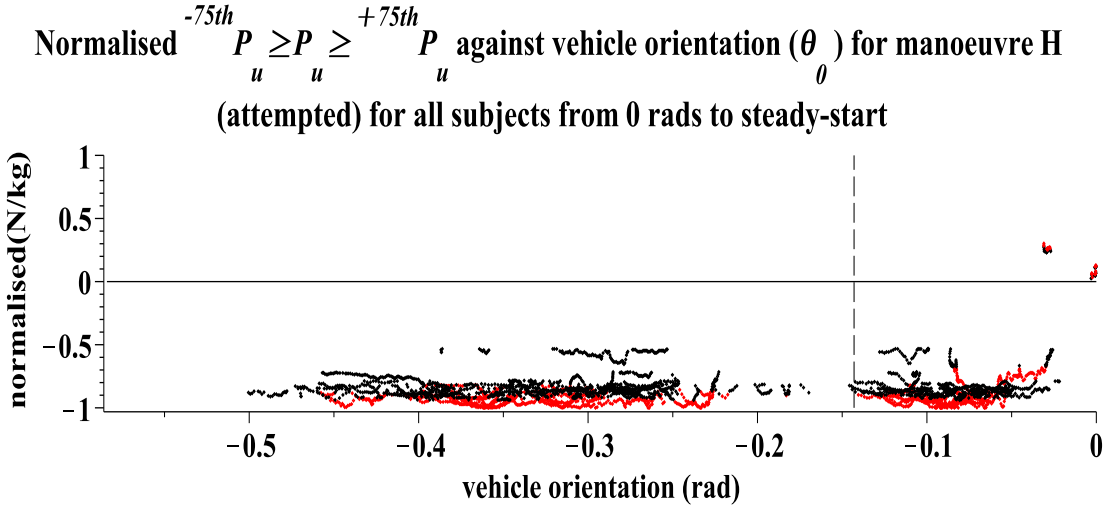

Figure D.70 – Occurrences of ${}^{-75th}_{ssi}P^{\mathrm{H}}_u \geq P_u > {}^{-90th}_{ssi}P^{\mathrm{H}}_u$ and of ${}^{+75th}_{ssi}P^{\mathrm{H}}_u \leq P_u < {}^{+90th}_{ssi}P^{\mathrm{H}}_u$ (both black markers) and, of $P_u < {}^{-90th}_{ssi}P^{\mathrm{H}}_u$ and of $P_u > {}^{+90th}_{ssi}P^{\mathrm{H}}_u$ (both red markers) in N/kg and normalised against each subject's maximum magnitude P_u against θ_0 for $\{{}_{ssi}\theta^{\mathrm{H}}_0\}$ for all subjects with $\theta_0 = -0.143$ indicated (dashed vertical) for manoeuvre H (a.)

which confirms the representativeness of Figure D.69 (page 352) in this respect. It is also evident the accumulated occurrences of ${}^{-75th}_{ssi}P^{\mathrm{H}}_u \geq P_u > {}^{-90th}_{ssi}P^{\mathrm{H}}_u$ for all subjects[H] are in two contiguous groups and that $\theta_0 = -0.143$ rad is at the end of the first contiguity: the next contiguity begins at $\theta \lesssim -0.25$ rad. An examination of the data shows that all subjects[H] contribute to the contiguous occurrences of ${}^{-75th}_{ssi}P^{\mathrm{H}}_u \geq P_u > {}^{-90th}_{ssi}P^{\mathrm{H}}_u$ in the initial period: occurrences for all subjects[H] are [30, 85, 26, 12, 15, 56, 31, 55, 76, 49, 49, 47, 47, 50, 54, 10] respectively. Thus for all subjects[H], despite any subject variations, the mechanism is so configured that subjects have occurrences of ${}^{-75th}_{ssi}P^{\mathrm{H}}_u \geq P_u > {}^{-90th}_{ssi}P^{\mathrm{H}}_u$ before $\theta_0 = -0.143$ rad followed by a local trough in the P_u magnitudes. Thus division of $\{{}_{ssi}\theta^{\mathrm{H}}_0\}$ at this location relates to a mechanical property of the system for manoeuvre H (a.). It is also noteworthy that this examination fails if the process is repeated with $P_u < {}^{-90th}_{ssi}P^{\mathrm{H}}_u$, i.e. not all subjects apply the largest magnitude of P_u in $\{{}_{ss1}\theta^{\mathrm{H}}_0\}$.

Figure D.71 (page 354) shows measures for $P_u \leq {}^{-90th}_{ss1}P^{\mathrm{H}}_u$ (N/kg) for all subjects[H] for $\{{}_{ss1}\theta^{\mathrm{H}}_0\}$. Representative values for the largest magnitude $P_u < 0$ are obtained as follows. For each subject[H] the measure for the minimum magnitude $P_u \leq {}^{-90th}_{ss1}P^{\mathrm{H}}_u$, denoted ${}^{-90th}_{ss1}P^{\mathrm{H}}_{umini}$, can be read and the minimum mag-

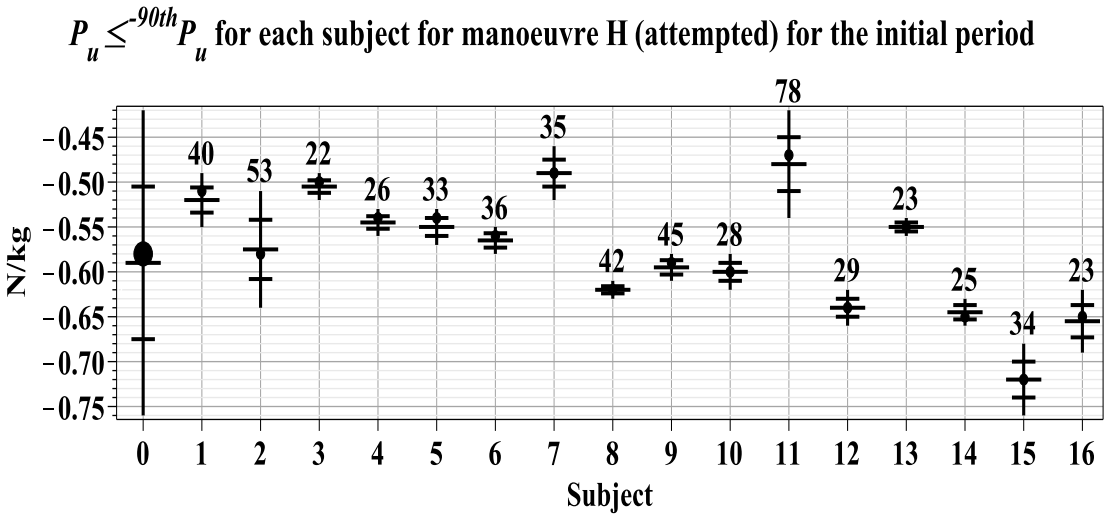

Figure D.71 – Shows for each subject[H] (i) for $\{{}_{ss1}\theta_0^{\mathrm{H}}\}$ (N/kg): a vertical line indicating the minimum magnitude measure ${}^{-90th}_{ss1}P^{\mathrm{H}}_{umini}$ to the maximum magnitude measure ${}^{-90th}_{ss1}P^{\mathrm{H}}_{umaxi}$, a solid circle indicating the mean ${}^{-90th}_{ss1}P^{\mathrm{H}}_{umini} \geq P_u \geq {}^{-90th}_{ss1}P^{\mathrm{H}}_{umaxi}$, the quarter divisions of the range (horizontal lines) and the number of occurrences of $P_u \geq {}^{-90th}_{ss1}P^{\mathrm{H}}_{u}$ shown above the range line. Subject[0] shows these measures with a solid circle indicating the mean of all the mean ${}^{-90th}_{ss1}P^{\mathrm{H}}_{umini} \geq P_u \geq {}^{-90th}_{ss1}P^{\mathrm{H}}_{umaxi}$.

nitude ${}^{-90th}_{ss1}P^{\mathrm{H}}_{umini}$ for all subjects[H], denoted ${}^{-90th}_{ss1}P^{\mathrm{H}}_{umin}$, is -0.42 N/kg (subject[11]). The maximum magnitude P_u for each subject[H], denoted ${}^{-90th}_{ss1}P^{\mathrm{H}}_{umaxi}$ can also be read and the maximum magnitude ${}^{-90th}_{ss1}P^{\mathrm{H}}_{umaxi}$ denoted ${}^{-90th}_{ss1}P^{\mathrm{H}}_{umax}$ is 0.76 N/kg (subjects[15]). The mean ${}^{-90th}_{ss1}P^{\mathrm{H}}_{umini} \geq P_u \geq {}^{-90th}_{ss1}P^{\mathrm{H}}_{umaxi}$ for each subject[H] is indicated by a solid circle and it can be seen, where the range magnitude is not too small, that these are located from first to the third quarter. Subject[0] shows the range from ${}^{-90th}_{ss1}P^{\mathrm{H}}_{umin}$ to ${}^{-90th}_{ss1}P^{\mathrm{H}}_{umax}$ with the mean for all the mean ${}^{-90th}_{ss1}P^{\mathrm{H}}_{umini} \geq P_u \geq {}^{-90th}_{ss1}P^{\mathrm{H}}_{umaxi}$ located approximately centrally as indicated by a solid circle. For each subject occurrences of $P_u \leq {}^{-90th}_{ss1}P^{L}_{u}$ are shown above the range line in Figure D.71: an examination of the data shows that these are approximately equal to $\frac{50}{10} \times t_i(\{{}_{ss1}\theta_0^{\mathrm{H}}\})$ for subjects[1, 2, 4, 5, 7, 10, 11, 14] who have a few measures for $P_u > 0$ and equal for subjects[3, 6, 8, 9, 12, 13, 15, 16] who do not.

It can also be seen from Figure D.71 that the range magnitude of 0.34 N/kg, ${}^{-90th}_{ss1}P^{\mathrm{H}}_{umax} - {}^{-90th}_{ss1}P^{\mathrm{H}}_{umin}$, arises from inter-subject variation (subjects[11] compared with subject[15]) and is not the result of the ${}^{-90th}_{ss1}P^{\mathrm{H}}_{umaxi} - {}^{-90th}_{ss1}P^{\mathrm{H}}_{umini}$ of a specific subject. While there are differences between subjects for the largest

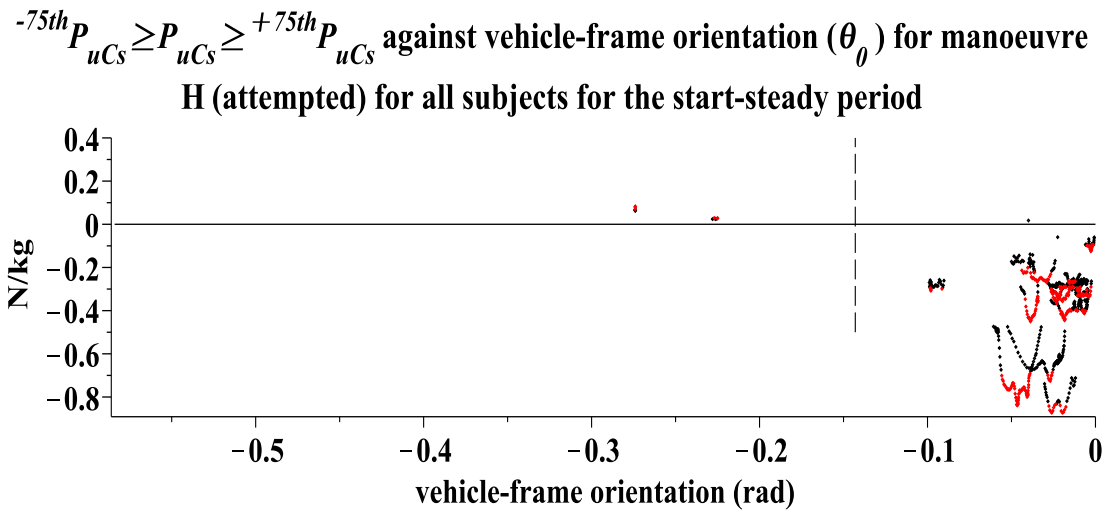

Figure D.72 – Occurrences of ${}^{-75th}_{ssi}P^{\mathrm{H}}_{uCs} \geq P_{uCs} > {}^{-90th}_{ssi}P^{\mathrm{H}}_{uCs}$ and of ${}^{+75th}_{ssi}P^{\mathrm{H}}_{uCs} \geq P_{uCs} < {}^{+90th}_{ssi}P^{\mathrm{H}}_{uCs}$ (both black markers) and, $P_{uCs} < {}^{-90th}_{ssi}P^{\mathrm{H}}_{uCs}$ and $P_{uCs} > {}^{+90th}_{ssi}P^{\mathrm{H}}_{uCs}$ (both red markers) in N/kg against θ_0 for all subjects[H] for $\{{}_{ssi}\theta^{\mathrm{H}}_0\}$with $\theta_0 = -0.143$ indicated (dashed vertical)

$P_u < {}^{-90th}_{ss1}P^{\mathrm{H}}_{u}$ the intra-subject range magnitude is relatively small. The inequality ${}^{-90th}_{ss1}P^{\mathrm{H}}_{umini} \geq P_u \geq {}^{-90th}_{ss1}P^{\mathrm{H}}_{umaxi}$ provides a representative range for each subject[H]. Additionally the inequality ${}^{+90th}_{ss1}P^{\mathrm{H}}_{umin} \geq P_u \geq {}^{-90th}_{ss1}P^{\mathrm{H}}_{umax}$ provides a representative range for all subjects[H] for the largest $P_u < 0$ for $\{{}_{ss1}\theta^{\mathrm{H}}_0\}$.

D.12.3. *Manouevre H (a.)* P_{uCs}

Figure D.72 (page 355) shows occurrences of ${}^{-75th}_{ssi}P^{\mathrm{H}}_{uCs} \geq P_{uCs} > {}^{-90th}_{ssi}P^{\mathrm{H}}_{uCs}$ and of ${}^{+75th}_{ssi}P^{\mathrm{H}}_{uCs} \geq P_{uCs} < {}^{+90th}_{ssi}P^{\mathrm{H}}_{uCs}$ (both black markers), and $P_{uCs} < {}^{-90th}_{ssi}P^{\mathrm{H}}_{uCs}$ and $P_{uCs} > {}^{+90th}_{ssi}P^{\mathrm{H}}_{uCs}$ (both red markers) in N/kg for all subjects: these measures are not normalised. A dashed vertical line indicates $\theta_0 = -0.143$ rad and this divides $\{{}_{ssi}\theta^{\mathrm{H}}_0\}$ into $\{{}_{ss1}\theta^{\mathrm{H}}_0\}$ and $\{{}_{ss2i}\theta^{\mathrm{H}}_0\}$ as previously defined.

It is evident that the occurrences and magnitudes of $P_{uCs} > 0$ are negligible and this confirms the representativeness of Figure D.69 (page 352) in this respect. Figure D.72 also indicates that $P_{uCs} < 0$ measures occur in $\{{}_{ss1}\theta^{\mathrm{H}}_0\}$.

Figure D.73 (page 356) shows measures for $P_{uCs} \leq {}^{-90th}_{ss1}P^{\mathrm{H}}_{uCs}$ (N/kg) for all subjects[H] for $\{{}_{ss1}\theta^{\mathrm{H}}_0\}$. Representative values for the largest magnitude P_{uCs} are obtained as follows. For each subject[H] with non-zero occurrences the measure for the minimum magnitude $P_{uCs} \leq {}^{-90th}_{ss1}P^{\mathrm{H}}_{uCs}$, denoted ${}^{-90th}_{ss1}P^{\mathrm{H}}_{uCsmini}$, may be read and the minimum magnitude ${}^{-90th}_{ss1}P^{\mathrm{H}}_{uCsmini}$ for all subjects[H], de-

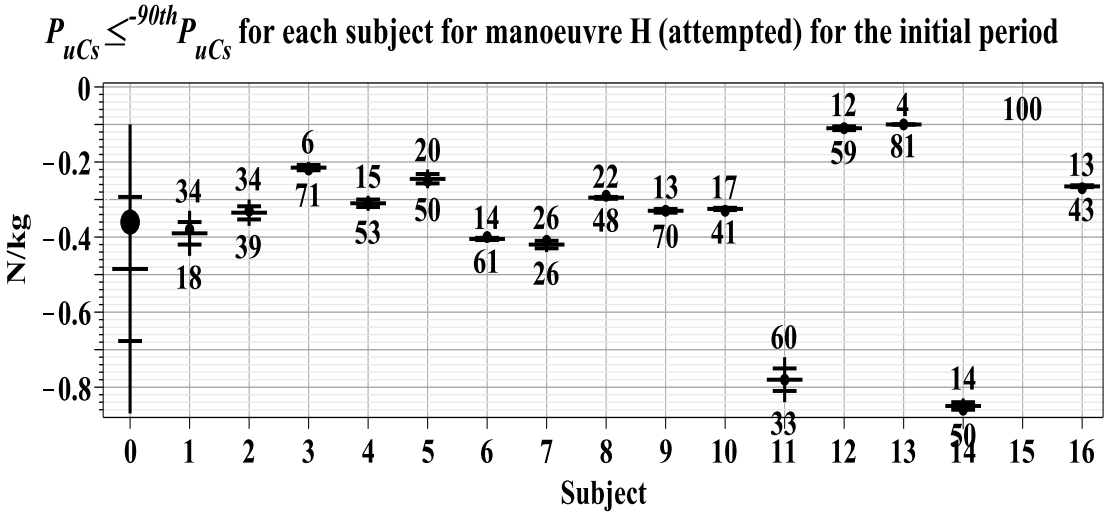

Figure D.73 – Shows for each subject[H] (i), for $\{{}_{ss1}\theta_0^{\mathrm{H}}\}$ in N/kg: a vertical line indicating the minimum magnitude measure ${}^{-90th}_{ss1}P^{\mathrm{H}}_{uCsmini}$ to the maximum magnitude measure ${}^{-90th}_{ss1}P^{\mathrm{H}}_{uCsmaxi}$, a solid circle indicating the mean ${}^{-90th}_{ss1}P^{\mathrm{H}}_{PuCsmini} \geq P_{uCs} \geq {}^{-90th}_{ss1}P^{\mathrm{H}}_{PuCsmaxi}$, the quarter divisions of the range (horizontal lines), the number of occurrences of $P_{uCs} \leq {}^{-90th}_{ss1}P^{\mathrm{H}}_{uCs}$ shown above the range line and the percentage of $P_{uCs} = 0$ (integer) below the range line. Subject[0] shows these measures with a solid circle indicating the mean of all the mean ${}^{-90th}_{ss1}P^{\mathrm{H}}_{PuCsmini} \geq P_{uCs} \geq {}^{-90th}_{ss1}P^{\mathrm{H}}_{PuCsmaxi}$.

noted ${}^{-90th}_{ss1}P^{\mathrm{H}}_{uCsmin}$, is -0.10 N/kg (subjects[12, 13]). The maximum magnitude P_{uCs} for each subject[H], denoted ${}^{-90th}_{ss1}P^{\mathrm{H}}_{uCsmaxi}$, may also be read and the maximum magnitude ${}^{-90th}_{ss1}P^{\mathrm{H}}_{uCsmaxi}$, denoted ${}^{-90th}_{ss1}P^{\mathrm{H}}_{uCsmax}$, is -0.87 N/kg (subject[14]). The mean ${}^{-90th}_{ss1}P^{\mathrm{H}}_{uCsmini} \geq P_{uCs} \geq {}^{-90th}_{ss1}P^{\mathrm{H}}_{uCsmaxi}$ for each subject[H] are indicated by a solid circle and it can be seen that these means, ignoring subjects where the range magnitude is relatively small, are located approximately centrally in the intra-subject range. Subject[0] shows the range of ${}^{-90th}_{ss1}P^{\mathrm{H}}_{uCsmin}$ to ${}^{-90th}_{ss1}P^{\mathrm{H}}_{uCsmax}$ and the mean of all the mean ${}^{-90th}_{ss1}P^{\mathrm{H}}_{uCsmini} \geq P_{uCs} \geq {}^{-90th}_{ss1}P^{\mathrm{H}}_{uCsmaxi}$ indicated by a solid circle can be seen to be located in the second quarter of the inter-subject range.

Figure D.73 shows occurrences of $P_{uCs} \leq {}^{-90th}_{ss1}P^{\mathrm{H}}_{uCs}$ above the range line and the percentage of $P_{uCs} = 0$ (integer) below the range line. Substantial variation is evident: subject[15] has 100% $P_{uCs} = 0$ (integer), and hence no occurrences of $P_{uCs} \leq {}^{-90th}_{ss1}P^{\mathrm{H}}_{uCs}$ where as subject[1] has 18% $P_{uCs} = 0$ (integer) and 34 occurrences of $P_{uCs} \leq {}^{-90th}_{ss1}P^{\mathrm{H}}_{uCs}$. In other words the attempt at manoeuvre[H] by some

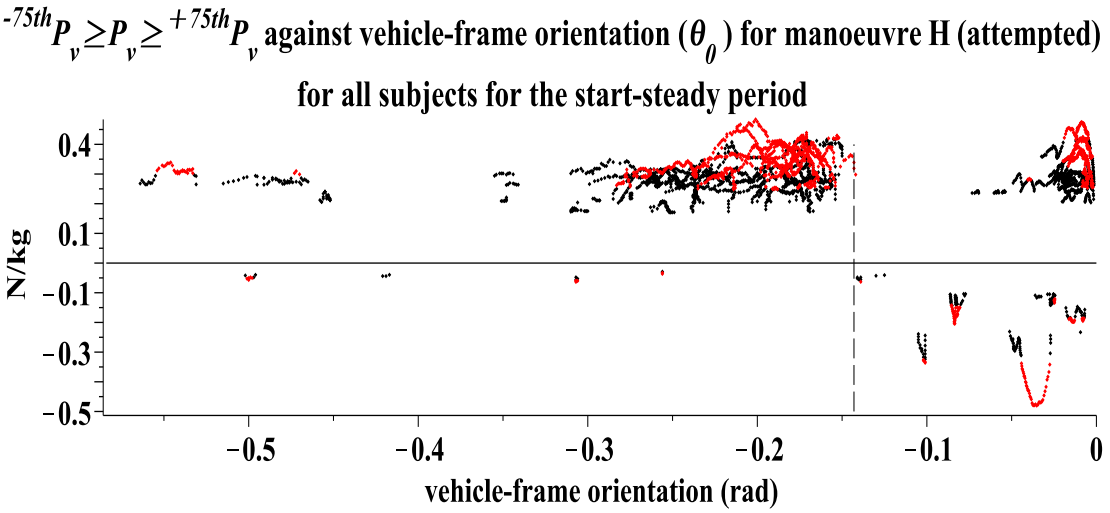

Figure D.74 – Occurrences of ${}^{-75th}_{ssi}P^{\mathrm{H}}_{v} \geq P_v > {}^{-90th}_{ssi}P^{\mathrm{H}}_{v}$ and of ${}^{+75th}_{ssi}P^{\mathrm{H}}_{v} \leq P_v < {}^{+90th}_{ssi}P^{\mathrm{H}}_{v}$ (both black markers) and, of $P_v < {}^{-90th}_{ssi}P^{\mathrm{H}}_{v}$ and of $P_v > {}^{+90th}_{ssi}P^{\mathrm{H}}_{v}$ (both red markers) in N/kg against θ_0 for $\{{}_{ssi}\theta^{\mathrm{H}}_{0}\}$ for all subjects[H] with $\theta_0 = -0.143$ line (dashed vertical) for manoeuvre H (a.)

subjects, to some extent, reduces the occurrences of the couple action.

It can also be seen from Figure D.73 (page 356) that the range magnitude of 0.77 N/kg, ${}^{-90th}_{ss1}P^{\mathrm{H}}_{uCsmax} - {}^{-90th}_{ss1}P^{\mathrm{H}}_{uCsmin}$, arises from inter-subject variation (subjects[12, 13] compared with subject[14]) and is not the result of the ${}^{-90th}_{ss1}P^{\mathrm{H}}_{uCsmaxi} - {}^{-90th}_{ss1}P^{\mathrm{H}}_{uCsmini}$ magnitude of a specific subject. There are therefore substantial differences between subjects for the largest magnitude $P_{uCs} < 0$. However, the inequality ${}^{-90th}_{ss1}P^{\mathrm{H}}_{uCsmini} \geq P_{uCs} \geq {}^{-90th}_{ss1}P^{\mathrm{H}}_{uCsmaxi}$ provides a representative range for each subject. In addition the inequality ${}^{-90th}_{ss1}P^{\mathrm{H}}_{uCsmin} \geq P_{uCs} \geq {}^{-90th}_{ss1}P^{\mathrm{H}}_{uCsmax}$ provides a representative range for all subjects[H].

D.12.4. *Manouevre H (a.) P_v*

Figure D.74 (page 357) shows occurrences of ${}^{-75th}_{ssi}P^{\mathrm{H}}_{v} \geq P_v > {}^{-90th}_{ssi}P^{\mathrm{H}}_{v}$ and of ${}^{+75th}_{ssi}P^{\mathrm{H}}_{v} \leq P_v < {}^{+90th}_{ssi}P^{\mathrm{H}}_{v}$ (both black markers) and, of $P_v < {}^{-90th}_{ssi}P^{\mathrm{H}}_{v}$ and of $P_v > {}^{+90th}_{ssi}P^{\mathrm{H}}_{v}$ (both red markers) for all subjects[H]. A dashed vertical line indicates $\theta_0 = -0.143$ rad and this divides $\{{}_{ssi}\theta^{\mathrm{H}}_{0}\}$ into $\{{}_{ss1}\theta^{\mathrm{H}}_{0}\}$ and $\{{}_{ss2i}\theta^{\mathrm{H}}_{0}\}$ as previously defined. It is evident from Figure D.74 that a cluster of $P_v > {}^{+75th}_{ssi}P^{\mathrm{H}}_{v}$ begin at the commencement of $\{{}_{ss2i}\theta^{\mathrm{H}}_{0}\}$ and this lends support to the interpretation that this period division relates to a mechanical property of the system for manoeuvre H (a.) as already observed with respect to P_u measures. It is also evident

that while non negligible measures of P_v occur in both signs the majority of peak magnitudes are positive.

Representative measures for the largest magnitude P_v can be obtained as follows. Figure D.75 (page 359) shows measures for ${}^{-90th}_{ss1}P^{\mathrm{H}}_{v} \geq P_v \geq {}^{+90th}_{ss1}P^{\mathrm{H}}_{v}$ (N/kg) for all subjects[H] with non-zero occurrences for $\{{}_{ss1}\theta^{\mathrm{H}}_{0}\}$. Representative values for the largest $P_v > 0$ are obtained as follows. For each subject[H] the measure for the minimum ${}^{+90th}_{ss1}P^{\mathrm{H}}_{v}$, denoted ${}^{+90th}_{ss1}P^{\mathrm{H}}_{vmini}$, can be read and the minimum ${}^{+90th}_{ss1}P^{\mathrm{H}}_{vmini}$ for all subjects[H], denoted ${}^{+90th}_{ss1}P^{\mathrm{H}}_{vmin}$, is 0.09 N/kg (subject[6]). The maximum P_v for each subject[H], denoted ${}^{+90th}_{ss1}P^{\mathrm{H}}_{vmaxi}$, can also be read and the maximum ${}^{+90th}_{ss1}P^{\mathrm{H}}_{vmaxi}$, denoted ${}^{+90th}_{ss1}P^{\mathrm{H}}_{vmax}$, is 0.48 N/kg (subject[5]). The mean ${}^{+90th}_{ss1}P^{\mathrm{H}}_{vmaxi} \leq P_v \leq {}^{+90th}_{ss1}P^{\mathrm{H}}_{vmaxi}$ for each subject[H] is indicated by a solid circle though the ranges are of such small magnitude that the location of the mean is immaterial. Occurrences of $P_v \geq {}^{+90th}_{ss1}P^{\mathrm{H}}_{v}$ are shown above the range line for $P_v > 0$ for each subject. Subject[0] shows the range from ${}^{+90th}_{ss1}P^{\mathrm{H}}_{vmin}$ to ${}^{+90th}_{ss1}P^{\mathrm{H}}_{vmax}$ with the mean for all the mean ${}^{+90th}_{ss1}P^{\mathrm{H}}_{vmini} \leq P_v \leq {}^{+90th}_{ss1}P^{\mathrm{H}}_{vmaxi}$ located approximately centrally as indicated by a solid circle.

It can also be seen from Figure D.75 that the range magnitude of 0.39 N/kg, ${}^{+90th}_{ss1}P^{\mathrm{H}}_{vmax} - {}^{+90th}_{ss1}P^{\mathrm{H}}_{vmin}$, arises from inter-subject variation (subject[6] compared with subject[5]) and is not the result of the ${}^{+90th}_{ss1}P^{\mathrm{H}}_{vmaxi} - {}^{+90th}_{ss1}P^{\mathrm{H}}_{vmini}$ of a specific subject. There are therefore substantial differences between subjects for the largest $P_v > 0$. However, the inequality ${}^{+90th}_{ss1}P^{\mathrm{H}}_{vmini} \leq P_v \leq {}^{+90th}_{ss1}P^{\mathrm{H}}_{vmaxi}$ provides a representative range for each of subjects[H]. Additionally the inequality ${}^{+90th}_{ss1}P^{\mathrm{H}}_{vmin} \leq P_v \leq {}^{+90th}_{ss1}P^{\mathrm{H}}_{vmax}$ provides a representative range for subjects[H] for the largest $P_v > 0$ for the initial period.

Representative values for the largest magnitude $P_v < 0$ are also read from Figure D.75. For each subject[H] with non-zero occurrences the measure for the minimum magnitude ${}^{-90th}_{ss1}P^{\mathrm{H}}_{v}$, denoted ${}^{-90th}_{ss1}P^{\mathrm{H}}_{vmini}$, can be read and the minimum magnitude ${}^{-90th}_{ss1}P^{\mathrm{H}}_{vmini}$ for all subjects[H] with more than one occurrences, denoted ${}^{-90th}_{ss1}P^{\mathrm{H}}_{vmin}$, is -0.12 N/kg (subject[14]). The maximum magnitude $P_v < 0$ for all subjects[H], denoted ${}^{-90th}_{ss1}P^{\mathrm{H}}_{vmaxi}$, can also be read and the maximum magnitude ${}^{-90th}_{ss1}P^{\mathrm{H}}_{vmaxi}$, denoted ${}^{-90th}_{ss1}P^{\mathrm{H}}_{vmax}$, is -0.48 N/kg (subject[11]). The mean ${}^{-90th}_{ss1}P^{\mathrm{H}}_{vmini} \geq P_v \geq {}^{-90th}_{ss1}P^{\mathrm{H}}_{vmaxi}$ for each subject[H] is indicated by a solid

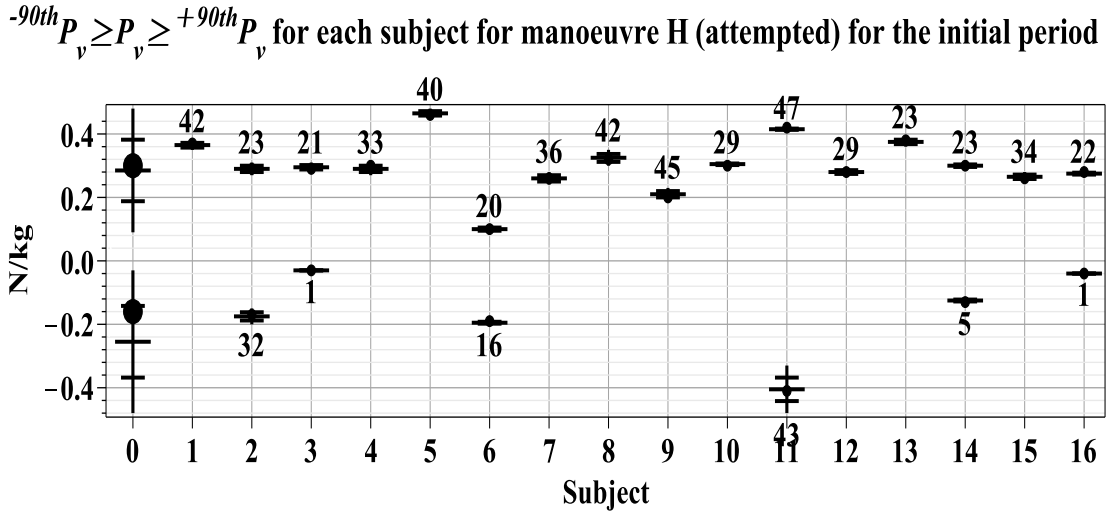

Figure D.75 – Shows for each subject[H] (i) for $\{{}_{ss1}\theta_0^{\mathrm{H}}\}$ in N/kg: for $P_v > 0$ a vertical line indicating the minimum magnitude measure ${}^{+90th}_{ss1}P^{\mathrm{H}}_{vmini}$ to the maximum magnitude measure ${}^{+90th}_{ss1}P^{\mathrm{H}}_{vmaxi}$, a solid circle indicating the mean ${}^{+90th}_{ss1}P^{\mathrm{H}}_{vmini} \leq P_v \leq {}^{+90th}_{ss1}P^{\mathrm{H}}_{vmaxi}$, the quarter divisions of the range (horizontal lines) and the number of occurrences of $P_v \geq {}^{+90th}_{ss1}P^{\mathrm{H}}_{v}$ shown above the range line: for $P_v < 0$ where there are non-zero occurrences, a vertical line indicating the minimum magnitude measure ${}^{-90th}_{ss1}P^{\mathrm{H}}_{vmini}$ to the maximum magnitude measure ${}^{-90th}_{ss1}P^{\mathrm{H}}_{vmaxi}$, a solid circle indicating the mean ${}^{-90th}_{ss1}P^{\mathrm{H}}_{vmaxi} \geq P_v \geq {}^{-90th}_{ss1}P^{\mathrm{H}}_{vmaxi}$, the quarter divisions of the range (horizontal lines) and the number of occurrences of $P_v \leq {}^{+90th}_{ss1}P^{\mathrm{H}}_{v}$ shown below the range line. Subject[0] shows these measures for all subjects[H] with: for $P_v > 0$ a solid circle indicating the mean of all the mean ${}^{+90th}_{ss1}P^{\mathrm{H}}_{vmini} \leq P_v \leq {}^{+90th}_{ss1}P^{\mathrm{H}}_{vmaxi}$ and for $P_v < 0$ with a solid circle indicating the mean of all the mean ${}^{-90th}_{ss1}P^{\mathrm{H}}_{vmini} \geq P_v \geq {}^{-90th}_{ss1}P^{\mathrm{H}}_{vmaxi}$.

circle but it can be seen that the ranges (excluding subject[11]) are of such small magnitude that the location is immaterial. The occurrences of $P_v \leq {}^{-90th}_{ss1}P^{\mathrm{H}}_{v}$ are shown below the range line. Subjects[3, 16] are disregarded as only a single occurrence is present. Subject[0] shows the range from ${}^{-90th}_{ss1}P^{\mathrm{H}}_{vmin}$ to ${}^{-90th}_{ss1}P^{\mathrm{H}}_{vmax}$ with the mean of all the mean ${}^{-90th}_{ss1}P^{\mathrm{H}}_{vmini} \geq P_v \geq {}^{-90th}_{ss1}P^{\mathrm{H}}_{vmaxi}$ indicated by a solid circle is approximately centrally located.

It can also be seen from Figure D.75 (page 359) that the range magnitude of 0.36 N/kg, ${}^{-90th}_{ss1}P^{\mathrm{H}}_{vmax} - {}^{-90th}_{ss1}P^{\mathrm{H}}_{vmin}$, arises from inter-subject variation (subject[10] compared with subject[14]) and is not the result of the ${}^{-90th}_{ss1}P^{\mathrm{H}}_{vmaxi} - {}^{-90th}_{ss1}P^{\mathrm{H}}_{vmini}$ of a specific subject. There are therefore differences between subjects for the largest magnitude $P_v < 0$. However, the inequality ${}^{-90th}_{ss1}P^{\mathrm{H}}_{vmini} \geq P_v \geq {}^{-90th}_{ss1}P^{\mathrm{H}}_{vmaxi}$

provides a representative range for each of subjects[2, 6, 11, 14]. Additionally the inequality ${}^{-90th}_{ss1}P^{\mathrm{H}}_{vmin} \geq P_v \geq {}^{-90th}_{ss1}P^{\mathrm{H}}_{vmax}$ (subject[0]) provides a representative range for all of subjects[2, 6, 11, 14] for the largest magnitude $P_v < 0$ for $\{{}_{ss1}\theta^{\mathrm{H}}_0\}$.

D.12.5. *Manouevre H (a.) the $P_v - P_{uCs}$ plane*

This final section uses the inequalities, as previously defined, to define a cuboid boundary for the largest magnitude measures for each and all subjects. As subjects[1, 3, 4, 5, 7, 8, 9, 10, 12, 13, 15, 16] had P_v measures in one sign and subjects[2, 6, 11, 14] had P_v measures in two signs this definition requires two sets of three inequalities as follows. For the first set of three inequalities for each of subjects[1,..., 16] the inequalities are:

$${}^{-90th}_{ss1}P^{\mathrm{H}}_{uCsmini} \geq P_{uCs} \geq {}^{-90th}_{ss1}P^{\mathrm{H}}_{uCsmaxi}$$ (page 355),

$${}^{+90th}_{ss1}P^{\mathrm{H}}_{vmini} \leq P_v \leq {}^{+90th}_{ss1}P^{\mathrm{H}}_{vmaxi}$$ (page 357) and

$${}^{-90th}_{ss1}P^{\mathrm{H}}_{umini} \geq P_u \geq {}^{-90th}_{ss1}P^{\mathrm{H}}_{umaxi}$$ (page 351).

For the second set of three inequalities for each of subjects[2, 6, 11, 14] the inequalities are as given for P_{uCs} and P_u above and

$${}^{-90th}_{ss1}P^{\mathrm{H}}_{vmini} \geq P_v \geq {}^{-90th}_{ss1}P^{\mathrm{H}}_{vmaxi}$$ (page 357).

A graphical representation of ${}^{large}_{ss1}\mathbf{P}^{\mathrm{H}}_i$ in the $P_v - P_{uCs}$ plane is shown in Figure D.76 (page 361): the construction follows the same process as described in Section 6.4.4 (page 149) for manoeuvre F (a.). These two sets of three inequalities define one cuboid boundary for each of subjects[1, 3, 4, 5, 7, 8, 9, 10, 12, 13, 15, 16] and two cuboid boundaries for all of subjects[2, 6, 11, 14] as they have P_v measures in both signs. These two inequality sets provide a representation of the largest magnitudes of handle-forces for manoeuvre H (a.) for $\{{}_{ss1}\theta^{\mathrm{D}}_0\}$ for each subject. These one set or two sets of three inequalities are denoted ${}^{large}_{ss1}\mathbf{P}^{\mathrm{D}}_i$ where i indicates the subject index.

Two sets of inequalities define the cuboid boundaries which enclose the measures for all, rather than each of, subjects[H] and this is achieved by removal of the i subscript from the above definitions as follows. For the first set of three inequalities for all of subjects[1,..., 16] the inequalities are:

$${}^{-90th}_{ss1}P^{\mathrm{H}}_{umin} \geq P_u \geq {}^{-90th}_{ss1}P^{\mathrm{H}}_{umax}$$

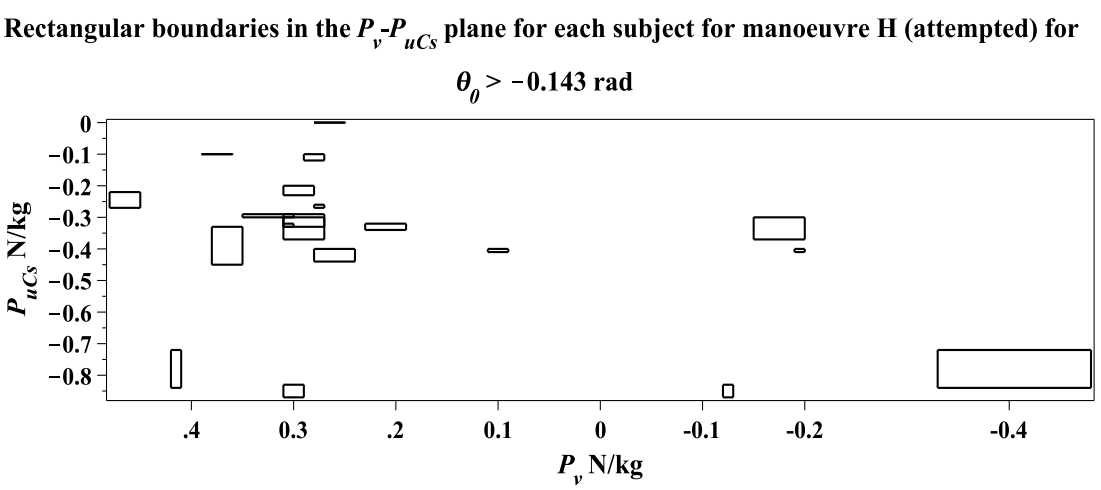

Figure D.76 – Shows, relating to $P_v > 0$, for each subject[H] (i) the four vertices of a rectangle are formed with a $[P_v, P_{uCs}]$ coordinate as follows: $[{}^{+90th}_{ss1}P^{\mathrm{H}}_{vmaxi}, {}^{-90th}_{ss1}P^{\mathrm{H}}_{uCsmini}]$, $[{}^{+90th}_{ss1}P^{\mathrm{H}}_{vmini}, {}^{-90th}_{ss1}P^{\mathrm{H}}_{uCsmini}]$, $[{}^{+90th}_{ss1}P^{\mathrm{H}}_{vmini}, {}^{-90th}_{ss1}P^{\mathrm{H}}_{uCsmaxi},]$, and $[{}^{+90th}_{ss1}P^{\mathrm{H}}_{vmaxi}, {}^{-90th}_{ss1}P^{\mathrm{H}}_{uCsmaxi}]$: dotted and dashed lines are used where required to isolate individual subjects: n=16. Relating to $P_v < 0$ for each subject[2, 6, 11, 14] the four vertices of a rectangle are formed with a $[P_v, P_{uCs}]$ coordinate as follows: $[{}^{-90th}_{ss1}P^{\mathrm{H}}_{vmini}, {}^{-90th}_{ss1}P^{\mathrm{H}}_{uCsmini}]$, $[{}^{-90th}_{ss1}P^{\mathrm{H}}_{vmaxi}, {}^{-90th}_{ss1}P^{\mathrm{H}}_{uCsmini}]$, $[{}^{-90th}_{ss1}P^{\mathrm{H}}_{vmaxi}, {}^{-90th}_{ss1}P^{\mathrm{H}}_{uCsmaxi},]$, and $[{}^{-90th}_{ss1}P^{\mathrm{H}}_{vmini}, {}^{-90th}_{ss1}P^{\mathrm{H}}_{uCsmaxi}]$: n=4.

$${}^{-90th}_{ss1}P^{\mathrm{H}}_{uCsmin} \geq P_{uCs} \geq {}^{-90th}_{ss1}P^{\mathrm{H}}_{uCsmax},$$

$${}^{+90th}_{ss1}P^{\mathrm{H}}_{vmin} \leq P_v \leq {}^{+90th}_{ss1}P^{\mathrm{H}}_{vmax} \text{ and}$$

and for each of subjects[2, 6, 11, 14] relating to $P_v < 0$ a second cuboid boundary is defined by a second set of three inequalities comprising of P_{uCs} and P_u as above and the inequality:

$${}^{-90th}_{ss1}P^{\mathrm{H}}_{vmin} \geq P_v \geq {}^{-90th}_{ss1}P^{\mathrm{H}}_{vmax}.$$

These two sets of three inequalities are denoted ${}^{large}_{ss1}\mathbf{P}^{\mathrm{H}}$. In conclusion ${}^{large}_{ss1}\mathbf{P}^{\mathrm{H}}$ provides a useful representation of the boundaries of the largest handle-forces for all subjects[H] for manoeuvre H (a.): the numerical values are:

$0.09 \leq P_v \leq 0.48$ (N/kg),

$-0.12 \geq P_v \geq -0.48$ (N/kg),

$-0.10 \geq P_{uCs} \geq -0.87$ (N/kg) and

$-0.42 \geq P_u \geq -0.76$ (N/kg).

D.13. **Manouevre E (attempted)**

A trailing super or sub script E in a symbol or 'all subjects[E]' indicates measures from subjects [1,. . . , 16].

D.13.1. *Manouevre E (a.) handle-force measures*

Examination of the handle-force measures will show that dividing the start-steady period at $\theta_0 = -0.085$ rad is useful and hence vehicle-frame orientation (θ_0) measures for manoeuvre[E] (a.) are defined for $-0.085 < \theta_0 < 0$ rad an initial period, denoted $\{_{ss1}\theta_0^{\mathrm{E}}\}$, and for a later period $\theta_{0steadi} < \theta_0 < -0.085$ rad, denoted $\{_{ss2i}\theta_0^{\mathrm{E}}\}$.

Figures D.78 and D.77 (page 363) illustrate the force measures for one subject[7] four features of which are common to all subjects[E]. Firstly, both occurrences and magnitudes of $P_{uCs} > 0$ are very small compared with $P_{uCs} < 0$. Secondly, the largest P_u magnitudes are relatively small compared with the largest P_{uCs} magnitudes. Thirdly, the largest P_v magnitudes are relatively small compared with the largest P_{uCs} magnitudes.

D.13.2. *Manouevre E (a.) P_{uCs}*

The presentation begins with P_{uCs}. Figure D.79 (page 364) shows occurrences of ${}^{-75th}_{ssi}P^{\mathrm{E}}_{uCs} \geq P_{uCs} > {}^{-90th}_{ssi}P^{\mathrm{E}}_{uCs}$ and of ${}^{+75th}_{ssi}P^{\mathrm{E}}_{uCs} \leq P_{uCs} < {}^{+90th}_{ssi}P^{\mathrm{E}}_{uCs}$ (both black markers), and $P_{uCs} \leq {}^{-90th}_{ssi}P^{\mathrm{E}}_{uCs}$ and $P_{uCs} \geq {}^{+90th}_{ssi}P^{\mathrm{E}}_{uCs}$ (both red markers) (N/kg) for all subjects[E] against θ_0: to assist inspection the measures for each subject are normalised against the subject's P_{uCs} peak magnitude for $\{_{ssi}\theta_0^{\mathrm{E}}\}$. A dashed vertical line indicates $\theta_0 = -0.084$ rad and this divides $\{_{ssi}\theta_0^{\mathrm{E}}\}$ into $\{_{ss1}\theta_0^{\mathrm{E}}\}$ and $\{_{ss2i}\theta_0^{\mathrm{E}}\}$ as previously defined. As Figure D.79 shows P_{uCs} normalised against the peak magnitude P_{uCs} it is evident that compared with $P_{uCs} < 0$, $P_{uCs} > 0$ are of very small magnitude and occurrences are very few and this confirms the representativeness of Figure D.78 (page 363) in this respect. It is also evident from Figure D.79 that the accumulated occurrences of $P_{uCs} \leq {}^{-90th}_{ssi}P^{\mathrm{E}}_{uCs}$ form a contiguity of peak magnitudes which terminates just before the termination of $\{_{ss1}\theta_0^{\mathrm{E}}\}$. Table D.4 (page 364) shows the $P_{uCs} \leq {}^{-90th}_{ssi}P^{\mathrm{E}}_{uCs}$ occurrences for the reduced angle range $\{_{ss1}\theta_0^{\mathrm{E}}\}$ i.e. $\theta_0 > -0.085$ rad: it is evident that all subjects have substantial occurrences of $P_{uCs} \leq {}^{-90th}_{ssi}P^{\mathrm{E}}_{uCs}$ for $\theta_0 > -0.085$ rad and that therefore

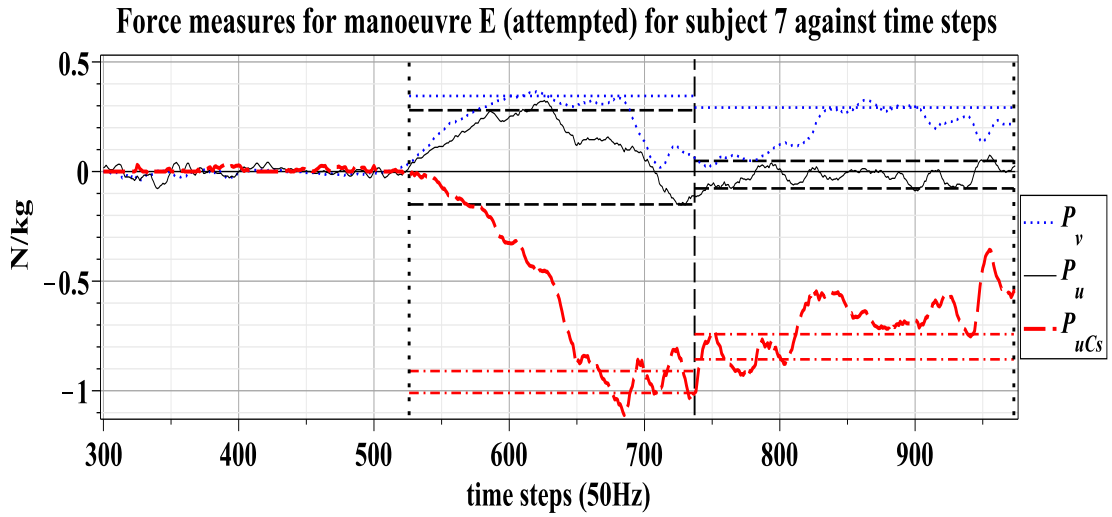

Figure D.77 – For subject[7] for manoeuvre[E] (a.), measures: P_v (dotted blue), P_u (thin black) and P_{uCs} (thick red dashed) in N/kg plotted against time-steps (approximately 0.02 seconds) with motion-start line (vertical black dotted: closest to left side), steady-start line (vertical black dotted: closest to right side), $\theta_0 = -0.085$ rad line (vertical black dashed). The following percentile lines are shown: ${}^{-90th}_{ssi}P^{\mathrm{E}}_{uCs}$ and ${}^{-75th}_{ssi}P^{\mathrm{E}}_{uCs}$ (horizontal red dash-dot), ${}^{-90th}_{ssi}P^{\mathrm{E}}_{u}$ and ${}^{+90th}_{ssi}P^{\mathrm{E}}_{u}$ (horizontal black dash) and ${}^{+90th}_{ssi}P^{\mathrm{E}}_{v}$ (horizontal blue dash).

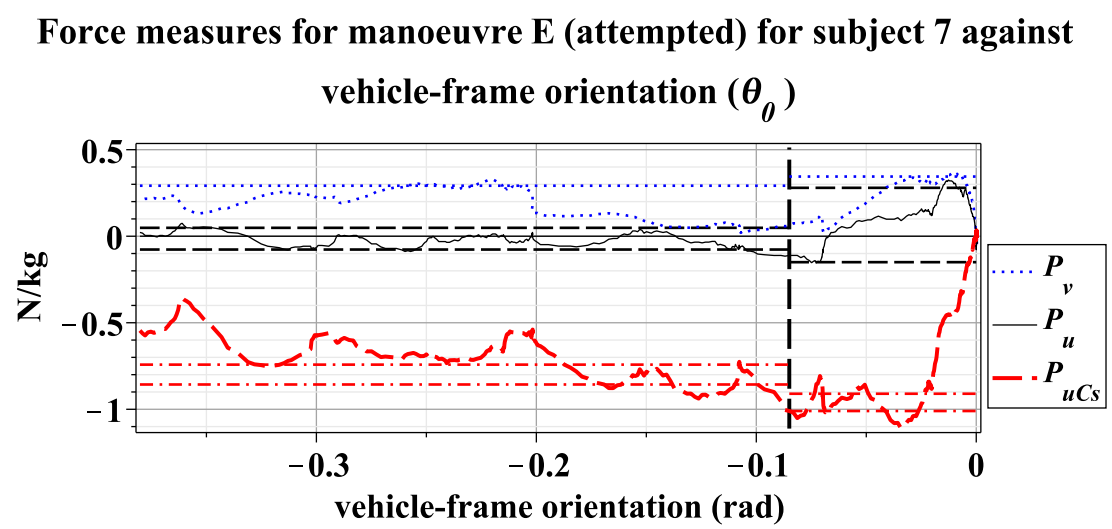

Figure D.78 – Shows for subject[7] for manoeuvre E (a.), measures plotted against θ_0 with other details as above.

the occurrences of $P_{uCs} \leq {}^{-90th}_{ssi}P^{\mathrm{E}}_{uCs}$ which are shown in Figure D.79 (page 364) for $\theta_0 < -0.085$ rad, i.e. for $\{{}_{ss2i}\theta^{\mathrm{E}}_0\}$ are not an initial $P_{uCs} \leq {}^{-90th}_{ssi}P^{\mathrm{E}}_{uCs}$ for any subject[E]. It follows that dividing $\{{}_{ssi}\theta^{\mathrm{E}}_0\}$ at $\theta_0 = -0.085$ rad provides a period ($\{{}_{ss1}\theta^{\mathrm{E}}_0\}$) in which the initial largest magnitudes of P_{uCs} are included for all subjects.

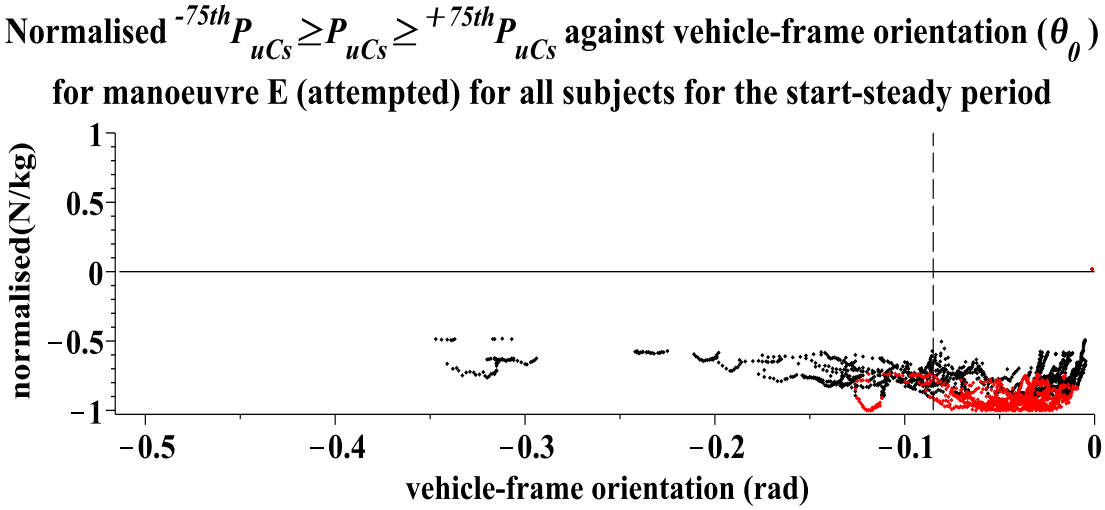

Figure D.79 – Occurrences of ${}^{-75th}_{ssi}P^{\mathrm{E}}_{uCs} \geq P_{uCs} > {}^{-90th}_{ssi}P^{\mathrm{E}}_{uCs}$ and of ${}^{+75th}_{ssi}P^{\mathrm{E}}_{uCs} \leq P_{uCs} < {}^{+90th}_{ssi}P^{\mathrm{E}}_{uCs}$ (both black markers) and, $P_{uCs} \leq {}^{-90th}_{ssi}P^{\mathrm{E}}_{uCs}$ and $P_{uCs} \geq {}^{+90th}_{ssi}P^{\mathrm{E}}_{uCs}$ (both red markers) in N/kg and normalised against each subject's maximum magnitude P_{uCs} against θ_0 for $\{{}_{ssi}\theta^{\mathrm{E}}_0\}$ for all subjects with $\theta_0 = -0.085$ indicated (dashed vertical) and normalised against each subject's maximum magnitude P_{uCs} for $\{{}_{ssi}\theta^{\mathrm{E}}_0\}$ for all subjects[E].

subject(i)	occurrences
1	71
2	64
3	39
4	56
5	53
6	92
7	48
8	75
9	56
10	61
11	81
12	58
13	39
14	70
15	58
16	36

Table D.4 – For each subject the occurrences of $P_{uCs} \leq {}^{-90th}_{ssi}P^{\mathrm{E}}_{uCs}$ for $\{{}_{ss1}\theta^{\mathrm{E}}_0\}$.

Thus, despite any variations, the mechanism is so configured that the majority of the largest magnitude P_{uCs} actions occur by $\theta_0 = -0.084$ rad and hence division of $\{{}_{ssi}\theta^{\mathrm{E}}_0\}$ at this location relates to a mechanical property of the system for manoeuvre E (a.).

Figure D.80 (page 365) shows measures for $P_{uCs} \leq {}^{-90th}_{ss1}P^{\mathrm{E}}_{uCs}$ (N/kg) for all subjects[E] for $\{{}_{ss1}\theta^{\mathrm{E}}_0\}$. Representative values for the largest magnitude

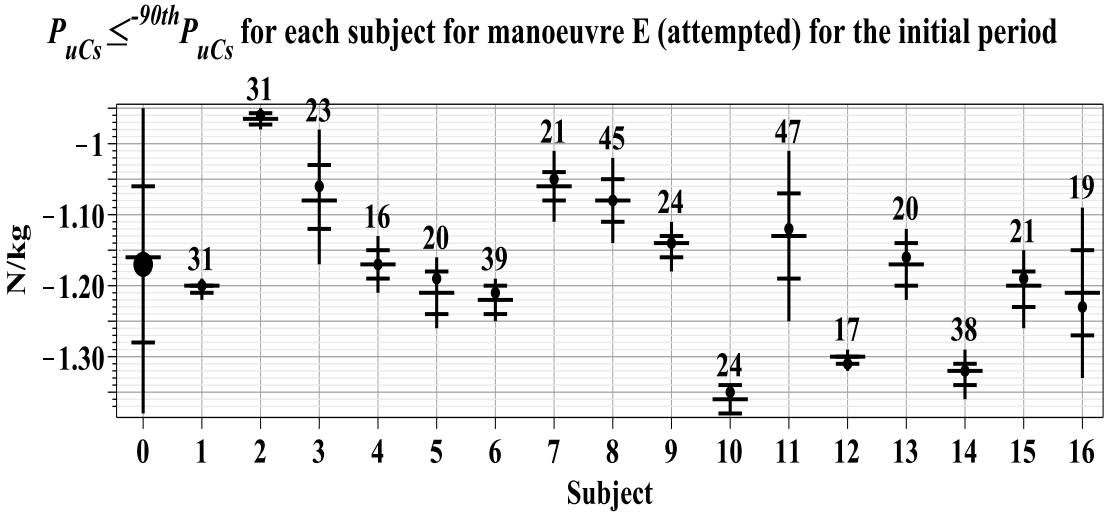

Figure D.80 – Shows for each subject[E] (i) for $\{{}_{ss1}\theta_0^{\mathrm{E}}\}$ (N/kg): a vertical line indicating the minimum magnitude ${}^{-90th}_{ss1}P^{\mathrm{E}}_{uCsmini}$ to the maximum magnitude ${}^{-90th}_{ss1}P^{\mathrm{E}}_{uCsmaxi}$, a solid circle indicating the mean ${}^{-90th}_{ss1}P^{\mathrm{E}}_{PuCsmini} \geq P_{uCs} \geq {}^{-90th}_{ss1}P^{\mathrm{E}}_{PuCsmaxi}$, the quarter divisions of the range (horizontal lines), the number of occurrences of $P_{uCs} \leq {}^{-90th}_{ss1}P^{\mathrm{E}}_{uCs}$ shown. Subject[0] shows these measures for all subjects[E] with a solid circle indicating the mean of all the mean ${}^{-90th}_{ss1}P^{\mathrm{E}}_{PuCsmini} \geq P_{uCs} \geq {}^{-90th}_{ss1}P^{\mathrm{E}}_{PuCsmaxi}$.

P_{uCs} are obtained as follows. For each subject[E] the measure for the minimum magnitude $P_{uCs} \leq {}^{-90th}_{ss1}P^{\mathrm{E}}_{uCs}$, denoted ${}^{-90th}_{ss1}P^{\mathrm{E}}_{uCsmini}$, may be read and the minimum magnitude ${}^{-90th}_{ss1}P^{\mathrm{E}}_{uCsmini}$ for all subjects[E], denoted ${}^{-90th}_{ss1}P^{\mathrm{E}}_{uCsmin}$, is -0.95 N/kg (subject[2]). The maximum magnitude P_{uCs} for each subject[E], denoted ${}^{-90th}_{ss1}P^{\mathrm{E}}_{uCsmaxi}$, may also be read and the maximum magnitude ${}^{-90th}_{ss1}P^{\mathrm{E}}_{uCsmaxi}$, denoted ${}^{-90th}_{ss1}P^{\mathrm{E}}_{uCsmax}$, is -1.38 N/kg (subject[10]). The mean ${}^{-90th}_{ss1}P^{\mathrm{E}}_{uCsmini} \geq P_{uCs} \geq {}^{-90th}_{ss1}P^{\mathrm{E}}_{uCsmaxi}$ for each subject[E] are indicated by a solid circle and it can be seen that these means are located in the second to third quarters of the intra-subject range. Subject[0] shows the range of ${}^{-90th}_{ss1}P^{\mathrm{E}}_{uCsmin}$ to ${}^{-90th}_{ss1}P^{\mathrm{E}}_{uCsmax}$ and the mean of all the mean ${}^{-90th}_{ss1}P^{\mathrm{E}}_{uCsmini} \geq P_{uCs} \geq {}^{-90th}_{ss1}P^{\mathrm{E}}_{uCsmaxi}$ indicated by a solid circle can be seen to be located centrally in the inter-subject range.

For each subject occurrences of $P_{uCs} \leq {}^{-90th}_{ss1}P^{\mathrm{E}}_{uCs}$ are shown above the range line in Figure D.80. An examination of the data (results not presented) shows that for $-0.084 < \theta_0 < -0.01$ rad apart from 10 occurrences of $P_{uCs} = 0$ (integer) for subject[11] all measures are for $P_{uCs} < 0$. Occurrences of $P_{uCs} \leq {}^{-90th}_{ss1}P^{\mathrm{E}}_{uCs}$ are approximately equal to $\frac{50}{10} \times t_i(\{{}_{ss1}\theta_0^{\mathrm{E}}\})$ for subjects [4, 6, 11, 14] who have $P_{uCs} > 0$ measures for $\theta_0 > -0.01$ and exactly equal for subjects[1, 3, 4, 5, 7,. . . , 10, 12, 13,

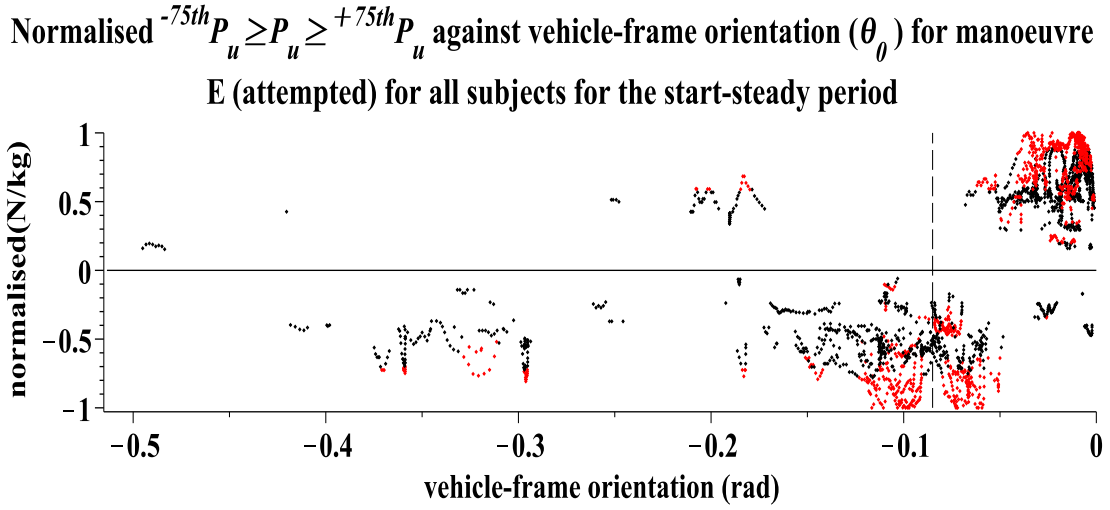

Figure D.81 – Occurrences of ${}^{-75th}_{ssi}P^{\mathrm{E}}_u \geq P_u > {}^{-90th}_{ssi}P^{\mathrm{E}}_u$ and of ${}^{+75th}_{ssi}P^{\mathrm{E}}_u \leq P_u < {}^{+90th}_{ssi}P^{\mathrm{E}}_u$ (both black markers) and, of $P_u \leq {}^{-90th}_{ssi}P^{\mathrm{E}}_u$ and of $P_u \geq {}^{+90th}_{ssi}P^{\mathrm{E}}_u$ (both red markers) in N/kg and normalised against each subject's maximum magnitude P_u against θ_0 for $\{{}_{ssi}\theta^{\mathrm{E}}_0\}$ for all subjects with $\theta_0 = -0.085$ indicated (dashed vertical) for manoeuvre E (a.).

15, 16] who do not.

It can also be seen from Figure D.80 (page 365) that the range magnitude of 0.43 N/kg, ${}^{-90th}_{ss1}P^{\mathrm{E}}_{uCsmax} - {}^{-90th}_{ss1}P^{\mathrm{E}}_{uCsmin}$, arises from inter-subject variation (subject[2] compared with subject[10]) and is not the result of the ${}^{-90th}_{ss1}P^{\mathrm{E}}_{uCsmaxi} - {}^{-90th}_{ss1}P^{\mathrm{E}}_{uCsmini}$ magnitude of a specific subject. There are therefore substantial differences between subjects for the largest magnitude $P_{uCs} < 0$. However, the inequality ${}^{-90th}_{ss1}P^{\mathrm{E}}_{uCsmini} \geq P_{uCs} \geq {}^{-90th}_{ss1}P^{\mathrm{E}}_{uCsmaxi}$ provides a representative range for each subject[E]. In addition the inequality ${}^{-90th}_{ss1}P^{\mathrm{E}}_{uCsmin} \geq P_{uCs} \geq {}^{-90th}_{ss1}P^{\mathrm{E}}_{uCsmax}$ provides a representative range for all subjects[E].

D.13.3. *Manouevre E (a.) P_u*

Figure D.81 (page 366) shows occurrences of ${}^{-75th}_{ssi}P^{\mathrm{E}}_u \geq P_u > {}^{-90th}_{ssi}P^{\mathrm{E}}_u$ and of ${}^{+75th}_{ssi}P^{\mathrm{E}}_u \leq P_u < {}^{+90th}_{ssi}P^{\mathrm{E}}_u$ (both black markers), and $P_u \leq {}^{-90th}_{ssi}P^{\mathrm{E}}_u$ and $P_u \geq {}^{+90th}_{ssi}P^{\mathrm{E}}_u$ (both red markers) (N/kg) for all subjects[E] against θ_0: to assist inspection the measures for each subject are normalised against the subject's P_u peak magnitude for $\{{}_{ssi}\theta^{\mathrm{E}}_0\}$. A dashed vertical line indicates $\theta_0 = -0.084$ rad and this divides $\{{}_{ssi}\theta^{\mathrm{E}}_0\}$ into $\{{}_{ss1}\theta^{\mathrm{E}}_0\}$ and $\{{}_{ss2i}\theta^{\mathrm{E}}_0\}$ as previously defined.

It can be seen from Figure D.81 that peak P_u occur in both signs for $\{{}_{ss1}\theta^{\mathrm{E}}_0\}$

and both signs are therefore taken into account in representing the largest magnitudes of P_u. It is also evident that close to $\theta_0 = -0.084$ rad measures of the largest magnitudes of $P_u < 0$ diminish compared with those immediately before and after and this adds support to the claim that the mechanism is distinctly configured at $\theta_0 = -0.084$ rad as presented with respect to P_{uCs}.

Figure D.82 (page 368) shows measures for ${}^{-90th}_{ss1}P^{\mathrm{E}}_{u} \geq P_u \geq {}^{+90th}_{ss1}P^{\mathrm{E}}_{u}$ (N/kg) for all subjects[E] for $\{{}_{ss1}\theta^{\mathrm{E}}_{0}\}$. Representative values for the largest $P_u > 0$ are obtained as follows. For each subject[E] the measure for the minimum ${}^{+90th}_{ss1}P^{\mathrm{E}}_{u}$, denoted ${}^{+90th}_{ss1}P^{\mathrm{E}}_{umini}$, can be read and the minimum ${}^{+90th}_{ss1}P^{\mathrm{E}}_{umini}$ for all subjects[E], denoted ${}^{+90th}_{ss1}P^{\mathrm{E}}_{umin}$, is 0.08 N/kg (subject[9]). The maximum P_u for each subject[E], denoted ${}^{+90th}_{ss1}P^{\mathrm{E}}_{umaxi}$, can also be read and the maximum ${}^{+90th}_{ss1}P^{\mathrm{E}}_{umaxi}$ denoted ${}^{+90th}_{ss1}P^{\mathrm{E}}_{umax}$ is 0.48 N/kg (subject[11]). The mean ${}^{+90th}_{ss1}P^{\mathrm{E}}_{umaxi} \leq P_u \leq {}^{+90th}_{ss1}P^{\mathrm{E}}_{umaxi}$ for each subject[E] is indicated by a solid circle but it can be seen that mostly the ranges are of such small magnitude that the location of the mean is immaterial. Occurrences of $P_u \geq {}^{+90th}_{ss1}P^{\mathrm{E}}_{u}$ are shown above the range line for $P_u > 0$ for each subject. Subject[0] shows the range from ${}^{+90th}_{ss1}P^{\mathrm{E}}_{umin}$ to ${}^{+90th}_{ss1}P^{\mathrm{E}}_{umax}$ with the mean for all the mean ${}^{+90th}_{ss1}P^{\mathrm{E}}_{umini} \leq P_u \leq {}^{+90th}_{ss1}P^{\mathrm{E}}_{umaxi}$ located in the second quarter as indicated by a solid circle.

It can also be seen from Figure D.82 (page 368) that the range magnitude of 0.40 N/kg, ${}^{+90th}_{ss1}P^{\mathrm{E}}_{umax} - {}^{+90th}_{ss1}P^{\mathrm{E}}_{umin}$, arises from inter-subject variation (subject[9] compared with subject[11]) and is not the result of the ${}^{+90th}_{ss1}P^{\mathrm{E}}_{umaxi} - {}^{+90th}_{ss1}P^{\mathrm{E}}_{umini}$ of a specific subject. There are therefore substantial differences between subjects for the largest $P_u > 0$. However, the inequality ${}^{+90th}_{ss1}P^{\mathrm{E}}_{umini} \leq P_u \leq {}^{+90th}_{ss1}P^{\mathrm{E}}_{umaxi}$ provides a representative range for each subject[E]. Additionally the inequality ${}^{+90th}_{ss1}P^{\mathrm{E}}_{umin} \leq P_u \leq {}^{+90th}_{ss1}P^{\mathrm{E}}_{umax}$ provides a representative range for subjects[E] for the largest $P_u > 0$ for $\{{}_{ss1}\theta^{\mathrm{E}}_{0}\}$.

Representative values for the largest magnitude $P_u < 0$ are also read from Figure D.82 (page 368). For each subject[E] with non-zero occurrences the measure for the minimum magnitude $P_u < {}^{-90th}_{ss1}P^{\mathrm{E}}_{u}$, denoted ${}^{-90th}_{ss1}P^{\mathrm{E}}_{umini}$, can be read and the minimum ${}^{-90th}_{ss1}P^{\mathrm{E}}_{umini}$ for all subjects[E] with non-zero occurrences, denoted ${}^{-90th}_{ss1}P^{\mathrm{E}}_{umin}$, is -0.08 N/kg (subject[9]). The maximum magnitude $P_u < 0$ for all subjects[E], denoted ${}^{-90th}_{ss1}P^{\mathrm{E}}_{umaxi}$, can also be read and the max-

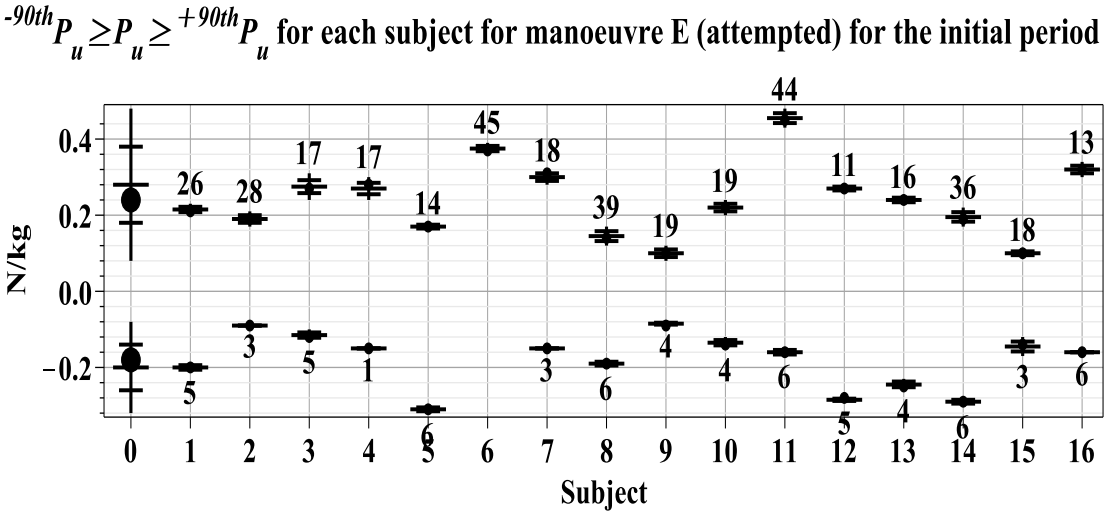

Figure D.82 – Shows for each subject[E] i for $\{{}_{ss1}\theta_0^{\mathrm{E}}\}$ (N/kg): for $P_u > 0$ a vertical line indicating the minimum magnitude measure ${}^{+90th}_{ss1}P^{\mathrm{E}}_{umini}$ to the maximum magnitude measure ${}^{+90th}_{ss1}P^{\mathrm{E}}_{umaxi}$, a solid circle indicating the mean ${}^{+90th}_{ss1}P^{\mathrm{E}}_{umini} \leq P_u \leq {}^{+90th}_{ss1}P^{\mathrm{E}}_{umaxi}$, the quarter divisions of the range (horizontal lines) and the number of occurrences of $P_u \geq {}^{+90th}_{ss1}P^{\mathrm{E}}_{u}$ shown above the range line: for $P_u < 0$ where there are non-zero occurrences, a vertical line indicating the minimum magnitude measure ${}^{-90th}_{ss1}P^{\mathrm{E}}_{umini}$ to the maximum magnitude measure ${}^{-90th}_{ss1}P^{\mathrm{E}}_{umaxi}$, a solid circle indicating the mean ${}^{-90th}_{ss1}P^{\mathrm{E}}_{umaxi} \geq P_u \geq {}^{-90th}_{ss1}P^{\mathrm{E}}_{umaxi}$, the quarter divisions of the range (horizontal lines) and the number of occurrences of $P_u \leq {}^{+90th}_{ss1}P^{\mathrm{E}}_{u}$ shown below the range line. Subject[0] shows these measures for all subjects[E] with: for $P_u > 0$ a solid circle indicating the mean of all the mean ${}^{+90th}_{ss1}P^{\mathrm{E}}_{umini} \leq P_u \leq {}^{+90th}_{ss1}P^{\mathrm{E}}_{umaxi}$ and for $P_u < 0$ for subjects with non-zero occurrences a solid circle indicating the mean of all the mean ${}^{-90th}_{ss1}P^{\mathrm{E}}_{umini} \geq P_u \geq {}^{-90th}_{ss1}P^{\mathrm{E}}_{umaxi}$.

imum ${}^{-90th}_{ss1}P^{\mathrm{E}}_{umaxi}$, denoted ${}^{-90th}_{ss1}P^{\mathrm{E}}_{umax}$, is −0.32 N/kg (subject[5]). The occurrences of $P_u \leq {}^{-90th}_{ss1}P^{\mathrm{E}}_{u}$ are shown below the range line. The mean ${}^{-90th}_{ss1}P^{\mathrm{E}}_{umini} \geq P_u \geq {}^{-90th}_{ss1}P^{\mathrm{E}}_{umaxi}$ for each subject[E] is indicated by a solid circle but it can be seen that the ranges are mostly of such small magnitude that the location is immaterial. Subject[0] shows the range from ${}^{-90th}_{ss1}P^{\mathrm{E}}_{umin}$ to ${}^{-90th}_{ss1}P^{\mathrm{E}}_{umax}$ with the mean of all the mean ${}^{-90th}_{ss1}P^{\mathrm{E}}_{umini} \geq P_u \geq {}^{-90th}_{ss1}P^{\mathrm{E}}_{umaxi}$ indicated by a solid circle is located in the second quarter.

Occurrences are shown below the range line and it can be seen that for all subjects[E] occurrences for $P_u < {}^{-90th}_{ss1}P^{\mathrm{E}}_{u}$ are fewer than for $P_u > {}^{+90th}_{ss1}P^{\mathrm{E}}_{u}$. It can also be seen from Figure D.82 (page 368) that the range magnitude of

0.26 N/kg, ${}^{-90th}_{ss1}P^{\mathrm{E}}_{umax} - {}^{-90th}_{ss1}P^{\mathrm{E}}_{umin}$, arises from inter-subject variation (subject[9]) compared with subject[5]) and is not the result of the ${}^{-90th}_{ss1}P^{\mathrm{E}}_{umaxi} - {}^{-90th}_{ss1}P^{\mathrm{E}}_{umini}$ of a specific subject. There are therefore differences between subjects for the largest magnitude $P_u < 0$. However, the inequality ${}^{-90th}_{ss1}P^{\mathrm{E}}_{umini} \geq P_u \geq {}^{-90th}_{ss1}P^{\mathrm{E}}_{umaxi}$ provides a representative range for each of subjects[1, 2, 3, 5, 7,..., 16]: disregarding subject[4] since one occurrences is not a range. Additionally the inequality ${}^{-90th}_{ss1}P^{\mathrm{E}}_{umin} \geq P_u \geq {}^{-90th}_{ss1}P^{\mathrm{E}}_{umax}$ provides a representative range for all of subjects[1, 2, 3, 5, 7,..., 16] for the largest $P_u < 0$ for $\{{}_{ss1}\theta^{\mathrm{E}}_0\}$.

Taking account of both signs the largest magnitude of P_u is given by ${}^{+90th}_{ss1}P^{\mathrm{E}}_{umax} = 0.37$ N/kg and the smallest magnitude for $P_{uCs} \leq {}^{-90th}_{ss1}P^{\mathrm{E}}_{uCsmin}$ is -0.95 N/kg and it is therefore concluded that the largest magnitudes of P_{uCs} are greater than the largest magnitudes of P_u and this confirms the representativeness of Figure D.78 (page 363) in this respect.

D.13.4. *Manouevre E (a.) P_v*

Figure D.83 (page 370) shows occurrences of ${}^{-75th}_{ssi}P^{\mathrm{E}}_{v} \geq P_v > {}^{-90th}_{ssi}P^{\mathrm{E}}_{v}$ and of ${}^{+75th}_{ssi}P^{\mathrm{E}}_{v} \leq P_v < {}^{+90th}_{ssi}P^{\mathrm{E}}_{v}$ (both black markers) and, of $P_v \leq {}^{-90th}_{ssi}P^{\mathrm{E}}_{v}$ and of $P_v \geq {}^{+90th}_{ssi}P^{\mathrm{E}}_{v}$ (both red markers) (N/kg) for all subjects[E] against θ_0: to assist inspection the measures for each subject are normalised against the subject's P_v peak magnitude for $\{{}_{ssi}\theta^{\mathrm{E}}_0\}$. A dashed vertical line indicates $\theta_0 = -0.084$ rad and this divides $\{{}_{ssi}\theta^{\mathrm{E}}_0\}$ into $\{{}_{ss1}\theta^{\mathrm{E}}_0\}$ and $\{{}_{ss2i}\theta^{\mathrm{E}}_0\}$ as previously defined.

The majority of $P_v \geq {}^{+75th}_{ssi}P^{\mathrm{E}}_{v}$ occur in two groups: firstly for $\theta_0 \gtrsim -0.085$ rad and secondly for $\theta_{0steadi} \lesssim \theta_0 \lesssim -0.2$ rad. For $P_v \leq {}^{-75th}_{ssi}P^{\mathrm{E}}_{v}$ the majority of occurrences are for $\theta_0 \gtrsim -0.085$ rad.

It is evident that P_v magnitudes and occurrences are non negligible in both signs so it follows that the representation of the largest magnitude P_v must consider both signs: this confirms the representativeness of Figure D.6 (page 289) in this respect.

Figure D.84 (page 372) shows measures for ${}^{-90th}_{ss1}P^{\mathrm{E}}_{v} \geq P_v \geq {}^{+90th}_{ss1}P^{\mathrm{E}}_{v}$ (N/kg) for all subjects[E] with non-zero occurrences for $\{{}_{ss1}\theta^{\mathrm{E}}_0\}$. Representative values for the largest $P_v > 0$ are obtained as follows. For each subject[E] the measure for the minimum ${}^{+90th}_{ss1}P^{\mathrm{E}}_{v}$, denoted ${}^{+90th}_{ss1}P^{\mathrm{E}}_{vmini}$, can be read and the min-

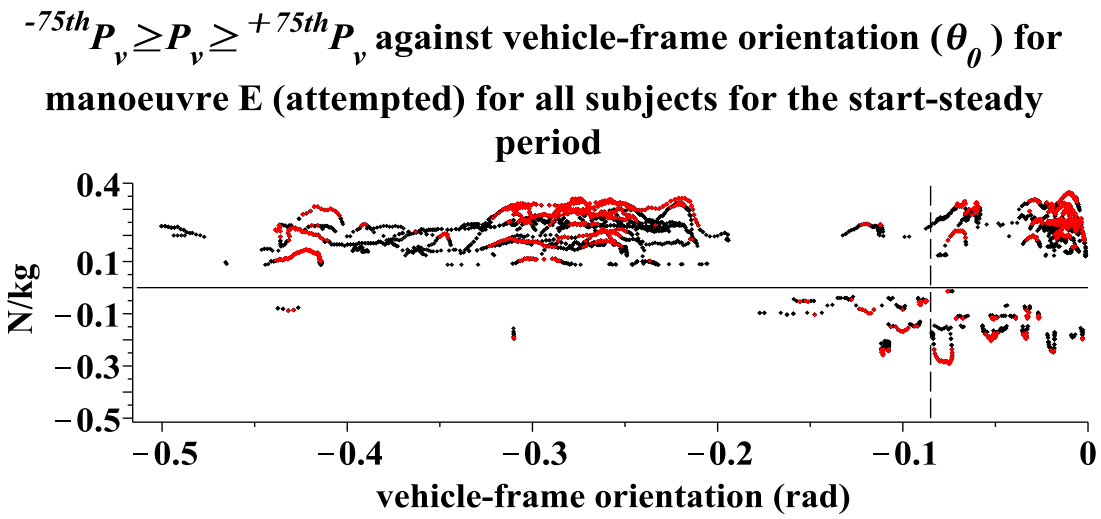

Figure D.83 – Occurrences of ${}^{-75th}_{ssi}P^{\mathrm{E}}_{v} \geq P_v > {}^{-90th}_{ssi}P^{\mathrm{E}}_{v}$ and of ${}^{+75th}_{ssi}P^{\mathrm{E}}_{v} \leq P_v < {}^{+90th}_{ssi}P^{\mathrm{E}}_{v}$ (both black markers) and, of $P_v \leq {}^{-90th}_{ssi}P^{\mathrm{E}}_{v}$ and of $P_v \geq {}^{+90th}_{ssi}P^{\mathrm{E}}_{v}$ (both red markers) in N/kg against θ_0 for ${}_{ssi}\theta^{\mathrm{E}}_{0}$ for all subjects[E].

imum ${}^{+90th}_{ss1}P^{\mathrm{E}}_{vmini}$ for all subjects[E], denoted ${}^{+90th}_{ss1}P^{\mathrm{E}}_{vmin}$, is 0.05 N/kg (subject[6]). The maximum P_v for each subject[E], denoted ${}^{+90th}_{ss1}P^{\mathrm{E}}_{vmaxi}$, can also be read and the maximum ${}^{+90th}_{ss1}P^{\mathrm{E}}_{vmaxi}$, denoted ${}^{+90th}_{ss1}P^{\mathrm{E}}_{vmax}$, is 0.37 N/kg (subject[7]). The mean ${}^{+90th}_{ss1}P^{\mathrm{E}}_{vmaxi} \leq P_v \leq {}^{+90th}_{ss1}P^{\mathrm{E}}_{vmaxi}$ for each subject[E] is indicated by a solid circle though most ranges are of such small magnitude that the location of the mean is immaterial. Occurrences of $P_v \geq {}^{+90th}_{ss1}P^{\mathrm{E}}_{v}$ are shown above the range line for $P_v > 0$ for each subject. Subject[0] shows the range from ${}^{+90th}_{ss1}P^{\mathrm{E}}_{vmin}$ to ${}^{+90th}_{ss1}P^{\mathrm{E}}_{vmax}$ with the mean for all the mean ${}^{+90th}_{ss1}P^{\mathrm{E}}_{vmini} \leq P_v \leq {}^{+90th}_{ss1}P^{\mathrm{E}}_{vmaxi}$ located approximately centrally as indicated by a solid circle.

It can also be seen from Figure D.84 (page 372) that the range magnitude of 0.35 N/kg, ${}^{+90th}_{ss1}P^{\mathrm{E}}_{vmax} - {}^{+90th}_{ss1}P^{\mathrm{E}}_{vmin}$, arises from inter-subject variation (subject[6] compared with subject[7]) and is not the result of the ${}^{+90th}_{ss1}P^{\mathrm{E}}_{vmaxi} - {}^{+90th}_{ss1}P^{\mathrm{E}}_{vmini}$ of a specific subject. There are therefore substantial differences between subjects for the largest $P_v > 0$. However, the inequality ${}^{+90th}_{ss1}P^{\mathrm{E}}_{vmini} \leq P_v \leq {}^{+90th}_{ss1}P^{\mathrm{E}}_{vmaxi}$ provides a representative range for each of subjects[E]. Additionally the inequality ${}^{+90th}_{ss1}P^{\mathrm{E}}_{vmin} \leq P_v \leq {}^{+90th}_{ss1}P^{\mathrm{E}}_{vmax}$ provides a representative range for all subjects[E] for the largest $P_v > 0$ for the $\{{}_{ss1}\theta^{\mathrm{E}}_{0}\}$.

Representative values for the largest magnitude $P_v < 0$ are also read from Figure D.84 (page 372). For each subject[E] with non-zero occurrences the meas-

ure for the minimum magnitude ${}^{-90th}_{ss1}P^{\mathrm{E}}_{v}$, denoted ${}^{-90th}_{ss1}P^{\mathrm{E}}_{vmini}$, can be read and the minimum magnitude ${}^{-90th}_{ss1}P^{\mathrm{E}}_{vmini}$ for all subjects[E] with non-zero occurrences, denoted ${}^{-90th}_{ss1}P^{\mathrm{E}}_{vmin}$, is, after rounding, -0.00 N/kg (subject[10]). The maximum magnitude $P_v < 0$ for all subjects[E], denoted ${}^{-90th}_{ss1}P^{\mathrm{E}}_{vmaxi}$ can also be read and the maximum magnitude ${}^{-90th}_{ss1}P^{\mathrm{E}}_{vmaxi}$, denoted ${}^{-90th}_{ss1}P^{\mathrm{E}}_{vmax}$, is -0.25 N/kg (subject[11]). The mean ${}^{-90th}_{ss1}P^{\mathrm{E}}_{vmini} \geq P_v \geq {}^{-90th}_{ss1}P^{\mathrm{E}}_{vmaxi}$ for each subject[E] is indicated by a solid circle but it can be seen that the ranges (excluding subjects[11, 16]) are of such small magnitude that the location is immaterial. The occurrences of $P_v \leq {}^{-90th}_{ss1}P^{\mathrm{E}}_{v}$ are shown below the range line. Subjects[4, 10, 13] are disregarded as only a single occurrence is present. Subject[0] shows the range from ${}^{-90th}_{ss1}P^{\mathrm{E}}_{vmin}$ to ${}^{-90th}_{ss1}P^{\mathrm{E}}_{vmax}$ with the mean of all the mean ${}^{-90th}_{ss1}P^{\mathrm{E}}_{vmini} \geq P_v \geq {}^{-90th}_{ss1}P^{\mathrm{E}}_{vmaxi}$ indicated by a solid circle is approximately centrally located.

It can also be seen from Figure D.84 (page 372) that the range magnitude of 0.15 N/kg, ${}^{-90th}_{ss1}P^{\mathrm{E}}_{vmax} - {}^{-90th}_{ss1}P^{\mathrm{E}}_{vmin}$, arises from inter-subject variation (subject[10] compared with subject[11]) and is not the result of the ${}^{-90th}_{ss1}P^{\mathrm{E}}_{vmaxi} - {}^{-90th}_{ss1}P^{\mathrm{E}}_{vmini}$ of a specific subject. There are therefore differences between subjects for the largest magnitude $P_v < 0$. However, the inequality ${}^{-90th}_{ss1}P^{\mathrm{E}}_{vmini} \geq P_v \geq {}^{-90th}_{ss1}P^{\mathrm{E}}_{vmaxi}$ provides a representative range for each of subjects[2, 3, 6, 9, 11, 12, 16]. Additionally the inequality ${}^{-90th}_{ss1}P^{\mathrm{E}}_{vmin} \geq P_v \geq {}^{-90th}_{ss1}P^{\mathrm{E}}_{vmax}$ (subject[0]) provides a representative range for all of subjects[2, 3, 6, 9, 11, 12, 16] for the largest magnitude $P_v < 0$ for $\{{}_{ss1}\theta^{\mathrm{E}}_{0}\}$.

Taking account of both signs the largest magnitude P_v is 0.37 N/kg and the smallest magnitude for $P_{uCs} \leq {}^{-90th}_{ss1}P^{\mathrm{E}}_{uCsmin}$ is 0.95 N/kg and therefore the largest magnitudes of P_{uCs} are greater than the largest magnitudes of P_v and this confirms the representativeness of Figure D.78 (page 363) in this respect.

D.13.5. *Manouevre E (a.) the $P_v - P_{uCs}$ plane*

This final section relating to manoeuvre E (a.) uses the inequalities, as previously defined, to define a cuboid boundary for the largest magnitude measures for each and all subjects. All subjects[E] had P_v measures for $P_v > 0$ and subjects[2, 3, 6, 9, 11, 12, 16] had measures for $P_v < 0$, and all subjects[E] had P_u measures for $P_u > 0$ and subjects[1, 2, 3, 5, 7,..., 16] had measures for $P_u < 0$: this

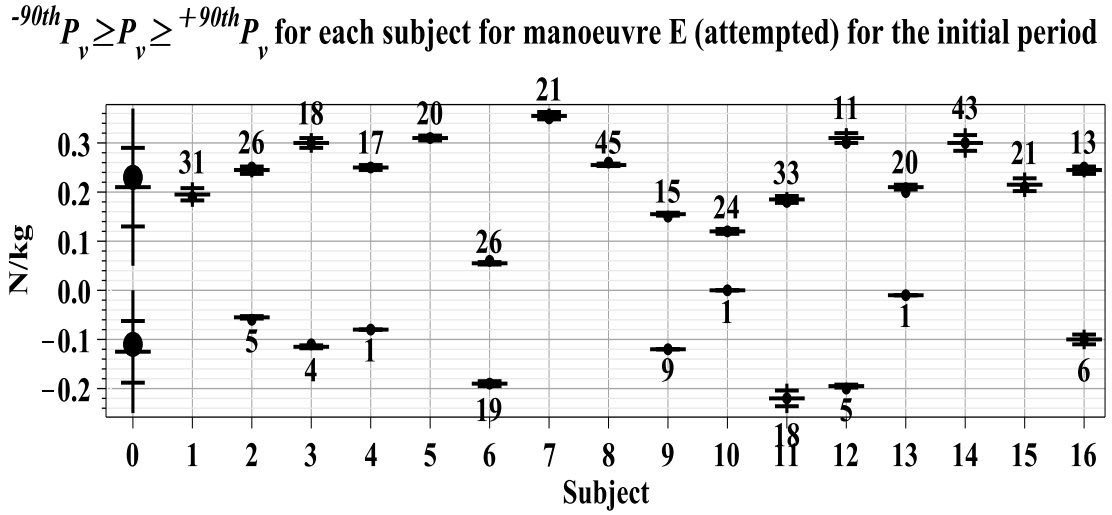

Figure D.84 – Shows for each subject[E] (i) for $\{{}_{ss1}\theta_0^{\mathrm{E}}\}$ (N/kg): for $P_v > 0$ a vertical line indicating the minimum magnitude measure ${}^{+90th}_{ss1}P^{\mathrm{E}}_{vmini}$ to the maximum magnitude measure ${}^{+90th}_{ss1}P^{\mathrm{E}}_{vmaxi}$, a solid circle indicating the mean ${}^{+90th}_{ss1}P^{\mathrm{E}}_{vmini} \leq P_v \leq {}^{+90th}_{ss1}P^{\mathrm{E}}_{vmaxi}$, the quarter divisions of the range (horizontal lines) and the number of occurrences of $P_v \geq {}^{+90th}_{ss1}P^{\mathrm{E}}_{v}$ shown above the range line: for $P_v < 0$ where there are non-zero occurrences, a vertical line indicating the minimum magnitude measure ${}^{-90th}_{ss1}P^{\mathrm{E}}_{vmini}$ to the maximum magnitude measure ${}^{-90th}_{ss1}P^{\mathrm{E}}_{vmaxi}$, a solid circle indicating the mean ${}^{-90th}_{ss1}P^{\mathrm{E}}_{vmini} \geq P_v \geq {}^{-90th}_{ss1}P^{\mathrm{E}}_{vmaxi}$, the quarter divisions of the range (horizontal lines) and the number of occurrences of $P_v \leq {}^{+90th}_{ss1}P^{\mathrm{E}}_{v}$ shown below the range line. Subject[0] shows these measures for all subjects[E]: for $P_v > 0$ with a solid circle indicating the mean of all the mean ${}^{+90th}_{ss1}P^{\mathrm{E}}_{vmini} \leq P_v \leq {}^{+90th}_{ss1}P^{\mathrm{E}}_{vmaxi}$ and for $P_v < 0$ with a solid circle indicating the mean of all the mean ${}^{-90th}_{ss1}P^{\mathrm{E}}_{vmini} \geq P_v \geq {}^{-90th}_{ss1}P^{\mathrm{E}}_{vmaxi}$.

definition requires four sets of three inequalities as follows. For the first set of three inequalities for each of subjects[1,..., 16] the inequalities are:

$${}^{-90th}_{ss1}P^{\mathrm{E}}_{uCsmini} \geq P_{uCs} \geq {}^{-90th}_{ss1}P^{\mathrm{E}}_{uCsmaxi},$$

$${}^{+90th}_{ss1}P^{\mathrm{E}}_{umini} \leq P_u \leq {}^{+90th}_{ss1}P^{\mathrm{E}}_{umaxi} \text{ and}$$

$${}^{+90th}_{ss1}P^{\mathrm{E}}_{vmini} \leq P_v \leq {}^{+90th}_{ss1}P^{\mathrm{E}}_{vmaxi}.$$

For the second set of three inequalities for each of subjects[1, 2, 3, 5, 7,..., 16] the inequalities are as given for P_{uCs} and P_v as above and

$${}^{-90th}_{ss1}P^{\mathrm{E}}_{umini} \geq P_u \geq {}^{-90th}_{ss1}P^{\mathrm{E}}_{umaxi}.$$

For the third set of three inequalities for each of subjects[2, 3, 6, 9, 11, 12, 16] the inequalities are as given for P_{uCs} and P_u as given in the first set and

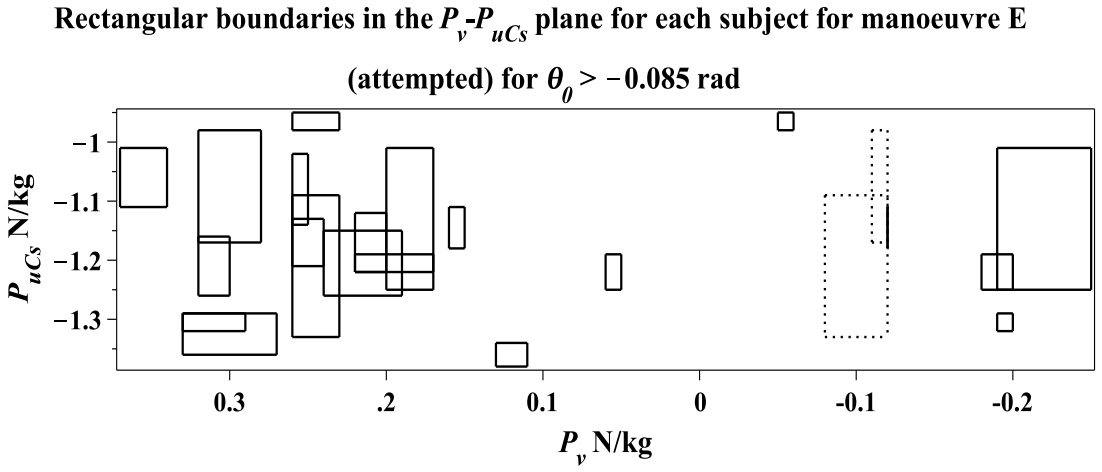

Figure D.85 – Shows, relating to $P_v > 0$, for each subject[E] the four vertices of a rectangle are formed with a $[P_v, P_{uCs}]$ coordinate as follows: $[{}^{+90th}_{ss1}P^{\mathrm{E}}_{vmaxi}, {}^{-90th}_{ss1}P^{\mathrm{E}}_{uCsmini}]$, $[{}^{+90th}_{ss1}P^{\mathrm{E}}_{vmini}, {}^{-90th}_{ss1}P^{\mathrm{E}}_{uCsmini}]$, $[{}^{+90th}_{ss1}P^{\mathrm{E}}_{vmini}, {}^{-90th}_{ss1}P^{\mathrm{E}}_{uCsmaxi},]$, and $[{}^{+90th}_{ss1}P^{\mathrm{E}}_{vmaxi}, {}^{-90th}_{ss1}P^{\mathrm{E}}_{uCsmaxi}]$: n=16. Relating to $P_v < 0$ for each subject[2, 3, 6, 9, 11, 12, 16] the four vertices of a rectangle are formed with a $[P_v, P_{uCs}]$ coordinate as follows: $[{}^{-90th}_{ss1}P^{\mathrm{E}}_{vmini}, {}^{-90th}_{ss1}P^{\mathrm{E}}_{uCsmini}]$, $[{}^{-90th}_{ss1}P^{\mathrm{E}}_{vmaxi}, {}^{-90th}_{ss1}P^{\mathrm{E}}_{uCsmini}]$, $[{}^{-90th}_{ss1}P^{\mathrm{E}}_{vmaxi}, {}^{-90th}_{ss1}P^{\mathrm{E}}_{uCsmaxi},]$, and $[{}^{-90th}_{ss1}P^{\mathrm{E}}_{vmini}, {}^{-90th}_{ss1}P^{\mathrm{E}}_{uCsmaxi}]$: subjects[9, 16] are shown as dotted boundaries in order to identify subject[3]: n=7.

$${}^{-90th}_{ss1}P^{\mathrm{E}}_{vmini} \geq P_v \geq {}^{-90th}_{ss1}P^{\mathrm{E}}_{vmaxi}.$$

For the fourth set of three inequalities for each of subjects[2, 3, 9, 11, 12, 16] the inequalities are as given for P_{uCs} in the first set, P_u as given in the second set and P_v as given in the third set.

One cuboid boundary is therefore defined for subject[4], two cuboid boundaries are defined for each of subjects[1, 5, 6, 7, 8, 10, 13, 14, 15] and four cuboid enclosures are defined for each of subjects[2, 3, 9, 11, 12, 16]: these provide a representation of the largest magnitudes of handle-forces for manoeuvre E (a.) for the $\{{}_{ss1}\theta^{\mathrm{E}}_0\}$ for each subject. These one, two or four sets of three inequalities are denoted ${}^{large}_{ss1}\mathbf{P}^{\mathrm{E}}_i$.

A graphical representation of ${}^{large}_{ss1}\mathbf{P}^{\mathrm{E}}_i$ in the $P_v - P_{uCs}$ plane is shown in Figure D.85 (page 373): the construction follows the same process as described in Section 6.4.4 (page 149) for manoeuvre F (a.) and subjects[9, 16] are shown as dotted boundaries in order to identify subject[3]

One, two or four sets of inequalities define the cuboid boundaries which

enclose the measures for all, rather than each of, subjects[E] can be determined by removal of the i subscript from the above definitions.

These four sets of three inequalities, comprising of five unique inequalities for all subjects[E], are denoted ${}^{large}_{ss1}\mathbf{P}^{\mathrm{E}}$. In conclusion ${}^{large}_{ss1}\mathbf{P}^{\mathrm{E}}$ provides a useful representation of the largest handle-forces for all subjects[E] for manoeuvre E (a.): the numerical values are:

$-0.95 \geq P_{uCs} \geq -1.38$ (N/kg) and

$0.08 \leq P_v \leq 0.48$ (N/kg),

$-0.08 \geq P_v \geq -0.32$ (N/kg),

$0.05 \leq P_u \leq 0.37$ (N/kg) and

$0.00 \geq P_u \geq -0.25$ (N/kg).

D.14. **Manoeuvre L (attempted)**

A trailing super or sub script L in a symbol or 'all subjects[L]' indicates measures from subjects [1,..., 14, 16]: subject[15] did not participate.

D.14.1. *Manoeuvre L (a.) handle-force measures*

Examination of the handle-force measures will show that dividing the start-steady period, denoted $\{{}_{ssi}\theta_0^{\mathrm{L}}\}$, at $\theta_0 = -0.108$ rad is useful and hence θ_0 measures for manoeuvre L (a.) are defined for the initial period $-0.108 < \theta_0 < 0$ rad, denoted $\{{}_{ss1}\theta_0^{\mathrm{L}}\}$, and for the later period $\theta_{0steadi} < \theta_0 < -0.108$ rad, denoted $\{{}_{ss2i}\theta_0^{\mathrm{L}}\}$. Figure D.87 (page 375) illustrates the force measures for one subject[9] two features of which are common to all subjects[L]. Firstly, there are no occurrences of $P_{uCs} > 0$ for $\{{}_{ss1}\theta_0^{\mathrm{L}}\}$. Secondly, there are no occurrences of $P_v < 0$.

D.14.2. *Manoeuvre L (a.) P_{uCs}*

The presentation begins with P_{uCs}. Figure D.88 (page 376) shows occurrences of ${}^{-75th}_{ssi}P^{\mathrm{L}}_{uCs} \geq P_{uCs} > {}^{-90th}_{ssi}P^{\mathrm{L}}_{uCs}$ and of ${}^{+75th}_{ssi}P^{\mathrm{L}}_{uCs} \leq P_{uCs} < {}^{+90th}_{ssi}P^{\mathrm{L}}_{uCs}$ (both black markers), and $P_{uCs} \leq {}^{-90th}_{ssi}P^{\mathrm{L}}_{uCs}$ and $P_{uCs} \geq {}^{+90th}_{ssi}P^{\mathrm{L}}_{uCs}$ (both red markers) in N/kg for all subjects[L]: to assist inspection the measures for each subject are normalised against the subject's P_{uCs} peak magnitude for $\{{}_{ssi}\theta_0^{\mathrm{L}}\}$. A dashed vertical line indicates $\theta_0 = -0.108$ rad and this divides $\{{}_{ssi}\theta_0^{\mathrm{L}}\}$ into $\{{}_{ss1}\theta_0^{\mathrm{L}}\}$ and $\{{}_{ss2i}\theta_0^{\mathrm{L}}\}$ as previously defined.

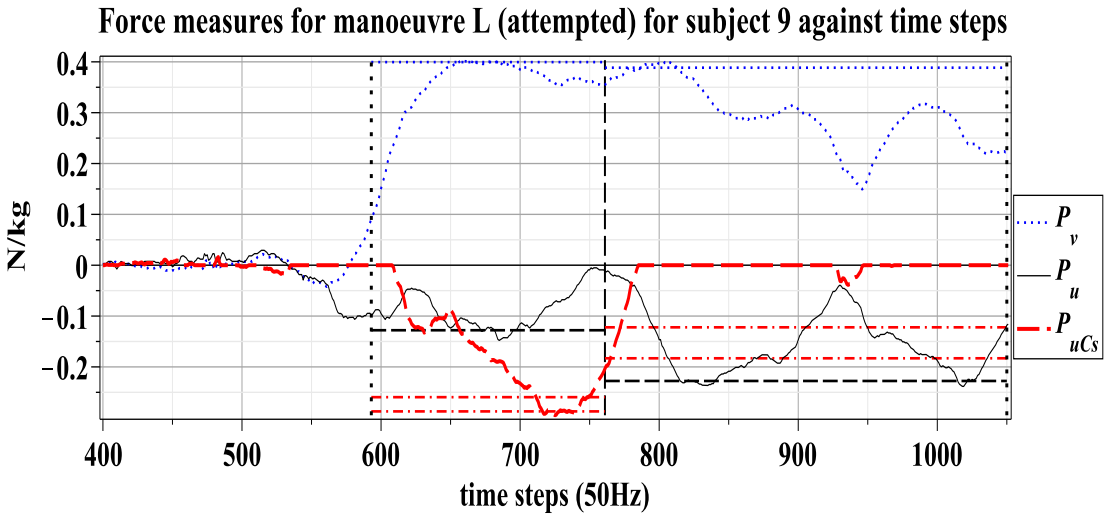

Figure D.86 – For subject[9] for the manoeuvre L (a.), measures: P_v (dotted blue), P_u (thin black) and P_{uCs} (thick red dashed) in N/kg plotted against time-steps (approximately 0.02 seconds) with motion-start line (vertical black dotted: closest to left side), steady-start line (vertical black dotted: closest to right side) and $\theta_0 = -0.108$ rad line (vertical black dashed). The following percentile lines are shown for the $\{{}_{ss1}\theta_0^{\mathrm{L}}\}$: ${}^{-90th}_{ss1}P^{\mathrm{L}}_{uCs}$ and ${}^{-75th}_{ss1}P^{\mathrm{L}}_{uCs}$ (horizontal red dash-dot), ${}^{-90th}_{ss1}P^{\mathrm{L}}_{u}$ (horizontal black dash) and ${}^{+90th}_{ss1}P^{\mathrm{L}}_{v}$ (horizontal blue dot): these percentile lines are also shown for $\{{}_{ss2i}\theta_0^{\mathrm{L}}\}$.

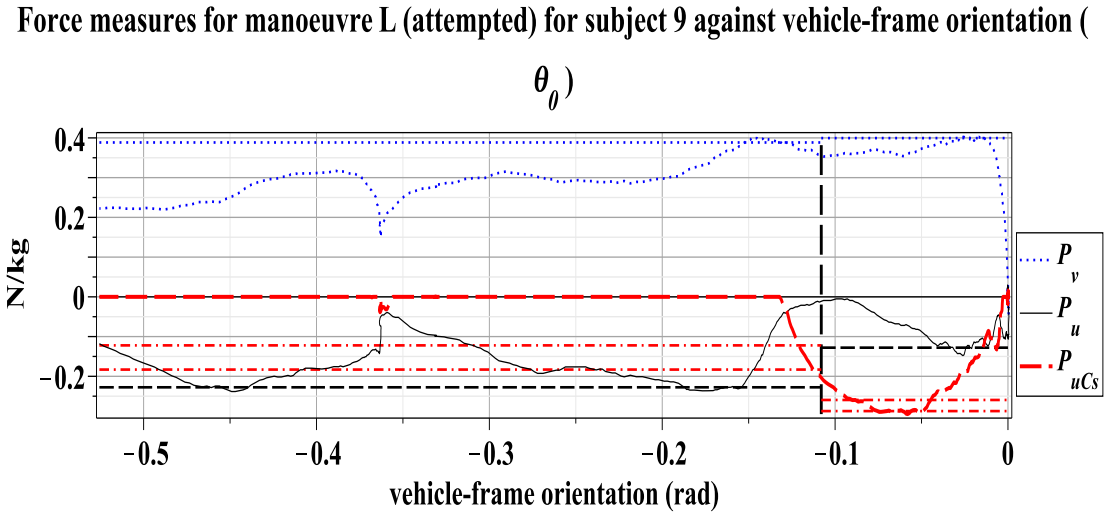

Figure D.87 – Shows for subject[9] for manoeuvre L (a.), measures plotted against θ_0 with other details as above.

Figure D.88 shows P_{uCs} normalised against peak magnitude so it is evident that $P_{uCs} > 0$ are of small magnitude compared with $P_{uCs} < 0$. Figure D.88 also indicates that the occurrences of $P_{uCs} > 0$ are small compared with $P_{uCs} < 0$ and an evaluation of the data shows that for all subjects[L] that there are no $P_{uCs} > 0$ for $\{{}_{ss1}\theta_0^{\mathrm{L}}\}$ and this confirms the representativeness of Figure D.87 (page 375) in

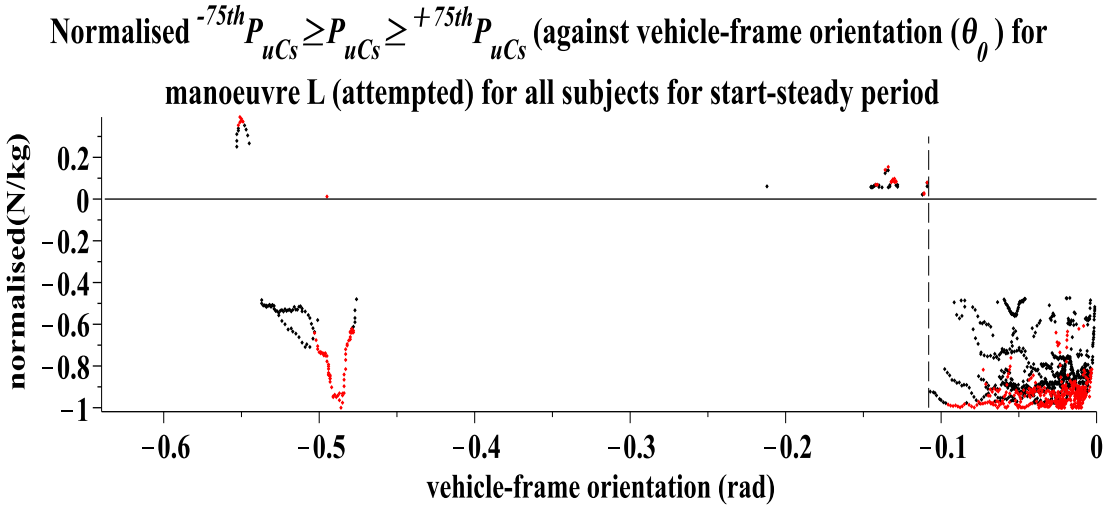

Figure D.88 – For the manoeuvre L (a.) occurrences of ${}^{-75th}_{ssi}P^{\mathrm{L}}_{uCs} \geq P_{uCs} > {}^{-90th}_{ssi}P^{\mathrm{L}}_{uCs}$ and of ${}^{+75th}_{ssi}P^{\mathrm{L}}_{uCs} \leq P_{uCs} < {}^{+90th}_{ssi}P^{\mathrm{L}}_{uCs}$ (both black markers) and, $P_{uCs} \leq {}^{-90th}_{ssi}P^{\mathrm{L}}_{uCs}$ and $P_{uCs} \geq {}^{+90th}_{ssi}P^{\mathrm{L}}_{uCs}$ (both red markers) in N/kg (normalised against each subject's maximum magnitude P_{uCs} for $\{{}_{ssi}\theta^{\mathrm{L}}_0\}$ against θ_0 for each subject: $\theta_0 = -0.108$ line indicated (dashed vertical).

this respect. Two further observations are made.

Firstly, it is evident that for $\{{}_{ss1}\theta^{\mathrm{L}}_0\}$ the accumulated occurrences of $P_{uCs} \leq {}^{-75th}_{ssi}P^{\mathrm{L}}_{uCs}$ for all subjects[L] are contiguous and that these include the peak magnitude measure for most though not all subjects[L]. Examination of the data (see PDF, Sensor Data) indicates that subject[6] is responsible for the peak close to −0.5 rad, the P_v and P_u measures also peak, and while this subject does not contribute to the contiguity for $\theta_0 > -0.475$ this subject does have P_{uCs} peak magnitude measures for $\{{}_{ss1}\theta^{\mathrm{L}}_0\}$, i.e. the signal is a typical shape for the initial period. Thus, disregarding the subject[6] exception, despite any variations between subjects, the mechanism is so configured that the contiguous occurrences of $P_{uCs} \leq {}^{-75th}_{ssi}P^{\mathrm{L}}_{uCs}$ are completed in $\{{}_{ss1}\theta^{\mathrm{L}}_0\}$ and thus the division of the start-steady period at $\theta_0 = -0.108$ rad relates to a mechanical property of the system.

Figure D.89 (page 377) shows measures for $P_{uCs} \leq {}^{-90th}_{ss1}P^{\mathrm{L}}_{uCs}$ (N/kg) for all subjects[L] for $\{{}_{ss1}\theta^{\mathrm{L}}_0\}$. Representative values for the largest magnitude P_{uCs} are obtained as follows. For each subject[L] the measure for the minimum $P_{uCs} \leq {}^{-90th}_{ss1}P^{\mathrm{L}}_{uCs}$, denoted ${}^{-90th}_{ss1}P^{\mathrm{L}}_{uCsmini}$, may be read and the minimum ${}^{-90th}_{ss1}P^{\mathrm{L}}_{uCsmini}$ for all subjects[L], denoted ${}^{-90th}_{ss1}P^{\mathrm{L}}_{uCsmin}$, is −0.28 N/kg (subject[7]). The maximum magnitude P_{uCs} for each subject[L], denoted ${}^{-90th}_{ss1}P^{\mathrm{L}}_{uCsmaxi}$, may also be read and the

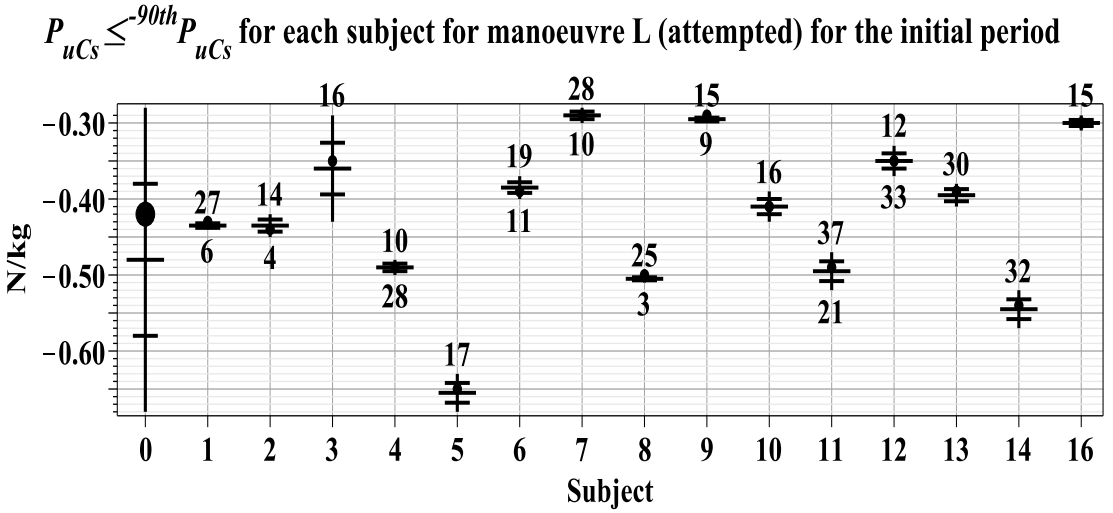

Figure D.89 – Shows for each subject[L] (i) for $\{{}_{ss1}\theta_0^{\mathrm{L}}\}$ in N/kg: a vertical line indicating the minimum magnitude ${}^{-90th}_{ss1}P^{\mathrm{L}}_{uCsmini}$ to the maximum magnitude ${}^{-90th}_{ss1}P^{\mathrm{L}}_{uCsmaxi}$, a solid circle indicating the mean ${}^{-90th}_{ss1}P^{\mathrm{L}}_{PuCsmini} \geq P_{uCs} \geq {}^{-90th}_{ss1}P^{\mathrm{L}}_{PuCsmaxi}$, the quarter divisions of the range (horizontal lines), the number of occurrences of $P_{uCs} \leq {}^{-90th}_{ss1}P^{\mathrm{L}}_{uCs}$ shown above the range line and the percentage of occurrences of $P_{uCs} = 0$ (integer) for $\{{}_{ss1}\theta_0^{\mathrm{L}}\}$ shown below the range line. Subject[0] shows these measures for all subjects[L] with a solid circle indicating the mean of all the mean ${}^{-90th}_{ss1}P^{\mathrm{L}}_{PuCsmini} \geq P_{uCs} \geq {}^{-90th}_{ss1}P^{\mathrm{L}}_{PuCsmaxi}$.

maximum ${}^{-90th}_{ss1}P^{\mathrm{L}}_{uCsmaxi}$, denoted ${}^{-90th}_{ss1}P^{\mathrm{L}}_{uCsmax}$, is −0.68 N/kg (subject[5]). The mean ${}^{-90th}_{ss1}P^{\mathrm{L}}_{uCsmini} \geq P_{uCs} \geq {}^{-90th}_{ss1}P^{\mathrm{L}}_{uCsmaxi}$ for each subject[L] are indicated by a solid circle and it can be seen that these means, ignoring subjects where the range magnitude is relatively small, are located in the first to third quarters of the intra-subject range. Subject[0] shows the range of ${}^{-90th}_{ss1}P^{\mathrm{L}}_{uCsmin}$ to ${}^{-90th}_{ss1}P^{\mathrm{L}}_{uCsmax}$ and the mean of all the mean ${}^{-90th}_{ss1}P^{\mathrm{L}}_{uCsmini} \geq P_{uCs} \geq {}^{-90th}_{ss1}P^{\mathrm{L}}_{uCsmaxi}$ indicated by a solid circle is located in the second quarter of the inter-subject range.

For each subject, occurrences of $P_{uCs} \leq {}^{-90th}_{ss1}P^{\mathrm{L}}_{uCs}$ are shown above the range line in Figure D.89 (page 377) and the percentage of occurrences of $P_{uCs} = 0$ (integer) are shown below the range line: zero occurrences are not shown. Substantial variation is evident: subjects[3, 10, 13, 14, 16] have no occurrences of $P_{uCs} = 0$ (integer) where as subject[12] has 33% $P_{uCs} = 0$ occurrences In other words the attempt at manoeuvre[L] by some subjects, to some extent, reduces the occurrences of the couple action.

It can also be seen from Figure D.89 (page 377) that the range mag-

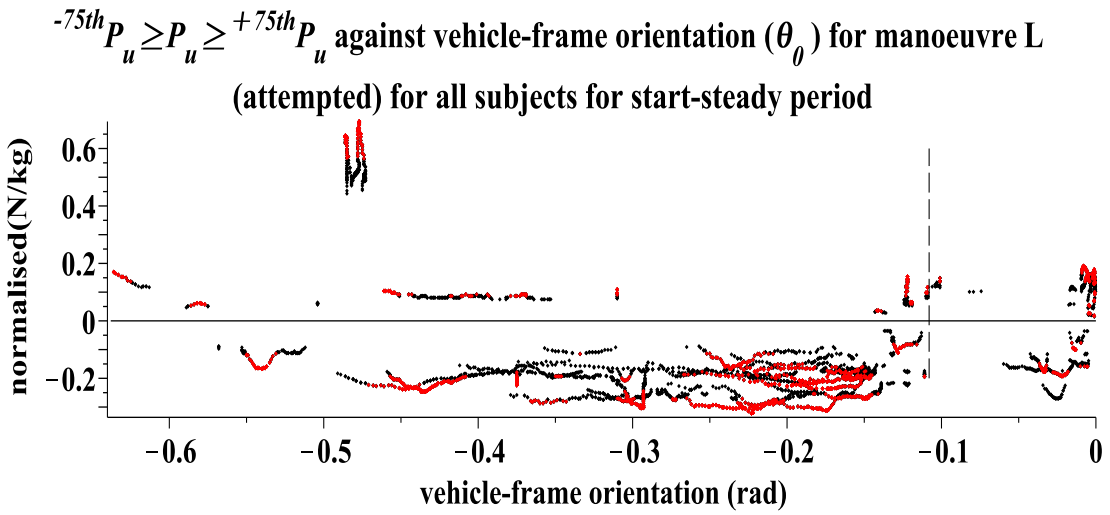

Figure D.90 – For the manoeuvre L (a.) occurrences of ${}^{-75th}_{ssi}P^{\mathrm{L}}_{u} \geq P_u > {}^{-90th}_{ssi}P^{\mathrm{L}}_{u}$ and of ${}^{+75th}_{ssi}P^{\mathrm{L}}_{u} \leq P_u < {}^{+90th}_{ssi}P^{\mathrm{L}}_{u}$ (both black markers) and, of $P_u \leq {}^{-90th}_{ssi}P^{\mathrm{L}}_{u}$ and of $P_u \geq {}^{+90th}_{ssi}P^{\mathrm{L}}_{u}$ (both red markers) in N/kg against θ_0 for $\{{}_{ssi}\theta^{\mathrm{L}}_{0}\}$ for each subject: $\theta_0 = -0.108$ line indicated (dashed vertical).

nitude of −0.40 N/kg, ${}^{-90th}_{ss1}P^{\mathrm{L}}_{uCsmax} - {}^{-90th}_{ss1}P^{\mathrm{L}}_{uCsmin}$, arises from inter-subject variation (subject[7] compared with subject[5]) and is not the result of the ${}^{-90th}_{ss1}P^{\mathrm{L}}_{uCsmaxi} - {}^{-90th}_{ss1}P^{\mathrm{L}}_{uCsmini}$ magnitude of a specific subject. There are therefore substantial differences between subjects for the largest magnitude $P_{uCs} < 0$. However, the inequality ${}^{-90th}_{ss1}P^{\mathrm{L}}_{uCsmini} \geq P_{uCs} \geq {}^{-90th}_{ss1}P^{\mathrm{L}}_{uCsmaxi}$ provides a representative range for each subject. In addition the inequality ${}^{-90th}_{ss1}P^{\mathrm{L}}_{uCsmin} \geq P_{uCs} \geq {}^{-90th}_{ss1}P^{\mathrm{L}}_{uCsmax}$ provides a representative range for all subjects[L].

D.14.3. *Manoeuvre L (a.)* P_u

Figure D.90 (page 378) shows occurrences of ${}^{-75th}_{ssi}P^{\mathrm{L}}_{u} \geq P_u > {}^{-90th}_{ssi}P^{\mathrm{L}}_{u}$ and of ${}^{+75th}_{ssi}P^{\mathrm{L}}_{u} \leq P_u < {}^{+90th}_{ssi}P^{\mathrm{L}}_{u}$ (both black markers) and, of $P_u \leq {}^{-90th}_{ssi}P^{\mathrm{L}}_{u}$ and of $P_u \geq {}^{+90th}_{ssi}P^{\mathrm{L}}_{u}$ (both red markers): these are the occurrences for all subjects[L]. As Figure D.90 does not show normalised P_u it is evident that, taking account of all subjects[L], that some peak measures in $\{{}_{ss1}\theta^{\mathrm{L}}_{0}\}$ can be of approximately equal magnitude but opposite signs and that therefore both signs of P_u should be considered.

Figure D.91 (page 380) shows measures for ${}^{-90th}_{ss1}P^{\mathrm{L}}_{u} \geq P_u \geq {}^{+90th}_{ss1}P^{\mathrm{L}}_{u}$ (N/kg) for all subjects[L] for $\{{}_{ss1}\theta^{\mathrm{L}}_{0}\}$. Subjects with a single occurrence are disregarded. Measures relating to $P_u > 0$ are considered first. Representative values for the

largest $P_u > 0$ are obtained as follows. For each subject[L] the measure for the minimum ${}^{+90th}_{ss1}P^{\mathrm{L}}_{u}$, denoted ${}^{+90th}_{ss1}P^{\mathrm{L}}_{umini}$, can be read and the minimum ${}^{+90th}_{ss1}P^{\mathrm{L}}_{umini}$ for all subjects[L] with non-zero occurrences, denoted ${}^{+90th}_{ss1}P^{\mathrm{L}}_{umin}$, is 0.02 N/kg (subjects[13]). The maximum P_u for each subject[L], denoted ${}^{+90th}_{ss1}P^{\mathrm{L}}_{umaxi}$ can also be read and the maximum ${}^{+90th}_{ss1}P^{\mathrm{L}}_{umaxi}$, denoted ${}^{+90th}_{ss1}P^{\mathrm{L}}_{umax}$, is 0.19 N/kg (subject[7]). The mean ${}^{+90th}_{ss1}P^{\mathrm{L}}_{umaxi} \leq P_u \leq {}^{+90th}_{ss1}P^{\mathrm{L}}_{umaxi}$ for each subject[L] is indicated by a solid circle but the ranges are of such small magnitude that the location of the mean is immaterial. Occurrences of $P_u \geq {}^{+90th}_{ss1}P^{\mathrm{L}}_{u}$ are shown above the range line for $P_u > 0$ for each subject. Subject[0] shows the range from ${}^{+90th}_{ss1}P^{\mathrm{L}}_{umin}$ to ${}^{+90th}_{ss1}P^{\mathrm{L}}_{umax}$ with the mean for all the mean ${}^{+90th}_{ss1}P^{\mathrm{L}}_{umini} \leq P_u \leq {}^{+90th}_{ss1}P^{\mathrm{L}}_{umaxi}$ is approximately centrally located in the inter-subject range as indicated by a solid circle.

It can also be seen from Figure D.91 (page 380) that the range magnitude of 0.17 N/kg, ${}^{+90th}_{ss1}P^{\mathrm{L}}_{umax} - {}^{+90th}_{ss1}P^{\mathrm{L}}_{umin}$, arises from inter-subject variation (subjects[13] compared with subject[7]) and is not the result of the ${}^{+90th}_{ss1}P^{\mathrm{L}}_{umaxi} - {}^{+90th}_{ss1}P^{\mathrm{L}}_{umini}$ of a specific subject. While there are differences between subjects for the largest $P_u > 0$ the intra-subject range magnitude is relatively small. The inequality ${}^{+90th}_{ss1}P^{\mathrm{L}}_{umini} \leq P_u \leq {}^{+90th}_{ss1}P^{\mathrm{L}}_{umaxi}$ provides a representative range for each subject[L]. Additionally the inequality ${}^{+90th}_{ss1}P^{\mathrm{L}}_{umin} \leq P_u \leq {}^{+90th}_{ss1}P^{\mathrm{L}}_{umax}$ (subject[0]) provides a representative range for all subjects[L] for the largest $P_u > 0$ for $\{{}_{ss1}\theta^{\mathrm{L}}_{0}\}$.

Representative values for the largest magnitude $P_u < 0$ are also read from Figure D.91 (page 380) from below the zero line. For each subject[L] the measure for the minimum magnitude ${}^{-90th}_{ss1}P^{\mathrm{L}}_{u}$, denoted ${}^{-90th}_{ss1}P^{\mathrm{L}}_{umini}$, can be read and the minimum ${}^{-90th}_{ss1}P^{\mathrm{L}}_{umini}$ for all subjects[L] with non-zero occurrences, denoted ${}^{-90th}_{ss1}P^{\mathrm{L}}_{umin}$, is -0.01 N/kg (subject[5]). The maximum magnitude $P_u < 0$ for all subjects[L], denoted ${}^{-90th}_{ss1}P^{\mathrm{L}}_{umaxi}$ can also be read and the maximum ${}^{-90th}_{ss1}P^{\mathrm{L}}_{umaxi}$, denoted ${}^{-90th}_{ss1}P^{\mathrm{L}}_{umax}$, is -0.27 N/kg (subject[16]). The occurrences of $P_u \leq {}^{-90th}_{ss1}P^{\mathrm{L}}_{u}$ are shown below the range line. The mean ${}^{-90th}_{ss1}P^{\mathrm{L}}_{umini} \geq P_u \geq {}^{-90th}_{ss1}P^{\mathrm{L}}_{umaxi}$ for each subject[L] is indicated by a solid circle but it can be seen that the ranges are of small magnitude and location is immaterial. Subject[0] shows ${}^{-90th}_{ss1}P^{\mathrm{L}}_{umin}$ and ${}^{-90th}_{ss1}P^{\mathrm{L}}_{umax}$ with the mean of all the mean ${}^{-90th}_{ss1}P^{\mathrm{L}}_{umini} \geq P_u \geq {}^{-90th}_{ss1}P^{\mathrm{L}}_{umaxi}$ approximately centrally located as indicated by a solid circle.

It can also be seen from Figure D.91 (page 380) that the range magnitude of

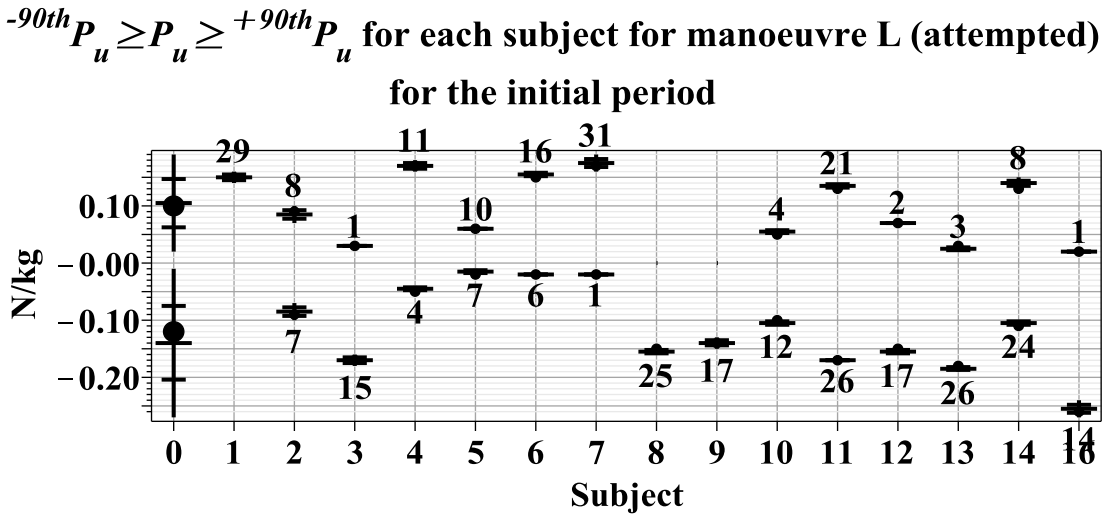

Figure D.91 – Shows for each subject[L] (i) for $\{{}_{ss1}\theta_0^{\mathrm{L}}\}$ in N/kg: for $P_u > 0$ a vertical line indicating the minimum measure ${}^{+90th}_{ss1}P^{\mathrm{L}}_{umini}$ to the maximum measure ${}^{+90th}_{ss1}P^{\mathrm{L}}_{umaxi}$, a solid circle indicating the mean ${}^{+90th}_{ss1}P^{\mathrm{L}}_{umini} \leq P_u \leq {}^{+90th}_{ss1}P^{\mathrm{L}}_{umaxi}$, the quarter divisions of the range (horizontal lines) and the number of occurrences of $P_u \geq {}^{+90th}_{ss1}P^{\mathrm{L}}_{u}$ shown above the range line: for $P_u < 0$ where there are non-zero occurrences, a vertical line indicating the minimum magnitude measure ${}^{-90th}_{ss1}P^{\mathrm{L}}_{umini}$ to the maximum magnitude measure ${}^{-90th}_{ss1}P^{\mathrm{L}}_{umaxi}$, a solid circle indicating the mean ${}^{-90th}_{ss1}P^{\mathrm{L}}_{umini} \geq P_u \geq {}^{-90th}_{ss1}P^{\mathrm{L}}_{umaxi}$, the quarter divisions of the range (horizontal lines) and the number of occurrences of $P_u \leq {}^{-90th}_{ss1}P^{\mathrm{L}}_{u}$ shown below the range line. Subject[0] shows these measures for all subjects[L]: for $P_u > 0$ with a solid circle indicating the mean of all the mean ${}^{+90th}_{ss1}P^{\mathrm{L}}_{umini} \leq P_u \leq {}^{+90th}_{ss1}P^{\mathrm{L}}_{umaxi}$ and for $P_u < 0$ with a solid circle indicating the mean of all the mean ${}^{-90th}_{ss1}P^{\mathrm{L}}_{umini} \geq P_u \geq {}^{-90th}_{ss1}P^{\mathrm{L}}_{umaxi}$.

0.28 N/kg, ${}^{-90th}_{ss1}P^{\mathrm{L}}_{umax} - {}^{-90th}_{ss1}P^{\mathrm{L}}_{umin}$, arises from inter-subject variation (subject[16] compared with subject[5]) and is not the result of the ${}^{-90th}_{ss1}P^{\mathrm{L}}_{umaxi} - {}^{-90th}_{ss1}P^{\mathrm{L}}_{umini}$ of a specific subject. There are therefore differences between subjects for the largest magnitude $P_u < 0$. There are also differences of occurrences: subject[13] has 26 occurrences where as subject[1] has zero. The inequality ${}^{-90th}_{ss1}P^{\mathrm{L}}_{umini} \leq P_u \leq {}^{-90th}_{ss1}P^{\mathrm{L}}_{umaxi}$ provides a representative range for each subject[L]. Additionally the inequality ${}^{-90th}_{ss1}P^{\mathrm{L}}_{umin} \leq P_u \leq {}^{-90th}_{ss1}P^{\mathrm{L}}_{umax}$ provides a representative range for the largest magnitudes for all subjects[L] with $P_u < 0$ measures. Taking account of both signs Figure D.91 shows that there is substantial variability between subjects[L].

D.14.4. *Manoeuvre L (a.) P_v*

Figure D.92 (page 381) shows occurrences of ${}^{-75th}_{ssi}P^{\mathrm{L}}_{v} \geq P_v > {}^{-90th}_{ssi}P^{\mathrm{L}}_{v}$ and of ${}^{+75th}_{ssi}P^{\mathrm{L}}_{v} \leq P_v < {}^{+90th}_{ssi}P^{\mathrm{L}}_{v}$ (both black markers) and, of $P_v \leq {}^{-90th}_{ssi}P^{\mathrm{L}}_{v}$ and

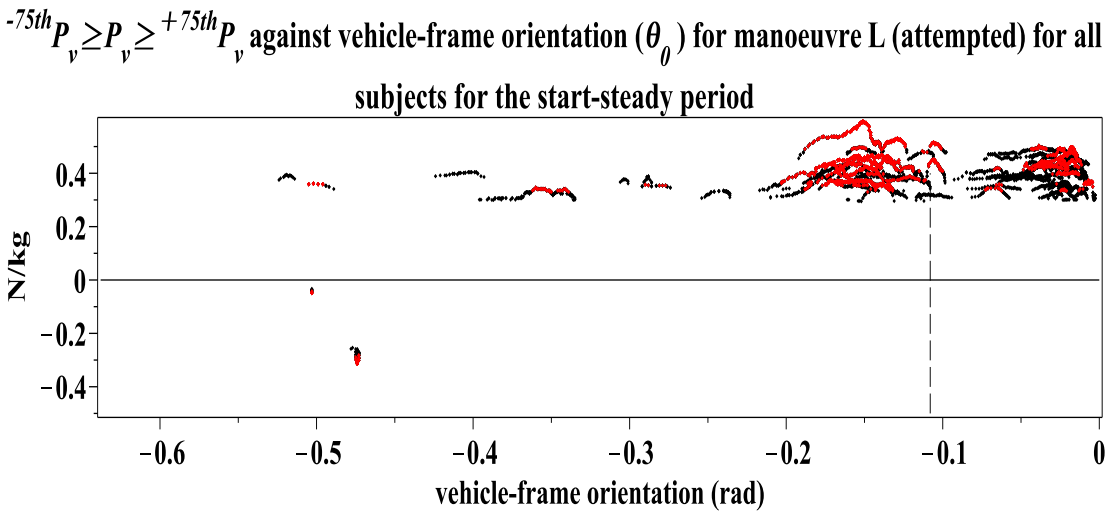

Figure D.92 – For the manoeuvre L (a.) occurrences of ${}^{-75th}_{ssi}P^{\mathrm{L}}_{v} \geq P_v > {}^{-90th}_{ssi}P^{\mathrm{L}}_{v}$ and of ${}^{+75th}_{ssi}P^{\mathrm{L}}_{v} \leq P_v < {}^{+90th}_{ssi}P^{\mathrm{L}}_{v}$ (both black markers) and, of $P_v \leq {}^{-90th}_{ssi}P^{\mathrm{L}}_{v}$ and of $P_v \geq {}^{+90th}_{ssi}P^{\mathrm{L}}_{v}$ (both red markers) in N/kg (normalised against each subject's maximum magnitude P_v for $\{{}_{ssi}\theta^{\mathrm{L}}_{0}\}$) against θ_0 for $\{{}_{ssi}\theta^{\mathrm{L}}_{0}\}$ for each subject: $\theta_0 = -0.108$ line indicated (dashed vertical).

of $P_v \geq {}^{+90th}_{ssi}P^{\mathrm{L}}_{v}$ (both red markers): these are the occurrences for all subjects[L]. It is evident that occurrences of $P_v < 0$ are few compared with the occurrences of $P_v > 0$. While occurrences of $P_v < 0$ exist for $\{{}_{ss1}\theta^{\mathrm{L}}_{0}\}$ these are disregarded in the presentation of results. Figure D.93 (page 382) shows measures for $P_v \geq {}^{+90th}_{ss1}P^{\mathrm{L}}_{v}$ (N/kg) for each subject[L] and for all subjects[L], denoted subject[0], for $\{{}_{ss1}\theta^{\mathrm{L}}_{0}\}$. Representative values for the largest P_v are obtained as follows. For each subject[L] the measure for the minimum ${}^{+90th}_{ss1}P^{\mathrm{L}}_{v}$, denoted ${}^{+90th}_{ss1}P^{\mathrm{L}}_{vmini}$, may be read and the minimum ${}^{+90th}_{ss1}P^{\mathrm{L}}_{vmini}$ for all subjects[L], denoted ${}^{+90th}_{ss1}P^{\mathrm{L}}_{vmin}$, is 0.33 N/kg (subject[6]). The maximum P_v for each subject[L], denoted ${}^{+90th}_{ss1}P^{\mathrm{L}}_{vmaxi}$, may also be read and the maximum ${}^{+90th}_{ss1}P^{\mathrm{L}}_{vmaxi}$ denoted ${}^{+90th}_{ss1}P^{\mathrm{L}}_{vmax}$ is 0.52 N/kg (subject[1]). The mean ${}^{+90th}_{ss1}P^{\mathrm{L}}_{vmaxi} \leq P_v \leq {}^{+90th}_{ss1}P^{\mathrm{L}}_{vmaxi}$ for each subject[L] is is indicated by a solid circle: it can be seen that these means are located variously in the intra-subject range but where range magnitudes are larger means are located in the second to third quarters. Subject[0] shows the range of the minimum ${}^{+90th}_{ss1}P^{\mathrm{L}}_{vmini}$ to the maximum ${}^{+90th}_{ss1}P^{\mathrm{L}}_{vmaxi}$ and the mean of all the mean ${}^{+90th}_{ss1}P^{\mathrm{L}}_{vmini} \leq P_v \leq {}^{+90th}_{ss1}P^{\mathrm{L}}_{vmaxi}$ is indicated by a solid circle and this is located approximately centrally in the inter-subject range.

It can also be seen from Figure D.93 (page 382) that the range magnitude of

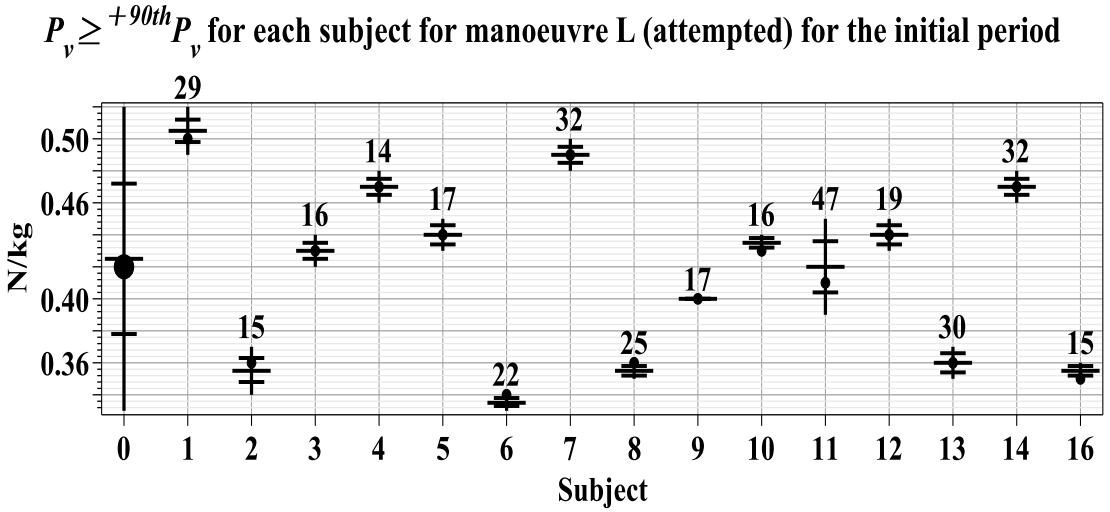

Figure D.93 – Shows for each subject[L] (i) for $\{{}_{ss1}\theta_0^{\mathrm{L}}\}$ in N/kg: a vertical line indicating the minimum measure ${}^{+90th}_{ss1}P^{\mathrm{L}}_{vmini}$ to the maximum measure ${}^{+90th}_{ss1}P^{\mathrm{L}}_{vmaxi}$, a solid circle indicating the mean ${}^{+90th}_{ss1}P^{\mathrm{L}}_{vmini} \leq P_v \leq {}^{+90th}_{ss1}P^{\mathrm{L}}_{vmaxi}$, the quarter divisions of the range (horizontal lines) and the number of occurrences of $P_v \geq {}^{+90th}_{ss1}P^{\mathrm{L}}_{v}$ shown above the range line. Subject[0] shows these measures for all subjects[L] with a solid circle indicating the mean of all the mean ${}^{+90th}_{ss1}P^{\mathrm{L}}_{vmini} \leq P_v \leq {}^{+90th}_{ss1}P^{\mathrm{L}}_{vmaxi}$.

0.19 N/kg, ${}^{+90th}_{ss1}P^{\mathrm{L}}_{vmax} - {}^{+90th}_{ss1}P^{\mathrm{L}}_{vmin}$, arises from inter-subject variation (subject[6] compared with subject[1]) and is not the result of the ${}^{+90th}_{ss1}P^{\mathrm{L}}_{vmaxi} - {}^{+90th}_{ss1}P^{\mathrm{L}}_{vmini}$ magnitude of a specific subject. There are therefore substantial differences between subjects for the magnitudes of the largest $P_v > 0$. However, the inequality ${}^{+90th}_{ss1}P^{\mathrm{L}}_{vmini} \leq P_v \leq {}^{+90th}_{ss1}P^{\mathrm{L}}_{vmaxi}$ provides a representative range for each subject[L]. Additionally the inequality ${}^{+90th}_{ss1}P^{\mathrm{L}}_{vmin} \leq P_v \leq {}^{+90th}_{ss1}P^{\mathrm{L}}_{vmax}$ provides a representative range for all subjects[L].

D.14.5. *Manoeuvre L (a.) the $P_v - P_{uCs}$ plane*

This final section relating to manoeuvre L (a.) uses the inequalities, as previously defined, to define a cuboid boundary for the largest magnitude measures for each and all subjects. As the P_u measure occurs in both signs two sets of three inequalities are required. For each of subjects[1, 2, 4, 5, 6, 7, 10, 11, 12, 13, 14] the following inequalities define the cuboid boundaries:

$${}^{-90th}_{ss1}P^{\mathrm{L}}_{uCsmini} \geq P_{uCs} \geq {}^{-90th}_{ss1}P^{\mathrm{L}}_{uCsmaxi},$$

$${}^{+90th}_{ss1}P^{\mathrm{L}}_{vmini} \leq P_v \leq {}^{+90th}_{ss1}P^{\mathrm{L}}_{vmaxi} \text{ and}$$

$${}^{+90th}_{ss1}P^{\mathrm{L}}_{umini} \leq P_u \leq {}^{+90th}_{ss1}P^{\mathrm{L}}_{umaxi}.$$

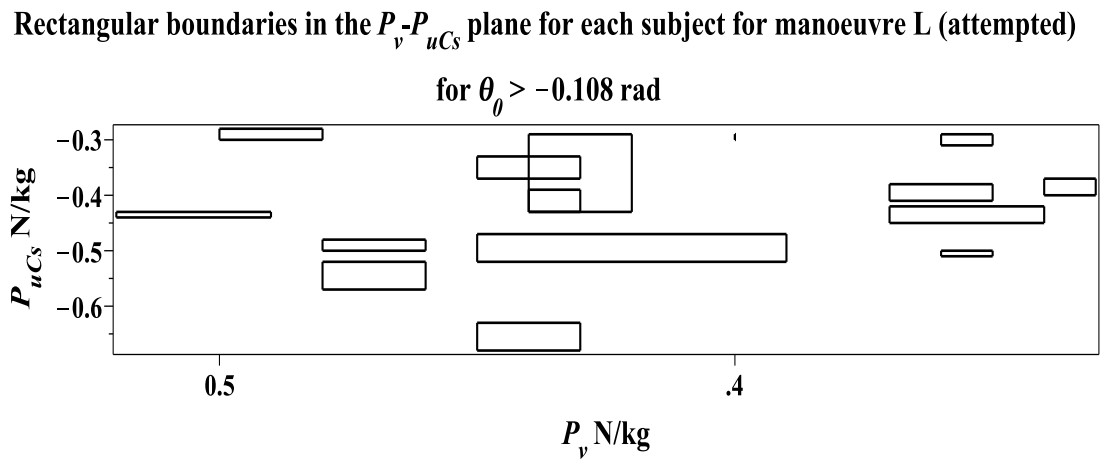

Figure D.94 – Rectangles formed with vertices of coordinates $[{}^{+90th}_{ss1}P^{\mathrm{L}}_{vmaxi}, {}^{-90th}_{ss1}P^{\mathrm{L}}_{uCsmini}]$, $[{}^{+90th}_{ss1}P^{\mathrm{L}}_{vmini}, {}^{-90th}_{ss1}P^{\mathrm{L}}_{uCsmini}]$, $[{}^{+90th}_{ss1}P^{\mathrm{L}}_{vmini}, {}^{-90th}_{ss1}P^{\mathrm{L}}_{uCsmaxi},]$, and $[{}^{+90th}_{ss1}P^{\mathrm{L}}_{vmaxi}, {}^{-90th}_{ss1}P^{\mathrm{L}}_{uCsmaxi}]$ for all subjects[L] i.e. n=15.

For subjects[2, 3, 4, 5, 6, 8, 9, 10, 11, 12, 13, 14, 16] the second set of three inequalities are as given for P_{uCs} and P_v above and

$${}^{-90th}_{ss1}P^{\mathrm{L}}_{umini} \geq P_u \geq {}^{-90th}_{ss1}P^{\mathrm{L}}_{umaxi}.$$

A graphical representation of ${}^{large}_{ss1}\mathbf{P}^{\mathrm{L}}_i$ in the $P_v - P_{uCs}$ plane is shown in Figure D.94 (page 383).

The cuboid boundaries which enclose the measures for all, rather than each of, subjects[L] can be determined by removal of the i subscript from the above definitions. These two sets of three inequalities for all subjects[L] are denoted ${}^{large}_{ss1}\mathbf{P}^{\mathrm{L}}$. In conclusion ${}^{large}_{ss1}\mathbf{P}^{\mathrm{L}}$ provides a useful representation of the largest handle-forces for all subjects[L] for manoeuvre L (a.). The numerical values are:

$0.33 \leq P_v \leq 0.52$ (N/kg),

$-0.28 \geq P_{uCs} \geq -0.68$ (N/kg),

$0.02 \leq P_u \leq 0.19$ (N/kg) and

$-0.01 \geq P_u \geq -0.27$ (N/kg).